

Polypyridyl Transition Metal Complexes for Application in Optoelectronic Devices: Characterization and Film Preparation Studies

Dissertation

zur Erlangung des akademischen Grades
doctor rerum naturalium (Dr. rer. nat.)



seit 1558

vorgelegt dem Rat der
Chemisch-Geowissenschaftlichen Fakultät
der Friedrich-Schiller-Universität Jena

von Diplom-Chemiker Christian Friebe
geboren am 06. April 1984 in Erfurt

Gefördert durch den Fonds der Chemischen Industrie (FCI), den Europäischen Sozialfonds (ESF) und die Thüringer Aufbaubank.

Gutachter:

1. Prof. Dr. Ulrich S. Schubert (Friedrich-Schiller-Universität Jena)
2. Jun.-Prof. Dr. Anna Ignaszak (Friedrich-Schiller-Universität Jena)
3. Prof. Dr. Biprajit Sarkar (Freie Universität Berlin)

Tag der öffentlichen Verteidigung: 02. Oktober 2013

„Wer die Weisheit sucht, ist ein weiser Mann; wer glaubt, sie gefunden zu haben, ist ein Narr.“ Lucius Annaeus Seneca

„Immer erscheinen die entscheidenden Ideen nachträglich als einfache und selbstverständliche.“ Stefan Zweig

Table of Contents

| | |
|---|----|
| Table of Contents | 1 |
| Documentation of Authorship | 2 |
| 1 Introduction | 5 |
| 2 Theoretical Background | 7 |
| 2.1 Metal complexes from 2,2':6',2''-terpyridines and 1 <i>H</i> -1,2,3-triazole-containing ligands | 7 |
| 2.2 Metallopolymers by electropolymerization | 10 |
| 2.3 Ruthenium(II) complexes in dye-sensitized solar cells | 13 |
| 3 Metallopolymers of π -Conjugated <i>Bis</i> -2,2':6',2''-terpyridines | 15 |
| 3.1 Zinc(II) metallopolymers..... | 16 |
| 3.2 Ruthenium(II) metallopolymers | 19 |
| 3.3 Inkjet printing of <i>bis</i> -2,2':6',2''-terpyridine metallopolymers..... | 19 |
| 4 Tridentate 1,2,3-Triazolyl Ligands in Ruthenium(II) Complexes..... | 23 |
| 4.1 Ruthenium(II) complexes of 1,2,3-triazolyl-containing cyclometalating ligands..... | 23 |
| 4.2 A ruthenium(II) complex of an abnormal carbene ligand | 30 |
| 4.3 Metallopolymers from ditopic 1,2,3-triazolyl-containing ligands..... | 31 |
| 4.4 Conclusion..... | 33 |
| 5 Metallopolymers of Ruthenium(II) Complexes of Tridentate Ligands through Electropolymerization | 35 |
| 5.1 Electropolymerization of ruthenium(II)-2,6-di(quinoline-8-yl)pyridine complexes..... | 35 |
| 5.2 Electropolymerization of cyclometalated ruthenium(II) complexes | 46 |
| Summary | 57 |
| Zusammenfassung..... | 59 |
| References | 61 |
| Publication List..... | 67 |
| Curriculum Vitae..... | 71 |
| Acknowledgements | 73 |
| Declaration of Authorship / Selbstständigkeitserklärung..... | 75 |
| Supplementary Information..... | 77 |
| List of Abbreviations..... | 85 |
| Publications A1–A11 | 87 |

Documentation of Authorship

This section contains a list of the individual authors' contributions to the publications reprinted in this thesis.

- A1) C. Friebe, M. D. Hager, A. Winter, U. S. Schubert, "Metal-containing polymers via electropolymerization", *Adv. Mater.* **2012**, *24*, 332–345.

C. Friebe: conception, preparation of the manuscript
A. Winter, M. D. Hager: correction of the manuscript, supervision
U. S. Schubert: correction of the manuscript, supervision

- A2) A. Wild, C. Friebe, A. Winter, M. D. Hager, U.-W. Grummt, U. S. Schubert, " π -Conjugated 2,2':6',2''-bis(terpyridines): Systematical tuning of the optical properties by variation of the linkage between the terpyridines and the π -conjugated system", *Eur. J. Org. Chem.* **2010**, 1859–1868.

A. Wild: conception, synthesis and characterization of the compounds, manuscript preparation
C. Friebe: thin-film preparation and characterization
U. W. Grummt: computational calculations, correction of the manuscript
A. Winter, M. D. Hager: correction of the manuscript, supervision
U. S. Schubert: correction of the manuscript, supervision

- A3) A. Wild, F. Schlütter, G. M. Pavlov, C. Friebe, G. Festag, A. Winter, M. D. Hager, V. Cimrová, U. S. Schubert, " π -Conjugated donor and donor-acceptor metallo-polymers", *Macromol. Rapid Commun.* **2010**, *31*, 868–874.

A. Wild: conception, preparation and characterization of compounds, thin-films, and devices, manuscript preparation
F. Schlütter: synthesis and characterization of compounds
G. M. Pavlov: AUC and viscosity measurements
C. Friebe: UV-vis absorption and emission measurements in solution
G. Festag: SEC measurements
A. Winter, M. D. Hager: correction of the manuscript, supervision
V. Cimrová: supervision of the device preparation
U. S. Schubert: correction of the manuscript, supervision

- A4) F. Schlütter, A. Wild, A. Winter, M. D. Hager, A. Baumgaertel, C. Friebe, U. S. Schubert, "Synthesis and characterization of new self-assembled metallo-polymers containing electron-withdrawing and electron-donating bis(terpyridine) zinc(II) moieties", *Macromolecules* **2010**, *43*, 2759–2771.

F. Schlütter: synthesis and characterization of the compounds, UV-vis absorption and emission measurements, manuscript preparation
A. Wild: synthesis and characterization of the compounds, CV measurements, preparation and characterization of thin films
A. Winter, M. D. Hager: correction of the manuscript, supervision
A. Baumgaertel: MALDI-TOF MS measurement
C. Friebe: UV-vis absorption and emission measurements
U. S. Schubert: correction of the manuscript, supervision

A5) C. Friebe, A. Wild, J. Perelaer, U. S. Schubert, "Inkjet printing of zinc(II) *bis*-2,2':6',2''-terpyridine metallopolymers: Printability and film-forming studies by a combinatorial thin-film library approach", *Macromol. Rapid Commun.* **2012**, *33*, 503–509.

C. Friebe: conception, inkjet printing and characterization of thin films, manuscript preparation
A. Wild: synthesis of the compounds
J. Perelaer: correction of the manuscript, supervision
U. S. Schubert: correction of the manuscript, supervision

A6) B. Schulze, D. Escudero, C. Friebe, R. Siebert, H. Görls, S. Sinn, M. Thomas, S. Mai, J. Popp, B. Dietzek, L. González, U. S. Schubert, "Ruthenium(II) photosensitizers of tridentate click-derived cyclometalating ligands: A joint experimental and computational study", *Chem. Eur. J.* **2012**, *18*, 4010–4025.

B. Schulze: conception, synthesis and characterization of compounds, preparation of the manuscript
D. Escudero: computational calculations, contribution to the manuscript preparation
C. Friebe: UV-vis absorption and emission, electrochemistry, spectro-electrochemistry, contribution to the manuscript preparation
R. Siebert: time- and temperature-dependent UV-vis emission measurements, contribution to the manuscript preparation
H. Görls: X-ray diffraction measurements
S. Sinn: synthesis of compounds
M. Thomas, S. Mai: computational calculations
J. Popp, B. Dietzek: correction of the manuscript, supervision
L. González: correction of the manuscript, supervision
U. S. Schubert: correction of the manuscript, supervision

A7) B. Schulze, D. Escudero, C. Friebe, R. Siebert, H. Görls, U. Köhn, E. Altuntas, A. Baumgaertel, M. D. Hager, A. Winter, B. Dietzek, J. Popp, L. González, U. S. Schubert, "A heteroleptic *bis*(tridentate) ruthenium(II) complex of a click-derived abnormal carbene pincer ligand with potential for photosensitizer application", *Chem. Eur. J.* **2011**, *17*, 5494–5498.

B. Schulze: conception, synthesis and characterization of compounds, preparation of the manuscript
D. Escudero: computational calculations, contribution to the manuscript preparation
C. Friebe: UV-vis absorption and emission, electrochemistry, spectro-electrochemistry, contribution to the manuscript preparation
R. Siebert: time-dependent emission measurements
H. Görls: X-ray diffraction measurements
U. Köhn: computational calculations
E. Altuntas: ESI MS measurements
A. Baumgaertel: MALDI MS measurements
M. D. Hager, A. Winter: correction of the manuscript
B. Dietzek, J. Popp: correction of the manuscript, supervision
L. González: correction of the manuscript, supervision
U. S. Schubert: correction of the manuscript, supervision

- A8) B. Schulze, C. Friebe, S. Hoepfner, G. M. Pavlov, A. Winter, M. D. Hager, U. S. Schubert, "Ruthenium(II) metallo-supramolecular polymers of click-derived tridentate ditopic ligands" *Macromol. Rapid Commun.* **2012**, *33*, 597–602.
- B. Schulze: conception, synthesis and characterization of compounds, preparation of the manuscript
 C. Friebe: UV-vis absorption and emission measurements, electrochemistry spectroelectrochemistry
 S. Hoepfner: AFM and TEM measurements
 G. M. Pavlov: analytical ultracentrifugation studies
 M. D. Hager, A. Winter: correction of the manuscript
 U. S. Schubert: correction of the manuscript, supervision
- A9) C. Friebe, H. Görls, M. Jäger, U. S. Schubert, "Linear metallopolymers from ruthenium(II)-2,6-di(quinolin-8-yl)pyridine complexes by electropolymerization – Formation of redox-stable and emissive films" *Eur. J. Inorg. Chem.* **2013**, 4191–4202.
- C. Friebe: conception, electropolymerization, UV-vis absorption and emission, electrochemistry, spectroelectrochemistry, manuscript preparation
 H. Görls: X-ray diffraction measurements
 M. Jäger: synthesis and characterization of compounds, computational calculations, contribution to the manuscript preparation
 U. S. Schubert: correction of the manuscript, supervision
- A10) C. Friebe, M. Jäger, U. S. Schubert, "Emitting electrode coatings with redox-switchable conductivity: Incorporation of ruthenium(II)-2,6-di(quinolin-8-yl)pyridine complexes into polythiophene by electropolymerization" *RSC Adv.* **2013**, *3*, 11686–11690.
- C. Friebe: conception, electropolymerization, UV-vis absorption and emission, electrochemistry, manuscript preparation
 M. Jäger: synthesis and characterization of compounds, contribution to the manuscript preparation
 U. S. Schubert: correction of the manuscript, supervision
- A11) C. Friebe, B. Schulze, H. Görls, M. Jäger, U. S. Schubert, "Designing cyclometalated ruthenium(II) complexes for anodic electropolymerization", *Chem. Eur. J.*, DOI: 10.1002/chem.201301439.
- C. Friebe: conception, electropolymerization, UV-vis absorption and emission, electrochemistry, spectroelectrochemistry, manuscript preparation
 B. Schulze: conception, synthesis and characterization of compounds, preparation of the manuscript
 H. Görls: X-ray diffraction measurements
 M. Jäger: computational calculations, contribution to the manuscript preparation
 U. S. Schubert: correction of the manuscript, supervision

1 Introduction

Nowadays, huge efforts are made to develop functional materials that are suitable for application in electro-optical devices. Namely the energy generation by photovoltaics,^[1] electroluminescent lighting devices,^[2] catalysis of organic and inorganic chemical reactions,^[3] water splitting, in particular with respect to photo-catalyzed hydrogen production,^[4] as well as sensing systems^[5] are in the focus of many scientific projects.

Due to the mankind's rising demand for energy, in particular the transformation of sunlight into electricity is of outstanding importance.^[6] Hence, various approaches have been developed to complement and even substitute the conventional inorganic semiconductors by alternative photosensitizers within solar cells, *e. g.* by inorganic nanoparticles,^[7] conducting organic polymers,^[8] as well as small-molecule and metal-complex systems.^[1b, 1e, 9] In this regard, namely ruthenium(II) polypyridyl complexes became highly prominent candidates for photosensitizers, in particular within Grätzel-type dye-sensitized solar cells (DSSCs), due to their efficient light absorptivity and high redox stability.^[10] However, the well-established parent systems ruthenium(II)-*tris*(2,2'-bipyridine) and ruthenium(II)-*bis*(2,2':6',2''-terpyridine) suffer from inherent drawbacks, namely the possibility of structural isomers and unfavorable photophysical characteristics, respectively.^[11] As a consequence, we synthesized and characterized ruthenium(II) complexes using novel tridentate polypyridyl-type ligands with optimized electrochemical and photophysical characteristics showing the potential for future photosensitizer application.

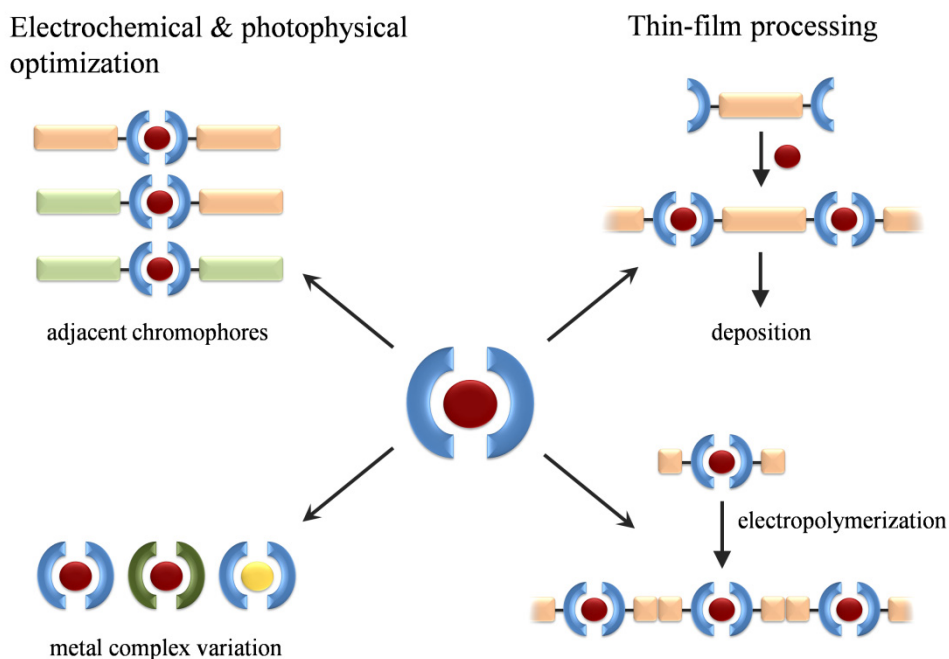


Figure 1.1. Schematic overview over the investigated *bis*-tridentate complexes presented in this thesis: (1) Manipulation of the electrochemical and photophysical properties by variation of ancillary chromophores and by modification of the complex moiety, *i. e.* the coordinating ligand or the metal. (2) Preparation of thin metallopolymer films either by the complexation of bifunctional ligands and subsequent deposition or by precipitation *via* electrochemical polymerization.

Additionally, in the course of the assembly of a final device, *i. e.* an operating solar cell, thin-film processability comes to the fore (Figure 1.1). In general, films of single small molecules and metal complexes suffer from brittleness and, in case of multi-compound mixtures, phase separation. In contrast, polymeric systems allow the formation of smooth and

homogenous thin films that are suitable for utilization in electro-optical devices. Here, the incorporation of metal complexes into metallopolymers, combining the photophysical and electrochemical characteristics of the monomers with the favorable solid-state properties of a polymer, represents a convenient method.^[12] Different procedures are possible: Firstly, the polymerization can be carried out through the complexation of bifunctional ligands. The thus obtained polymers can be processed using conventional film-preparation methods (*e. g.* spin-coating, doctor blading, inkjet printing). On the other hand, metal complexes can be prepared that carry suitable functionalities for a subsequent, efficient coupling. In particular, the electrochemical polymerization of metal complexes represents a versatile approach since it allows the direct coating of surfaces during the polymerization process. In this thesis, both approaches, the complexation of *bis*-polypyridyl ligands with ruthenium(II) ions as well as the electropolymerization of the respective complexes, are presented.

In view of energy shortage, also efficient lighting, *i. e.* energy-to-light transformation, represents a highly significant topic. Organic and polymer-based light-emitting diodes (OLEDs and PLEDs) became more and more popular since their introduction over twenty years ago.^[13] Here, a promising approach is the usage of small, organic, and π -conjugated molecules whose electro-optical properties can be easily tuned *via* chemical functionalization.^[14] Again, to allow a facile thin-film processability, the formation of polymers from the functional small molecules is intended using the metallopolymer concept, *i. e.* applying bifunctional, π -conjugated ligands for metal complexation. Since the ligands already possess the aimed photophysical and electrochemical features themselves, a metal ion should be used that does not interact extensively with the ligands' electronic system and works only as linking unit. Here, metallopolymers based on zinc(II) ions, exhibiting a closed, thus stable, d^{10} outer-shell electron configuration, represent a suitable choice. Hence, zinc(II)-containing polymers possessing π -conjugated *bis*(2,2':6',2''-terpyridine) ligands were prepared and characterized with regard to a future application in electroluminescent devices. Additionally, their thin-film processability will be elaborated within combinatorial inkjet-printing studies.

2 Theoretical Background

Parts of this chapter have been published: A1) C. Friebe, M. D. Hager, A. Winter, U. S. Schubert, *Adv. Mater.* **2012**, *24*, 332–345.

2.1 Metal complexes from 2,2':6',2''-terpyridines and 1*H*-1,2,3-triazole-containing ligands

Polypyridyl-type ligands have gained much interest since they provide stable complexes with various metal ions as well as noteworthy photophysical and electrochemical characteristics. In particular, ligand systems based on the 2,2':6',2''-terpyridine (tpy) unit are extensively used to build up molecular and supramolecular structures and represent the current benchmark in the field of tridentate polypyridyl-type ligands.^[11a, 15] However, there are plenty of competing analogue systems, achieved by substituting pyridyl units for alternative aryl moieties, offering advantages regarding synthetic access and inherent properties.^[16] A promising, relatively young type of ligands is the 1*H*-1,2,3-triazole-containing one, firstly introduced for the purpose of metal complexation as tridentate 2,6-*bis*(1-alkyl-1*H*-1,2,3-triazol-4-yl)pyridine by Flood and Hecht in 2007.^[17] Since then, this ligand has received much attention generating bidentate and cyclometalating as well as cationic and abnormal carbene offshoots.^[18]

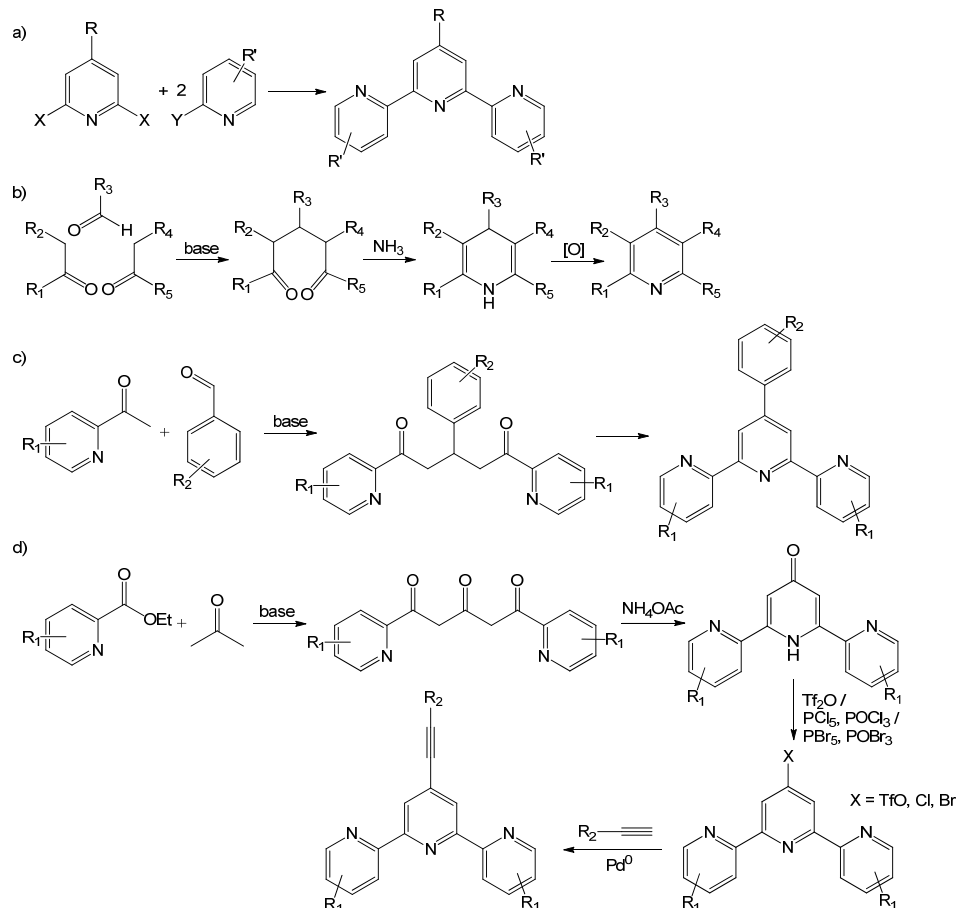
In this thesis, monomeric and polymeric metal complex systems bearing terpyridines or 1,2,3-triazole-containing ligands are studied, in particular with regard to their optical and electrochemical characteristics. This section introduces fundamental basics in terms of general synthesis routes and properties of the respective metal complexes and metallopolymers.

2.1.1 Synthetic routes towards 2,2':6',2''-terpyridine- and 1*H*-1,2,3-triazole-based ligands and related ruthenium(II) and zinc(II) complexes

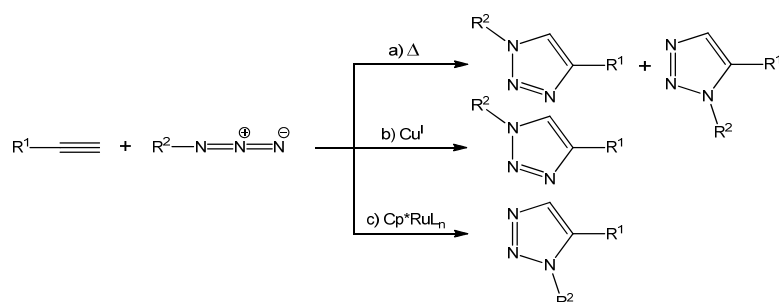
The first synthesis of a 2,2':6',2''-terpyridine is dated to 1932, when Morgan and Burstall isolated small amounts as by-product of the oxidative coupling of pyridine with FeCl₃.^[19] In the meantime, several synthesis methods have been developed for the directed preparation of terpyridines with a variety of functionalities. Cross-coupling reactions, *e. g.* the Ullmann reaction, coupling of lithium-species, palladium(0)-catalyzed Suzuki and Stille reaction, have been used to couple pyridines and 2,2'-bipyridines (Scheme 2.1a).^[20] However, procedures that involve the assembly of at least one pyridine ring are used much more frequently.^[15c, 21] Besides conventional pyridine-derivative synthesis protocols, *e. g.* of Hantzsch^[22] and Tschischibabin^[23] type, the most common synthesis route is the Kröhnke-type condensation,^[24] which bases upon the reaction of 2-acetylpyridine with an aromatic aldehyde leading to 4'-aryl-substituted 2,2':6',2''-terpyridines (Scheme 2.1b, c). Since many functional groups are tolerated under the reaction conditions, various protocols have been developed based on the original Kröhnke procedure.^[25] In particular with regard to the introduction of photophysically interesting π -conjugated substituents, the syntheses of halide-,^[26] alkyne- (Ziessel type, Scheme 2.1d),^[27] vinyl-,^[28] and azide-functionalized^[29] terpyridines have to be highlighted.

Replacing outer pyridyl rings by 1,2,3-triazole heterocycles led to a new class of terpyridine alternatives, which has established over the last five years.^[16a] The synthesis is based on the 1,3-cycloaddition of alkynes and organic azides, which was developed by Huisgen *et al.* during the 1960s (Scheme 2.2).^[30] However, the thermally induced Huisgen-type reaction produces mixtures of 1,4- and 1,5-disubstituted-1,2,3-triazoles, being inapplicable for the directed synthesis of defined systems. Hence, metal-catalyzed versions were developed, namely the

copper(I)-catalyzed 1,3-cycloaddition of alkynes and azides (CuAAC), designed independently by Meldal^[31] and Sharpless,^[32] and the ruthenium(II)-based catalysis by Fokin,^[33] leading selectively to 1,4- and 1,5-substitution patterns, respectively. Being formerly used as an innocent linking unit, the 1,2,3-triazole became a popular fragment within functional assemblies because of its interesting structural and electronic properties.^[34] Namely the usage as pyridyl analogue in metal-coordinating ligands led to an entire new group of metal complexes.^[17, 18c, 35]



Scheme 2.1. 2,2':6',2''-Terpyridine synthesis routes: a) General representation of cross-coupling reactions (X, Y: *e. g.* halide, SnR₃, BR₂, Li, pyridyl), b) general scheme of synthesis *via* condensation buildup of the central pyridyl ring, and c) Kröhnke-type condensation, and d) Ziesel-type procedure.

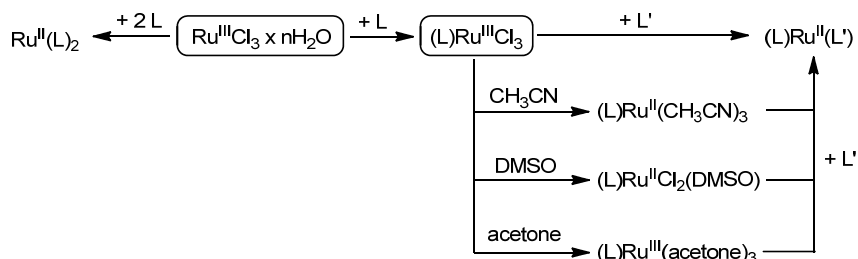


Scheme 2.2. 1,3-Cycloaddition of alkynes and azides: a) Thermal reaction producing stereoisomer mixtures, b) 1,4-isomer-selective copper(I) catalysis, and c) 1,5-isomer-selective ruthenium catalysis.

This work particularly focuses on complexes of tridentate ligands with ruthenium(II) and zinc(II) ions. Ruthenium(II) forms *bis*-complexes with terpyridine-like tridentate ligands, which possess high thermodynamic and kinetic stabilities.^[36] Thus, a two-step synthesis is possible, enabling the preparation of heteroleptic assemblies (Scheme 2.3). On the other hand, harsh reaction conditions are generally required, which can be avoided, *e. g.* by applying

microwave irradiation^[37] or converting the initial ruthenium(III) trichloride *mono*-complex to a more reactive species carrying acetone,^[38] DMSO,^[26a, 39] or acetonitrile^[40] ligands.

In comparison to ruthenium(II), *bis*-2,2':6',2''-terpyridine complexes of zinc(II) show both reduced stability and increased lability^[41] because of metal-ligand interactions that are dominated by an ionic character due to the filled d¹⁰ shell of zinc(II) in contrast to an intense orbital exchange for d⁶-ruthenium(II) systems. Especially the high lability impedes the usage of particular solution-based characterization methods, *e. g.* size-exclusion chromatography (SEC),^[15b] as well as the formation of defined heteroleptic complexes. In general, the synthesis bases upon the reaction of a zinc(II) salt, *e. g.* Zn(AcO)₂, ZnCl₂, Zn(OTf)₂, with the ligand in a 1:2 ratio.^[42]



Scheme 2.3. Complexation of ruthenium with tridentate ligands towards homoleptic and heteroleptic complexes. For the latter route, the initially formed trichloride *mono*-complex precursor is either converted directly by reaction with a second ligand or firstly transformed to a more reactive form.

2.1.2 Photophysical and electrochemical properties of ruthenium(II) and zinc(II) complexes of 2,2':6',2''-terpyridine- and 1*H*-1,2,3-triazole-based ligands

The photophysical characteristics of ruthenium(II) complexes of terpyridine-analogue ligands are based on the interaction of metal-centered d orbitals with the π system of the ligands as well as on independent contributions of both. In Figure 2.1, a respective molecular orbital (MO) scheme is depicted.^[37a] The highest occupied molecular orbitals (HOMOs) are located in general on the metal, namely on the t_{2g}-type orbitals, while the lowest unoccupied molecular orbitals (LUMOs) are formed by ligand π^* orbitals. Thus, the visible, low-energy region of the UV-vis absorption spectrum is dominated by metal-to-ligand charge-transfer (MLCT) transitions.^[11a, 43] At higher energies, also transitions located solely either on the metal (metal-centered, MC) or one ligand (ligand-centered, LC) appear. The luminescence behavior is likewise determined by MLCT transitions – occurring emission arises from low-lying ³MLCT states – but also by competing MC-based relaxation. In particular, after excitation of the system *via* light absorption, it relaxes to the lowest excited singlet state, namely a ¹MLCT state, followed by intersystem crossing (ISC) towards the lowest, emissive ³MLCT state. However, in case of Ru(tpy)₂-analogue complexes, the ³MC states are also easily available, since the structural and electronic conditions enable an efficient coupling, *i. e.* a low crossing barrier towards the ³MLCTs due to large spatial orbital overlap and / or low energy difference (Figure 2.1).^[4c, 11a, 44] Since, in turn, the ³MC states couple efficiently with the ground state (GS) leading to radiationless internal-conversion (IC), these complexes show in general low photoluminescence quantum yields and very short lifetimes.^[11] Different strategies to overcome this limitation have been developed mainly focusing on the enlargement of the ³MLCT–³MC energy gap, *i. e.* stabilization of the ³MLCT state, destabilization of the ³MC state, or both. The most promising approaches are based on the incorporation of strong electron donors *via* cyclometalation^[16d, 45] or *N*-heterocyclic carbenes,^[16c] and structural modifications,^[16b, 46] whereas additional energy-storing chromophores only enhance the apparent lifetime.^[47] The

electrochemical properties are also determined by both metal(II) center and surrounding ligand assembly. In general, the Ru^{III}/Ru^{II} redox couple dominates the anodic electrochemistry of the complexes while ligand-centered processes determine the reduction behavior.^[11b]

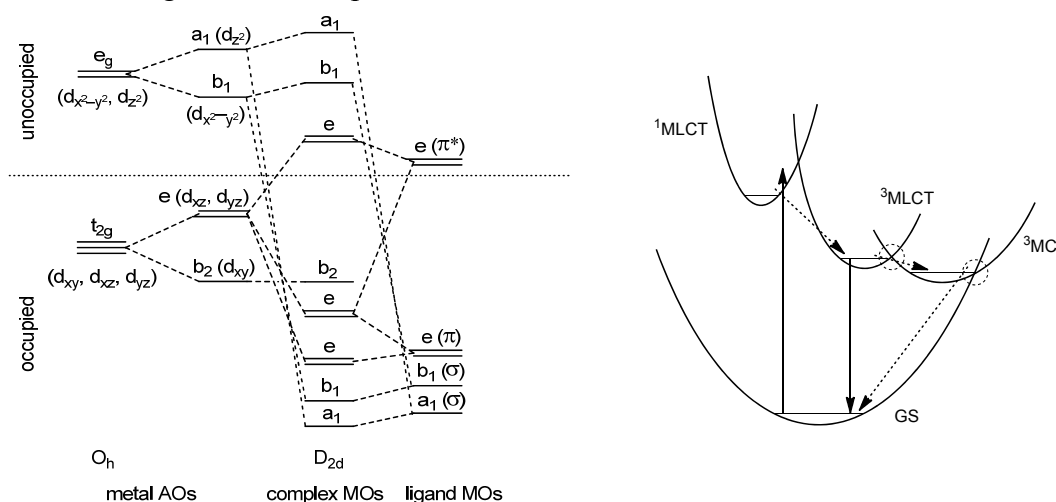


Figure 2.1. Qualitative MO scheme of the Ru(tpy)₂²⁺ complex (left) and qualitative potential energy surfaces for analogue complexes (right; solid arrows indicate radiative, dashed arrows non-radiative transitions, dashed circles display low energy barriers enabling efficient ³MC-mediated deactivation).

In contrast, the respective zinc(II) complexes reflect, in principle, the ligands' photophysical and electrochemical characteristics. The stable d¹⁰ closed shell of the zinc(II) ion prevents extensive interactions of the metal- and the ligand-based electron orbitals.^[42a, 42b] Thus, UV-vis absorption and emission spectra show only (mainly $\pi\pi^*$ -based) LC-transition bands; electrochemical studies reveal redox signals being typical for the ligands.

2.2 Metallopolymers by electropolymerization

In various cases, metal-containing compounds need to form thin coatings. Thereby, a suitable approach is the formation of metal-containing polymers directly onto respective surfaces *via* electropolymerization. This method offers several advantages compared to common polymerization techniques.^[48] Firstly, solubility problems, which often complicate thin-film processing, are avoided since the polymer itself is formed directly on the respective surface – only the monomers have to be dissolved, which is far easier to achieve in most cases. Secondly, the required time and instrumental effort to obtain a polymer film is low in comparison to alternative procedures. Thirdly, the thickness of electropolymerized films is easily controllable and simply determined through the polymerization time.

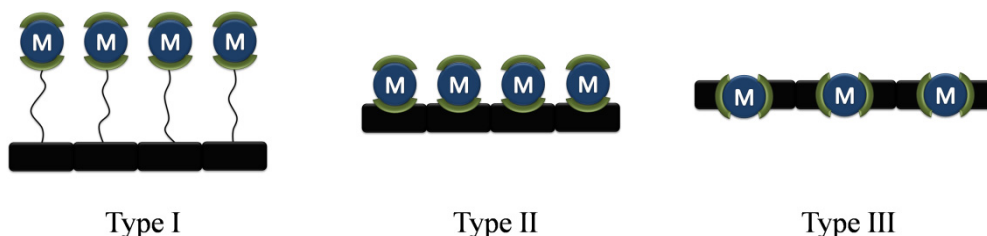


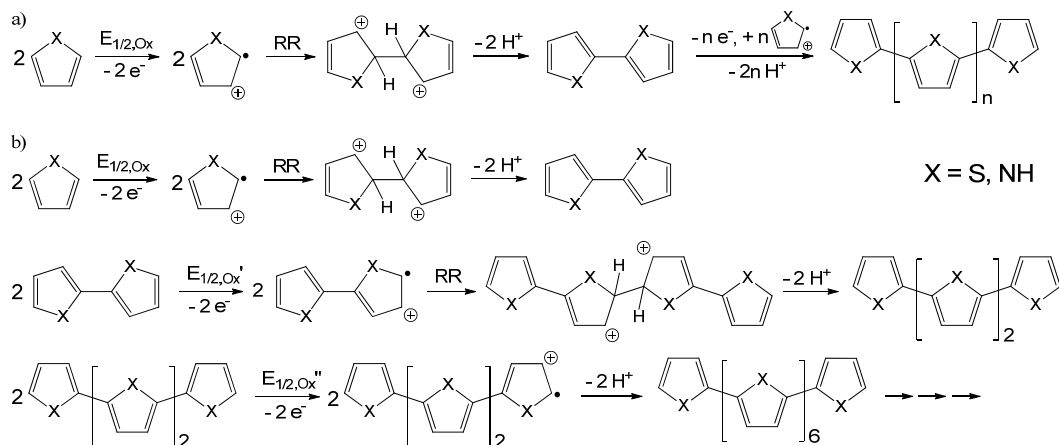
Figure 2.2. Possible arrangements of metal ions within metal-containing polymers.

In order to carry out an electrochemical polymerization, the metal complex has to be linked to an electropolymerizable moiety. The monomer unit can be incorporated into the polymer in different ways to obtain various types of metallopolymers. It can be coupled by a non-conjugated spacer (*e. g.* alkyl, ester, or ether linkages), so that the properties of the metal complex is

mostly unchanged in the course of polymer formation. Alternatively, the monomer can be attached directly to the complex ligand, either in a way to arrange the metal ions laterally on the polymer chain or to include them as an essential, linking part of the backbone (Figure 2.2). In the latter cases, a significant interaction between metal and polymer system as well as between the metal centers is present, with the largest mutual influences for the latter kind. Wolf classified such systems as metal-containing polymers of Type I, II, and III, respectively.^[49]

2.2.1 Mechanistic aspects

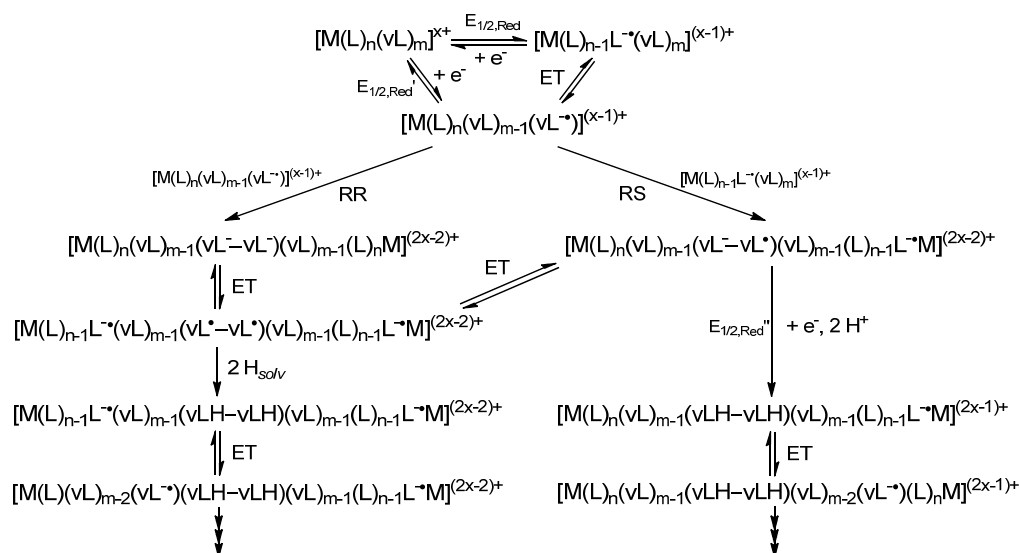
A widespread method is the oxidative coupling of 5-membered heterocycles, such as pyrrole, thiophene, 3,4-ethylenedioxythiophene (EDOT), and other aromatic systems (*e. g.* aniline). Although several versions have been proposed,^[50] it is generally believed that the first step of the electropolymerization, as soon as the respective potential is achieved, is the formation of radical cations through a one-electron oxidation of the aromatic ring, followed by radical-radical coupling (RR) and subsequent deprotonation leading to dimeric species.^[51] According to the original mechanism suggested by Diaz *et al.* in 1981 (Scheme 2.4a),^[52] the polymerization propagates by continuous chain growth through coupling of monomeric radical cations to oligomer radicals. Since the dimers and oligomers are more easily oxidizable than the monomers, their radical cations are formed immediately under the applied voltages. However, experimental and theoretical investigations showed that a coupling of oligomeric and monomeric radical cations is rather unlikely due to a decrease of radical reactivity and lowered deprotonation ability of their σ -coupling products with increasing chain length causing favored monomer-monomer coupling.^[53] By contrast, the coupling of oligomeric radical cations is supposed leading from dimers to tetramers to octamers etc. (Scheme 2.4b).^[48b, 54] At a critical chain length, the solubility is so low that the deposition process starts and film formation occurs.



Scheme 2.4. Proposed chain-growth mechanisms for the oxidative electropolymerization: a) Chain growth by addition of radical monomers and b) chain growth by coupling of oligomers.

Although oxidative methods are used in most of the cases, electropolymerization can also be carried out cathodically. The most common example is the reduction of vinyl-substituted pyridyl and polypyridyl complexes. The vinyl-possessing ligand can be reduced either directly or, depending on the order of reduction potentials, through electron transfer (ET) from a previously reduced ancillary ligand (Scheme 2.5).^[55] Subsequently, the generated vinyl radical anion reacts with a second vinyl radical anion (RR) or couples to the vinyl group of a complex having a radical ancillary ligand (radical-substrate coupling, RS). Again, the reducibilities of the ligand moieties determine the present species and, thus, the particular mechanism. The RR

path firstly leads to a vinyl-vinyl diradical possessing reduced ancillary ligands *via* electron transfer, followed by hydrogen abstraction from the solvent and a further electron transfer that generates again an anionic vinyl radical being able to continue the polymerization process. If the RS route is dominant, the formed vinyl-ancillary ligand diradical can either convert to the vinyl-vinyl diradical, following subsequently the previously described mechanism, or is further reduced, if the required reduction potential is applied. Reduction and associated protonation yield the dimer featuring a radical ancillary ligand that is able to transfer its unpaired electron to another vinyl ligand, thus, enabling further chain growth.



Scheme 2.5. Mechanism of the reductive electropolymerization of vinyl-pyridyl metal complexes (M: *e. g.* Fe, Ru, Os ($x = 2$) or Co, Cr ($x = 3$); L: *e. g.* py, bpy, tpy; vL: *e. g.* vinyl-py, vinyl-bpy).

2.2.2 Experimental remarks

Potential- and galvanostatic as well as potentiodynamic procedures can be used for electropolymerization. While the underlying polymerization mechanism remains the same,^[56] the solid-state morphology is influenced significantly by the chosen technique. However, which method offers a better homogeneity and substrate adhesion for the generated films depends on the particular polymerized system.^[57] The used electrode material complies with the targeted application of the polymerized material. For electrochemical characterization of the polymer, standard working electrodes, made of glassy carbon, platinum, gold, etc., are used. With regard to spectroscopic characterization or optical devices, transparent electrode materials, *e. g.* indium-doped tin oxide (ITO) or fluorine-doped tin oxide (FTO), have to be used.^[58] In case of anodic polymerization approaches using aromatic electropolymerizable moieties, Lewis acids (*e. g.* $BF_3 \cdot OEt_2$, Al_2O_3) are added occasionally to lower the related oxidation potentials. Thus, polymerization is possible in a wider range of electrolytes, on the one hand, and overoxidation of the resulting polymer is prevented, on the other hand.^[59]

The characterization of the prepared polymers starts already during the polymerization process, since the current and potential curve in case of potentiostatic and galvanostatic procedures, respectively, or the CV for potentiodynamic polymerizations provide first information about changing electrochemical response and the polymer growth. Furthermore, non-electrochemical methods can be used for online monitoring of the electropolymerization, *e. g.* UV-vis and IR spectroelectrochemistry for the spectral characterization of intermediates or electrochemical quartz crystal microbalance (EQCM) measurements to follow the film

growth. Post-synthesis characterization includes different electrochemical investigations, namely cyclic voltammetry, differential pulse polarography (DPP), or (*in situ*) conductivity measurements. Additionally, spectroscopic methods (UV-vis, NIR, IR, Raman, EPR) are applied either on the unmodified film or spectroelectrochemically. For a detailed film characterization, X-ray photoelectron spectroscopy (XPS), solid-state NMR spectroscopy, or transmission and scanning electron microscopy (TEM, SEM) are used.

2.3 Ruthenium(II) complexes in dye-sensitized solar cells

With regard to light-to-energy conversion, dye-sensitized solar cells have gained much attention since they were firstly introduced by O'Regan and Grätzel in 1991^[10b] and, meanwhile, devices showing efficiencies up to 11% could be prepared.^[60] The Grätzel-type DSSC bases on a mesoporous TiO₂ semiconductor film, which possesses an electronic band gap of about 3 eV itself, corresponding to UV-light absorption, and that is, therefore, equipped with a layer of a photosensitizer, which allows the absorption of low-energy visible light leading to charge injection into the TiO₂ conduction band. A redox mediator (*e. g.* I₃⁻/I⁻), which is contained in the surrounding electrolyte, accounts for the regenerating reduction of the oxidized dye and is reduced itself at the adjacent counter electrode (Figure 2.3).^[10a]

Ruthenium(II)-polypyridyl complexes currently represent the favored sensitizer dyes due to their ability to perform efficient light absorption and subsequent charge separation, resulting in the oxidized metal ion and a reduced ligand system. Variations of the latter one, through introduction of functionalities and substitution of pyridine rings by alternative aromatic cycles, allow comprehensive fine-tuning of the UV-vis properties and electrochemical characteristics of the complexes to fulfill the demands of a solar cell photosensitizer: Firstly, a large fraction of the solar spectrum should be absorbed, meaning that the longest-wavelength absorption needs to be in the visible-red or even the NIR region. Secondly, the sensitizer's redox potentials must allow efficient electron injection and dye regeneration. The injection process is determined by the gap between the excited-state oxidation potential of the dye and the conduction band edge of the TiO₂. The latter one can be strongly influenced by the electrolyte since particular ions, *e. g.* Li⁺, are able to be inserted into the mesoporous semiconductor lattice increasing its surface charge and causing a lowered required energy for electrons to pass into the conduction band. That way, shifts of the band edge by about 1 eV are possible.^[10a, 61] Furthermore, the lifetimes of the photo-excited states of the sensitizer have to be long enough to permit charge migration towards the semiconductor's conduction band. Dependent on the conduction band edge, thus on the used electrolyte, injection half times in the region of 0.1 to 1 ns were identified,^[62] so that excited-state lifetimes of several nanoseconds are sufficient in general.

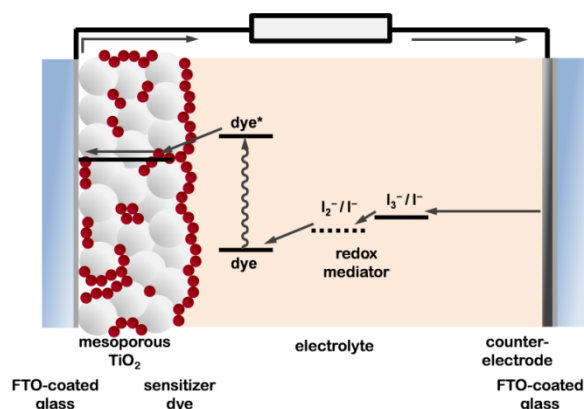


Figure 2.3. Schematic overview of a dye-sensitized solar cell with a simplified energy diagram.

3 Metallopolymers of π -Conjugated *Bis-2,2':6',2''-terpyridines*

Parts of this chapter have been published: A2) A. Wild, C. Friebe, A. Winter, M. D. Hager, U.-W. Grummt, U. S. Schubert, *Eur. J. Org. Chem.* **2010**, 1859–1868; A3) A. Wild, F. Schlütter, G. M. Pavlov, C. Friebe, G. Festag, A. Winter, M. D. Hager, V. Cimrová, U. S. Schubert, *Macromol. Rapid Commun.* **2010**, *31*, 868–874; A4) F. Schlütter, A. Wild, A. Winter, M. D. Hager, A. Baumgaertel, C. Friebe, U. S. Schubert, *Macromolecules* **2010**, *43*, 2759–2771; A5) C. Friebe, A. Wild, J. Perelaer, U. S. Schubert, *Macromol. Rapid Commun.* **2012**, *33*, 503–509.

Complexation of π -conjugated *bis-2,2':6',2''-terpyridines* by transition metal ions provides metallopolymers that combine the benefits of the used π -conjugated systems (*i. e.* favorable optical and electrochemical properties) with those of polymers (*i. e.* thin-film processability), both being essential for a potential application in electro-optical devices.^[15b, 63] A library of *bis-terpyridines* that possess different spacers and their respective zinc(II) and ruthenium(II) metallopolymers were synthesized and characterized to investigate spectroscopic and electrochemical structure-property-relationships.

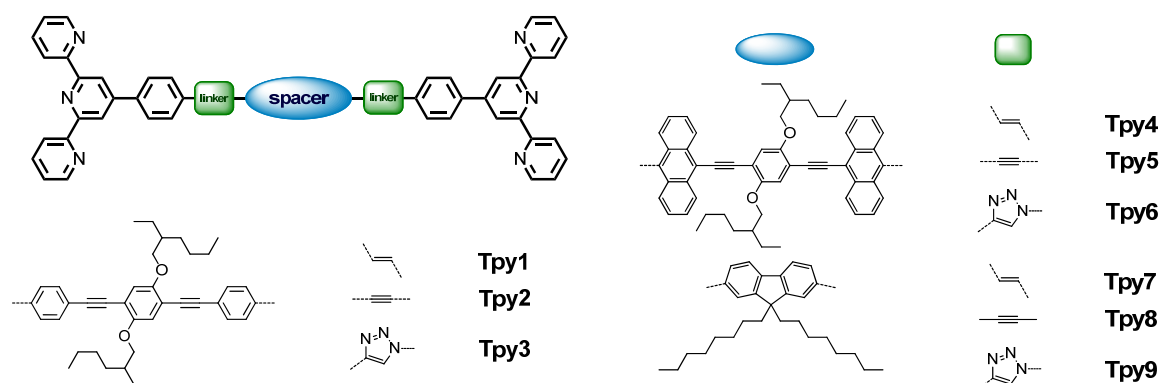


Figure 3.1. Schematic representation of the studied electron-donor *bis-2,2':6',2''-terpyridines*.

Thus, π -conjugated *bis-2,2':6',2''-terpyridines* with varying chromophore moieties and different linking units were studied (Figure 3.1 and 3.2, and Table 3.1). The variation of the latter causes spectral shifts depending on the conjugation efficiency of the linker. Since the double bond turned out to show a higher degree of conjugation than the triple bond,^[64] in general, the double bond-containing species feature a bathochromically shifted absorption. On the other hand, calculations revealed that the *1H-1,2,3-triazole* building block diminishes π -conjugation. Therefore, the *bis-terpyridines* having triazole linkers exhibit blue shifts compared to their double- and triple-bond counterparts. Here, the double bond- and anthracene-containing system (**Tpy4**) represents an exception; the steric hindrance caused by the bulky anthracene unit leads to a disturbed conjugation, also in the case of the double-bond linker. For the central moiety, both electron-donor (**Tpy1** to **Tpy9**) and electron-donor-acceptor (**Tpy10** to **Tpy20**) blocks were used, reflected in the generally higher absorption wavelengths for the latter compounds.

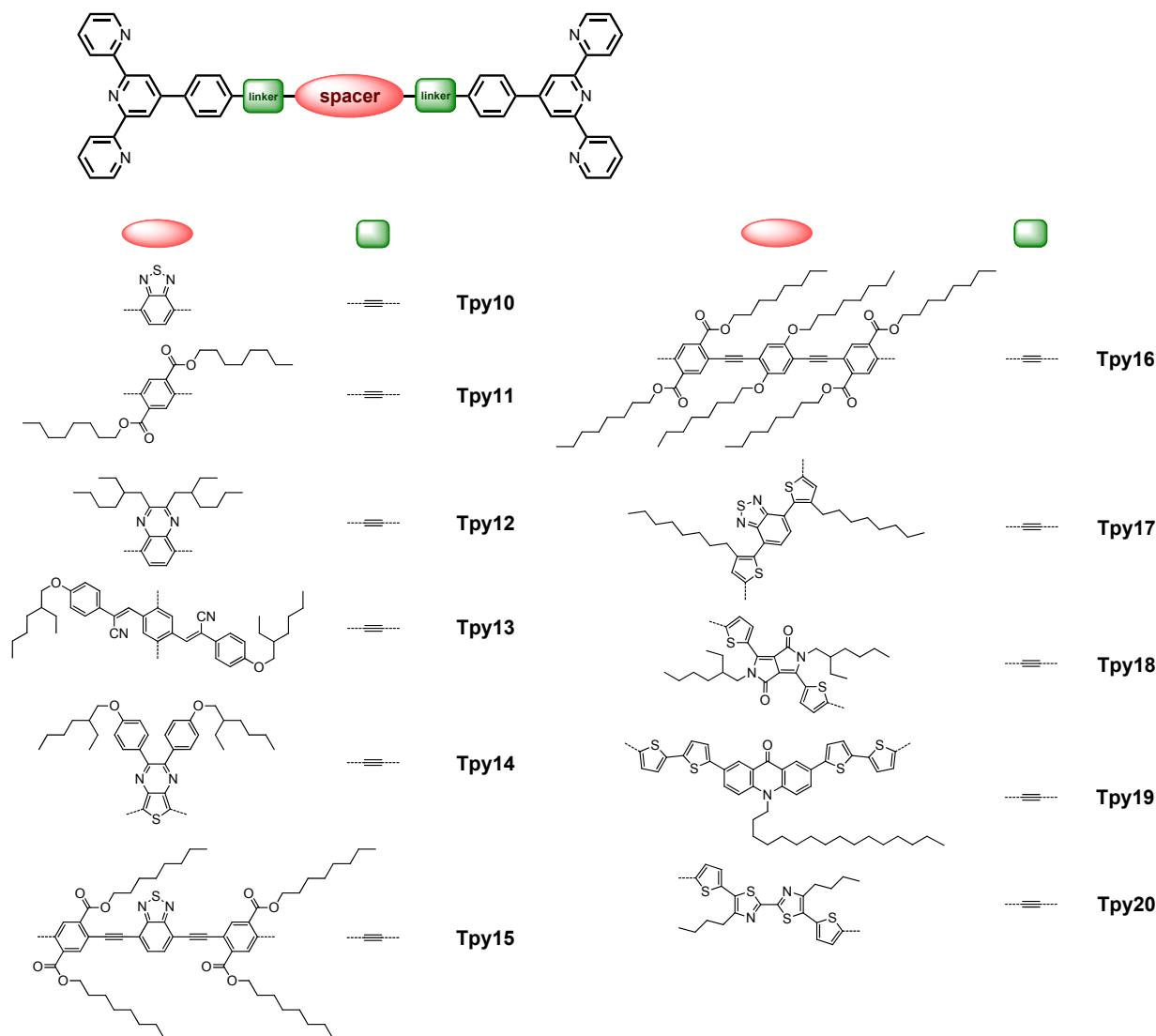


Figure 3.2. Schematic representation of the studied electron-donor-acceptor *bis-2,2':6',2''-terpyridines*.

Table 3.1. UV-vis spectroscopic characteristics of *bis-2,2':6',2''-terpyridines* (10^{-6} M in CHCl_3).

| Cmpd. | λ_{Abs} [nm] | ϵ [$\text{M}^{-1}\cdot\text{cm}^{-1}$] | λ_{PL} [nm] | Φ_{PL} | Cmpd. | λ_{Abs} [nm] | ϵ [$\text{M}^{-1}\cdot\text{cm}^{-1}$] | λ_{PL} [nm] | Φ_{PL} |
|--------------|--------------------------------|--|-------------------------------|--------------------|--------------|--------------------------------|--|-------------------------------|--------------------|
| Tpy1 | 399 | 100,700 | 450 | 0.85 | Tpy11 | 373 | 59,300 | 424 | 0.63 |
| Tpy2 | 392 | 77,400 | 438 | 0.75 | Tpy12 | 395 | 30,100 | 443 | 0.68 |
| Tpy3 | 384 | 56,400 | 424 | 0.77 | Tpy13 | 401 | 88,000 | 484 | 0.37 |
| Tpy4 | 478 | 99,700 | 545 | 0.12 | Tpy14 | 498 | 20,200 | 587 | 0.69 |
| Tpy5 | 503 | 45,400 | 553 | 0.25 | Tpy15 | 433 | 32,300 | 498 | 0.65 |
| Tpy6 | 482 | 51,200 | 510 | 0.72 | Tpy16 | 427 | 23,900 | 490 | 0.57 |
| Tpy7 | 399 | 98,900 | 444 | 0.88 | Tpy17 | 439 | 10,900 | 599 | 0.30 |
| Tpy8 | 369 | 91,200 | 404 | 0.77 | Tpy18 | 616 | 68,300 | 643 | – ^a |
| Tpy9 | 328 | 89,300 | 378 | 0.55 | Tpy19 | 415 | 81,900 | 548 | – ^a |
| Tpy10 | 423 | 20,700 | 503 | 0.79 | Tpy20 | 450 | 106,100 | 553 | – ^a |

^a Not measured.

3.1 Zinc(II) metallopolymers

Subsequently, the *bis-2,2':6',2''-terpyridines* were used to form metallopolymers *via* complexation with Zn^{2+} and Ru^{2+} ions (Figure 3.3). Thus, both *homo-* as well as *random-* (Zn^{2+}) and *alt-co-*polymers (Ru^{2+}) were formed.

On the one hand, the usage of zinc(II) ions leads to the formation of dynamic polymers, *i. e.* the polymer chains are re-opened easily under ambient conditions in solution since the

zinc-terpyridine complex is kinetically labile.^[41] Thus, *co*-polymers can be prepared by simply mixing different metallopolymer solutions, but the characterization of the polymer chains is significantly more difficult. On the other hand, the stable d^{10} outer-shell configuration of the Zn^{2+} ion impedes an electronic interaction between the metal orbitals and the π system of the ligands. Hence, the electro-optical characteristics of the polymers mirror the properties of the used π -conjugated systems (Table 3.2). Nevertheless, both hypsochromic and bathochromic shifts through metallopolymerization are present. In general, an electron-poor central moiety (*e. g.* for **Tpy10** to **Tpy16**) leads to a blue shift of UV-vis absorption since the low electron density at the center of the ligand causes the stabilization of molecular orbitals located there. Thus, the system's LUMO is located at the center while the HOMO resides at the more electron-rich terpyridine unit (Figure 3.4). Consequently, complexation, which leads to lowered electron density within terpyridine-related orbitals, causes stabilization of the HOMO and, therefore, a hypsochromic shift of absorption. In contrast, for zinc(II) metallopolymers with electron-rich π -conjugated ligands, a red shift was reported for most cases.^[65] In case of ligands with an intrinsic donor-acceptor system within the central unit (*i. e.* systems possessing electron-poor building blocks as well as electron-rich thiophene rings, **Tpy17** to **Tpy20**), the localization of terpyridine-based molecular orbitals cannot be evaluated that easy, so that the character of the spectral shift through complexation deviates from the proposed model.

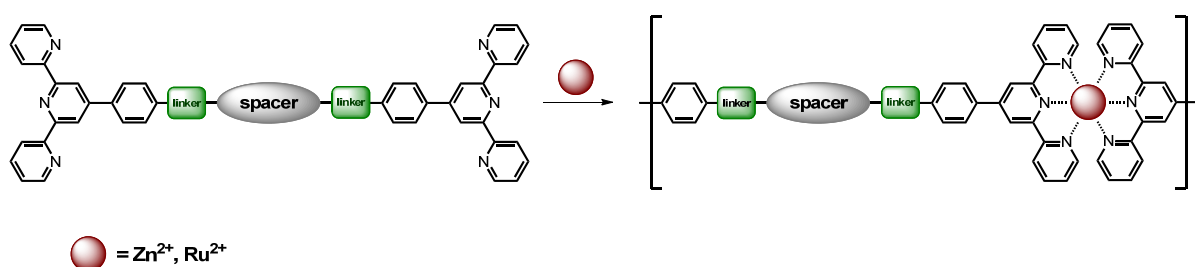


Figure 3.3. General representation of the metallopolymer formation from *bis*-2,2':6',2''-terpyridines (counter ions are omitted).

Table 3.2. UV-vis spectroscopic characteristics of zinc(II)- and ruthenium(II)-*bis*-2,2':6',2''-terpyridine metallopolymers (10^{-6} M in DMF); $\Delta = \tilde{\nu}_{\text{Polymer}} - \tilde{\nu}_{\text{Monomer}}$.

| Cmpd. | λ_{Abs} [nm] | ϵ [$M^{-1} \cdot \text{cm}^{-1}$] ^a | λ_{PL} [nm] | Φ_{PL} | Δ_{Abs} [cm^{-1}] |
|---|-----------------------------|---|----------------------------|--------------------|--|
| [Zn(Tpy1)] _n (PF ₆) _{2n} | 399 | 52,800 | 452 | 0.70 | 0 |
| [Zn(Tpy8)] _n (PF ₆) _{2n} | 369 | 82,300 | 409 | 0.95 | 0 |
| [Zn(Tpy10)] _n (PF ₆) _{2n} | 415 | 9,900 | 513 | 0.66 | 460 |
| [Zn(Tpy11)] _n (PF ₆) _{2n} | 362 | 27,400 | 424 | 0.43 | 820 |
| [Zn(Tpy12)] _n (PF ₆) _{2n} | 392 | 17,500 | 443 | 0.53 | 190 |
| [Zn(Tpy13)] _n (PF ₆) _{2n} | 397 | 23,500 | 446 | 0.26 | 250 |
| [Zn(Tpy14)] _n (PF ₆) _{2n} | 485 | 3,300 | 586 | 0.42 | 540 |
| [Zn(Tpy15)] _n (PF ₆) _{2n} | 405 | 26,900 | 511 | 0.31 | 1,600 |
| [Zn(Tpy16)] _n (PF ₆) _{2n} | 411 | 2,400 | 518 | 0.18 | 910 |
| [Zn(Tpy17)] _n (PF ₆) _{2n} | 429 | 28,700 | 605 | – ^b | 530 |
| [Zn(Tpy18)] _n (PF ₆) _{2n} | 618 | 13,200 | 640 | – ^b | –50 |
| [Zn(Tpy19)] _n (PF ₆) _{2n} | 421 | 65,900 | 517 | – ^b | –340 |
| [Zn(Tpy20)] _n (PF ₆) _{2n} | 454 | 64,500 | 561 | – ^b | –200 |
| [Zn(Tpy10) _{0.5} (Tpy1) _{0.5}] _n (PF ₆) _{2n} | 404 | 45,400 | 453 | 0.90 | – |
| [Zn(Tpy12) _{0.5} (Tpy8) _{0.5}] _n (PF ₆) _{2n} | 369 | 56,300 | 432 | 0.81 | – |
| [Ru(Tpy8)] _n (PF ₆) _{2n} | 505 ^c | 53,000 | – ^d | – ^d | – |
| [Ru(Tpy12) _{0.5} (Tpy8) _{0.5}] _n (PF ₆) _{2n} | 505 ^c | 57,500 | – ^d | – ^d | – |

^a Per monomer unit. ^b Not measured. ^c Additional MLCT transitions. ^d Not detectable.

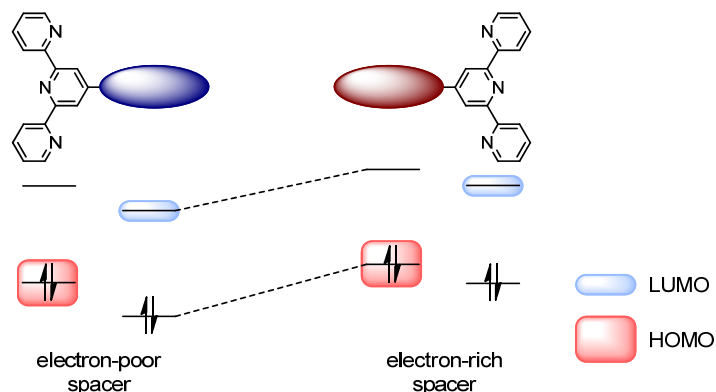


Figure 3.4. Model of the HOMO-LUMO distribution for *bis-2,2':6',2''-terpyridines* with either an electron-poor or an electron-rich π -conjugated spacer.

Besides the *homo*-polymers, also *random-co*-polymers were prepared. In each case, an electron-rich and an electron-poor monomer were chosen for *co*-polymerization to create donor-acceptor systems, which enable an intra-chain electron transfer. In particular, an alkoxybenzene (**Tpy1**) and a fluorene (**Tpy8**) core were used as electron-donor and a benzothiadiazole (**Tpy10**) and a quinoxaline (**Tpy12**) unit as electron-acceptor moieties. The UV-vis absorption properties of the *co*-polymers resemble in principle mixtures of the respective *homo*-polymers (Figure 3.5). UV-vis emission was dominated by the electron-poor (*i. e.* electron-accepting) chromophores when exciting the system at a wavelength with equivalent extinction coefficients for acceptor and donor moieties, indicating energy transfer from the electron-rich to the electron-poor parts of the *co*-polymers.

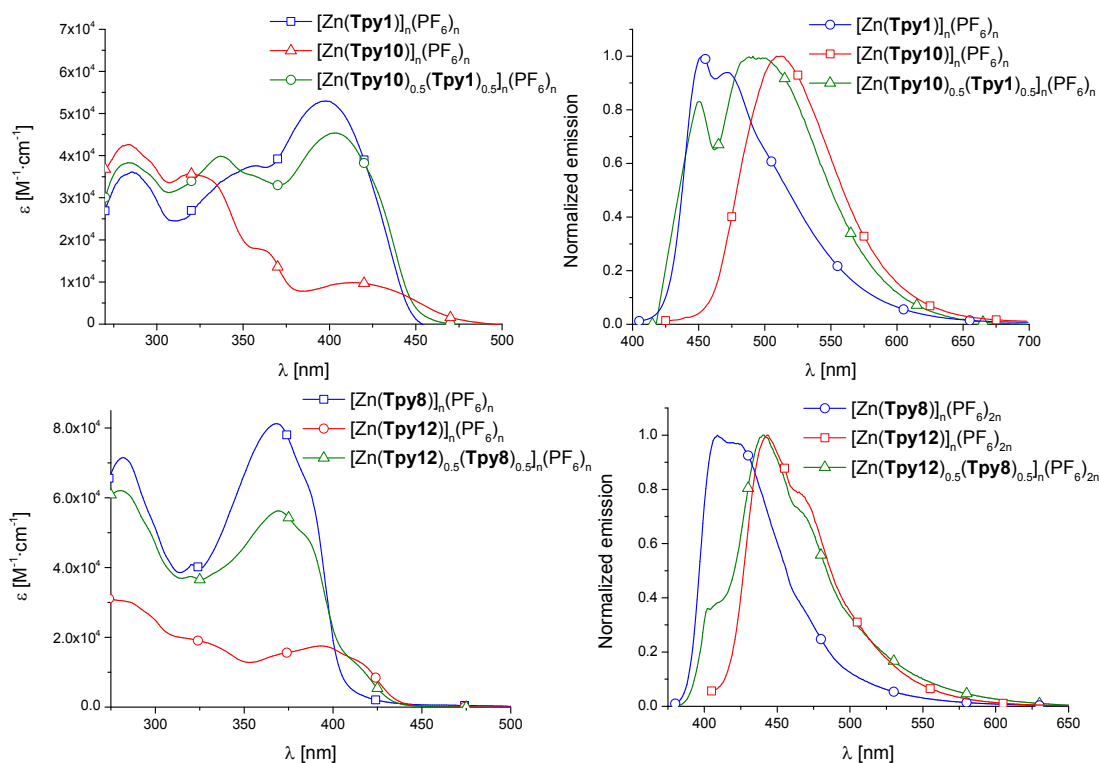


Figure 3.5. UV-vis absorption (left) and emission (right) spectra of *random-co*- and *homo*-polymers. Excitation of the latter at the λ_{Abs} maximum, $[\text{Zn}(\text{Tpy}10)_{0.5}(\text{Tpy}1)_{0.5}]_n(\text{PF}_6)_{2n}$ at 440 nm and $[\text{Zn}(\text{Tpy}12)_{0.5}(\text{Tpy}8)_{0.5}]_n(\text{PF}_6)_{2n}$ at 400 nm (equivalent extinction coefficients of the *homo*-polymers). All measurements were performed in DMF with concentrations of 10^{-6} M (per monomer unit).

3.2 Ruthenium(II) metallopolymers

Using ruthenium(II) instead of zinc(II) ions leads to significantly different metallopolymers. The ruthenium(II)-terpyridine *bis*-complex moiety, which possesses high stability constants and inert kinetics,^[36] allows for the formation of stable polymer chains enabling a comprehensive characterization, *e. g.* by size-exclusion chromatography (SEC), analytical ultracentrifugation (AUC), and viscosimetry.^[63b] Furthermore, since Ru²⁺ exhibits a d⁶ outer-shell, strong orbital interactions between the metal ion and the ligand's π system occur. Thus, additional electronic transitions, mainly metal-to-ligand charge-transfers, are possible, causing further bands in the UV-vis absorption spectra of the systems. Hence, intense absorptions are present around 505 nm for both investigated polymers (Figure 3.6). Since those low-energy MLCT transitions are located mainly on the ruthenium(II)-terpyridine unit, both peak wavelength and extinction coefficient are similar for the ruthenium(II) metallopolymers investigated herein. Likewise due to the localization of the lowest-energy transitions on the Ru(tpy)₂ moiety, UV-vis emission could not be observed because of the known efficient interaction of the triplet metal-to-ligand charge-transfer (³MLCT) excited state with the triplet metal-centered (³MC) states of the ruthenium(II) center and their fast and radiationless deactivation towards the singlet ground state in common ruthenium(II)-terpyridine systems.^[44b, 66]

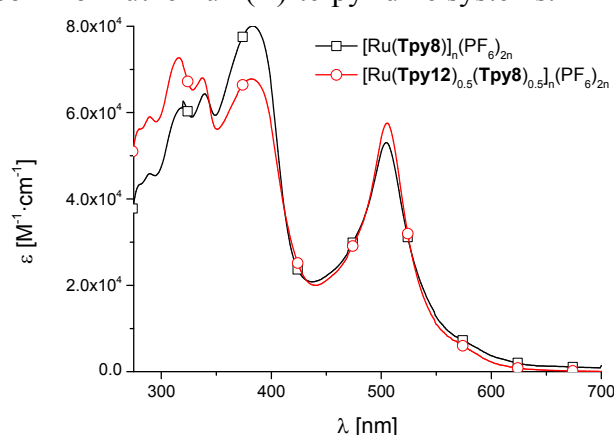


Figure 3.6. UV-vis absorption spectra of *homo*- and *random-co*-polymers of ruthenium(II) and *bis*-2,2':6',2''-terpyridines (10⁻⁶ M (per monomer unit) in DMF).

3.3 Inkjet printing of *bis*-2,2':6',2''-terpyridine metallopolymers

In several studies the properties of thin films of terpyridine metallopolymers were investigated using spin-coating for film preparation.^[42a, 65b, 65d] Beside the advantage of a low effort for the preparation of thin films, spin-coating suffers from several drawbacks, *e. g.* high material consumption and the lack of a possible combinatorial workflow.^[67] Alternatively, inkjet printing can be applied, offering an efficient material usage, flexible change of processing conditions, and deposition of defined patterns without the necessity of template masks.^[68] Inkjet printing is accepted as a selective and highly efficient material deposition tool for a wide range of applications, *e. g.* for printed electronics, organic photovoltaics, sensor systems, thin-film transistors, and radio frequency identification (RFID) tags.^[69] Furthermore, inkjet printing has been used for the screening of numerous compounds and processing parameters.^[70] By using inkjet printing, thin-film libraries can be prepared and film properties can be studied systematically in a fast, reproducible and simple manner with high materials efficiency.^[71]

Hence, a combinatorial screening of the preparation of thin films of three zinc(II)-*bis*-2,2':6',2''-terpyridine metallopolymers using the inkjet printing technique was carried out.

Namely $[\text{Zn}(\text{Tpy8})]_n(\text{PF}_6)_{2n}$, $[\text{Zn}(\text{Tpy17})]_n(\text{PF}_6)_{2n}$, and $[\text{Zn}(\text{Tpy18})]_n(\text{PF}_6)_{2n}$ were chosen since their combined emission spectra cover the whole visible spectrum. The influence of the solvent system, dot spacing, and substrate temperature on the film homogeneity and thickness as well as the UV-vis absorption and emission properties was investigated in a combinatorial, two-dimensional approach varying multiple parameters at the same time to identify optimum parameters for the preparation of smooth thin films. In contrast to a one-dimensional variation of settings, synergic interactions between different variables could be recognized.^[71-72]

The obtained data revealed the following optimum printing conditions for the investigated polymers: Firstly, the dot spacing should be within the range from 58 to 79 μm . A mixture of DMF and acetophenone with a volume ratio of 9 to 1 revealed to be the most convenient solvent system to achieve homogenous films with reduced formation of rings and edging. Furthermore, elevated substrate temperatures of 40 to 50 $^\circ\text{C}$ were necessary for an appropriate drying behavior of the printed films. An optical profilometer (see also Figure 3.7) was used to determine the thicknesses of $[\text{Zn}(\text{Tpy17})]_n(\text{PF}_6)_{2n}$ and $[\text{Zn}(\text{Tpy18})]_n(\text{PF}_6)_{2n}$ films (Table 3.3). For both polymers and substrate temperatures, a decreasing film thickness was observed upon increasing the dot spacing. Values of 100 to 200 nm, suitable for OLED and PV devices,^[71] can be obtained with dot spacings from 79 to 93 μm for both polymers. Notably, the substrate temperature showed a large influence on the standard deviation, *i. e.* the reproducibility.

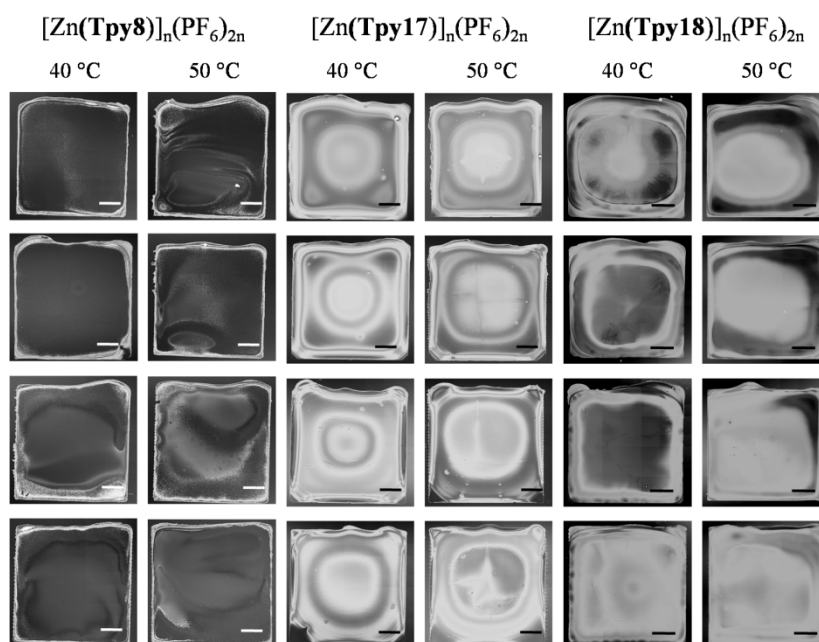


Figure 3.7. Optical profiler images of films of $[\text{Zn}(\text{Tpy8})]_n(\text{PF}_6)_{2n}$, $[\text{Zn}(\text{Tpy17})]_n(\text{PF}_6)_{2n}$, and $[\text{Zn}(\text{Tpy18})]_n(\text{PF}_6)_{2n}$ inkjet-printed with dot spacings of, from top to down, 50 μm , 58 μm , 68 μm , and 79 μm . Solvent system was DMF / AcPh with a volume ratio of 9 to 1. Substrate temperature was 40 $^\circ\text{C}$ and 50 $^\circ\text{C}$. The included scale bars correspond to 1 mm.

Subsequently, UV-vis absorption and emission of the films, printed using optimized conditions, were determined (Figure 3.8). The solution absorption of $[\text{Zn}(\text{Tpy8})]_n(\text{PF}_6)_{2n}$ features a low-energy band at 370 nm, with the respective film exhibiting a red shift of 2,600 cm^{-1} to 410 nm, which is most likely due to a π - π stacking of the fluorene-containing moieties within the solid state causing a stabilized excited state.

Table 3.3. Film thickness values and standard deviations obtained at different substrate temperatures and dot spacings. Printed from DMF / AcPh 9:1.

| Cmpd. | Substrate temperature [°C] | Dot spacing [μm] | Thickness [nm] | Standard deviation [%] |
|---|----------------------------|-------------------------------|----------------|------------------------|
| $[\text{Zn}(\text{Tpy17})]_n(\text{PF}_6)_{2n}$ | 40 | 50 | 451 | 7.3 |
| | | 58 | 396 | 12.5 |
| | | 68 | 279 | 4.8 |
| | | 79 | 274 | 8.6 |
| | 50 | 50 | 536 | 6.7 |
| | | 58 | 372 | 7.5 |
| | | 68 | 252 | 8.9 |
| | | 79 | 168 | 15.5 |
| $[\text{Zn}(\text{Tpy18})]_n(\text{PF}_6)_{2n}$ | 40 | 50 | 509 | 10.7 |
| | | 58 | 388 | 41.8 |
| | | 68 | 275 | 33.5 |
| | | 79 | 153 | 36.2 |
| | 50 | 50 | 307 | 10.4 |
| | | 58 | 251 | 1.9 |
| | | 68 | 207 | 6.8 |
| | | 79 | 196 | 4.8 |

Emission studies showed a structured peak at 409 nm in solution and a broad, structureless solid-state emission at 530 nm, with a Stokes shift of $2,600\text{ cm}^{-1}$ and $5,600\text{ cm}^{-1}$, respectively. In conjunction with the mentioned smoothed band structure, excimer formation is indicated.^[73] $[\text{Zn}(\text{Tpy17})]_n(\text{PF}_6)_{2n}$ possesses only a small bathochromic shift between the solution and the printed film due to a less efficient stacking of the metallopolymer chains. UV-vis absorption and emission show shifts from 430 nm to 445 nm and from 605 to 630 nm, respectively. Solution and film feature large Stokes shifts of $6,600\text{ cm}^{-1}$ and broad, unstructured emission bands, caused by the charge-transfer characteristic, namely intra-ligand charge transfers (ICT), of the low-energy transitions.^[74] Also $[\text{Zn}(\text{Tpy17})]_n(\text{PF}_6)_{2n}$ possesses only marginal changes between solution and film characteristics. The absorption maximum at around 570 nm remains constant, whereas a low-energy shoulder shifts from 615 to 650 nm. Emission could not be observed, most likely due to a shift to the NIR region, thus not detectable with the available measurement setup.

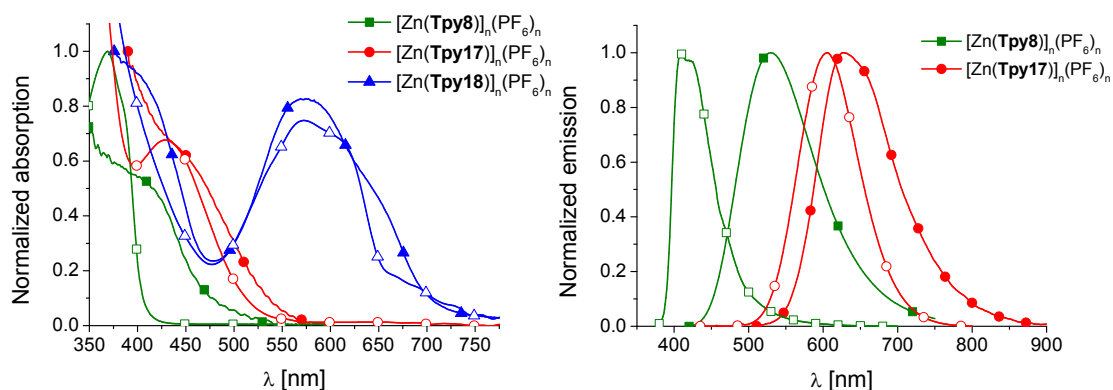


Figure 3.8. Normalized UV-vis absorption (left) and emission (right) spectra of inkjet-printed zinc(II) metallopolymer films (solid symbols) and the respective solutions (hollow symbols; 10^{-6} M in DMF).

4 Tridentate 1,2,3-Triazolyl Ligands in Ruthenium(II) Complexes

Parts of this chapter have been published: A6) B. Schulze, D. Escudero, C. Friebe, R. Siebert, H. Görls, S. Sinn, M. Thomas, S. Mai, J. Popp, B. Dietzek, L. González, U. S. Schubert, *Chem. Eur. J.* **2012**, *18*, 4010–4025; A7) B. Schulze, D. Escudero, C. Friebe, R. Siebert, H. Görls, U. Köhn, E. Altuntas, A. Baumgaertel, M. D. Hager, A. Winter, B. Dietzek, J. Popp, L. González, U. S. Schubert, *Chem. Eur. J.* **2011**, *17*, 5494–5498; A8) B. Schulze, C. Friebe, S. Hoepfner, G. M. Pavlov, A. Winter, M. D. Hager, U. S. Schubert, *Macromol. Rapid Commun.* **2012**, *33*, 597–602.

The 1,2,3-triazolyl moiety became a popular building block for the assembly of bi- and tridentate ligands during the last years acting as aromatic nitrogen-donor unit and, thus, replacing the conventional pyridyl ring. Besides common 2,2':6',2''-terpyridine and 2,2'-bipyridine analogues, *i. e.* N[^]N[^]N- and N[^]N-type ligands, respectively,^[35e, 75] also approaches including cyclometalating,^[18d, 34b] (abnormal) carbene,^[18e, 76] and cationic triazolium^[77] and anionic triazolate^[78] units were established.

With respect to their photophysical and electrochemical characteristics, we recently studied ruthenium(II) complexes of tridentate, N[^]N[^]N-type 2,6-bis(1*H*-1,2,3-triazol-4-yl)pyridine ligands to form homoleptic and, with terpyridine, heteroleptic complexes.^[18c] However, although the incorporation of the triazole moiety, based upon the 1,3-dipolar cycloaddition of alkynes and azides, enables the convenient and modular assembly of ligands, the photophysical properties turned out to be insufficient regarding the aspired application as photosensitizer. In particular the short-wavelength-dominated UV-vis absorption spectra, which cover only a narrow region of the visible spectrum, and the very short room-temperature excited-state lifetimes, impeding favored continuative processes, limit the applicability. Consequently, different concepts were applied to enhance the photophysical features, namely introducing anionic donors, on the one hand, and mesoionic carbenes, on the other hand.

4.1 Ruthenium(II) complexes of 1,2,3-triazolyl-containing cyclometalating ligands

The main reason for the low excited-state lifetimes of ruthenium(II) complexes with tridentate N[^]N[^]N-type ligands is the strong coupling of ³MLCT states, accountable for the lowest excited state, to ³MC states, which enable efficient, radiationless deactivation towards the ground state.^[4c, 11a, 44] Cyclometalation represents a well-established approach to overcome this problem since the introduction of a covalent carbon-metal bond is considered to cause a significant destabilization of antibonding metal-centered molecular orbitals leading to a raised energetic difference between the ³MLCT and ³MC states and, thus, a diminished coupling.^[45b, 45c] Besides the enhanced excited-state lifetime, the cyclometalation induces a decreased HOMO-LUMO energy gap, causing a bathochromically shifted longest-wavelength absorption, compared to the N[^]N[^]N counterpart, so that a larger fraction of the visible light can be absorbed. Hence, the cyclometalated complexes are much more suitable for photovoltaics.

Therefore, a series of cyclometalating, 1,2,3-triazole-containing tridentate ligands and heteroleptic ruthenium(II) complexes thereof possessing 2,2':6',2''-terpyridines as adjacent ligand was synthesized and characterized. In Figure 4.1, the respective complexes, accompanied by the correlated intention with regard to an application in Grätzel-type dye-sensitized solar cells, are depicted.

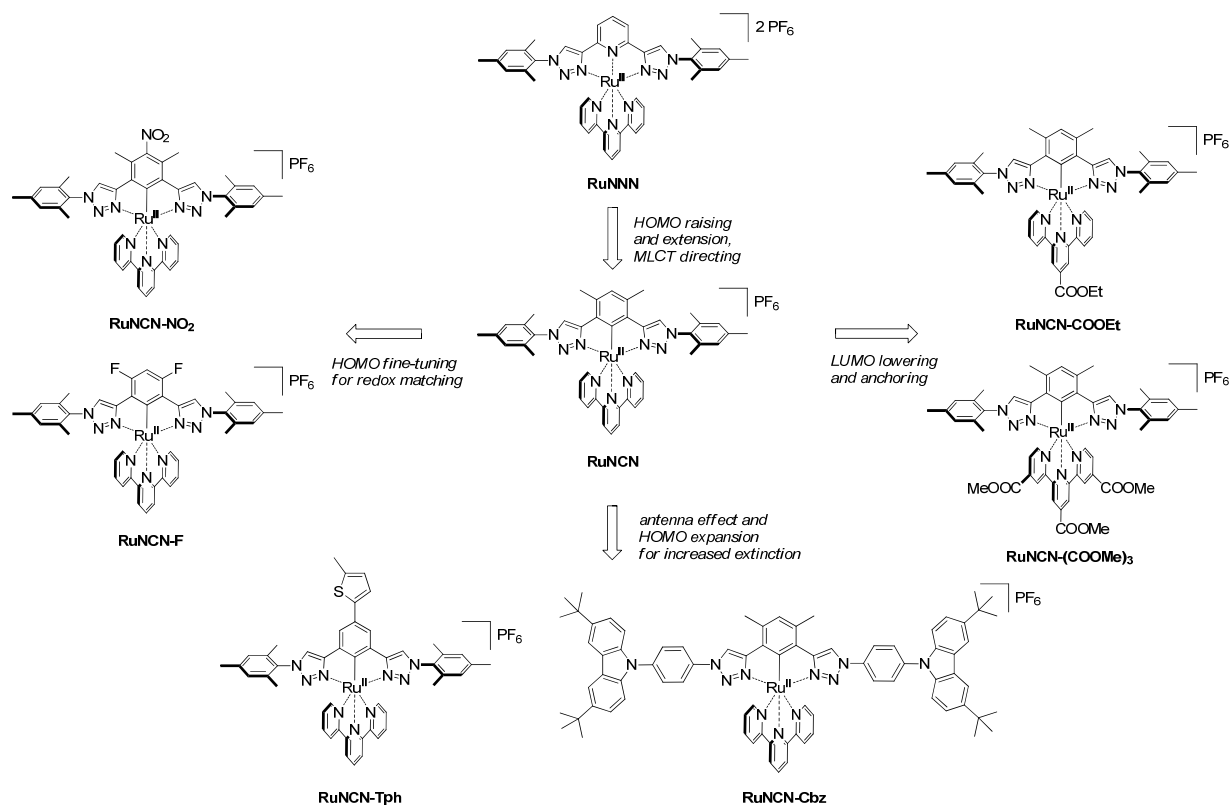


Figure 4.1. Overview over the synthesized cyclometalated 1,2,3-triazolyl-containing ruthenium(II) complexes and related synthetic strategies.

4.1.1 Photophysical characterization

Concerning the suitability for the designated usage as a solar-cell photosensitizer, the photophysical properties play a crucial role. The most important optical characteristics are depicted in Figure 4.2 and Table 4.1. Comparison of the N^NN-type complex **RuNNN** with the parent cyclometalated counterpart **RuNCN** reveals, first of all, a significant red shift as well as a broadening of the longest-wavelength UV-vis absorption band. According to computational simulations, these changes are due to a destabilization of the HOMOs, being also located on the metal center, due to the strong electron-donating ability of the anionic carbon. On the other hand, the expected enhancement of the photoluminescence behavior could be observed: At room temperature, a quantum yield of 6.1×10^{-5} and an excited-state lifetime of 4.1 ns were determined, while **RuNNN** showed no detectable emission at ambient conditions at all. The reason for this is most likely a destabilized ³MC state, usually responsible for a fast, radiationless deactivation of the excited state; further findings in this regard will be presented later.

To adjust the properties of the prototypic complex system, different substituents were introduced. A thiophene unit and carbazole moieties were installed at the 4-position of the central phenyl ring and the 1-positions of the triazoles, respectively, to intensify the light absorption capability. In case of the thiophene-functionalized **RuNCN-Tph**, the extinction coefficient is significantly increased due to the expansion of the HOMO, being also located on the central phenyl unit, towards the thiophene causing an enlarged optical cross section. This assumption was confirmed by DFT calculations. In contrast, the carbazole moieties of **RuNCN-Cbz**, attached *via* a phenyl ring to the triazoles, constitute additional chromophores that are not included in the existing set of molecular orbitals. Thus, only further LC transitions appear and the overall extinction coefficient in the short-wavelength region below 450 nm is

increased, while the MLCT absorption remains unchanged. Both complexes showed room-temperature emission with comparable luminescence wavelengths and excited-state lifetimes.

Mainly with respect to the fine-tuning of the electrochemistry (*vide infra*), electron-withdrawing fluoro and nitro groups were coupled to the central ring. Both substitutions cause stabilization of the HOMO, leading to a slight blue shift of the longest-wavelength absorption of about 700 cm^{-1} for **RuNCN-F** and **RuNCN-NO₂**. Moreover, the emission is blue-shifted by about 870 cm^{-1} for **RuNCN-NO₂**, while the fluoro-substituted complex showed no measurable room-temperature luminescence (*vide infra* for low-temperature emission).

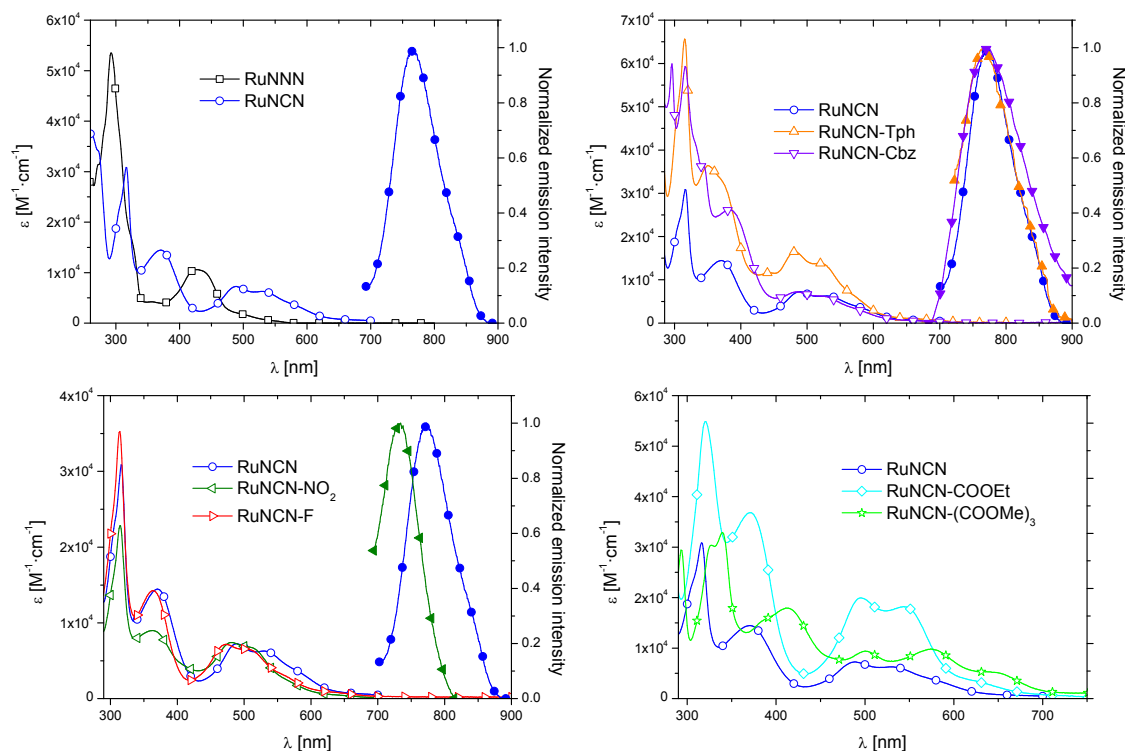


Figure 4.2. UV-vis absorption and emission spectra of cyclometalated 1,2,3-triazoly- containing ruthenium(II) complexes. All measurements were performed in CH₃CN with concentrations of 10^{-6} M .

Finally, to study the behavior of the complexes immobilized on the TiO₂ surface within a dye-sensitized solar cell *via* carboxylate groups, the complexes **RuNCN-COOEt** and **RuNCN-(COOMe)₃** were prepared and investigated. They bear one carboxylic ethyl ester and three methyl ester groups, respectively, at the adjacent terpyridine and serve as models for adsorbed species. Besides their primary role as linking unit, also a considerable influence of the ester groups on the electro-optical properties of the dyes is apparent. Since they act as π -conjugated electron acceptors, the terpyridine-based LUMO is stabilized and a red shift of the lowest-energy absorption by about 500 and $3,000\text{ cm}^{-1}$, respectively, was observed, leading to an almost full coverage of the visible spectrum in the latter case. Furthermore, the extinction coefficient increases for both complexes in comparison to the parent **RuNCN** since the MLCT transition dipole moment, directing from the cyclometalating ligand and the metal center to the terpyridine ligand, is enhanced. Photoluminescence could not be measured, most likely due to the too low wavelength detection limit of the used instrument ($< 900\text{ nm}$).

Additionally, photoluminescence measurements at 77 K were carried out (Table 4.1). The ester-substituted **RuNCN-COOEt** and **RuNCN-(COOMe)₃** showed no detectable emission, most likely due to a too low wavelength detection limit of the used instrumental setup. For the remaining complexes, including **RuNNN**, emissions were measured that are blue-shifted

compared to room temperature due to the rigidochromic effect, *i. e.* the rigid matrix of the frozen solvent prevents structural reorganization and, thus, stabilization of the excited state, causing a larger energy gap.^[79] The comparison of the 77-K emission of **RuNCN** to its non-cyclometalated counterpart reveals a red shift of 3,500 cm⁻¹, due to the destabilized HOMO in the former case. Introduction of the electron-withdrawing fluoro and nitro substituents, which are expected to stabilize the HOMO, indeed lead to a hypsochromic shift of 1,100 cm⁻¹, while the thiophene and the carbazole groups change the emission only marginally.

Table 4.1. Photophysical data of cyclometalated 1,2,3-triazolyl-containing ruthenium(II) complexes. The literature values of the [Ru(tpy)₂](PF₆)₂ complex are added for comparison.^[45b]

| Cmpd. | 298 K | 77 K | | | | |
|--|---|---|---|------------------|---|---------------------------------------|
| | λ_{Abs} [nm] (ϵ [$10^3 \text{ M}^{-1} \cdot \text{cm}^{-1}$]) ^a | λ_{PL} [nm] ^a | Φ_{PL} [10^{-5}] ^{a,b} | τ [ns] | λ_{PL} [nm] ^c | τ [μs] ^c |
| [Ru(tpy)₂](PF₆)₂ | 308 (63.4), 475 (14.7) | – | – | 0.25 | 603 | – |
| RuNNN | 325s, 428 (10.6), 500 (1.8) | – | – | – | 574 | 14 |
| RuNCN | 371 (14.5), 488 (7.3), 532 (6.3) | 751 | 6.1 | 4.1 | 719 | 4.1 |
| RuNCN-Tph | 350 (36.4), 482 (16.5), 518 (13.8) | 745 | 5.3 | 4.1 ^d | 722 | 4.3 |
| RuNCN-Cbz | 384 (26.2), 485 (7.3), 523 (6.3) | 750 | 25 | 6.7 ^d | 712 | 4.5 |
| RuNCN-NO₂ | 365 (9.0), 483 (7.4), 511 (6.8) | 705 | 10 | 5.3 | 667 | 5.2 |
| RuNCN-F | 363 (14.3), 473 (7.2), 507 (6.5) | – | – | 0.5 ^d | 661 | 5.8 |
| RuNCN-COOEt | 372 (36.8), 495 (19.9), 546 (18.2) | – ^e | – | – | – ^e | – |
| RuNCN-(COOMe)₃ | 413 (17.9), 500 (9.4), 574 (9.8), 641 (5.3) | – ^e | – | – | – ^e | – |

^a 10^{-6} M in deaerated CH₃CN. ^b Determined using [Ru(dqp)₂](PF₆)₂ in EtOH:MeOH (4:1) with $\Phi_{\text{PL}} = 2.0\%$ as a reference.^[80] ^c In *n*-butyronitrile glass. ^d Extrapolated from the temperature-dependent phosphorescence lifetime measurements. ^e The instrumental detection limit is about 800 nm.

For a more detailed study of the deactivation processes, excited-state lifetimes were determined for temperatures from 160 to 300 K. Careful analyses of the obtained lifetime-temperature curves reveals key values of the deactivation of the excited state. Namely, transition rate constants related to the non-activated deactivation from the lowest ³MLCT (radiative and non-radiative, k_{MLCT}), *via* the ³MC (activated, non-radiative, k_{MC}), and, except for **RuNCN-NO₂** and **RuNCN-F**, from a second, slightly more energy-rich MLCT state (activated, non-radiative, k_{MLCT2}) towards the ground state and the respective energy differences between the former one and the latter ones (ΔE_{MC} and ΔE_{MLCT2}) could be determined by fitting an Arrhenius-type expression to the data:

$$\tau(T) = \frac{1}{k_r + \sum k_{\text{nr}}} = \frac{1}{k_{\text{MLCT}} + k_{\text{MC}} \cdot e^{-\Delta E_{\text{MC}}/k_{\text{B}}T} + k_{\text{MLCT2}} \cdot e^{-\Delta E_{\text{MLCT2}}/k_{\text{B}}T}}$$

The obtained values (Table 4.2) result in two main conclusions: Firstly, compared to [Ru(tpy)₂]²⁺,^[40a] the energy gap separating the emitting ³MLCT and the ³MC is only negligibly higher for the cyclometalated species and even lower for its functionalized derivatives. However, the lifetime-limiting k_{MC} transition rate constants are significantly decreased by one to two magnitudes indicating a less efficient coupling of the ³MC and the ground state,^[81] hence being responsible for raised luminescence quantum yields and excited-state lifetimes, in particular at room temperature. Secondly, **RuNCN-NO₂** and **RuNCN-F** show the lowest ³MLCT-³MC gaps, reflecting the electron-withdrawing, thus MC-stabilizing, characteristic of their substituents. Notably, fluoro groups cause an even smaller gap than the nitro ones since they only affect orbitals of the metal center and the cyclometalating ligand, while the nitro group

also features a strong stabilizing influence on the terpyridine and, hence, on the MLCT states. Thus, no room-temperature emission is observable for **RuNCN-F**, but for **RuNCN-NO₂**.

Table 4.2. Characteristic values of the deactivation process of cyclometalated 1,2,3-triazolyl-containing ruthenium(II) complexes obtained from temperature-dependent lifetime measurements. Literature values of ruthenium(II)-*bis*(2,2':6',2''-terpyridine) complex for comparison.^[40a]

| Cmpd. | $k_{\text{MLCT}} [\text{s}^{-1}]$ | $k_{\text{MC}} [\text{s}^{-1}]$ | $\Delta E_{\text{MC}} [\text{cm}^{-1}]$ | $k_{\text{MLCT2}} [\text{s}^{-1}]$ | $\Delta E_{\text{MLCT2}} [\text{cm}^{-1}]$ |
|--|-----------------------------------|---------------------------------|---|------------------------------------|--|
| [Ru(tpy) ₂](PF ₆) ₂ | 6.5×10^4 | 2.0×10^{13} | 1,700 | 2.1×10^7 | 720 |
| RuNCN | 2.44×10^5 | 1.1×10^{12} | 1,830 | 3.11×10^8 | 350 |
| RuNCN-Tph | 2.33×10^5 | 1.89×10^{11} | 1,450 | 1.42×10^8 | 240 |
| RuNCN-Cbz | 2.22×10^5 | 2.04×10^{11} | 1,570 | 1.33×10^8 | 270 |
| RuNCN-NO₂ | 1.92×10^5 | 6.63×10^{11} | 1,400 | – | – |
| RuNCN-F | 1.72×10^5 | 9.74×10^{11} | 1,290 | – | – |

To conclude, the introduction of cyclometalation led to several improvements of the photo-physical features: The destabilization of the HOMO by the strongly σ - and π -electron-donating cyclometalating ligand caused a lowered energy gap, leading to a broadened UV-vis spectrum, which enables a more efficient absorption of sunlight. Emission measurements revealed a diminished radiationless excited-state relaxation *via* ³MC states. Thus, the excited-state lifetimes are raised allowing, *e. g.*, charge injection into a semiconductor to occur.

4.1.2 Electrochemical characterization

Application of a sensitizer in solar cells requires a careful tuning of ground-state and excited-state redox potentials with respect to the regenerating redox couple (that is I₂^{•-}/I⁻ with 0.79 V *vs.* NHE,^[82] 0.17 V *vs.* Fc⁺/Fc) and the semiconductor's conduction band edge (that is TiO₂ with -0.7 V *vs.* NHE,^[10a, 83] -1.3 V *vs.* Fc⁺/Fc), respectively. Hence, cyclic voltammetry was carried out to determine the respective characteristics (Figure 4.3 and Table 4.3).

First of all, the comparison of the cyclometalated **RuNCN** to its N[^]N[^]N-type analogue **RuNNN** reveals a cathodic shift of the oxidation potential by about 900 mV, caused by the strong σ - and π -donor ability of the cyclometalating moiety and by the strong electronic repulsion of the carbanion.^[45c] Noteworthy, DFT calculations show that the enhanced interaction of the ligand with the metal ion leads to a HOMO that is not only located on the ruthenium, but also on the cyclometalating ligand. Likewise, the first reduction, being located on the terpyridine ligand, is shifted by about 260 mV towards lower potentials due to an increased π back donation from the more electron-rich ruthenium(II) ion.^[45b] Under CV conditions, the first oxidation and reduction processes are fully reversible for **RuNCN**.

To gain optimized systems for solar cells, tuning the redox potentials is necessary. This was realized *via* introduction of nitro and fluoro groups at the central ring.^[16d] Their electron-acceptor ability stabilizes the HOMO, leading to oxidation potentials that are anodically shifted by 180 and 230 mV, respectively. In contrast, the reduction of **RuNCN-F** is only negligibly changed, whereas the nitro substituent causes a significant anodic shift of 160 mV since its π -acceptor character causes weakening of the π donation of the carbanion and, hence, of the π back donation towards the terpyridine from the less electron-rich ruthenium(II) center.

The introduction of the thiophene and carbazole moieties has only insignificant effects on the oxidation and reduction potentials, but causes irreversibility of the reduction processes.

The ester-functionalized complexes **RuNCN-COOEt** and **RuNCN-(COOMe)₃** feature significant anodic shifts of the reduction potentials of about 190 and 430 mV, respectively, due

to stabilization of the terpyridine-based LUMO. Furthermore, the π -accepting esters increase the overall π -acceptor strength of the polypyridyl ligand leading to a shift of the oxidation towards higher potentials by about 80 and 180 mV, respectively.

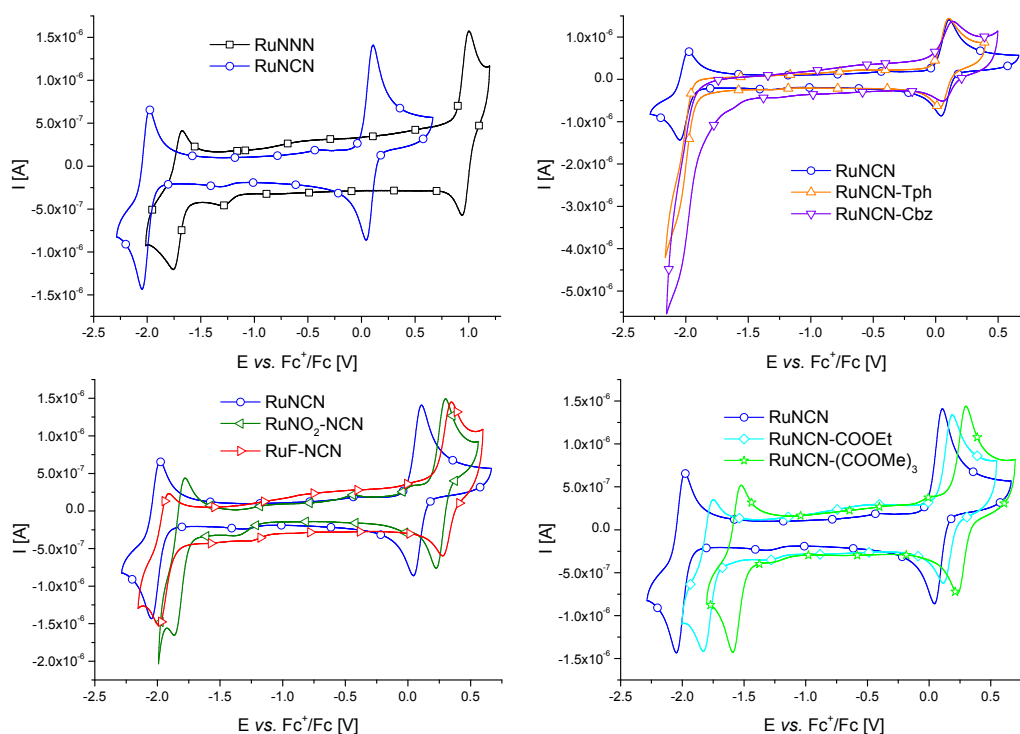


Figure 4.3. Cyclic voltammograms of cyclometalated 1,2,3-triazolyl-containing ruthenium(II) complexes. All measurements were performed in CH_3CN with concentrations of 10^{-4} M and 0.1 M Bu_4NPF_6 .

The systems studied herein showed redox potentials being convenient for the use in the widespread $\text{TiO}_2 / \text{I}_2^{\bullet-} / \text{I}^-$ redox system of a dye-sensitized solar cell. However, the $\text{Ru}^{\text{III}}/\text{Ru}^{\text{II}}$ redox potential of the parent **RuNCN** turned out to be slightly below the $\text{I}_2^{\bullet-}/\text{I}^-$ potential, but could be shifted to higher values by introduction of suitable functionalizations ($-\text{F}$, $-\text{NO}_2$). Also, the reversibility of the crucial oxidation process was shown, at least on the timescale of a CV experiment – further studies dealing with this problem are presented in the next section.

Table 4.3. Electrochemical data of cyclometalated 1,2,3-triazolyl-containing ruthenium(II) complexes.

| Cmpd. | $E_{1/2,\text{Ox}}$ [V] ($\frac{i_{p,a}}{i_{p,c}}$, ΔE_p [mV]) ^a | $E_{1/2,\text{Red}}$ [V] ($\frac{i_{p,a}}{i_{p,c}}$, ΔE_p [mV]) ^a | $E_{\text{S}^*,\text{Ox}}$ [V] ^b | E_{HOMO} [eV] ^c | E_{LUMO} [eV] ^c | $E_{\text{gap,el}}$ [eV] | $E_{\text{gap,opt}}$ [eV] |
|----------------------------------|--|---|---|-------------------------------------|-------------------------------------|--------------------------|---------------------------|
| RuNNN | 0.98 (1.1, 74) | -1.72 (0.9, 80) | -1.22 | -5.78 | -3.22 | 2.56 | 2.20 |
| RuNCN | 0.08 (1.0, 67) | -1.98 (1.0, 71) | -1.83 | -4.88 | -2.91 | 1.97 | 1.91 |
| RuNCN-Tph | 0.07 (1.0, 69) | -1.97 (irrev.) ^b | -1.93 | -4.87 | -2.93 | 1.94 | 2.00 |
| RuNCN-Cbz | 0.10 (1.0, 83) | -1.97 (irrev.) ^b | -1.84 | -4.89 | -3.00 | 1.89 | 1.94 |
| RuNCN-NO₂ | 0.26 (1.0, 76) | -1.82 (1.0, 88) | -1.77 | -5.07 | -3.11 | 1.96 | 2.03 |
| RuNCN-F | 0.31 (1.0, 74) | -1.95 (1.0, 79) | -1.67 | -5.12 | -2.97 | 2.15 | 1.98 |
| RuNCN-COOEt | 0.16 (1.0, 70) | -1.79 (1.1, 80) | -1.74 | -4.96 | -3.14 | 1.82 | 1.90 |
| RuNCN-(COOMe)₃ | 0.26 (1.0, 71) | -1.56 (1.0, 71) | -1.51 | -5.06 | -3.37 | 1.69 | 1.77 |

^a In CH_3CN with 0.1 M Bu_4NPF_6 ; vs. Fc^+/Fc . ^b Calculated using $E_{\text{S}^*,\text{Ox}} = E_{1/2,\text{Ox}} - (E_{\text{gap,opt}}/e)$. ^c Calculated using $E_{\text{HOMO/LUMO}} = [-(E_{\text{onset,Ox/Red}} - E_{\text{onset,Fc}^+/\text{Fc}}) - 4.8]\text{e}$. ^d Irreversible process; $E_{1/2}$ obtained from DPP spectra.

4.1.3 Spectroelectrochemical characterization

To gain more detailed insights into the electrochemistry of the cyclometalated ruthenium(II) complexes, UV-vis-NIR spectroelectrochemical measurements were executed (Figure 4.4 for **RuNCN** and Supplementary Information for the remaining complexes). For all complexes, the spectral development during the oxidation reveals several isosbestic points, indicating the presence of only two species and well-defined reactions. Generally, the changes involve a decrease of MLCT bands between 350 and 600 nm, caused by depopulation of the metal / ligand-based HOMO, and the appearance of additional broad signals between 600 and 850 nm (up to 1,000 nm in case of **RuNCN-(COOMe)₃**), attributed to emerging LMCT transitions. Here, **RuNCN-F** is an exception showing no changes beyond 600 nm, probably because of a very low transition dipole moment. Likewise, for **RuNCN-NO₂**, only very weak transitions occur. In contrast, for **RuNCN-Tph**, the appearance of two intense absorption signals around 450 and 900 nm can be observed, being assigned to MLCT ($d_{\text{Ru}} \rightarrow [\text{d}_{\text{Ru}} / \pi_{\text{NCN}}]^+$) and LMCT transitions involving thiophene-located π orbitals, which possess a large orbital overlap with the $d_{\text{Ru}} / \pi_{\text{NCN}}$ SOMO. Noteworthy, all oxidized species reproduce the initial spectra almost completely by re-reduction, approving the oxidation processes to be fully reversible.

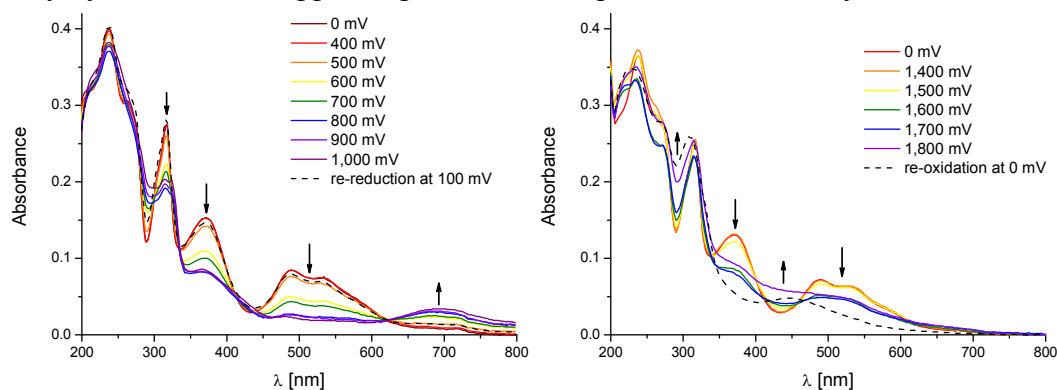


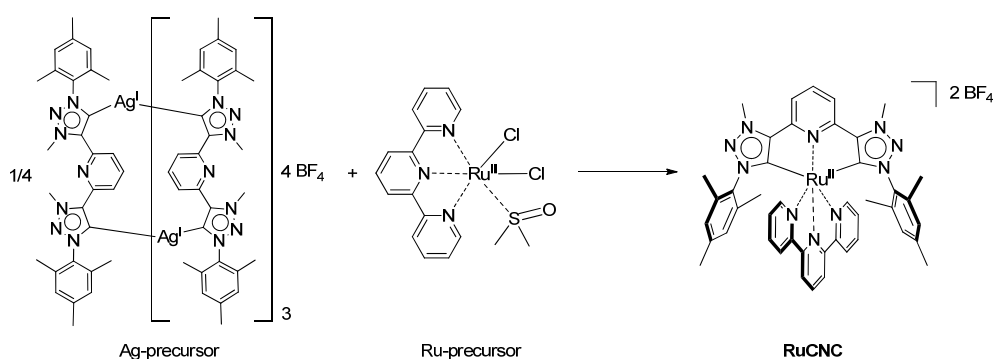
Figure 4.4. UV-vis spectroelectrochemical investigation on the oxidation (left) and reduction (right) process of **RuNCN** (voltage varied between 400 and 1,000 mV and -1,400 and -1,800 mV vs. AgCl/Ag, respectively; 10^{-5} M in CH_3CN with 0.1 M Bu_4NPF_6).

The first, terpyridine-located reductions ($\text{tpy} \rightarrow \text{tpy}^{\bullet-}$), which were measured only for the complexes showing reversibility in the CV, reveal a less-defined reduction in spectroelectrochemical measurements. Again, a signal decrease is apparent in the MLCT / MLLCT region that is caused by the population of π^*_{tpy} orbitals, being the acceptor for the longest-wavelength transition processes. Additionally, absorbance increases in the region at around 450 nm and several changes occur in the UV region, both originating from arising and disappearing or shifted LC and LLCT transitions. Notably, the initial complex could not be successfully recovered *via* re-oxidation for every complex except for **RuNCN-(COOMe)₃**. The three electron-withdrawing ester groups at the terpyridine ligand enable an enhanced stabilization of the electron-rich reduced $\text{tpy}^{\bullet-}$ moiety allowing full regeneration.

As already realized for the absorption and emission studies as well as for electrochemistry, the spectroelectrochemical experiments demonstrated the suitability of the investigated ruthenium(II) complexes for application in dye-sensitized solar cells, revealing the stability of the oxidized states, which represent one of the key steps in a solar cell's working cycle.

4.2 A ruthenium(II) complex of an abnormal carbene ligand

Installing *N*-heterocyclic carbenes (NHCs) in the ligand system represents a further alternative to manipulate the electronic structure of the complex aiming at prolonged excited-state lifetimes.^[16c, 84] Classical NHC ligands are strong σ donors and π acceptors causing ^3MC destabilization, but also increasing MLCT energy, leading to an undesired UV-vis blue shift. In contrast, abnormal or mesoionic carbenes feature an even stronger σ donation accompanied with a modest π -acceptor strength.^[18e, 76] Thus, as a further photosensitizer candidate, the heteroleptic ruthenium(II) complex **RuCNC**, possessing a tridentate ligand that contains mesoionic carbene 1,2,3-triazolylidene units, was synthesized. The ligand was derived from a 2,6-*bis*(1-mesityl-1*H*-1,2,3-triazol-4-yl)pyridine *via* selective methylation with Meerwein's salt and was converted into a silver(I) precursor complex with silver(I) oxide. The heteroleptic complex was prepared by subsequent reaction with the [Ru(tpy)(DMSO)Cl₂] precursor (Scheme 4.1).



Scheme 4.1. Schematic representation of the synthesis of the heteroleptic ruthenium(II)-1,2,3-triazolylidene complex **RuCNC** from a respective silver(I) and ruthenium(II)-terpyridine precursor.

For photosensitizer usage, both spectroscopic and electrochemical characteristics are essential (Figure 4.5). UV-vis measurements revealed absorption features up to 550 nm, assigned to MLCT transitions by calculations, with a maximum extinction coefficient of $10,000 \text{ M}^{-1}\cdot\text{cm}^{-1}$ at 463 nm, comparable to [Ru(tpy)₂](PF₆)₂ and significantly red-shifted compared to **RuNNN** (see Table 4.1). In contrast to both, **RuCNC** shows room-temperature emission at 643 nm with a quantum yield of 5.5% and excited-state lifetimes of 630 ns, both being in the range of [Ru(bpy)₃](PF₆)₂ ($\Phi_{\text{PL}} = 6.2\%$; $\tau = 860 \text{ ns}$).^[85] The DFT computations revealed that the ^3MC state is, as intended, significantly destabilized due to the strong σ -donor strength of the abnormal NHC, causing the suppression of the ^3MC -mediated radiationless deactivation. Hence, the triazolylidene complex combines the long-wavelength, efficient light absorption, the defined structure, and the high stability of the N[^]N[^]N-type systems with the convenient excited-state characteristics of the bidentate [Ru(bpy)₃](PF₆)₂.

Regarding the complex' electrochemical characteristics, cyclic voltammetry was executed and revealed a reversible oxidation process, located on the ruthenium(II), according to related computations, with a half-wave potential of 0.60 V *vs.* Fc⁺/Fc, cathodically shifted compared to the N[^]N[^]N-type complexes (0.90 V for [Ru(tpy)₂](PF₆)₂, 0.98 V for **RuNNN**) due to the σ -donor characteristic of the mesoionic carbene moieties, which causes destabilization of the metal-located HOMO. Likewise, the first reduction, being assigned to the terpyridine ligand, shows a cathodic half-wave-potential shift towards -1.95 V (-1.64 V for [Ru(tpy)₂](PF₆)₂, -1.72 V for **RuNNN**), so that, in total, the energy gap remains the same compared to the homoleptic terpyridine complex, as already indicated by the UV-vis absorption spectra.

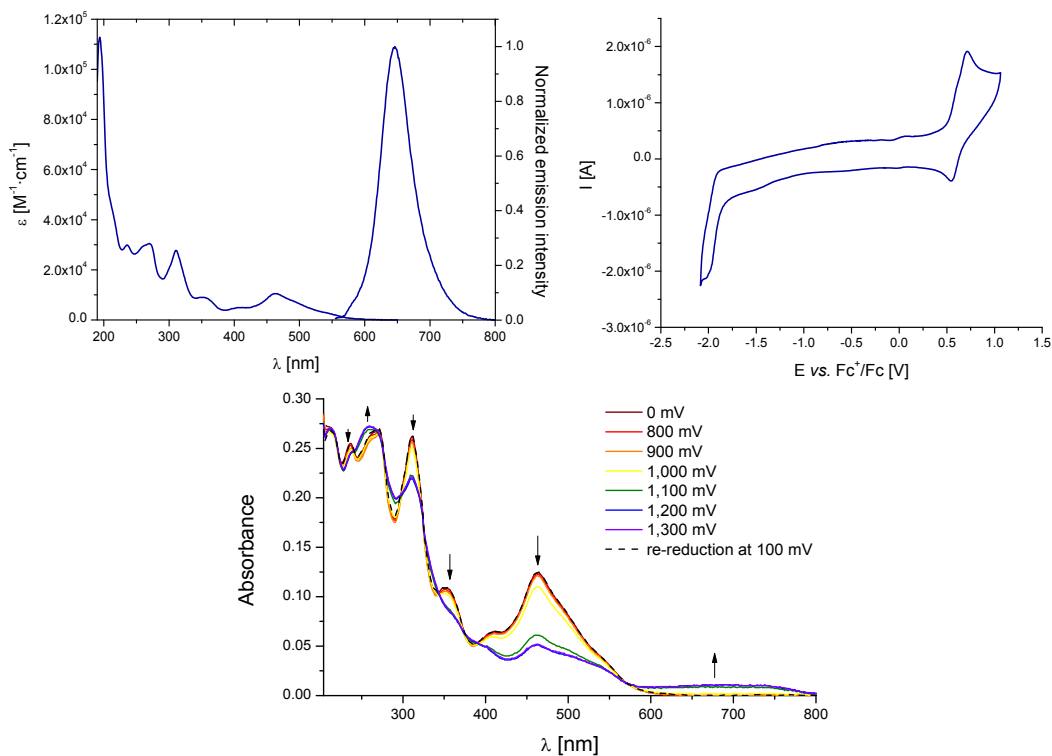


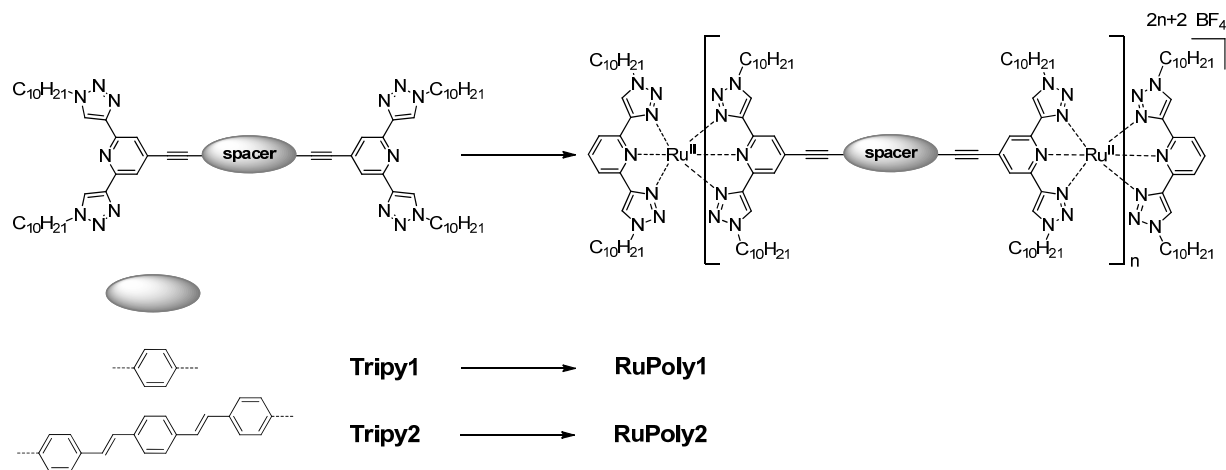
Figure 4.5. Optical and electrochemical characterization of **RuCNC**: UV-vis absorption and emission spectrum (top left, 10^{-6} M in deaerated CH_3CN), CVs of the first redox processes (top right, 10^{-4} M in CH_3CN with 0.1 M Bu_4NPF_6), and UV-vis spectroelectrochemical study of the oxidation process (bottom, voltage between 800 and 1,300 mV vs. AgCl/Ag ; 10^{-5} M in CH_3CN with 0.1 M Bu_4NPF_6).

For a more detailed characterization of the electrochemical processes, namely the oxidation, UV-vis spectroelectrochemical experiments were carried out (Figure 4.5). The oxidation of the complex leads to a bleaching of the MLCT region of the absorption spectrum, due to depopulation of the metal-based HOMO. Additionally, a broad band occurs between 600 and 800 nm, assigned to LMCT transitions from low-lying ligand-based π orbitals towards empty metal d orbitals, while in the LC region below 330 nm, no significant changes of band structure and position occur. The spectral changes during the oxidation exhibits several isosbestic points, which indicate a defined reaction with only one product species. Furthermore, re-reduction of the oxidized complex regenerates the initial spectrum completely confirming the redox stability of the system and, thus, its suitability to act as a photosensitizer.

4.3 Metallopolymers from ditopic 1,2,3-triazolyl-containing ligands

Metallopolymers derived by ruthenium(II) complexation of ditopic, π -conjugated ligands provide the combined optical and electrochemical characteristics of the ruthenium(II) complex as well as the bridging π system with favorable polymer properties, in particular with regard to a thin-film processability.^[12a, 86] Two ligand systems with two 2,6-bis(1-decyl-1*H*-1,2,3-triazol-4-yl)pyridine units, linked *via* different π -conjugated bridges, were prepared (Scheme 4.2).

The formation of polymer chains was confirmed by SEC and AUC investigations, whereupon the latter exhibited absolute molar masses of $36,000 \text{ g}\cdot\text{mol}^{-1}$ and $29,000 \text{ g}\cdot\text{mol}^{-1}$ for **RuPoly1** and **RuPoly2**, respectively. Additionally, the polymers were studied in the solid state by AFM and TEM measurements indicating the assembly of rod-like aggregate structures with chain lengths of 120 to 200 nm and 100 to 150 nm, respectively.



Scheme 4.2. Schematic representation of the synthesis of ruthenium(II) metallopolymer of ditopic 2,6-*bis*(1*H*-1,2,3-triazol-4-yl)pyridine ligands.

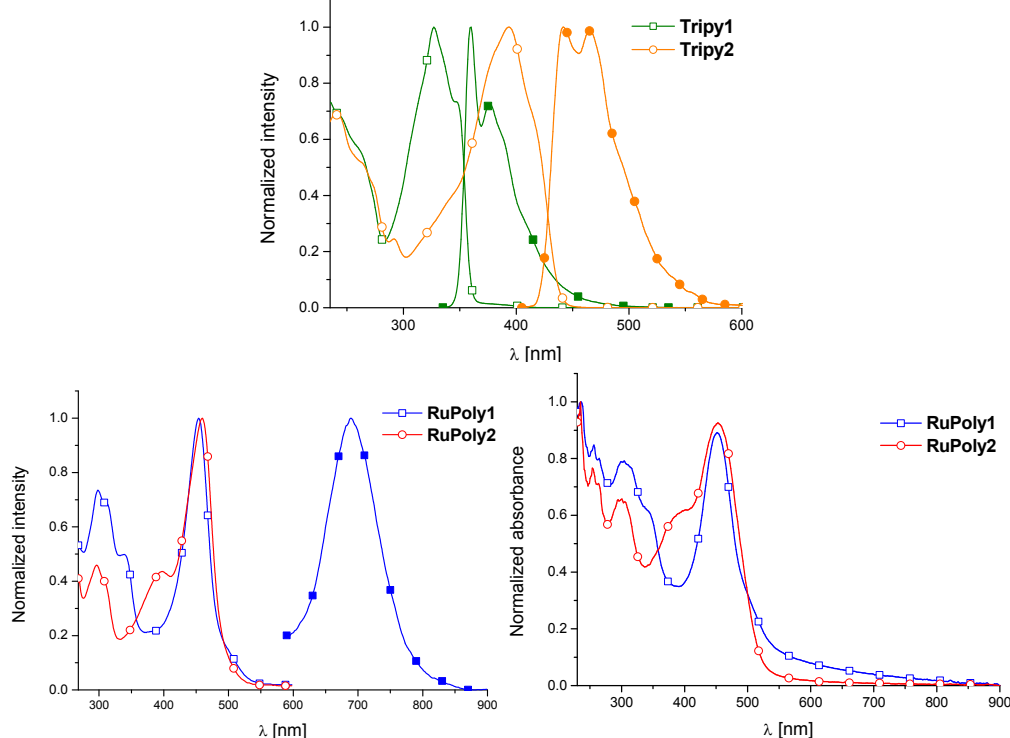


Figure 4.6. UV-vis absorption (hollow symbols) and emission (solid symbols) spectra of ditopic *bis*(2,6-*bis*(1*H*-1,2,3-triazol-4-yl)pyridine) ligands (top, 10^{-6} M in CH_2Cl_2) and of the respective ruthenium(II) metallopolymer in solution (bottom left, 10^{-6} M in DMF) and of drop-casted thin films (bottom, right).

The photophysical characterization of the ligands and the metallopolymer (Figure 4.6) show intense absorption and high photoluminescence quantum yields for the ligands (0.53 for **Tripy1**, 0.97 for **Tripy2**). The larger π -conjugated system of **Tripy2** causes a red-shifted absorption and emission compared to **Tripy1** as well as increased extinction coefficients. Introduction of ruthenium(II) causes the occurrence of an MLCT transition at 450 nm (Figure 4.6), red-shifted in comparison to the non-substituted homoleptic ruthenium(II) 2,6-*bis*(1-decyl-1*H*-1,2,3-triazol-4-yl)pyridine complex ($\lambda_{\text{Abs}} = 400$ nm)^[17b, 18c] most-likely due to a stabilization of the MLCT state by the attached π -conjugated bridge. Furthermore, a weak room-temperature emission ($\Phi_{\text{PL}} = 2 \times 10^{-5}$) appears for **RuPoly1** since the thus increased MLCT-MC gap diminishes radiationless deactivation.^[11a, 63d] UV-vis absorption measurements of thin polymer films resembled in principle the characteristics of the solution spectra.

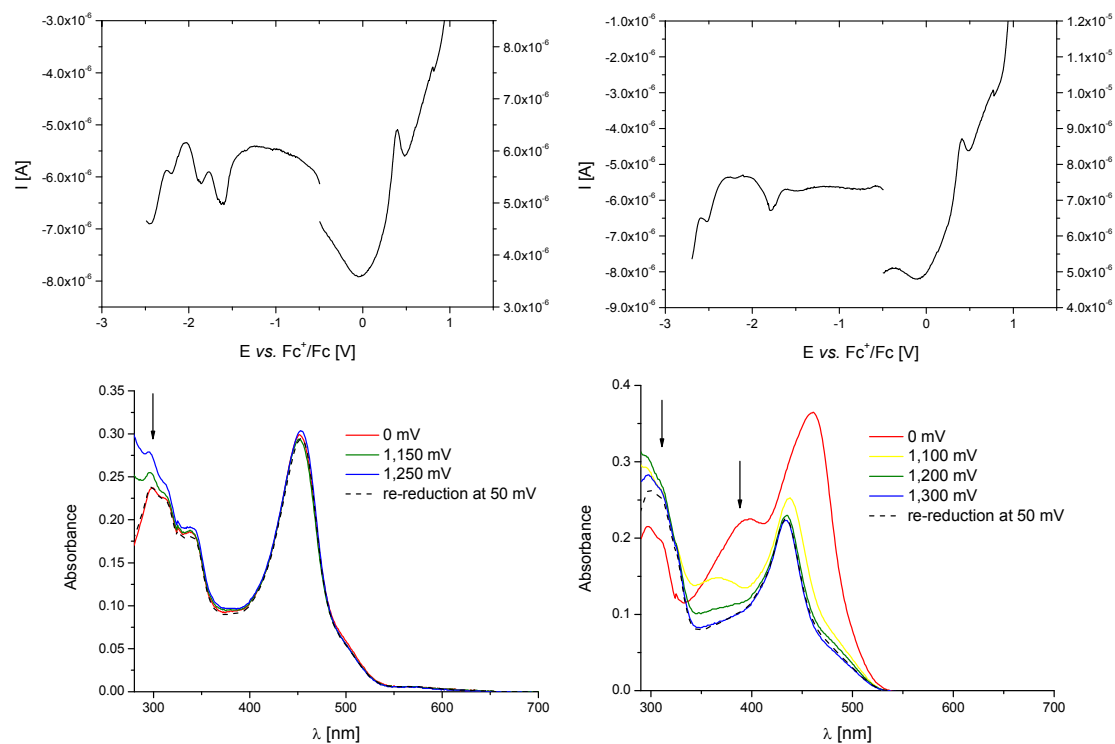


Figure 4.7. DPP spectra (top) and UV-vis spectral changes during the first oxidation process (bottom) for **RuPoly1** (left) and **RuPoly2** (right) (10^{-5} M in DMA with 0.1 M Bu_4NPF_6).

Electrochemical characterization of the polymers, depicted in Figure 4.7, was accomplished, due to solubility reasons, in DMA allowing measurements only up to 0.9 V vs. Fc^+/Fc . Thus, only one redox process at 0.40 V vs. Fc^+/Fc could be identified for both systems, corresponding to the π -conjugated ligand according to spectroelectrochemical studies (Figure 4.7, bottom). Additionally, several cathodic signals occur for **RuPoly1** (−1.60 V, −1.85 V, −2.20 V, and −2.45 V) and **RuPoly2** (−1.78 V and −2.50 V). Comparison with the homoleptic, non-substituted parent complex^[17b, 18c] allows the assignment of the reduction processes at around −1.80 V to the 2,6-*bis*(1-decyl-1*H*-1,2,3-triazol-4-yl)pyridine moiety while further reductions are most likely related to the π -conjugated bridge.

4.4 Conclusion

The tridentate $\text{N}^{\wedge}\text{N}^{\wedge}\text{N}$ -type 2,6-*bis*(1*H*-1,2,3-triazol-4-yl)pyridine ligand^[17, 18c] was modified to enhance the photo-electrochemical properties of its ruthenium(II) complexes as well as the solid-state processability. The former aim could be accomplished either by replacing the central pyridine ring by an anionic, cyclometalating phenyl moiety or by converting the 1,2,3-triazolyl rings to the mesoionic triazolylidene carbenes. Both approaches resulted in heteroleptic complexes with elongated excited-state lifetimes allowing application as photosensitizer. The synthesis of ditopic, π -conjugated *bis*(2,6-*bis*(1*H*-1,2,3-triazol-4-yl)pyridine) ligands enabled the integration of homoleptic ruthenium(II) complexes in metallopolymers combining the electro-optical characteristics of the metal complex and the conjugated π system and, furthermore, facilitating the preparation of thin films, which is crucial for device assembly.

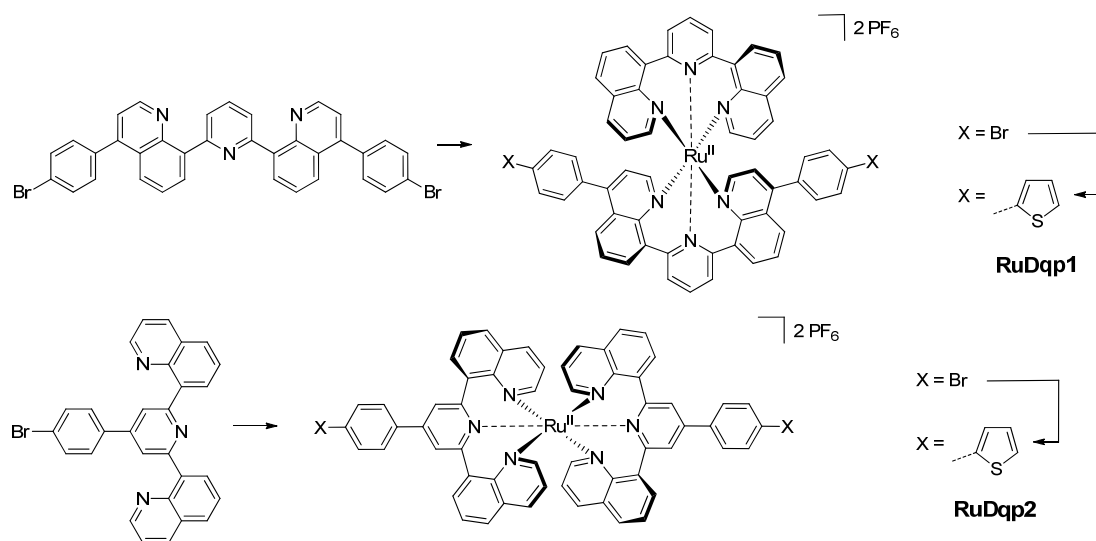
5 Metallopolymers of Ruthenium(II) Complexes of Tridentate Ligands through Electropolymerization

Parts of this chapter have been published: A9) C. Friebe, H. Görls, M. Jäger, U. S. Schubert, *Eur. J. Inorg. Chem.* **2013**, 4191–4202; A10) C. Friebe, M. Jäger, U. S. Schubert, *RSC Adv.* **2013**, 3, 11686–11690; A11) C. Friebe, B. Schulze, H. Görls, M. Jäger, U. S. Schubert, *Chem. Eur. J.*, DOI: 10.1002/chem.201301439.

For the incorporation of electrochemically and optically active ruthenium(II) complexes into device architectures, particularly into photovoltaics, the preparation of thin, homogenous films, enabling efficient charge transport, is required. Since it allows the direct and defined deposition of metal-containing polymer films onto electrode surfaces from monomer solutions, electropolymerization represents a convenient technique for this purpose.^[48a, 49b] Consequently, ruthenium(II) complexes that had been already established as suitable photosensitizer systems, namely of 2,6-di(quinoline-8-yl)pyridine^[87] and 2,6-bis(1*H*-1,2,3-triazol-4-yl)benzene ligands (see Chapter 4.1), were equipped with electropolymerizable 2-thienyl units. Their ability to undergo electropolymerization was subsequently studied and the achieved polymers were characterized to evaluate a possible usage in electro-optical devices.

5.1 Electropolymerization of ruthenium(II)-2,6-di(quinoline-8-yl)pyridine complexes

Ruthenium(II) complexes of 2,6-di(quinoline-8-yl)pyridine (dqp) ligands feature remarkable photophysical properties. In particular, excited-state lifetimes in the μs region combined with a broad UV-vis absorption spectrum make them highly promising candidates for the usage as photosensitizers.^[87] Hence, we synthesized two Ru(dqp)₂ complexes possessing electropolymerizable thien-2-yl units (Scheme 5.1), where the functionalization was carried out either at the 4-position of the two quinoline moieties of one ligand or at the 4-position of the central pyridine rings of both ligands to result in heteroleptic and homoleptic complexes, respectively. The obtained complexes were consequently used for the electrochemical formation of type-II and type-III metallo-*homo*- and, including thiophene, metallo-*co*-polymers.



Scheme 5.1. Schematic representation of the synthesis of Ru(dqp)₂ complexes **RuDqp1** and **RuDqp2** possessing thien-2-yl units.

5.1.1 Photophysical and electrochemical characteristics of monomeric complexes

The ruthenium(II) complexes were studied by UV-vis absorption and emission spectroscopy, by cyclic voltammetry (Figure 5.1 and Table 5.1) and by UV-vis-NIR spectroelectrochemistry. The UV-vis absorption spectrum of **RuDqp1** shows a characteristic band structure in the visible region with MLCT as well as MC and LC transitions, according to related DFT calculations. Complex **RuDqp2** features a similar spectrum, but displays a pronounced low-energy shoulder and an additional band at 425 nm. Room-temperature luminescence studies revealed structureless emission bands; the respective data is presented in Table 5.1.

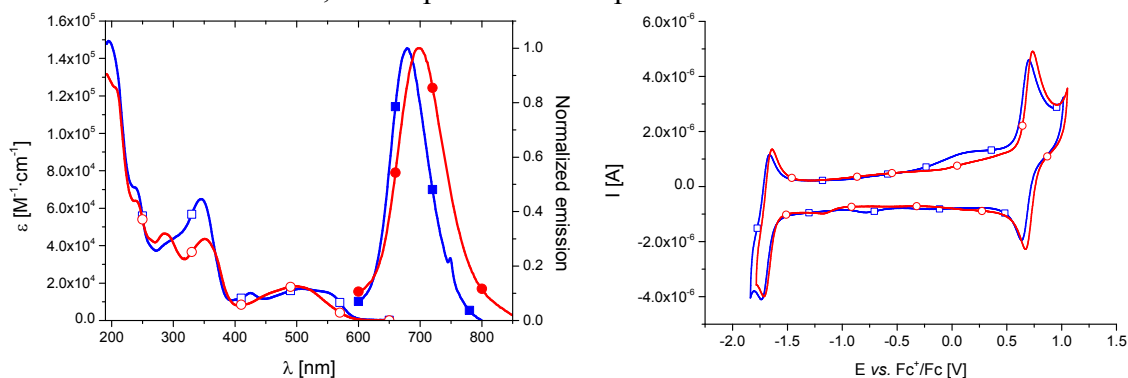


Figure 5.1. UV-vis absorption (hollow symbols) and emission (solid symbols) spectra (left, 10^{-6} M in CH_3CN) and cyclic voltammograms (right, 10^{-4} M in CH_3CN with 0.1 M Bu_4NPF_6) of the monomeric complexes **RuDqp1** (red) and **RuDqp2** (blue).

Cyclic voltammetry measurements revealed fully reversible first oxidation couples for both complexes (Table 5.1), attributed to the single-electron $\text{Ru}^{\text{III}}/\text{Ru}^{\text{II}}$ process. A second, irreversible oxidation wave was observed at around 1.3 V, being assigned to the formation of thiophene radical moieties and in full agreement with computational calculations. The first reduction signals were found at around -1.70 V and displayed a reversible behavior.

Table 5.1. UV-vis spectroscopic properties and electrochemical data of the monomer complexes (in CH_3CN , 10^{-6} M for UV-vis spectroscopy, 10^{-4} M with 0.1 M Bu_4NPF_6 for electrochemistry).

| Cmpd. | λ_{Abs} [nm] ^a (ϵ [$10^3 \text{ M}^{-1} \cdot \text{cm}^{-1}$]) | λ_{PL} [nm] | Φ_{PL} [%] ^b | $E_{1/2}$ ^c [V] ($\frac{i_{\text{p,a}}}{i_{\text{p,c}}}$, ΔE_{p} [mV]) | |
|---------------|---|----------------------------|-------------------------------------|--|------------------|
| | | | | 2+ → 3+ | 2+ → 1+ |
| RuDqp1 | 521s (16.6), 500 (18.5), 350 (43.9), 285 (46.4) | 698 | 0.8 | 0.70 (1.05, 70) | -1.68 (0.94, 79) |
| RuDqp2 | 553s (15.0), 507 (17.1), 425 (14.7), 345 (64.7), 290 (41.7) | 678 | 3.1 | 0.67 (1.06, 68) | -1.70 (0.90, 73) |

^a s = shoulder. ^b Measured using $[\text{Ru}(\text{dqp})_2](\text{PF}_6)_2$ ($\Phi_{\text{PL}} = 2\%$ in $\text{MeOH}:\text{EtOH}$ 1:4) as reference.^[87b]

^c Measured vs. Fc^+/Fc redox couple.

UV-vis-NIR spectroelectrochemical measurements showed the spectral changes during the oxidation process. The spectra of monomer **RuDqp1** exhibited a decrease of the longest-wavelength absorption band at around 510 nm, related to MLCT transitions. This is in accordance to the assignment of the first oxidation to the $\text{Ru}^{\text{III}}/\text{Ru}^{\text{II}}$ couple since applying an oxidizing potential should cause depopulation of the respective metal-located orbital leading to the observed weakening of the identified MLCT transitions. Simultaneously, a broad band arises in the region between 600 and 1,100 nm peaking at 800 nm, which is attributed to transitions from energetically lower lying orbitals to the SOMO. For complex **RuDqp2**, applying an oxidative potential led to disappearing absorption bands between 400 and 600 nm; again, the removal of electrons from a metal-based orbital that is involved in the long-

wavelength transitions is held to be responsible for the observed bleaching. As for the heteroleptic counterpart, a very broad NIR absorption appeared peaking at 800 nm.

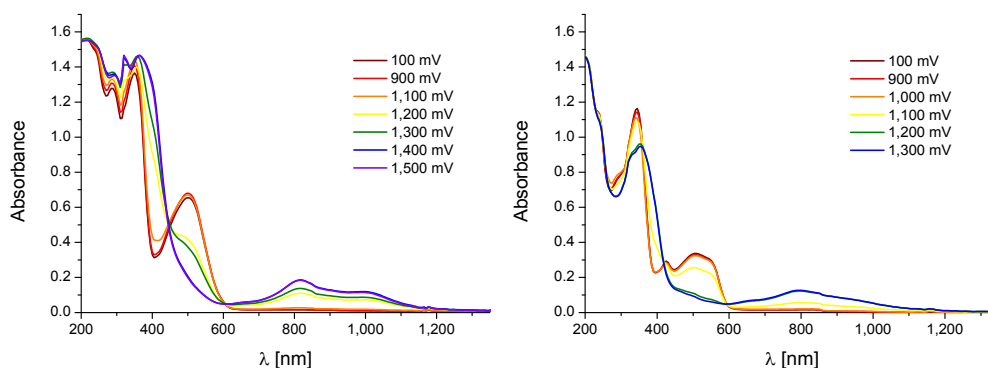
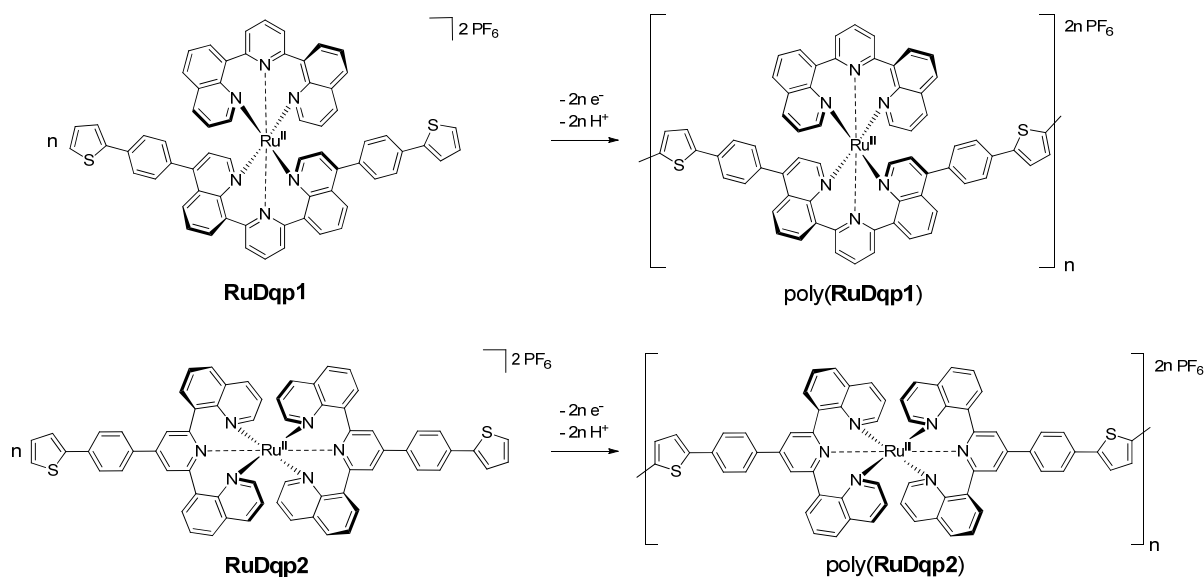


Figure 5.2. UV-vis-NIR spectroelectrochemical studies of the first oxidation processes of **RuDqp1** (left) and **RuDqp2** (right) (10^{-5} M in CH_3CN with 0.1 M Bu_4NPF_6).

5.1.2 Electrochemical *homo*-polymerization

The electropolymerization (Scheme 5.2) was carried out in acetonitrile containing 5 vol.-% of $\text{BF}_3 \cdot \text{OEt}_2$ and 0.1 M Bu_4NPF_6 . The potential was cycled between -0.5 V and 1.5 V vs. Fc^+/Fc to oxidize the thiophene moiety at around 1.2 V and form reactive thienyl cation radicals.



Scheme 5.2. Schematic representation of the proposed electro-*homo*-polymerization of complexes **RuDqp1** and **RuDqp2**.

The CV development for the first 50 cycles is presented in Figure 5.3 and exhibits a well-defined growth of the characteristic electrochemical response at 0.7 V, related to the $\text{Ru}^{\text{III}}/\text{Ru}^{\text{II}}$ redox process, while the peak current of the thienyl oxidation signal decreases over the first cycles due to consumption of monomeric complexes. Noteworthy, after two cycles, a small cathodic peak occurs at 0.9 V being assigned to the re-reduction of residual oxidized thienyl moieties that did not react due to the depletion of monomer, *i. e.* the loss of potential reaction partners. At around the 15th cycle, the polymerization rate is diminished, most likely due to the completed coverage of the electrode surface and, thus, a decreased charge transport.^[88]

The elemental composition of the films could be confirmed by XPS analysis; a Ru:S ratio of 1:2.1 and 1:1.9 for poly(**RuDqp1**) and poly(**RuDqp2**), respectively, was determined.

5.1.3 Electrochemical and photophysical characterization of the *homo*-polymer films

The CVs of the first anodic processes of the *homo*-polymers are depicted in Figure 5.4 and Table 5.2. In case of poly(**RuDqp1**), the half-wave potential is shifted slightly in comparison to the monomer towards 0.76 V vs. Fc^+/Fc . Noteworthy, related DFT calculations suggested involvement of the *bis*-thiophene unit in the redox process, which cannot be completely excluded since the respective potential of *bis*-phenylthienyl is close to the observed potential.^[89] The process is reversible with the same charge current for oxidation and reduction. The linear relationship of peak current and scan rate up to $500 \text{ mV}\cdot\text{s}^{-1}$ indicates the formation of a conductive film where redox processes are only weakly limited by charge diffusion.^[48b, 90] The redox signal of poly(**RuDqp2**) at 0.72 V is also defined and reversible. In contrast, the peak-current-scan-rate function is linear up to the highest applied scan rate of $2,000 \text{ mV}\cdot\text{s}^{-1}$, indicating a higher charge mobility than for poly(**RuDqp1**), supported by smaller $E_{p,a}-E_{p,c}$ peak splits.

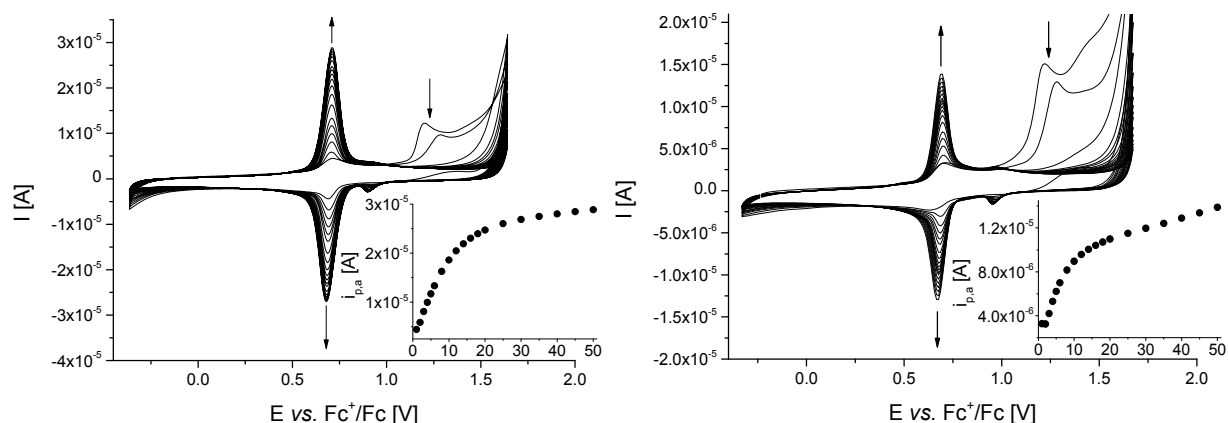


Figure 5.3. First 50 CV cycles of the electro-*homo*-polymerization and peak current increase at 0.70 V with cycle number (insets) of complex **RuDqp1** (left) and **RuDqp2** (right) (glassy carbon disk electrode, 10^{-4} M in CH_3CN with 5 vol.-% $\text{BF}_3\cdot\text{OEt}_2$ and 0.1 M Bu_4NPF_6).

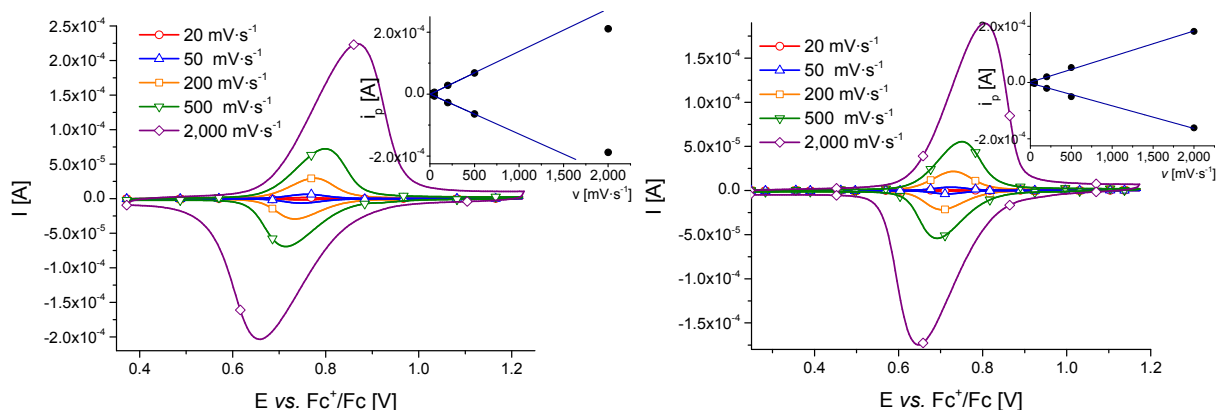


Figure 5.4. Cyclic voltammograms of the electropolymerized films applying different scan rates and peak-current dependence on the used scan rate (inset) of polymers poly(**RuDqp1**) (left) and poly(**RuDqp2**) (right) (coated glassy-carbon electrode in CH_3CN with 0.1 M Bu_4NPF_6).

Figure 5.5 shows the UV-vis absorption and emission spectra of the *homo*-polymer and monomer films. Poly(**RuDqp1**) and its monomer reveal a significant bathochromic shift of the absorption of $1,400 \text{ cm}^{-1}$ and $1,000 \text{ cm}^{-1}$, respectively, compared to the monomer solution, but only negligible differences between the monomer and the polymer films. Similarly, the film absorption of poly(**RuDqp2**) exhibits a large red shift between the dissolved monomer complex **RuDqp2** and its spin-coated film, while only a small shift of 500 cm^{-1} occurs for the

polymer compared to the monomer film. The additional peak at 425 nm, which was observed for **RuDqp2** in solution, is also present for the films as an absorption shoulder at 430 nm.

Table 5.2. UV-vis spectroscopic properties and electrochemical data of the *homo*-polymer films and UV-vis characteristics of the monomers for comparison (films on ITO-coated glass substrates).

| Cmpd. | $E_{1/2,ox}^a$ | $\lambda_{Abs,Poly}$ | $\lambda_{Abs,Mono}^b$ | $\lambda_{PL,Poly}$ | $\lambda_{PL,Mono}^b$ |
|-----------------------|----------------|----------------------|------------------------|---------------------|-----------------------|
| | [V] | [nm] | [nm] | [nm] | [nm] |
| poly(RuDqp1) | 0.76 | 537 | 527 | 767 | 746 |
| poly(RuDqp2) | 0.72 | 567 | 551 | 745 | 717 |

^a Measured vs. Fc^+/Fc redox couple. ^b UV-vis properties of spin-coated monomer films.

Both polymeric films showed weak photoluminescence. In comparison to the complexes in solution, the solid-state emissions of the spin-coated monomers are bathochromically shifted by approximately 800 to 900 cm^{-1} , and for the electropolymerized films by around $1,300\text{ cm}^{-1}$. The spectral shifts towards higher wavelengths were observed likewise for ruthenium(II)-polypyridyl systems in previous studies and are assigned to the presence of low-energy trap sites, which are available *via* electronic interaction between the ligand π systems of the closely packed complexes in the solid state.^[91] In case of the polymerized systems, an even more efficient interaction is plausible, leading to the more pronounced red shift. However, no significant effect of the conjugation path on the excited-state properties was found.

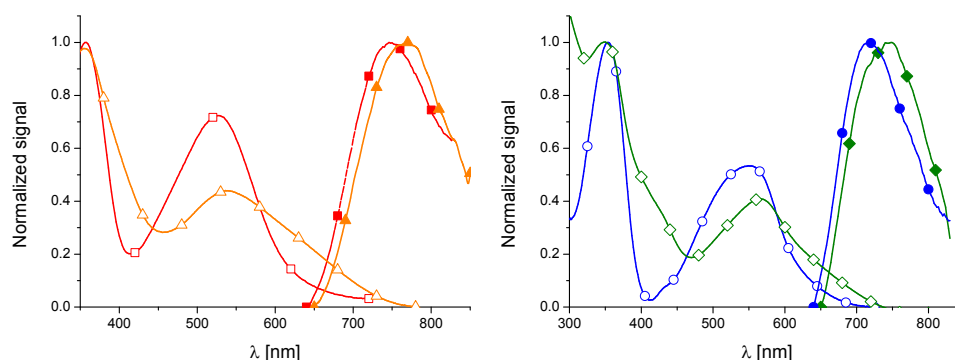


Figure 5.5. UV-vis absorption (hollow symbols) and emission (solid symbols) spectra of films of poly(**RuDqp1**) (orange) and **RuDqp1** (red) (left) and poly(**RuDqp2**) (green) and **RuDqp2** (blue) (right) on ITO-coated glass substrates.

The electrosynthesized *homo*-polymer films were furthermore studied by UV-vis-NIR spectroelectrochemistry (Figure 5.6). Poly(**RuDqp1**) showed a bleaching of the low-energy MLCT absorption band, caused by depletion of the respective metal-located orbitals, as well as the appearance of a broad band between 600 and $1,100\text{ nm}$, similar to the monomer species. The color of the polymer film changes from deep red to light yellow. Applying a potential being able to re-reduce the oxidized species recovered the starting spectrum; the repeatable change of film transmission at 515 and 810 nm with switching potential over 20 cycles indicates a reversible and stable redox process with switching times (defined by achieving 95% of the full transmission change^[92]) of around 2 s . Respective oxidation of poly(**RuDqp2**) films likewise caused the vanishing of bands between 400 and 600 nm and the increase of absorption intensity in the NIR region with a peak at 800 nm . The re-reduction produced the initial spectrum nearly completely and, over 20 cycles, a reversible and stable redox switching with response times of around 2.5 s could be observed. Comparison to the respective monomer complexes exhibited principle consistency of the observed changes upon oxidation.

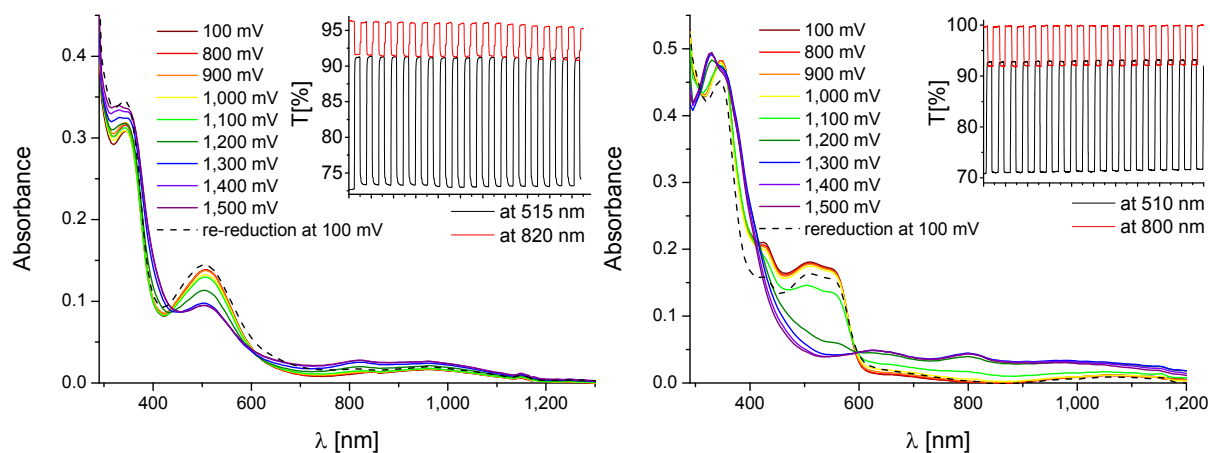
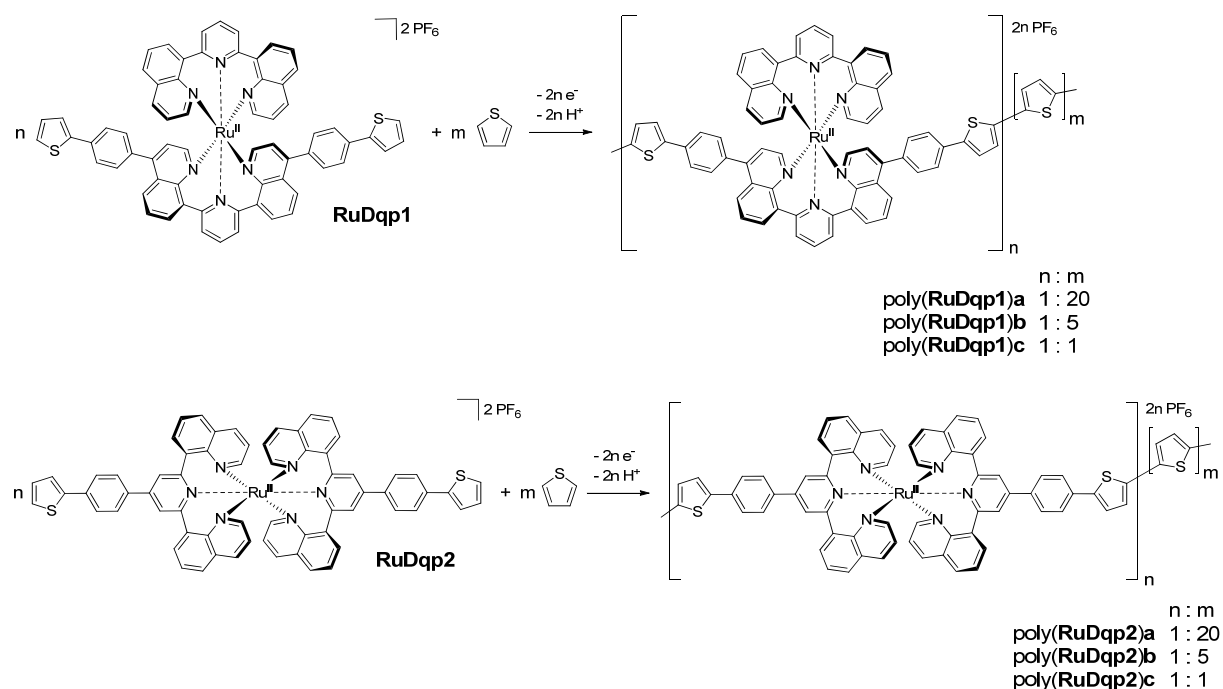


Figure 5.6. UV-vis-NIR spectral changes during the oxidation of poly(**RuDqp1**) (left) and poly(**RuDqp2**) (right) films on ITO-coated glass as well as change of transmission at selected wavelengths over 20 cycles of switching between initial and oxidized state (insets).

5.1.4 Electrochemical *co*-polymerization

In addition to the preparation of *homo*-polymers, *co*-polymers were prepared by incorporating **RuDqp1** and **RuDqp2** in polythiophene (Scheme 5.3). Therefore, different ratios of the respective complex and thiophene were used for potentiodynamic electropolymerization.



Scheme 5.3. Proposed electro-*co*-polymerization of **RuDqp1**, **RuDqp2**, and thiophene.

The applied potential was cycled between -0.1 V and 1.5 V vs. Fc^+/Fc to oxidize both the complex-appendant 2-thienyl moieties and the free thiophene to form reactive radicals. The resulting CV changes for the *co*-polymerization of **RuDqp1** and thiophene are depicted in Figure 5.7, for **RuDqp2** and thiophene in Figure 5.8. Generally, a steady increase of the current with a slope decrease after 15 to 20 cycles can be observed for all systems. However, the changes differ significantly between the different *co*-monomer ratios. In case of the 1:20-polymerizations, broad redox waves appear due to various overlapping, chain-length-dependent redox states of the formed oligothiophene.^[49b, 93] The CVs of the 1:1-mixtures match, in principle, the corresponding *homo*-polymerization (see Figure 5.3) exhibiting the rise of a

sharp signal of the complex' Ru^{III}/Ru^{II} couple as well as an additional reduction signal at 0.9 V assigned to unreacted thienyl radicals. For a ratio of 1:5, the electrochemical response is still ruthenium-dominated, but broadened due to the incorporation of oligothiophene chains.

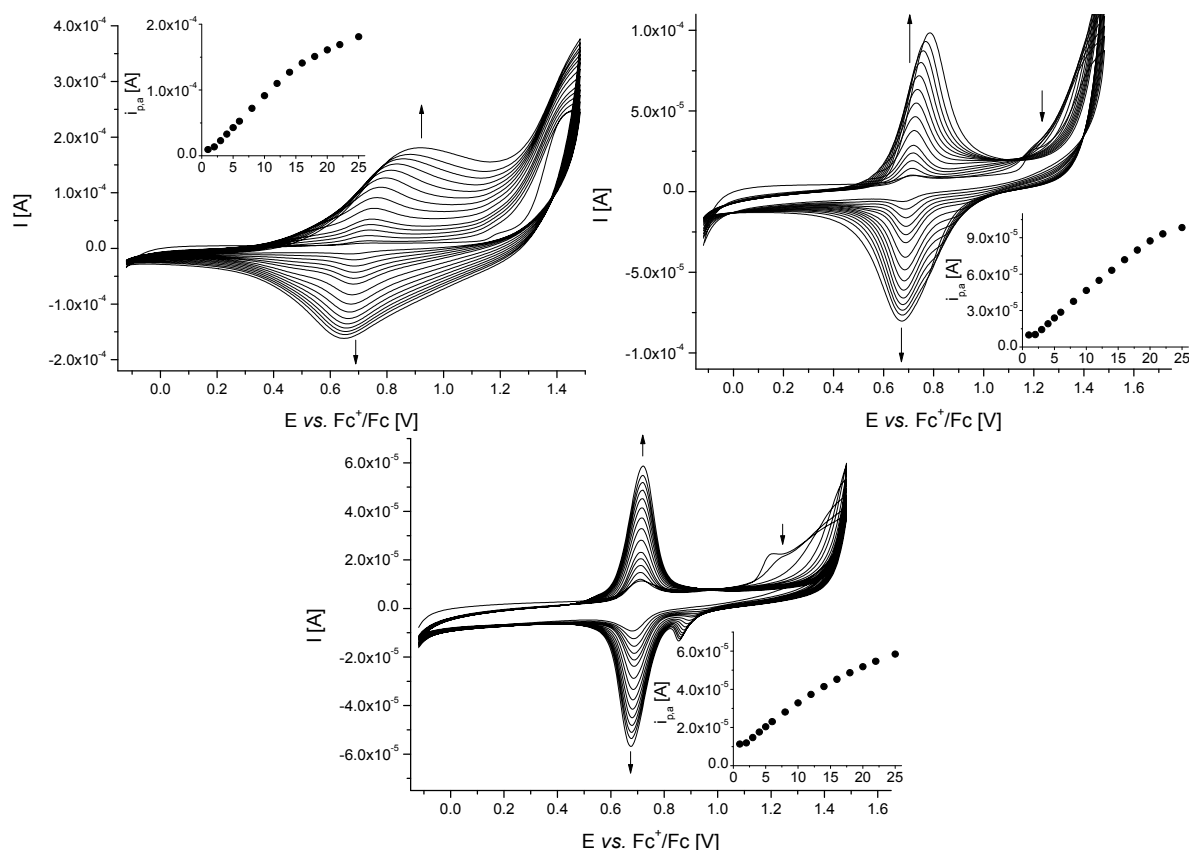


Figure 5.7. First 25 CV cycles of the electro-*co*-polymerization and peak current increase with cycle number (insets) of complex **RuDqp1** with thiophene at ratios of 1:20 (top left), 1:5 (top right), and 1:1 (bottom) (platinum disk electrode, 10^{-4} M in CH_3CN with 5 vol.-% $\text{BF}_3\cdot\text{OEt}_2$ and 0.1 M Bu_4NPF_6).

5.1.5 Electrochemical and photophysical characterization of the *co*-polymer films

The films were subsequently characterized by cyclic voltammetry and UV-vis spectroscopy. In Figure 5.9 and 5.10, the CVs of the *co*-polymer films obtained from **RuDqp1** and **RuDqp2**, respectively, are shown. The voltammograms of the 1:20-*co*-polymers are dominated by polythiophene, as already observed during the polymerization. Additionally, they show decreased electrochemical stability indicated by a decreasing peak current during cycling. For both complex assemblies, increasing their content led to a more stable behavior with fully reversible, ruthenium-based redox signals at 0.77 V and 0.74 V for poly(**RuDqp1**)**b** and poly(**RuDqp2**)**b**, respectively, at least at scan rates of $50 \text{ mV}\cdot\text{s}^{-1}$ and lower. Higher scan rates caused broader redox waves and larger peak splits, indicating hindered electron transfer processes. In case of a 1:1 ratio, the metal complex' characteristics determine the CV, *i. e.* a fully reversible redox process emerges at 0.74 V and 0.70 V for poly(**RuDqp1**)**c** and poly(**RuDqp2**)**c**, respectively, featuring a linear peak-current-scan-rate relation up to $500 \text{ mV}\cdot\text{s}^{-1}$ as well as small peak splits (10 mV for $20 \text{ mV}\cdot\text{s}^{-1}$). Both findings suggest the formation of conductive films with redox processes that are only weakly limited by charge diffusion.^[48b, 90]

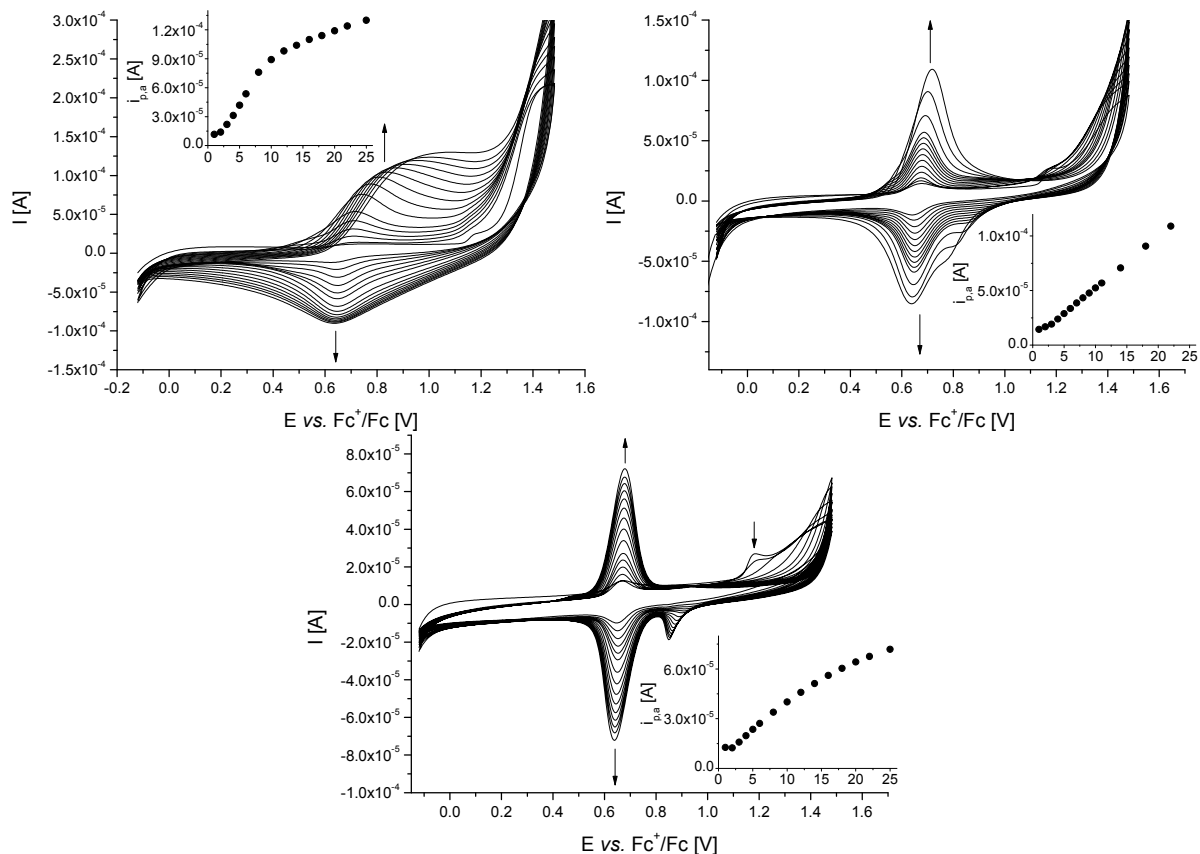


Figure 5.8. First 25 CV cycles of the electro-*co*-polymerization and peak current increase with cycle number (insets) of complex **RuDqp2** with thiophene at ratios of 1:20 (top left), 1:5 (top right), and 1:1 (bottom) (platinum disk electrode, 10^{-4} M in CH_3CN with 5 vol.-% $\text{BF}_3 \cdot \text{OEt}_2$ and 0.1 M Bu_4NPF_6).

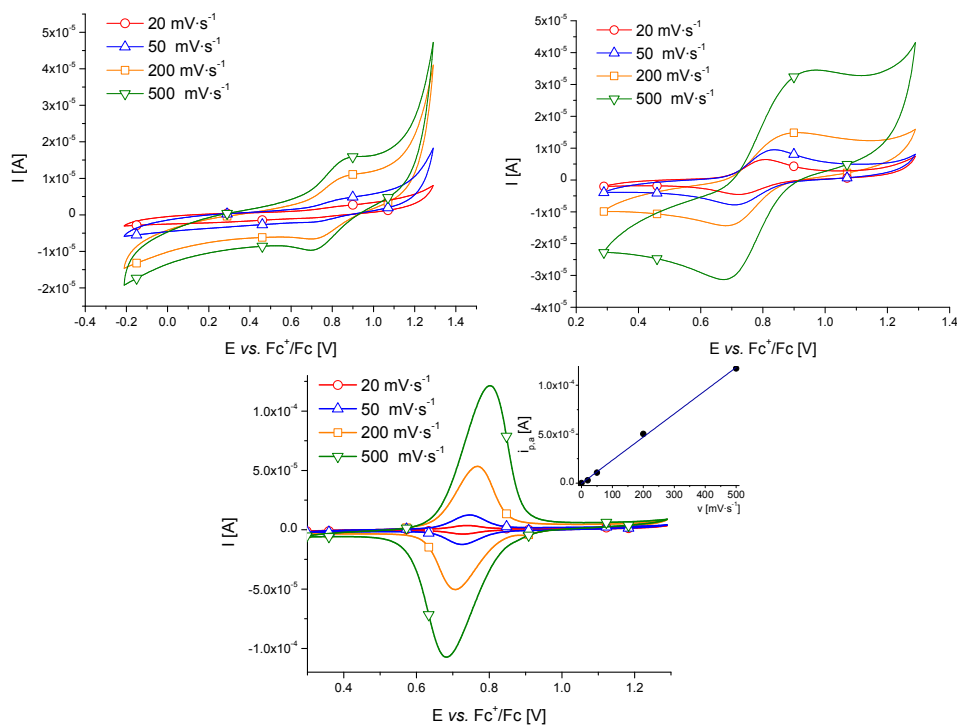


Figure 5.9. CVs of electropolymerized *co*-polymer films poly(**RuDqp1**)**a** (top left), poly(**RuDqp1**)**b** (top right), and poly(**RuDqp1**)**c** (bottom) applying different scan rates and peak-current dependence for poly(**RuDqp1**)**c** (inset) (coated platinum disk electrode in CH_3CN with 0.1 M Bu_4NPF_6).

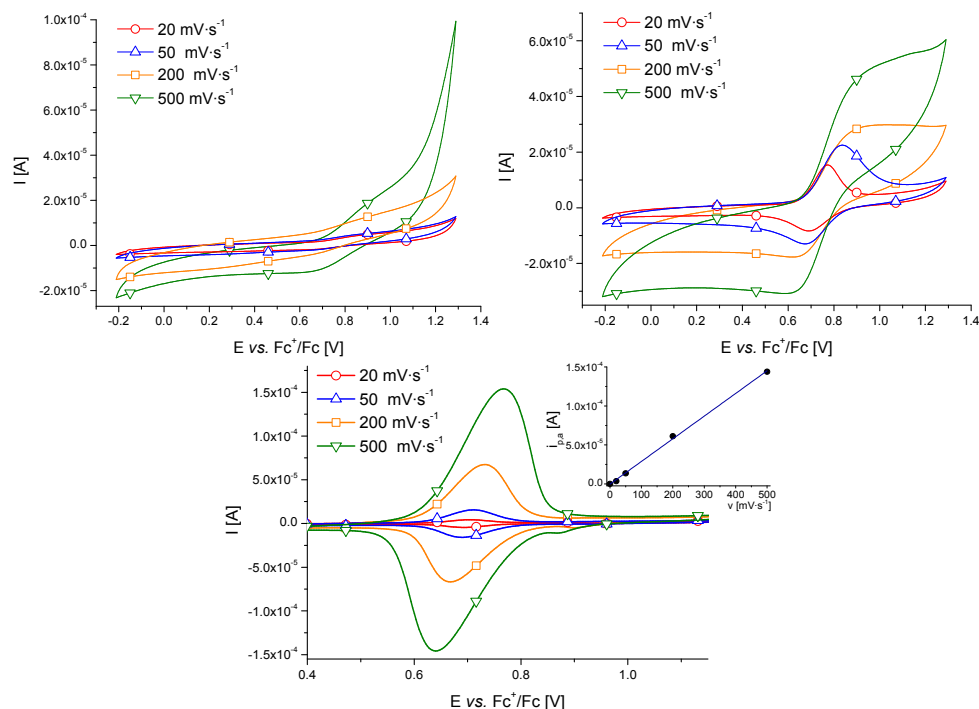


Figure 5.10. CVs of electropolymerized *co*-polymer films poly(**RuDqp2**)**a** (top left), poly(**RuDqp2**)**b** (top right), and poly(**RuDqp2**)**c** (bottom) applying different scan rates and peak-current dependence for poly(**RuDqp2**)**c** (inset) (coated platinum disk electrode in CH₃CN with 0.1 M Bu₄NPF₆).

By the admixing thiophene with a ratio of 1:5, the UV-vis absorption reveals a blue shift compared to their *homo*-polymers to 520 nm and 510 nm for poly(**RuDqp1**)**b** and poly(**RuDqp2**)**b**, respectively. For the 1:20-ratio *co*-polymers, the typical broad band of polythiophene appears,^[93] *i. e.* a maximum at 450 nm and a long-wavelength shoulder at 600 nm. UV-vis emission measurements under ambient conditions display peaks at 760 and 735 nm for the **RuDqp1**- and **RuDqp2**-based polymers, respectively. The signals do not shift with changing thiophene content indicating that the emission is based on the ruthenium(II) complex with an insignificant effect of the thiophene units.

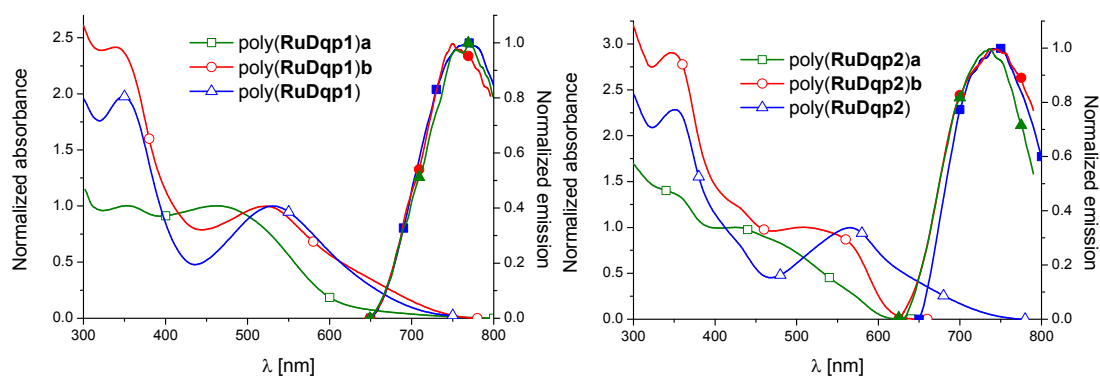


Figure 5.11. UV-vis absorption (hollow symbols) and emission (solid symbols) spectra of *co*- and *homo*-polymers from **RuDqp1** (left) and **RuDqp2** (right) (films on ITO-coated glass).

5.1.6 Characterization of the polymer films by electrochemical impedance spectroscopy

Electrochemical impedance spectroscopy was used to elucidate the charge-transfer characteristics of the polymer films.^[94] Particularly, the changes in the electrical conductivity of the different monomer ratios were deduced for varying degrees of film oxidation. The resulting Nyquist plots display two semi-circles and a straight line at lower frequencies (see the Supple-

mentary Information). The first semi-circle, spanning from $\text{Re}(Z)$ of 60 to 500 Ω , remains unaffected by varying dc potential and polymer, and represents the charge transfer between electrolyte and polymer. It is best described by an equivalent-circuit element of a resistor (R), corresponding to the interfacial charge-transport resistance, and a parallel constant-phase element (CPE), representing the interface charging and accounting also for film inhomogeneities.^[94a] The second semi-circle varies vastly with changing dc potential and reflects the charge transport within the polymer. It can be also fitted by an R-CPE element where the resistor equates the film's bulk resistance while the CPE correlates to its charge-separation capacitance. The affiliated straight line represents the Warburg impedance reflecting ion diffusion, necessary to sustain electroneutrality within the film (Figure 5.12).

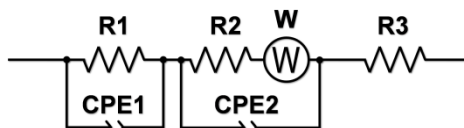


Figure 5.12. Equivalent circuit to fit the EIS data (R1: Electrolyte-polymer charge-transfer resistance, CPE1: Electrolyte-polymer interface charging, R2: Polymer film charge-transport resistance, CPE2: Polymer film charge-separation capacitance, W: Warburg impedance, R3: electrolyte resistance).

Analysis of the second semi-circles yields the electron-transfer resistance and the electrical conductivity of the polymer film for different oxidation levels. Figure 5.13 illustrates the conductivity-potential behavior for the first polymer series. In case of the polythiophene-dominated poly(**RuDqp1**)**a**, the conductivity increases from the onset of oxidation and reaches a peak value of $1.5 \times 10^{-5} \text{ S} \cdot \text{cm}^{-1}$. However, the backward scan shows a significantly lower conductivity ($2 \times 10^{-6} \text{ S} \cdot \text{cm}^{-1}$), attributed to overoxidation of the polythiophene moieties and the associated degradation of the conjugated π systems.^[48b, 95] The conductivities correspond directly to the product of charge mobility and charge concentration,^[94a, 96] hence, the oxidation of the film introduces charge carriers leading to an increased conductance of the holes, but if too many units are oxidized, the conductivity drops again, because less accepting sites are present. In line, poly(**RuDqp1**)**b** shows a later onset of increasing conductivity peaking at $5 \times 10^{-6} \text{ S} \cdot \text{cm}^{-1}$ at the half-wave potential of the $\text{Ru}^{\text{III}}/\text{Ru}^{\text{II}}$ redox process. The reverse scan showed a pronounced decrease of conductivity with a small peak at $10^{-6} \text{ S} \cdot \text{cm}^{-1}$, again, most likely due to anodic degradation of the polythiophene's conjugated π system. The 1:1 polymer poly(**RuDqp1**)**c** exhibits a similar behavior, but the higher ruthenium content leads to almost reversible redox chemistry with a comparable conductivity of up to $5 \times 10^{-6} \text{ S} \cdot \text{cm}^{-1}$. In case of the *homo*-polymer, the conductivity reaches a maximum of about $1.5 \times 10^{-5} \text{ S} \cdot \text{cm}^{-1}$ for a dc potential of 700 mV corresponding to the half-wave potential of the $\text{Ru}^{\text{III}}/\text{Ru}^{\text{II}}$ redox process. At this potential, the maximum conductance is expected due to the optimal 1:1 ratio of charge-accepting and charge-carrying units, *i. e.* $\text{Ru}^{\text{III}}:\text{Ru}^{\text{II}}$ centers.^[96]

The polymers derived from **RuDqp2** exhibit a similar behavior (Figure 5.14). Poly(**RuDqp2**)**a** and poly(**RuDqp2**)**b** show a vast conductivity drop during the backward scan decreasing from $10^{-5} \text{ S} \cdot \text{cm}^{-1}$ and $3 \times 10^{-6} \text{ S} \cdot \text{cm}^{-1}$, respectively, to $10^{-6} \text{ S} \cdot \text{cm}^{-1}$. Again, this behavior is attributed to the diminished π conjugation within the polythiophene chains caused by electrochemical degradation. For the 1:1 *co*-polymer and the *homo*-polymer, the ruthenium(II) unit is determinant, leading to a sharp increase of conductivity when oxidizing the metal complex with peak values of $8 \times 10^{-6} \text{ S} \cdot \text{cm}^{-1}$ and $1.3 \times 10^{-5} \text{ S} \cdot \text{cm}^{-1}$, respectively. During the backward scans the behavior turns out to be reversible without any significant loss in conductivity.

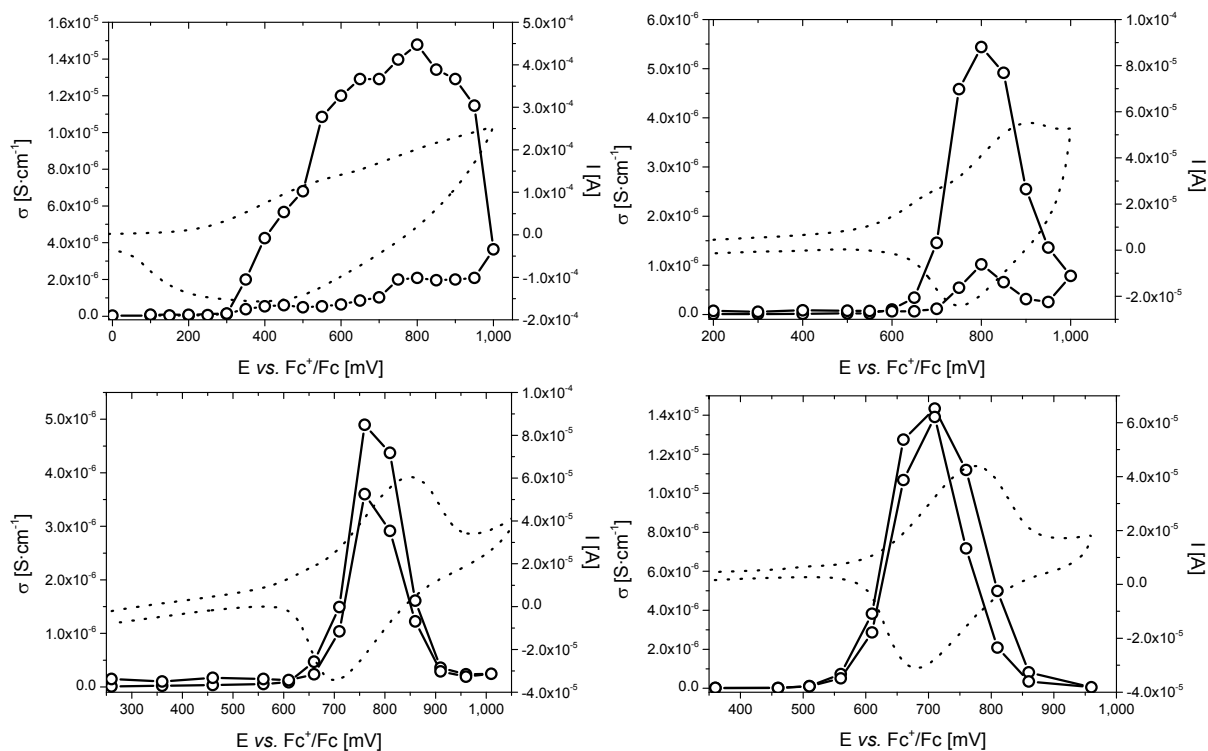


Figure 5.13. Conductivities of poly(**RuDqp1**)a (top left), poly(**RuDqp1**)b (top right), poly(**RuDqp1**)c (bottom left), and poly(**RuDqp1**) (bottom right) films on a platinum electrode depending on the applied potential (solid line; dotted line: respective CV).

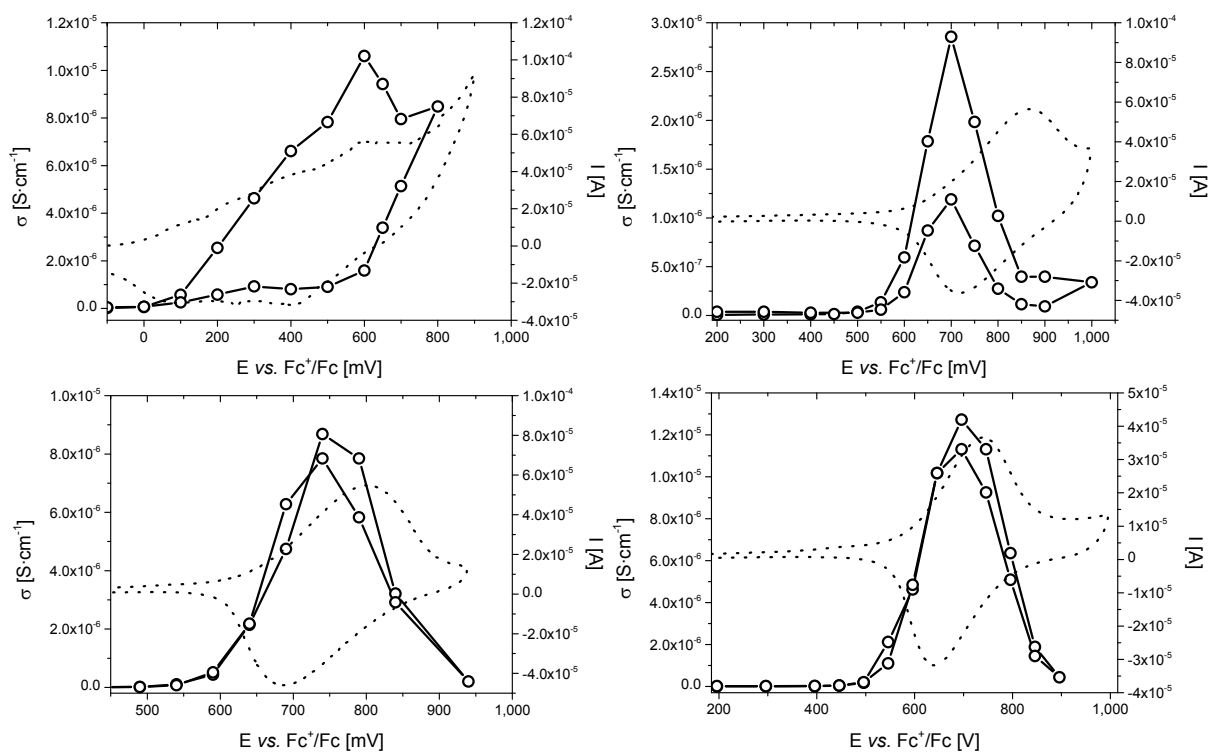


Figure 5.14. Conductivities of poly(**RuDqp2**)a (top left), poly(**RuDqp2**)b (top right), poly(**RuDqp2**)c (bottom left), and poly(**RuDqp2**) (bottom right) films on a platinum electrode depending on the applied potential (solid line; dotted line: respective CV).

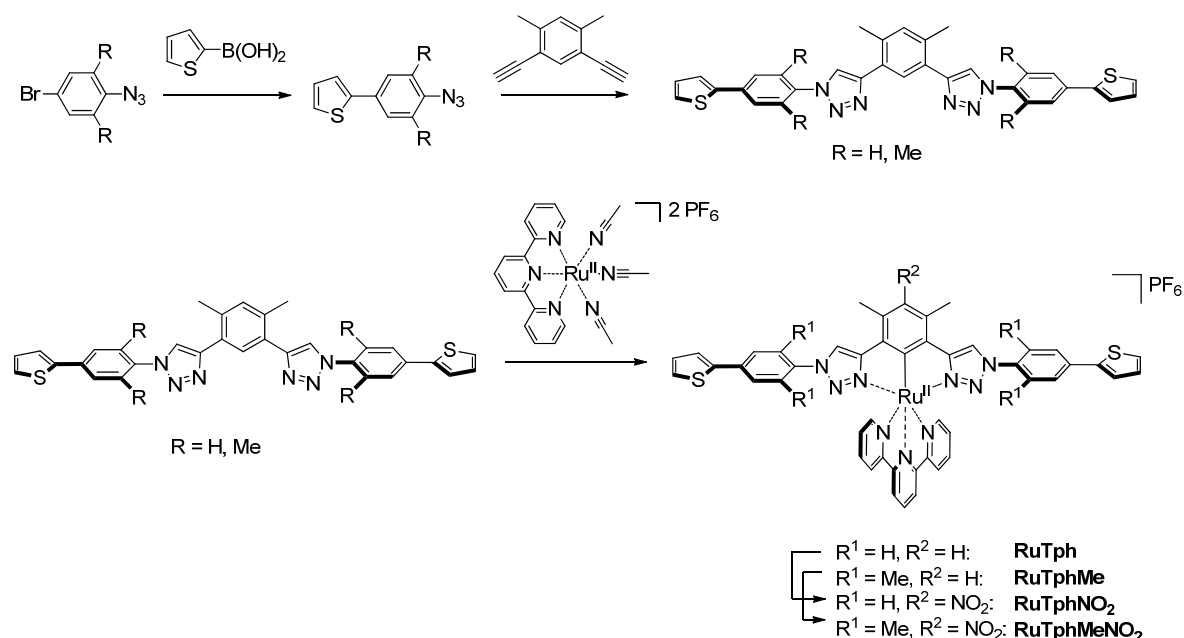
To conclude, electropolymerization was applied to realize a facile electrode coating with ruthenium(II)-dqp-containing *homo*- and thiophene-*co*-polymers. The films exhibited promising photo-redox properties, *i.e.* room-temperature emission, redox-switchability, and electrical conductivities, making them suitable for usage in electro-optical applications.

5.2 Electropolymerization of cyclometalated ruthenium(II) complexes

In Chapter 4.1, complexes based on a cyclometalating, tridentate ligand that possesses 1,2,3-triazole moieties is presented. Subsequently, such complexes were equipped with electropolymerizable 2-thienyl units (Scheme 5.4). Two motifs were applied: One with additional methyl groups at the linking phenyl rings, one without. The additional steric hindrance within the former complex should impede a full conjugation through the whole aromatic system, which should be possible in the latter one. In the further process, nitro groups were directly attached to the cyclometalating ring for redox optimization (*vide infra*), using $\text{Cu}(\text{NO}_3)_2$.^[97]

5.2.1 Characterization of the monomer complexes

The complexes were electrochemically characterized; the obtained CVs and the first redox potentials are depicted in Figure 5.15 and Table 5.3, respectively (for DPPs comprising the full available potential range, see the Supplementary Information). The CVs of **RuTph** and **RuTphMe** reveal a reversible redox process, assigned to a mixed ruthenium- and cyclometalating ligand-based orbital (see Chapter 4.1.2). In the region from 1.1 to 1.4 V, further, overlapping signals appear, including the thienyl oxidation that is necessary for the electropolymerization process. The first ligand-based redox process appears at -2.04 V for **RuTph** and at -2.06 V for **RuTphMe** and is irreversible in both cases. For **RuTphMeNO₂** and **RuTphNO₂**, both the first oxidation and the first reduction potentials are anodically shifted by about 200 mV (see Table 5.3) due to the electron-withdrawing influence of the nitro group. As for the nitro-free counterparts, the first, reversible anodic signal is assigned to the mixed ruthenium(II) / cyclometalating ligand moiety. A second oxidation appears at 1.2 V, most likely related to the formation of the thienyl radical cations. In contrast to the preceding complexes, the first reduction is reversible and a further process occurs at -2.10 V.



Scheme 5.4. Schematic representation of the synthesis of the 2-thienyl-functionalized cyclometalated ruthenium(II) complexes.

In Figure 5.15, the UV-vis absorption spectra of the monomers are depicted. They exhibit bands between 450 and 700 nm, which are assigned to MLCT and MLLCT transitions. For **RuTphMeNO₂** and **RuTphNO₂**, these bands are blue-shifted due to the electron-withdrawing

ability of the nitro group, which causes a stabilization of the HOMOs being located on the cyclometalating ligand and the metal ion (see Chapter 4.1.1). An additional band can be found at 400 nm. Here, the introduction of methyl groups at the peripheral phenyl rings causes a hypsochromic shift as well as a decreasing extinction coefficient. This is most likely because of a diminished π conjugation within the triazole-phenyl-thienyl fragment due to steric repulsion between the methyl groups and the 1,2,3-triazole rings precluding a complete co-planarization. Emission measurements revealed photoluminescence peaks at around 740 nm for the nitro-free **RuTph** and **RuTphMe**, while the emission maxima for the nitro-substituted species are, as expected, blue-shifted by about 900 to 1,000 cm^{-1} (see Table 5.3).

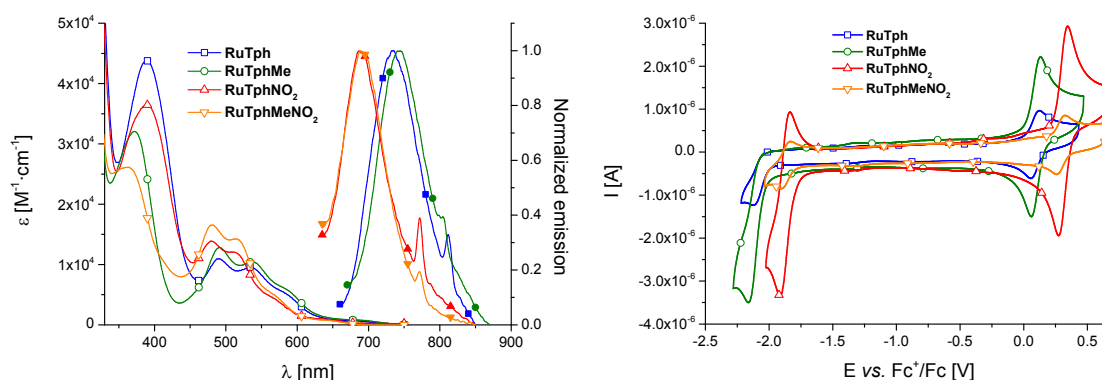


Figure 5.15. UV-vis absorption (hollow symbols) and emission (solid symbols) spectra (left, 10^{-6} M in CH_2Cl_2) and cyclic voltammograms (right, 10^{-4} M in CH_2Cl_2 with 0.1 M Bu_4NPF_6) of the monomeric complexes **RuTph** (blue), **RuTphMe** (green), **RuTphNO₂** (red) and **RuTphMeNO₂** (orange).

Table 5.3. UV-vis spectroscopic and electrochemical characteristics of the monomer complexes (10^{-6} M in CH_2Cl_2 and 10^{-4} M in CH_2Cl_2 with 0.1 M Bu_4NPF_6 , respectively).

| Complex | λ_{Abs} [nm] (ϵ [$10^3 \text{ M}^{-1}\cdot\text{cm}^{-1}$]) ^a | λ_{PL} [nm] | $E_{1/2}$ [V] ($\frac{i_{p,a}}{i_{p,c}}$, ΔE_p [mV]) ^b | |
|------------------------------|---|----------------------------|---|-----------------------------|
| | | | $1+ \rightarrow 2+$ | $1+ \rightarrow 0$ |
| RuTph | 685s (0.7), 586s (5.0), 533 (9.5), 491 (11.0), 388 (43.8) | 733 | 0.10 (1.05, 65) | -2.04 (irrev.) ^c |
| RuTphMe | 689s (0.8), 590s (5.5), 536 (10.5), 491 (12.8), 372 (32.1) | 743 | 0.10 (1.0, 74) | -2.06 (irrev.) ^c |
| RuTphNO₂ | 645s (0.7), 570s (4.0), 507 (11.8), 479 (13.7), 389 (36.3) | 689 | 0.29 (1.0, 67) | -1.87 (1.0, 75) |
| RuTphMeNO₂ | 642s (0.7), 560s (5.6), 515 (14.3), 482 (16.5), 361 (26.1) | 690 | 0.31 (1.0, 72) | -1.88 (1.05, 78) |

^a s = shoulder ^b Potentials vs. Fc^+/Fc . ^c Obtained from DPP spectra.

5.2.2 Electropolymerization

Electropolymerization experiments were carried out potentiodynamically in different solvents using 0.1 M Bu_4NPF_6 as electrolyte. The first studies were performed in acetonitrile. Including the region at 1.2 to 1.4 V, both **RuTph** and **RuTphMe** showed a rapid decrease of all redox signals indicating decomposition (Figure 5.16). Since changing the potential range or scan rate did not lead to successful polymerization, the solvent was changed to dichloromethane. For **RuTphMe**, the CV development was divided in two phases: During the first eleven cycles, an increase of the ruthenium-based redox signal was observed, indicating the formation of the desired polymer, which was, however, accompanied by rising of additional signals at -0.1 and 0.9 V, suggesting the formation of polymeric byproducts (Figure 5.17). After the eleventh cycle, the redox signals in the region between -0.4 and 0.4 V start to decrease, which is, again,

most likely due to the electrochemical decomposition of the formed compounds. For **RuTphMe**, likewise, additional redox processes appear at around -0.2 V, but already during the third cycle, a signal decrease, *i. e.* decomposition, starts. Also involving the usage of Lewis acids (*e. g.* $\text{BF}_3 \cdot \text{OEt}_2$, borate esters)^[59] or weak bases (*e. g.* water, 2,6-di-*tert*-butylpyridine)^[48b] did not result in a successful polymerization.

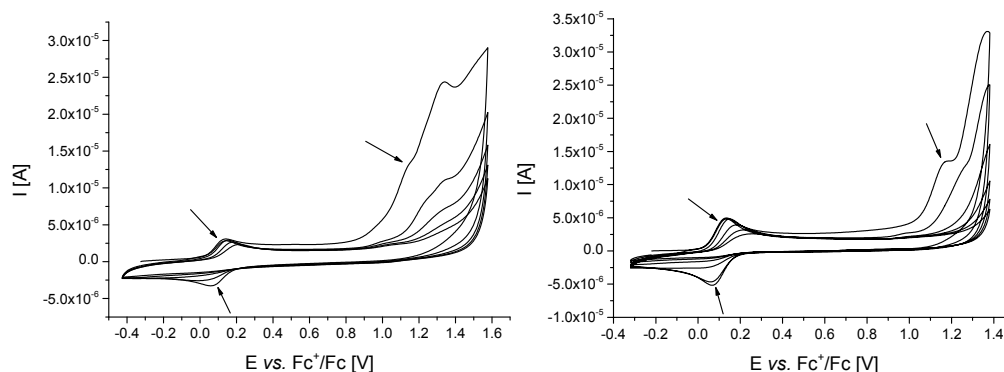


Figure 5.16. CV development during the electropolymerization attempts for **RuTph** (left) and **RuTphMe** (right) in CH_3CN (10^{-4} M with 0.1 M Bu_4NPF_6).

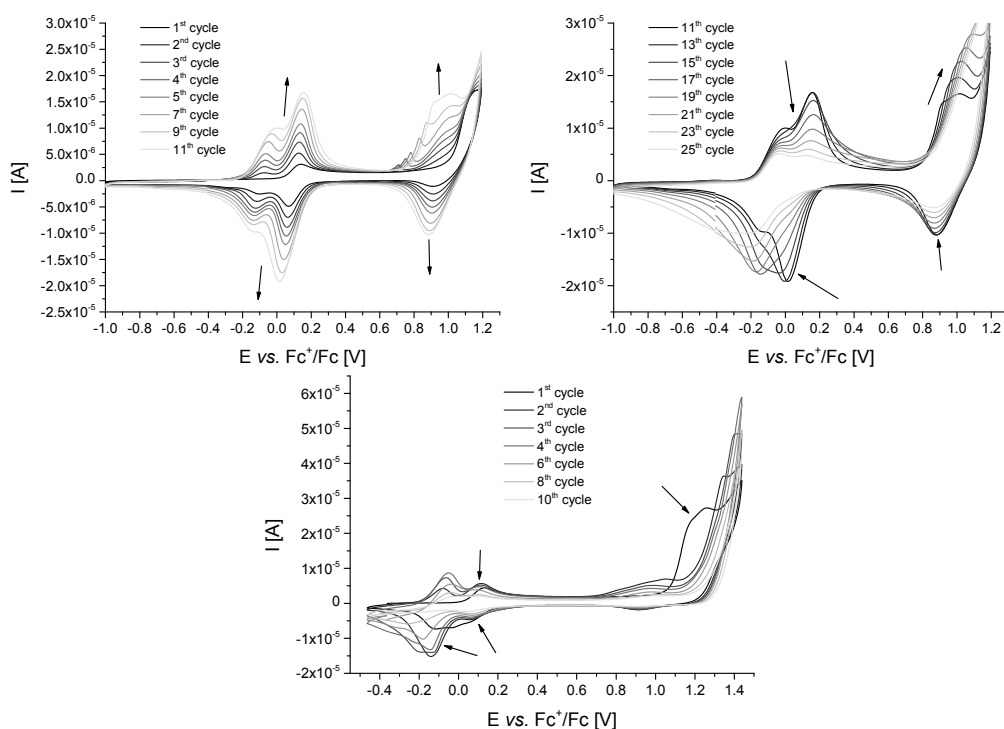


Figure 5.17. CV development during electropolymerization attempts for **RuTph** (top; 1st to 11th and 11th to 25th cycle) and **RuTphMe** (bottom) in CH_2Cl_2 (10^{-4} M with 0.1 M Bu_4NPF_6).

It is assumed that the decomposition is caused by an inherent electrochemical process of the complexes. This assumption was supported by comparison of the CVs of the thienyl-equipped systems with their parent complex **RuNCN** (Figure 5.18), revealing a further, irreversible redox process at around 1.2 V that is overlaid by the thienyl-based signals. Thus, oxidation of the thienyl units would not be possible without inducing an irreversible oxidation reaction of the complex core moiety. To overcome this problem, attempts to shift the respective irreversible oxidation potential beyond the thienyl's one were undertaken. For this purpose, a nitro group was introduced at the 4-position of the central phenyl ring of the cyclometalating ligand to increase the redox potentials as observable for the respective thiophene-free parent

complex (Figure 5.18). Indeed, the DPP spectra of the consequently synthesized nitro-containing complexes **RuTphMeNO₂** and **RuTphNO₂** reveal one separate signal at 1.15 V (see the Supplementary Information), which is assumed to be related to the thienyl oxidation. Notably, an oxidative dimerization reaction, as described in literature,^[38b, 98] was excluded by electropolymerization experiments using the 4-bromo-functionalized **RuTph** complex, which resulted likewise in non-defined electrochemical processes (see the Supplementary Information).

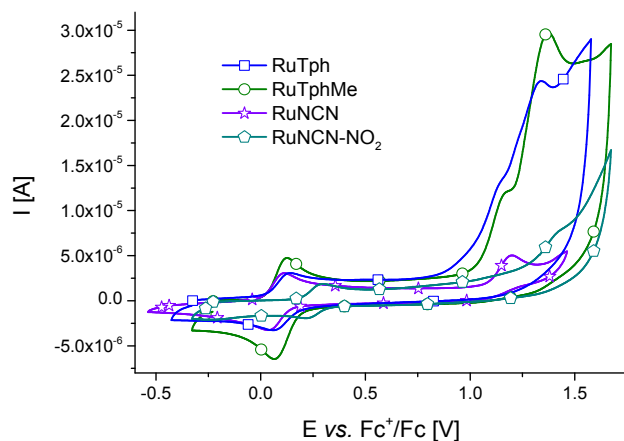


Figure 5.18. Cyclic voltammogram depicting the oxidation processes of **RuTph** and **RuTphMe** in comparison to the parent **RuNCN** and **RuNCN-NO₂** (10^{-4} M in CH_3CN with 0.1 M Bu_4NPF_6).

Hence, the electropolymerization of **RuTphMeNO₂** in dichloromethane was studied. In Figure 5.19, the respective cyclic voltammograms are shown. The peak current of the first oxidation of the complex rises during the first five to ten cycles, as expected for a successful electropolymerization. However, the slope is comparatively low, indicating a low polymerization rate, and decreases afterwards, reaching a plateau at the 20th cycle. Hence, the obtained films are very thin. Nevertheless, their characterization by cyclic voltammetry as well as UV-vis absorption spectroscopy was possible. In Figure 5.20, the respective spectra are presented. The CV shows a fully reversible first redox process with a half-wave potential of 0.28 V, slightly cathodically shifted compared to the dissolved monomer complex. Furthermore, the peak current grows linearly with increasing scan rate up to $500 \text{ mV}\cdot\text{s}^{-1}$, indicating the formation of conductive films with only weakly diffusion-controlled charge migration.^[48b, 90]

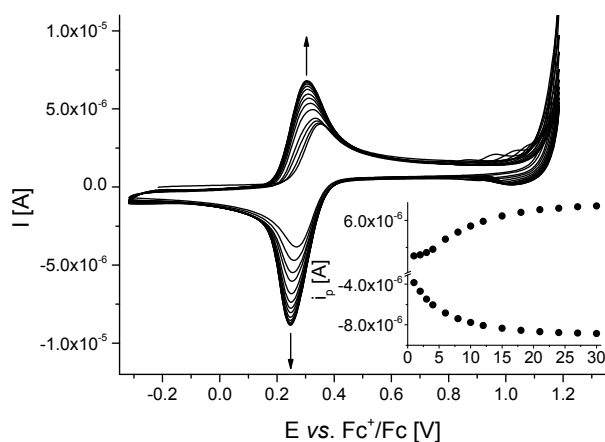


Figure 5.19. CV and peak-current development during the electropolymerization of **RuTphMeNO₂** in CH_2Cl_2 (10^{-4} M with 0.1 M Bu_4NPF_6).

Comparison of the UV-vis absorption spectrum of the polymer film with the monomer showed an only negligible red shift of the MLCT maximum of 110 cm^{-1} from 520 nm for the drop-casted monomer film to 523 nm for the polymer film, accompanied by a broadening and a loss of band structure (Figure 5.20). An additional intense peak arises at 341 nm , assigned to LC transitions located on the *bis*-phenylthienyl moieties, which are only present in the polymer.^[89] Unfortunately, spectroelectrochemical investigations could not be executed since the obtained films were too thin to yield an observable absorption signal with the used setup.

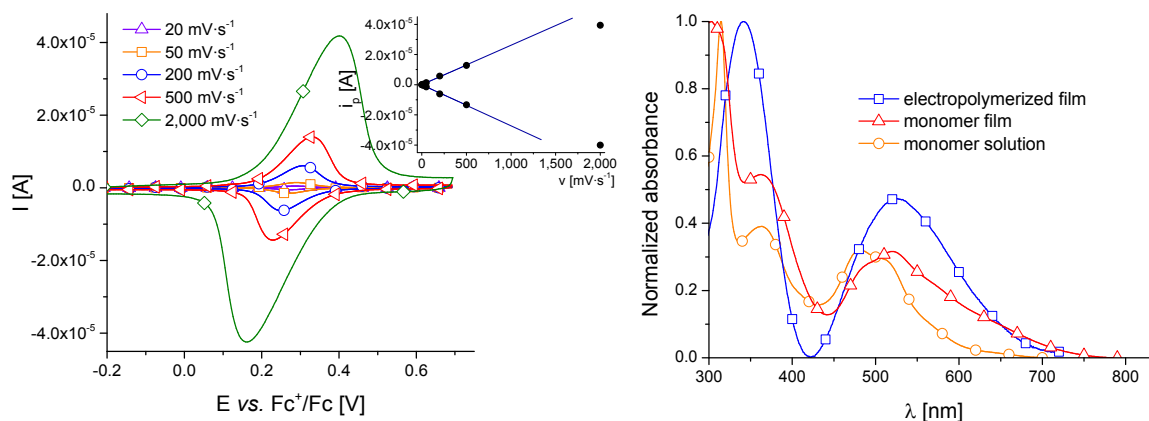


Figure 5.20. Characterization of **RuTphMeNO₂** films: CVs of the first oxidation at different scan rates (left; on glassy carbon in CH_2Cl_2 with $0.1\text{ M Bu}_4\text{NPF}_6$) and UV-vis absorption compared to the drop-casted (ITO-coated glass) and the dissolved monomer (10^{-6} M in CH_2Cl_2) (right).

In a similar manner, anodic polymerization attempts were carried out for the non-methylated congener **RuTphNO₂**. Notably, only relatively low concentrations (around $50\text{ }\mu\text{g}\cdot\text{mL}^{-1}$ or $5\cdot 10^{-5}\text{ M}$) could be applied due to the poor solubility of the complex. However, in contrast to its methylated counterpart, a linear increase for the monitored peak current occurred at least up to the 30th cycle (Figure 5.21), indicating the formation of a polymeric film. Comparative experiments with low concentrations for **RuTphMeNO₂** resulted, as for the described studies with higher concentrations, in a limited polymerization. Additional signals appeared at 0.45 and -0.05 V , which are tentatively assigned to non-reacted radicals that were not incorporated into the polymer. Subsequently, electropolymerization studies on the nitro-functionalized complexes with higher vertex potentials were carried out, which resulted in a non-defined process, as observed for the non-nitro species (see the Supplementary Information). Thus, the enhanced electropolymerization ability upon nitro-functionalization is indeed attributed to shifted redox potentials, but not to blocked reaction sites.

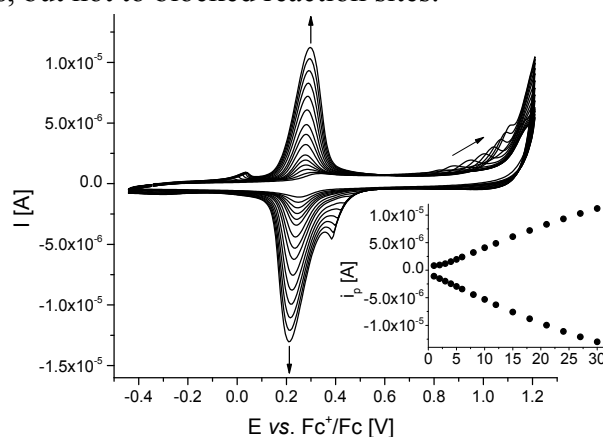


Figure 5.21. CV and peak-current development during the electropolymerization of **RuTphNO₂** in CH_2Cl_2 (10^{-5} M with $0.1\text{ M Bu}_4\text{NPF}_6$).

CV characterization displays a fully reversible redox signal at 0.25 V, slightly cathodically shifted with respect to its monomer and the **RuTphMeNO₂** polymer. As for the latter, the peak-current-scan-rate relationship shows a linear behavior up to 500 mV·s⁻¹. Notably, the accompanying signals at 0.45 and -0.05 V are not present for the film, supporting the assignment to non-reacted species.

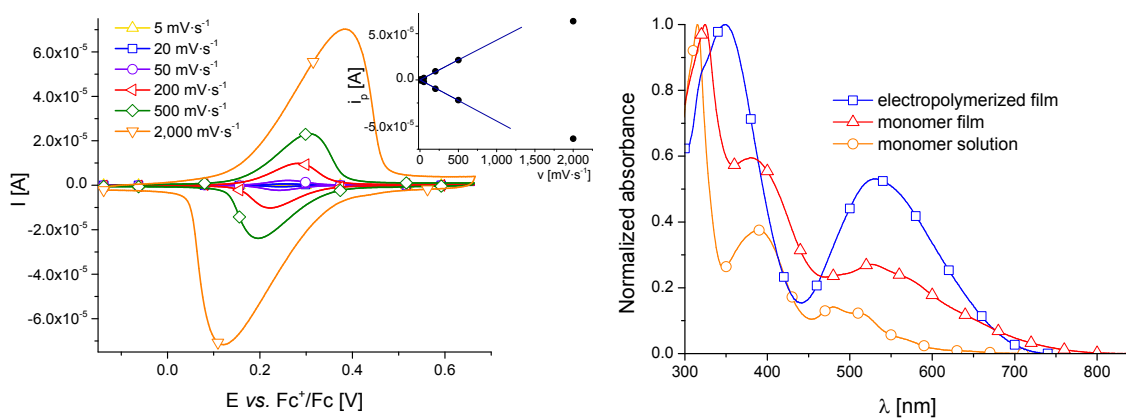


Figure 5.22. Characterization of **RuTphNO₂** films: CVs of the first oxidation at different scan rates (left, on glassy carbon in CH₂Cl₂ with 0.1 M Bu₄NPF₆) and UV-vis absorption compared to the drop-casted (on ITO-coated glass) and the dissolved monomer (right, 10⁻⁶ M in CH₂Cl₂).

UV-vis absorption measurements exhibited a prominent MLCT band at 531 nm, slightly red-shifted by 220 cm⁻¹ compared to the monomer film (Figure 5.22) and by 290 cm⁻¹ with respect to the methylated analog, suggesting a higher degree of conjugation. Likewise, the additional peak that is present in the UV region, assigned to *bis*-phenylthienyl units formed through the polymerization,^[89] is red-shifted by 590 cm⁻¹ to 348 nm. UV-vis-NIR spectroelectrochemical studies on the polymer film (Figure 5.23) for the redox process at 0.25 V resemble the characteristic features of the present cyclometalated ruthenium(II) complex, namely a bleaching of the MLCT absorption, on the one hand, and the rise of a broad and weak band between 700 and 900 nm (see Chapter 4.1.3). Repeated switching between the initial and the oxidized state turned out to be reversible for at least 30 cycles, proving the redox stability of the polymer film, and revealed switching times of 1.8 s.

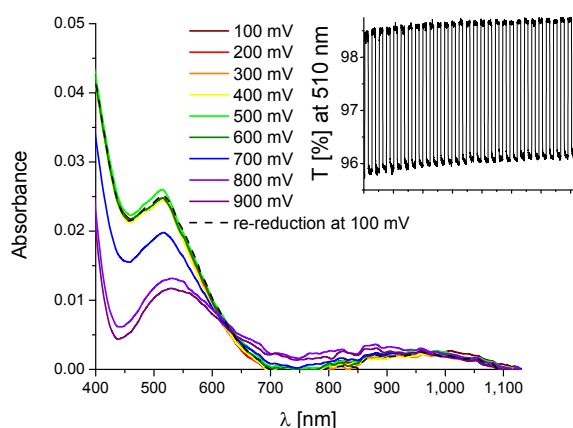


Figure 5.23. Spectral change of **RuTphNO₂** polymer film during oxidation and for 30 cycles of switching between initial and oxidized state (on ITO-coated glass in CH₂Cl₂ with 0.1 M Bu₄NPF₆).

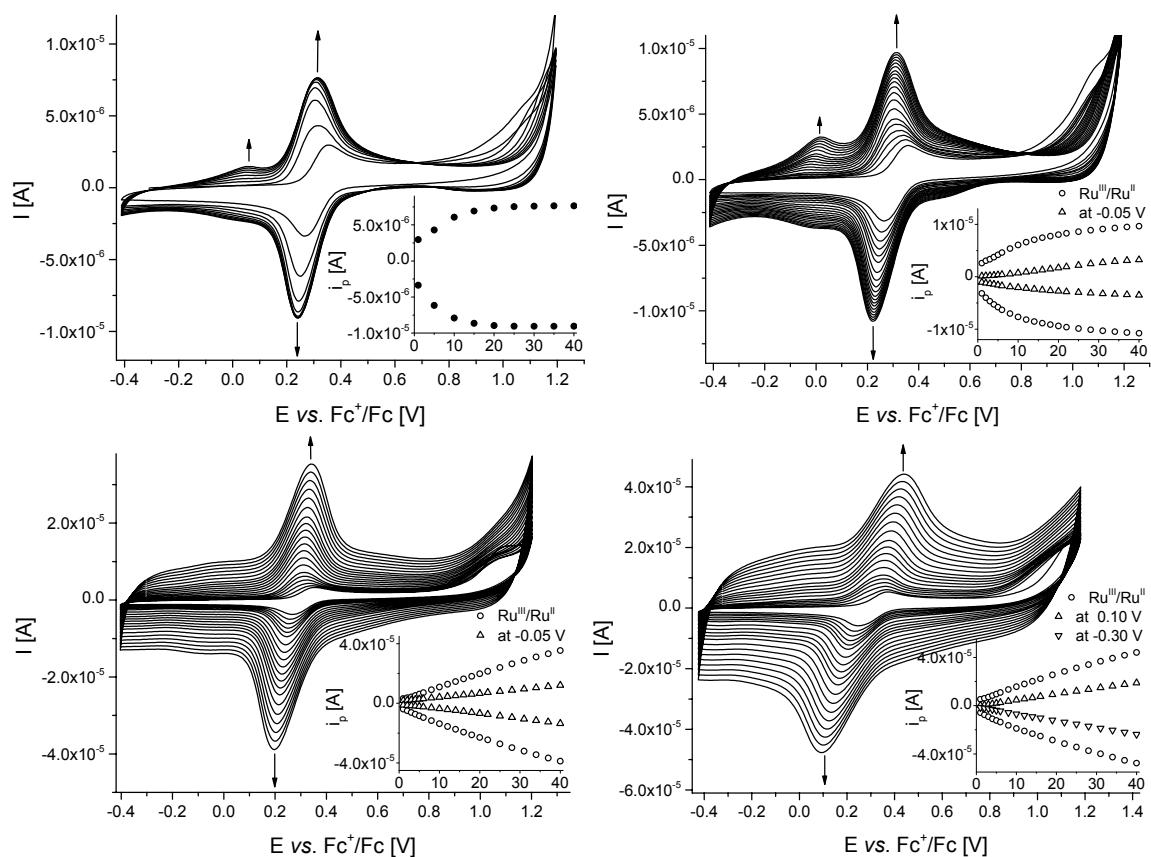


Figure 5.24. CV and peak-current development during the *co*-electropolymerization of **RuTphMeNO₂** with EDOT in CH₂Cl₂ (10⁻⁴ M with 0.1 M Bu₄NPF₆) using molar ratios of 5:1, 2:1, 1:1, and 1:5.

5.2.3 *Co*-polymers

To further enhance the electropolymerization performance of the **RuTphMeNO₂** complex, *co*-polymerization with 3,4-ethylenedioxythiophene (EDOT) as *co*-monomer was carried out. Different molar monomer ratios were used for potentiodynamic anodic polymerization (Figure 5.24). A 5:1 complex-EDOT ratio did not improve the polymerization process at all. Like for the pure complex, the peak-current development indicates an interruption around the 15th cycle. However, an additional plateau arises between -0.2 and 0.6 V, assigned to the formation of PEDOT (see the Supplementary Information for comparison). For a ratio of 2:1, an enhanced PEDOT generation is observable, but still, the slope of the Ru^{III}/Ru^{II}-based peak-current increase is reduced after 15 cycles and the further current development parallels the pure PEDOT-based one, indicating that only PEDOT is formed from that cycle on and no more complex is included. Increasing the EDOT ratio to 50% leads to a significantly improved polymerization: The Ru^{III}/Ru^{II}-related current increases linearly at least up to the 40th cycle, indicating that the ruthenium(II) moiety is still incorporated into the *co*-polymer. A similar behavior was observed for an excess of EDOT, namely for a ruthenium(II)-EDOT ratio of 1:5, with an expectedly higher current for the PEDOT-related background. This way, *co*-polymer films containing the cyclometalated ruthenium(II) complex could be prepared and characterized.

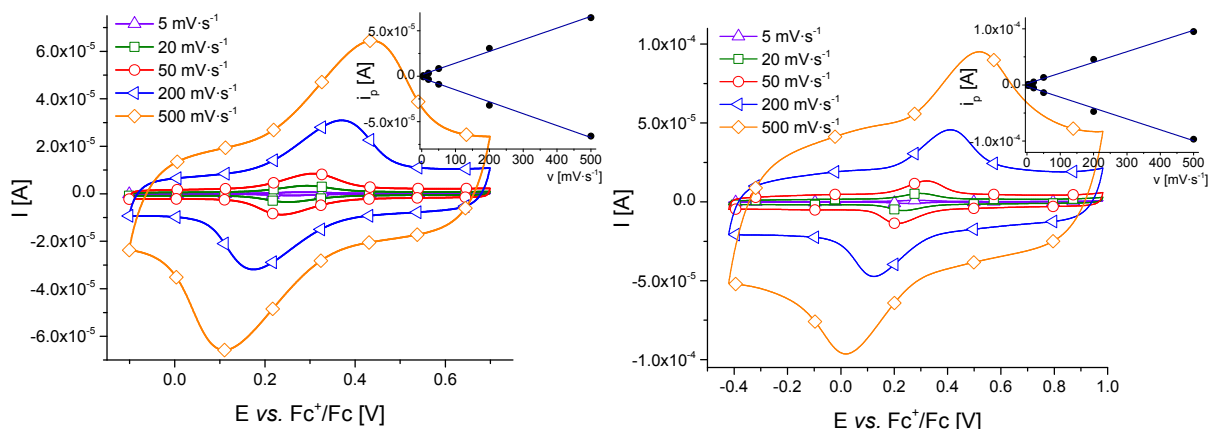


Figure 5.25. CVs of electropolymerized *co*-polymer films from **RuTphMeNO₂** and EDOT showing the first oxidation at different scan rates as well as relationship between peak currents and scan rate (films on glassy-carbon disk electrode in CH₂Cl₂ with 0.1 M Bu₄NPF₆) for molar ratios of 1:1 and 1:5.

Cyclic voltammetry revealed a reversible redox process for both the 1:1 and the 1:5 *co*-polymer at 0.27 V accompanied by a broad redox current assigned to PEDOT. In both cases, the peak-current-scan-rate relationship is linear up to 500 mV·s⁻¹ (Figure 5.25). The UV-vis absorption spectra of the *co*-polymer films show absorption peaks at 523 nm and 341 nm, accompanied by a broad band in the NIR region (Figure 5.26). With increasing EDOT content, the relative intensity of the latter rises, assigned to a growing content of PEDOT moieties, which exhibit strong NIR absorption (see the Supplementary Information). Simultaneously, the peak at 341 nm, related to *bis*-phenylthienyl moieties, decreases with respect to the MLCT band since the *bis*-thienyl bridges are replaced by *oligo*-EDOT blocks for the *co*-polymers. UV-vis-NIR spectroelectrochemical studies of the *co*-polymer films showed a combination of RuNCN and PEDOT characteristics, *i. e.* the vanishing of the MLCT band between 400 and 600 nm and the rise of a broad, intense band in the NIR region, respectively. In the long-wavelength visible region, also the metal complex' behavior, *i. e.* the formation of a new absorption band, is dominant, but superimposed by a PEDOT-related absorption decrease (see the Supplementary Information). Notably, for the 1:1 *co*-polymer the PEDOT-based NIR absorption is blue-shifted with respect to the 1:5 polymer, indicating the presence of shorter *oligo*-EDOT chains, which possess a smaller conjugated π system, while the 1:5 system exhibits an NIR absorption maximum similar to the pure-PEDOT reference study. Applying a re-reducing potential recovered the initial spectrum in both cases and, similarly, monitoring the UV-vis transmission while repeatedly changing between oxidizing and re-reducing potential showed reversible and stable redox switchability for at least 30 cycles.

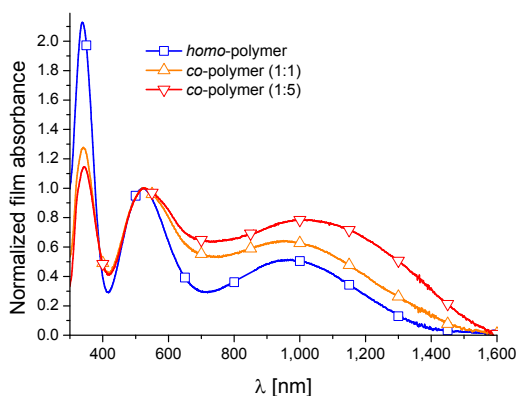


Figure 5.26. UV-vis absorption spectra of *homo*- and *co*-polymer films of **RuTphMeNO₂** (ITO-coated glass).

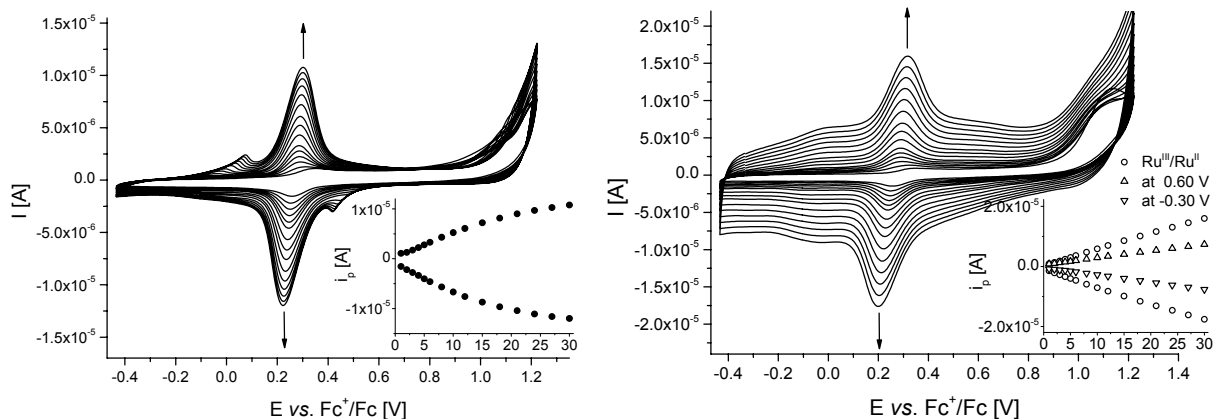


Figure 5.27. CV and peak-current development during the *co*-electropolymerization of **RuTphNO₂** with EDOT in CH₂Cl₂ (10⁻⁵ M with 0.1 M Bu₄NPF₆) using molar ratios of 1:1 and 1:5.

Like for its methylated analogue, *co*-polymers of **RuTphNO₂** and EDOT were electrochemically prepared using molar ratios of 1:1 and 1:5. As shown in Figure 5.27, for an equimolar ratio, only marginal differences, namely a small current plateau between -0.2 and 0.5 V, occur compared to the *homo*-polymerization. This behavior is most likely attributed to the low concentration (below 10⁻⁴ M) of the EDOT due to the low complex solubility. In contrast, the fivefold EDOT excess led to the distinct formation of PEDOT moieties, indicated by the development of a broad current plateau. As for **RuTphMeNO₂**, the peak current that corresponds to the Ru^{III}/Ru^{II} redox couple increases faster than the subjacent PEDOT-related current, showing that ruthenium(II) complex and EDOT are polymerized.

Subsequent electrochemical and UV-vis spectroscopic characterization (shown in Figure 5.28 and 5.29) confirmed the achieved findings: Both CV and UV-vis absorption spectrum of the 1:1 polymer resemble in principle the *homo*-polymer's ones, while the films from the higher EDOT ratio revealed a significant PEDOT influence, namely a broad current plateau in the CV and an enhanced absorption in the NIR region. Remarkably, in contrast to its methylated counterpart, a notable red shift of the MLCT absorption by 1,300 cm⁻¹ between the *homo*-polymer and the 1:5 *co*-polymer appears, suggesting an at least partial interaction between the metal complex centers and the *poly*- and *oligo*-EDOT moieties.

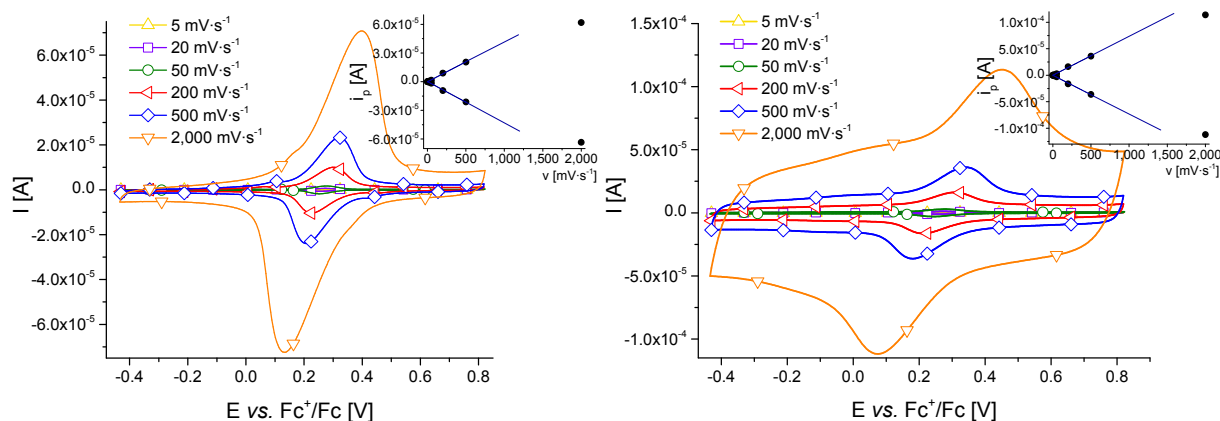


Figure 5.28. CVs of electropolymerized *co*-polymer films from **RuTphNO₂** and EDOT showing the first oxidation at different scan rates as well as relationship between peak currents and scan rate (films on glassy-carbon disk electrode in CH₂Cl₂ with 0.1 M Bu₄NPF₆) for molar ratios of 1:1 and 1:5.

UV-vis-NIR spectroelectrochemical studies on the *co*-polymer films (see the Supplementary Information) revealed the typical spectral changes during oxidation: For the ruthenium(II)-complex-dominated 1:1 polymer, as soon as the oxidation of the metal center starts the MLCT

absorption band at around 500 nm vanishes, while a very broad, weak absorption arises beyond 600 nm, which spans, in contrast to the *homo*-polymer, the region up to 1,600 nm, attributed to the incorporated *oligo*-EDOT chains. However, their influence is significantly smaller than for the 1:1 *co*-polymer of **RuTphMeNO₂** and an isosbestic point at 590 nm, which was not present for the other *co*-polymer, supports the presence of only one electrooptically determinant species. In case of the 1:5 *co*-polymer, both the metal complex moiety and PEDOT determine the spectra; a decrease of the complex' MLCT absorption between 400 and 600 nm is accompanied by an emerging strong NIR absorption peaking at 1,350 nm. Re-reduction of the polymer films recovered the initial absorption spectra demonstrating the redox stability of the systems. However, for the 1:5 *co*-polymer, repetitive switching of the redox state over 30 cycles showed a diminished maximum absorption change to 95% of the initial value.

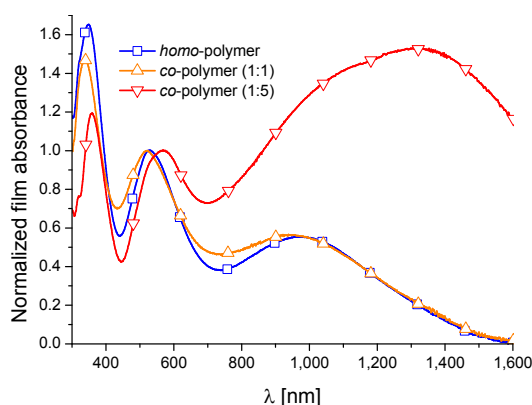


Figure 5.29. UV-vis absorption spectra of *homo*- and *co*-polymer films of **RuTphNO₂** (ITO-coated glass).

To conclude, cyclometalated, 1,2,3-triazole-containing ruthenium(II) complexes could be eventually electropolymerized. Oxidative decomposition of the thiophene-equipped parent complexes at polymerizing potentials could be overcome *via* anodic shifting of the respective redox potentials by introduction of a nitro group at the cyclometalating phenyl ring. The obtained polymer films showed broad, long-wavelength UV-vis absorption and a reversible redox switchability. The usage of EDOT as *co*-monomer for *co*-electropolymerization led to further improvement of the polymerization performance and resulted in films that combined the optical features of the ruthenium(II) complexes and PEDOT.

Summary

For application in electrooptical devices, *e. g.* for solar cells, lighting, and sensors, materials have to be developed that feature optimized properties with regard to their photophysics, *i. e.* light-absorption ability, emission efficiency, etc., and their electrochemistry. In this respect, transition metal complexes based on polypyridyl-type ligands have proven their suitability to work as a basic structural motif for the assembly of photoredox-active systems.

Using *bis*-functionalized ligands, the 2,2':6',2''-terpyridine parent complex allows the buildup of metallopolymers through the complexation of appropriate metal ions, like zinc(II) or ruthenium(II). Thereby, the former preserves the optical and electronic properties of the *bis*-terpyridine since the d^{10} -metal does not interact with the electronic system of the ligand. Thus, the photophysical characteristics of the metallopolymer can be straightforwardly modified by manipulation of the bridging moiety that links the two 2,2':6',2''-terpyridine units. Consequently, *bis*-terpyridines with varying π -conjugated linker moieties were synthesized and characterized. The library of π systems was chosen to cover a large range of the visible spectrum with respect to their absorption and emission ability, thus including both electron-poor and electron-rich building blocks. Hence, zinc(II) metallopolymers showing absorption and emission maxima from 362 to 618 nm and 409 to 640 nm, respectively, could be obtained possessing photoluminescence quantum yields from 18% up to 95%.

Another promising metal ion for metallopolymer formation is the ruthenium(II). In contrast to zinc(II), its outer electron shells interact with the π system of the complexing polypyridyl system, constituting intense charge-transfer transitions from the metal to the ligand (MLCT) and, thus, enabling a broader light-absorption range. Furthermore, ruthenium(II)-2,2':6',2''-terpyridine metallopolymers feature significantly enhanced complex stabilities compared to the zinc(II) systems, but suffer from nearly annihilated photoluminescence. A *homo*- and a *co*-ruthenium(II) metallopolymer was synthesized reflecting the UV-vis absorption characteristics of the π -conjugated linker complemented by an MLCT absorption at 505 nm.

Additionally, inkjet-printing studies on selected zinc(II) metallopolymers were successfully carried out, which proved the thin-film processability of the polymer systems by inkjet techniques.

In particular for photosensitizer application in solar-cell devices, namely in the so-called dye-sensitized solar cells (DSSC), ruthenium(II) complexes of polypyridyl-type ligands are of great interest. Since the parent 2,2':6',2''-terpyridine complex suffers from low excited-state lifetimes (around 0.25 ns), which impede efficient charge generation within solar cells, descendants were developed possessing electron-donating polypyridyl-type alternatives. Hence, cyclometalating ligands were synthesized possessing the 1,2,3-triazole motif, which can be easily introduced *via* the copper(I)-catalyzed azide-alkyne 1,3-cycloaddition and allows the modular functionalization of the ligand, instead of pyridine rings. Different substitution patterns were applied with regard to an optimization for the intended solar-cell usage (*e. g.* NO_2 and F for redox modification, thiophene and carbazole for enhanced UV-vis absorption). The respective heteroleptic ruthenium(II) complexes showed broad light absorption up to 700 nm and excited-state lifetimes of around 6 ns. Furthermore, electrochemical studies revealed a high stability of the oxidized state, which is a key step in the DSSC working cycle.

Beside the cyclometalation approach, mesoionic carbenes represent a further promising possibility for the modification of ruthenium(II)-polypyridyl complexes with strong electron

donors regarding the photosensitizer suitability. Again, the 1,2,3-triazole moiety provided the basis for the ligand assembly. The prepared mesoionic-carbene ruthenium(II) complex featured room-temperature photoluminescence at 643 nm with a quantum yield of 5.5% and a high excited-state lifetime of 630 ns as well as a reversible, stable redox chemistry.

The *bis*-1,2,3-triazole-pyridine moiety could also be used to compose π -conjugated *bis*-functionalized ligands for the formation of metallopolymers *via* the complexation of ruthenium(II).

For the preparation of thin films of metal complexes that are of photophysical and electrochemical interest, which is crucial for various electrooptical applications, electropolymerization represents a sophisticated method since it allows the deposition of defined layers from a metal complex solution directly onto an electrode surface. The respective complexes have to be functionalized with electropolymerizable groups, which can electrochemically form reactive radicals enabling the coupling of towards insoluble (metallo)polymer chains.

Two ruthenium(II)-2,6-di(quinoline-8-yl)pyridine complexes, which had shown favorable photophysical and redox characteristics, were equipped with electropolymerizable thiophene units. Anodic polymerization could be successfully executed and the resulting films showed a broad UV-vis absorption as well as room-temperature photoluminescence at around 750 nm. Furthermore, (spectro)electrochemical experiments revealed redox stability and switchability as well as electrochromicity in the visible and NIR region, while electrochemical impedance spectroscopy showed redox-switchable electrical conductivity for the investigated polymers.

The cyclometalated 1,2,3-triazole-containing ruthenium(II) complexes were likewise employed for electropolymerization studies. Thiophene-functionalized derivatives of the parent complex were studied at first, but underwent electrochemical decomposition at the applied potentials due to a second, irreversible oxidation of the system. Hence, a nitro group was introduced at the ligand core to modify the involved redox potentials, namely to shift the decomposing process beyond the potential that is required for electropolymerization. The thus functionalized cyclometalating ruthenium(II) complexes could be successfully polymerized resulting in thin films featuring long-wavelength visible absorption and electrochemical stability. A further improvement of the polymerization ability could be attained by the incorporation of 3,4-ethylenedioxythiophene moieties to form *co*-polymers.

The metal-polypyridyl systems, both (metallo)polymers and single complexes, that are presented in this thesis showed favorable photophysical and electrochemical characteristics with regard to photosensitizing (Ru^{II}) and light emitting (Zn^{II}). Furthermore, they revealed the capability for efficient thin-film processing using either inkjet printing or deposition by electrochemical polymerization. Thus, the compounds studied herein represent promising candidates for a potential future application in electrooptical devices, in particular in solar cells and light-emitting diodes.

Zusammenfassung

Hinsichtlich des Einsatzes in elektrooptischen Anwendung, wie Solarzellen, Leuchtmittel oder Sensorsysteme, ist es notwendig, Materialien mit optimierten photophysikalischen Eigenschaften, d. h. maximierte Lichtabsorption, effiziente Emission etc., zu entwickeln. Dabei hat sich herausgestellt, dass es sich bei Übergangsmetallkomplexe von Polypyridylliganden um geeignete Bausteine für photoredoxaktive Systeme handelt.

Die Einführung zweier 2,2':6',2''-Terpyridineinheiten in Liganden gestattet den Aufbau von Metallopolymeren durch die Komplexierung von Metallionen, wie Zink(II) oder Ruthenium(II). Ersteres ermöglicht die Herstellung von Systemen, die die elektrooptischen Eigenschaften der verwendeten *Bis*-2,2':6',2''-Terpyridineinheiten widerspiegeln, da das d^{10} -System Zink(II) nicht mit dem Elektronenorbitalen des Liganden wechselwirkt. Eine Manipulation der Eigenschaften des Polymers ist in diesen Fällen durch entsprechende Anpassungen an den Liganden, genauer an den verbrückenden Einheiten, möglich. Aus diesem Grund wurde eine Serie von *Bisterpyridinen* mit unterschiedlichen, elektronenarmen als auch -reichen, π -konjugierten Brückenbausteinen synthetisiert, wobei diese so gewählt wurden, dass ihre UV/Vis-Spektren einen möglichst großen Bereich des sichtbaren Lichts abdeckten. Derart konnten Metallopolymere mit Absorptionsmaxima zwischen 362 und 618 nm und Emissionen zwischen 409 und 640 nm sowie Quantenausbeuten bis 95% hergestellt werden.

Weiterhin ist die Verwendung von Ruthenium(II)-ionen möglich. Diese wechselwirken, im Gegensatz zu Zink(II), mit dem π -System des Liganden und generieren so zusätzliche, intensive elektronische Übergänge (MLCTs) die eine breitere Lichtabsorption ermöglichen. Desweiteren weisen Ruthenium(II)-Komplexe von Terpyridinen, im Vergleich zu entsprechenden Zink(II)-Komplexen, höhere Komplexstabilitäten auf, zeigen jedoch keine Photolumineszenz. Zwei der *Bisterpyridine* wurden ausgewählt und ein *Homo*- sowie ein *Co*-metallopolymer wurden synthetisiert, wobei die UV/Vis-Absorptionen die Merkmale der Liganden kombiniert mit zusätzlichen MLCT-Banden bei 505 nm aufwiesen.

Außerdem konnte die Möglichkeit der Herstellung dünner Filme ausgewählter Zink(II)-metallopolymere mit Hilfe der Tintenstrahl Drucktechnik erfolgreich demonstriert werden.

Monomere Ruthenium(II)-Polypyridylkomplexe stellen eine verbreitete Substanzklasse für den Einsatz als Photosensibilisator in farbstoffsensibilisierten Solarzellen (DSSCs) dar. Der ursprüngliche Terpyridinmodellkomplex weist dabei jedoch extrem kurze Lebenszeiten des angeregten Zustandes auf, wodurch eine effiziente Ladungserzeugung in der Solarzelle verhindert wird. Eine Möglichkeit, diesen Nachteil zu überwinden, ist die Einführung starker Elektronendonoren im Ligandensystem, beispielsweise durch Cyclometallierung. Es wurden cyclometallisierende Liganden synthetisiert, die 1,2,3-Triazole an Stelle der Pyridine enthalten, welche elegant mit Hilfe der Kupfer(I)-katalysierten Azid-Alkin-1,3-Cycloaddition eingeführt werden können und dadurch den modularen Einbau unterschiedlicher Funktionalitäten erlauben. Hinsichtlich der Optimierung für die Verwendung in DSSCs wurden verschiedene Substituenten, wie NO_2 und Fluor für die Modifizierung der elektrochemischen oder Thiophen und Carbazol für die photophysikalischen Eigenschaften, am Ligandengerüst angebracht. Die entsprechenden heteroleptischen Ruthenium(II)-Komplexe zeigten beinahe panchromatische Absorption bis 700 nm, Lebensdauern der angeregten Zustände bis 6 ns sowie reversible Redoxprozesse, was sie zu vielversprechenden Solarzellenkandidaten macht.

Der Einbau mesoionischer Carbene stellt eine weitere Möglichkeit der Modifikation von Ruthenium(II)-Polypyridylkomplexen zur Verbesserung der optoelektronischen Eigenschaften dar. Auf Basis des *Bis*-(1,2,3-Triazolyl)pyridins wurde ein Ligand für die Herstellung eines mesoionischen Carbenkomplexes des Ruthenium(II) entwickelt, welcher Raumtemperatur-emission mit einem Maximum bei 643 nm, einer Quantenausbeute von 5.5% und einer Lebensdauer des angeregten Zustandes von 630 ns zeigt sowie eine hohe Stabilität der oxidierten Form aufweist. Dadurch erweist sich seine Eignung als Photosensibilisator.

Zusätzlich wurden Ruthenium(II)-Metallopolymere, welche auf zweifach *Bis*-(1,2,3-Triazolyl)pyridin-funktionaliserten, π -konjugierten Liganden basieren, synthetisiert.

Für einen Einsatz der Komplexe in elektrooptischen Anwendungen ist typischerweise die Herstellung von dünnen, definierten Filmen von entscheidender Bedeutung. Dabei stellt die Elektropolymerisation eine elegante Methode dar, die ein direktes Abscheiden von entsprechenden (Metallo)Polymerfilmen aus Monomerkomplexlösungen auf Elektrodenoberflächen ermöglicht. Dafür müssen die Systeme zuvor mit elektropolymerisierbaren Gruppen ausgestattet werden, die die elektrochemische Generierung von reaktiven Radikalen ermöglichen, welche durch Radikalkopplung zur Bildung von Polymeren führen.

Ruthenium(II)-2,6-Di(quinolin-8-yl)pyridin-Komplexe haben sich auf Grund ihrer hervorragenden photophysikalischen und elektrochemischen Eigenschaften als außerordentlich geeignet für Solarzellenanwendungen erwiesen. Folgerichtig wurden zwei solcher Komplexe, funktionalisiert mit elektropolymerisierbaren Thiopheneinheiten, erfolgreich anodisch polymerisiert. Die resultierenden Filme zeigten eine effiziente UV/Vis-Absorption sowie Raumtemperaturlumineszenz bei ca. 750 nm. Elektro- und spektroelektrochemische Untersuchungen erwiesen eine hohe Redoxstabilität sowie Elektrochromizität. Elektrochemische Impedanzspektroskopie zeigte zudem eine redoxschaltbare elektrische Leitfähigkeit.

Ebenso wurden die cyclometallierten 1,2,3-triazolbasierten Ruthenium(II)-komplexe einer Elektropolymerisationsstudie unterzogen. Hierfür wurden zunächst zwei thiophenfunktionalisierte Derivate des unmodifizierten Modellkomplexes untersucht, doch verhinderten in diesen Fällen Zersetzungsreaktionen unter den notwendigen elektrischen Potentialen eine erfolgreiche Polymerisation. Aus diesem Grund wurden Nitrogruppen in das Ligandensystem eingeführt, die die für die Zersetzung verantwortlichen Redoxpotentiale zu höheren Werten verschieben sollten. Die dergleichen funktionalisierten Komplexe konnten daraufhin erfolgreich polymerisiert werden und ergaben dünne Polymerfilme, die eine breite Lichtabsorption sowie Redoxstabilität aufwiesen. Weitere Verbesserung des Polymerisationsverhaltens konnte durch den Einsatz von 3,4-Ethylendioxythiophen als *Co*-monomer erzielt werden.

Die in dieser Arbeit vorgestellten Metall-Polypyridyl-Systeme, sowohl die (Metallo)Polymere als auch die monomeren Metallkomplexe, wiesen photoelektrochemische Eigenschaften auf, die sie als geeignete Kandidaten für Photosensibilisierung (Ru^{II}) und Lichterzeugung (Zn^{II}) auszeichnen. Außerdem konnte ihre Eignung für die Verarbeitung in dünnen Filmen demonstriert werden, wobei zum einen die Herstellung der Schichten aus bereits vorgefertigten Polymeren mittels Tintenstrahldruck, zum anderen die Präparation von Elektrodenbeschichtungen durch Elektropolymerisation zum Einsatz kam. Die untersuchten Verbindungen stellen daher vielversprechende Materialien für eine zukünftige Verwendung in elektrooptischen Bauteilen, speziell in Solarzellen und LEDs, dar.

References

- [1] a) G. Dennler, M. C. Scharber, C. J. Brabec, *Adv. Mater.* **2009**, *21*, 1323–1338; b) M. K. Nazeeruddin, M. Grätzel, in *Photofunctional Transition Metal Complexes, Vol. 123* (Ed.: V. W. W. Yam), Springer, Berlin, **2007**, p. 113–175; c) H. Hoppe, N. S. Sariciftci, *J. Mater. Res.* **2004**, *19*, 1924–1945; d) M. Grätzel, *J. Photoch. Photobio. C* **2003**, *4*, 145–153; e) A. Hagfeldt, M. Grätzel, *Acc. Chem. Res.* **2000**, *33*, 269–277.
- [2] a) P.-T. Chou, Y. Chi, *Chem. Eur. J.* **2007**, *13*, 380–395; b) R. C. Evans, P. Douglas, C. J. Winscom, *Coord. Chem. Rev.* **2006**, *250*, 2093–2126; c) E. Holder, B. M. W. Langeveld, U. S. Schubert, *Adv. Mater.* **2005**, *17*, 1109–1121; d) A. P. Kulkarni, C. J. Tonzola, A. Babel, S. A. Jenekhe, *Chem. Mater.* **2004**, *16*, 4556–4573; e) L. Akcelrud, *Prog. Polym. Sci.* **2003**, *28*, 875–962; f) L. S. Hung, C. H. Chen, *Mater. Sci. Eng.* **2002**, *39*, 143–222.
- [3] a) J.-M. Savéant, *Chem. Rev.* **2008**, *108*, 2348–2378; b) F. Bedioui, S. Griveau, T. Nyokong, A. J. Appleby, C. A. Caro, M. Gulppi, G. Ochoa, J. H. Zagal, *Phys. Chem. Chem. Phys.* **2007**, *9*, 3383–3396.
- [4] a) R. Brimblecombe, G. C. Dismukes, G. F. Swiegers, L. Spiccia, *Dalton Trans.* **2009**, 9374–9384; b) M. Wang, Y. Na, M. Gorlov, L. Sun, *Dalton Trans.* **2009**, 6458–6467; c) J. H. Alstrum-Acevedo, M. K. Brennaman, T. J. Meyer, *Inorg. Chem.* **2005**, *44*, 6802–6827.
- [5] a) U. Lange, N. V. Roznyatovskaya, V. M. Mirsky, *Anal. Chim. Acta* **2008**, *614*, 1–26; b) X. Luo, A. Morrin, A. J. Killard, M. R. Smyth, *Electroanalysis* **2006**, *18*, 319–326; c) C. W. Rogers, M. O. Wolf, *Coord. Chem. Rev.* **2002**, *233–234*, 341–350; d) P. D. Beer, P. A. Gale, *Angew. Chem. Int. Ed.* **2001**, *40*, 486–516; e) D. T. McQuade, A. E. Pullen, T. M. Swager, *Chem. Rev.* **2000**, *100*, 2537–2574.
- [6] a) N. Armaroli, V. Balzani, *Angew. Chem. Int. Ed.* **2007**, *46*, 52–66; b) N. S. Lewis, D. G. Nocera, *Proc. Natl. Acad. Sci. U.S.A.* **2006**, *103*, 15729–15735.
- [7] a) I. Robel, V. Subramanian, M. Kuno, P. V. Kamat, *J. Am. Chem. Soc.* **2006**, *128*, 2385–2393; b) J. B. Baxter, E. S. Aydil, *Appl. Phys. Lett.* **2005**, *86*, 053114.
- [8] a) S. Günes, H. Neugebauer, N. S. Sariciftci, *Chem. Rev.* **2007**, *107*, 1324–1338; b) K. M. Coakley, M. D. McGehee, *Chem. Mater.* **2004**, *16*, 4533–4542; c) C. J. Brabec, N. S. Sariciftci, J. C. Hummelen, *Adv. Funct. Mater.* **2001**, *11*, 15–26.
- [9] a) M. Riede, T. Mueller, W. Tress, R. Schueppel, K. Leo, *Nanotechnology* **2008**, *19*, 424001; b) P. Peumans, A. Yakimov, S. R. Forrest, *J. Appl. Phys.* **2003**, *93*, 3693–3723.
- [10] a) A. Hagfeldt, G. Boschloo, L. Sun, L. Kloo, H. Pettersson, *Chem. Rev.* **2010**, *110*, 6595–6663; b) B. O'Regan, M. Grätzel, *Nature* **1991**, *353*, 737–740.
- [11] a) J.-P. Sauvage, J.-P. Collin, J.-C. Chambron, S. Guillerez, C. Coudret, V. Balzani, F. Barigelletti, L. De Cola, L. Flamigni, *Chem. Rev.* **1994**, *94*, 993–1019; b) A. Juris, V. Balzani, F. Barigelletti, S. Campagna, P. Belser, A. von Zelewsky, *Coord. Chem. Rev.* **1988**, *84*, 85–277.
- [12] a) G. R. Whittell, I. Manners, *Adv. Mater.* **2007**, *19*, 3439–3468; b) P. G. Pickup, *J. Mater. Chem.* **1999**, *9*, 1641–1653.
- [13] a) J. H. Burroughes, D. D. C. Bradley, A. R. Brown, R. N. Marks, K. Mackay, R. H. Friend, P. L. Burns, A. B. Holmes, *Nature* **1990**, *347*, 539–541; b) C. W. Tang, S. A. VanSlyke, *Appl. Phys. Lett.* **1987**, *51*, 913–915.
- [14] C.-L. Ho, W.-Y. Wong, *Coord. Chem. Rev.* **2011**, *255*, 2469–2502.
- [15] a) A. Wild, A. Winter, F. Schlütter, U. S. Schubert, *Chem. Soc. Rev.* **2011**, *40*, 1459–1511; b) U. S. Schubert, A. Winter, G. R. Newkome, *Terpyridine-based Materials for Catalytic, Optoelectronic and Life Science Applications*, Wiley-VCH, Weinheim, **2011**; c) H. Hofmeier, U. S. Schubert, *Chem. Soc. Rev.* **2004**, *33*, 373–399; d) E. C. Constable, *Adv. Inorg. Chem.* **1986**, *30*, 69–121.

- [16] a) J. D. Crowley, D. A. McMorran, in *Click Triazoles, Vol. 28* (Ed.: J. Košmrlj), Springer, Berlin, Heidelberg, **2012**, p. 31–83; b) L. Hammarström, O. Johansson, *Coord. Chem. Rev.* **2010**, *254*, 2546–2559; c) H.-J. Park, K. H. Kim, S. Y. Choi, H.-M. Kim, W. I. Lee, Y. K. Kang, Y. K. Chung, *Inorg. Chem.* **2010**, *49*, 7340–7352; d) P. G. Bomben, K. C. D. Robson, P. A. Sedach, C. P. Berlinguette, *Inorg. Chem.* **2009**, *48*, 9631–9643.
- [17] a) R. M. Meudtner, M. Ostermeier, R. Goddard, C. Limberg, S. Hecht, *Chem. Eur. J.* **2007**, *13*, 9834–9840; b) Y. Li, J. C. Huffman, A. H. Flood, *Chem. Commun.* **2007**, 2692–2694.
- [18] a) M. Mydlak, C. Bizzarri, D. Hartmann, W. Sarfert, G. Schmid, L. De Cola, *Adv. Funct. Mater.* **2010**, *20*, 1812–1820; b) G. Guisado-Barrios, J. Bouffard, B. Donnadieu, G. Bertrand, *Angew. Chem. Int. Ed.* **2010**, *49*, 4759–4762; c) B. Schulze, C. Friebe, M. D. Hager, A. Winter, R. Hoogenboom, H. Görls, U. S. Schubert, *Dalton Trans.* **2009**, 787–794; d) B. Beyer, C. Ulbricht, D. Escudero, C. Friebe, A. Winter, L. González, U. S. Schubert, *Organometallics* **2009**, *28*, 5478–5488; e) P. Mathew, A. Neels, M. Albrecht, *J. Am. Chem. Soc.* **2008**, *130*, 13534–13535; f) M. Obata, A. Kitamura, A. Mori, C. Kameyama, J. A. Czaplewska, R. Tanaka, I. Kinoshita, T. Kusumoto, H. Hashimoto, M. Harada, Y. Mikata, T. Funabiki, S. Yano, *Dalton Trans.* **2008**, 3292–3300.
- [19] G. T. Morgan, F. H. Burstall, *J. Chem. Soc.* **1932**, 20–30.
- [20] a) M. Heller, U. S. Schubert, *J. Org. Chem.* **2002**, *67*, 8269–8272; b) U. S. Schubert, C. Eschbaumer, G. Hochwimmer, *Synthesis* **1999**, *1999*, 779–782; c) D. J. Cárdenas, J.-P. Sauvage, *Synlett* **1996**, *1996*, 916–918; d) T. Kauffmann, J. König, A. Woltermann, *Chem. Ber.* **1976**, *109*, 3864–3868.
- [21] A. M. W. Cargill Thompson, *Coord. Chem. Rev.* **1997**, *160*, 1–52.
- [22] C. Hollins, *Synthesis of Nitrogen Ring Compounds*, Ernest Benn Ltd., London, **1924**.
- [23] A. E. Tschitschibabin, *J. Prakt. Chem.* **1924**, *107*, 122–128.
- [24] F. Kröhnke, *Synthesis* **1976**, *1976*, 1–24.
- [25] a) S. V. Jadhav, P. G. Ingole, H. C. Bajaj, *Synth. Commun.* **2010**, *40*, 1142–1148; b) S. Tu, R. Jia, B. Jiang, J. Zhang, Y. Zhang, C. Yao, S. Ji, *Tetrahedron* **2007**, *63*, 381–388; c) A. Winter, A. M. J. van den Berg, R. Hoogenboom, G. Kickelbick, U. S. Schubert, *Synthesis* **2006**, *2006*, 2873–2878; d) C. B. Smith, C. L. Raston, A. N. Sobolev, *Green Chem.* **2005**, *7*, 650–654; e) S. Tu, T. Li, F. Shi, F. Fang, S. Zhu, X. Wei, Z. Zong, *Chem. Lett.* **2005**, *34*, 732–733; f) I. Sasaki, J. C. Daran, G. G. A. Balavoine, *Synthesis* **1999**, 815–820.
- [26] a) V. Grosshenny, R. Ziessel, *J. Organomet. Chem.* **1993**, *453*, C19–C22; b) K. T. Potts, D. Konwar, *J. Org. Chem.* **1991**, *56*, 4815–4816; c) E. C. Constable, M. D. Ward, *Dalton Trans.* **1990**, 1405–1409.
- [27] a) A. Khatyr, R. Ziessel, *J. Org. Chem.* **2000**, *65*, 3126–3134; b) R. Ziessel, M. Hissler, A. El-ghayoury, A. Harriman, *Coord. Chem. Rev.* **1998**, *178–180*, 1251–1298; c) A. Harriman, R. Ziessel, *Chem. Commun.* **1996**, 1707–1716.
- [28] a) A. Scarpaci, C. Monnereau, N. Hergué, E. Blart, S. Legoupy, F. Odobel, A. Gorfo, J. Pérez-Moreno, K. Clays, I. Asselberghs, *Dalton Trans.* **2009**, 4538–4546; b) P. Kadjane, L. Charbonnière, F. Camerel, P. Lainé, R. Ziessel, *J. Fluoresc.* **2008**, *18*, 119–129; c) F. Dumur, C. R. Mayer, E. Dumas, F. Miomandre, M. Frigoli, F. Sécheresse, *Org. Lett.* **2007**, *10*, 321–324; d) G. Pickaert, R. Ziessel, *Tetrahedron Lett.* **1998**, *39*, 3497–3500.
- [29] R.-A. Fallahpour, M. Neuburger, M. Zehnder, *Synthesis* **1999**, 1051–1055.
- [30] a) R. Huisgen, *Helv. Chim. Acta* **1967**, *50*, 2421–2439; b) R. Huisgen, G. Szeimies, L. Möbius, *Chem. Ber.* **1967**, *100*, 2494–2507; c) R. Huisgen, *Angew. Chem. Int. Ed.* **1963**, *2*, 565–598.
- [31] C. W. Tornøe, C. Christensen, M. Meldal, *J. Org. Chem.* **2002**, *67*, 3057–3064.

- [32] V. V. Rostovtsev, L. G. Green, V. V. Fokin, K. B. Sharpless, *Angew. Chem. Int. Ed.* **2002**, *41*, 2596–2599.
- [33] L. Zhang, X. Chen, P. Xue, H. H. Y. Sun, I. D. Williams, K. B. Sharpless, V. V. Fokin, G. Jia, *J. Am. Chem. Soc.* **2005**, *127*, 15998–15999.
- [34] a) M. Juriček, P. H. J. Kouwer, A. E. Rowan, *Chem. Commun.* **2011**, *47*, 8740–8749; b) B. M. J. M. Suijkerbuijk, B. N. H. Aerts, H. P. Dijkstra, M. Lutz, A. L. Spek, G. van Koten, R. J. M. Klein Gebbink, *Dalton Trans.* **2007**, 1273–1276.
- [35] a) S. Liu, P. Müller, M. K. Takase, T. M. Swager, *Inorg. Chem.* **2011**, *50*, 7598–7609; b) T. Romero, R. A. Orenes, A. Espinosa, A. Tárraga, P. Molina, *Inorg. Chem.* **2011**, *50*, 8214–8224; c) M. Ostermeier, M.-A. Berlin, R. M. Meudtner, S. Demeshko, F. Meyer, C. Limberg, S. Hecht, *Chem. Eur. J.* **2010**, *16*, 10202–10213; d) R. Lalrempuia, N. D. McDaniel, H. Müller-Bunz, S. Bernhard, M. Albrecht, *Angew. Chem. Int. Ed.* **2010**, *49*, 9765–9768; e) J. T. Fletcher, B. J. Bumgarner, N. D. Engels, D. A. Skoglund, *Organometallics* **2008**, *27*, 5430–5433.
- [36] M. A. R. Meier, B. G. G. Lohmeijer, U. S. Schubert, *J. Mass. Spectrom.* **2003**, *38*, 510–516.
- [37] a) M. Ziegler, V. Monney, H. Stoeckli-Evans, A. Von Zelewsky, I. Sasaki, G. Dupic, J.-C. Daran, G. G. A. Balavoine, *Dalton Trans.* **1999**, 667–676; b) T. Matsumura-Inoue, M. Tanabe, T. Minami, T. Ohashi, *Chem. Lett.* **1994**, *23*, 2443–2446.
- [38] a) J.-P. Collin, P. Lainé, J.-P. Launay, J.-P. Sauvage, A. Sour, *Chem. Commun.* **1993**, 434–435; b) M. Beley, J.-P. Collin, R. Louis, B. Metz, J.-P. Sauvage, *J. Am. Chem. Soc.* **1991**, *113*, 8521–8522.
- [39] M. Hissler, A. El-ghayoury, A. Harriman, R. Ziessel, *Angew. Chem. Int. Ed.* **1998**, *37*, 1717–1720.
- [40] a) A. C. Benniston, A. Harriman, D. J. Lawrie, A. Mayeux, *Phys. Chem. Chem. Phys.* **2004**, *6*, 51–57; b) A. Amini, K. Bates, A. C. Benniston, D. J. Lawrie, E. Soubeyrand-Lenoir, *Tetrahedron Lett.* **2003**, *44*, 8245–8247.
- [41] R. H. Holyer, C. D. Hubbard, S. F. A. Kettle, R. G. Wilkins, *Inorg. Chem.* **1966**, *5*, 622–625.
- [42] a) R. Dobrawa, M. Lysetska, P. Ballester, M. Grüne, F. Würthner, *Macromolecules* **2005**, *38*, 1315–1325; b) G. Albano, V. Balzani, E. C. Constable, M. Maestri, D. R. Smith, *Inorg. Chim. Acta* **1998**, *277*, 225–231; c) E. C. Constable, J. Lewis, M. C. Liptrot, P. R. Raithby, *Inorg. Chim. Acta* **1990**, *178*, 47–54.
- [43] M. L. Stone, G. A. Crosby, *Chem. Phys. Lett.* **1981**, *79*, 169–173.
- [44] a) I. M. Dixon, F. Alary, J.-L. Heully, *Dalton Trans.* **2010**, *39*, 10959–10966; b) O. A. Borg, S. S. M. C. Godinho, M. J. Lundqvist, S. Lunell, P. Persson, *J. Phys. Chem. A* **2008**, *112*, 4470–4476.
- [45] a) M. Jäger, A. Smeigh, F. Lombeck, H. Görls, J.-P. Collin, J.-P. Sauvage, L. Hammarström, O. Johansson, *Inorg. Chem.* **2009**, *49*, 374–376; b) S. H. Wadman, M. Lutz, D. M. Tooke, A. L. Spek, F. Hartl, R. W. A. Havenith, G. P. M. van Klink, G. van Koten, *Inorg. Chem.* **2009**, *48*, 1887–1900; c) J.-P. Collin, M. Beley, J.-P. Sauvage, F. Barigelletti, *Inorg. Chim. Acta* **1991**, *186*, 91–93.
- [46] a) A. Breivogel, C. Förster, K. Heinze, *Inorg. Chem.* **2010**, *49*, 7052–7056; b) F. Schramm, V. Meded, H. Fliegl, K. Fink, O. Fuhr, Z. Qu, W. Klopper, S. Finn, T. E. Keyes, M. Ruben, *Inorg. Chem.* **2009**, *48*, 5677–5684.
- [47] a) J. Wang, Y.-Q. Fang, L. Bourget-Merle, M. I. J. Polson, G. S. Hanan, A. Juris, F. Loiseau, S. Campagna, *Chem. Eur. J.* **2006**, *12*, 8539–8548; b) J. Wang, G. S. Hanan, F. Loiseau, S. Campagna, *Chem. Commun.* **2004**, 2068–2069.
- [48] a) C. Friebe, M. D. Hager, A. Winter, U. S. Schubert, *Adv. Mater.* **2012**, *24*, 332–345; b) J. Heinze, B. A. Frontana-Urbe, S. Ludwigs, *Chem. Rev.* **2010**, *110*, 4724–4771.
- [49] a) M. O. Wolf, in *Handbook of Thiophene-Based Materials* (Eds.: I. F. Perepichka, D. F. Perepichka), John Wiley & Sons, Chichester, **2009**, p. 293–319; b) M. O. Wolf, *J.*

- Inorg. Organomet. Polym. Mater.* **2006**, *16*, 189–199; c) M. O. Wolf, *Adv. Mater.* **2001**, *13*, 545–553.
- [50] a) S. Sadki, P. Schottland, N. Brodie, G. Sabouraud, *Chem. Soc. Rev.* **2000**, *29*, 283–293; b) K.-J. Kim, H.-S. Song, J.-D. Kim, J.-K. Chon, *Bull. Korean Chem. Soc.* **1988**, *9*, 248–251; c) S. Asavapiriyant, G. K. Chandler, G. A. Gunawardena, D. Pletcher, *J. Electroanal. Chem.* **1984**, *177*, 229–244.
- [51] a) J. Heinze, C. Willmann, P. Bäuerle, *Angew. Chem. Int. Ed.* **2001**, *40*, 2861–2864; b) C. P. Andrieux, P. Audebert, P. Hapiot, J.-M. Savéant, *J. Phys. Chem.* **1991**, *95*, 10158–10164.
- [52] A. F. Diaz, J. I. Castillo, J. A. Logan, W.-Y. Lee, *J. Electroanal. Chem.* **1981**, *129*, 115–132.
- [53] J. Heinze, H. John, M. Dietrich, P. Tschuncky, *Synth. Met.* **2001**, *119*, 49–52.
- [54] J. Heinze, in *Encyclopedia of Electrochemistry, Vol. 8* (Eds.: A. J. Bard, M. Stratmann), Wiley-VCH, Weinheim, **2004**, p. 605–643.
- [55] J. M. Calvert, R. H. Schmehl, B. P. Sullivan, J. S. Facci, T. J. Meyer, R. W. Murray, *Inorg. Chem.* **1983**, *22*, 2151–2162.
- [56] V. Ruiz, Á. Colina, A. Heras, J. López-Palacios, *Electrochim. Acta* **2004**, *50*, 59–67.
- [57] a) J. V. Sanchez, R. Diaz, P. Herrasti, P. Ocon, *Polym. J.* **2001**, *33*, 514–521; b) T. F. Otero, E. De Larreta, *Synth. Met.* **1988**, *26*, 79–88.
- [58] C. Pinheiro, A. J. Parola, F. Pina, J. Fonseca, C. Freire, *Sol. Energy Mater. Sol. Cells* **2008**, *92*, 980–985.
- [59] a) W. Chen, G. Xue, *Prog. Polym. Sci.* **2005**, *30*, 783–811; b) S. Jin, G. Xue, *Macromolecules* **1997**, *30*, 5753–5757.
- [60] a) C.-C. Chou, K.-L. Wu, Y. Chi, W.-P. Hu, S. J. Yu, G.-H. Lee, C.-L. Lin, P.-T. Chou, *Angew. Chem. Int. Ed.* **2011**, *50*, 2054–2058; b) H. Tributsch, *Coord. Chem. Rev.* **2004**, *248*, 1511–1530; c) M. K. Nazeeruddin, P. Péchy, T. Renouard, S. M. Zakeeruddin, R. Humphry-Baker, P. Comte, P. Liska, L. Cevey, E. Costa, V. Shklover, L. Spiccia, G. B. Deacon, C. A. Bignozzi, M. Grätzel, *J. Am. Chem. Soc.* **2001**, *123*, 1613–1624.
- [61] G. Redmond, D. Fitzmaurice, *J. Phys. Chem.* **1993**, *97*, 1426–1430.
- [62] S. E. Koops, B. C. O'Regan, P. R. F. Barnes, J. R. Durrant, *J. Am. Chem. Soc.* **2009**, *131*, 4808–4818.
- [63] a) R. Shunmugam, G. J. Gabriel, K. A. Aamer, G. N. Tew, *Macromol. Rapid Commun.* **2010**, *31*, 784–793; b) A. Wild, F. Schlütter, G. M. Pavlov, C. Friebe, G. Festag, A. Winter, M. D. Hager, V. Cimrová, U. S. Schubert, *Macromol. Rapid Commun.* **2010**, *31*, 868–874; c) E. C. Constable, *Chem. Soc. Rev.* **2007**, *36*, 246–253; d) E. A. Medlycott, G. S. Hanan, *Chem. Soc. Rev.* **2005**, *34*, 133–142.
- [64] a) A. Winter, C. Friebe, M. Chiper, U. S. Schubert, M. Presselt, B. Dietzek, M. Schmitt, J. Popp, *ChemPhysChem* **2009**, *10*, 787–798; b) A. P. H. J. Schenning, A. C. Tsipis, S. C. J. Meskers, D. Beljonne, E. W. Meijer, J. L. Brédas, *Chem. Mater.* **2002**, *14*, 1362–1368.
- [65] a) A. Winter, C. Friebe, M. Chiper, M. D. Hager, U. S. Schubert, *J. Polym. Sci., Part A: Polym. Chem.* **2009**, *47*, 4083–4098; b) A. Winter, C. Friebe, M. D. Hager, U. S. Schubert, *Macromol. Rapid Commun.* **2008**, *29*, 1679–1686; c) Y.-Y. Chen, H.-C. Lin, *Polymer* **2007**, *48*, 5268–5278; d) S.-C. Yu, C.-C. Kwok, W.-K. Chan, C.-M. Che, *Adv. Mater.* **2003**, *15*, 1643–1647.
- [66] a) A. Amini, A. Harriman, A. Mayeux, *Phys. Chem. Chem. Phys.* **2004**, *6*, 1157–1164; b) D. W. Fink, W. E. Ohnesorge, *J. Am. Chem. Soc.* **1969**, *91*, 4995–4998.
- [67] F. C. Krebs, *Sol. Energy Mater. Sol. Cells* **2009**, *93*, 394–412.
- [68] M. Singh, H. M. Haverinen, P. Dhagat, G. E. Jabbour, *Adv. Mater.* **2010**, *22*, 673–685.
- [69] J. Perelaer, P. J. Smith, D. Mager, D. Soltman, S. K. Volkman, V. Subramanian, J. G. Korvink, U. S. Schubert, *J. Mater. Chem.* **2010**, *20*, 8446–8453.
- [70] C. J. Brabec, S. Gowrisanker, J. J. M. Halls, D. Laird, S. Jia, S. P. Williams, *Adv. Mater.* **2010**, *22*, 3839–3856.

- [71] A. Teichler, R. Eckardt, C. Friebe, J. Perelaer, U. S. Schubert, *Thin Solid Films* **2011**, *519*, 3695–3702.
- [72] E. Tekin, B. J. de Gans, U. S. Schubert, *J. Mater. Chem.* **2004**, *14*, 2627–2632.
- [73] S. A. Jenekhe, J. A. Osaheni, *Science* **1994**, *265*, 765–768.
- [74] W.-Y. Wong, C.-L. Ho, *Acc. Chem. Res.* **2010**, *43*, 1246–1256.
- [75] a) D. Schweinfurth, R. Pattacini, S. Strobel, B. Sarkar, *Dalton Trans.* **2009**, 9291–9297; b) B. Happ, C. Friebe, A. Winter, M. D. Hager, R. Hoogenboom, U. S. Schubert, *Chem. Asian J.* **2009**, *4*, 154–163; c) E. Orselli, R. Q. Albuquerque, P. M. Fransen, R. Fröhlich, H. M. Janssen, L. De Cola, *J. Mater. Chem.* **2008**, *18*, 4579–4590.
- [76] K. J. Kilpin, U. S. D. Paul, A.-L. Lee, J. D. Crowley, *Chem. Commun.* **2011**, *47*, 328–330.
- [77] B. Schulze, C. Friebe, M. D. Hager, W. Günther, U. Köhn, B. O. Jahn, H. Görls, U. S. Schubert, *Org. Lett.* **2010**, *12*, 2710–2713.
- [78] C. Richardson, C. M. Fitchett, F. R. Keene, P. J. Steel, *Dalton Trans.* **2008**, 2534–2537.
- [79] F. Barigelletti, P. Belser, A. Von Zelewsky, A. Juris, V. Balzani, *J. Phys. Chem.* **1985**, *89*, 3680–3684.
- [80] M. Abrahamsson, M. Jäger, R. J. Kumar, T. Österman, P. Persson, H.-C. Becker, O. Johansson, L. Hammarström, *J. Am. Chem. Soc.* **2008**, *130*, 15533–15542.
- [81] a) F. Barigelletti, A. Juris, V. Balzani, P. Belser, A. Von Zelewsky, *J. Phys. Chem.* **1987**, *91*, 1095–1098; b) W. F. Wacholtz, R. A. Auerbach, R. H. Schmehl, *Inorg. Chem.* **1986**, *25*, 227–234; c) G. H. Allen, R. P. White, D. P. Rillema, T. J. Meyer, *J. Am. Chem. Soc.* **1984**, *106*, 2613–2620.
- [82] G. Boschloo, E. A. Gibson, A. Hagfeldt, *J. Phys. Chem. Lett.* **2011**, *2*, 3016–3020.
- [83] A. Listorti, B. O'Regan, J. R. Durrant, *Chem. Mater.* **2011**, *23*, 3381–3399.
- [84] a) F. E. Hahn, M. C. Jahnke, *Angew. Chem. Int. Ed.* **2008**, *47*, 3122–3172; b) S. U. Son, K. H. Park, Y.-S. Lee, B. Y. Kim, C. H. Choi, M. S. Lah, Y. H. Jang, D.-J. Jang, Y. K. Chung, *Inorg. Chem.* **2004**, *43*, 6896–6898; c) W. A. Herrmann, *Angew. Chem. Int. Ed.* **2002**, *41*, 1290–1309.
- [85] B. Durham, J. V. Caspar, J. K. Nagle, T. J. Meyer, *J. Am. Chem. Soc.* **1982**, *104*, 4803–4810.
- [86] a) B. J. Holliday, T. M. Swager, *Chem. Commun.* **2005**, 23–36; b) R. J. Forster, J. G. Vos, *Macromolecules* **1990**, *23*, 4372–4377.
- [87] a) M. Jäger, R. J. Kumar, H. Görls, J. Bergquist, O. Johansson, *Inorg. Chem.* **2009**, *48*, 3228–3238; b) M. Abrahamsson, M. Jäger, T. Österman, L. Eriksson, P. Persson, H.-C. Becker, O. Johansson, L. Hammarström, *J. Am. Chem. Soc.* **2006**, *128*, 12616–12617.
- [88] P. J. Hochgesang, R. D. Bereman, *Inorg. Chim. Acta* **1988**, *149*, 69–76.
- [89] J. J. Apperloo, L. B. Groenendaal, H. Verheyen, M. Jayakannan, R. A. J. Janssen, A. Dkhissi, D. Beljonne, R. Lazzaroni, J.-L. Brédas, *Chem. Eur. J.* **2002**, *8*, 2384–2396.
- [90] A. J. Bard, L. R. Faulkner, *Electrochemical Methods*, 2nd ed., John Wiley & Sons, Inc., New York, **2001**.
- [91] a) M. Devenney, L. A. Worl, S. Gould, A. Guadalupe, B. P. Sullivan, J. V. Caspar, R. L. Leasure, J. R. Gardner, T. J. Meyer, *J. Phys. Chem. A* **1997**, *101*, 4535–4540; b) J. L. Colón, C. Y. Yang, A. Clearfield, C. R. Martin, *J. Phys. Chem.* **1988**, *92*, 5777–5781.
- [92] C. L. Gaupp, D. M. Welsh, R. D. Rauh, J. R. Reynolds, *Chem. Mater.* **2002**, *14*, 3964–3970.
- [93] K. Kaneto, K. Yoshino, Y. Inuishi, *Solid State Commun.* **1983**, *46*, 389–391.
- [94] a) J. F. Rubinson, Y. P. Kayinamura, *Chem. Soc. Rev.* **2009**, *38*, 3339–3347; b) C. H. Hamann, A. Hamnett, W. Vielstich, *Electrochemistry*, 2nd ed., Wiley-VCH, Weinheim, **2007**; c) B. W. Johnson, D. C. Read, P. Christensen, A. Hamnett, R. D. Armstrong, *J. Electroanal. Chem.* **1994**, *364*, 103–109.
- [95] a) A. Zykwincka, W. Domagala, B. Pilawa, M. Lapkowski, *Electrochim. Acta* **2005**, *50*, 1625–1633; b) U. Barsch, F. Beck, *Electrochim. Acta* **1996**, *41*, 1761–1771; c) Z. Qi, P. G. Pickup, *Anal. Chem.* **1993**, *65*, 696–703.

- [96] C. E. D. Chidsey, R. W. Murray, *J. Phys. Chem.* **1986**, *90*, 1479–1484.
- [97] M. Gagliardo, D. J. M. Snelders, P. A. Chase, R. J. M. Klein Gebbink, G. P. M. van Klink, G. van Koten, *Angew. Chem. Int. Ed.* **2007**, *46*, 8558–8573.
- [98] W.-W. Yang, J. Yao, Y.-W. Zhong, *Organometallics* **2012**, *31*, 1035–1041.

Publication List

Refereed publications in scientific journals

1. A. Winter, C. Friebe, M. D. Hager, U. S. Schubert, “Advancing the solid state properties of metallo-supramolecular materials: Poly(ϵ -caprolactone) modified π -conjugated *bis*(terpyridine)s and their Zn(II) based metallo-polymers “, *Macromol. Rapid Commun.* **2008**, *29*, 1679–1686.
2. M. Presselt, B. Dietzek, M. Schmitt, J. Popp, A. Winter, M. Chiper, C. Friebe, U. S. Schubert, “Zinc(II) *bis*terpyridine complexes: The influence of the cation on the π -conjugation between terpyridine and the lateral phenyl substituent”, *J. Phys. Chem. C* **2008**, *112*, 18651–18660.
3. B. Happ, C. Friebe, A. Winter, M. D. Hager, R. Hoogenboom, U. S. Schubert, “2-(1*H*-1,2,3-Triazol-4-yl)-pyridine ligands as alternatives to 2,2'-bipyridines in ruthenium(II) complexes”, *Chem. Asian J.* **2009**, *4*, 154–163.
4. B. Schulze, C. Friebe, M. D. Hager, A. Winter, R. Hoogenboom, H. Görls, U. S. Schubert, “2,2':6',2''-Terpyridine meets 2,6-*bis*(1*H*-1,2,3-triazol-4-yl)pyridine: Tuning the electro-optical properties of ruthenium(II) complexes”, *Dalton Trans.* **2009**, 787–794.
5. A. Winter, C. Friebe, M. D. Hager, U. S. Schubert, “Synthesis of rigid π -conjugated mono-, *bis*-, *tris*-, and *tetrakis*(terpyridine)s: Influence of the degree and pattern of substitution on the photophysical properties”, *Eur. J. Org. Chem.* **2009**, 801–809.
6. A. Winter, C. Friebe, M. Chiper, U. S. Schubert, M. Presselt, B. Dietzek, M. Schmitt, J. Popp, “Synthesis, characterization, and electro-optical properties of Zn^{II} complexes with π -conjugated terpyridine ligands”, *ChemPhysChem* **2009**, *10*, 787–798.
7. A. Winter, C. Friebe, M. Chiper, M. D. Hager, U. S. Schubert, “Self-assembly of π -conjugated *bis*(terpyridine) ligands with zinc(II) ions: New metallosupramolecular materials for optoelectronic applications”, *J. Polym. Sci., Part A: Polym. Chem.* **2009**, *47*, 4083–4098.
8. B. Beyer, C. Ulbricht, C. Friebe, A. Winter, U. S. Schubert, D. Escudero, L. González, “Phenyl-1*H*-[1,2,3]triazoles as new cyclometallating ligands for iridium(III) complexes”, *Organometallics*, **2009**, *28*, 5478–5488.
9. C. Ulbricht, B. Beyer, C. Friebe, A. Winter, U. S. Schubert, “Recent developments in the application of phosphorescent iridium(III) complex systems”, *Adv. Mater.* **2009**, *21*, 4418–4441.
10. B. Happ, C. Friebe, A. Winter, M. D. Hager, U. S. Schubert, „Click chemistry meets polymerization: Controlled incorporation of an easily accessible ruthenium(II) complex into a PMMA backbone via RAFT copolymerization”, *Eur. Polym. J.*, **2009**, *45*, 3433–3441.
11. F. Schlütter, A. Wild, A. Winter, M. D. Hager, A. Baumgaertel, C. Friebe, U. S. Schubert, “Synthesis and characterization of new self-assembled metallo-polymers containing electron-withdrawing and electron-donating *bis*(terpyridine) zinc(II) moieties”, *Macromolecules* **2010**, *43*, 2759–2771.

12. A. Wild, C. Friebe, A. Winter, M. D. Hager, U.-W. Grummt, U. S. Schubert, “ π -Conjugated 2,2':6',2''-bis(terpyridines): Systematical tuning of the optical properties by variation of the linkage between the terpyridines and the π -conjugated system”, *Eur. J. Org. Chem.* **2010**, 1859–1868.
13. A. Wild, F. Schlütter, G. M. Pavlov, C. Friebe, G. Festag, A. Winter, M. D. Hager, V. Cimrová, U. S. Schubert, “ π -Conjugated donor and donor-acceptor metallo-polymers”, *Macromol. Rapid Commun.* **2010**, *31*, 868–874.
14. A. Wild, S. Hornig, F. Schlütter, J. Vitz, C. Friebe, M. D. Hager, A. Winter, U. S. Schubert, “Complexation of terpyridine-containing dextrans: Toward water-soluble supramolecular structures”, *Macromol. Rapid Commun.* **2010**, *31*, 921–927.
15. B. Schulze, C. Friebe, M. D. Hager, W. Günther, U. Köhn, B. O. Jahn, H. Görls, U. S. Schubert, “Anion complexation by triazolium "ligands": Mono- and bis-tridentate complexes of sulfate”, *Org. Lett.* **2010**, *12*, 2710–2713.
16. B. Happ, D. Escudero, M. D. Hager, C. Friebe, A. Winter, H. Görls, E. Altuntas, L. González, U. S. Schubert, “N-Heterocyclic donor- and acceptor-type ligands based on 2-(1H-[1,2,3]triazol-4-yl)pyridines and their ruthenium(II) complexes”, *J. Org. Chem.* **2010**, *75*, 4025–4038.
17. A. Teichler, R. Eckardt, S. Hoepfner, C. Friebe, J. Perelaer, A. Senes, M. Morana, C. J. Brabec, U. S. Schubert, “Combinatorial screening of polymer:fullerene blends for organic solar cells by inkjet printing”, *Adv. Energy Mater.* **2011**, *1*, 105–114.
18. B. Happ, G. M. Pavlov, E. Altuntas, C. Friebe, M. D. Hager, A. Winter, H. Görls, W. Günther, U. S. Schubert, “Self-assembly of 3,6-bis(4-triazolyl)pyridazine ligands with copper(I) and silver(I) ions: Time-dependant 2D-NOESY and ultracentrifuge measurements”, *Chem. Asian J.* **2011**, *6*, 873–880.
19. A. Teichler, R. Eckardt, C. Friebe, J. Perelaer, U. S. Schubert, “Film formation properties of inkjet-printed poly(phenylene-ethynylene)-poly(phenylene-vinylene)s”, *Thin Solid Films* **2011**, *519*, 3695–3702.
20. R. Menzel, A. Breul, C. Pietsch, J. Schäfer, C. Friebe, E. Täuscher, D. Weiß, B. Dietzek, J. Popp, R. Beckert, U. S. Schubert, “Blue-emitting polymers based on 4-hydroxythiazoles incorporated in a methacrylate backbone”, *Macromol. Chem. Phys.* **2011**, *212*, 840–848.
21. B. Schulze, D. Escudero, C. Friebe, R. Siebert, H. Görls, U. Köhn, E. Altuntas, A. Baumgaertel, M. D. Hager, A. Winter, B. Dietzek, J. Popp, L. González, U. S. Schubert, “A heteroleptic bis(tridentate) ruthenium(II) complex of a click-derived abnormal carbene pincer ligand with potential for photosensitizer application“, *Chem. Eur. J.* **2011**, *17*, 5494–5498.
22. A. Q. Daraosheh, U.-P. Apfel, H. Görls, C. Friebe, U. S. Schubert, M. El-khateeb, G. Mloston, W. Weigand, “New approach to [FeFe]-hydrogenase models using aromatic thioketones”, *Eur. J. Inorg. Chem.* **2012**, 318–326.
23. C. Friebe, M. D. Hager, A. Winter, U. S. Schubert, “Metal-containing polymers via electropolymerization”, *Adv. Mater.* **2012**, *24*, 332–345.
24. B. Schulze, D. Escudero, C. Friebe, R. Siebert, H. Görls, S. Sinn, M. Thomas, S. Mai, J. Popp, B. Dietzek, L. González, U. S. Schubert, “Ruthenium(II) photosensitizers of

tridentate click-derived cyclometalating ligands: A joint experimental and computational study“, *Chem. Eur. J.* **2012**, *18*, 4010–4025.

25. C. Friebe, A. Wild, J. Perelaer, U. S. Schubert, “Inkjet printing of zinc(II) *bis*-2,2':6',2"-terpyridine metallopolymers: Printability and film-forming studies by a combinatorial thin-film library approach” *Macromol. Rapid Commun.* **2012**, *33*, 503–509.
26. B. Schulze, C. Friebe, S. Hoepfner, G. M. Pavlov, A. Winter, M. D. Hager, U. S. Schubert, “Ruthenium(II) metallo-supramolecular polymers of click-derived tridentate ditopic ligands”, *Macromol. Rapid Commun.* **2012**, *33*, 597–602.
27. A. M. Breul, J. Schäfer, C. Friebe, F. Schlütter, R. M. Paulus, G. Festag, M. D. Hager, A. Winter, B. Dietzek, J. Popp, U. S. Schubert, “Synthesis and characterization of poly(methyl methacrylate) backbone polymers containing side-chain pendant ruthenium(II) *bis*-terpyridine complexes with an elongated conjugated system”, *Macromol. Chem. Phys.* **2012**, *213*, 808–819.
28. B. Happ, J. Schäfer, C. Friebe, H. Görls, A. Winter, M. D. Hager, B. Dietzek, J. Popp, U. S. Schubert, “Chelating fluorene dyes as mono- and ditopic 2-(1*H*-1,2,3-triazol-4-yl)pyridine ligands and their corresponding ruthenium(II) complexes”, *Synthesis*, **2012**, *44*, 2287–2294.
29. R. Schroot, C. Friebe, E. Altuntas, S. Crotty, M. Jäger, U. S. Schubert, “Nitroxide-mediated polymerization of styrenic triaryl amines and chain-end functionalization with a ruthenium complex: Toward tailored photoredox-active architectures”, *Macromolecules*, **2013**, *46*, 2039–2048.
30. C. Friebe, M. Jäger, U. S. Schubert, “Emitting electrode coatings with redox-switchable conductivity: Incorporation of ruthenium(II)-2,6-di(quinolin-8-yl)pyridine complexes into polythiophene by electropolymerization”, *RSC Adv.* **2013**, *3*, 11686–11690.
31. C. Friebe, H. Görls, M. Jäger, U. S. Schubert, “Linear metallopolymers from ruthenium(II)-2,6-di(quinolin-8-yl)pyridine complexes by electropolymerization – Formation of redox-stable and emissive films“, *Eur. J. Inorg. Chem.* **2013**, 4191–4202.
32. C. Friebe, B. Schulze, H. Görls, M. Jäger, U. S. Schubert, “Designing cyclometalated ruthenium(II) complexes for anodic electropolymerization”, *Chem. Eur. J.*, DOI: 10.1002/chem.201301439.
33. B. Schulze, D. G. Brown, K. C. D. Robson, C. Friebe, E. Birckner, C. P. Berlinguette, U. S. Schubert, “Cyclometalated ruthenium(II) complexes featuring tridentate click-derived ligands for dye-sensitized solar cell applications”, *Chem. Eur. J.* **2013**, *19*, 14171–14180.

Non-refereed publications

1. B. Schulze, C. Friebe, M. D. Hager, A. Winter, R. Hoogenboom, H. Görls, U. S. Schubert, “2,2':6',2"-Terpyridine meets 2,6-*bis*(1*H*-1,2,3-triazol-4-yl)pyridine: Tuning the optical properties of ruthenium(II) complexes”, *Polym. Prepr. (Am. Chem. Soc., Div. Polym. Chem.)* **2009**, *50*(2), 252–253.
2. B. Happ, M. D. Hager, A. Winter, C. Friebe, R. Hoogenboom, U. S. Schubert, “Alternative bipyridines analogs via click chemistry”, *Polym. Prepr. (Am. Chem. Soc., Div. Polym. Chem.)* **2009**, *50*(2), 254–255.

3. C. Friebe, M. Chiper, M. D. Hager, A. Winter, U. S. Schubert, "Designing photoactive polymeric systems using zinc(II)-bis(terpyridine)-linkers", *Polym. Prepr. (Am. Chem. Soc., Div. Polym. Chem.)* **2009**, 50(2), 266–267.
4. A. Winter, F. Schlütter, A. Wild, C. Friebe, M. D. Hager, U. S. Schubert, "Rigid π -conjugated 2,2',6',2"-terpyridines with donor- and / or acceptor-moieties", *Polym. Prepr. (Am. Chem. Soc., Div. Polym. Chem.)* **2009**, 50(2), 335–336.
5. C. Friebe, B. Beyer, C. Ulbricht, A. Winter, U. S. Schubert, "Phenyl-1*H*-[1,2,3]triazoles as new cyclometalating ligands for phosphorescent iridium(III) complexes", *Polym. Prepr. (Am. Chem. Soc., Div. Polym. Chem.)* **2009**, 50(2), 561–562.
6. B. Schulze, C. Friebe, M. D. Hager, A. Winter, U. S. Schubert, " π -Conjugated spacer bridged ditopic 2',6'-bis(1*H*-1,2,3-triazol-4-yl)pyridines", *Polym. Prepr. (Am. Chem. Soc., Div. Polym. Chem.)* **2009**, 50(2), 575–576.
7. A. Winter, R. Siebert, D. Akimov, C. Friebe, M. Schmitt, B. Dietzek, J. Popp, U. S. Schubert, "Toward new photovoltaic materials: Rigid π -conjugated 2,2':6',2"-terpyridines - synthesis, characterization and ultrafast photoinduced dynamics", *Polym. Prepr. (Am. Chem. Soc., Div. Polym. Chem.)* **2009**, 50(2), 719–720.
8. B. Schulze, C. Friebe, S. Hoepfner, G. M. Pavlov, M. D. Hager, A. Winter, U. S. Schubert, "Ruthenium(II) and platinum(II) metallopolymers of ditopic π -conjugated clicked ligands - towards printable optoelectronics", *Polym. Prepr. (Am. Chem. Soc., Div. Polym. Chem.)* **2011**, 52(2), 917–918.

Posters

1. *Designing photoactive polymeric systems using zinc(II)-bis(terpyridine)-linkers*, ORCHEM 2008, Weimar, Germany, 01.09. – 03.09.2008, C. Friebe, M. Chiper, M. D. Hager, A. Winter, U. S. Schubert.
2. *Phenyl-1*H*-[1,2,3]triazoles as new cyclometalating ligands for phosphorescent iridium(III) complexes*, 238th ACS National Meeting, Washington, D. C., U. S., 16.08. – 20.08.2009, C. Friebe, B. Beyer, C. Ulbricht, A. Winter, U. S. Schubert.

Oral presentations

1. *Designing photoactive polymeric systems using bis(terpyridine)-linkers*, 238th ACS National Meeting, Washington, D. C., U. S., 16.08. – 20.08.2009.

Curriculum Vitae

- 06.04.1984 Born in Erfurt, Germany
- 1990 – 2002 School education in Erfurt, Germany
- 10/2002 – 06/2003 Military service
- 10/2003 – 09/2008 Study of chemistry at the Friedrich Schiller University, Jena, Germany
- 11/2007 – 09/2008 “Diplom” (equivalent to master thesis) under the supervision of Prof. U. S. Schubert, Friedrich Schiller University Jena, Germany (the practical work was performed at the Eindhoven University of Technology, Eindhoven, The Netherlands): “Electro-optical investigations on transition metal complexes and metallo-polymers”
- 10/2008 – 10/2013 Ph.D. student, Laboratory of Organic and Macromolecular Chemistry (IOMC), Friedrich Schiller University Jena, Germany
- 08/2009 – 07/2011 Scholarship of the Fonds der Chemischen Industrie

Jena, den 23.10.2013

Christian Friebe

Acknowledgements

This thesis would not have been possible without the continuous support, help, advice, and encouragement of a lot of people.

First of all, I want to thank Prof. Dr. U. S. Schubert for the opportunity to perform the work that constitutes the foundation for this thesis in his versatile and well-equipped working group. I appreciate the continuous support and, in particular, the patience waiting for the first first-author publications.

Furthermore, I would like to thank Jun.-Prof. Dr. A. Ignaszak and Prof. Dr. B. Sarkar for carefully reading this thesis and preparing a reference letter.

Several people supported me over the years by experimental work as well as by helpful advices and discussions and a complete list would go beyond the scope. However, I hereby want to acknowledge some of them, who strongly impacted my work:

Above all, I would like to express my sincere gratitude to Benjamin Schulze, Michael Jäger, and Andreas Wild whose extensive synthetic efforts provided the basis for my investigations and with whom I had a lot of long and substantial discussions being essential for the development of this thesis.

Furthermore, my thanks go to Andreas Winter and Martin Hager for their support and advice, in particular with respect to various organizational issues.

Prof. Dr. A. Ignaszak additionally deserves my gratitude for providing me with her equipment and electrochemical knowledge.

For introduction and advice concerning inkjet printing, my thanks go to the inkjet team, in particular to Anke Teichler, Jolke Perelaer, and Joe Delaney.

Further appreciations go to Ronald Siebert for the performance of time-dependent spectroscopy experiments, Georges M. Pavlov for his analytical-ultracentrifugation studies, and Bernd Schröter for XPS characterization.

I also want to thank the administrative team, consisting of Anja Helbig, Tanja Wagner, and Sylvia Braunsdorf, who kept the place running all the time as well as Uwe Köhn who handled all my chemical orders as fast as possible.

My work was furthermore strongly facilitated by the harmonious and motivating ambience that was present in the offices 308 and 317.

I am also highly grateful to Benni, Uli, and Micha for the pleasant time we could spend together beside our investigations, in particular the regular lunch sessions.

Last, but in no way least, I greatly thank my parents and my sister who supported me throughout all the years of my studies.

Declaration of Authorship / Selbstständigkeitserklärung

Ich erkläre, dass ich die vorliegende Arbeit selbstständig und unter Verwendung der angegebenen Hilfsmittel, persönlichen Mitteilungen und Quellen angefertigt habe.

I certify that the work presented here is, to the best of my knowledge and belief, original and the result of my own investigations, except as acknowledged, and has not been submitted, either in part or whole, for a degree at this or any other university.

Jena, den 23.10.2013

Christian Friebe

Supplementary Information

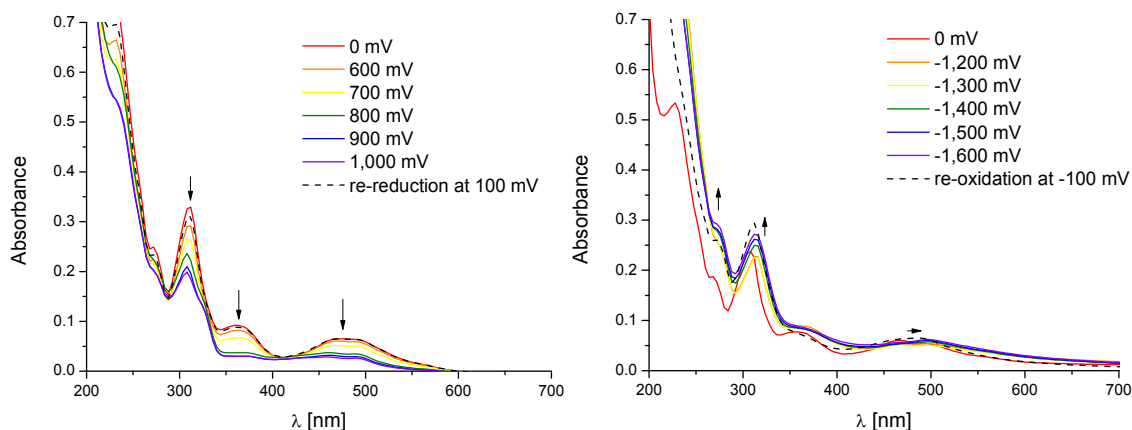


Figure S1. UV-vis spectroelectrochemical investigation on the oxidation (left) and reduction (right) process of **RuNCN-F** (voltage varied from 400 to 1,000 mV and $-1,200$ to $-1,600$ mV vs. AgCl/Ag, respectively; 10^{-5} M in CH_3CN with 0.1 M Bu_4NPF_6).

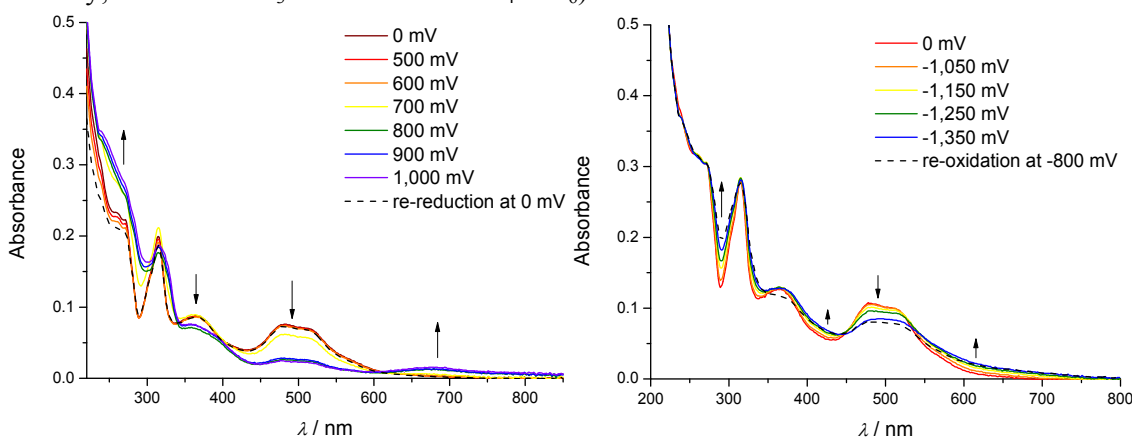


Figure S2. UV-vis spectroelectrochemical investigation on the oxidation (left) and reduction (right) process of **RuNCN-NO₂** (voltage varied from 500 to 1,000 mV and $-1,050$ to $-1,350$ mV vs. AgCl/Ag, respectively; 10^{-5} M in CH_3CN with 0.1 M Bu_4NPF_6).

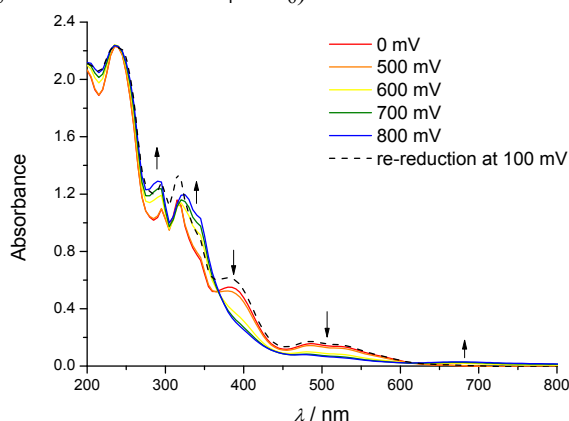


Figure S3. UV-vis spectroelectrochemical investigation on the oxidation process of **RuNCN-Cbz** (voltage varied from 500 to 800 mV vs. AgCl/Ag; 10^{-5} M in CH_3CN with 0.1 M Bu_4NPF_6).

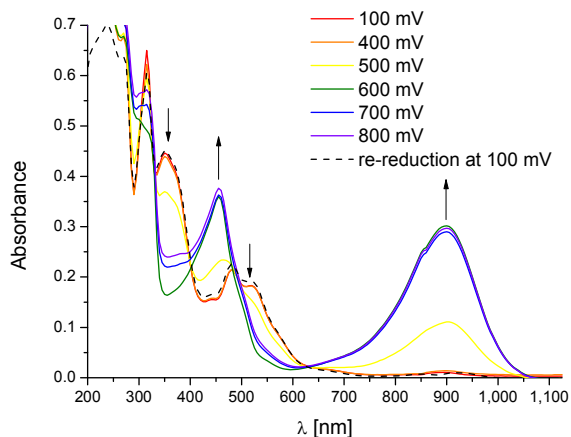


Figure S4. UV-vis spectroelectrochemical investigation on the oxidation process of **RuNCN-Tph** (voltage varied from 400 to 800 mV vs. AgCl/Ag; 10^{-5} M in CH_3CN with 0.1 M Bu_4NPF_6).

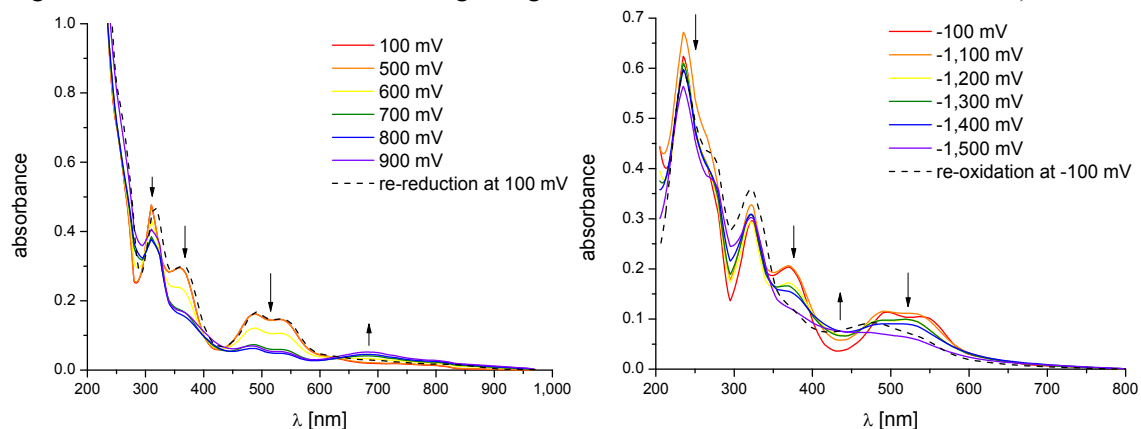


Figure S5. UV-vis spectroelectrochemical investigation on the oxidation (left) and reduction (right) process of **RuNCN-COOEt** (voltage varied from 500 to 900 mV and $-1,100$ to $-1,500$ mV vs. AgCl/Ag, respectively; 10^{-5} M in CH_3CN with 0.1 M Bu_4NPF_6).

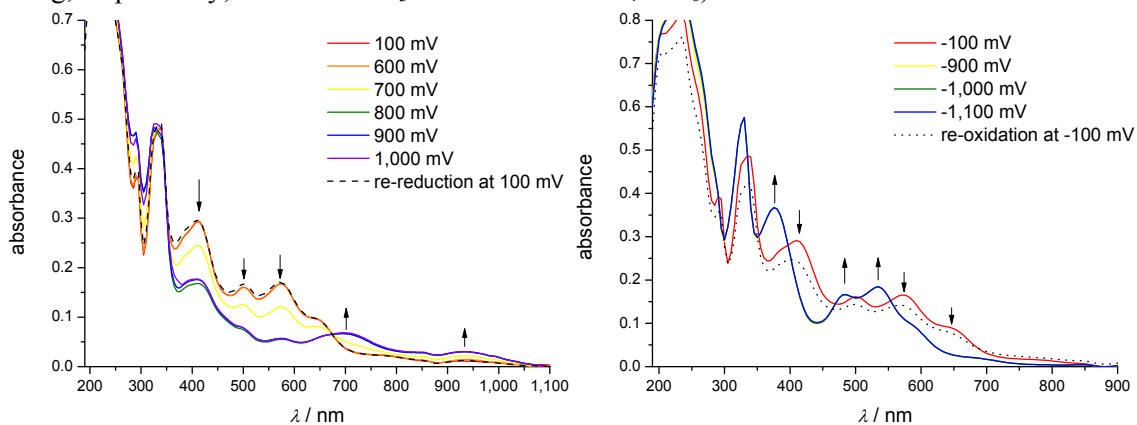


Figure S6. UV-vis spectroelectrochemical investigation on the oxidation (left) and reduction (right) process of **RuNCN-(COOMe)₃** (voltage varied from 600 to 1,000 mV and -900 to $-1,100$ mV vs. AgCl/Ag, respectively; 10^{-5} M in CH_3CN with 0.1 M Bu_4NPF_6).

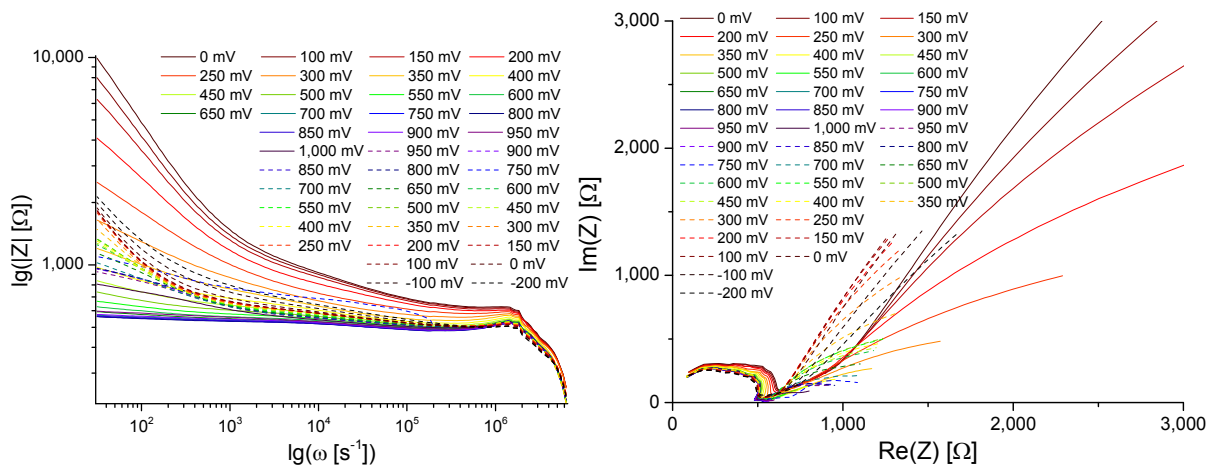


Figure S7. Bode (left) and Nyquist (right) plot of electrochemical impedance spectroscopy of poly(**RuDqp1**)a (potentials vs. Fc^+/Fc , solid lines indicate increasing potential, dashed lines decreasing potential).

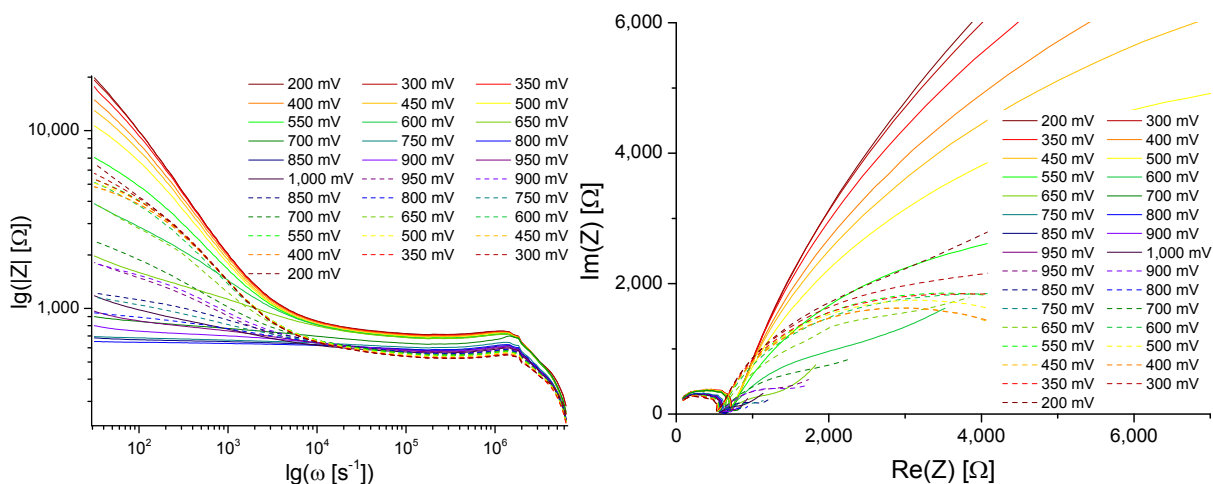


Figure S8. Bode (left) and Nyquist (right) plot of electrochemical impedance spectroscopy of poly(**RuDqp1**)b (potentials vs. Fc^+/Fc , solid lines indicate increasing potential, dashed lines decreasing potential).

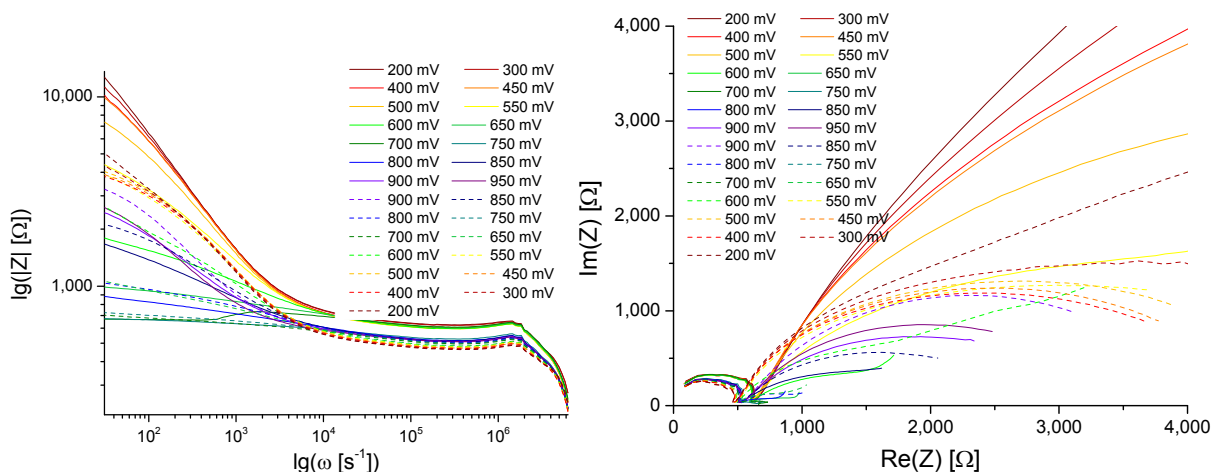


Figure S9. Bode (left) and Nyquist (right) plot of electrochemical impedance spectroscopy of poly(**RuDqp1**)c (potentials vs. Fc^+/Fc , solid lines indicate increasing potential, dashed lines decreasing potential).

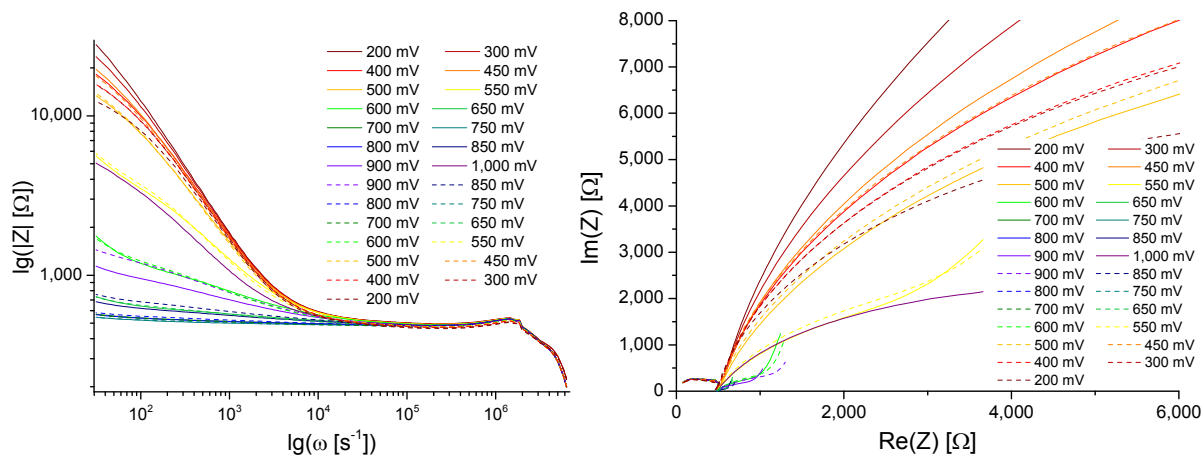


Figure S10. Bode (left) and Nyquist (right) plot of electrochemical impedance spectroscopy of poly(**RuDqp1**) (potentials vs. Fc^+/Fc , solid lines indicate increasing potential, dashed lines decreasing potential).

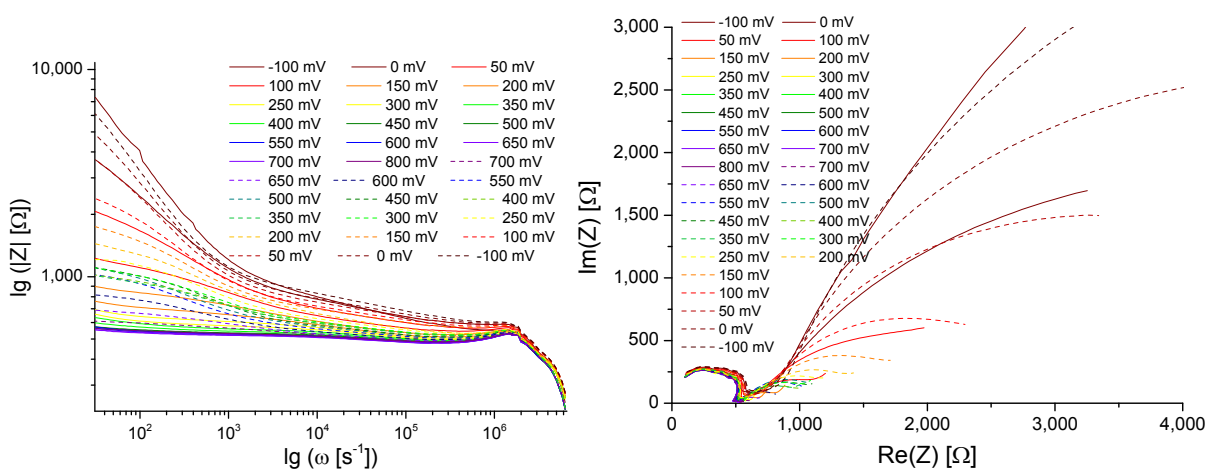


Figure S11. Bode (left) and Nyquist (right) plot of electrochemical impedance spectroscopy of poly(**RuDqp2**)a (potentials vs. Fc^+/Fc , solid lines indicate increasing potential, dashed lines decreasing potential).

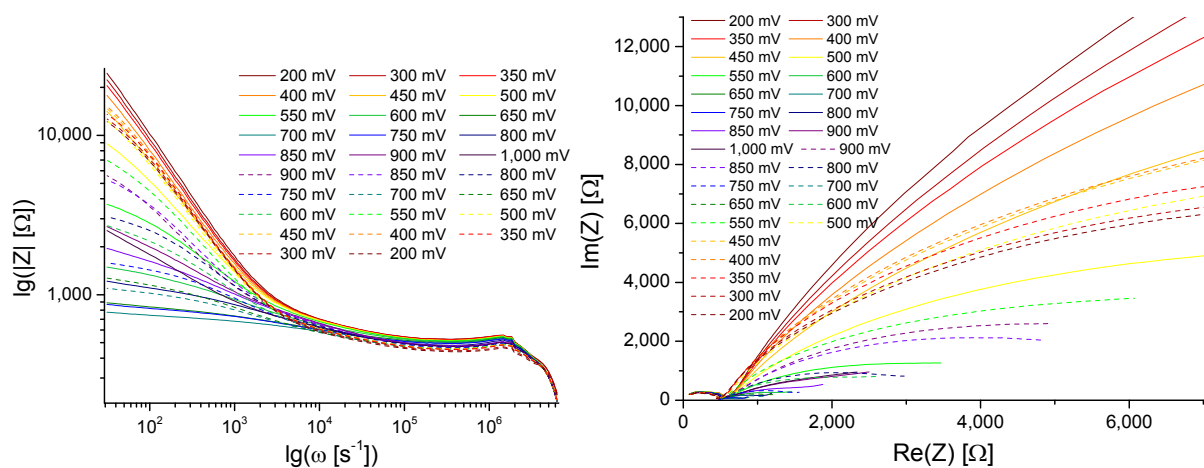


Figure S12. Bode (left) and Nyquist (right) plot of electrochemical impedance spectroscopy of poly(**RuDqp2**)b (potentials vs. Fc^+/Fc , solid lines indicate increasing potential, dashed lines decreasing potential).

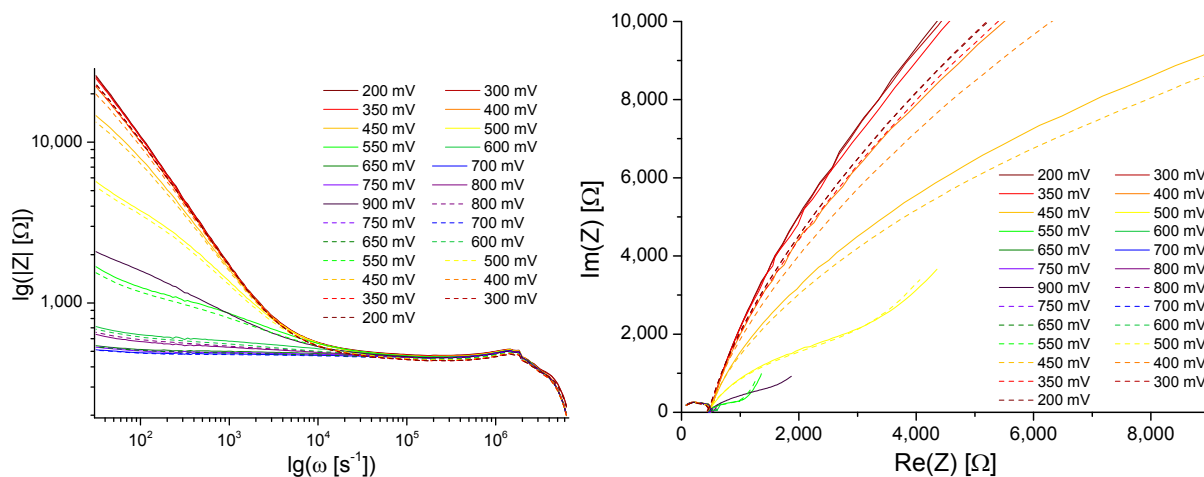


Figure S13. Bode (left) and Nyquist (right) plot of electrochemical impedance spectroscopy of poly(**RuDqp2**)c (potentials vs. Fc^+/Fc , solid lines indicate increasing potential, dashed lines decreasing potential).

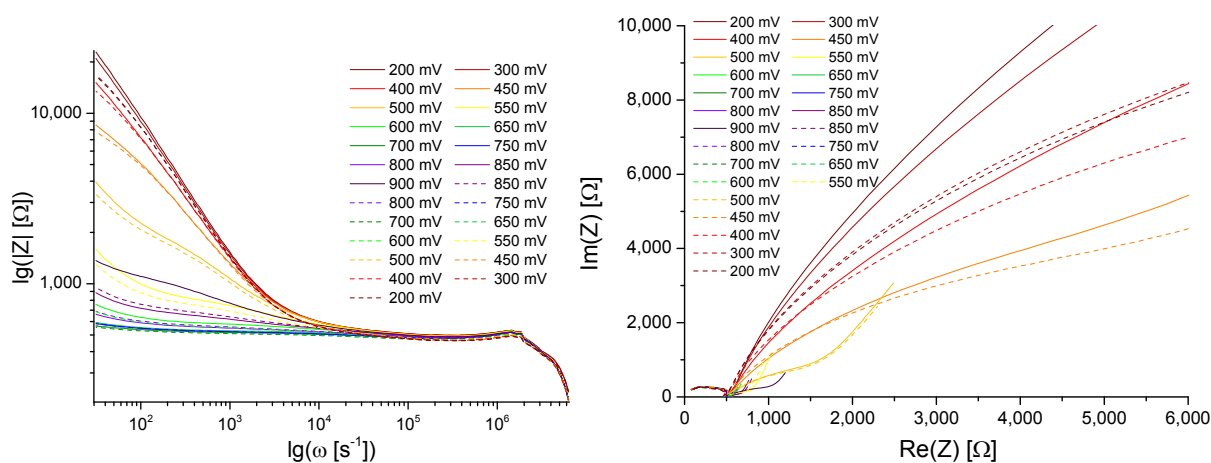


Figure S14. Bode (left) and Nyquist (right) plot of electrochemical impedance spectroscopy of poly(**RuDqp2**) (potentials vs. Fc^+/Fc , solid lines indicate increasing potential, dashed lines decreasing potential).

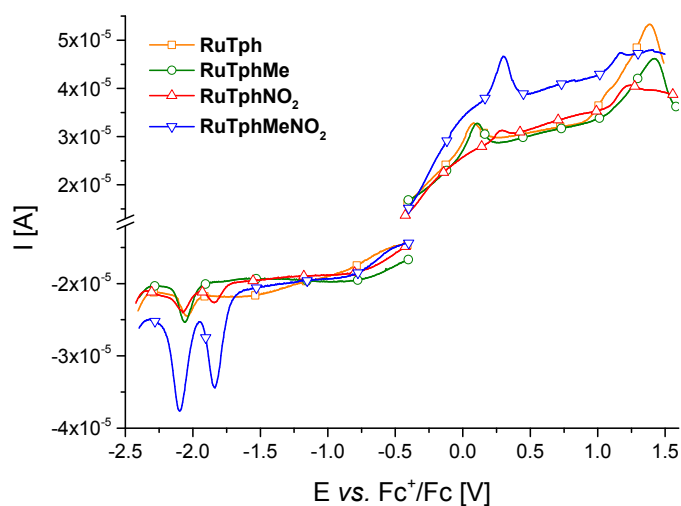


Figure S15. Differential pulse polarograms of cyclometalated complexes used for electropolymerization (10^{-5} M in CH_2Cl_2 with 0.1 M Bu_4NPF_6).

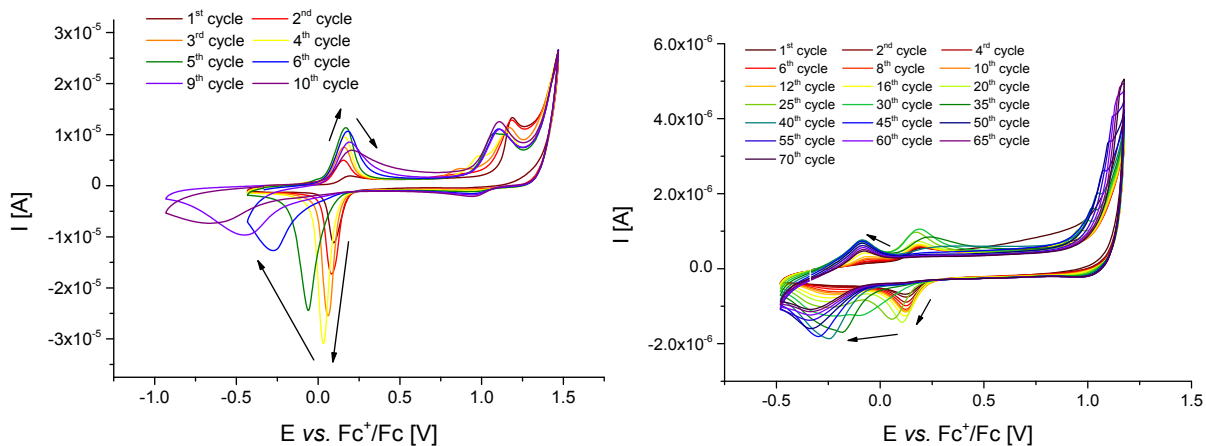


Figure S16. Electropolymerization attempts for bromo-functionalized **RuTph** applying end potentials of 1.5 (left) and 1.2 V (right) (10^{-4} M in CH_2Cl_2 with 0.1 M Bu_4NPF_6).

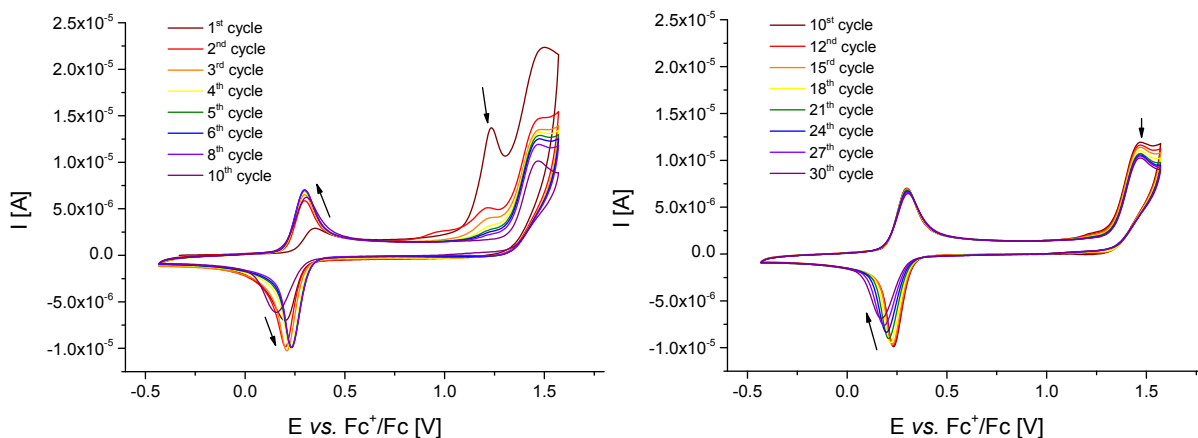


Figure S17. Electropolymerization attempts for **RuTphMeNO₂** applying a higher end potential (10^{-4} M in CH_2Cl_2 with 0.1 M Bu_4NPF_6).

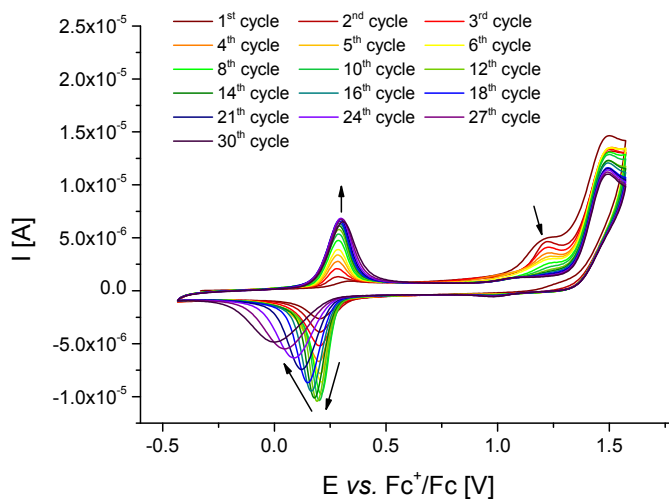


Figure S18. Electropolymerization attempt for **RuTphNO₂** applying a higher end potential (10^{-4} M in CH_2Cl_2 with 0.1 M Bu_4NPF_6).

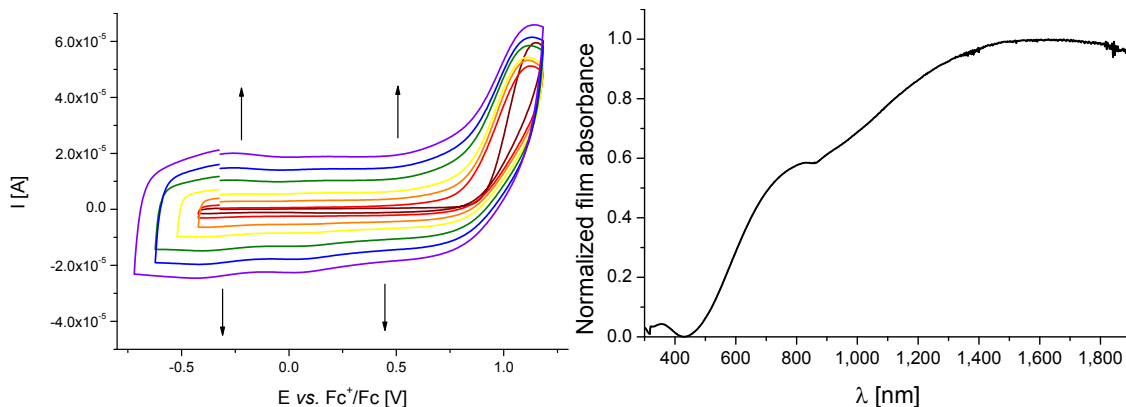


Figure S19. Electropolymerization of EDOT in CH₂Cl₂ (left, 10⁻⁴ M with 0.1 M Bu₄NPF₆) and UV-vis absorption spectrum of a PEDOT film on ITO-coated glass obtained by electropolymerization of EDOT (right).

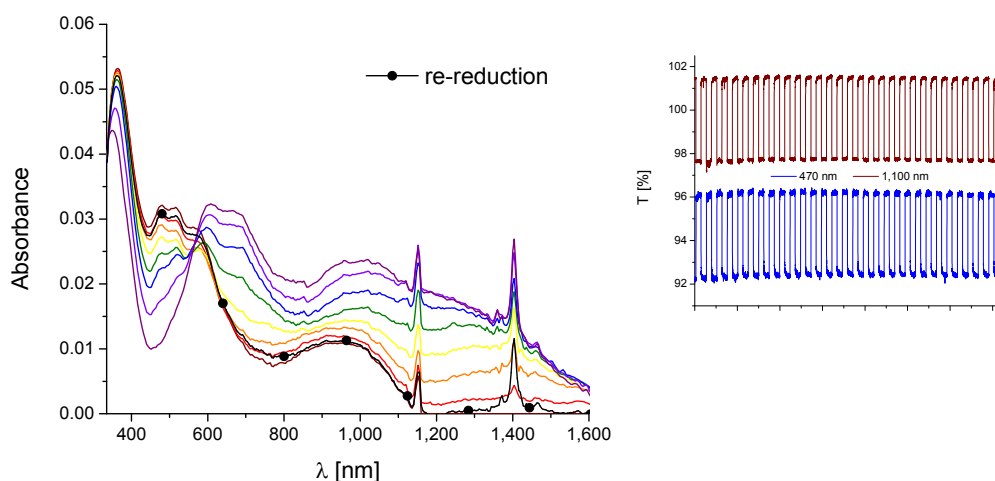


Figure S20. Change of the UV-vis absorption spectrum of an electropolymerized film of *co*-polymer of RuTphMeNO₂ and EDOT (1:1) during the oxidation up to 400 mV (left) and change of transmission at 470 and 1,100 nm over 30 cycles of switching between initial and oxidized state (right) (film on ITO-coated glass in CH₂Cl₂ with 0.1 M Bu₄NPF₆).

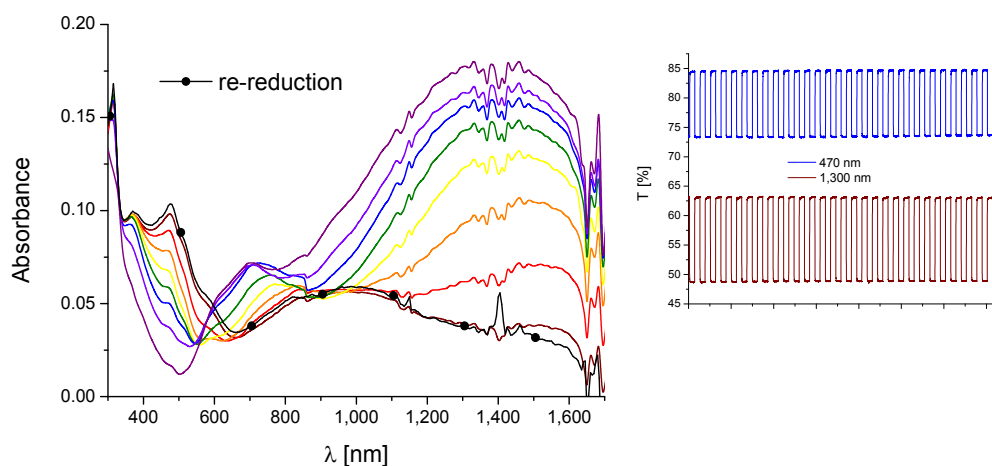


Figure S21. Change of the UV-vis absorption spectrum of an electropolymerized film of *co*-polymer of RuTphMeNO₂ and EDOT (1:5) during the oxidation up to 400 mV (left) and change of transmission at 470 and 1,300 nm over 30 cycles of switching between initial and oxidized state (right) (film on ITO-coated glass in CH₂Cl₂ with 0.1 M Bu₄NPF₆).

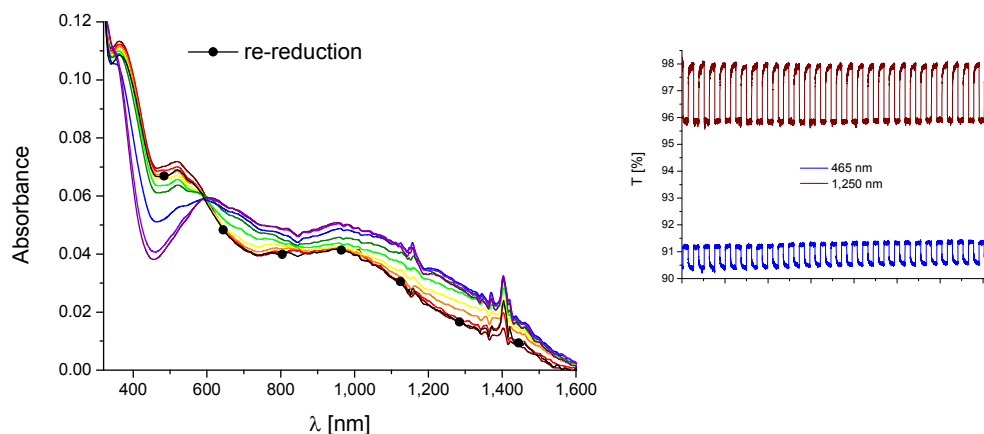


Figure S22. Change of the UV-vis absorption spectrum of an electropolymerized film of *co*-polymer of **RuTphNO₂** and EDOT (1:1) during the oxidation up to 400 mV (left) and change of transmission at 465 and 1,250 nm over 30 cycles of switching between initial and oxidized state (right) (film on ITO-coated glass in CH₂Cl₂ with 0.1 M Bu₄NPF₆).

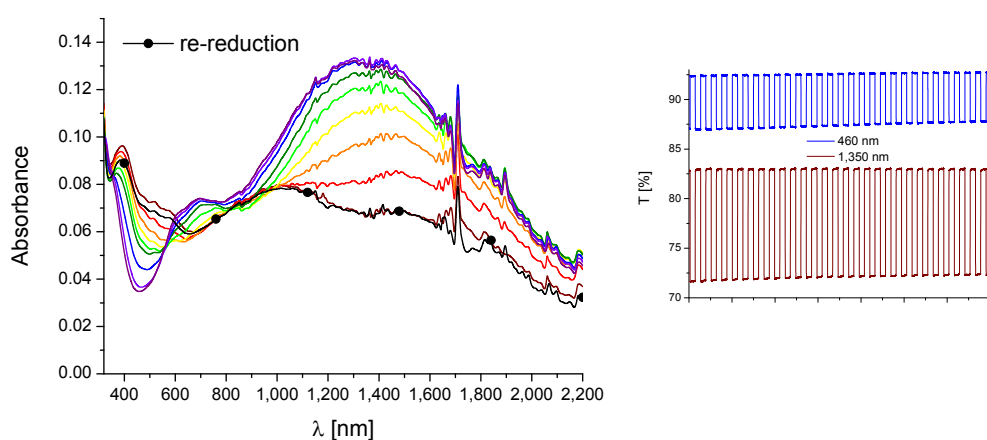


Figure S23. Change of the UV-vis absorption spectrum of an electropolymerized film of *co*-polymer of **RuTphNO₂** and EDOT (1:5) during the oxidation up to 400 mV (left) change of transmission at 460 and 1,350 nm over 30 cycles of switching between initial and oxidized state (right) (film on ITO-coated glass in CH₂Cl₂ with 0.1 M Bu₄NPF₆).

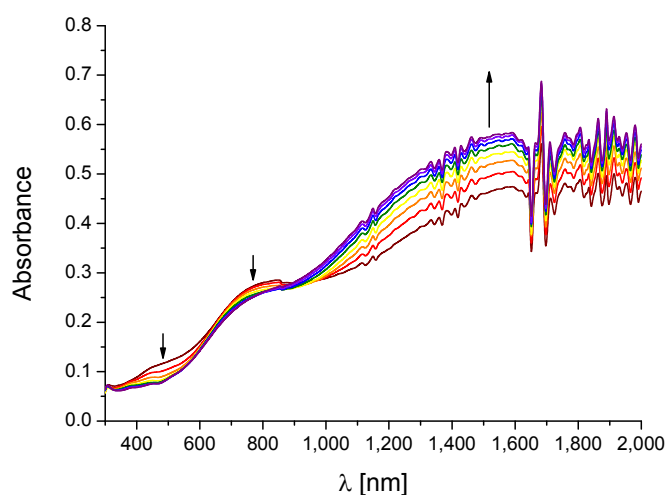


Figure S24. Change of the UV-vis absorption spectrum of an electropolymerized PEDOT film during the oxidation up to 400 mV (film on ITO-coated glass in CH₂Cl₂ with 0.1 M Bu₄NPF₆).

List of Abbreviations

| | |
|------------------------|--|
| AUC | analytical ultracentrifugation |
| bpy | 2,2'-bipyridine |
| CuAAC | copper(I)-catalyzed azide-alkyne 1,3-cycloaddition |
| CV | cyclic voltammetry |
| DFT | density functional theory |
| DMA | <i>N,N</i> -dimethyl acetamide |
| DMF | <i>N,N</i> -dimethyl formamide |
| DMSO | dimethyl sulfoxide |
| DPP | differential pulse polarography |
| dqp | 2,6-di(quinoline-8-yl)pyridine |
| DSSC | dye-sensitized solar cell |
| $E_{1/2}$ | half-wave redox potential |
| EDOT | 3,4-ethylenedioxythiophene |
| E_{gap} | band gap |
| EIS | electrochemical impedance spectroscopy |
| el | electrochemical |
| EQCM | electrochemical quartz crystal microbalance |
| E_p | peak potential |
| EPR | electron paramagnetic resonance |
| $E_{S^*,\text{Ox}}$ | excited-state redox potential |
| ET | electron transfer |
| ε | extinction coefficient |
| Fc | ferrocene |
| FTO | fluorine-doped tin oxide |
| GS | electronic ground state |
| HOMO | highest occupied molecular orbital |
| IC | internal conversion |
| ICT | intra-ligand charge transfer |
| i_p | peak current |
| IR | infra-red |
| ISC | intersystem crossing |
| ITO | indium-doped tin oxide |
| LC | ligand-centered |
| LLCT | ligand-to-ligand charge transfer |
| LMCT | ligand-to-metal charge transfer |
| LUMO | lowest unoccupied molecular orbital |
| λ_{Abs} | absorption wavelength |
| λ_{PL} | photoluminescence wavelength |
| M | mol per liter |
| MC | metal-centered |
| MLCT | metal-to-ligand charge-transfer |
| MO | molecular orbital |
| NIR | near infra-red |
| NHC | <i>N</i> -heterocyclic carbene |

| | |
|--------------------|-----------------------------------|
| NHE | normal hydrogen electrode |
| OLED | organic light-emitting diode |
| opt | optical |
| Ox | oxidation |
| PLED | polymer light-emitting diode |
| PV | photovoltaic |
| py | pyridine |
| Φ_{PL} | photoluminescence quantum yield |
| Red | reduction |
| RFID | radio frequency identification |
| RR | radical-radical coupling |
| RS | radical-substrate coupling |
| SEC | size-exclusion chromatography |
| SEM | scanning electron microscopy |
| SOMO | singly occupied molecular orbital |
| σ | electrical conductivity |
| T | transmission |
| TEM | transmission electron microscopy |
| tpy | 2,2':6',2''-terpyridine |
| τ | excited-state lifetime |
| UV-vis | ultra-violet and visible |
| XPS | X-ray photoelectron |

Publications A1–A11

Publication A1: “Metal-containing polymers via
electropolymerization”

Christian Friebe, Martin D. Hager, Andreas Winter,
Ulrich S. Schubert

Adv. Mater. **2012**, *24*, 332–345.

Reprinted with permission from: WILEY-VCH Weinheim (Copyright 2012)

Metal-Containing Polymers via Electropolymerization

Christian Friebe, Martin D. Hager, Andreas Winter, and Ulrich S. Schubert*

Electropolymerization represents a suitable and well-established approach for the assembly of polymer structures, in particular with regard to the formation of thin, insoluble films. Utilization of monomers that are functionalized with metal complex units allows the combination of structural and functional benefits of polymers and metal moieties. Since a broad range of both electropolymerizable monomers and metal complexes are available, various structures and, thus, applications are possible. Recent developments in the field of synthesis and potential applications of metal-functionalized polymers obtained via electropolymerization are presented, highlighting the significant advances in this field of research.

1. Introduction

Metal complexes offer highly versatile application possibilities in the area of catalysis,^[1] energy generation^[2] and water-splitting,^[3] lighting,^[4] and sensor materials.^[5] In various cases, the metal-containing compounds need to be processed in the solid state, forming thin films and coatings, e.g., on electrode surfaces or nanoparticles. Among other deposition procedures, e.g., spin-coating, inkjet printing, doctor blading, and drop-casting, a suitable approach is the formation of metal-containing polymeric systems directly onto the material to be coated via electropolymerization. This method offers several advantages compared to common polymerization techniques. Firstly, solubility problems, which often complicate thin-film processing, are avoided since the polymer itself is formed directly on the respective surface while only the corresponding monomers have to be dissolved; this is far easier to achieve in most cases. Secondly, the required time and instrumental effort to obtain a polymer film that is suitable for further investigations is low in comparison to alternative polymerization procedures. In this regard, another benefit is the easily controllable thickness of electropolymerized films that can be simply determined through the polymerization duration.

C. Friebe, Dr. M. D. Hager, Dr. A. Winter, Prof. U. S. Schubert
Laboratory of Organic and Macromolecular Chemistry (IOMC)
Friedrich-Schiller-University Jena
Humboldtstr. 10, 07743 Jena, Germany
E-mail: ulrich.schubert@uni-jena.de

C. Friebe, Dr. M. D. Hager, Dr. A. Winter, Prof. U. S. Schubert
Jena Center for Soft Matter (JCSM)
Humboldtstr. 10, 07743 Jena, Germany
C. Friebe, Dr. M. D. Hager, Dr. A. Winter,
Prof. U. S. Schubert

Dutch Polymer Institute (DPI)
P.O. Box 902, 5600 AX Eindhoven, Netherlands



DOI: 10.1002/adma.201103420

In order to carry out an electrochemical polymerization, the respective metal complex has to be linked to an electropolymerizable monomer moiety, e.g., thiophene, pyrrole, aniline, or vinyl groups. Thereby, the monomer unit can be incorporated into the polymer in different ways to obtain different kinds of metallopolymers. On the one hand, it can be coupled by a non-conjugated spacer (e.g., alkyl chains, ester, or ether linkages) so that the properties of the metal complexes are mostly unchanged in the course of polymer formation. On the other hand, the monomer can be attached directly to the ligand of

the complex, either in a way to arrange the metal ions laterally on the polymer chain or to include them as an essential linking part of the backbone (Figure 1). In these cases, a significant interaction between metal and polymer system as well as between the different metal centers is present, whereupon the largest mutual influences can be observed in the latter kind. Wolf classified such systems as metal-containing polymers of type I, II, and III, respectively.^[6] Another class (designated type IV) is represented by polymer systems where the backbone consists solely of the metal atoms (e.g., Ru⁰ and Rh⁰). They can also be obtained by electropolymerization of respective metal precursor complexes and enable an even higher level of metal-metal interactions. Furthermore, the usage of suitable monomers allows the combination of different polymer types leading to the formation of cross-linked networks.

2. Mechanistic Aspects

A widespread method is the electropolymerization achieved via oxidative coupling mainly of 5-membered heterocycles, such as

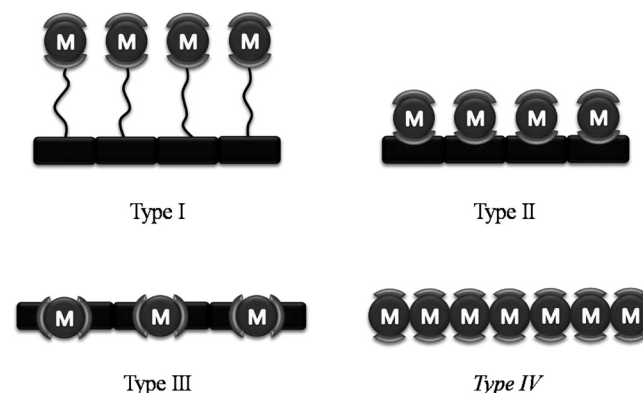


Figure 1. Possible arrangements of metal ions within metal-containing polymers (classification according to Wolf^[6]).

pyrrole, thiophene, and 3,4-ethylenedioxythiophene (EDOT), but also of other aromatic systems (e.g., aniline). Although several variants have been proposed,^[7] it is generally believed that the first step of the anodic electropolymerization, as soon as the respective oxidation potential is achieved, is the formation of radical cations through a one-electron oxidation of the aromatic ring, followed by radical–radical coupling (RR) and subsequent deprotonation leading to dimeric species.^[8] According to the original mechanism suggested by Diaz et al. already in 1981,^[9] the polymerization propagates by continuous chain growth through coupling of monomeric radical cations to oligomeric radicals (Scheme 1a). Since the dimers and higher oligomers are more easily oxidized than their corresponding monomers, their radical cations are formed immediately under the applied voltages. However, more recent experimental and theoretical investigations showed that a coupling of oligomeric and monomeric radical cations is rather unlikely due to the decrease of radical reactivity and lowered deprotonation ability of their σ -coupling products with increasing chain length causing highly preferred monomer–monomer instead of monomer–oligomer coupling.^[10] In contrast, the coupling of oligomeric radical cations is supposed, which leads from dimers to tetramers to octamers and so forth (Scheme 1b).^[11] At a certain chain length, the solubility is thus low enough that the deposition process starts and film formation occurs.

Although oxidative methods are used in the majority of cases, electropolymerization can also be carried out cathodically. The most common example is the reduction of vinyl-substituted pyridyl and polypyridyl complexes. As proposed by Murray and co-workers,^[12] the vinyl-possessing ligand can be reduced either directly or, depending on the order of reduction potentials, through electron transfer (ET) from a previously reduced ancillary ligand, e.g., pyridine (py), 2,2'-bipyridine (bpy), and 2,2':6',2''-terpyridine (tpy) (Scheme 2). Subsequently, the generated vinyl radical anion reacts with a second vinyl radical anion (RR) or couples to the vinyl group of a complex having a radical ancillary ligand (radical–substrate coupling, RS). Again, the reducibility of the ligand moieties determines the present species and, thus, the particular mechanism. The RR path firstly leads via electron transfer to a vinyl–vinyl diradical possessing reduced ancillary ligands, followed by hydrogen abstraction from the solvent and a further electron transfer that generates again an anionic vinyl radical being able to continue the polymerization process. If the RS route is dominant, the formed vinyl-ancillary ligand diradical can either convert to the vinyl–vinyl diradical, following subsequently the previously described mechanism, or, if the required reduction potential is applied, is further reduced. Reduction and associated protonation yield the dimer featuring a radical ancillary ligand that is able to transfer its unpaired electron to another vinyl ligand, thus, enabling further chain growth.

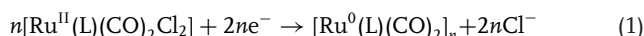
Whereas metallopolymers of type I, II, and III can be generated either oxidatively or reductively, depending on the used electropolymerizable monomer, metal-backbone polymers (type IV) are built up exclusively through cathodic electropolymerization. For this purpose, the metal center of a suitable precursor, e.g., $[\text{Ru}^{\text{II}}(\text{L})(\text{CO})_2\text{Cl}_2]$, is reduced electrochemically to form dimers, tetramers and eventually polymers by generating metal–metal bonds (Equation 1).^[13]



Christian Friebe was born in Erfurt (Germany) and studied chemistry at the Friedrich-Schiller-University Jena (Germany) where he graduated in organometallic chemistry in 2008. Currently, he is working on his PhD thesis, focusing on the electrochemical and spectroscopic characterization of transition metal complexes, at the Friedrich-Schiller-University Jena under the supervision of Prof. U. S. Schubert.



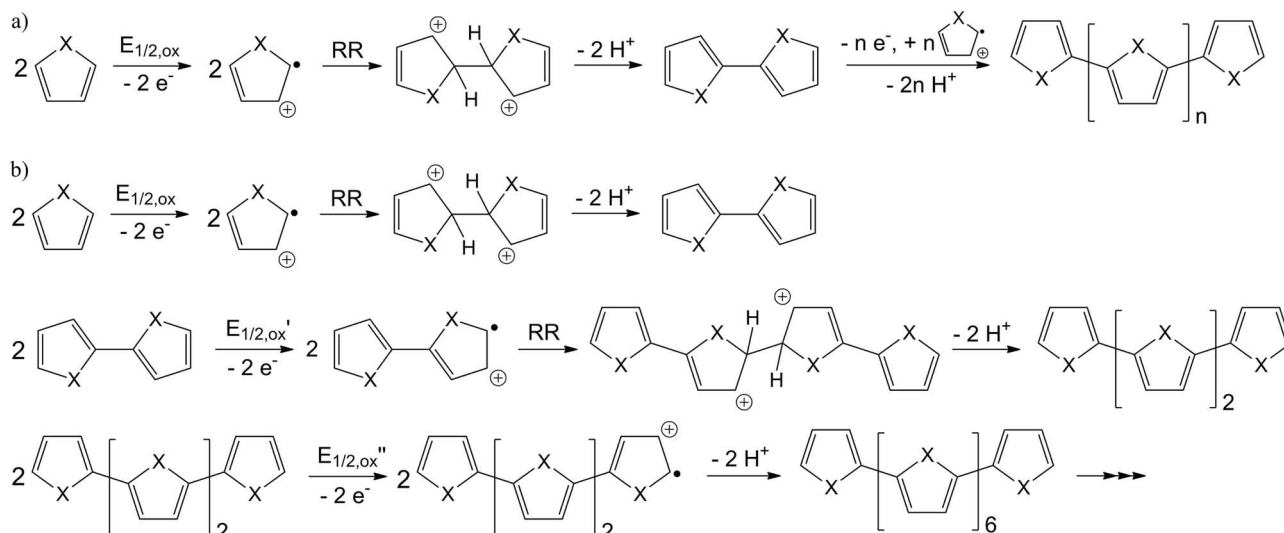
Ulrich S. Schubert studied chemistry at the Universities of Frankfurt and Bayreuth (Germany) and the Virginia Commonwealth University, Richmond (USA). His PhD work was performed with Profs. C. D. Eisenbach (Bayreuth, Germany) and G. R. Newkome (Florida, USA). He did postdoctoral research with Prof. J.-M. Lehn (Université Strasbourg (France)), moved to the Munich University of Technology (Germany) to obtain his habilitation, and from 1999 to 2000 held a temporary position at the Center for NanoScience (CeNS) at the LMU Munich. From 2000 to 2007, he was Full Professor at the Eindhoven University of Technology. He is now Full Professor at the Friedrich-Schiller-University Jena.



With these diverse techniques on hand, a wide range of possibilities for the formation of metal-containing polymers via electrochemical deposition are available.

3. Experimental Remarks

Different electrochemical techniques can be applied for electropolymerization: potenti- and galvanostatic methods on the one hand and potentiodynamic on the other hand. While the polymerization mechanism itself remains the same, regardless of whether the voltage or electric current is held constant or changed cyclically,^[14] the solid-state morphology is influenced significantly by the chosen technique. However, whether the generated films exhibit a better homogeneity and substrate adhesion in the case of static or dynamic experiments depends on the particular polymerized system.^[15] Additionally, the electrochemical state of the achieved polymer differs. While a

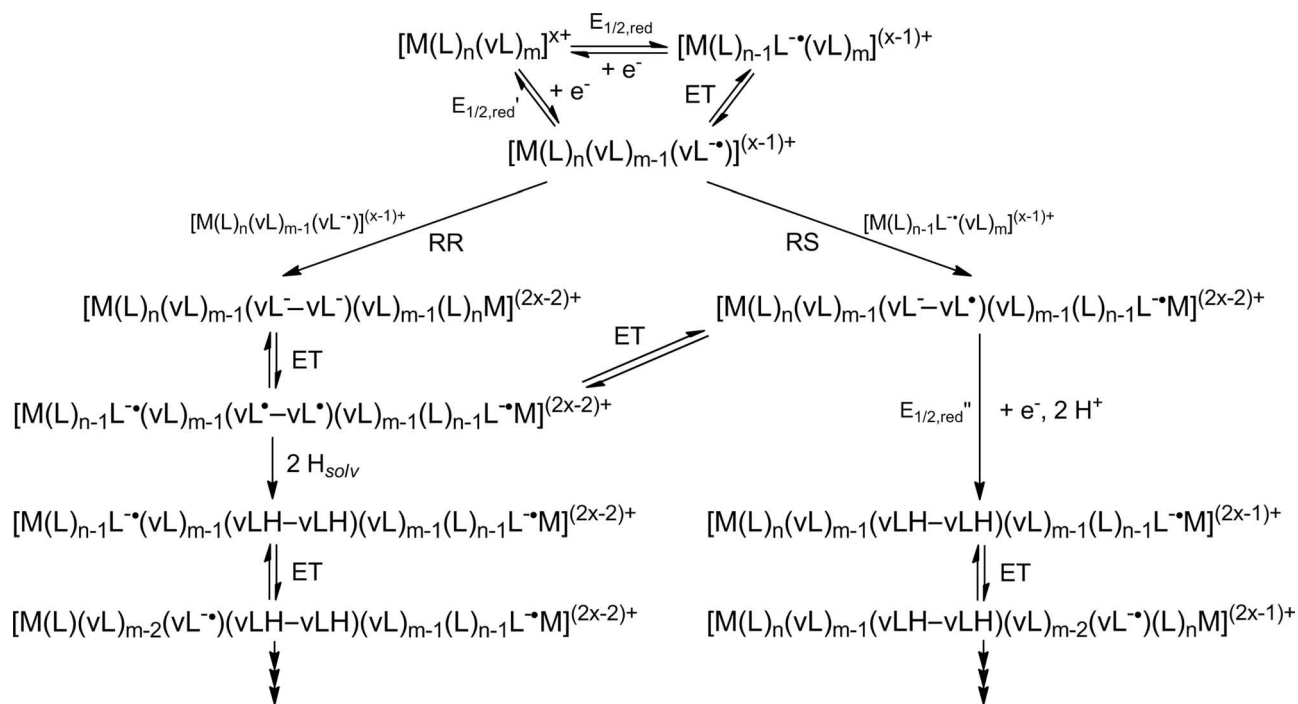


Scheme 1. Proposed chain-growth mechanisms for the oxidative electropolymerization (X = S, NH). a) Chain growth by addition of radical monomers. b) Chain growth by coupling of oligomers.

system synthesized by galvanostatic polymerization is charged and can still undergo structural modifications via electrochemical treatment, a polymer that was formed through potential cycling is available in its uncharged ground state and, because of the continuous potential variation during polymerization, generally remains stable against electrochemical post-synthesis modification attempts.^[16]

The utilized electrode material depends on the particular aim, i.e., on the targeted application of the electropolymerized

material. For a simple proof of principle and electrochemical characterization of the polymeric film, standard working electrodes, for instance made of glassy carbon, platinum, or gold, are used. With regard to spectroscopic characterization or usage in optical devices (polymer light-emitting diodes (PLEDs), solar cells, or electrochromic components), transparent electrode materials, e.g., indium tin oxide (ITO) or fluorine-doped tin oxide (FTO), have to be used.^[17] Furthermore, to achieve specific electrode properties, special materials are applied, such



Scheme 2. Mechanism of reductive electropolymerization of vinyl-pyridyl transition metal complexes (M: e.g., Fe, Ru, Os ($x = 2$) or Co, Cr ($x = 3$); L: e.g., py, bpy, tpy; vL: e.g., vinyl-py, vinyl-bpy).^[12]

as carbon nanotubes^[18] or semiconductor photocathodes (e.g., zinc-doped indium phosphide).^[19]

The characterization of the obtained polymer already begins during the polymerization process. The current and potential curves in case of potentiostatic and galvanostatic procedures, respectively, or the cyclic voltammograms for potentiodynamic polymerizations provide the first information about polymer growth and change of electrochemical response. Furthermore, non-electrochemical methods can be used for online monitoring of the electropolymerization process, e.g., UV-vis and IR spectroelectrochemistry for the spectral characterization of intermediates or electrochemical quartz crystal microbalance (EQCM) measurements to follow directly the film growth during polymerization. Post-synthesis film characterization includes different electrochemical investigations, namely cyclic voltammetry, differential pulse polarography (DPP), or in situ conductivity measurements. Additionally, spectroscopic methods (UV-vis, NIR, IR, Raman, electron paramagnetic resonance (EPR)) are applied either on the unmodified film or spectroelectrochemically. For detailed film characterization, X-ray photoelectron spectroscopy (XPS), solid-state NMR, or transmission and scanning electron microscopy (TEM, SEM) are used.

4. Polymers Containing Polypyridyl Complexes

Beside the parent pyridine (py), its descendents 2,2'-bipyridine (bpy) and 2,2':6',2''-terpyridine (tpy) are the most commonly used polypyridyl ligands to form metal complexes due to their high stabilities with various metal ions, functionalizability, and easy synthetic access. In particular, metal complexes of terpyridine and its derivatives are able to form well-defined macromolecular structures, which make them interesting building blocks for functional polymeric architectures.^[20] Hence, a wide range of polypyridyl complexes containing different metal ions were incorporated into polymers via electropolymerization (Table 1).

Substituted terpyridines, bipyridines, phenanthrolines, and pyridines were applied to generate type-III metallopolymers featuring iron(II),^[21] ruthenium(II),^[22] and osmium(II)^[22a,22c] ions within the polymer backbone using different kinds of polymerizable monomers. Constable, Forster, and co-workers investigated the influence of the size of the monomer on the reactivity and conductivity of the polymers using thienyl, bithienyl, and terthienyl substituents within homoleptic ruthenium(II) and osmium(II) terpyridine complexes.^[22a] Both $[\text{Ru}(\text{ttpy})_2]^{2+}$ and $[\text{Os}(\text{ttpy})_2]^{2+}$, possessing a thiophen-2-yl ring in 4'-position of each terpyridine, formed highly reactive radical cations during the polymerization requiring elaborated experimental conditions (i.e., stringent exclusion of water and usage of $\text{BF}_3 \cdot \text{OEt}_2$ as solvent); in contrast, bi- and terthienyl compounds could be electropolymerized easily (Figure 2). In situ conductivity measurements revealed a strongly enhanced charge transfer within the oxidized metallopolymers, if the difference between the metal-center and bridge oxidation potential was minimized. Elsewhere, Forster and Meyer utilized uncommon reaction media, namely ionic liquids^[22b] and SiO_2 sol-gel films,^[22c] for the polymerization of aminophenanthroline and vinylbipyridine complexes, respectively.

Type-II polymers were synthesized using heteroleptic polypyridyl complexes carrying two polymerizable moieties at one ligand, leading to its incorporation into the polymer backbone. Ruthenium(II), iridium(III), and europium(III) complexes were used to produce metal-containing polymers.^[23] The introduction of an emissive iridium(III) complex into a polymer structure by Holliday and co-workers, aiming at its application in PLEDs, surprisingly led to a non-emissive system.^[23a] This behavior was explained by a stabilized ligand-centered triplet state that makes a charge transfer to the metal triplet state less favorable. Another approach to achieve suitable materials for PLEDs was the deployment of rare earth metal ion complexes, namely using europium(III), resulting in polymer films showing strong, purely metal-based photoluminescence.^[23b]

Metallopolymers possessing complexes incorporated in pendant side chains (type I) involved, in addition to ruthenium(II) systems,^[18a,24] cobalt(II)^[25] and copper(II)^[26] complexes. Aiming at the development of photoelectrochemical sensors, Cosnier and co-workers executed the electropolymerization of pyrrole-functionalized ruthenium(II)-tris-2,2'-bipyridine (one or three disubstituted ligands) on multiwalled carbon nanotube (MWCNT) electrodes (Figure 3).^[18a] The authors reported enhanced polymerization yields and enlarged electroactivity of the generated coated surfaces in comparison to usual platinum electrodes. Gold nanoparticles were functionalized with both a ruthenium polypyridyl complex ($[\text{Ru}(\text{tpy})_2]^{2+}$) and an electropolymerizable pyrrole (1) by Fujihara and co-workers (Figure 4) to fabricate electrodes coated with metal nanocomposite films.^[24a]

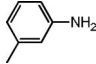
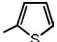
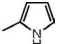
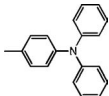
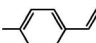
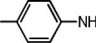
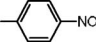
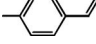
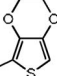
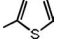
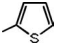
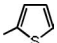
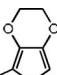
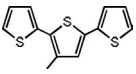
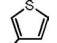

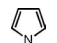

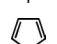
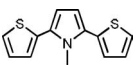
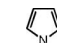
Polymers featuring a metal backbone with laterally attached 2,2'-bipyridine ligands were obtained from suitable precursors containing ruthenium(II),^[13b,19,27] rhenium(II),^[28] and osmium(II)^[29] centers. Wasberg and co-workers investigated the mechanism of polymerization of the $[\text{Ru}(\text{bpy})(\text{CO})_2\text{Cl}_2]$ complex.^[13b,27a] The polymers were applied successfully to coat electrodes electrochemically with ruthenium(0)-metallopolymers for the purpose of catalytic CO_2 reduction.^[19,27e] Additionally, electrically conducting polymer chains with conductivities up to $0.3 \text{ S} \cdot \text{cm}^{-1}$ could be achieved via partial oxidation of the metal backbone.^[27b] Another approach worth mentioning, also targeting at the electrocatalytic reduction of CO_2 , is the work of Chardon-Noblat, Deronzier, and co-workers who synthesized a $[\text{Ru}(\text{bpy})(\text{CO})_2(\text{CH}_3\text{CN})_2]^{2+}$ dimer with an electropolymerizable pyrrole moiety covalently linked to the 2,2'-bipyridine unit enabling two separate polymerization processes, a cathodic and an anodic one, that allowed the controlled formation of cross-linked polymers.^[27e]

5. Metallocenes in Electropolymerized Systems

Metallocenes exhibit remarkable electronic and optical properties making them versatile building blocks for the incorporation into polymer systems^[30] and, consequently, for electrochemical polymerization. Ferrocene and its derivatives represent the most common metallocenes applied in polymeric systems,^[31] but also other metals such as cobalt^[32] or tantalum^[33] are used.

Toppare and co-workers incorporated ferrocene units into quinoxaline-containing conjugated polymers that were built up by electropolymerization of EDOT units. The achieved

Table 1. Polypyridyl complexes assembled within electropolymerized polymers (italics indicate: ligands linked to electropolymerization monomer).

| Metal complex | Polymerizable unit | Polymer type ^{a)} | Ref. |
|---|--|----------------------------|----------------|
| [Fe(<i>tpy</i>) ₂] ²⁺ |  | I, III | [21a] |
| [Fe(<i>phen</i>) ₃] ²⁺ | Imidazolidine | III | [21b] |
| [Ru(<i>tpy</i>) ₂] ²⁺ , [Os(<i>tpy</i>) ₂] ²⁺ |  | III | [22a] |
| [Ru(<i>tpy</i>) ₂] ²⁺ |  | III | [22d] |
| [Ru(<i>tpy</i>) ₂] ²⁺ |  | I, III | [22e] |
| [Ru(<i>bpy</i>) ₃] ²⁺ , [Os(<i>bpy</i>) ₃] ²⁺ |  | I, III | [22c] |
| [Ru(<i>phen</i>) ₃] ²⁺ |  | III | [22b] |
| [Ru(<i>phen</i>) ₂ (<i>py</i> Cl)] ⁺ |  | III | [22f] |
| [Ru(<i>py</i>) ₄ Cl ₂] |  | III | [22g,22h] |
| [Ru(<i>tpy</i>)(<i>bpp</i>)] ²⁺ |  | II | [23c] |
| [Ru(<i>bpm</i>) ₃] ²⁺ |  | II, III | [23d] |
| [Ru(<i>bpy</i>) ₂ (<i>bpm</i>)] ²⁺ |  | II | [23d] |
| [Ir(<i>ppy</i>) ₂ (<i>phen</i>)] ⁺ |  | II | [23a] |
| [Eu(DBM) ₃ (<i>phen</i>)] |  | II | [23b] |
| [Co(DBSQ) ₂ (<i>bpy</i>)] |  | I | [25] |
| [Cu(<i>py-NH</i>) ₂] ²⁺ |  | I | [26] |
| [Ru(<i>tpy</i>)(<i>tpy</i>)] ²⁺ |  | I | [24a] |
| [Ru(<i>bpy</i>) ₂ (<i>py</i> Cl)] ⁺ |  | I | [24b] |
| [Ru(<i>bpy</i>) ₃] ²⁺ |  | I, III | [18a] |
| [Ru(<i>bpy</i>) ₂ (<i>bpy</i>)] ²⁺ |  | I | [18a] |
| [Ru(<i>phen</i>)(DMSO) ₂ Cl ₂] |  | I | [24c] |
| [Ru(<i>bpy</i>)(CO) ₂] | Ru | IV | [13b,19,27a–d] |
| [Ru(<i>bpy</i>)(CO) ₂] |  Ru, | I, IV | [27e] |
| [Rh ₂ (μ-OOCCH ₃)(<i>phen</i>) ₂] ²⁺ | Rh | IV | [28] |
| [Os(<i>bpy</i>)(CO) ₂] | Os | IV | [29] |

^{a)}Networks are marked by the combination of two types.

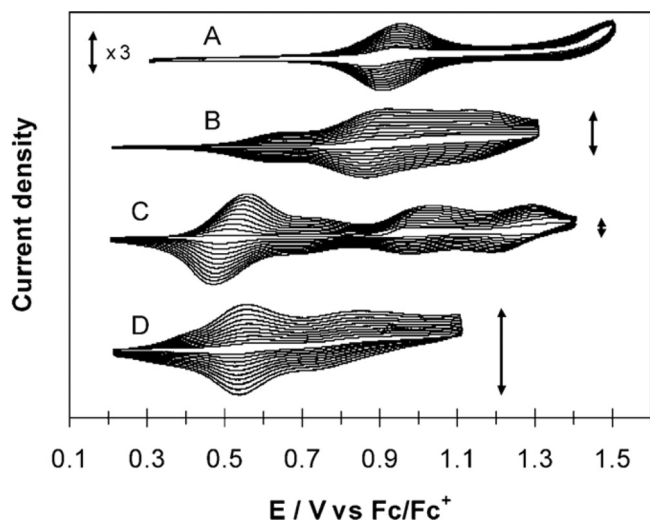


Figure 2. Anodic electropolymerization of $[\text{Ru}^{\text{II}}(\text{tpy})_2]$ with mono- (A) and bithienyl (B) units and $[\text{Os}^{\text{II}}(\text{tpy})_2]$ with bi- (C) and terthienyl (D) moieties, deposited from $4 \times 10^{-4} \text{ mol}\cdot\text{L}^{-1}$ solution using scan rate of $0.1 \text{ V}\cdot\text{s}^{-1}$. Reproduced with permission.^[22a] Copyright 2005, American Chemical Society.

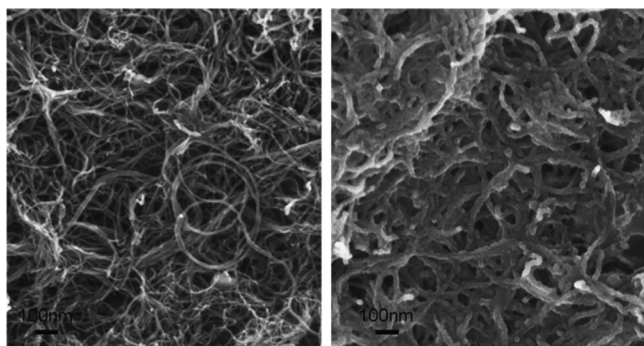


Figure 3. SEM images of MWCNT electrodes (left) and MWCNT electrodes that were coated via electropolymerization of pyrrole-functionalized ruthenium(II)-tris-2,2'-bipyridine (right). Reproduced with permission.^[18a] Copyright 2011, Elsevier.

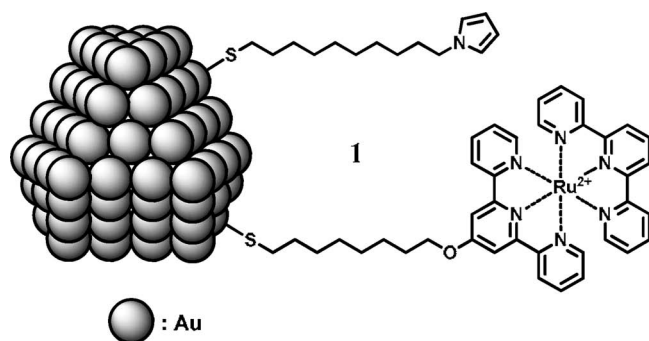


Figure 4. Functionalized gold nanoparticle 1.^[24a]

polymers showed electrochromic characteristics thus being promising candidates for the application in display devices (Figure 5).^[31a,31b] Furthermore, an electrochemically synthesized

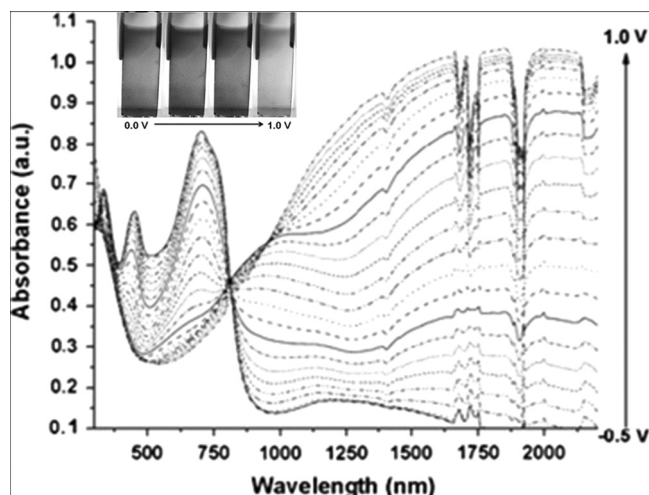


Figure 5. UV-vis spectroelectrochemistry of poly(5,8-bis(2,3-dihydrothieno[3,4-b][1,4]dioxin-5-yl)-2-(phenyl)-3-ferrocenylquinoxaline) between -0.5 V and 1.0 V (on ITO-coated glass, in $0.1 \text{ mol}\cdot\text{L}^{-1} \text{ Bu}_4\text{NPF}_6$ solution). Reproduced with permission.^[31b] Copyright 2011, Elsevier.

type-III polymer possessing ferrocene and triarylamine moieties was utilized as the hole-injection layer of PLEDs by Leung and co-workers leading to light-emitting devices exhibiting turn-on voltages 1.5 V lower than respective poly(3,4-ethyleneoxythiophene):poly(styrenesulfonate) (PEDOT:PSS) reference devices.^[31c] The synthesis of conducting type-II polymers containing azaferrrocene or cobalt cyclopentadienyl cyclobutadiene was in the focus of the work of Swager and co-workers (Figure 6).^[31d,32] The authors systematically investigated the influence of the length of the conjugated spacer within the polymers 2a to 2d on the charge transfer mechanism and, thus, on the in situ conductivity, finding a lowered conductivity onset for decreased spacer lengths most probably due to a superexchange mechanism.

6. Polymers with N-Macrocycle Metal Complexes

Nitrogen-containing macrocycle ligands, e.g., porphyrin (porph), phthalocyanine (phcy), and 1,4,8,11-tetraazacyclotetradecane (cyclam), form highly stable metal complexes exhibiting interesting catalytic, optical, and electrochemical properties^[34] and, thus, are usable building blocks for the preparation of a variety of electropolymerized polymers (Table 2).

Johannes and co-workers synthesized porphyrin complexes of nickel(II), cobalt(II), copper(II), and zinc(II) connected to

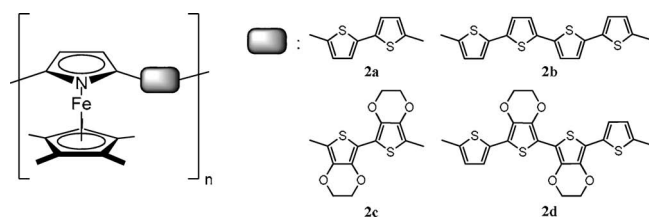
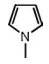
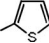
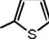
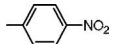
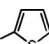
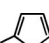
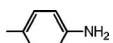
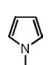
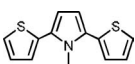
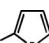
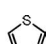

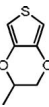
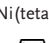
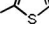
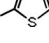


Figure 6. Azaferrrocene-containing polymers 2a–2d used for conductivity investigations by Swager et al.^[31d]

Table 2. N-Macrocycle metal complexes incorporated into polymers by electropolymerization.

| Metal complex | Polymerizable unit | Polymer type | Ref. |
|---|---|--------------|-------|
| [Mn(porph)] | porph | III | [18b] |
| [Fe(porph)] | porph | III | [18b] |
| [Co(porph)(CN) ₂] |  | I | [36] |
| [Co(porph)] |  | I, III | [35a] |
| [Co(porph)] | porph | III | [18b] |
| [Ni(porph)] |  | I, III | [35b] |
| [Ni(porph)] |  | I | [22f] |
| [Cu(porph)] |  | III | [35a] |
| [Zn(porph)] |  | I, III | [35a] |
| [Zn(porph)] | C ₆₀ /Pd | I | [38] |
| [Pt(porph)] |  | III | [37] |
| [Mn(phcya)] |  | I | [41] |
| [Zn(phcya)] |  | I | [39] |
| [Ru(phcya)(py) ₂] ^{a)} |  | II, III | [40] |
| [Co(cyclam)] |  | I | [42a] |
| [Ni(cyclam)] |  | I | [42b] |
| [Cu(cyclam)] |  | I | [42c] |
| [Ni(teta)] | [Ni(teta)] | III | [43] |
| [Fe(N ₆)] |  | III | [44] |
| [Co(N ₆)] |  | III | [44] |
| [Ru(N ₆)] |  | III | [44] |

^{a)}Polymerization monomers are linked to the pyridine units.

either two bis- and monothiophene units or one terthiophene to achieve type-III and type-I polymers by electropolymerization, respectively.^[35] Although porphyrin acts as a conjugation breaker, weak electronic communication between the metal complex moiety and the thiophene units could still be observed. The cobalt(II)-complex-containing polymer behaved exceptionally since the incorporated complex could be

oxidized easier than the thiophene moiety and, thus, the electropolymerization process and the optical and electrochemical properties of the resulting polymer differed significantly from the other complex-containing polymers. Vitamin B₁₂ derivatives featuring pyrrole rings were used by Abrantes and co-workers to coat platinum surfaces with regard to application in catalytic oxygen reduction reactions.^[36] Pursuing the same

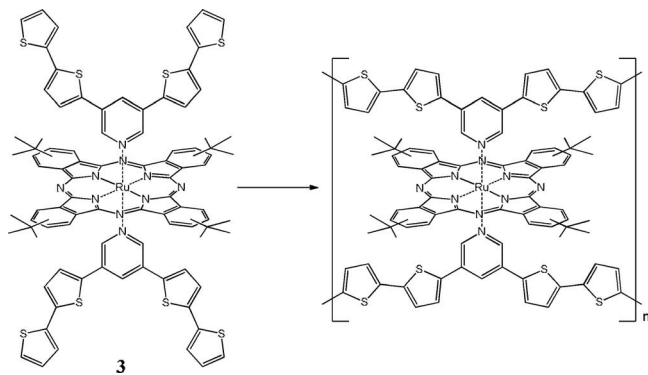


Figure 7. Electropolymerization of ruthenium(II) phthalocyanine complex **3** to construct polythiophene-phthalocyanine networks.^[40]

goal, Schuhmann and co-workers prepared manganese, iron, and cobalt porphyrin complexes for electrochemical deposition onto MWCNTs.^[18b] In particular the manganese systems, possessing multiple available oxidation states, led to a remarkable enhancement of the oxygen reduction due to a limited hydrogen peroxide production. With respect to another catalytic application, namely the electrocatalytic reduction of nitrite anions, polymers containing both nickel(II) porphyrin and ruthenium(II) polypyridyl moieties were synthesized successfully by Isaacs and co-workers.^[22f] Beside catalytic purposes, metal porphyrin complexes also represent suitable systems for sensor applications. Thus, Holmes-Smith et al. investigated a platinum(II) porphyrin complex exhibiting aniline units for electropolymerization experiments.^[37] The respective polymers showed an oxygen-induced photoluminescence quenching (Stern-Volmer constant of 5.0 atm^{-1} , response time of 0.5 s), hence providing a convenient material for O_2 sensing. Winkler, D'Souza, Balch, and co-workers combined an electrochemically available fullerene palladium polymer (vide infra) with a zinc(II) porphyrin complex.^[38] Also the porphyrin-like phthalocyanine can be used to create electropolymerizable metal complexes. Önal and co-workers prepared zinc(II) phthalocyanine complexes with pendant 2,5-di(thiophen-2-yl)-1*H*-pyrrol-1-yl groups and prepared electrochromic polymers.^[39] A polymer network was synthesized by Krompiec, Łapkowski, and co-workers using the ruthenium(II) phthalocyanine system **3** with two additional pyridine ligands with pendant bithiophene groups (**Figure 7**).^[40] As already presented for porphyrin

complexes, phthalocyanine systems can be used for oxygen reduction, as shown by the group of Bedioui who synthesized polymer films from manganese phthalocyanines possessing covalently linked pyrroles.^[41]

In addition to porphyrin and its analogs, other *N*-macrocycles are capable ligands for electropolymerizable metal complexes. The cyclam ligand was used to create cobalt(III)-, nickel(II)-, and copper(II)-containing type-I polymers.^[42] Ganesan and co-workers employed the cyclam derivative *meso*-5,5,7,12,12,14-hexamethyl-1,4,8,11-tetraazacyclotetradecane (teta) for the complexation of nickel(II) and electrochemical coating of different types of electrodes, namely glassy carbon, Nafion-modified glassy carbon as well as glassy carbon electrodes with Nafion-stabilized silver and gold nanoparticles.^[43] The modified electrodes enabled an improved catalytic oxidation of glucose; in particular, the incorporation of nanoparticles enhanced the electron transfer ability of the obtained polymer film. Defined layer-by-layer deposition of the iron(II)-, cobalt(II)-, and ruthenium(II)-containing polymers **4** was shown by Lee and co-workers using a thiophene-substituted hexadentate *tris*(dioximate) macrocycle, thus receiving metal-containing conducting polymer structures (**Figure 8**).^[44]

7. Salen Systems in Electropolymerized Polymers

In particular with regard to applications in catalysis,^[45] the *N,N'*-bis(salicylidene)ethylenediamine (salen) ligand represents a frequently used building block. Usually type-II conjugated polymers are built up using salen for incorporation of various metal ions like iron(III),^[46] nickel(II),^[17,47] cobalt(II),^[47a,48] copper(II),^[17,30,47b,49] zinc(II)^[50] as well as vanadium(IV),^[47b] chromium(II),^[47a,51] cadmium(II),^[52] palladium(II),^[17] and even gallium(III).^[50,53]

The group of Schulz synthesized chiral salen complexes that contained thiophene rings. The resulting polymers were successfully tested as heterogenous, enantioselective catalysts for Nozaki–Hiyama–Kishi^[47a] and hetero-Diels–Alder^[51] reactions. Furthermore, the reduction of hydrogen peroxide could be catalyzed using a film of polymerized copper(II) *N,N'*-bis(3-methoxysalicylidene)-2-aminobenzylamine complex by Demetgül and co-workers,^[49a] whereas Teixeira and Dadamos prepared Cu(salen)-coated platinum electrodes for the catalytic oxidation of sulfite anions.^[49b] In both cases, the metal-salen moiety was electropolymerized directly. Although the mechanism

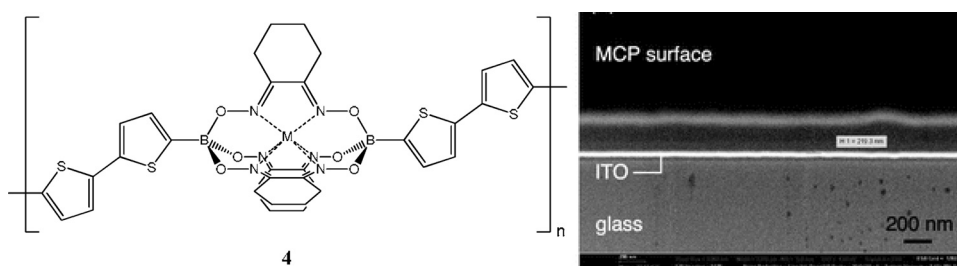


Figure 8. Polymer containing a hexadentate macrocycle **4** [$\text{M}(\text{N}_6)$] ($\text{M} = \text{Fe}^{\text{II}}, \text{Co}^{\text{II}}, \text{Ru}^{\text{II}}$) (left). Cross-sectional field emission SEM image of a poly[$\text{Fe}(\text{N}_6)$]/poly[$\text{Co}(\text{N}_6)$] bilayer (right; MCP: metal-containing conducting polymer). Reproduced with permission.^[44] Copyright 2010, American Chemical Society.

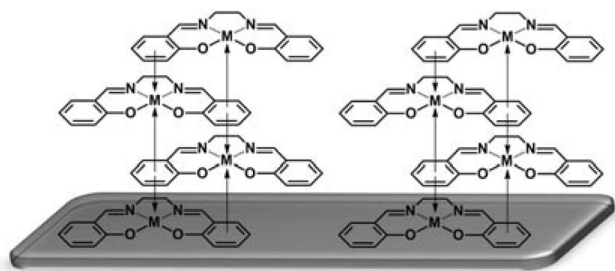


Figure 9. Stacking of metal salen complexes on the working electrode through anodic electropolymerization.^[49b,54]

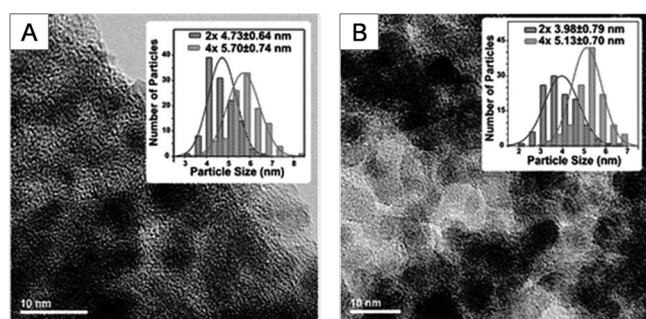


Figure 10. TEM images of CdS nanoparticles grown within a polymer of cadmium(II) salen bithienyl complex (A) and a copolymer with bithiophene (B). Insets: Size distributions of the nanoparticles. Reproduced with permission.^[52] Copyright 2009, American Chemical Society.

is still not completely understood, the formation of single stacks formed by the interaction of the electron-rich aromatic rings with the metal centers is proposed (Figure 9),^[49b,54] thus allowing electropolymerization without usage of common electropolymerizable monomer units.

In addition to catalytic applications, also other utilization possibilities were presented. Swager and co-workers polymerized an EDOT-functionalized cobalt(II) salen complex and investigated the resistive response to nitric oxides regarding the usage in sensor devices.^[48] Holliday and co-workers prepared cadmium(II) and gallium(III) salen polymers whose metal centers act as seed points for the growth of CdS and Ga₂S₃ nanoparticles, respectively (Figure 10).^[52,53] Hence, hybrid

materials containing semiconducting nanoparticles directly attached to conducting conjugated polymers could be achieved enabling strong metal–polymer interactions. With regard to flexible displays or similar applications, Pinheiro et al. deposited electrochromic polymers from nickel(II), copper(II), and palladium(II) salen complexes onto ITO-coated poly(ethylene terephthalate) (PET) foils (Figure 11).^[17] Detailed chromaticity studies revealed coloration efficiencies of about 80, 160, and 175 cm²·C⁻¹.

8. Thiolate Complexes

Complexes of dithiolate ligands (Figure 12) were integrated in electropolymerized polymers mainly to achieve semiconductor materials. Rocco and co-workers investigated polypyrroles doped with the metal complexes of 1,3-dithiole-2-thione-4,5-dithiolate (5, dmit) via electropolymerization from a pyrrole/[M(dmit)_n]²⁻ solution.^[55] Semiconductor conductivities of 2 × 10⁻³ to 4 × 10⁻³ S·cm⁻¹ for nickel(II), palladium(II), and platinum(II) complexes and 6 × 10⁻⁷ S·cm⁻¹ for the tin(IV) species were measured. The different orders of magnitude were caused by the different geometries; while the square-planar systems allows a parallel arrangement of metal complexes and polymer, an octahedral geometry impedes a unidirectional orientation.^[55a] On the other hand the release of the anion by anion exchange during redox cycling could be obtained. Murphy and co-workers described the electropolymerization of 1,2-ethylenedithiolate nickel(II) complexes 6 exhibiting either a 2- or 3-thienyl moiety.^[56] While the system containing 2-substituted thiophene rings could not be polymerized electrochemically, the 3-thienyl-bearing complex was able to be polymerized readily within both a homopolymer system and a copolymer with thiophene, whereupon the latter one showed significant conductivity. Elsewhere, Skabara and co-workers synthesized nickel(II), palladium(II), and gold(III) complexes of thiophene-3,4-dithiolate exhibiting 2-thienyl, 4-methoxy-phenyl, and 5-methyl-2-thienyl units at the thiophene 2- and 5-positions.^[57] The resulting electropolymerizable terthiophene species 7 were polymerized and yielded polymers featuring mainly polythiophene-based electrochemistry for palladium(II) and gold(III), in contrast to metal-dithiolate-determined electrochemical properties for the nickel(II) system.

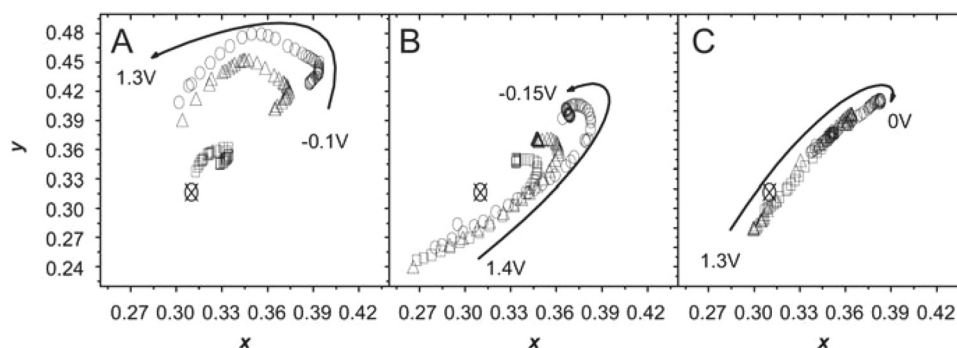


Figure 11. Chromaticity coordinates of electropolymerized Pd^{II} (A), Cu^{II} (B), and Ni^{II} (C) salen systems depending on the applied voltage. Films were deposited with 10 (open circles), 5 (open triangles), and 2 (open square) cycles. Reproduced with permission.^[17] Copyright 2008, Elsevier.

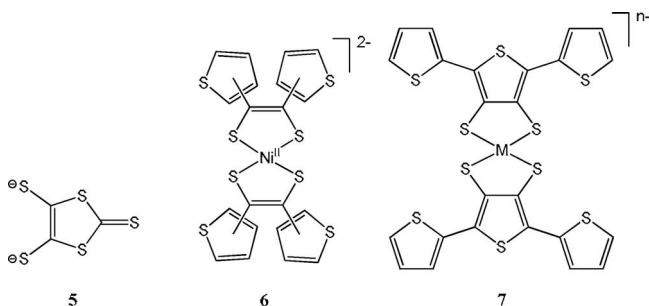


Figure 12. Dithiolate ligand **5** and complexes **6** and **7** used within electropolymerized polymers ($M = \text{Ni}^{\text{II}}$, Pd^{II} , Au^{III}).^[55–57]

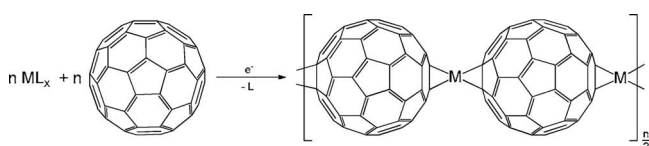


Figure 13. Formation of fullerene metallopolymer [M: e.g., Pd, Pt, $\text{Rh}(\text{CF}_3\text{COO})_2$, or $\text{Ir}(\text{CO})_2$].

9. Fullerene Metallopolymer

Fullerenes can be polymerized using different ways depending on the targeted applications.^[58] Electrochemical reduction of suitable transition metal complexes can be used to form metallopolymer with alternating metal and fullerene units (Figure 13). Targeting materials intended for energy storage,

thus requiring mainly high electrochemical stabilities, high capacitances, and high conductivities, Winkler and co-workers synthesized several polymers formed from C_{60} and C_{70} fullerenes and $[\text{Pd}(\text{CH}_3\text{COO})_2]$, $[\text{Pt}(\mu\text{-Cl})\text{Cl}(\text{C}_2\text{H}_4)]_2$, $[\text{Rh}(\text{CF}_3\text{COO})_2]_2$, and $\text{IrCl}(\text{CO})_2(p\text{-toluidine})$ (Figure 14).^[59] In comparison to their C_{60} counterparts, C_{70} fullerenes showed a higher polymerization efficiency. Respective polymers exhibited more reversible reduction processes and films with higher porosities and higher capacitance values. Comparing the different metals that were used, the rhodium/fullerene system showed the best polymerization performance and palladium/fullerene films exhibited the highest rates of charge-transfer processes.^[59a] Further studies focused on the redox stability of the palladium/ C_{60} system, revealing an increased stability through incorporation of palladium particles into the film,^[59b] and the coating of MWCNTs with fullerene metallopolymer leading to an enhanced capacitance of the resulting solid-state systems.^[59c] Balch and co-workers polymerized C_{60} fullerenes linked covalently to zinc(II) porphyrin complexes electrochemically with palladium(II) acetate, leading to polymers that combine the redox properties of fullerene and metal porphyrin moieties.^[38]

10. Other Systems

In addition to the presented classes of metal complexes, other systems have also been used for the incorporation into polymers by electropolymerization.

With respect to catalytic applications and optoelectronic materials, transition metal complexes featuring strongly

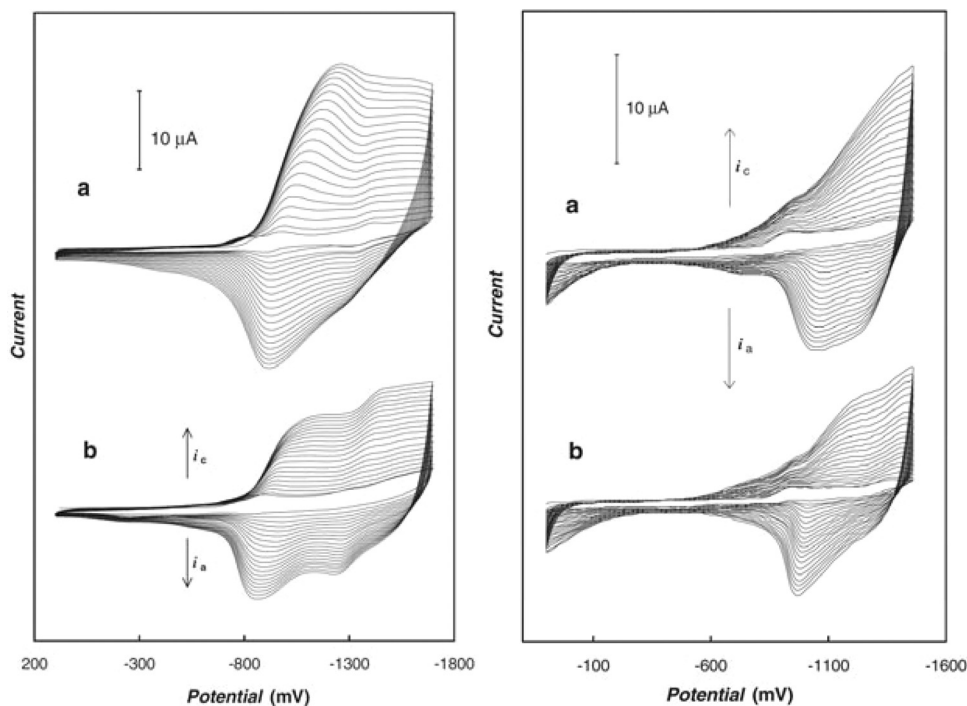


Figure 14. Potentiodynamic polymerization of C_{60} (a) and C_{70} (b) and $[\text{Pd}(\text{CH}_3\text{COO})_2]$ (left) and $[\text{Rh}(\text{CF}_3\text{COO})_2]_2$ (right) onto a gold electrode from acetonitrile/toluene (1:4) solution with $0.1 \text{ mol}\cdot\text{L}^{-1} \text{ Bu}_4\text{NClO}_4$. Reproduced with permission.^[59a] Copyright 2008, Springer.

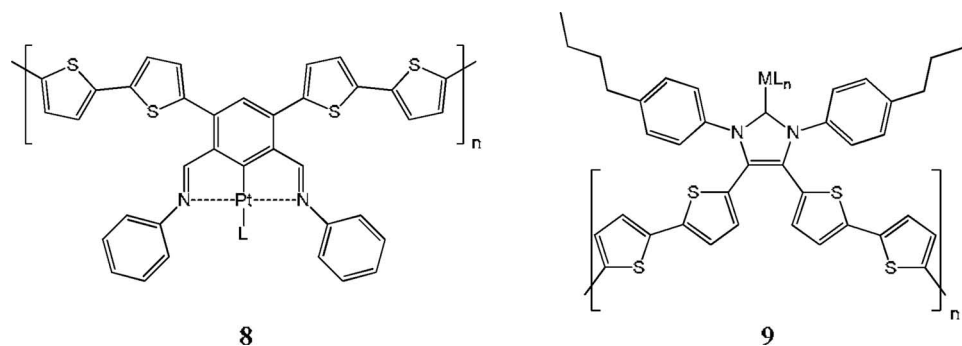


Figure 15. Electrochemically synthesized polymers featuring cyclometalated (**8**) and NHC complexes (**9**, $M = Au^I, Ag^I, Ir^I$).^[62,63]

electron-donating ligands, namely cyclometalating ligands^[60] and *N*-heterocyclic carbenes (NHCs),^[61] have gained more and more interest. A cyclometalated platinum(II) complex was electropolymerized by Holliday and co-workers to form the conducting type-II polymer **8** (Figure 15).^[62] Cowley and co-workers integrated imidazolylidene complexes of gold(I), silver(I), and iridium(I) in the electrochemically prepared polymers **9** exhibiting electrochromism.^[63]

Aiming at the electrochemical detection of copper(II) ions, Taher and Mohadesi developed a polypyrrole with incorporated 4,5-dihydroxy-3-(*p*-sulfophenylazo)-2,7-naphthalene disulfonic acid anions. The resulting film, deposited onto an electrode, was able to selectively complex copper(II) ions and, thus, to preconcentrate them on the electrode surface. Thus, the detection limit of consequent anodic stripping analysis could be lowered to $1.1 \text{ ng} \cdot \text{mL}^{-1}$ ($1.7 \times 10^{-8} \text{ mol} \cdot \text{L}^{-1}$).^[64] Based on the same concept, Moutet and co-workers prepared electrodes coated electrochemically with polymers from ((3-pyrrol-1-yl)propyl) malonic acid^[65] and 1,2-ethylene-*bis*[*N*-((3-(pyrrole-1-yl)propyl) carbamoyl)methyl]-glycine^[66] for the detection of copper(II), lead(II), cadmium(II), and mercury(II) ions (Figure 16). By this means, they could achieve detection limits of $5 \times 10^{-9} \text{ mol} \cdot \text{L}^{-1}$ (Cu^{2+}) to $5 \times 10^{-10} \text{ mol} \cdot \text{L}^{-1}$ (Pb^{2+}).

The same group synthesized poly(pyrrole-carboxylate)s containing coordinated nickel(II) ions. The polymer could be

applied for the electrocatalytic hydrogenation of ketones and enones in aqueous media providing a significant improvement of the catalytic activity compared to respective polymer anion/nickel cation hybrid materials.^[67] A (diamino-oligothiophene) palladium complex was synthesized and electropolymerized by Wolf and co-workers in order to achieve a new heterogeneous catalyst for cross-coupling reactions.^[68] Hence, the obtained polymer films could be used successfully for the catalysis of Suzuki-, Sonogashira-, and Heck-type reactions. The electrocatalytic reduction of protons to hydrogen, with an overpotential reduction of 230 mV by using electrodes coated with the electropolymerized cobalt(III) *bis*(dicarbollide) complexes **10** (Figure 17), was presented by Vicente and co-workers.^[69] Electrocatalytic oxidation of methanol was studied by Ojani et al. The authors coated the surface of a carbon paste electrode with an electrochemically synthesized poly(1,5-diaminonaphthalene) and coordinated nickel(II) ions by dipping into a nickel chloride solution. The electrochemically created nickel(III) state showed the ability to oxidize methanol.^[70]

Mono- and dinuclear ruthenium(II) carboxylate complexes possessing thiophenes were reported by the group of Aquino, but only the derivatives with bithiophene units were able to undergo anodic polymerization.^[71] Wolf and co-workers prepared gold(I) complexes bearing phosphine and acetylide ligands with terthiophene moieties, which enabled electropolymerization.^[72]

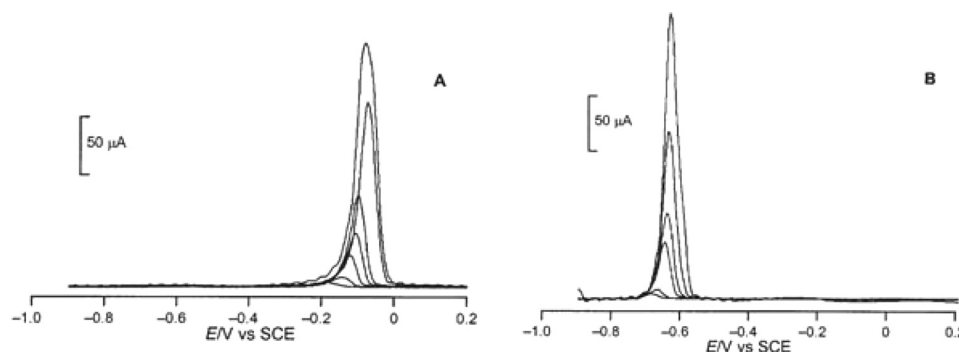


Figure 16. Square-wave voltammograms of a poly(((3-pyrrol-1-yl)propyl)malonic acid)-modified carbon disk electrode in acetate-buffered (pH 4.4) solution with different concentrations of copper(II) (A) and lead(II) (B) ions (5×10^{-8} to $5 \times 10^{-6} \text{ mol} \cdot \text{L}^{-1}$) after accumulation times of 10 min. Reproduced with permission.^[65] Copyright 2005, John Wiley and Sons.

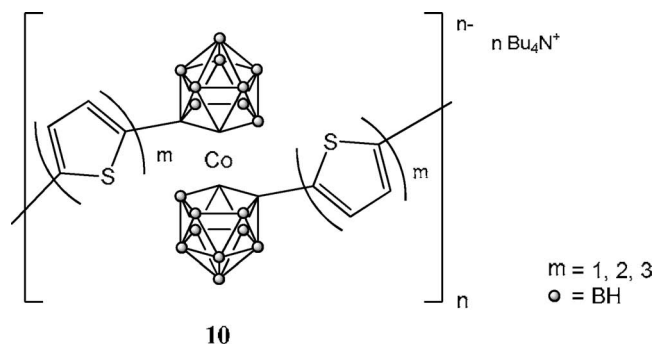


Figure 17. Cobalt(III) bis(dicarbollide) polymer **10** used for electrocatalytic proton reduction.^[69]

Gold(I) complexes of alkynethiolate ligands were synthesized by Laguna, Cerrada et al. 2-Thienyl substituents allowed the consequent electrochemical preparation of type-III polymers.^[73] An EDOT-functionalized diphenylphosphine was used to coordinate platinum(II) and palladium(II). Higgins et al. showed the electropolymerizability of the resulting complexes forming copolymers with the capability to be utilized as catalytic systems.^[74] Veith and co-workers prepared metal alcoholate complexes from tri(thiophen-2-yl)methanol with neodymium(III) and europium(III). Again, only the bithiophene species could be polymerized anodically.^[75] With regard to spin-crossover materials, an octahedral iron(II) complex possessing two thiocyanate and two *N*-((pyridin-2-yl)methylidene)-2,5-bis(thiophen-2-yl)aniline ligands was electropolymerized by Lemaire and co-workers, revealing conductivity and electrochromicity.^[76]

11. Conclusions

A broad range of metal-containing systems, including polypyridyl complexes, metallocenes, porphyrin, and salen compounds, has been incorporated into polymeric frameworks by applying electropolymerization techniques. In particular, heterogeneous catalysis using polymer-coated electrodes, optical applications (displays and solar cells), and the assembly of conducting polymer chains were in the focus of the studies discussed herein. The demonstrated pool of applicable materials based mainly on the large assortment of usable monomers, varying from the common oxidizable aromatics (thiophene, pyrrole, aniline etc.) to unusual assemblies such as metal-metal polymers or fullerene/metal polymers. Thus, the polymerization conditions can be adapted to various types of materials and proposed applications.

Hence, the future potential of electrochemically synthesized metal-containing polymers appears highly promising. In principle, almost every metal complex that needs to be processed in a thin film on an electrode surface, regarding its particular application intention, represents an appropriate candidate for the incorporation into an electropolymerized polymer. Furthermore, extended combination of different, “orthogonal” electropolymerization monomers would allow the stepwise construction of polymer networks and, thus, the formation of more defined systems.

Acknowledgements

C.F. is grateful to the Fonds der Chemischen Industrie for a PhD scholarship. Furthermore, financial support of this study by the Dutch Polymer Institute (DPI, technology area HTE), the German Federal Ministry of Education and Research (Excellence Research and Innovation in East Germany: PhoNa), and the Thüringer Ministerium für Bildung, Wissenschaft und Kultur (Grant No. B 514-09049: PhotoMic) is kindly acknowledged.

Received: September 5, 2011
Published online: December 20, 2011

- [1] a) J.-M. Savéant, *Chem. Rev.* **2008**, *108*, 2348; b) F. Bedioui, S. Griveau, T. Nyokong, A. J. Appleby, C. A. Caro, M. Gulppi, G. Ochoa, J. H. Zagal, *Phys. Chem. Chem. Phys.* **2007**, *9*, 3383.
- [2] a) A. Hagfeldt, M. Grätzel, *Acc. Chem. Res.* **2000**, *33*, 269; b) M. K. Nazeeruddin, M. Grätzel, in *Photofunctional Transition Metal Complexes*, Vol. 123 (Ed: V. W. W. Yam), Springer, Berlin **2007**, p. 113.
- [3] a) J. H. Alstrum-Acevedo, M. K. Brennaman, T. J. Meyer, *Inorg. Chem.* **2005**, *44*, 6802; b) R. Brimblecombe, G. C. Dismukes, G. F. Swiegers, L. Spiccia, *Dalton Trans.* **2009**, 9374; c) M. Wang, Y. Na, M. Gorlov, L. Sun, *Dalton Trans.* **2009**, 6458.
- [4] a) E. Holder, B. M. W. Langeveld, U. S. Schubert, *Adv. Mater.* **2005**, *17*, 1109; b) R. C. Evans, P. Douglas, C. J. Winscom, *Coord. Chem. Rev.* **2006**, *250*, 2093; c) P.-T. Chou, Y. Chi, *Chem. Eur. J.* **2007**, *13*, 380.
- [5] C. W. Rogers, M. O. Wolf, *Coord. Chem. Rev.* **2002**, *233–234*, 341.
- [6] a) M. O. Wolf, *Adv. Mater.* **2001**, *13*, 545; b) M. O. Wolf, *J. Inorg. Organomet. Polym. Mater.* **2006**, *16*, 189; c) M. O. Wolf, in *Handbook of Thiophene-Based Materials* (Eds: I. F. Perepichka, D. F. Perepichka), John Wiley & Sons, Chichester **2009**, p. 293.
- [7] a) S. Sadki, P. Schottland, N. Brodie, G. Sabouraud, *Chem. Soc. Rev.* **2000**, *29*, 283; b) K.-J. Kim, H.-S. Song, J.-D. Kim, J.-K. Chon, *Bull. Korean Chem. Soc.* **1988**, *9*, 248; c) S. Asavapiriyant, G. K. Chandler, G. A. Gunawardena, D. Pletcher, *J. Electroanal. Chem.* **1984**, *177*, 229.
- [8] a) C. P. Andrieux, P. Audebert, P. Hapiot, J.-M. Savéant, *J. Phys. Chem.* **1991**, *95*, 10158; b) J. Heinze, C. Willmann, P. Bäuerle, *Angew. Chem. Int. Ed.* **2001**, *40*, 2861.
- [9] A. F. Diaz, J. I. Castillo, J. A. Logan, W.-Y. Lee, *J. Electroanal. Chem.* **1981**, *129*, 115.
- [10] J. Heinze, H. John, M. Dietrich, P. Tschuncky, *Synth. Met.* **2001**, *119*, 49.
- [11] a) J. Heinze, in *Encyclopedia of Electrochemistry*, Vol. 8 (Eds: A. J. Bard, M. Stratmann), Wiley-VCH, Weinheim **2004**, p. 605–643; b) J. Heinze, B. A. Frontana-Urbe, S. Ludwigs, *Chem. Rev.* **2010**, *110*, 4724.
- [12] J. M. Calvert, R. H. Schmehl, B. P. Sullivan, J. S. Facci, T. J. Meyer, R. W. Murray, *Inorg. Chem.* **1983**, *22*, 2151.
- [13] a) S. Myllynen, M. Wasberg, E. Eskelinen, M. Haukka, T. A. Pakkanen, *J. Electroanal. Chem.* **2001**, *506*, 115; b) S. Myllynen, M. Wasberg, *J. Electroanal. Chem.* **2008**, *623*, 93.
- [14] V. Ruiz, Á. Colina, A. Heras, J. López-Palacios, *Electrochim. Acta* **2004**, *50*, 59.
- [15] a) T. F. Otero, E. De Larreta, *Synth. Met.* **1988**, *26*, 79; b) J. V. Sanchez, R. Diaz, P. Herrasti, P. Ocon, *Polym. J.* **2001**, *33*, 514.
- [16] M. Zhou, J. Heinze, *Electrochim. Acta* **1999**, *44*, 1733.
- [17] C. Pinheiro, A. J. Parola, F. Pina, J. Fonseca, C. Freire, *Sol. Energy Mater. Sol. Cells* **2008**, *92*, 980.
- [18] a) A. Le Goff, M. Holzinger, S. Cosnier, *Electrochim. Acta* **2011**, *56*, 3633; b) A. Okunola, B. Kowalewska, M. Bron, P. J. Kulesza, W. Schuhmann, *Electrochim. Acta* **2009**, *54*, 1954.

- [19] T. Arai, S. Sato, K. Uemura, T. Morikawa, T. Kajino, T. Motohiro, *Chem. Commun.* **2010**, 46, 6944.
- [20] a) A. Wild, A. Winter, F. Schlütter, U. S. Schubert, *Chem. Soc. Rev.* **2011**, 40, 1459; b) U. S. Schubert, A. Winter, G. R. Newkome, *Terpyridine-based Materials*, Wiley-VCH, Weinheim **2011**.
- [21] a) G. Chiericato Júnior, A. P. S. Silva, *Polyhedron* **2008**, 27, 1860; b) C. García, D. Villagra, F. Caruso, M. Rossi, B. Matsuhiro, L. Mendoza, M. J. Aguirre, M. Isaacs, *Inorg. Chem. Commun.* **2009**, 12, 392.
- [22] a) J. Hjelm, R. W. Handel, A. Hagfeldt, E. C. Constable, C. E. Housecroft, R. J. Forster, *Inorg. Chem.* **2005**, 44, 1073; b) A. Venkatanarayanan, A.-M. Spehar-Délèze, L. Dennany, Y. Pellegrin, T. E. Keyes, R. J. Forster, *Langmuir* **2008**, 24, 11233; c) J. Yang, M. Sykora, T. J. Meyer, *Inorg. Chem.* **2005**, 44, 3396; d) M. Abboud, D. Kalinina, P. G. Potvin, *Inorg. Chim. Acta* **2009**, 362, 4953; e) D. Qiu, Q. Zhao, X. Bao, K. Liu, H. Wang, Y. Guo, L. Zhang, J. Zeng, H. Wang, *Inorg. Chem. Commun.* **2011**, 14, 296; f) P. A. Dreyse, M. A. Isaacs, P. E. Iturriaga, D. A. Villagra, M. J. Aguirre, C. P. Kubiak, S. D. Glover, J. C. Goeltz, *J. Electroanal. Chem.* **2010**, 648, 98; g) M. C. E. Bandeira, J. A. Crayston, N. S. Conçalves, L. K. Noda, A. Glidle, C. V. Franco, *J. Solid State Electrochem.* **2007**, 11, 231; h) M. C. E. Bandeira, J. A. Crayston, C. V. Franco, A. Glidle, *Phys. Chem. Phys.* **2007**, 9, 1003.
- [23] a) T. W. Hesterberg, X. Yang, B. J. Holliday, *Polyhedron* **2010**, 29, 110; b) X.-Y. Chen, X. Yang, B. J. Holliday, *J. Am. Chem. Soc.* **2008**, 130, 1546; c) X. J. Zhu, B. J. Holliday, *Macromol. Rapid Commun.* **2010**, 31, 904; d) S. Dufresne, G. S. Hanan, W. G. Skene, *J. Phys. Chem. B* **2007**, 111, 11407.
- [24] a) M. Ito, T. Tsukatani, H. Fujihara, *J. Mater. Chem.* **2005**, 15, 960; b) K. Foster, T. McCormac, *Electroanalysis* **2007**, 19, 1509; c) S. Kannan, J. I. Son, J. Yang, Y.-B. Shim, *Bull. Korean Chem. Soc.* **2011**, 32, 1341.
- [25] T. J. O'Sullivan, B. Djukic, P. A. Dube, M. T. Lemaire, *Chem. Commun.* **2009**, 1903.
- [26] S. J. Howell, C. S. Day, R. E. Nofle, *Inorg. Chim. Acta* **2005**, 358, 3711.
- [27] a) S. Myllynen, M. Wasberg, M. Haukka, *J. Electroanal. Chem.* **2006**, 586, 217; b) S. Myllynen, M. Wasberg, *Electrochem. Commun.* **2009**, 11, 1453; c) F. Hartl, A. K. Renfrew, F. Lafalet, T. Mahabiersing, M. J. Calhorda, S. Chardon-Noblat, M. Haukka, A. Deronzier, *Inorg. Chem.* **2009**, 48, 8233; d) G. Gerbaud, J.-M. Mouesca, S. Hediger, S. Chardon-Noblat, F. Lafalet, A. Deronzier, M. Bardet, *Phys. Chem. Chem. Phys.* **2010**, 12, 15428; e) S. Chardon-Noblat, A. Pellissier, G. Cripps, A. Deronzier, *J. Electroanal. Chem.* **2006**, 597, 28.
- [28] F. Lafalet, S. Chardon-Noblat, C. Duboc, A. Deronzier, F. P. Pruchnik, M. Rak, *Dalton Trans.* **2008**, 2149.
- [29] S. Chardon-Noblat, A. Deronzier, F. Hartl, J. van Slageren, T. Mahabiersing, *Eur. J. Inorg. Chem.* **2001**, 613.
- [30] M. A. Vorotyntsev, S. V. Vasilyeva, *Adv. Colloid Interface Sci.* **2008**, 139, 97.
- [31] a) Ş. Özdemir, A. Balan, D. Baran, Ö. Doğan, L. Toppare, *J. Electroanal. Chem.* **2010**, 648, 184; b) Ş. Özdemir, A. Balan, D. Baran, Ö. Doğan, L. Toppare, *React. Funct. Polym.* **2011**, 71, 168; c) C. C. Chiang, H.-C. Chen, C.-s. Lee, M.-k. Leung, K.-R. Lin, K.-H. Hsieh, *Chem. Mater.* **2008**, 20, 540; d) P. D. Byrne, P. Müller, T. M. Swager, *Langmuir* **2006**, 22, 10596; e) G. E. Collis, A. K. Burrell, E. J. Blandford, D. L. Officer, *Tetrahedron* **2007**, 63, 11141.
- [32] P. D. Byrne, D. Lee, P. Müller, T. M. Swager, *Synth. Met.* **2006**, 156, 784.
- [33] M. Skompska, M. A. Vorotyntsev, J. Goux, P. Le Gendre, C. Moise, *Electrochim. Acta* **2008**, 53, 3844.
- [34] a) C. J. Fowler, J. L. Sessler, V. M. Lynch, J. Waluk, A. Gebauer, J. Lex, A. Heger, F. Zuniga-y-Rivero, E. Vogel, *Chem. Eur. J.* **2002**, 8, 3485; b) W. M. Campbell, A. K. Burrell, D. L. Officer, K. W. Jolley, *Coord. Chem. Rev.* **2004**, 248, 1363; c) I. Spasojević, I. Batinić-Haberle, *Inorg. Chim. Acta* **2001**, 317, 230.
- [35] a) M. J. Zöllner, E. Becker, U. Jahn, W. Kowalsky, H.-H. Johannes, *Eur. J. Org. Chem.* **2010**, 4426; b) M. J. Zöllner, J. S. Frähmcke, M. Elstner, U. Jahn, P. G. Jones, E. Becker, W. Kowalsky, H.-H. Johannes, *Macromol. Chem. Phys.* **2010**, 211, 359.
- [36] R. Fraga, J. P. Correia, R. Keese, L. M. Abrantes, *Electrochim. Acta* **2005**, 50, 1653.
- [37] A. S. Holmes-Smith, X. Zheng, M. Uttamlal, *Meas. Sci. Technol.* **2006**, 17, 3328.
- [38] M. Plonska, K. Winkler, S. Gadde, F. D'Souza, A. L. Balch, *Electroanalysis* **2006**, 18, 841.
- [39] A. Yavuz, B. Bezgin, L. Aras, A. M. Önal, *J. Electroanal. Chem.* **2010**, 639, 116.
- [40] M. Krompiec, S. Krompiec, I. Grudzka, M. Filapek, Ł. Skórka, T. Flak, M. Łapkowski, *Electrochim. Acta* **2011**, 56, 6824.
- [41] N. P. Rodrigues, J. Obirai, T. Nyokong, F. Bedioui, *Electroanalysis* **2005**, 17, 186.
- [42] a) P. V. Bernhardt, N. L. Kilah, *Polyhedron* **2007**, 26, 392; b) F. Mouffouk, A. Demetriou, S. J. Higgins, R. J. Nichols, *Inorg. Chim. Acta* **2006**, 359, 3491; c) K. Velauthamurthy, S. J. Higgins, R. M. G. Rajapakse, H. M. N. Bandara, M. Shimomura, *Electrochim. Acta* **2010**, 56, 326.
- [43] U. P. Azad, V. Ganesan, *Electroanalysis* **2010**, 22, 575.
- [44] W. Liu, W. Huang, M. Pink, D. Lee, *J. Am. Chem. Soc.* **2010**, 132, 11844.
- [45] a) P. G. Cozzi, *Chem. Soc. Rev.* **2004**, 33, 410; b) K. C. Gupta, A. Kumar Sutar, C.-C. Lin, *Coord. Chem. Rev.* **2009**, 253, 1926.
- [46] B. Djukic, M. T. Lemaire, *Inorg. Chem.* **2009**, 48, 10489.
- [47] a) A. Voituriez, M. Mellah, E. Schulz, *Synth. Met.* **2006**, 156, 166; b) A. Pietrangelo, B. C. Sih, B. N. Boden, Z. Wang, Q. Li, K. C. Chou, M. J. MacLachlan, M. O. Wolf, *Adv. Mater.* **2008**, 20, 2280; c) J.-L. Li, F. Gao, Y.-K. Zhang, L.-Z. He, G.-M. Han, X.-D. Wang, *Acta Phys. Chim. Sin.* **2010**, 26, 2647.
- [48] B. J. Holliday, T. B. Stanford, T. M. Swager, *Chem. Mater.* **2006**, 18, 5649.
- [49] a) D. Deletioğlu, S. Yalçinkaya, C. Demetgül, M. Timur, S. Serin, *Mater. Chem. Phys.* **2011**, 128, 500; b) T. R. L. Dadasos, M. F. S. Teixeira, *Electrochim. Acta* **2009**, 54, 4552; c) C. Demetgül, D. Deletioğlu, F. Karaca, S. Yalçinkaya, M. Timur, S. Serin, *J. Coord. Chem.* **2010**, 63, 2181.
- [50] M. L. Mejía, J. H. Rivers, S. F. Swingle, Z. Lu, X. Yang, M. Findlater, G. Reeske, B. J. Holliday, *Main Group Chem.* **2010**, 9, 167.
- [51] a) A. Zulauf, M. Mellah, R. Guillot, E. Schulz, *Eur. J. Org. Chem.* **2008**, 2118; b) M. Mellah, B. Ansel, F. Patureau, A. Voituriez, E. Schulz, *J. Mol. Catal. A: Chem.* **2007**, 272, 20.
- [52] M. L. Mejía, K. Agapiou, X. Yang, B. J. Holliday, *J. Am. Chem. Soc.* **2009**, 131, 18196.
- [53] M. L. Mejía, G. Reeske, B. J. Holliday, *Chem. Commun.* **2010**, 46, 5355.
- [54] S. V. Vasil'eva, I. A. Chepurnaya, S. A. Logvinov, P. V. Gaman'kov, A. M. Timonov, *Russ. J. Electrochem.* **2003**, 39, 310.
- [55] a) A. G. B. da Cruz, J. L. Wardell, A. M. Rocco, *J. Mater. Sci.* **2008**, 43, 5823; b) A. G. B. da Cruz, J. L. Wardell, M. V. D. Rangel, R. A. Simão, A. M. Rocco, *Synth. Met.* **2007**, 157, 80; c) A. G. B. da Cruz, J. L. Wardell, R. A. Simão, A. M. Rocco, *Electrochim. Acta* **2007**, 52, 1899; d) C. Arantes, A. M. Rocco, M. L. M. Rocco, *J. Mol. Struct.* **2010**, 969, 220.
- [56] T. Anjos, S. J. Roberts-Bleming, A. Charlton, N. Robertson, A. R. Mount, S. J. Coles, M. B. Hursthouse, M. Kalaji, P. J. Murphy, *J. Mater. Chem.* **2008**, 18, 475.
- [57] P. J. Skabara, C. Pozo-Gonzalo, N. Lardié, M. Laguna, E. Cerrada, A. Luquin, B. González, S. J. Coles, M. B. Hursthouse, R. W. Harrington, W. Clegg, *Dalton Trans.* **2008**, 3070.

- [58] K. Winkler, A. L. Balch, W. Kutner, *J. Solid State Electrochem.* **2006**, *10*, 761.
- [59] a) E. Grodzka, J. Grabowska, M. Wysocka-Żółopa, K. Winkler, *J. Solid State Electrochem.* **2008**, *12*, 1267; b) E. Grodzka, M. Nieciecka, K. Winkler, *J. Solid State Electrochem.* **2008**, *12*, 215; c) E. Grodzka, P. Pieta, P. Dłużewski, W. Kutner, K. Winkler, *Electrochim. Acta* **2009**, *54*, 5621.
- [60] M. Albrecht, *Chem. Rev.* **2009**, *110*, 576.
- [61] a) O. Schuster, L. Yang, H. G. Raubenheimer, M. Albrecht, *Chem. Rev.* **2009**, *109*, 3445; b) G. Guisado-Barrios, J. Bouffard, B. Donnadieu, G. Bertrand, *Angew. Chem. Int. Ed.* **2010**, *49*, 4759.
- [62] K. M. Milum, Y. N. Kim, B. J. Holliday, *Chem. Mater.* **2010**, *22*, 2414.
- [63] a) A. B. Powell, C. W. Bielawski, A. H. Cowley, *J. Am. Chem. Soc.* **2009**, *131*, 18232; b) A. B. Powell, C. W. Bielawski, A. H. Cowley, *J. Am. Chem. Soc.* **2010**, *132*, 10184; c) A. B. Powell, C. W. Bielawski, A. H. Cowley, *Comments Inorg. Chem.* **2010**, *31*, 75.
- [64] A. Mohadesi, M. A. Taher, *Anal. Sci.* **2007**, *23*, 969.
- [65] M. Heitzmann, L. Basaez, F. Brovelli, C. Bucher, D. Limosin, E. Pereira, B. L. Rivas, G. Royal, E. Saint-Aman, J.-C. Moutet, *Electroanalysis* **2005**, *17*, 1970.
- [66] M. Heitzmann, C. Bucher, J.-C. Moutet, E. Pereira, B. L. Rivas, G. Royal, E. Saint-Aman, *Electrochim. Acta* **2007**, *52*, 3082.
- [67] T. Melki, A. Zouaoui, B. Bendemagh, I. M. F. de Oliveira, G. F. de Oliveira, J.-C. Leprêtre, C. Bucher, J.-C. Moutet, *J. Braz. Chem. Soc.* **2009**, *20*, 1523.
- [68] a) V. G. Albano, M. Bandini, C. Moorlag, F. Piccinelli, A. Pietrangelo, S. Tommasi, A. Umani-Ronchi, M. O. Wolf, *Organometallics* **2007**, *26*, 4373; b) M. Bandini, A. Pietrangelo, R. Sinisi, A. Umani-Ronchi, M. O. Wolf, *Eur. J. Org. Chem.* **2009**, 3554.
- [69] B. Fabre, E. Hao, Z. M. Lejeune, E. K. Amuhaya, F. Barrière, J. C. Garno, M. G. H. Vicente, *Appl. Mater. Interface* **2010**, *2*, 691.
- [70] R. Ojani, J. B. Raoof, S. R. H. Zavvarmahalleh, *Electrochim. Acta* **2008**, *53*, 2402.
- [71] A. H. Murray, Z. Yue, A. I. Wallbank, T. S. Cameron, R. Vadavi, B. J. MacLean, M. A. S. Aquino, *Polyhedron* **2008**, *27*, 1270.
- [72] A. M. Kuchison, M. O. Wolf, B. O. Patrick, *Inorg. Chem.* **2010**, *49*, 8802.
- [73] N. Lardiés, I. Romeo, E. Cerrada, M. Laguna, P. J. Skabara, *Dalton Trans.* **2007**, 5329.
- [74] K. Velauthamurthy, S. J. Higgins, R. M. G. Rajapakse, J. Bacsá, H. vanZalinge, R. J. Nichols, W. Haiss, *J. Mater. Chem.* **2009**, *19*, 1850.
- [75] M. Veith, C. Belot, V. Huch, H. L. Cui, L. Guyard, M. Knorr, C. Wickleder, *Eur. J. Inorg. Chem.* **2010**, 879.
- [76] B. Djukic, T. Seda, S. I. Gorelsky, A. J. Lough, M. T. Lemaire, *Inorg. Chem.* **2011**, *50*, 7334.

Publication A2: “ π -Conjugated 2,2':6',2''-bis(terpyridines):
Systematical tuning of the optical properties by variation of
the linkage between the terpyridines and the π -conjugated
system”

Andreas Wild, Christian Friebe, Andreas Winter, Martin D. Hager,
Ulrich-Walter Grummt, Ulrich S. Schubert

Eur. J. Org. Chem. **2010**, 1859–1868.

Reprinted with permission from: WILEY-VCH Weinheim (Copyright 2010)

π -Conjugated 2,2':6',2''-Bis(terpyridines): Systematical Tuning of the Optical Properties by Variation of the Linkage between the Terpyridines and the π -Conjugated System

Andreas Wild,^[a,b] Christian Friebe,^[a] Andreas Winter,^[b,c] Martin D. Hager,^[a,b]
Ulrich-Walter Grummt,^[d] and Ulrich S. Schubert^{*[a,b,c]}

Keywords: Conjugation / Supramolecular chemistry / UV/Vis spectroscopy / Density functional calculations

2,2':6',2''-Terpyridines bearing well-defined π -conjugated substituents at the 4'-position are known to exhibit interesting electronic and optical properties. The systematic variation of both the spacer unit and the linker in conjugated bis(terpyridines) has resulted in a library of π -conjugated systems, enabling the study of the structure–property relationships of these materials. We have proven the Huisgen 1,3-dipolar cycloaddition reaction to be a versatile tool for connecting conjugated systems, even though the conjugation is hindered by the introduced triazole moiety. All the terpyrid-

ine derivatives were fully characterized by ¹H and ¹³C NMR spectroscopy, UV/Vis absorption and emission measurements as well as MALDI-TOF MS. Thin films of the materials were produced by spin-coating and subsequently characterized. Because tuning of the band gap of the materials over a wide range is possible, quantum yields of up to 85 % and extinction coefficients of around 100000 M⁻¹cm⁻¹ could be observed, the compounds might be promising candidates for the design of new functional supramolecular materials.

Introduction

In recent years there has been an enormous growth of interest in the field of supramolecular architectures consisting of small molecules held together by weak, reversible, non-covalent interactions.^[1,2] Oligopyridyl ligands and their transition-metal complexes, which have found applications in several areas of modern research, are examples of such systems.^[3–13] 2,2':6',2''-Terpyridines bearing well-defined π -conjugated substituents at the 4'-position are known to exhibit attractive electronic and optical properties.^[6,8,10,14–25] When two 2,2':6',2''-terpyridine units are introduced at either end of a rigid conjugated spacer, the resulting ditopic bis(terpyridine) ligand enables the synthesis of metallo-supramolecular polymers by coordination with different metal ions. Several publications dealing with the synthesis and characterization of such conjugated terpyrid-

ine systems have recently been published, but the spacer and/or connecting units utilized were generally not varied significantly nor in any systematic way.^[6,15,17,26,27] To enable the preparation of metallo-polymers exhibiting absorption over a wide range of the visible spectrum, we aimed to tune the band gap of our systems in an easy and systematic manner. The exchange of a phenyl moiety of the conjugated substituent by, for example, an anthracene or fluorene, enables the variation of the absorption of the derived terpyridyl system over a range of more than 100 nm. But not only the type of spacer unit affects the photophysical properties of these materials, but also the linker connecting the spacer to the terpyridine units, required for later introduction into supramolecular assemblies. This allows the synthesis of materials that show tailor-made optical properties. As a continuation of previous work in the field of π -conjugated terpyridines and their applications in supramolecular chemistry,^[27–29] in which we synthesized systems with different geometries^[30,31] and introduced the Huisgen reaction to the field of conjugated terpyridines,^[32] we have studied the effect of the systematic variation of both the spacer unit and the linker in conjugated bis(terpyridines). This should allow the elucidation of selected structure–property relationships of these materials. Furthermore, the knowledge gained by this investigation will facilitate the synthesis of materials that show tailor-made properties for applications in organic light-emitting diodes (OLEDs) and photovoltaic (PV) devices. This can be achieved by using a defined ratio of monomers showing complementary absorption spectra in combination with suitable transition-metal ions.

[a] Laboratory of Organic and Macromolecular Chemistry, Friedrich-Schiller-University Jena, Humboldtstr. 10, 07743 Jena, Germany
Fax: +49-3641-9482-02
E-mail: ulrich.schubert@uni-jena.de
www.schubert-group.com

[b] Dutch Polymer Institute (DPI), P. O. Box 902, 5600 AX Eindhoven, The Netherlands

[c] Laboratory of Macromolecular Chemistry and Nanoscience, Eindhoven University of Technology, P. O. Box 513, 5600 MB Eindhoven, The Netherlands

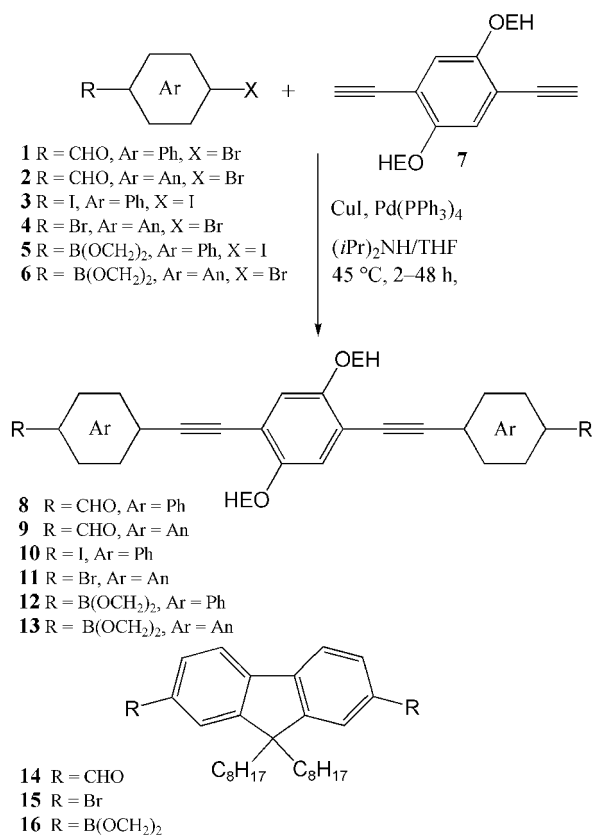
[d] Institute of Physical Chemistry, Friedrich-Schiller-University Jena, Lessingstr. 10, 07743 Jena, Germany

Supporting information for this article is available on the WWW under <http://dx.doi.org/10.1002/ejoc.200901112>.

Results and Discussion

Synthesis of Bis(terpyridines)

To investigate the influence of the electron-rich aromatic systems anthracene (**9**, **11** and **13**) and fluorene (**14**–**16**) as part of the π -conjugated system in bis(terpyridines) and to determine differences with their phenyl-containing counterparts (**8**, **10** and **12**), we initially synthesized the different conjugated spacer units by the approach shown in Scheme 1. The use of branched 2-ethylhexyl (EH) alkyl chains lead to soluble products, despite their linear and stiff geometry. By choosing different end-group functionalities we were able to investigate the effect of the connecting unit between the spacer and the terpyridine moiety. The general reaction scheme for the synthesis of the bis(terpyridines) **T8**–**T16** by linking functionalized 4'-phenyl-2,2':6',2''-terpyridines **17** and **18** to the spacer units **8**–**16** is shown in Figure 1.



Scheme 1. Schematic representation of the structures and synthesis of the spacer units **8**–**16**.

By using halogen end-groups, the systems were coupled to a terpyridine derivative bearing an ethynyl functionality (**17**) by Sonogashira reaction to yield the conjugated bis(terpyridines) **T10**, **T11** and **T15**. The Huisgen 1,3-dipolar cycloaddition reaction^[33] under Cu^I catalysis, one of the so-called “click” reactions,^[34–38] was used to connect the terpyridine and the spacer in the cases of compounds **T12**, **T13** and **T16**. Again, **17** was used and “clicked” to the diazides of the aromatic systems synthesized in situ from the glycol

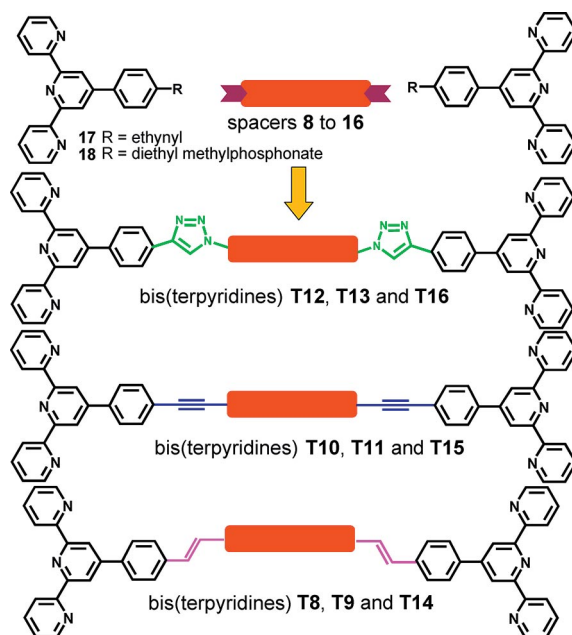


Figure 1. Schematic representation of the conversion of the conjugated spacer units **8**–**16** to bis(terpyridines) **T8**–**T16**.

boronates **12**, **13** and **16**.^[39] These reactions were performed in a two-step one-pot procedure by first forming the azide at room temperature and then performing the Huisgen reaction at 100 °C using microwave heating. It was shown that both reactions can be carried out at room temperature, but under these conditions longer reaction times were required. Finally, the spacer was connected to the terpyridines through a C=C double bond by Horner–Wadsworth–Emmons (HWE) condensation of dialdehydes **8**, **9** or **14** with a phosphonate-functionalized terpyridine (**18**)^[27] to yield the systems **T8**, **T9** and **T14**.

All the terpyridine derivatives shown in this contribution were fully characterized by ¹H and ¹³C NMR spectroscopy, absorption and emission spectroscopy in dilute solutions and as thin films as well as by MALDI-TOF mass spec-

Table 1. Synthesis of the bis(terpyridines) **T8**–**T16**.^[a]

| Code | Spacer | Linker | Yield [%] |
|------------|--------|--------------------|-----------|
| T8 | | double bond | 79 |
| T10 | | triple bond | 77 |
| T12 | | 1,2,3 triazol-4-yl | 54 |
| T9 | | double bond | 87 |
| T11 | | triple bond | 72 |
| T13 | | 1,2,3 triazol-4-yl | 44 |
| T14 | | double bond | 79 |
| T15 | | triple bond | 81 |
| T16 | | 1,2,3 triazol-4-yl | 74 |

[a] Experimental details are given in the Supporting Information.

trometry. Additionally, several spacer and ligand systems were investigated by temperature-dependent absorption spectroscopy. Table 1 provides an overview of the synthesized systems, their spacer and linker units and the isolated yields.

Photophysical Properties

The photophysical properties of the π -conjugated terpyridines were investigated in detail by absorption and emission spectroscopy in solution (Table 2). In addition, we prepared thin films of the materials by spin-coating to study the optical properties in the solid state. Figure 2 shows the absorption and emission spectra of the phenyl-containing bis(terpyridines) **T8**, **T10** and **T12**, connected to the spacer units through a double bond, triple bond and 1*H*-1,2,3-triazole, respectively, and illustrates the effect of the conjugated linker. As also summarized in Table 2, the longest-wavelength absorption maximum shows a constant bathochromic shift of around 7 nm on going from the conjugated spacer unit without terpyridines (**10**, $\lambda_{\text{abs}} = 377$ nm) to the triazole-connected system (**T12**, $\lambda_{\text{abs}} = 384$ nm), the triple bond linked (**T10**, $\lambda_{\text{abs}} = 392$ nm) and the system containing the double bond (**T8**, $\lambda_{\text{abs}} = 399$ nm). The molar extinction coefficient increases in the same way. It has been proven by DFT calculations and experiments that a double bond next to a terpyridine unit leads to a higher degree of conjugation than in the case of a triple bond.^[40–42] This general trend can be verified by the experimental values reported herein. The fluorescence spectra show a strong $S_{10} \rightarrow S_{00}$ transition and a $S_{10} \rightarrow S_{01}$ transition as a shoulder. The emission maxima exhibit the same general trends as the absorption maxima.

Table 2. Selected photophysical properties of compounds **10**, **11**, **15** and **T8–T16** in dilute solution (10^{-6} M in CHCl_3 , 25 °C).

| Code | λ_{abs} [nm] | ϵ [$\text{M}^{-1} \text{cm}^{-1}$] | λ_{PL} [nm] | $\Phi_{\text{PL}}^{\text{[a]}}$ |
|------------|-----------------------------|---|----------------------------|---------------------------------|
| 10 | 377 | 38000 | 418 | 0.70 |
| T8 | 399 | 100700 | 450 | 0.85 |
| T10 | 392 | 77400 | 438 | 0.75 |
| T12 | 384 | 56400 | 424 | 0.77 |
| 11 | 477 | 44200 | 500 | 0.73 |
| T9 | 478 | 99700 | 545 | 0.12 |
| T11 | 503 | 45400 | 553 | 0.25 |
| T13 | 482 | 51200 | 510 | 0.72 |
| 15 | 315 | 30800 | 330 | 0.24 |
| T14 | 399 | 98900 | 444 | 0.88 |
| T15 | 369 | 91200 | 404 | 0.77 |
| T16 | 328 | 89300 | 378 | 0.55 |

[a] Absolute fluorescence quantum yield.

Within this series, the quantum yield in solution is the highest for the double-bond-containing bis(terpyridine) **T8** ($\Phi_{\text{PL}} = 0.85$). Because no other structural parameters have been changed, the changes in optical properties can be unambiguously explained by the different linker units. The value of the absorption maximum is an indication of the conjugation length of the systems studied. Therefore, the surprisingly small bathochromic shift observed for **T12**

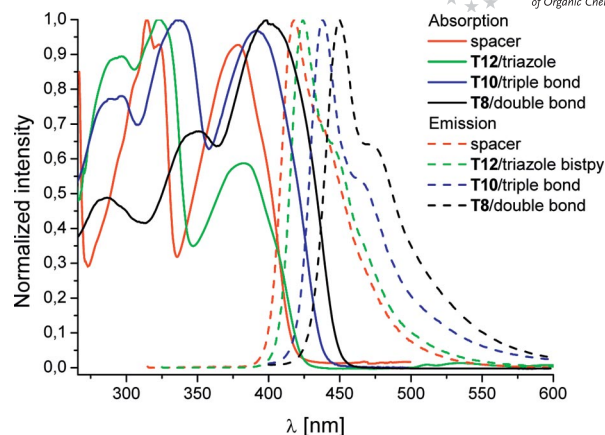


Figure 2. Normalized absorption and emission spectra of terpyridines **T8**, **T10** and **T12** and the spacer **10**. For all measurements: CHCl_3 , 10^{-6} M, 25 °C.

compared with the spacer **10** can be explained by a non-optimal conjugation through the 1*H*-1,2,3-triazole moiety. This assumption was confirmed by calculations and will be described in the Calculations section of this contribution in detail (see below). In the cases of **T10** and **T8**, the intensities of the longest wavelength bands also increase significantly compared with the one around $\lambda_{\text{abs}} = 320$ –350 nm, which can be confirmed by the extinction coefficients (Table 2).

This trend can also be seen for the fluorene-containing bis(terpyridine) systems **T14–T16** (Figure 3, Table 2). In these systems no torsion is possible in the spacer unit itself and, therefore, all changes in the geometry have to occur in the connecting unit. Compared with the fluorene spacer unit (**15**), the longest-wavelength absorption maximum of the system connected by two triazole units (**T16**) is shifted by 13 nm. The introduction of a triple (**T15**, $\lambda_{\text{abs}} = 369$ nm, $\lambda_{\text{PL}} = 404$ nm) or a double bond (**T14**, $\lambda_{\text{abs}} = 399$ nm, $\lambda_{\text{PL}} = 444$ nm) leads to the expected redshift in the absorption and emission.

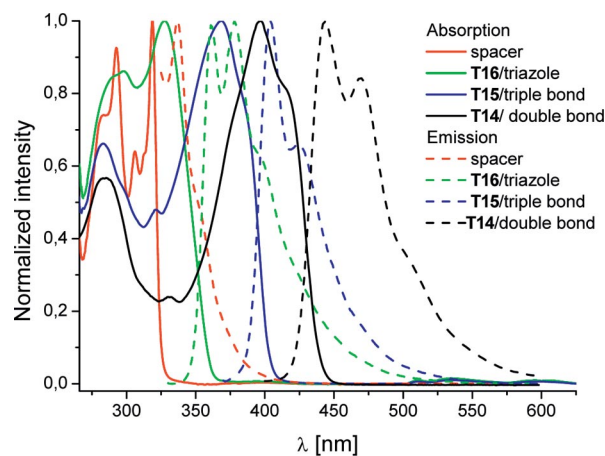


Figure 3. Normalized absorption and emission spectra of the spacer **15** and the bis(terpyridines) **T14–T16**. For all measurements: CHCl_3 , 10^{-6} M, 25 °C.

When comparing the spectra of the anthracene-containing systems with each other, it is obvious that the spacer unit **11** ($\lambda_{\text{abs}} = 477$ nm), the triazole- (**T13**) ($\lambda_{\text{abs}} = 482$ nm) and double-bond- (**T9**) ($\lambda_{\text{abs}} = 478$ nm)-connected systems exhibit absorption maxima in the same region, but for different reasons. The connection of a triazole to the anthracene unit also leads, in addition to the electronic situation previously discussed for **T12** and **T16**, to decreased conjugation due to steric hindrance. We have calculated that the interaction between the hydrogen atoms at the 1- and 8-positions of the anthracene and the triazole leads to an energetic minimum at a dihedral angle of around 85° .

It has already been shown in the case of PPE/PPV-type polymers that a double bond connected to an anthracene unit at the 9- or 10-position leads to a torsion and, thereby, hindered conjugation in the ground state.^[43] This assumption was confirmed by analysing the emission spectra. Systems **11** ($\Delta v_{\text{af}} = 1000$ cm^{-1}) and **T13** ($\Delta v_{\text{af}} = 1100$ cm^{-1}) exhibit small Stokes shifts, whereas **T9** ($\Delta v_{\text{af}} = 2600$ cm^{-1}) shows a clearly larger shift as well as a remarkably low quantum yield and an unstructured emission band, which can be explained by the planarization of the conjugated system in the excited state and thus a large geometrical rearrangement. Consequently, steric effects are absent in the excited state, but electronic effects still hinder full conjugation in the case of **T13**. When the spacer unit is connected by triple bonds to the terpyridines (**T11**), the absorption is shifted to $\lambda_{\text{abs}} = 503$ nm as no steric or electronic effects hinder the conjugation in this case. As expected, the emission maximum appears in the same region as for **T9** (Figure 4).

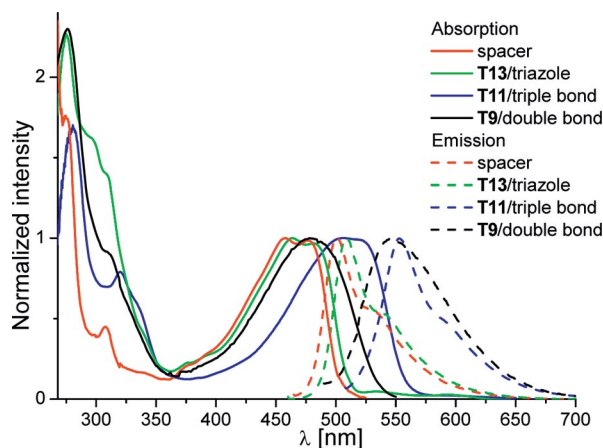


Figure 4. Normalized absorption and emission spectra of the spacer **11** and the bis(terpyridines) **T9**, **T11** and **T13**. For all measurements: CHCl_3 , 10^{-6} M, 25°C .

The photophysical properties were also investigated in the solid state. In particular, the fluorene-containing bis(terpyridines) **T14–T16** were chosen because of their good solubility and film-forming properties. Thin films were prepared by spin-coating onto glass slides from solutions of 10 mg/mL of the respective compound in chlorobenzene. The absorption and emission data obtained are summarized in

Figure 5 and Table 3. A comparison of the data for dilute solutions and the solid state show that the absorption properties remain in principle the same: only small shifts of $220\text{--}460$ cm^{-1} were observed (Table 3). In contrast, the solid-state emission spectra exhibit large bathochromic shifts of $3725\text{--}5300$ cm^{-1} in comparison with the solution spectra. Additional shoulders are observed on the short-wavelength side of the luminescence bands, which exhibit energy differences of $740\text{--}830$ cm^{-1} compared with the solution emission maxima. Moreover, the photoluminescence quantum yields Φ_{PL} show a notable decrease from 0.88, 0.77 and 0.55 in

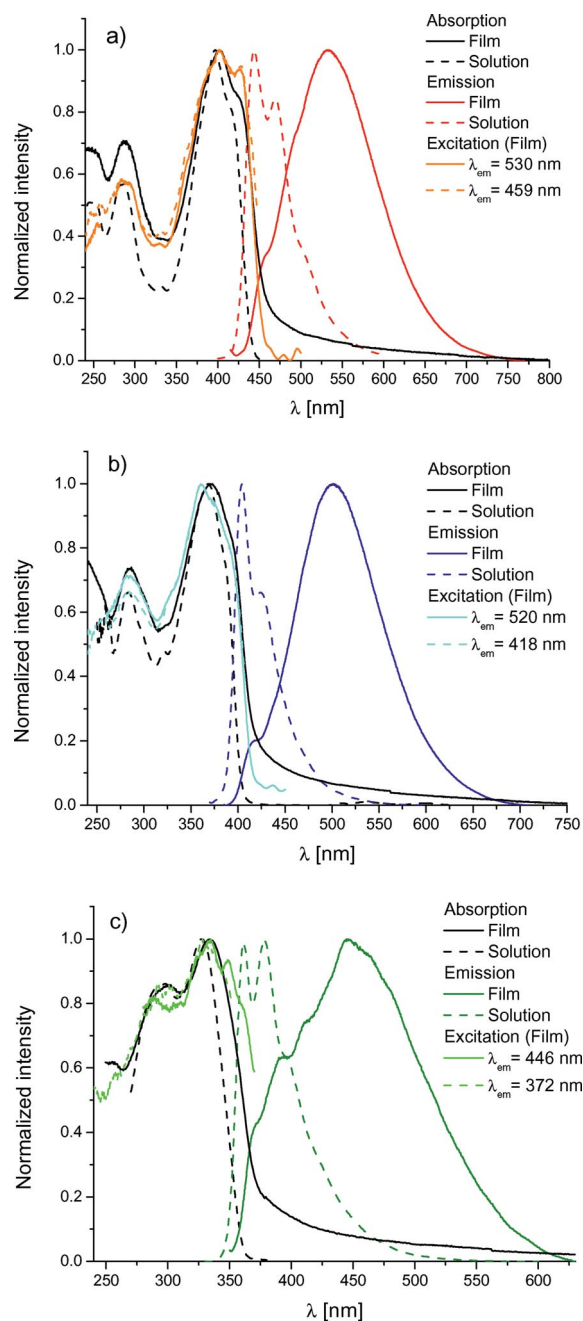


Figure 5. UV/Vis absorption, emission and excitation spectra of a) **T14**, b) **T15** and c) **T16** in solution (10^{-6} M in CHCl_3 , 25°C) and as thin films.

solution to 0.14, 0.26 and 0.07 in the films, respectively. This behaviour can be explained by the formation of excimers (or larger aggregated excited species), as described in the literature.^[44] In this process an excited species forms a dimeric system with a non-excited one. Because excimers mostly possess cofacial sandwich-type configurations, the planar π -conjugated systems presented in this work are pre-eminently suited to form such species. Excimer formation leads to the appearance of an additional emission band that is both redshifted and unstructured (as can be observed in Figure 5) as well as to rapidly decreased photoluminescence quantum yields. The observed short-wavelength shoulders, which can be attributed to monomer emission, and the fact that excitation spectra with different emission wavelengths remain in principle constant support our assumption of excimer formation. In addition, the formation of excimers seems to be strongly dependent on film morphology; although different thin-film samples were prepared in the same way, they show slightly different intensity ratios between excimer and monomer emissions.

Table 3. Photophysical properties of compounds **T14–T16** in dilute solution (10^{-6} M in CHCl_3 , 25 °C) and as thin films.

| | λ_{abs} [nm] | | λ_{PL} [nm] | | Φ_{PL} [a] | |
|------------|-----------------------------|------|----------------------------|---------------------|------------------------|------|
| | Solution | Film | Solution | Film ^[b] | Solution | Film |
| T14 | 397 | 401 | 442 | 532, 457s | 0.88 | 0.14 |
| T15 | 368 | 371 | 404 | 500, 418s | 0.77 | 0.26 |
| T16 | 327 | 332 | 378, 360 | 445, 390s, 371s | 0.55 | 0.07 |

[a] Absolute fluorescence quantum yield. [b] s: short-wavelength shoulder.

Calculations

All the bis(terpyridines) described in this paper may be regarded as more or less conjugated multichromophoric π systems. The π conjugation may not extend over the entire molecule, but may be disturbed by torsional disorder and also by potential sinks within the chain. Standard quantum chemical calculations were performed in order to interpret the spectroscopic findings, to localize the essential chromophores and to identify rotational disorder. Density functional theory at the B3LYP/6-31g(d) level of theory was applied to all full geometry optimizations using the GAUSSIAN03 program package.^[45] For computational ease, the 2-ethylhexyloxy substituents and the octyl substituents in the fluorene-containing compounds were replaced by hydroxy groups and hydrogen atoms, respectively. Electronic transitions were calculated with the help of time-dependent density functional theory implemented in the same package. From an inspection of the frontier orbitals we may draw a series of qualitative conclusions, although the HOMO/LUMO configuration interaction (CI) coefficients for the S_1 state are only close to 0.66 throughout.

The π system of the terminal phenylterpyridine moiety is only negligibly involved in the frontier orbitals of **T10–T13**. The triazole units of **T12** and **T13** do not contribute to the frontier orbitals either (see also Figure 6).

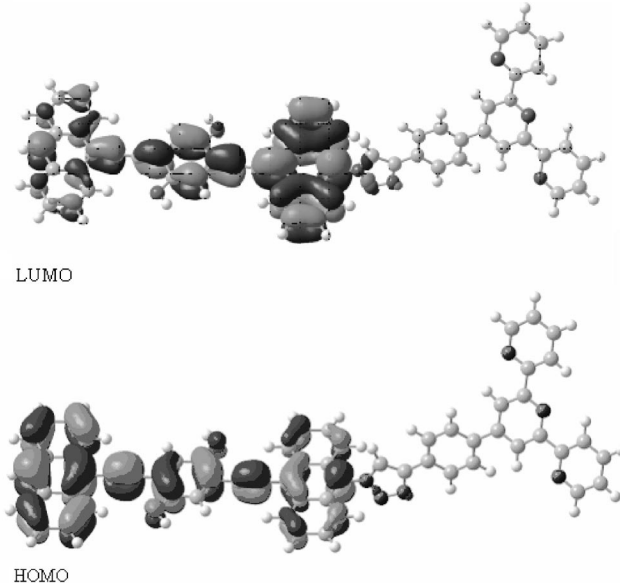


Figure 6. Representation of the LUMO (top) and HOMO (bottom) of **T13**.

In other words, the chromophores of **T12** and **T13** can be identified as the spacer unit consisting of three arylenes linked by two ethynylene moieties. The same conclusion has to be drawn from a pairwise comparison of the absorption and emission spectra of the bis(terpyridine) with the corresponding spacer molecule (i.e., **T12/8** and **T13/9**). With the vinylene-linked bis(terpyridines) **T8** and **T9**, the HOMO extends well into the phenylene ring adjacent to the terpyridine and even the π orbitals of the middle pyridine rings are involved in the LUMO.^[46] This part of the π system is essentially flat in the case of **T8**. In **T9**, steric hindrance between the vinylene protons and two anthracene protons causes a tilt of about 70° between the planes of the anthracene and the phenylene moieties, as determined by structure optimization. Nevertheless, mediated by the vinylene moiety, conjugation also extends to the middle pyridine rings. The planes of the central part of the linker and the terpyridine are essentially perpendicular to each other. As a result of the larger size of the LUMO, one might expect some symmetric charge transfer from the centre of the molecules to the periphery. With the fluorene-containing bis(terpyridines) **T14** and **T15**, the frontier orbitals include the phenylene rings attached to the middle pyridine ring. The π system is essentially flat and the triazole moieties in **T16** do not interrupt the conjugation (Figure 7). The middle pyridine rings of **T14** and **T15** contribute significantly more to the LUMOs than to the HOMOs. Again, we can conclude that some symmetric charge transfer occurs from the centre of the molecules to the periphery upon excitation.

In addition, we recorded absorption spectra at low temperatures. The data have been interpreted by exemplarily comparing the calculated and experimental positions of the longest wavelength transitions of **T13** and its spacer unit **13**. When comparing the theoretical results ($\lambda_{\text{max}} = 551$ nm;

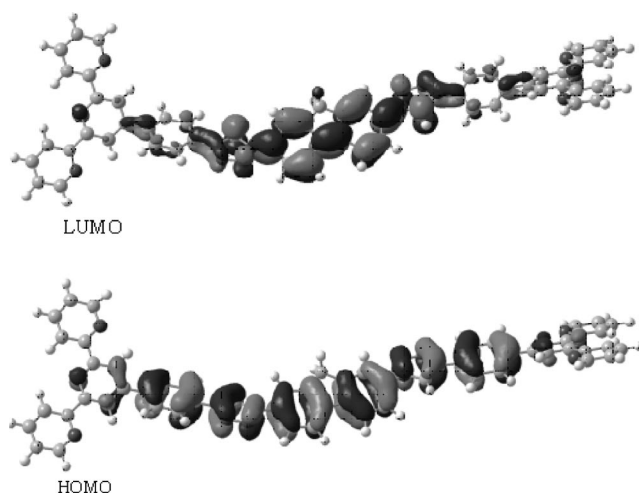


Figure 7. Representation of the LUMO (top) and HOMO (bottom) of **T16**.

oscillator strength of 1.362) with the experimental ones ($\lambda_{\text{max}, 20\text{ }^\circ\text{C}} = 482\text{ nm}$, $\lambda_{\text{max}, -200\text{ }^\circ\text{C}} = 502\text{ nm}$), we have to take into consideration the fact that theory only predicts transitions for the ideal structure whereas the experiment at room temperature in solution gives an average ensemble of strongly torsionally disordered systems. Hence, the low-temperature spectra of samples with partially frozen tor-

sional motion compare significantly better with the computational model. An example of the thermochromism is presented in Figure 8. Furthermore, it is well known that DFT underestimates the energy difference between the S_1 and S_0 states for large extended π systems.^[47]

Because the temperature-dependent spectra of the spacer **13** and the corresponding bis(terpyridine) **T13** are nearly the same we have to conclude that the torsional disorder is caused by the ethynylene links. The very different internal torsional barriers of 9-(triazol-4'-yl)anthracene and (triazol-4'-yl)benzene, calculated as 54 and 17.5 kJ/mol, respectively, apparently have only a negligible influence on the overall spectra. The spectral behaviour, including fluorescence, closely resembles the findings with arylene-ethynylene/arylene-vinylene copolymers and their low-molecular-mass model compounds, which have recently been reviewed.^[48]

Conclusions

In this contribution we have described the synthesis of a series of bis(terpyridines) containing phenyl, anthracene and fluorene systems. To be able to compare the results of a photophysical study of these compounds in detail we varied both the spacer unit as well as the connecting unit between the spacer and the terpyridine moiety in a systematic manner. In this way we found that 1*H*-1,2,3-triazole is invaluable for the connection of conjugated systems under mild conditions at room temperature. As a result of the non-optimal conjugation through this connecting unit, the resulting ligands exhibit the most hypsochromic-shifted absorption maxima. Through DFT calculations we have proven this explanation and also shown the fluorene system to be able to overlap with the p orbital of the tertiary nitrogen atom of the triazole and therefore extend the conjugation, which is also confirmed by the absorption spectra. A comparison of the absorption spectra of the systems studied herein with the same conjugated backbone shows the possibility of tuning the absorption maximum over a range of about 80 nm by just varying the connecting unit. In addition, the emission colour could easily be changed, which is an important consideration when aiming to synthesize ligands with potential applications as emitting layers in LED devices. The thin films of the ligands showed a very high tendency towards excimer formation and thus broad emission spectra and high Stokes shifts. Thus, this approach allows the synthesis of materials with tailor-made optical properties. Moreover, the corresponding metal complexes may be used for the construction of OLEDs and solar cells (for the first results of a study in this direction see, for example, ref.^[49]).

Experimental Section

Materials: All reagents were purchased from commercial sources and were used without further purification unless specified. Solvents were dried and distilled according to standard procedures.

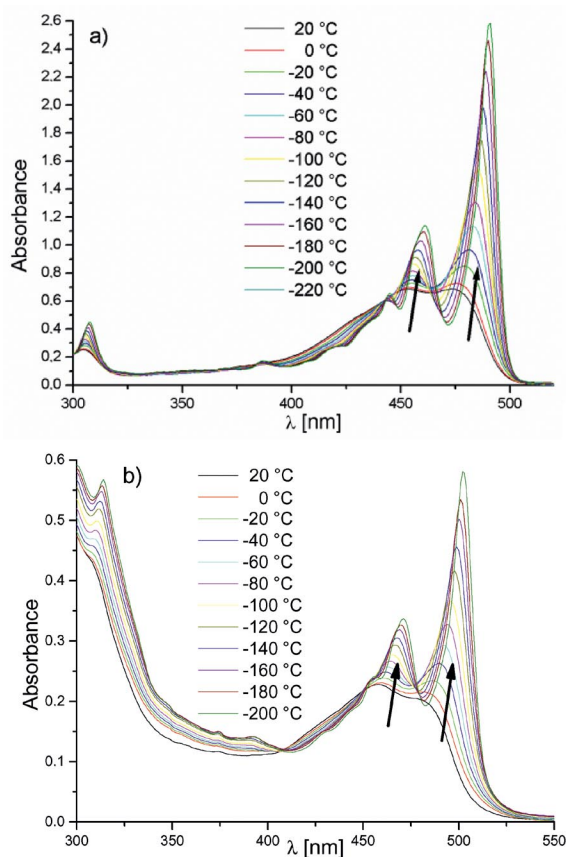


Figure 8. Temperature-dependent absorption spectra of a) **13** and b) **T13** 10^{-5} to 10^{-6} M in 2-methyltetrahydrofuran.

Unless otherwise specified, solvents or solutions were degassed by bubbling with argon 1 h prior to use. Compounds **2**, **7**, **14–18**, **T14** and **T15** were prepared following previously published protocols.^[17,27,43] All the terpyridine derivatives were purified by flash column chromatography (neutral alumina, CH₂Cl₂/MeOH as eluent) or preparative size-exclusion chromatography (BioBeads[®] S-X5, toluene as eluent). The commercially available boronic acids **5** and **6** were converted into the corresponding ethylene glycol boronate by heating with ethylene glycol at reflux in toluene.

Instrumentation: ¹H and ¹³C NMR spectra were obtained in deuterated chloroform at 25 °C using a Bruker DRX 400 or AC 250 instrument. UV/Vis absorption spectra were recorded in dilute CHCl₃ solutions with a Analytik Jena SPECORD 250 spectrometer. Emission spectra were measured with a Jasco FP-6500 spectrometer. Absolute quantum yields were determined by using a Hamamatsu C 10027 Photonic Multi-Channel Analyzer. UV/Vis absorption spectra of spin-coated films were obtained using a Perkin–Elmer UV/Vis/NIR Lambda 19 spectrometer; the emission data were recorded with a Hitachi F-4500 fluorescence spectrometer. MALDI-TOF mass spectra were obtained with an Ultraflex III TOF/TOF mass spectrometer with dithranol as matrix in reflector mode. Elemental analyses were carried out with a CHN-932 Auto-matic Leco instrument.

Synthesis of the π -Conjugated Spacer Units by Sonogashira Reaction: The aryl halide **1**, **2**, **5** or **6** (6.3 mmol) was dissolved in a mixture of THF (20 mL) and diisopropylamine (10 mL). CuI (23 mg, 0.12 mmol) and [Pd(PPh₃)₄] (139 mg, 0.12 mmol) were added and the mixture was heated to 45 °C. A degassed solution of **7** (1.15 g, 3 mmol) in THF (10 mL) was added dropwise. The reaction mixture was stirred at 45 °C for 2–48 h. After cooling, the precipitate was removed by filtration. The solvent was then removed and the residue was redissolved in CHCl₃, washed with a sat. NH₄Cl solution and water, dried with MgSO₄ and the solution concentrated. In the case of aryl halides **4** and **5** a larger excess (15 mmol) was used to avoid polycondensation. Owing to their instability towards water, the spacer units **12** and **13** were not washed with water.

4,4'-[2,5-Bis(2-Ethylhexyloxy)-1,4-phenylene]bis(ethynediyl)-dibenzaldehyde (8**):** The reaction of 4-bromobenzaldehyde (**1**; 1.17 g, 6.3 mmol) and 1,4-bis(2-ethylhexyloxy)-2,5-diethynylbenzene (**7**; 1.15 g, 3 mmol) was carried out according to the general procedure. The crude product was purified by column chromatography (silica gel, toluene/heptane, 5:1) and recrystallization from acetone to yield **8** as a yellow substance (1.31 g, 74%). ¹H NMR (250 MHz, CDCl₃): δ = 10.02 (s, 2 H, CHO), 7.87 (AA', 4 H), 7.66 (XX', 4 H), 7.04 (s, 2 H, C_{phenyl}-H), 3.94 (d, ³J = 5.5 Hz, 2 H, OCH₂), 1.80 (m_c, ³J = 6.1 Hz, 2 H, CH), 1.67–1.23 (m, 16 H, CH₂), 0.99 (t, ³J = 7.4 Hz, 6 H, ethyl-CH₃), 0.90 (t, ³J = 6.9 Hz, 6 H, hexyl-CH₃) ppm. ¹³C NMR (62.9 MHz, CDCl₃): δ = 191.32 (CHO), 154.06 (C_{phenyl}-OR), 135.41, 131.96, 129.72, 129.57, 116.52, 113.84 (C_{phenyl}), 94.18, 90.12 (C \equiv C), 71.97 (OCH₂), 39.62 (CH), 30.87, 30.68, 29.14, 24.02, 23.05 (CH₂), 14.05 (ethyl-CH₃), 11.27 (hexyl-CH₃) ppm. MS (MALDI-TOF, dithranol): m/z = 591.36 [M + H]⁺. C₄₀H₄₆O₄ (590.79): calcd. C 81.32, H 7.85; found C 81.38, H 7.80.

10,10'-[2,5-Bis(2-ethylhexyloxy)-1,4-phenylene]bis(ethynediyl)-dianthracene-9-carbaldehyde (9**):** The reaction of 9-bromoanthracene-10-carbaldehyde (**2**; 1.80 g, 6.3 mmol) and **7** (1.15 g, 3 mmol) was carried out according to the general procedure. The crude product was purified by column chromatography (silica gel, CHCl₃) to yield **9** a red substance (759 mg, 32%). ¹H NMR (400 MHz, CDCl₃): δ = 11.56 (s, 2 H, CHO), 8.97 (dd, 4 H), 7.73

(m_c, 4 H), 7.36 (s, 2 H, C_{phenyl}-H), 4.18 (d, ³J = 5.6 Hz, 4 H, OCH₂), 2.03 (m_c, 2 H, CH), 1.80–1.26 (m, 16 H, CH₂), 1.02 (t, ³J = 7.6 Hz, 6 H, ethyl-CH₃), 0.86 (t, ³J = 6.8 Hz, 6 H, hexyl-CH₃) ppm. ¹³C NMR (100 MHz, CDCl₃): δ = 192.94 (CHO), 154.29 (C_{phenyl}-OR), 131.92, 131.39, 128.99, 128.08, 126.58, 125.87, 125.25, 123.94, 116.26, 114.31 (C_{aryl}), 101.61, 92.30 (C \equiv C), 71.97 (OCH₂), 39.69 (CH), 30.45, 29.12, 23.86, 23.03 (CH₂), 13.99 (ethyl-CH₃), 11.08 (hexyl-CH₃) ppm. MS (MALDI-TOF, dithranol): m/z = 791.43 [M + H]⁺. C₅₆H₅₄O₄ (791.03): calcd. C 85.03, H 6.88; found C 84.02, H 6.99.

4,4'-[2,5-Bis(2-ethylhexyloxy)-1,4-phenylene]bis(ethynediyl)bis(1-iodobenzene) (10**):** The reaction of 1,4-diiodobenzene (**3**; 4.95 g, 15 mmol) and **7** (1.15 g, 3 mmol) was carried out according to the general procedure. The crude product was purified by column chromatography (silica gel, toluene/heptane, 2:1) and recrystallization from acetone to yield **10** as a yellow substance (708 mg, 30%). ¹H NMR (250 MHz, CDCl₃): δ = 7.69 (d, ³J = 8.3 Hz, 4 H), 7.23 (d, ³J = 8.5 Hz, 4 H), 6.99 (s, 2 H), 3.90 (d, ³J = 5.5 Hz, 4 H, OCH₂), 1.78 (m_c, 2 H, CH), 1.64–1.21 (m, 16 H, CH₂), 0.96 (t, ³J = 7.3 Hz, 6 H, ethyl-CH₃), 0.88 (t, ³J = 7.4 Hz, 6 H, hexyl-CH₃) ppm. ¹³C NMR (62.9 MHz, CDCl₃): δ = 153.85 (C_{phenyl}-OR), 137.50, 132.95, 123.03, 116.47, 113.79, 94.04, 93.90, 87.47 (C_{aryl}, C \equiv C), 71.98 (OCH₂), 39.61 (CH), 30.66, 29.68, 29.14, 27.01, 23.05 (CH₂), 14.06 (ethyl-CH₃), 11.26 (hexyl-CH₃) ppm. MS (MALDI-TOF, dithranol): m/z = 786.15 [M]⁺. C₃₈H₄₄I₂O₂ (786.56): calcd. C 58.03, H 5.64, I 32.27; found C 59.03, H 5.98, I 31.56.

10,10'-[2,5-Bis(2-ethylhexyloxy)-1,4-phenylene]bis(ethynediyl)bis(9-bromoanthracene) (11**):** The reaction of 9,10-dibromoanthracene (**4**; 5.04 g, 15 mmol) and **7** (1.15 g, 3 mmol) was carried out according to the general procedure. The crude product was purified by column chromatography (silica gel, CH₂Cl₂) to yield **11** as a red substance (616 mg, 23%). ¹H NMR (400 MHz, CDCl₃): δ = 8.87 (m_c, 4 H), 8.62 (m_c, 4 H), 7.70–7.64 (m, 8 H), 7.34 (s, 2 H), 4.17–4.13 (m, 4 H, OCH₂), 2.00 (m_c, 2 H, CH), 1.78–1.28 (m, 16 H, CH₂), 1.01 (t, ³J = 7.6 Hz, 6 H, ethyl-CH₃), 0.85 (t, ³J = 7.2 Hz, 6 H, hexyl-CH₃) ppm. ¹³C NMR (62.9 MHz, CDCl₃): δ = 153.97 (C_{phenyl}-OR), 132.98, 130.34, 128.20, 127.62, 127.45, 126.71, 124.16, 118.66, 116.05, 114.14 (C_{aryl}), 98.84, 91.84 (C \equiv C), 71.83 (OCH₂), 39.67 (CH), 30.42, 29.68, 29.11, 23.82, 23.04 (CH₂), 14.02 (ethyl-CH₃), 11.07 (hexyl-CH₃) ppm. MS (MALDI-TOF, dithranol): m/z = 890.24 [M]⁺. C₅₄H₅₂Br₂O₂ (892.80): calcd. C 72.65, H 5.87, Br 17.90; found C 72.87, H 6.06, Br 17.54.

2,2'-[4,4'-[2,5-Bis(2-ethylhexyloxy)-1,4-phenylene]bis(ethynediyl)-bis(4,1-phenylene)]di-1,3,2-dioxaborolane (12**):** The reaction of 2-(4-iodophenyl)-1,3,2-dioxaborolane (**5**; 1.73 g, 6.3 mmol) and **7** (1.15 g, 3 mmol) was carried out according to the general procedure. The crude product was purified by recrystallization from THF to yield **12** as a yellow substance (1.62 g, 79%). ¹H NMR (250 MHz, CDCl₃): δ = 7.80 (d, ³J = 8.0 Hz, 4 H), 7.54 (d, ³J = 7.5 Hz, 4 H), 7.02 (s, 2 H), 4.39 [s, 8 H, B(OCH₂)₂], 3.92 (d, ³J = 5.8 Hz, 4 H, OCH₂), 1.80 (m_c, 2 H, CH), 1.67–1.26 (m, 16 H, CH₂), 0.97 (t, ³J = 7.5 Hz, 6 H, ethyl-CH₃), 0.88 (t, ³J = 7.3 Hz, 6 H, hexyl-CH₃) ppm. ¹³C NMR (62.9 MHz, CDCl₃): δ = 153.90 (C_{phenyl}-OR), 134.64, 130.81, 126.48, 116.60, 113.91 (C_{aryl}), 94.86, 87.63 (C \equiv C), 72.05 (OCH₂), 66.12 [(OCH₂)₂], 39.65 (CH), 30.68, 29.17, 24.01, 23.08 (CH₂), 14.09 (ethyl-CH₃), 11.29 (hexyl-CH₃) ppm. C₄₂H₅₂B₂O₆ (674.48): calcd. C 74.79, H 7.77; found C 75.12, H 7.97.

2,2'-[10,10'-[2,5-Bis(2-ethylhexyloxy)-1,4-phenylene]bis(ethynediyl)-bis(anthracene-10,9-diyl)]di-1,3,2-dioxaborolane (13**):** The reaction of 2-(10-bromoanthracen-9-yl)-1,3,2-dioxaborolane (**6**; 2.06 g,

6.3 mmol) and **7** (1.15 g, 3 mmol) was carried out according to the general procedure. The crude product was purified by recrystallization from toluene to yield **13** as a red substance (2.13 g, 81%). ¹H NMR (250 MHz, CDCl₃): δ = 8.80 (d, ³J = 7.8 Hz, 4 H), 8.33 (d, ³J = 7.3 Hz, 4 H), 7.66–7.54 (m, 8 H), 7.34 (s, 2 H), 4.68 [s, 8 H, B(OCH₂)₂], 4.15 (d, ³J = 5.38 Hz, 4 H, OCH₂), 2.02 (m_c, 2 H, CH), 1.80–1.22 (m, 16 H, CH₂), 1.00 (t, ³J = 7.5 Hz, 6 H, ethyl-CH₃), 0.85 (t, ³J = 7.0 Hz, 6 H, hexyl-CH₃) ppm. ¹³C NMR (62.9 MHz, CDCl₃): δ = 153.98 (C_{phenyl}-OR), 135.32, 131.87, 129.01, 127.66, 126.10, 126.03, 120.66, 116.16, 114.20 (C_{aryl}), 98.86, 92.36 (C≡C), 71.84 (OCH₂), 66.27 [(OCH₂)₂], 39.66 (CH), 30.42, 29.11, 23.82, 23.05 (CH₂), 14.04 (ethyl-CH₃), 11.08 (hexyl-CH₃) ppm. C₅₈H₆₀B₂O₆ (874.72): calcd. C 79.64, H 6.91; found C 79.92, H 7.12.

Synthesis of Bis(terpyridines) by Horner–Wadsworth–Emmons (HWE) Reaction: KO^tBu (34 mg, 0.3 mmol) was added to a solution of a dialdehyde **8**, **9** or **14** (0.2 mmol) and **18** (184 mg, 0.4 mmol) in toluene (20 mL). The reaction mixture was heated at reflux for 3 h and subsequently quenched with an aq. 10% HCl solution (10 mL). The organic phase was separated and washed with distilled water. The organic phase was dried with MgSO₄ and then evaporated. The crude product was purified as described above.

4,4'-(4,4'-(1E,1'E)-2,2'-{4,4'-[2,5-Bis(2-ethylhexyloxy)-1,4-phenylene]bis(ethynediyl)bis(4,1-phenylene)}bis(ethene-2,1-diyl)bis(4,1-phenylene))bis(2,2':6',2''-terpyridin-4-yl) (T8): The reaction of **8** (118 mg, 0.2 mmol) and diethyl 4-(2,2':6',2''-terpyridin-4'-yl)benzylphosphonate (**18**; 184 mg, 0.4 mmol) was carried out according to the general procedure for the HWE reaction. After purification **T8** was obtained as a yellow substance (192 mg, 79%). ¹H NMR (400 MHz, CDCl₃): δ = 8.78 (s, 4 H, tpy-H^{3',5'}), 8.75 (d, ³J = 5.0 Hz, 4 H, tpy-H^{3,3''}), 8.69 (d, ³J = 8.0 Hz, 4 H, tpy-H^{6,6''}), 7.95 (AA', 4 H), 7.90 (t, ³J = 7.8 Hz, 4 H, tpy-H^{4,4''}), 7.66 (XX', 4 H), 7.54 (AA'XX', 4 H), 7.38 (t, ³J = 5.2 Hz, 4 H, tpy-H^{5,5''}), 7.21 (s, 4 H), 7.04 (s, 2 H, C_{phenyl}-H), 3.95 (d, ³J = 5.5 Hz, 4 H, OCH₂), 1.84 (m_c, 2 H, CH), 1.73–1.22 (m, 16 H, CH₂), 1.01 (t, ³J = 7.3 Hz, 6 H, ethyl-CH₃), 0.92 (t, ³J = 6.8 Hz, 6 H, hexyl-CH₃) ppm. ¹³C NMR (100 MHz, CDCl₃): δ = 154.30, 156.00, 153.92, 149.63, 149.13, 137.95, 137.70, 137.07, 136.87, 131.89, 128.88, 128.84, 127.65, 127.14, 126.54, 123.82, 122.84, 121.40, 118.57, 116.63, 114.03 (C_{phenyl}), 95.07, 87.32 (C≡C), 72.12 (OCH₂), 39.71 (CH), 30.72, 29.21, 24.07, 23.09 (CH₂), 14.09 (ethyl-CH₃), 11.31 (hexyl-CH₃) ppm. MS (MALDI-TOF, dithranol): *m/z* = 1201.62 [M + H]⁺. C₈₄H₇₆N₆O₂ (1201.54): calcd. C 83.97, H 6.38, N 6.99; found C 84.21, H 6.52, N 6.73.

4,4'-(4,4'-(1E,1'E)-2,2'-{10,10'-[2,5-Bis(2-ethylhexyloxy)-1,4-phenylene]bis(ethynediyl)bis(anthracene-10,9-diyl)}bis(ethene-2,1-diyl)bis(4,1-phenylene))bis(2,2':6',2''-terpyridin-4-yl) (T9): The reaction of **9** (158 mg, 0.2 mmol) and **18** (184 mg, 0.4 mmol) was carried out according to the general procedure for the HWE reaction. After purification **T9** was obtained as an orange substance (238 mg, 87%). ¹H NMR (300 MHz, CDCl₃): δ = 8.92 (d, ³J = 8.6 Hz, 4 H, C_{anth}-H), 8.84 (s, 4 H, tpy-H^{3',5'}), 8.78 (d, ³J = 5.4 Hz, 4 H, tpy-H^{3,3''}), 8.72 (d, ³J = 8.1 Hz, 4 H, H^{6,6''}), 8.46 (m, 4 H, C_{anth}-H), 8.10–8.01 (m, AA', CH=CH, 6 H), 7.92 (t, ³J = 7.6 Hz, 4 H, tpy-H^{4,4''}), 7.83 (XX', 4 H), 7.70–7.52 (m, C_{anth}-H, 8 H), 7.40 (t, ³J = 5.42 Hz, 4 H, tpy-H^{5,5''}), 7.33 (s, 2 H, C_{phenyl}-H), 7.07 (d, ³J = 16.5 Hz, 2 H), 4.16 (d, ³J = 5.6 Hz, 4 H, OCH₂), 2.05 (m_c, ³J = 6.2 Hz, 2 H, CH), 1.83–1.26 (m, 16 H, CH₂), 1.03 (t, ³J = 7.2 Hz, 6 H, ethyl-CH₃), 0.87 (t, ³J = 6.9 Hz, 6 H, hexyl-CH₃) ppm. The ¹³C NMR spectrum could not be measured due to the low solubility of **T9**. MS (MALDI-TOF, dithranol): *m/z* = 1402.75 [M +

H]⁺. C₁₀₀H₈₄N₆O₂ (1401.78): calcd. C 85.68, H 6.04, N 6.00; found C 85.92, H 6.32, N 5.82.

Synthesis of Bis(terpyridines) by Sonogashira Reaction: CuI (6 mg, 0.032 mmol) and [Pd(PPh₃)₄] (18 mg, 0.016 mmol) were added to a solution of the dihalide derivative **10**, **11** or **15** (0.2 mmol) and **17** (133 mg, 0.4 mmol) in a mixture of THF (5 mL) and diisopropylamine (2 mL) and the mixture was stirred at 45 °C for 24 h. After cooling, the precipitate was removed by filtration. The solvent was removed and the residue was redissolved in CHCl₃, washed with a sat. NH₄Cl solution and water, dried with MgSO₄ and concentrated. The crude product was purified as described above.

4,4'-(4,4'-{4,4'-[2,5-Bis(2-ethylhexyloxy)-1,4-phenylene]bis(ethynediyl)bis(4,1-phenylene)}bis(ethene-2,2':6',2''-terpyridin-4-yl) (T10): The reaction of **10** (157 mg, 0.2 mmol) and 4'-(4-ethynylphenyl)-2,2':6',2''-terpyridine (**17**; 133 mg, 0.4 mmol) was carried out according to the general procedure for the Sonogashira reaction. After purification **T10** was obtained as an orange substance (180 mg, 77%). ¹H NMR (400 MHz, CDCl₃): δ = 8.69 (s, 4 H, tpy-H^{3',5'}), 8.67 (d, ³J = 4.8 Hz, 4 H, tpy-H^{3,3''}), 8.60 (d, ³J = 8.0 Hz, 4 H, tpy-H^{6,6''}), 7.85 (AA', 4 H), 7.81 (t, ³J = 7.6 Hz, 4 H, tpy-H^{4,4''}), 7.60 (XX', 4 H), 7.46 (AA'XX', 8 H), 7.29 (t, ³J = 6.0 Hz, 4 H, tpy-H^{5,5''}), 7.00 (s, 2 H, C_{phenyl}-H), 3.87 (d, ³J = 5.6 Hz, 4 H, OCH₂), 1.75 (m_c, 2 H, CH), 1.60–1.21 (m, 16 H, CH₂), 0.92 (t, ³J = 7.6 Hz, 6 H, ethyl-CH₃), 0.84 (t, ³J = 7.2 Hz, 6 H, hexyl-CH₃) ppm. ¹³C NMR (100 MHz, CDCl₃): δ = 156.18, 156.11, 153.96, 149.35, 149.16, 138.40, 136.87, 132.18, 131.59, 131.48, 127.31, 123.88, 123.86, 123.58, 122.90, 121.37, 118.68, 116.62, 113.97 (C_{phenyl}), 94.65, 91.03, 90.67, 88.18 (C≡C), 72.12 (OCH₂), 39.69 (CH), 30.72, 29.20, 24.06, 23.09 (CH₂), 14.08 (ethyl-CH₃), 11.30 (hexyl-CH₃) ppm. MS (MALDI-TOF, dithranol): *m/z* = 1198.59 [M + H]⁺. C₈₄H₇₂N₆O₂ (1197.51): calcd. C 84.25, H 6.06, N 7.02; found C 84.42, H 6.29, N 6.69.

4,4'-(4,4'-{10,10'-[2,5-Bis(2-ethylhexyloxy)-1,4-phenylene]bis(ethynediyl)bis(anthracene-10,9-diyl)}bis(ethynediyl)bis(4,1-phenylene))bis(2,2':6',2''-terpyridin-4-yl) (T11): The reaction of **11** (179 mg, 0.2 mmol) and **17** (133 mg, 0.4 mmol) was carried out according to the general procedure for the Sonogashira reaction. After purification **T11** was obtained as a red substance (196 mg, 72%). ¹H NMR (400 MHz, CDCl₃): δ = 8.90–8.69 (m, 20 H), 7.97 (AA'XX', 8 H), 7.91 (t, ³J = 7.5 Hz, 4 H, tpy-H^{4,4''}), 7.76–7.65 (m, 8 H), 7.39 (t, ³J = 5.9 Hz, 4 H, tpy-H^{5,5''}), 7.32 (s, 2 H, C_{phenyl}-H), 4.16 (d, ³J = 5.3 Hz, 4 H, OCH₂), 2.04 (m_c, 2 H, CH), 1.84–1.22 (m, 16 H, CH₂), 1.03 (t, ³J = 7.5 Hz, 6 H, ethyl-CH₃), 0.87 (t, ³J = 7.0 Hz, 6 H, hexyl-CH₃) ppm. The ¹³C NMR spectrum could not be measured due to the low solubility of **T11**. MS (MALDI-TOF, dithranol): *m/z* = 1398.68 [M + H]⁺. C₁₀₀H₈₀N₆O₂ (1397.74): calcd. C 85.93, H 5.77, N 6.01; found C 86.21, H 6.02, N 5.82.

Synthesis of Bis(terpyridines) by “Click” Reaction: NaN₃ (32 mg, 0.5 mmol) and anhydrous CuSO₄ (16 mg, 0.1 mmol) were suspended in MeOH (2 mL). Subsequently, the aromatic glycol boronate **12**, **13** or **16** (0.2 mmol) was added. The mixture was stirred vigorously at room temperature until full conversion of the boronic acid ester (TLC monitoring). Subsequently, H₂O (0.1 mL), ethanol (2 mL), sodium ascorbate (4 mg, 0.02 mmol), CuI (38 mg, 0.2 mmol) and **18** (133 mg, 0.4 mmol) were added. The resulting mixture was heated under microwave irradiation at 100 °C for 1 h. After cooling, H₂O (15 mL) was added and the precipitate was collected by filtration. The precipitate was washed with *N*-(2-hydroxyethyl)ethylenediamine-*N,N',N'*-triacetic acid (HEDTA) solution (10 mL) and water. The residue was extracted with toluene and the

solution was dried with MgSO_4 and then evaporated. The crude product was purified as mentioned above.

4,4'-[4,4'-(1,1'-{4,4'-[2,5-Bis(2-ethylhexyloxy)-1,4-phenylene]bis(ethynediyl)bis(4,1-phenylene)}bis[1*H*-[1,2,3]-triazole-4,1-diyl])bis(4,1-phenylene)]bis(2,2':6',2''-terpyridine) (T12): The reaction of **12** (135 mg, 0.2 mmol) and **17** (133 mg, 0.4 mmol) was carried out according to the general procedure for the “click” reaction. After purification **T12** was obtained as a white substance (139 mg, 54%). $^1\text{H NMR}$ (400 MHz, CDCl_3): δ = 8.76 (s, 4 H, tpy- $\text{H}^{3',5'}$), 8.70 (d, 3J = 5.4 Hz, 4 H, tpy- $\text{H}^{3',3''}$), 8.62 (d, 3J = 8.2 Hz, 4 H, tpy- $\text{H}^{6,6''}$), 8.20 (s, 2 H), 7.99 (AA'XX', 8 H), 7.82 (t, 3J = 7.5 Hz, 4 H, tpy- $\text{H}^{4,4''}$), 7.77 (AA', 4 H), 7.65 (XX', 4 H), 7.29 (t, 3J = 4.8 Hz, 4 H, tpy- $\text{H}^{5,5''}$), 7.01 (s, 2 H, $\text{C}_{\text{phenyl}}\text{-H}$), 3.93 (m_{c} , 4 H, OCH_2), 1.79 (m_{c} , 2 H CH), 1.65–1.27 (m, 16 H, CH_2), 0.97 (t, 3J = 7.8 Hz, 6 H, ethyl- CH_3), 0.88 (t, 3J = 7.2 Hz, 6 H, hexyl- CH_3) ppm. $^{13}\text{C NMR}$ (100 MHz, CDCl_3): δ = 156.46, 156.22, 154.24, 149.60, 149.12, 148.12, 138.75, 136.63, 136.45, 132.85, 130.90, 127.87, 126.42, 124.41, 123.63, 121.31, 120.29, 118.73, 117.46, 117.09, 114.23 (C_{aryl}), 93.60, 88.31, ($\text{C}\equiv\text{C}$), 72.54 (OCH_2), 39.89 (CH), 30.79, 29.20, 24.18, 22.97 (CH_2), 13.85 (ethyl- CH_3), 11.19 (hexyl- CH_3) ppm. MS (MALDI-TOF, dithranol): m/z = 1283.67 [$\text{M} + \text{H}$] $^+$. $\text{C}_{84}\text{H}_{74}\text{N}_{12}\text{O}_2$ (1283.57): calcd. C 78.60, H 5.81, N 13.09; found C 78.84, H 6.09, N 13.01.

4,4'-[4,4'-(1,1'-{10,10'-[2,5-Bis(2-ethylhexyloxy)-1,4-phenylene]bis(ethynediyl)bis(anthracene-10,9-diyl)}bis[1*H*-[1,2,3]triazole-4,1-diyl])bis(4,1-phenylene)]bis(2,2':6',2''-terpyridin-4-yl) (T13): The reaction of **13** (175 mg, 0.2 mmol) and **17** (133 mg, 0.4 mmol) was carried out according to the general procedure for the “click” reaction. After purification **T13** was obtained as an off-white substance (131 mg, 44%). $^1\text{H NMR}$ (400 MHz, CDCl_3): δ = 8.92 (d, 3J = 8.8 Hz, 4 H) 8.81 (s, 4 H, tpy- $\text{H}^{3',5'}$), 8.74 (d, 3J = 4.4 Hz, 4 H, tpy- $\text{H}^{3',3''}$), 8.67 (d, 3J = 8.0 Hz, 4 H, tpy- $\text{H}^{6,6''}$), 8.30 (s, 2 H), 8.07 (AA'XX', 8 H), 7.87 (t, 3J = 7.5 Hz, 4 H, tpy- $\text{H}^{4,4''}$), 7.68 (t, 3J = 8.0 Hz, 4 H), 7.59 (t, 3J = 6.4 Hz, 4 H), 7.47–7.44 (m, 4 H), 7.34 (t, 3J = 6.2 Hz, 4 H, tpy- $\text{H}^{5,5''}$) 7.28 (s, 2 H, $\text{C}_{\text{phenyl}}\text{-H}$), 4.12 (d, 3J = 5.8 Hz, 4 H, OCH_2), 2.00 (m_{c} , 2 H, CH), 1.81–1.22 (m, 16 H, CH_2), 1.01 (t, 3J = 7.8 Hz, 6 H, ethyl- CH_3), 0.85 (t, 3J = 7.2 Hz, 6 H, hexyl- CH_3) ppm. $^{13}\text{C NMR}$ (100 MHz, CDCl_3): δ = 156.29, 156.13, 154.15, 149.54, 149.16, 147.40, 138.44, 136.86, 132.18, 130.94, 128.67, 128.29, 128.18, 127.91, 127.51, 126.99, 126.44, 124.56, 123.85, 122.64, 121.68, 121.41, 118.67, 116.22, 114.20 (C_{aryl}), 99.97, 91.56 ($\text{C}\equiv\text{C}$), 72.04 (OCH_2), 39.78 (CH), 30.51, 29.18, 23.93, 23.09 (CH_2), 14.05 (ethyl- CH_3), 11.13 (hexyl- CH_3) ppm. MS (MALDI-TOF, dithranol): m/z = 1483.74 [$\text{M} + \text{H}$] $^+$. $\text{C}_{100}\text{H}_{82}\text{N}_{12}\text{O}_2$ (1483.80): calcd. C 80.95, H 5.57, N 11.33; found C 81.18, H 5.64, N 10.89.

4,4'-(4,4'-(1,1'-[9,9-Dioctyl-9*H*-fluorene-2,7-diyl)bis(1*H*-[1,2,3]-triazole-4,1-diyl)bis(4,1-phenylene))bis(2,2':6',2''-terpyridin-4-yl) (T16): The reaction of 2,2'-(9,9-dioctyl-9*H*-fluorene-2,7-diyl)di-1,3,2-dioxaborolane (**16**; 106 mg, 0.2 mmol) and **17** (133 mg, 0.4 mmol) was carried out according to the general procedure for the “click” reaction. After purification **T16** was obtained as a white substance (169 mg, 74%). $^1\text{H NMR}$ (400 MHz, CDCl_3): δ = 8.82 (s, 4 H, tpy- $\text{H}^{3',5'}$), 8.77 (d, 3J = 3.6 Hz, 4 H, tpy- $\text{H}^{3',3''}$), 8.70 (d, 3J = 8.0 Hz, 4 H, tpy- $\text{H}^{6,6''}$), 8.38 (s, 2 H), 8.08 (AA'XX', 8 H), 7.92–7.80 (m, 10 H), 7.38 (t, 3J = 6.0 Hz, 4 H, tpy- $\text{H}^{5,5''}$) 2.15 (m_{c} , 4 H, CH_2), 1.20–0.99 (m, 20 H, CH_2), 0.80 (t, 3J = 7.2 Hz, 6 H, CH_3), 0.77–0.69 (m, 4 H, CH_2) ppm. $^{13}\text{C NMR}$ (100 MHz, CDCl_3): δ = 156.22, 156.06, 153.06, 149.58, 149.18, 147.96, 140.39, 138.40, 136.94, 136.57, 130.95, 127.92, 126.38, 123.94, 121.43, 121.20, 119.57, 118.66, 118.06, 115.31 (C_{aryl}), 56.33, 40.36, 31.77, 29.96, 29.30, 29.24, 23.94, 22.60, 14.09 ppm. MS (MALDI-TOF,

dithranol): m/z = 1139.55 [$\text{M} + \text{H}$] $^+$. $\text{C}_{75}\text{H}_{70}\text{N}_{12}$ (1139.44): calcd. C 79.06, H 6.19, N 14.75; found C 79.08, H 6.18, N 14.70.

Supporting Information (see also the footnote on the first page of this article): $^1\text{H NMR}$ and MALDI-TOF MS spectra of the bis(terpyridines) **T8–T16**.

Acknowledgments

Financial support of this work by the Dutch Polymer Institute, the Nederlandse Organisatie voor Wetenschappelijk Onderzoek (VICI award to U. S. S.), the Fonds der Chemischen Industrie and the Deutsche Forschungsgemeinschaft (DFG) is kindly acknowledged. Furthermore, the authors want to thank Anja Baumgartel for MALDI-TOF MS measurements, Alfred Jacobi for the low-temperature absorption measurements and Beate Lentvogt for the elemental analyses.

- [1] J.-M. Lehn, *Supramolecular Chemistry – Concepts and Chemistry*, VCH, Weinheim, 1995.
- [2] U. S. Schubert, C. Eschbaumer, *Angew. Chem. Int. Ed.* **2002**, *41*, 2893–2926.
- [3] V. Banjoko, Y. Q. Xu, E. Mintz, Y. Pang, *Polymer* **2009**, *50*, 2001–2009.
- [4] A. Maier, A. R. Rabindranath, B. Tieke, *Chem. Mater.* **2009**, *21*, 3668–3676.
- [5] A. A. Stefopoulos, E. K. Pefkianakis, K. Papagelis, A. K. Andreopoulos, J. K. Kallitsis, *J. Polym. Sci., Part A: Polym. Chem.* **2009**, *47*, 2551–2559.
- [6] Y. Y. Chen, Y. T. Tao, H. C. Lin, *Macromolecules* **2006**, *39*, 8559–8566.
- [7] W. G. Weng, Z. Li, A. M. Jamieson, S. J. Rowan, *Macromolecules* **2009**, *42*, 236–246.
- [8] A. H. Flood, J. F. Stoddart, D. W. Steuerman, J. R. Heath, *Science* **2004**, *306*, 2055–2056.
- [9] V. Balzani, P. Ceroni, A. Juris, M. Venturi, S. Campagna, F. Puntorieri, S. Serroni, *Coord. Chem. Rev.* **2001**, *219*, 545–572.
- [10] F. Barigelletti, L. Flamigni, *Chem. Soc. Rev.* **2000**, *29*, 1–12.
- [11] R. Ziessel, M. Hissler, A. El-Ghayoury, A. Harriman, *Coord. Chem. Rev.* **1998**, *178*, 1251–1298.
- [12] C. D. Eisenbach, U. S. Schubert, *Macromolecules* **1993**, *26*, 7372–7374.
- [13] G. Hochwimmer, O. Nuyken, U. S. Schubert, *Macromol. Rapid Commun.* **1998**, *19*, 309–313.
- [14] U. S. Schubert, H. Hofmeier, G. R. Newkome, *Modern Terpyridine Chemistry*, Wiley-VCH, Weinheim, 2006.
- [15] Y. Y. Chen, H. C. Lin, *Polymer* **2007**, *48*, 5268–5278.
- [16] S. H. Hwang, C. N. Moorefield, P. S. Wang, J. Y. Kim, S. W. Lee, G. R. Newkome, *Inorg. Chim. Acta* **2007**, *360*, 1780–1784.
- [17] S. C. Yuan, H. B. Chen, Y. Zhang, J. Pei, *Org. Lett.* **2006**, *8*, 5700–5704.
- [18] U. S. Schubert, C. Eschbaumer, O. Hien, P. R. Andres, *Tetrahedron Lett.* **2001**, *42*, 4705–4707.
- [19] S. Schmatloch, A. M. J. van den Berg, A. S. Alexeev, H. Hofmeier, U. S. Schubert, *Macromolecules* **2003**, *36*, 9943–9949.
- [20] U. S. Schubert, O. Hien, C. Eschbaumer, *Macromol. Rapid Commun.* **2000**, *21*, 1156–1161.
- [21] B. G. G. Lohmeijer, U. S. Schubert, *Macromol. Chem. Phys.* **2003**, *204*, 1072–1078.
- [22] M. Heller, U. S. Schubert, *Macromol. Rapid Commun.* **2001**, *22*, 1358–1363.
- [23] U. S. Schubert, S. Schmatloch, A. A. Precup, *Des. Monomers Polym.* **2002**, *5*, 211–221.
- [24] H. Hofmeier, U. S. Schubert, *Chem. Soc. Rev.* **2004**, *33*, 373–399.
- [25] H. Hofmeier, U. S. Schubert, *Macromol. Chem. Phys.* **2003**, *204*, 1391–1397.
- [26] P. D. Vellis, J. A. Mikroyannidis, C. N. Lo, C. S. Hsu, *J. Polym. Sci., Part A: Polym. Chem.* **2008**, *46*, 7702–7712.

- [27] A. Winter, D. A. M. Egbe, U. S. Schubert, *Org. Lett.* **2007**, *9*, 2345–2348.
- [28] A. Winter, C. Friebe, M. Chiper, M. D. Hager, U. S. Schubert, *J. Polym. Sci., Part A: Polym. Chem.* **2009**, *47*, 4083–4098.
- [29] A. Winter, C. Friebe, M. D. Hager, U. S. Schubert, *Macromol. Rapid Commun.* **2008**, *29*, 1679–1686.
- [30] J. F. Gohy, M. Chiper, P. Guillet, C. A. Fustin, S. Hoepfner, A. Winter, R. Hoogenboom, U. S. Schubert, *Soft Matter* **2009**, *5*, 2954–2961.
- [31] A. Winter, C. Friebe, M. D. Hager, U. S. Schubert, *Eur. J. Org. Chem.* **2009**, 801–809.
- [32] A. Winter, A. Wild, R. Hoogenboom, M. W. M. Fijten, M. D. Hager, R. A. Fallahpour, U. S. Schubert, *Synthesis* **2009**, 1506–1512.
- [33] R. Huisgen, R. Knorr, L. Mobius, G. Szeimies, *Chem. Ber.* **1965**, *98*, 4014–4021.
- [34] H. C. Kolb, M. G. Finn, K. B. Sharpless, *Angew. Chem. Int. Ed.* **2001**, *40*, 2004–2021.
- [35] C. R. Becer, R. Hoogenboom, U. S. Schubert, *Angew. Chem. Int. Ed.* **2009**, *48*, 4900–4908.
- [36] B. Schulze, C. Friebe, M. D. Hager, A. Winter, R. Hoogenboom, H. Gols, U. S. Schubert, *Dalton Trans.* **2009**, 787–794.
- [37] B. Happ, C. Friebe, A. Winter, M. D. Hager, R. Hoogenboom, U. S. Schubert, *Chem. Asian J.* **2009**, *4*, 154–163.
- [38] D. Fournier, R. Hoogenboom, U. S. Schubert, *Chem. Soc. Rev.* **2007**, *36*, 1369–1380.
- [39] C. Z. Tao, X. Cui, J. Li, A. X. Liu, L. Liu, Q. X. Guo, *Tetrahedron Lett.* **2007**, *48*, 3525–3529.
- [40] T. M. Swager, C. J. Gil, M. S. Wrighton, *J. Phys. Chem.* **1995**, *99*, 4886–4893.
- [41] A. P. H. J. Schenning, A. C. Tsipis, S. C. J. Meskers, D. Beljonne, E. W. Meijer, J. L. Bredas, *Chem. Mater.* **2002**, *14*, 1362–1368.
- [42] A. Winter, C. Friebe, M. Chiper, U. S. Schubert, M. Presselt, B. Dietzek, M. Schmitt, J. Popp, *ChemPhysChem* **2009**, *10*, 787–798.
- [43] A. Wild, D. A. M. Egbe, E. Birckner, V. Cimrova, R. Baumann, U. W. Grummt, U. S. Schubert, *J. Polym. Sci., Part A: Polym. Chem.* **2009**, *47*, 2243–2261.
- [44] A. Moliton, R. C. Hiorns, *Polym. Int.* **2004**, *53*, 1397–1412.
- [45] M. J. Frisch, G. W. Trucks, H. B. Schlegel, G. E. Scuseria, M. A. Robb, J. R. Cheeseman, J. A. Montgomery Jr., T. Vreven, K. N. Kudin, J. C. Burant, J. M. Millam, S. S. Iyengar, J. Tomasi, V. Barone, B. Mennucci, M. Cossi, G. Scalmani, N. Rega, G. A. Petersson, H. Nakatsuji, M. Hada, M. Ehara, K. Toyota, R. Fukuda, J. Hasegawa, M. Ishida, T. Nakajima, Y. Honda, O. Kitao, H. Nakai, M. Klene, X. Li, J. E. Knox, H. P. Hratchian, J. B. Cross, V. Bakken, C. Adamo, J. Jaramillo, R. Gomperts, R. E. Stratmann, O. Yazyev, A. J. Austin, R. Cammi, C. Pomelli, J. W. Ochterski, P. Y. Ayala, K. Morokuma, G. A. Voth, P. Salvador, J. J. Dannenberg, V. G. Zakrzewski, S. Dapprich, A. D. Daniels, M. C. Strain, O. Farkas, D. K. Malick, A. D. Rabuck, K. Raghavachari, J. B. Foresman, J. V. Ortiz, Q. Cui, A. G. Baboul, S. Clifford, J. Cioslowski, B. B. Stefanov, G. Liu, A. Liashenko, P. Piskorz, I. Komaromi, R. L. Martin, D. J. Fox, T. Keith, M. A. Al-Laham, C. Y. Peng, A. Nanayakkara, M. Challacombe, P. M. W. Gill, B. Johnson, W. Chen, M. W. Wong, C. Gonzalez, J. A. Pople, *Gaussian 03, Revision D.01*, Gaussian, Inc., Wallingford, CT, **2004**.
- [46] As a result of technical difficulties, the orbital images of **T8** were constructed from a single-point calculation of a truncated molecule. The four outer pyridyl rings of the fully optimized molecule were replaced by hydrogen atoms.
- [47] Z. L. Cai, K. Sendt, J. R. Reimers, *J. Chem. Phys.* **2002**, *117*, 5543–5549.
- [48] D. A. M. Egbe, B. Carbonnier, E. Birckner, U. W. Grummt, *Prog. Polym. Sci.* **2009**, 1023–1067.
- [49] A. Wild, F. Schlütter, G. M. Pavlov, C. Friebe, G. Festag, A. Winter, M. D. Hager, V. Cimrová, U. S. Schubert, *Macromol. Rapid Commun.*, DOI: 10.1002/marc.200900889.

Received: September 30, 2009

Published Online: February 23, 2010

Publication A3: “ π -Conjugated donor and donor-acceptor
metallo-polymers”

Andreas Wild, Florian Schlütter, Georges M. Pavlov, Christian Friebe,
Grit Festag, Andreas Winter, Martin D. Hager, Vera Cimrová,
Ulrich S. Schubert

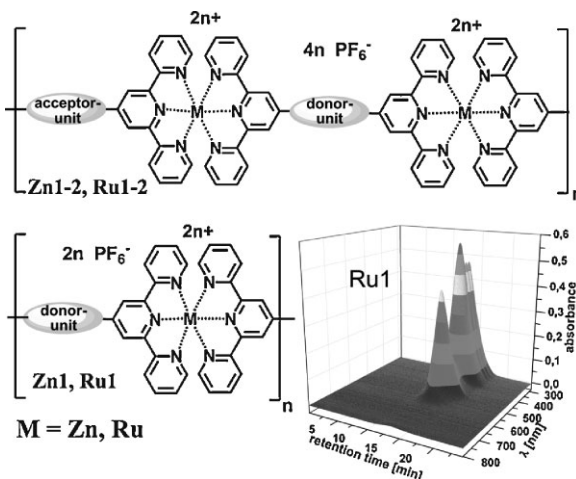
Macromol. Rapid Commun. **2010**, *31*, 868–874.

Reprinted with permission from: WILEY-VCH Weinheim (Copyright 2010)

π -Conjugated Donor and Donor–Acceptor Metallo-Polymers^a

Andreas Wild, Florian Schlütter, Georges M. Pavlov, Christian Friebe, Grit Festag, Andreas Winter, Martin D. Hager, Vera Cimrová, Ulrich S. Schubert*

Two zinc(II)- and two ruthenium(II) containing π -conjugated metallo-polymers were synthesized and characterized in detail. We could prove by SEC, analytical ultracentrifugation (AUC) and viscosimetry the ruthenium(II) metallo-polymers to be high molar mass materials ($M_{fs} = 20\,000\text{ g}\cdot\text{mol}^{-1}$ **Ru1-2**; $M_{fs} = 34\,000\text{ g}\cdot\text{mol}^{-1}$ **Ru1**) exhibiting intrinsic viscosities of up to $[\eta] = 192\text{ cm}^3\cdot\text{g}^{-1}$. Applying spin-coating we produced homogeneous films of the polymers and could, subsequently, investigate the photo-physical properties in the solid state. Introducing the Ru(II) metallo-polymers mixed with PCBM[60] as photoactive layer in bulk-heterojunction solar cells resulted in very low efficiencies due to morphology problems.



U. S. Schubert, A. Wild, F. Schlütter, G. M. Pavlov, C. Friebe, G. Festag, M. D. Hager
Laboratory of Organic and Macromolecular Chemistry, Friedrich-Schiller-University Jena, Humboldtstr.10, D-07743 Jena, Germany
Fax: (+49) 0 3641 9482 02; E-mail: ulrich.schubert@uni-jena.de
U. S. Schubert, A. Wild, A. Winter, G. M. Pavlov, M. D. Hager
Dutch Polymer Institute (DPI), P.O. Box 902, 5600 AX Eindhoven, The Netherlands

U. S. Schubert, A. Winter, G. M. Pavlov
Laboratory of Macromolecular Chemistry and Nanoscience, Eindhoven University of Technology, P.O. Box 513, 5600 MB Eindhoven, The Netherlands

V. Cimrová
Institute of Macromolecular Chemistry, Academy of Sciences of the Czech Republic, v.v.i, Heyrovského nám. 2, 162 06 Prague 6, Czech Republic

^a Supporting information for this article is available at the bottom of the article's abstract page, which can be accessed from the journal's homepage at <http://www.mrc-journal.de>, or from the author.

Introduction

The development of supramolecular chemistry introduced a new perspective to modern chemistry and material science by applying non-covalent interactions in a directed way to organize molecular building blocks forming supramolecular architectures.^[1–5] Terpyridine ligands are highly effective complexing agents and key templates in this particular field of research.^[5–11] Combining such ligands substituted in 4'-position with a π -conjugated spacer and suitable transition metal ions (e.g., Ru^{II}, Zn^{II}, Fe^{II}, or Ni^{II}) leads to the formation of linear, rodlike polynuclear polymers.^[12–20] The great potential of the bisterpyridine metallo-polymers is the versatility one can achieve using these substances. In particular, one can combine the defined optical properties of small organic molecules (e.g., color tunability, no structural defects) with the processing advantages of polymers (i.e., good film forming properties).

When using different metal ions (in particular Ru^{II}, Zn^{II}, Ir^{III}) one can adapt the same monomer to yield polymers featuring a broad range of properties depending on the employed metal ion. The incorporation of a ruthenium(II) complex into a conjugated polymer has the potential to facilitate the charge carrier generation. Such metal complexes usually exhibit a reversible Ru^{II}/Ru^{III} redox process and some ligand-centered redox processes. In addition, a ruthenium complex incorporated into a polymer will influence the optical as well as the electronic properties of the polymer due to its characteristic metal-to-ligand charge transfer (MLCT) transition around 500 nm, thus extending the absorption range of the material. The usage of Zn^{II} ions leads to metallo-polymers being potential interesting light-emitting materials in OLEDs;^[14,15,21–23] moreover, also Ir-containing polymers are of special interest for this purpose.^[24–26] In recent years, π -conjugated polymer semiconductors with donor–acceptor (D–A) architectures have attracted considerable attention, since their electro-optical properties make them promising candidates for potential applications in the fields of organic electronics.^[27–29] In this contribution we describe the synthesis and characterization of four metallo-polymers containing either zinc(II) or ruthenium(II) ions in the main chain. By using different polymerization methods we were able to synthesize, beside the *homo*-polymers (**Zn1**, **Ru1**), also a statistical (**Zn1-2**) and an alternating (**Ru1-2**) copolymer of our materials. These materials were studied in detail and we could prove in particular **Ru1** to possess a high degree of polymerization. Furthermore, first photovoltaic devices were produced out of these materials.

Experimental Part

Materials

All reagents were purchased from commercial sources and used without further purification unless specified. Solvents were dried and distilled according to standard procedures. Compounds **1** and **2** were prepared following previously published protocols.^[30,31] Details on the synthesis of the polymers, the instrumentation and device preparation are given in the Supporting Information.

Results and Discussion

Synthesis and Characterization

To synthesize the zinc(II) containing polymers the respective bisterpyridine(s) (**1,2**) were reacted with Zn(OAc)₂ × 2 H₂O in N-methylpyrrolidone (NMP) for 24 h at 110 °C followed by an anion exchange with an excess of NH₄PF₆.^{14,15,21–23} Using this protocol we produced, beside solely donor (**Zn1**) also statistical copolymers of

donor and acceptor systems (**Zn1-2**) (Scheme 1). The selected ligands **1** and **2** exhibit a preferably large overlap of the absorption of the acceptor part (quinoxaline unit) with the emission of the donor unit (fluorene unit). As a consequence, an energy transfer between the monomer units is more favorable. The molar mass of the resulting Zn^{II} metallo-polymers could not be determined, caused by the weak binding strength of the terpyridine ligand to the metal ion.^[4] However, characterization by ¹H NMR spectroscopy indicated the formation of the desired metallo-polymers by broadened signals of the terpyridine ligand, which is a characteristic feature of polymeric materials, as well as by the absence of the signals from the uncomplexed terpyridine unit.

Utilizing ruthenium(II) ions instead of zinc(II) ions it is possible to synthesize, beside the *homo*- and statistical, also alternating copolymers of donor and acceptor units (Scheme 1). The ruthenium(II) *homo*-polymer **Ru1** was synthesized by reacting **1** with Ru(DMSO)₄Cl₂ in a mixture of *n*-butanol/*N,N*-dimethyl-acetamide (DMA) for 24 h under heating to reflux, followed by an anion exchange with excess of NH₄PF₆ and precipitations in a methanol/water mixture and diethyl ether, respectively. The copolymer **Ru1-2** was synthesized in a two step procedure. First monomer **1** was reacted with an excess of RuCl₃ hydrate to yield the ruthenium(III) precursor **3**. Subsequently, this complex was heated with the second monomer (**2**) in a *n*-butanol/DMA mixture for 24 h under reflux. Anion exchange and purification were carried out as in the case of **Ru1** and the resulting polymers were characterized by UV–Vis absorption and emission measurements in thin film and solution, cyclic voltammetry (CV), ¹H NMR spectroscopy, elemental analysis, size exclusion chromatography (SEC) as well as AUC measurements.

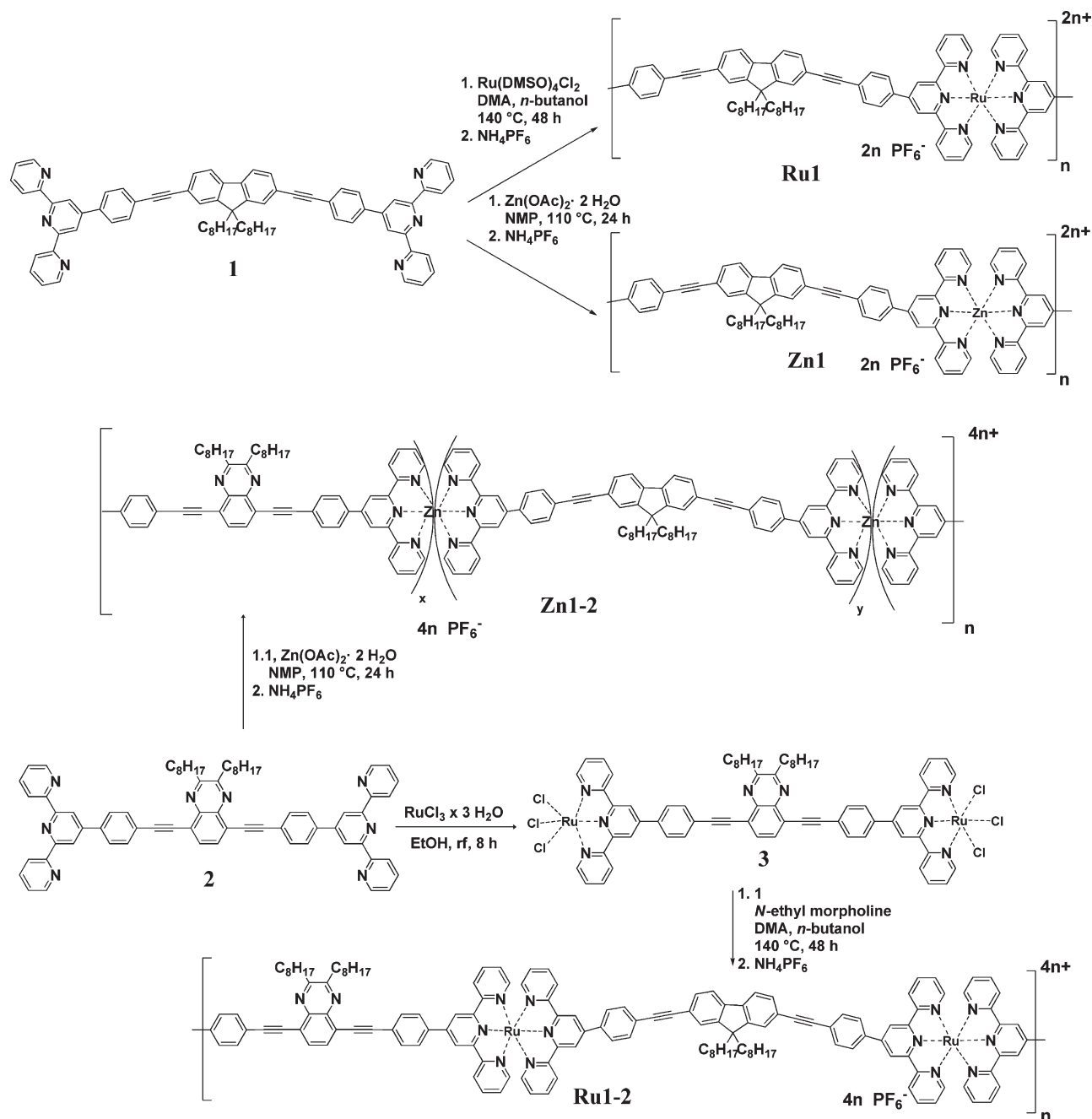
Electrochemical Properties

The electrochemical properties of the *homo*-polymers (**Zn1**, **Ru1**) and copolymers (**Zn1-2** and **Ru1-2**) as summarized in Table 1 were obtained from thin films of the materials coated on Pt wires (0.1 M TBAPF₆ in CH₃CN; scan rate 50 mV · s⁻¹).

The Zn^{II} polymers (**Zn1** and **Zn1-2**) exhibited reversible reduction peaks between –1.33 and –1.77 V. These peaks were attributed to the reduction of terpyridyl-based moieties.^[14,21,23] As anticipated no significant oxidation processes were observed up to 1.5 V. The lowest unoccupied molecular orbital (LUMO) levels were estimated from the first reduction wave and referenced to the energy level of ferrocene, according to Equation (1a).

$$E_{\text{LUMO}} = [-(E_{\text{red}} - E_{\text{reference}}) - 4.8] \text{eV} \quad (1a)$$

$$E_{\text{HOMO}} = [-(E_{\text{ox}} - E_{\text{reference}}) - 4.8] \text{eV} \quad (1b)$$



■ Scheme 1. Schematic representation of the synthesis of homo- (**Zn1**, **Ru1**) and donor-acceptor copolymers (**Zn1-2**, **Ru1-2**).

The LUMO levels calculated that way were around -3.50 eV (Table 1). Due to the absence of oxidation potentials, the estimation of the corresponding ionization energy (highest occupied molecular orbital, HOMO) according to Equation (1b) and, consequently, the calculation of the electrochemical band gap were not possible. Therefore, the band gap of the metallo-polymers was derived from the UV-Vis absorption spectra by extrapolation of the 0–0 transition of the longest wavelength absorption

band. This energy band gap was strongly influenced by the nature of the π -conjugated spacer unit.^[21,31] Considering this, the photophysical properties of such Zn^{II} containing metallo-polymers can be tuned via the electro-optical properties of the chromophore. The ruthenium(II) polymers showed, beside two reversible reduction peaks around -1.38 and -1.60 eV , one oxidation wave at 0.89 eV , corresponding to the $\text{Ru}^{\text{II}}/\text{Ru}^{\text{III}}$ couple and, thus, representing the HOMO of the polymer. Both types of

Table 1. Electrochemical properties of the *homo*-polymers (**Zn1** and **Ru1**) and copolymers (**Zn1-2** and **Ru1-2**).

| Polymer | $E_{1/2}^{\text{red}}$ ^{a)} | $E_{\text{onset}}^{\text{red}}$ | $E_{1/2}^{\text{ox}}$ ^{b)} | $E_{\text{onset}}^{\text{ox}}$ | E_{LUMO} ^{c)} | E_{HOMO} ^{c)} | E_g^{ec} ^{d)} |
|--------------|--------------------------------------|---------------------------------|-------------------------------------|--------------------------------|---------------------------------|---------------------------------|---------------------------------|
| | V | V | V | V | eV | eV | eV |
| Zn1 | −1.33 | −1.27 | | | −3.42 (−3.48) | n.a. | |
| Zn1-2 | −1.33, −1.73 | −1.25 | | | −3.41 (−3.50) | n.a. | |
| Ru1-2 | −1.38, −1.60 | −1.27 | 0.89 | 0.73 | −3.37 (−3.48) | −5.64 (−5.48) | 2.27 (2.00) |
| Ru1 | −1.39, −1.62 | −1.25 | 0.89 | 0.76 | −3.36 (−3.50) | −5.64 (−5.51) | 2.28 (2.01) |

^{a)} $E_{1/2}^{\text{red}}$ values were obtained from the first and second reduction peaks averaging the anodic and cathodic peak potentials measured versus Ag/Ag^+ , $E_{1/2} = (E_{\text{pa}} + E_{\text{pc}})/2$; ^{b)} $E_{1/2}^{\text{ox}}$ values were obtained from the first oxidation peaks averaging the anodic and cathodic peak potentials measured versus Ag/Ag^+ , $E_{1/2} = (E_{\text{pa}} + E_{\text{pc}})/2$; ^{c)} E_{LUMO} and E_{HOMO} were calculated from the first reduction and oxidation peaks according to Equation 1 using $E_{\text{red}} = E_{1/2}^{\text{red}}$ ($E_{\text{onset}}^{\text{red}}$) and $E_{\text{ox}} = E_{1/2}^{\text{ox}}$ ($E_{\text{onset}}^{\text{ox}}$); ^{d)} $E_g^{\text{ec}} = |E_{\text{HOMO}} - E_{\text{LUMO}}|$ using $E_{1/2}$ (E_{onset}) values.

metallo-polymers (i.e., possessing Zn^{II} or Ru^{II}) exhibited a reversible color change during the reduction. The Zn^{II} polymers changed their color from yellow, over red to black, and the Ru^{II} polymers from red to black. The reversibility of these color changes makes them interesting systems for potential electro-optical applications.

Photophysical Properties

Further investigation of the *homo*-polymers (**Zn1** and **Ru1**) and copolymers (**Zn1-2** and **Ru1-2**) was carried out by UV–Vis absorption and photoluminescence (PL) spectroscopy, both in solution and in thin films, respectively.

In general, all Zn^{II} polymers showed – in agreement with the observations for the corresponding *bis*terpyridines **1** and **2** – characteristic absorptions between 270 and 450 nm (See Table 2). As expected, the Zn^{II} cores, featuring a filled d^{10} electron shell, do not participate in the transitions.

A combination of **1** and **2** as donor–acceptor pair was chosen for the statistical copolymer **Zn1-2** since it exhibited a preferably large overlap of the absorption spectrum of the acceptor part with the emission spectrum of the donor unit. The absolute quantum yields (Φ_{PL}) of the materials were determined. In case of the *homo*-polymer **Zn1**, both an increase of Φ_{PL} (**1**: $\Phi_{\text{PL}} = 0.77$; **Zn1**: $\Phi_{\text{PL}} = 0.95$) and a 20 nm red-shift of the PL maximum (λ_{PL}) was observed upon complexation. Such a behavior might be attributed to a HOMO that is located mainly at the electron-rich central chromophore and a LUMO localized on the electron-deficient metal-coordinated terpyridine moieties.^[14,22] Comparing the absorption spectra of the Zn^{II} metallo-polymers, a bathochromic shift was obvious when changing from solution to films. The absorption spectra of the pure ligand **1** ($\lambda_{\text{abs}} = 368$ nm) and the corresponding zinc polymer **Zn1** ($\lambda_{\text{abs}} = 369$ nm) did not show any conjugation effect, even when measuring at higher

Table 2. Photophysical properties of *homo*-polymers (**Zn1**, **Ru1**) and *random*-copolymers (**Zn1-2** and **Ru1-2**).

| Polymer | λ_{abs} ^{a)} | | λ_{PL} ^{a)} | | $\epsilon \times 10^{4\text{a,b)}$ | Φ_{PL} ^{c)} | $\Delta\nu_{\text{af}}$ ^{d)} | E_g^{opte} |
|--------------|--------------------------------------|---------------------------------------|-------------------------------------|------|------------------------------------|----------------------------------|---------------------------------------|---------------------|
| | nm | | nm | | | | | |
| | Solution | Film | Solution | Film | | | | |
| Zn1-2 | 369, 320, 281 | 383, 344, 288, 234 | 432, 409(s) | 523 | 11.25 | 0.81 | 4 000/7 000 | 2.91 |
| Zn1 | 369, 321, 282 | 390, 340 322, 288, 235 | 424(s), 409 | 522 | 8.25 | 0.95 | 3 500/6 500 | 3.08 |
| Ru1-2 | 505, 382, 338, 316, 289 | 501, 380(s), 334, 316, 278, 234(s) | | | 11.50 | | | 2.15 |
| Ru1 | 505, 383, 340, 320, 290 | 502, 363, 336, 318, 288, 234 | | | 5.30 | | | 2.13 |

^{a)}For all solution spectra: 10^{-6} M in DMF; (s) = shoulder; ^{b)}Extinction coefficients at the lowest-energy absorption band; per repeating unit; ^{c)}Absolute quantum yields in solution; ^{d)} $\Delta\nu_{\text{af}} = 1/\lambda_{\text{a}} - 1/\lambda_{\text{f}}$; solution/film; ^{e)} $E_g^{\text{opt}} = hc/\lambda_{0.1\text{max}}$; solution.

absorbances ($A = 2$). Furthermore, it is known from literature that the Zn^{II} cores do not participate in the transitions, due to the filled d^{10} electron shell.^[32] In thin films the polymer chains lie open and flat, thereby improving the π -stacking between neighboring chains and aggregation occurs. The enhanced planarization of the conjugated backbone gave rise to the bathochromic shift of the absorption spectra of the polymers **Zn1** and **Zn1-2** in the solid state (Figure 1) as compared to their dilute solutions. Beside the bathochromic shift also a new band at around $\lambda_{abs} = 340$ nm appears in case of both zinc-coordination polymers. In contrast, the Ru^{II} polymers **Ru1** and **Ru1-2** did not show any bathochromic shift, when comparing thin film and solution spectra. Here, the position of the absorption maxima did not change, just the intensities of the bands themselves differ comparing solution and thin films. The absorption band around $\lambda_{abs} = 380$ nm, representing the $\pi-\pi^*$ transition of the π -conjugated ligand, was more intensive in solution, whereas the signals at higher energy, in particular for **Ru1**, appeared less intensive.

Molecular Hydrodynamics Study

The samples were studied by SEC, velocity sedimentation using AUC^[33,34] and by the measurement of the intrinsic viscosity (Figure 2). Velocity sedimentation was studied for three concentrations of each sample (0.4 to 0.01 $mg \cdot mL^{-1}$; $c_{max}/c_{min} \geq 40$) in DMA containing 0.8 mol-% NH_4PF_6 . The molar masses were calculated from the modified Svedberg relationship (Equation (2))^[35]

$$M_{fs} = 9\pi^{1/2} N_A ([s](f/f_{sph})_0)^{3/2} v^{1/2} \quad (2)$$

where $[s] = s_0 \eta_0 / (1 - v\rho_0)$ is the intrinsic sedimentation coefficient, $(f/f_{sph})_0$ the frictional ratio, v the partial specific volume, and N_A is the Avogadro number.

The main peaks contain around 80% of sample substance; the rest may be treated as the high molar mass shoulder (Figure 2, top Left). This kind of distributions finds a qualitative confirmation in

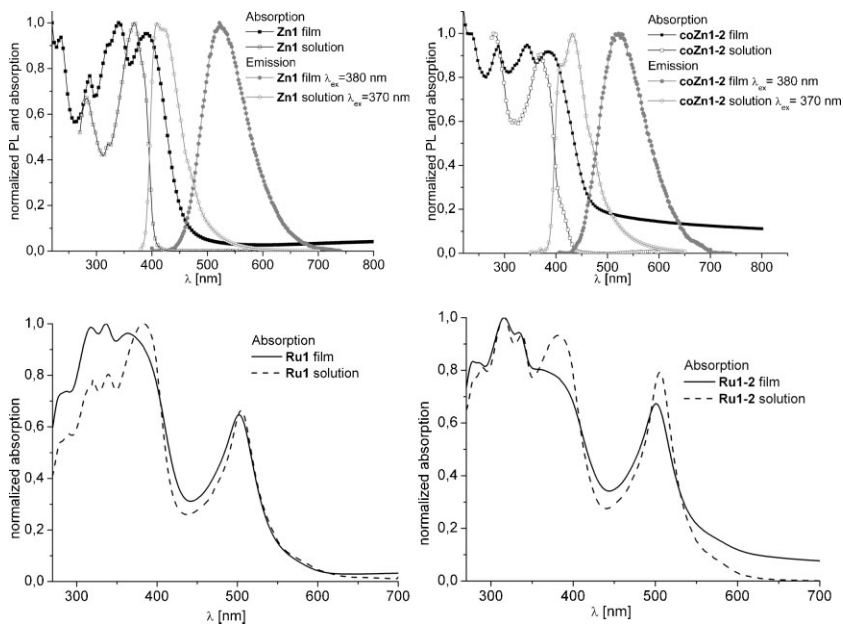


Figure 1. Normalized UV-Vis absorption and PL spectra of **Zn1** (top, left) and **Zn1-2** (top, right) in solution (dashed line) and thin film (straight line), as well as **Ru1** (bottom, left) and **Ru1-2** (bottom, right).

the SEC data. Both ruthenium(II) polymers (**Ru1** and **Ru1-2**) were suitable for SEC experiments using DMA containing 0.8 mol-% NH_4PF_6 as eluent. The response was detected by using both a refractive index (RI) as well as a photo-diode

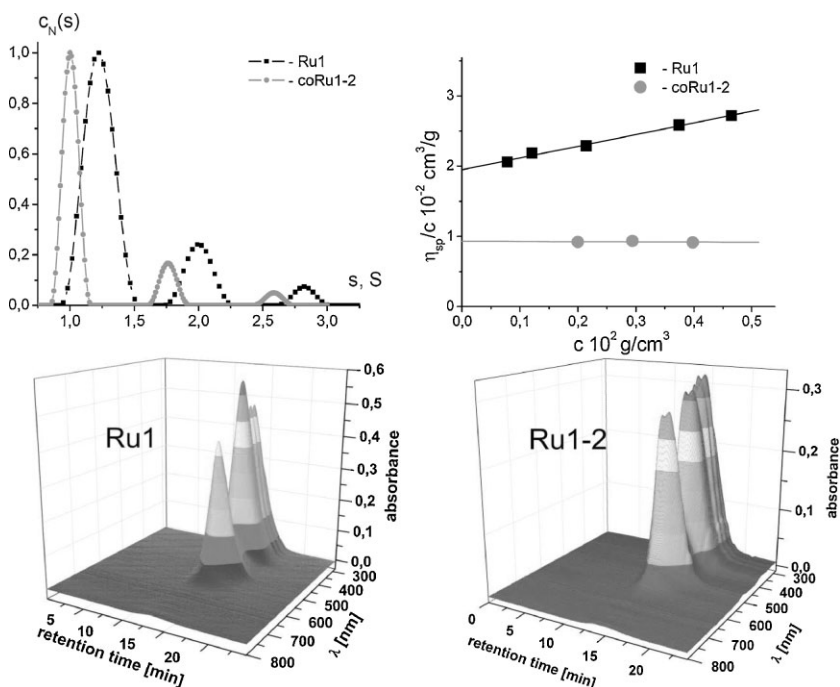


Figure 2. Top: Results of velocity sedimentation experiments of **Ru1** and **Ru1-2**: Corresponding differential distribution of the sample obtained from the sedimentation profiles (black **Ru1**, red **Ru1-2**) (left) and viscosity plots (right). Bottom: SEC traces of **Ru1** (left) and **Ru1-2** (right) using a PDA detector.

Table 3. Hydrodynamic characteristics and molar masses of **Ru1** and **Ru1-2** estimated from velocity sedimentation and SEC data.

| Polymer | $[\eta]$ $\text{cm}^3 \cdot \text{g}^{-1}$ | s_0 S | f/f_{sph} | M_{fs} $\text{g} \cdot \text{mol}^{-1}$ | \bar{M}_n (SEC) ^{a)} $\text{g} \cdot \text{mol}^{-1}$ |
|--------------|---|------------|--------------------|---|---|
| Ru1-2 | 90 | 1.2 | 2.6 | 20 000 | 38 000 |
| Ru1 | 192 | 1.4 | 3.3 | 34 000 | 88 000 |

^{a)}Values obtained from SEC using UV detection and polystyrene standards.

array (PDA) detector. The obtained chromatograms are depicted in Figure 2. Both spectra show the typical shape of a ruthenium-terpyridine containing system confirmed by the characteristic MLCT absorption band at around 500 nm. Furthermore, the hydrodynamic behavior of **Ru1** and **Ru1-2** was analyzed by viscosimetry experiments in DMA solutions containing 0.02 M NH_4PF_6 , where intermolecular Coulomb-type interactions between the charged macromolecules are screened out and polyelectrolyte effects are not manifested. Intrinsic viscosities were obtained from the Huggins and Kramer plots of up $[\eta] = 192 \text{ cm}^3 \cdot \text{g}^{-1}$. These relatively high levels of $[\eta]$ values are characteristics for linear high molar mass compounds.^[36] The $[\eta]$ value is related with molar mass and size (volume) of dissolved macromolecules by the Flory–Fox relation: $[\eta] = \Phi \langle h^2 \rangle^{3/2} / M$, where $\langle h^2 \rangle$ is the average square of the end-to-end distances, and Φ is the Flory hydrodynamic parameter. The obtained $[\eta]$ values may also characterize a relatively high asymmetry of the studied supramolecules in solutions. This assumption is validated by the differences in the molar mass estimation from the SEC and the AUC data (Table 3) which might be caused by a higher equilibrium rigidity of supramolecular chains in comparison with polystyrene chains. However, to obtain the quantitative characteristic of the equilibrium rigidity of supramolecular chains (the persistence length) it is required to study a series of supramolecular chains of different lengths; this will be targeted in the future.

Conclusion

In this contribution the synthesis and detailed characterization of two zinc(II) and two ruthenium(II) containing metallo-polymers were described. We could prove by SEC, AUC and viscosimetry the high degree of polymerization of **Ru1**. The absolute molar mass values, obtained by the sedimentation technique, allow a comparison to the relative values from SEC. Moreover, homogeneous films of the pristine polymers could be produced, but unfortunately spin-coating of the polymer:PCBM[60] mixtures lead to very rough surfaces, and therefore 50% of the built devices were not working. Optimization of the poly-

mer:PCBM[60] mixtures and the π -conjugated spacer units will be targeted in the future to obtain new materials showing tailor-made properties for applications in OLEDs and PV devices.

Acknowledgements: Financial support of this work by the *Dutch Polymer Institute, the Deutsche Forschungsgemeinschaft, the European Science Foundation (project number 2977), the Nederlandse Organisatie voor Wetenschappelijk Onderzoek (VICI award for U.S.S.), the Ministry of Education, Youth and Sports of the Czech Republic (grant No.1M06031), and the Grant Agency of the Academy of Sciences of the Czech Republic (grant No. IAA4050409)* is kindly acknowledged.

Received: December 14, 2009; Revised: February 1, 2010;
Published online: April 16, 2010; DOI: 10.1002/marc.200900889

Keywords: analytical ultracentrifugation; conducting polymers; metallo-polymers; solar cells; supramolecular structures

- [1] J. M. Lehn, *Supramolecular Chemistry - Concepts and Chemistry*, VCH, Weinheim, Germany 1995.
- [2] J. M. Lehn, *Angew. Chem., Int. Ed.* **1988**, *27*, 89.
- [3] J. M. Lehn, *Science* **2002**, *295*, 2400.
- [4] U. S. Schubert, H. Hofmeier, G. R. Newkome, *Modern Terpyridine Chemistry*, Wiley-VCH, Weinheim, Germany 2006.
- [5] H. Hofmeier, S. Schmatloch, D. Wouters, U. S. Schubert, *Macromol. Chem. Phys.* **2003**, *204*, 2197.
- [6] U. S. Schubert, S. Schmatloch, A. A. Precup, *Des. Monomers Polym.* **2002**, *5*, 211.
- [7] S. Schmatloch, A. M. J. van den Berg, A. S. Alexeev, H. Hofmeier, U. S. Schubert, *Macromolecules* **2003**, *36*, 9943.
- [8] U. S. Schubert, C. Eschbaumer, G. Hochwimmer, *Synthesis* **1999**, 779.
- [9] U. S. Schubert, C. Eschbaumer, *Angew. Chem., Int. Ed.* **2002**, *41*, 2893.
- [10] B. G. G. Lohmeijer, U. S. Schubert, *Macromol. Chem. Phys.* **2003**, *204*, 1072.
- [11] M. Heller, U. S. Schubert, *Macromol. Rapid Commun.* **2001**, *22*, 1358.
- [12] S. Kelch, M. Rehahn, *Macromolecules* **1999**, *32*, 5818.
- [13] R. Dobrawa, F. Würthner, *J. Polym. Sci., Part A: Polym. Chem.* **2005**, *43*, 4981.

- [14] P. D. Vellis, J. A. Mikroyannidis, C. N. Lo, C. S. Hsu, *J. Polym. Sci., Part A: Polym. Chem.* **2008**, *46*, 7702.
- [15] A. Winter, C. Friebe, M. Chiper, M. D. Hager, U. S. Schubert, *J. Polym. Sci., Part A: Polym. Chem.* **2009**, *47*, 4083.
- [16] K. Y. K. Man, H. L. Wong, W. K. Chan, A. B. Djuricic, E. Beach, S. Rozeveld, *Langmuir* **2006**, *22*, 3368.
- [17] S. Flores-Torres, G. R. Hutchison, L. J. Soltzberg, H. D. Abruna, *J. Am. Chem. Soc.* **2006**, *128*, 1513.
- [18] E. C. Constable, C. Thompson, *J. Chem. Soc., Dalton* **1992**, 3467.
- [19] E. C. Constable, A. M. W. Cargil Thompson, *J. Chem. Soc., Chem. Commun.* **1992**, 617.
- [20] D. G. Kurth, M. Higuchi, *Soft Matter* **2006**, *2*, 915.
- [21] S. C. Yu, C. C. Kwok, W. K. Chan, C. M. Che, *Adv. Mater.* **2003**, *15*, 1643.
- [22] Y. Y. Chen, Y. T. Tao, H. C. Lin, *Macromolecules* **2006**, *39*, 8559.
- [23] Y. Y. Chen, H. C. Lin, *Polymer* **2007**, *48*, 5268.
- [24] C. Ulbricht, B. Beyer, C. Friebe, A. Winter, U. S. Schubert, *Adv. Mater.* **2009**, *21*, 4418.
- [25] V. Marin, E. Holder, R. Hoogenboom, U. S. Schubert, *J. Polym. Sci., Part A: Polym. Chem.* **2004**, *42*, 4153.
- [26] E. Holder, B. M. W. Langeveld, U. S. Schubert, *Adv. Mater.* **2005**, *17*, 1109.
- [27] S. Günes, H. Neugebauer, N. S. Sariciftci, *Chem. Rev.* **2007**, *107*, 1324.
- [28] A. C. Grimsdale, K. L. Chan, R. E. Martin, P. G. Jokisz, A. B. Holmes, *Chem. Rev.* **2009**, *109*, 897.
- [29] K. Müllen, U. Scherf, *Organic Light Emitting Devices*, Wiley-VCH, Weinheim, Germany 2006.
- [30] A. Wild, C. Friebe, A. Winter, M. D. Hager, U.-W. Grummt, U. S. Schubert, *Eur. J. Org. Chem.* **2010**, 1859.
- [31] F. Schlütter, A. Wild, A. Winter, M. D. Hager, C. Friebe, U. S. Schubert, *Macromolecules* **2010**, *43*, 2759.
- [32] M. Chiper, *Advanced supramolecular assemblies based on terpyridine metal complexes*, Ph.D. Thesis, Eindhoven University of Technology (Eindhoven) December, 2008.
- [33] D. Schubert, C. Tziatzios, P. Schuck, U. S. Schubert, *Chem. Eur. J.* **1999**, *5*, 1377.
- [34] M. Rasa, U. S. Schubert, *Soft Matter* **2006**, *2*, 561.
- [35] G. M. Pavlov, D. Amoros, C. Ott, I. I. Zaitseva, J. G. de la Torre, U. S. Schubert, *Macromolecules* **2009**, *42*, 7447.
- [36] S. Kelch, M. Rehahn, *Chem. Commun.* **1999**, 1123.

Publication A4: “Synthesis and characterization of new self-assembled metallo-polymers containing electron-withdrawing and electron-donating *bis*(terpyridine) zinc(II) moieties”

Florian Schlütter, Andreas Wild, Andreas Winter, Martin D. Hager, Anja Baumgaertel, Christian Friebe, Ulrich S. Schubert

Macromolecules **2010**, *43*, 2759–2771.

Reprinted with permission from: American Chemical Society (Copyright 2010)

Synthesis and Characterization of New Self-Assembled Metallo-Polymers Containing Electron-Withdrawing and Electron-Donating Bis(terpyridine) Zinc(II) Moieties

Florian Schlütter,[†] Andreas Wild,^{†,‡} Andreas Winter,^{‡,§} Martin D. Hager,^{†,‡}
Anja Baumgaertel,^{†,‡} Christian Friebe,^{†,‡} and Ulrich S. Schubert^{*,†,‡,§}

[†]Laboratory of Organic and Macromolecular Chemistry, Friedrich-Schiller-University Jena, Humboldtstr. 10, 07743 Jena, Germany, [‡]Dutch Polymer Institute (DPI), P.O. Box 902, 5600 AX Eindhoven, The Netherlands, and [§]Laboratory of Macromolecular Chemistry and Nanoscience, Eindhoven University of Technology, P.O. Box 513, 5600 MB Eindhoven, The Netherlands

Received September 26, 2009; Revised Manuscript Received January 17, 2010

ABSTRACT: A series of rigid π -conjugated bis(terpyridines) (**M1–M7**) bearing electron-acceptor spacer units in 4'-position was synthesized in moderate to high yields by Pd⁰-catalyzed Sonogashira cross-coupling reactions. The compounds were fully characterized by NMR spectroscopy, MALDI-TOF mass spectrometry, elemental analysis and their photophysical properties were discussed in detail. These new bis(terpyridines) were applied for the self-assembly reaction with Zn^{II} ions to form metallo-homo polymers (**P1–P7**). Broadened NMR signals and UV-vis titration experiments confirmed the successful polymerization. The electro-optical properties of the materials were investigated in detail. Band gaps up to 2.08 eV and bright blue to orange photoluminescence with quantum yields of 18 to 66% were observed strongly depending on the nature of the π -conjugated bis(terpyridine) system. In combination with electron-donor ditopic terpyridine ligands (**MD1** and **MD2**), two Zn^{II} random copolymers (**R1** and **R2**) were synthesized. These materials were investigated by UV-vis absorption and photoluminescence experiments in dilute solution and in the solid state, prepared by spin-coating from DMF solutions. Thereby, random copolymer **R2** featured an energy transfer from the donor to the acceptor part in dilute solution.

Introduction

In the extensive search for new materials for optoelectronic applications, metal–ligand coordination has gained much interest in the last decades.^{1–3} By varying the metal–ligand combination, the properties of such supramolecular assemblies can be tuned, not only with respect to their binding strength, reversibility and solubility, but also with respect to their optoelectronic properties.^{4–10}

Therefore, several *N*-heterocyclic ligands, e.g., 2,2'-bipyridine, 1,10-phenanthroline, and, in particular, [2,2':6',2'']-terpyridine, attracted much interest as supramolecular templates due to their high binding affinity towards many transition metal ions in low oxidation states, through $d\pi-p\pi^*$ bonding and the prevention of Δ/Λ -chirality compared to 2,2'-bipyridine metal complexes.^{11,12} This work focuses on [2,2':6',2'']-terpyridines bearing π -conjugated substituents in 4'-position,^{8,12–15} which are showing interesting photophysical as well as electrochemical properties. Furthermore, bis(terpyridines) allow the electronic communication between the metal-complexed terpyridine units pointing out their potential in the design of functional materials.^{9,10,16–19} In combination with transition metal ions [2,2':6',2'']-terpyridines form distorted octahedral complexes showing different stabilities from kinetically inert (e.g., Ru^{II} and Ni^{II}) to labile (e.g., Zn^{II}).^{10,20} With respect to this, the availability and the low costs of zinc(II) ions show a considerable advantage compared with the other potential metals.

Such metal complexes have found numerous applications as luminescent sensors in molecular biology and medical diagnostics, as photocatalysts, effective materials in self-assembled molecular devices as well as molecular wires.^{21,22} The combination of the properties of [M(tpy)]²⁺ complexes (i.e., optical, electrochemical, magnetic properties) with the versatile properties of organic polymers (i.e., mechanical properties, solubility, processability) leads to fascinating possibilities.^{2,23–25} The group of Constable and Thompson developed an approach for the utilization of ditopic [2,2':6',2'']-terpyridines as building blocks for the self-assembly with transition metal ions to metallo-polymers and -oligomers.²⁶ Beside highly stable Ru^{II} metallo-polymers, Zn^{II} terpyridine metallo-polymers gained recently interest due to their well-defined structures and enhanced photo- and electroluminescent properties at room temperature.^{23,27,28} Therefore, Zn^{II} containing metallo-polymers are promising materials for potential applications, e.g., in organic light-emitting diodes (OLED). Such systems provide large equilibrium constants, which are essential for the thermodynamic driven polymer formation.^{9,10,29} In previous work in this field, the group of Würthner showed the metal-directed self-assembly of highly fluorescent [2,2':6',2'']-terpyridine bearing perylene bisimide in 4'-position to photoactive metallo-polymers and presented their spectroscopic and structural properties.^{9,19} Lin et al. applied fluorene substituted ditopic [2,2':6',2'']-terpyridines for the synthesis of Zn^{II} containing metallo-homopolymers and metallo-alt-copolymers.^{23,28} According to Che and Cao, the incorporation of [2,2':6',2'']-terpyridine Zn^{II} moieties into different main-chain structures leads to a variety from violet to yellow colors with high PL quantum yields.^{30,31} Furthermore, we

*Author for correspondence. Telephone: +49(0) 3641 948200. Fax: +49(0) 3641 948202. E-mail: ulrich.schubert@uni-jena.de.

showed several types of bis(terpyridines) bearing electron-donating π -conjugated spacer units with remarkable photophysical properties and used them as building blocks for the construction of Zn^{II} containing metallo-polymers.^{24,32,33} We could improve the film-forming ability of such systems by incorporating polymer side-chains to π -conjugated bis(terpyridines).¹⁶

In continuation of this work, we focused on the synthesis of bis(terpyridine) building blocks with electron-accepting π -conjugated spacer units, which should significantly influence the optical properties and, lead in combination with the established electron-donor units, towards supramolecular low band gap materials.³⁴ Potential photovoltaic materials, e.g., π -conjugated systems, have to cover the red and near-infrared ranges of the terrestrial solar spectrum, based on the maximum photon flux density of the sunlight, located at approximately 700 nm (bandgap, $E_g \approx 1.77$ eV). Hence, it is desirable to develop π -conjugated systems with broader absorptions by reducing their E_g values.³⁵ The combination of electron-acceptors with electron-donors leads to a significant decrease of the distance (bandgap, E_g) between the highest occupied molecular orbital (HOMO) of the donor and the lowest unoccupied molecular orbital (LUMO) of the acceptor, which results in a bathochromic shift of the absorption.^{34,35} Therefore, we attached well-known strong electron-acceptors, e.g., [2,1,3]benzothiadiazole, terephthalates, thieno[3,4-*b*]pyrazine, quinoxaline as well as a nitrile-groups containing system to the [2,2':6',2'']-terpyridine in 4'-position using the Pd⁰-catalyzed *Sonogashira* cross-coupling reaction.

These ditopic ligands were polymerized via the coordination of Zn^{II} ions into the corresponding metallo-homo polymers. Furthermore, two statistical metallo-random polymers were synthesized in combination with ditopic terpyridine ligands containing π -conjugated electron-donating spacers. This combination should lead to a transfer of energy from the excited donor part to the acceptor moiety, which can consequently relax under emission. The investigation of energy as well as electron transfer processes is crucial for the understanding of the photosynthetic processes and the design of artificial light-to-energy conversion systems.^{36,37} Besides that, an efficient energy transfer process allows long-range information transmission, which could be applied in the development of molecular devices and machines for information technology.³⁸

The photophysical and electrochemical properties of the new type of bis(terpyridines) and their corresponding metallo-polymeric materials are discussed in detail.

Experimental Section

Materials and General Experimental Details. All chemicals were purchased from Aldrich, Acros Organics and Alfa Aesar and were of reagent grade and used as received, unless otherwise specified. The solvents were purchased from Biosolve, Aldrich and Acros Organics and were dried and distilled according to standard procedures. Chromatographic separation was performed with standardized silica gel 60 (Merck) and aluminum oxide 90 neutral (Molekula). The reaction progress was controlled by thin layer chromatography (TLC) using aluminum sheets precoated with silica gel 60 F₂₅₄ (Merck) and aluminum oxide 60 F₂₅₄ neutral (Macherey-Nagel).

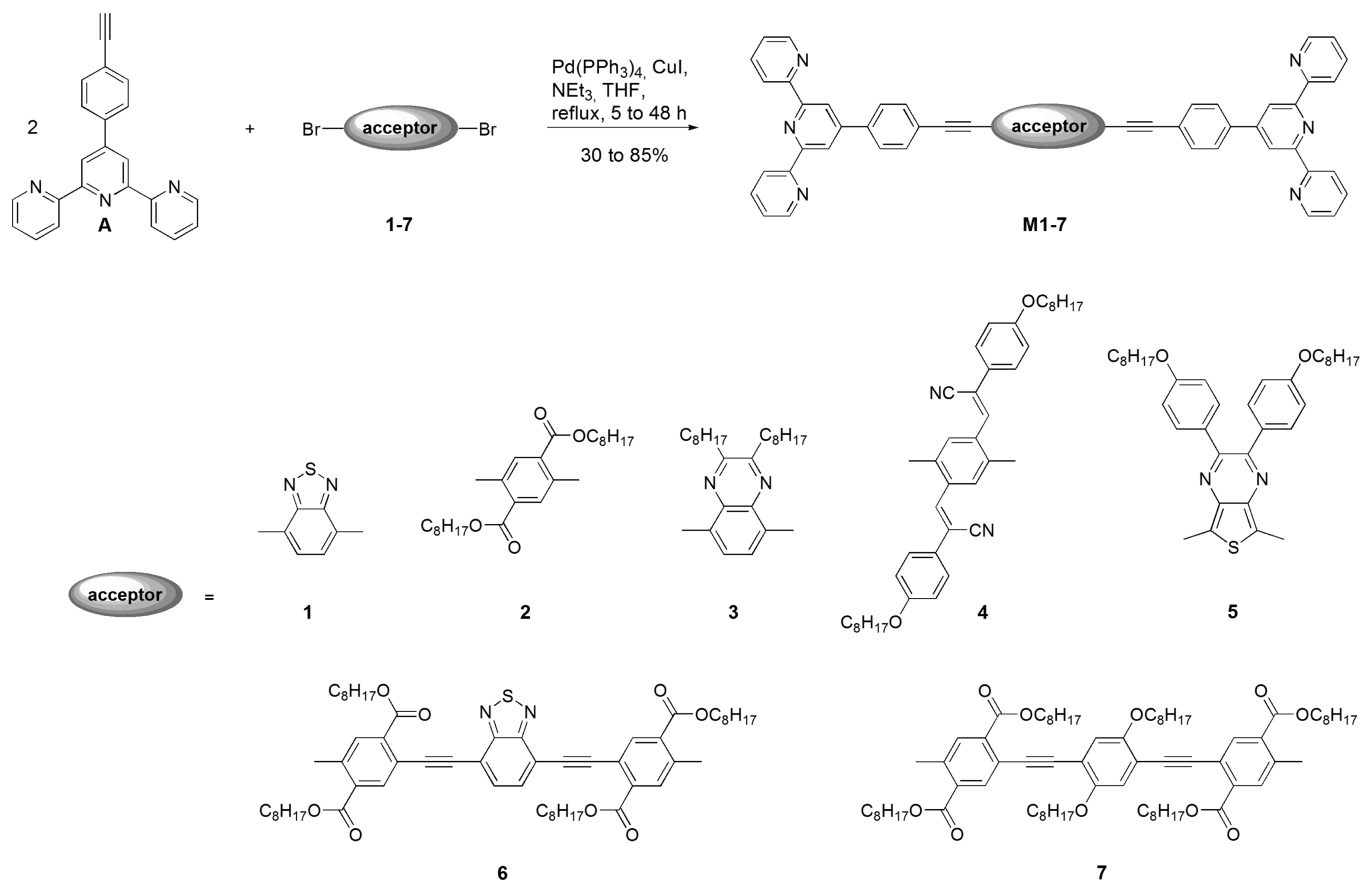
4'-(4-Ethynylphenyl)-[2,2':6',2'']terpyridine (**A**),^{39–41} 4,7-dibromo-[2,1,3]benzothiadiazole (**1**),⁴² dioctyl 2,5-dibromoterephthalate (**2**),⁴³ 5,8-dibromo-2,3-bis(2-ethylhexyl)quinoxaline (**3**),^{44,45} (2Z,2'Z)-3,3'-(2,5-dibromo-1,4-phenylene)bis(2-(4-(2-ethylhexyloxy)phenyl)acrylonitrile) (**4**),^{46,47} 5,7-dibromo-2,3-bis(4-(octyloxy)phenyl)thieno[3,4-*b*]pyrazine (**5**),^{48,49} tetraoctyl 5,5'-([2,1,3]benzothiadiazole-4,7-diyl)bis(ethyne-2,1-diyl)bis(2-bromoterephthalate) (**6**), and tetraoctyl 5,5'-(2,5-bis(octyloxy)-1,4-phenylene)bis(ethyne-2,1-diyl)bis(2-bromoterephthalate) (**7**) were prepared according to the literature (see the Supporting Information for the detailed

synthetic procedures and characterization). The synthesis of 4'-(4-((1*E*,7*E*)-4-(2-(4-(2-(4-((*E*)-4-([2,2':6',2'']terpyridine-4'-yl)-styryl)phenyl)ethynyl)-2,5-bis(2-ethylhexyloxy)phenyl)ethynyl)-styryl)-phenyl)-[2,2':6',2'']terpyridine (**MD1**) and 2,7-bis(4-([2,2':6',2'']terpyridine-4'-yl)phenyl)ethynyl)-9,9-bis(octyloxy)-9*H*-fluorene (**MD2**) as well as their Zn^{II} metallo-homo polymers is reported elsewhere.⁵⁰

Instrumentation. 1D (¹H, ¹³C) and 2D (¹H–¹H gCOSY, HSQC, HMBC) nuclear magnetic resonance (NMR) spectra were recorded on a Bruker Cryomagnēt BZH 400 (400 MHz), Bruker AC 300 (300 MHz) or Bruker AC 250 (250 MHz) instrument at 298 K. Chemical shifts are reported in parts per million (ppm, δ scale) relative to the residual signal of the deuterated solvent. Coupling constants are given in Hz. UV–vis absorption and photoluminescence (PL) emission spectroscopy were performed on an Analytik Jena SPECORD 250 and Jasco FP-6500 spectrometer, respectively, at 298 K. Absolute photoluminescence quantum yields were evaluated at 298 K on a Hamamatsu photonic multi-channel analyzer C 10027. For these techniques 10^{–6}–10^{–5} M solutions in chloroform or *N,N*-dimethylformamide (DMF) were used. Matrix-assisted laser desorption/ionization time-of-flight (MALDI–TOF) mass spectra were obtained from an Ultraflex III TOF/TOF mass spectrometer with dithranol as matrix in reflector as well as linear mode. Elemental analyses were carried out on a CHN-932 Automat Leco instrument. Cyclic voltammetry (CV) measurements were performed using a PA4 polarographic analyzer (Laboratory instruments, Prague, Czech Republic) with a three electrode cell. Platinum (Pt) wire electrodes were used as both working and counter electrodes and a nonaqueous Ag/Ag⁺ electrode (Ag in 0.1 M AgNO₃ solution) was used as reference electrode. Thin films coated onto Pt electrodes from acetonitrile solutions containing 0.1 M tetra-*n*-butylammonium hexafluorophosphate ((TBA)PF₆) were used for these measurements. All measurements and film preparations were performed under nitrogen atmosphere within a glovebox. Polymer thin films were prepared by spin-coating polymer solutions from DMF (20 mg/mL) using a spin-coating rate of 1000 rpm for 100 s onto silica fused substrates for optical studies. The glass slides were ultrasonicated in 2% Helmanex-solution (Helma) and 2-propanol for 20 min, in between washed 12 times with distilled water, and finally placed into an ethanol solution and dried using nitrogen. UV–vis absorption and PL emission spectra of these thin films were measured with a Hitachi F-4500 fluorescence spectrophotometer. Layer thicknesses were measured outside the glovebox using a KLA-Tencor P-10 profilometer.

General Procedure for the Synthesis of the Bis(terpyridine) Monomers (M1–M7). To an argon-degassed mixture of 4'-(4-ethynylphenyl)-[2,2':6',2'']terpyridine (**A**, 0.50 mmol) and an aromatic bromide (**1–7**, 0.25 mmol) in dry THF (30 mL) and dry triethylamine or diisopropylamine (10 mL) were added tetrakis(triphenylphosphine)palladium(0) (10 mol %) and copper(I) iodide (10 mol %), and the reaction mixture was refluxed until TLC indicated complete conversion (5 to 48 h). After the reaction had cooled to room temperature, the precipitated ammonia salt was filtered off and washed intensively with THF. Subsequently, dichloromethane was added and the solution was washed with saturated aqueous NH₄Cl/EDTA solution and dried over anhydrous MgSO₄. After removal of the solvents, the product was precipitated from methanol. Further purification was achieved by column chromatography (aluminum oxide, CH₂Cl₂ as eluent).

4,7-Bis((4-([2,2':6',2'']terpyridine-4'-yl)phenyl)ethynyl)[2,1,3]-benzothiadiazole (M1). According to the above-mentioned general procedure, **M1** was obtained after filtration from the reaction mixture, intensive washing with water and repeated recrystallization from large amounts of chloroform as orange solid (169 mg, 85%). ¹H and ¹³C NMR spectra could not be obtained due to the very low solubility of **M1** in organic solvents. MALDI–TOF MS (dithranol): *m/z* = 799.25 (100%, [M + H]⁺). Anal. Calcd for C₅₂H₃₀N₈S: C, 78.18; H, 3.78; N, 14.03; S, 4.01. Found: C, 77.98; H, 4.02; N, 14.21; S, 3.76.

Scheme 1. Schematic Representation of the Synthesis of Bis(terpyridines) M1–M7 Using Pd⁰-Catalyzed Sonogashira Cross-Coupling Reactions

(*m_c*, H^{3',5'}). Anal. Calcd for C₇₀H₆₄F₁₂N₈P₂Zn: C, 61.25; H, 4.70; N, 8.16. Found: C, 60.71; H, 4.13; N, 7.58.

Metallo-Homo Polymer P4: {[Zn(M4)](PF₆)₂}_{*n*}. According to the above-mentioned procedure, homo polymer **P4** was obtained after three times precipitation as yellow solid (8 mg, 20%).⁵¹ ¹H NMR (DMSO-*d*₆, 300 MHz, δ): 0.85 (*m_c*, CH₃), 1.04–1.54 (*m*, CH₂), 3.08 (*m_c*, O–CH₂), 7.05 (*m_c*, H^{aryl}), 7.52 (*m_c*, H^{5,5'}), 7.93 (*m_c*, H^{6,6'}), 8.30 (*m_c*, H^{aryl}), 8.60 (*m_c*, H^{4,4'}), 8.79 (*m_c*, H^{aryl}), 9.13 (*m_c*, H^{3,3'}), 9.34 (*m_c*, H^{3',5'}). Anal. Calcd for C₈₆H₇₄F₁₂N₈O₂P₂Zn: C, 64.28; H, 4.64; N, 6.97. Found: C, 63.78; H, 4.04; N, 6.77.

Metallo-Homo Polymer P5: {[Zn(M5)](PF₆)₂}_{*n*}. According to the above-mentioned procedure, homo polymer **P5** was obtained as orange solid (21 mg, 54%). ¹H NMR (DMSO-*d*₆, 300 MHz, δ): 0.84 (*m_c*, CH₃), 0.99–1.47 (*m*, CH₂), 3.99 (*m_c*, O–CH₂), 7.07 (*m_c*, H^{aryl}), 7.52 (*m_c*, H^{5,5'}), 7.97 (*m_c*, H^{6,6'}), 8.03 (*m_c*, H^{aryl}), 8.30 (*m_c*, H^{4,4'}), 8.76 (*m_c*, H^{aryl}), 9.19 (*m_c*, H^{3,3'}), 9.48 (*m_c*, H^{3',5'}). Anal. Calcd for C₈₀H₇₀F₁₂N₈O₂P₂SZn: C, 61.48; H, 4.51; N, 7.17; S, 2.05. Found: C, 60.63; H, 3.58; N, 6.64; S, 1.65.

Metallo-homo polymer P6: {[Zn(M6)](PF₆)₂}_{*n*}. According to the above-mentioned procedure, homo polymer **P6** was obtained after three times precipitation as yellow solid (23 mg, 48%).⁵¹ ¹H NMR (DMSO-*d*₆, 300 MHz, δ): 0.75 (*m_c*, CH₃), 0.98–1.48 (*m*, CH₂), 4.40 (*m_c*, O–CH₂), 7.52 (*m_c*, H^{5,5'}), 8.06 (*m_c*, H^{6,6'}), 8.08 (*m_c*, H^{aryl}), 8.30 (*m_c*, H^{4,4'}), 8.68 (*m_c*, H^{aryl}), 8.77 (*m_c*, H^{aryl}), 9.15 (*m_c*, H^{3,3'}), 9.41 (*m_c*, H^{3',5'}). Anal. Calcd for C₁₀₄H₁₀₂F₁₂N₈O₈P₂SZn: C, 63.11; H, 5.19; N, 5.66; S, 1.62. Found: C, 62.47; H, 4.78; N, 5.37; S, 1.22.

Metallo-Homo Polymer P7: {[Zn(M7)](PF₆)₂}_{*n*}. According to the above-mentioned procedure, homo polymer **P7** was obtained as yellow solid (44 mg, 82%). ¹H NMR (DMSO-*d*₆, 300 MHz, δ): 0.76 (*m_c*, CH₃), 0.97–1.53 (*m*, CH₂), 4.18 (*m_c*, O–CH₂), 4.40 (*m_c*, O–CH₂), 7.55 (*m_c*, H^{5,5'}), 8.04 (*m_c*, H^{6,6'}),

8.08 (*m_c*, H^{aryl}), 8.31 (*m_c*, H^{4,4'}), 8.69 (*m_c*, H^{aryl}), 8.77 (*m_c*, H^{aryl}), 9.16 (*m_c*, H^{3,3'}), 9.45 (*m_c*, H^{3',5'}). Anal. Calcd for C₁₂₀H₁₃₆F₁₂N₆O₁₀P₂Zn: C, 66.18; H, 6.29; N, 3.86. Found: C, 65.35; H, 4.23; N, 3.37.

Metallo-Random Copolymer R1: {[Zn(M1)](PF₆)₂]_{*n*}{[Zn(MD1)](PF₆)₂]_{*m*}. According to the above-mentioned procedure, random copolymer **R1** was obtained as yellow solid (42 mg, 68%). ¹H NMR (DMSO-*d*₆, 300 MHz, δ): 0.90 (*m_c*, CH₃), 0.99 (*m_c*, CH₃), 1.26–1.80 (*m*, CH₂), 4.01 (*m_c*, O–CH₂), 7.56 (*m_c*, H^{5,5'}), 7.78 (*m_c*, H^{aryl}), 7.99 (*m_c*, H^{6,6'}), 8.13 (*m_c*, H^{aryl}), 8.32 (*m_c*, H^{4,4'}), 8.58 (*m_c*, H^{aryl}), 8.74 (*m_c*, H^{aryl}), 8.78 (*m_c*, H^{aryl}), 9.15 (*m_c*, H^{3,3'}), 9.41 (*m_c*, H^{3',5'}).

Metallo-Random Copolymer R2: {[Zn(M3)](PF₆)₂]_{*n*}{[Zn(MD2)](PF₆)₂]_{*m*}. According to the above-mentioned procedure, random copolymer **R2** was obtained as green-yellow solid (48 mg, 70%). ¹H NMR (DMSO-*d*₆, 300 MHz, δ): 0.80 (*m_c*, CH₃), 0.94–1.57 (*m*, CH₂), 3.14 (*m_c*, O–CH₂), 7.54 (*m_c*, H^{5,5'}), 7.66 (*m_c*, H^{aryl}), 7.78 (*m_c*, H^{aryl}), 7.99 (*m_c*, H^{6,6'}), 8.06 (*m_c*, H^{aryl}), 8.31 (*m_c*, H^{4,4'}), 8.58 (*m_c*, H^{aryl}), 8.69 (*m_c*, H^{aryl}), 8.77 (*m_c*, H^{aryl}), 9.18 (*m_c*, H^{3,3'}), 9.47 (*m_c*, H^{3',5'}).

Results and Discussion

Synthesis and Characterization of Monomers M1–M7.

The synthetic route towards the ditopic bis(terpyridine) monomers **M1–M7** is illustrated in Scheme 1. The acceptor-type spacer units (**1–7**) were synthesized in multistep procedures, starting from commercial available compounds (see the Supporting Information for details). According to Scheme 1, the aromatic dibromides **1–7** were reacted with two equivalents of 4'-(4-ethynylphenyl)-[2,2':6',2'']terpyridine (**A**) under Pd⁰-catalyzed Sonogashira cross-coupling conditions. After precipitation from methanol and column chromatographic purification, the bis(terpyridines)

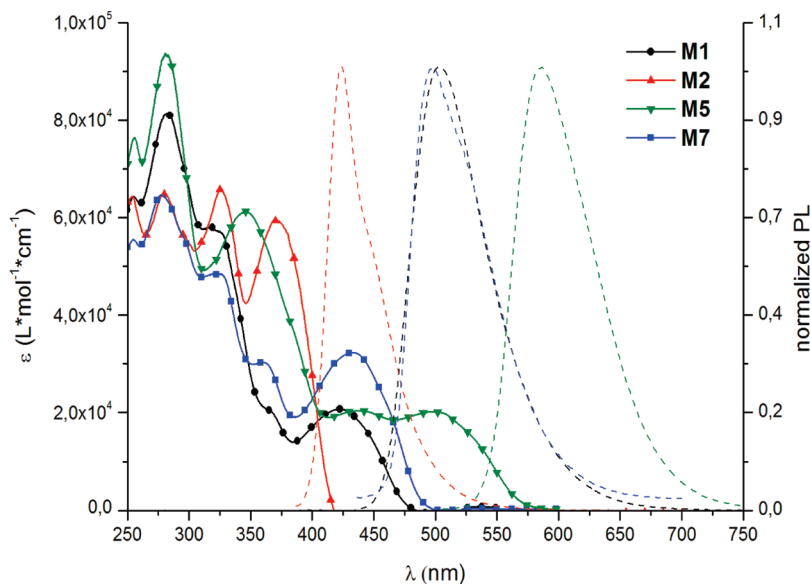


Figure 1. UV-vis absorption (solid lines) and normalized photoluminescence spectra (dashed line) of selected bis(terpyridines). For all spectra: 10^{-6} M in CHCl_3 , room temperature.

Table 1. Selected Photophysical Properties of Bis(terpyridines) M1–M7

| bis(terpyridine) | $\lambda_{\text{abs,max}}^a$ (nm) | $\lambda_{\text{PL,max}}^a$ (nm) | $\epsilon \times 10^4^{a,b}$ ($\text{M}^{-1} \cdot \text{cm}^{-1}$) | $\Phi_{\text{PL}}^{a,c}$ | Stokes shift (cm^{-1}) | $E_g^{\text{opt } d}$ (eV) |
|------------------|-----------------------------------|----------------------------------|---|--------------------------|-----------------------------------|----------------------------|
| M1 | 423, 365, 316, 282 | 503 | 2.07 | 0.79 | 3760 | 2.62 |
| M2 | 373, 325, 279, 254 | 424 | 5.93 | 0.63 | 3225 | 3.00 |
| M3 | 395, 317, 267, 252 | 443 | 3.01 | 0.68 | 2743 | 2.83 |
| M4 | 401(s), 354, 283, 253 | 484, 509(s) | 8.80 | 0.37 | 4277 | 2.74 |
| M5 | 498, 440, 346, 281, 255 | 587 | 2.02 | 0.69 | 3045 | 2.17 |
| M6 | 433, 361, 322, 279, 255 | 498 | 3.23 | 0.65 | 3014 | 2.58 |
| M7 | 427, 361, 328, 283 | 490 | 2.39 | 0.57 | 3011 | 2.56 |

^a For all spectra: 10^{-6} M in chloroform; (s) = shoulder. ^b Extinction coefficients of the lowest-energy absorption band. ^c Absolute quantum yields, uncorrected with respect to reabsorption. ^d $E_g^{\text{opt}} = h \cdot c / \lambda_{0.1\text{max}}$.

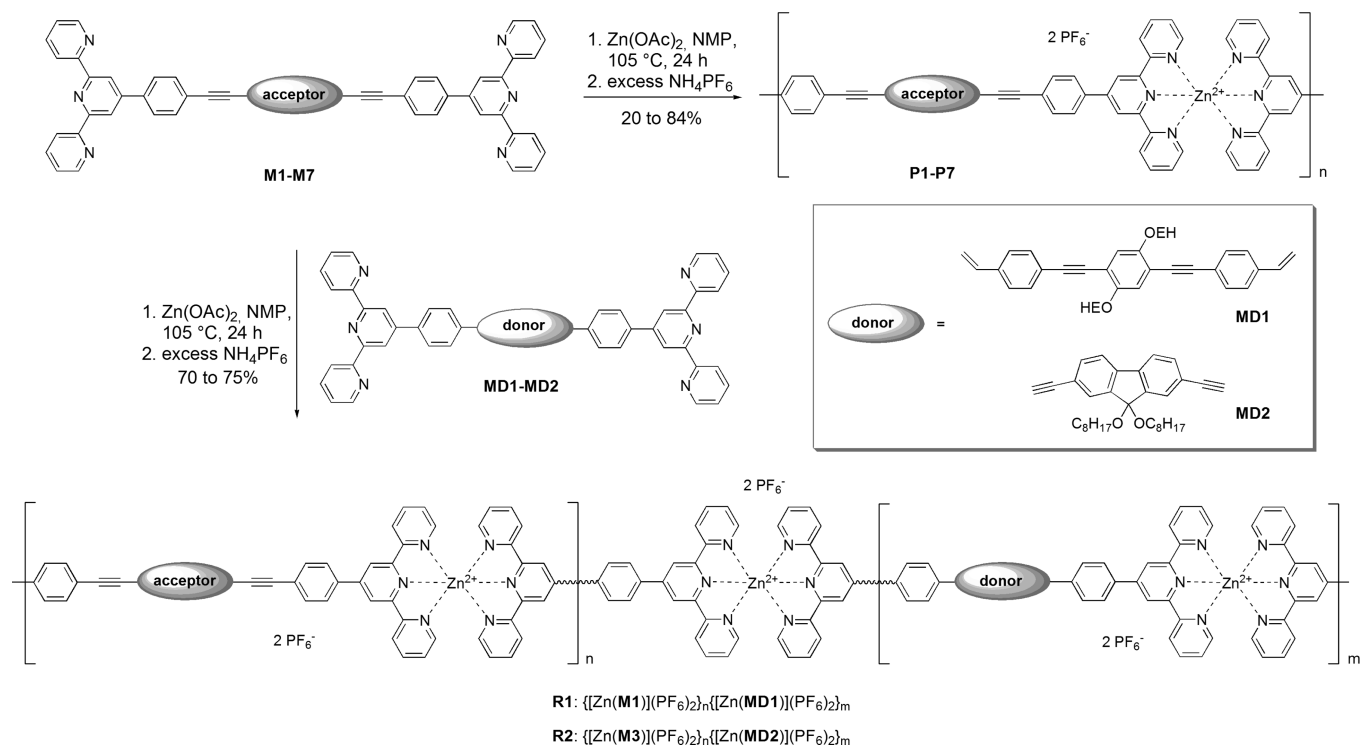
M1–M7 were obtained in moderate to good yields and fully characterized by NMR, UV-vis absorption, and photoluminescence spectroscopy as well as MALDI-TOF mass spectrometry and elemental analysis. The photophysical properties of **M1–M7** are summarized in Figure 1 and Table 1.

In order to investigate the influence of the electron-acceptor spacers and the length of the π -conjugated system on the photophysical properties of bis(terpyridines) **M1–M7**, UV-vis absorption and photoluminescence spectra were measured. In accordance with the literature, the absorption spectra of the ditopic ligands **M1–M7** featured two intense band regions.^{2,9,10,32,33,52} The bands at about 250 to 350 nm were assigned to the characteristic π - π^* transitions of the terpyridine moieties and show high extinction coefficients (ϵ) up to $95,000 \text{ M}^{-1} \cdot \text{cm}^{-1}$.^{23,28,33,52} Furthermore, the spectra are characterized by an intensive band in the visible region ($\lambda_{\text{abs}} = 370$ – 498 nm) corresponding to π - π^* transitions of the overall π -conjugated system with extinction coefficients up to $88,000 \text{ M}^{-1} \cdot \text{cm}^{-1}$. However, in comparison to all other synthesized systems, bis(terpyridine) **M5** showed the most pronounced bathochromic shift of the absorption maximum and, thereby, the smallest optical energy band gap, although **M5** bears *n*-octyl chains which are known to disturb rigidity and planarity.⁴⁸ This indicates a strong electronic interaction of the lateral electron-rich *p*-dialkoxy-benzene substituents with the electron-poor thieno[3,4-*b*]pyrazine unit, resulting in a push-pull effect. In consequence of this interaction, the quinoid contribution to the electronic structure of the ground state is increased, resulting in a destabilization of the

HOMO energy location with a simultaneous stabilization of the LUMO energy location, which induces a significantly lowered energy band gap and a strong red-shift of the absorption, as observed. The dimension of this bathochromic shift correlates well with the intensity of the intramolecular charge transfer.³⁴ The π -extended systems **M6** and **M7** also exhibit a bathochromic shift as well as a lowered energy band gap, in comparison to their analogues with smaller spacer units (**M1** and **M2**). In particular, the comparison of **M6** and **M1** reveals that the influence of the π -extension is partially compensated by a steric hindrance due to the alkyl chains, which results only in a small red-shift of the absorption maximum of about 10 nm. The increase of the extinction coefficient of **M6** relative to **M1** can be ascribed to an increasing absorption cross section of the central chromophores within the bis(terpyridines).³³

The photoluminescence spectra and absolute quantum yields were obtained by excitation at the lowest-energy absorption maxima of the bis(terpyridine) systems. In dilute solution, emission maxima in the range of 392 to 587 nm, corresponding to Stokes shifts between 2700 and 4500 cm^{-1} , were observed. The large Stokes shift of bis(terpyridine) **M4** (4300 cm^{-1}) can be explained by a more extended conjugation in the excited state in comparison to the other systems.^{33,50} Theoretical calculations on these systems would help to investigate this behavior further.

In general, the photoluminescence properties are equally influenced by the electronic structure as previously discussed for the UV-vis absorption behavior. Again, bis(terpyridine) **M5** showed the most distinctive bathochromic shift of the

Scheme 2. Schematic Representation of the Metallo-Polymerization of M1–M7 to the Homo Polymers P1–P7 (Top) and Random Copolymers R1 and R2 (Bottom)

emission maximum, thus the effects mentioned above have to be considered again. As a consequence of its Stokes shift (3000 cm^{-1}), **M5** emits with an intensive orange-red color ($\lambda_{\text{PL,max}} = 587 \text{ nm}$).

By incorporation of electron-rich dialkoxy-benzene sub-units into the spacer (push–pull effect) and the resulting elongation of the π -conjugation, the emission maximum of **M7** (bright green emission) is notably red-shifted in comparison to the structurally related bis(terpyridine) **M2** (blue emission).

All ditopic ligands featured high quantum yields (Φ_{PL}) in the range of 40 to 80%. The highest quantum yields were obtained for bis(terpyridines) **M1** and **M5**.

Synthesis of the Zinc(II)-Containing Metallo-Polymers. The synthesis of the Zn^{II} -based metallo-polymers is depicted in Scheme 2. The metallo-polymerization by self-assembly was carried out according to methods described in literature.^{9,16,23} Bis(terpyridines) **M1–M7** were heated with zinc(II) acetate at an exact stoichiometric ratio of 1:1 in *N*-methylpyrrolidone (NMP), followed by subsequent anion exchange with ammonium hexafluorophosphate to yield the metallo-homo polymers **P1–P7**. In the case of the random copolymers (**R1** and **R2**) donor-type bis(terpyridines)⁵⁰ with a dialkoxy-benzene (**MD1**) and a fluorene spacer unit (**MD2**), respectively, were utilized in combination with the acceptor-type bis(terpyridines) (**M1** and **M3**). Here, both ditopic ligands were used in a 1:1 ratio in order to obtain metallo-copolymers with a 50% content of each monomer. Since, no signals are separated in the NMR spectra of **R1** and **R2**, we could not apply a selective integration in order to get information about the arrangement of the monomers (alternating/random) along the polymer chains. For this purpose, we assume a random distribution in both copolymers (**R1** and **R2**).

The resulting polymers were purified by repeated precipitation from NMP in diethyl ether and dried in vacuum, leading to homo polymers **P1–P7** (yield: 20–84%) and

random copolymers **R1** and **R2** (yields: 75% and 70%, respectively). Because of the reactivity of Zn^{II} ions and the stability of the bis(terpyridine)– Zn^{II} moieties, the self-assembly process occurs under comparably mild conditions.^{23,24}

In comparison to the monomers **M2–M7** (**M1** was hardly soluble itself), all metallo-polymers showed a significantly decreased solubility in common organic solvents. This behavior is mainly caused by the highly linear-rigid structure of the polymer backbone as well as by the involved charged metal ions attached leading to solubility only in highly polar aprotic solvents, e.g., DMSO, DMF, NMP, or acetonitrile.^{9,23,24}

The molar mass of the resulting polymers could not yet be determined because both size exclusion chromatography (SEC) and MALDI–TOF mass spectrometry were not usable for the characterization of Zn^{II} -based metallo-polymers. In contrast to related ruthenium(II)- or nickel(II)-containing metallo-polymers,⁵³ Zn^{II} -based systems are not stable under the measurement conditions owing to a considerably weaker binding strength of the terpyridine ligand to the metal ion.²

However, characterization by ^1H NMR spectroscopy indicated the formation of the desired metallo-polymers by broadened signals of the terpyridine ligand, which is a typically feature of polymeric materials, as well as by the absence of the signals from the uncomplexed terpyridine unit (Figure 2). Additionally, this behavior proves that the polymeric structure remains unaffected in polar solvents. Furthermore, and in accordance with the literature, a clear downfield shift of the (5,5''), (4,4''), (3,3'')- and (3',5'')-terpyridine signals, upon coordination to the Zn^{II} ions, was observed.^{9,19,23,24} The (6,6'')-terpyridine signals are significantly upfield shifted due to the location above the ring plane of the adjacent ligand. These assignments are based on the comparison of the spectra to those reported for related homoleptic Zn^{II} model complexes.^{9,24} A calculation of the molar mass of the metallo-polymers via the integration of

end group-signals was not possible due to the absence of any end group-signals. However, considering the typical limit of the NMR spectroscopy ($\approx 5\%$), the synthesized metallo-polymers should consist of more than 30 repeating units [for comparison, see ref 60]. Hence, the molar mass of **P1–P7** was estimated to be not less than 25 000 to 50 000 g/mol.

Additionally, elemental analysis of the obtained metallo-polymers provides an indication that the relative composition is close to the expected stoichiometric ratio of 1:1 for the Zn^{II} ions and bis(terpyridine) ligands.

For further characterization of the homo polymers **P1–P7**, UV–vis titration experiments were carried out to confirm their supramolecular structure (Figure 3). It is known from the literature that the formation of linear metallo-polymers can be controlled by the exact stoichiometric ratio of metal ion to ditopic ligand.^{9,24,28} Upon

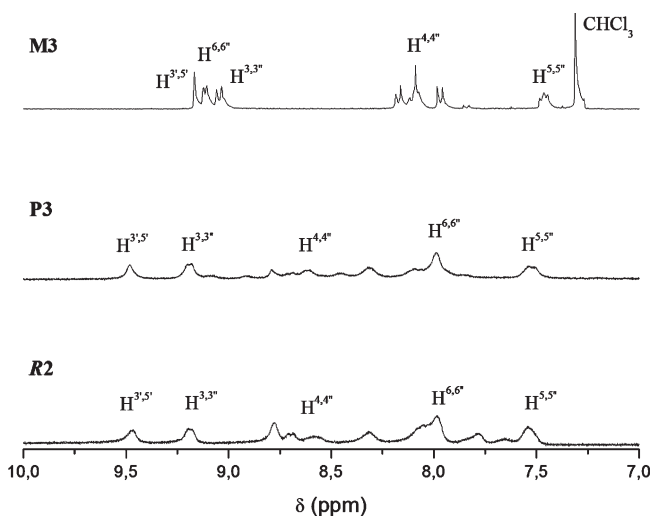


Figure 2. ^1H NMR spectra (aromatic region) of bis(terpyridine) **M3** (top, CDCl_3), homo polymer **P3** (middle, $\text{DMSO-}d_6$) and random copolymer **R2** (bottom, $\text{DMSO-}d_6$). The signals belonging to the terpyridine moiety are assigned; the other signals correspond to the π -conjugated spacer. For all spectra: 300 MHz, room temperature.

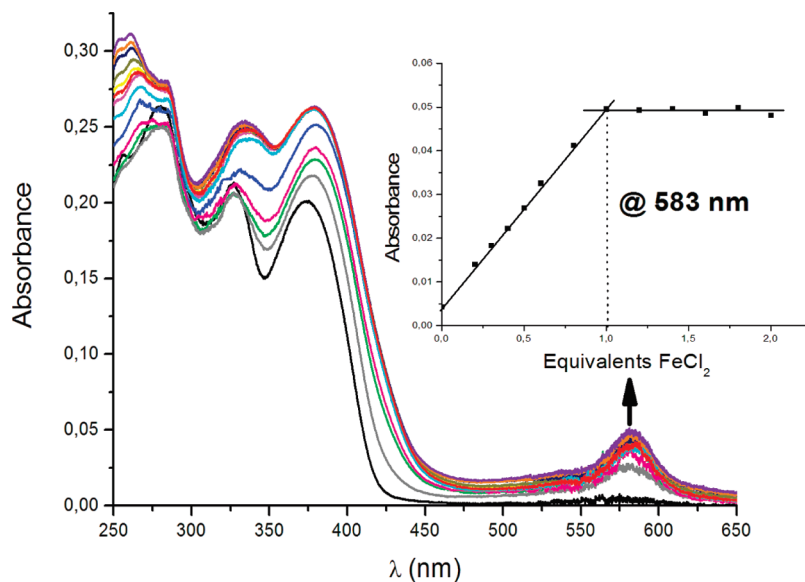


Figure 3. UV–vis absorption spectra acquired upon the titration of monomer **M2** (10^{-5} M in chloroform) with FeCl_2 (10^{-4} M in methanol). The absorbance at the MLCT band (583 nm) as a function of added FeCl_2 solution is shown as an inset.

stepwise addition of Fe^{II} to a solution of bis(terpyridine) **M2**, the absorption spectra revealed the appearance of a metal-to-ligand charge-transfer (MLCT) band at 583 nm, characteristic for iron(II)-based supramolecular assemblies. Furthermore, a shift of three other absorption bands at 373, 333, and 260 nm could be observed. The intensity of the MLCT band is increasing linearly up to a stoichiometric ratio of 1:1, which indicates the formation of a metallo-polymer.

The absence of any shoulder at the π – π^* transition of the whole π -conjugated system at 373 nm with increasing addition of Fe^{II} ions accommodates to the fact that an electron-withdrawing spacer unit is attached to the terpyridine. Usually this circumstance is attributed to a charge-transfer occurring between electron-rich spacer units and the electron deficient metal-coordinated terpyridine moiety.^{23,28}

The titration experiments clearly revealed that at a 1:1 ratio of metal ion to bis(terpyridine) ligand a supramolecular assembly is formed. Depolymerization beyond the point of equivalence^{23,24} has not been observed in the present case due to the stable $\text{Fe}^{\text{II}}(\text{tpy})_2$ moiety.

Electrochemical Properties. Applying cyclic voltammetry, the energy levels of the HOMO, corresponding to the ionization potential, and of the LUMO, corresponding to the electron affinity, can be estimated. The electrochemical properties of the homo polymers (**P1–P7**) and random copolymers (**R1** and **R2**) were obtained from thin films of the materials coated on Pt wires and are summarized in Table 2 and Figure 4.

All homo polymers (**P1–P7**) and both random copolymers (**R1** and **R2**) exhibited quasi-reversible reduction peaks between -1.29 and -1.65 V at scans up to -2.5 V. In agreement with the literature, these waves were attributed to the reduction of the terpyridine moiety and the attached π -conjugated spacer unit inside the polymers.^{23,24,28} Furthermore, most of the metallo-polymers featured distinct reduction waves at more negative potentials. As expected, no significant oxidation processes were observed up to 1.5 V. Because of the stable d^{10} electron configuration of the Zn^{II} metal centers, oxidation is difficult to observe.^{23,24,28} The estimated LUMO levels are based on the first reduction wave

Table 2. Electrochemical Properties of the Homo Polymers P1–P7 and the Random Copolymers R1 and R2, respectively

| polymer | $E_{1/2}^{red a}$ (V) | $E_{onset}^{red a}$ (V) | LUMO ^b (eV) | HOMO ^c (eV) | $E_g^{opt d}$ (eV) |
|-----------|-----------------------|-------------------------|------------------------|------------------------|--------------------|
| P1 | −1.44, −1.81, −2.05 | −1.69 | −3.16 | −5.75 | 2.59 |
| P2 | −1.29, −1.60 | −1.49 | −3.36 | −6.21 | 2.85 |
| P3 | −1.29, −1.62 | −1.49 | −3.36 | −6.14 | 2.78 |
| P4 | −1.61, −2.16 | −1.68 | −3.17 | −5.90 | 2.73 |
| P5 | −1.65, −2.19 | −1.63 | −3.22 | −5.30 | 2.08 |
| P6 | −1.61, −2.01 | −1.62 | −3.23 | −5.56 | 2.33 |
| P7 | −1.65 | −1.45 | −3.40 | −5.91 | 2.51 |
| R1 | −1.54, −1.87 | −1.73 | −3.12 | −5.88 | 2.76 |
| R2 | −1.29, −1.66, −1.95 | −1.54 | −3.31 | −6.22 | 2.91 |

^a Half-wave potential of the reduction waves (films (0.1 M (TBA)PF₆ in CH₃CN) coated on Pt wires, scan rate 50 mV·s^{−1}); potentials are reported versus a Ag/Ag⁺ electrode (Ag in 0.1 M AgNO₃ solution). ^b LUMO levels were calculated from the measured first reduction potential versus Fc/Fc⁺ according to eq 1. ^c HOMO levels were calculated from the optical band gap E_g^{opt} and the respective LUMO levels. ^d $E_g^{opt} = h \cdot c / \lambda_{0.1max}$.

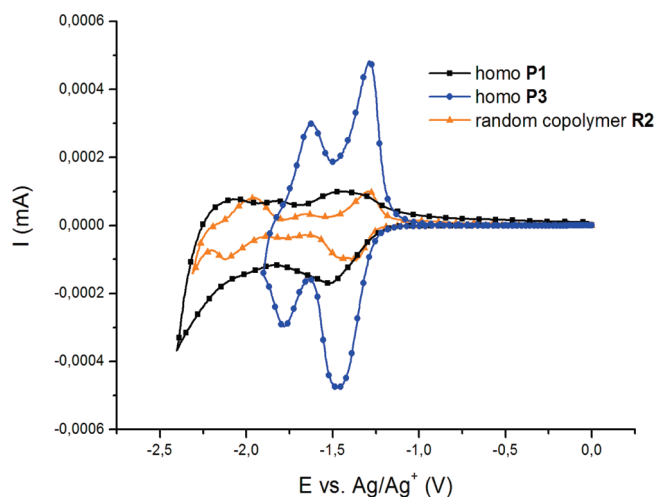


Figure 4. Cyclic voltammograms of selected metallo-polymers (cathodic scans are shown). For all measurements: films (0.1 M (TBA)PF₆ in CH₃CN), coated on Pt wires, scan rate 50 mV/s.

and on the reference energy level of ferrocene, according to eq 1.⁵⁴

$$E^{LUMO} = [-(E_{onset}^{red} - E_{onset}^{reference}) - 4.8] \text{ eV} \quad (1)$$

The LUMO levels range between −3.12 and −3.40 eV. Since no oxidation potentials could be determined, the corresponding estimation of the ionization potential (i.e., the HOMO energy level) and the electrochemical band gap could not be derived. Therefore, the optical energy band gaps of the metallo-polymers were estimated from the UV–vis absorption spectra by extrapolating to the 0–0 transition of the longest wavelength absorption band (at 10% of the absorption maximum). They ranged from 2.08 to 2.85 eV and were strongly influenced by the nature of the attached π -conjugated spacer unit. In order to obtain any information about the HOMO levels of the Zn^{II} metallo-polymers, the calculated optical band gaps E_g^{opt} and LUMO levels were used for the estimation. HOMO levels from −5.30 to −6.22 eV were derived. Taking this into account, the photophysical and electrochemical properties of the metallo-polymers can be tuned by variation of the chromophore, which was shown representatively for the small energy band gap of homo polymer **P5**.

Photophysical Properties. Further investigation on the photophysical properties of homo polymers **P1–P7** and, in particular, of the random copolymers **R1** and **R2**, was carried out by UV–vis absorption and photoluminescence spectroscopy. The spectroscopic data are summarized in Table 3 and Figures 5–7. In general, all metallo-polymers showed in agreement with the observations for the bis(terpyridines)

M1–M7 — characteristic absorptions between 250 and 480 nm, where the transitions at higher energy correspond to the terpyridine motive itself and the lower energy transitions to absorptions of the whole π -conjugated system. As expected, the Zn^{II} cores do not participate in the transitions, due to the filled d¹⁰ electron shell. Furthermore, a mostly hypsochromic shift of the π – π^* transition of 5 to 25 nm compared to the free bis(terpyridines) was observed. As reported for Zn^{II}-based metallo-polymers with electron-donating spacer units, a charge-transfer (CT) between electron-rich central units and the metal-coordinated electron-deficient terpyridine unit causes a red-shift in absorption.⁵⁵ In the present cases, the central chromophores consist of electron-withdrawing groups which are not able to undergo such CT processes with the terpyridine units. Inductive effects, which are caused by the complexed metal ion, do not compensate the missing CT and, therefore, result in a small blue-shift of the absorption bands. Additionally, the UV–vis absorption data of the metallo-polymers revealed a considerable decrease of the values of the extinction coefficients (Tables 1 and 2), which might be caused by a parallel arrangement of the dipole moments of the bis(terpyridine) units within the polymer backbone.²⁴

Homo polymer **P5** resembled this behavior impressively with a decrease in the extinction coefficient of about one order of magnitude. It simultaneously exhibits the highest absorption wavelength ($\lambda_{abs} = 485$ nm) and, therefore, the smallest distance between the HOMO and the LUMO energy level. On the other hand, homo polymer **P2** possesses the lowest absorption wavelength ($\lambda_{abs} = 362$ nm), equivalent with the largest HOMO–LUMO energy band gap. The values for E_g^{opt} were obtained by extrapolating the tails of the lowest energy absorption edge to the 0–0 transition as mentioned above.

The homo polymers (**P1–P7**) covered a wide range of PL emission maxima from 424 to 586 nm (Figure 5, dashed line), which strongly depends on the effective π -conjugation length and push–pull effects in the case of homo polymer **P5** (see above). Also absolute photoluminescence quantum yields (Φ_{PL}) of the materials were determined. In the case of the homo polymers, a decrease of Φ_{PL} in comparison to the ditopic terpyridine ligands **M1–M7** upon complexation was observed (**M1–M7**, $\Phi_{PL} = 0.37$ – 0.79 ; **P1–P7**, $\Phi_{PL} = 0.18$ – 0.66). Whereas **P7** showed only a third of the value measured for the corresponding bis(terpyridine) **M7**, only a small decrease of 15% was detected for **P3** relative to **M3**.

In comparison to conventional π -conjugated polymers bearing similar backbone units, the metallo-polymers exhibited higher PL quantum yields. The group of Klemm obtained for similar thieno[3,4-*b*]pyrazine-bearing π -conjugated polymers Φ_{PL} values in solution of about 0.15, which correlates with a 3-fold larger value for **P5**.^{49,56} In addition,

Table 3. Selected Photophysical Properties of the Homo Polymers P1–P7 and the Random Copolymers R1 and R2, respectively

| polymer | $\lambda_{\text{abs,max}}^a$ (nm) | $\lambda_{\text{PL,max}}^a$ (nm) | $\epsilon \times 10^4^{a,b}$ ($\text{M}^{-1} \cdot \text{cm}^{-1}$) | $\Phi_{\text{PL}}^{a,c}$ | Stokes shift (cm^{-1}) | $E_g^{\text{opt } d}$ (eV) |
|-----------|-----------------------------------|----------------------------------|---|--------------------------|-----------------------------------|----------------------------|
| P1 | 415, 359, 321, 284 | 513 | 0.99 | 0.66 | 4603 | 2.59 |
| P2 | 362, 325, 279 | 424 | 2.74 | 0.43 | 4039 | 2.85 |
| P3 | 392, 322, 288 | 443 | 1.75 | 0.53 | 2937 | 2.78 |
| P4 | 397 (s), 362, 331, 284 | 446 | 2.35 | 0.26 | 2767 | 2.73 |
| P5 | 485 (s), 400 324 (s), 288 | 586 | 0.33 | 0.42 | 3554 | 2.08 |
| P6 | 405, 317, 284 | 511 | 2.69 | 0.31 | 5122 | 2.33 |
| P7 | 411, 326, 284 | 518 | 2.24 | 0.18 | 5026 | 2.51 |
| R1 | 404, 337, 284 | 453, 470 (s) | 9.07 | 0.90 | 2677 | 2.76 |
| R2 | 369, 320, 281 | 409 (s), 432 | 11.25 | 0.81 | 3952 | 2.91 |

^a For all spectra: 10^{-6} M in DMF; (s) = shoulder. ^b Extinction coefficients at the lowest-energy absorption band. ^c Absolute quantum yields, uncorrected with respect to reabsorption. ^d $E_g^{\text{opt}} = hc/\lambda_{0.1\text{max}}$.

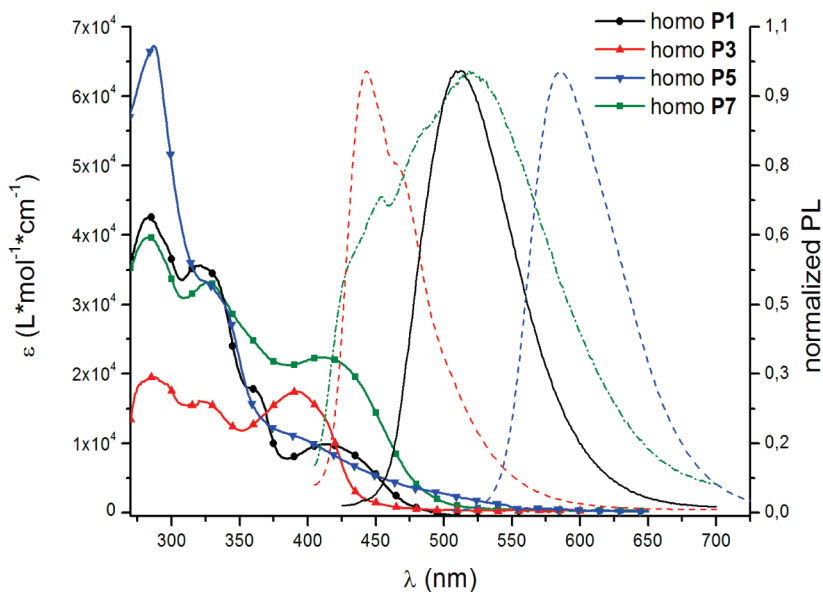


Figure 5. UV–vis absorption (solid line) and normalized photoluminescence spectra (dashed line) of selected homo polymers. For all spectra: 10^{-6} M in DMF, room temperature.

Chen et al. reported Φ_{PL} values of [2,1,3]benzothiadiazole- and quinoxaline-bearing π -conjugated polymers of about 0.19 and 0.22, respectively.⁵⁷ Compared to these π -conjugated polymers, metallo-polymers **P1** and **P3** ($\Phi_{\text{PL}} = 0.66$ to 0.53) emit much more efficiently.

Moreover, the random copolymers **R1** and **R2** were characterized by UV–vis absorption and PL spectroscopy in order to study the influence of a donor- and acceptor-bridged bis(terpyridine) within one Zn^{II} metallo-polymer (Figures 6 and 7).

Therefore, the UV–vis absorption spectra of the individual donor- and acceptor-based homo polymers (**P8**⁵⁸ and **P1**, respectively) were compared to that of random copolymer **R1** (Figure 6, top). Additionally, the spectra of both homo polymers were numerically summed up. The resulting spectrum showed good conformity of the appearing bands with the experimental spectrum of **R1**, but less accordance with the measured extinction coefficients. The latter fact might be a hint for a deviation from the exact 1:1 ratio of the monomeric bis(terpyridines) (**M1** and **MD1**) within the present random copolymer **R1**, attributed to a small excess of the **MD1**. The overall UV–vis absorption spectrum of **R1** is dominated by three bands between 250 to 420 nm, corresponding to the aforementioned characteristic transitions. Because of the large difference in the extinction coefficient between donor-type (**P8**) and acceptor-type homo polymer (**P1**) ($\epsilon = 5.3 \times 10^4 \text{ M}^{-1} \cdot \text{cm}^{-1}$ and $\epsilon = 0.99 \times 10^4 \text{ M}^{-1} \cdot \text{cm}^{-1}$, respectively), the extinction of the π - π^* transi-

tion of the random copolymer **R1** is predominated by the donor-part. The same applies also for the PL emission of **R1**. Excitation at the lowest energy absorption band of random copolymer **R1** ($\lambda_{\text{ex}} = 404$ nm) prefers considerably the PL emission of the electron-donating part. By means of varying the excitation wavelengths to smaller extinction differences, e.g., $\lambda_{\text{ex}} = 440$ nm (Figure 6, bottom), and by measuring the PL emission of different molar ratios of the ditopic monomers (**MD1** and **M1**, see Figure 6, middle left), the emission behavior of the random copolymer **R1** could be attributed mainly to the large extinction coefficient. At wavelengths with almost equivalent extinction coefficients (e.g., $\lambda_{\text{abs}} = 440$ nm) the PL emission of the acceptor is dominating. This leads to the assumption that the very high quantum yield of **R1** ($\Phi_{\text{PL}} = 0.90$) is caused by both parts and that an energy transfer from the donor to the acceptor moiety within the random copolymer **R1** is not favored.

Consequently, a second donor–acceptor pair was chosen for random copolymer **R2**, which exhibits a preferably large overlap of acceptor absorption with the emission of the donor unit, in order to achieve similar energies for several vibronic transitions of the donor and the acceptor, leading to a resonant coupling. These are requirements to obtain an energy transfer, in particular of the Förster-type (FRET).^{36,37} From the materials at hand, the acceptor-based bis(terpyridine) **M3** with a quinoxaline spacer-unit and a donor-based bis(terpyridine) bearing a fluorene-moiety (**MD2**,⁵⁸ see Scheme 2) provide these conditions. The position of the

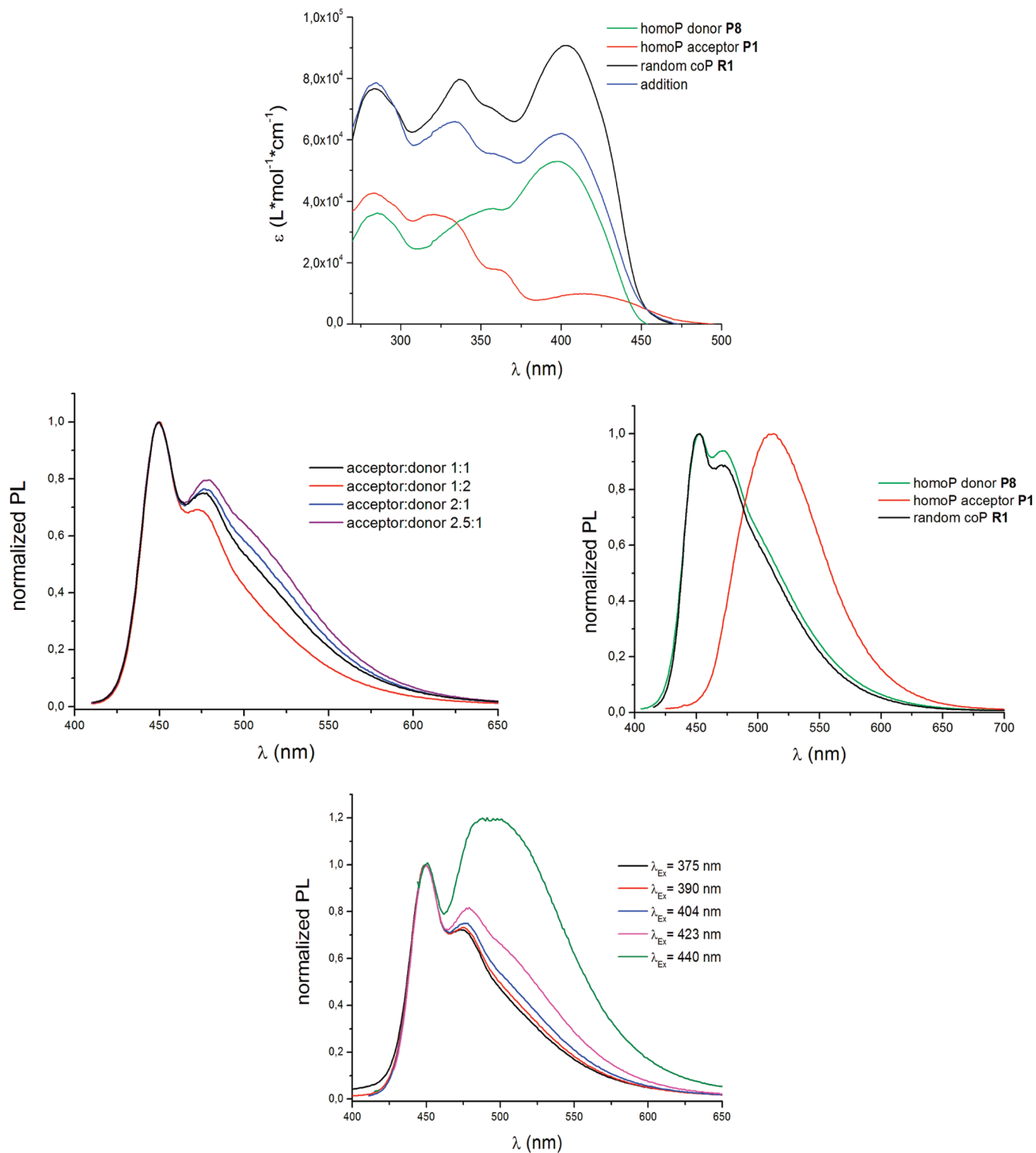


Figure 6. Top: UV-vis absorption spectra of random copolymer **R1** compared to the homo polymers of the acceptor-based bis(terpyridine) (**P1**) and the donor-based bis(terpyridine) (**P8**).⁵⁸ Middle left: Normalized PL spectra obtained at different acceptor (**M1**) to donor (**MD1**) ratios. Middle right: Normalized PL spectra of **R1** compared to the homo polymers of the acceptor-based (**P1**) and the donor-based bis(terpyridine) (**P8**). Bottom: Normalized PL spectra of **R1** at different excitation wavelengths. For all spectra: (10^{-6} M in DMF).

PL emission maximum of the donor bis(terpyridine) ($\lambda_{PL} = 403$ nm) is almost at the same wavelength as the π - π^* transition of the π -conjugated system of the acceptor **M3** ($\lambda_{abs} = 396$ nm). Additionally, the extinction coefficients are in a comparable order of magnitude.

Therefore, the UV-vis absorption spectra of both monomers were measured and numerically added (Figure 7, top).

The resulting spectrum is almost identical to the measured UV-vis absorption spectrum of random copolymer **R2**, both in band positions and in the extinction coefficients. This is an indication for an almost 1:1 ratio of the donor and acceptor within the synthesized copolymer. As for **R1**, the typical π - π^* transitions of the terpyridine and the whole π -conjugated system were obtained for **R2**. The longest

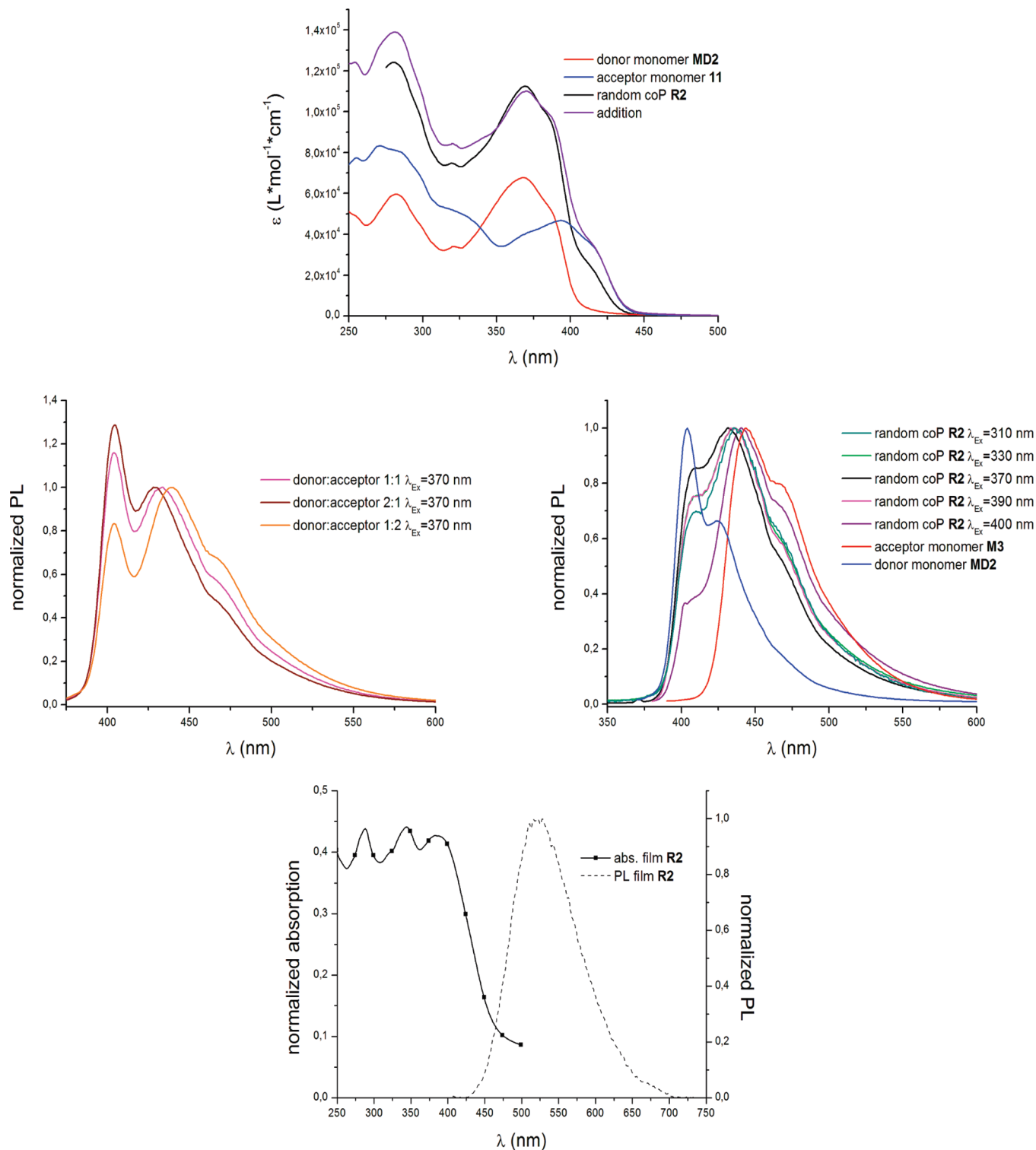


Figure 7. Top: UV-vis absorption spectra of **R2** compared to the acceptor-based bis(terpyridine) (**M3**) and the donor-based bis(terpyridine) (**MD2**).⁵⁸ Middle left: Normalized PL spectra obtained at different acceptor (**M3**) to donor (**MD2**) ratios. Middle right: Normalized PL spectra of **R2** at different excitation wavelengths compared to the monomers **M3** and **MD2**. Bottom: UV-vis absorption and photoluminescence (PL) spectra of random copolymer **R2** in the solid state (80 nm thickness). For all spectra: 10^{-6} M in DMF, respectively, spin coated from DMF solution (20 mg/mL, 1000 rpm, 100 s).

wavelength absorption band of random copolymer **R2** is located at 370 nm with a shoulder at 411 nm, induced by the long wavelength flank of the acceptor system.

In order to gain further insight into the behavior of random copolymer **R2** at the excited state, the PL properties were investigated. In a first experiment the donor- and acceptor-monomers (**MD2** and **M3**) were mixed in different

molar ratios (Figure 7, middle left) and excited at their longest wavelength absorption maximum. At a 1:1 ratio the emission originating from the donor bis(terpyridine) (**MD2**) is slightly dominating due to the larger extinction coefficient at 370 nm, which inverses with increasing acceptor portion. Consequently, the PL behavior of the mixtures of **MD2** and **M3** is only an addition of both monomers and

no energy transfer was observed. Nevertheless, excitation at the longest absorption band wavelength of the random copolymer **R2** resulted in a completely different PL emission spectrum (Figure 7, middle right). In this case, the emission attributed to the acceptor-unit, though slightly red-shifted, was clearly dominating. Only a shoulder confirms the emission originating from the donor-part. Both, decreasing as well as increasing the excitation wavelength, lead to a further reduction of the donor-based emission. At $\lambda_{\text{ex}} = 370$ nm the emission ratio of the acceptor- to the donor-unit is 1:0.85, although the ratio of the extinction coefficients at this particular wavelength (1:1.66) indicates a larger absorption of the donor.

This circumstance can be explained by a radiationless transfer of energy from the excited donor moieties in random copolymer **R2** to the electron-accepting units.^{36,37,59} This leads to the excitation of the acceptor-parts, which are now able to deactivate under emission of the transferred energy.³⁶ The fact that a simple mixture of the involved monomers (**MD2** and **M3**) revealed no indication for an energy transfer whereas the corresponding Zn^{II}-based random copolymer is able to do, shows that the central Zn^{II}-terpyridine moieties play a crucial role for the mediation of such a transfer.

In order to obtain information about the applicability of Zn^{II} metallo-polymers as OLED devices, the solid-state properties are crucial. Therefore, the photophysical properties of random copolymer **R2** in the solid state were additionally investigated. Low solubility of all synthesized metallo-polymers in common organic solvents was observed. Spin-coating from DMF solution (20 mg/mL, 1000 rpm, 100 s) was applied, resulting in a homogeneous film (80 nm thickness) of random copolymer **R2** which was used for the UV-vis absorption and photoluminescence measurements (Figure 7, bottom). The spectra reveal a slight hypsochromic shift (10 nm) of the absorption maximum in comparison to those observed in solution. However, the PL maximum shows a bathochromic shift of 90 nm in comparison to the solution of random copolymer **R2**. In accordance with the literature, this large Stokes shift of about 7000 cm⁻¹ can be attributed to strong intermolecular π - π -interactions of the metallo-polymeric chains. This behavior results from a very close orientation in the solid state, which prefers a disturbance among themselves and destabilizes occupied orbitals.^{24,28,30}

Conclusion

In summary, a logical synthesis route for a set of π -conjugated bis(terpyridine) ligands bearing electron-withdrawing spacer units and their corresponding main chain metallo-homo polymers was developed. The formation of the metallo-polymers was concluded from the broadened ¹H NMR signals as well as from UV-vis titration experiments. ¹H NMR provides an estimation of the molar mass of approximately 25 000–50 000 g/mol. Apparently, the electro-optical properties of the monomers as well as of the homo polymers are strongly influenced by the nature of the attached π -conjugated spacer unit and shows some distinct differences in comparison to related electron-donating Zn^{II} metallo-polymers. Furthermore, two donor-acceptor random copolymers were synthesized and their electro-optical properties were investigated by UV-vis absorption as well as PL spectroscopy. Thereby, random copolymer **R2** featured an energy transfer from the donor to the acceptor unit, which was confirmed by various emission experiments in solution. The central role of the Zn^{II}-terpyridine moiety within the materials was concluded from these results. Furthermore, the solid-state properties of random copolymer **R2** were investigated in order to

obtain information about the potential applicability of Zn^{II} metallo-polymers as OLED devices.

The herein synthesized metallo-polymers (homo and random) show promising properties with respect to potential opto-electronic applications in OLED or PLED devices.

Acknowledgment. The authors acknowledge the financial support from the Dutch Polymer Institute (DPI), the Nederlandse Organisatie voor Wetenschappelijk Onderzoek (NWO, VICI award for U.S.S.), the Fonds der Chemischen Industrie and the Freistaat Thüringen. We also thank Vera Cimrová (cyclic voltammetry: Institute of Macromolecular Chemistry, Academy of Science of the Czech Republic, Prague, Czech Republic) and Beate Lentvogt (elemental analysis) for the help with the respective measurements.

Supporting Information Available: Text giving full experimental details and characterization of the aromatic dibromides (**1–7**), bis(terpyridines) (**M1–M7**) and metallo-polymers (**P1–P7**, **R1**, **R2**) including reaction schemes and structures, and figures showing NMR and MALDI-TOF mass spectra of bis(terpyridines) (**M1–M7**). This material is available free of charge via the Internet at <http://pubs.acs.org>.

References and Notes

- Lehn, J. M. *Angew. Chem., Int. Ed.* **1988**, *27*, 89–112.
- Schubert, U. S.; Hofmeier, H.; Newkome, G. R. *Modern Terpyridine Chemistry*; VCH Wiley: Weinheim, Germany, 2006.
- Lehn, J.-M. *Supramolecular Chemistry—Concepts and Chemistry*; VCH Wiley: Weinheim, Germany, 1995.
- Balzani, V.; Juris, A.; Venturi, M.; Campagna, S.; Serroni, S. *Chem. Rev.* **1996**, *96*, 759–833.
- Eisenbach, C. D.; Schubert, U. S. *Macromolecules* **1993**, *23*, 7372–7374.
- Newkome, G. R.; Wang, P. S.; Moorefield, C. N.; Cho, T. J.; Mohapatra, P. P.; Li, S. N.; Hwang, S. H.; Lukoyanova, O.; Echegoyen, L.; Palagallo, J. A.; Iancu, V.; Hla, S. W. *Science* **2006**, *312*, 1782–1785.
- Hofmeier, H.; Schmatloch, S.; Wouters, D.; Schubert, U. S. *Macromol. Chem. Phys.* **2003**, *204*, 2197–2203.
- Lohmeijer, B. G. G.; Schubert, U. S. *Macromol. Chem. Phys.* **2003**, *204*, 1072–1078.
- Dobrawa, R.; Lysetska, M.; Ballester, P.; Grüne, M.; Würthner, F. *Macromolecules* **2005**, *38*, 1315–1325.
- Dobrawa, R.; Würthner, F. *J. Polym. Sci., Part A: Polym. Chem.* **2005**, *43*, 4981–4995.
- Schubert, U. S.; Eschbaumer, C. *Angew. Chem., Int. Ed.* **2002**, *41*, 2893–2926.
- Bonnet, S.; Collin, J. P.; Koizumi, M.; Mobian, P.; Sauvage, J. P. *Adv. Mater.* **2006**, *18*, 1239–1250.
- Schmatloch, S.; van den Berg, A. M. J.; Alexeev, A. S.; Hofmeier, H.; Schubert, U. S. *Macromolecules* **2003**, *36*, 9943–9949.
- Schubert, U. S.; Schmatloch, S.; Precup, A. A. *Des. Monomers Polym.* **2002**, *5*, 211–221.
- Schubert, U. S.; Hien, O.; Eschbaumer, C. *Macromol. Rapid Commun.* **2000**, *21*, 1156–1161.
- Winter, A.; Friebe, C.; Hager, M. D.; Schubert, U. S. *Macromol. Rapid Commun.* **2008**, *29*, 1679–1686.
- Hissler, M.; El-ghayoury, A.; Harriman, A.; Ziessel, R. *Angew. Chem., Int. Ed.* **1998**, *37*, 1717–1720.
- Sauvage, J. P.; Collin, J. P.; Chambron, J. C.; Guillerez, S.; Coudret, C.; Balzani, V.; Barigelletti, F.; Decola, L.; Flamigni, L. *Chem. Rev.* **1994**, *94*, 993–1019.
- Dobrawa, R.; Würthner, F. *Chem. Commun.* **2002**, 1878–1879.
- Flores-Torres, S.; Hutchison, G. R.; Soltzberg, L. J.; Abruna, H. D. *J. Am. Chem. Soc.* **2006**, *128*, 1513–1522.
- Erkkila, K. E.; Odom, D. T.; Barton, J. K. *Chem. Rev.* **1999**, *99*, 2777–2795.
- Barigelletti, F.; Flamigni, L. *Chem. Soc. Rev.* **2000**, *29*, 1–12.
- Chen, Y. Y.; Tao, Y. T.; Lin, H. C. *Macromolecules* **2006**, *39*, 8559–8566.
- Winter, A.; Friebe, C.; Chiper, M.; Hager, M. D.; Schubert, U. S. *J. Polym. Sci., Part A: Polym. Chem.* **2009**, *47*, 4083–4098.

- (25) Manners, I. *Science* **2001**, *294*, 1664–1666.
- (26) Constable, E. C.; Thompson, A. M. W. C. *J. Chem. Soc., Chem. Commun.* **1992**, 617–619.
- (27) Vellis, P. D.; Mikroyannidis, J. A.; Lo, C. N.; Hsu, C. S. *J. Polym. Sci., Part A: Polym. Chem.* **2008**, *46*, 7702–7712.
- (28) Chen, Y. Y.; Lin, H. C. *J. Polym. Sci., Part A: Polym. Chem.* **2007**, *45*, 3243–3255.
- (29) Parameswar, K. I.; Beck, B.; Weder, C.; Rowan, S. J. *Chem. Commun.* **2005**, 319–321.
- (30) Yu, S.-C.; Kwok, C.-C.; Chan, W.-K.; Che, C.-M. *Adv. Mater.* **2003**, *15*, 1643–1647.
- (31) Huang, F.; Wu, H.; Wang, D.; Wang, W.; Cao, Y. *Chem. Mater.* **2004**, *16*, 708–712.
- (32) Winter, A.; Egbe, D. A. M.; Schubert, U. S. *Org. Lett.* **2007**, *9*, 2345–2348.
- (33) Winter, A.; Friebe, C.; Hager, M. D.; Schubert, U. S. *Eur. J. Org. Chem.* **2009**, 801–809.
- (34) Roncali, J. *Chem. Rev.* **1997**, *97*, 173–205.
- (35) Cheng, Y. J.; Yang, S. H.; Hsu, C. S. *Chem. Rev.* **2009**, *109*, 5868–5923.
- (36) Förster, T. *Annal. Phys.* **1948**, *6*, 55–75.
- (37) Lakowicz, J. R. *Principles of Fluorescence Spectroscopy*; Kluwer Academic/Plenum: New York, 1999.
- (38) Santoni, M.-P.; Medlycott, E. A.; Hanan, G. S.; Hasenknopf, B.; Proust, A.; Nastasi, F.; Campagna, S.; Chiorboli, C.; Argazzi, R.; Scandola, F. *Dalton Trans.* **2009**, 3964–3970.
- (39) Winter, A.; van den Berg, A. M. J.; Hoogenboom, R.; Kickelbick, G.; Schubert, U. S. *Synthesis* **2006**, 2873–2878.
- (40) Wang, J. H.; Hanan, G. S. *Synlett* **2005**, 1251–1254.
- (41) Smith, C. B.; Raston, C. L.; Sobolev, A. N. *Green Chem* **2005**, *7*, 650–654.
- (42) Pilgram, K.; Zupan, M.; Skiles, R. *J. Heterocycl. Chem.* **1970**, *7*, 629–640.
- (43) Bartholome, D. Ph.D. Thesis. Friedrich-Schiller-University Jena, Jena, Germany, **2007**.
- (44) Karsten, B. P.; Viani, L.; Gierschner, J.; Cornil, J.; Janssen, R. A. J. *J. Phys. Chem.* **2008**, *112*, 10764–10773.
- (45) Huo, L. J.; Tan, Z. A.; Zhou, Y.; Zhou, E. J.; Han, M. F.; Li, Y. F. *Macromol. Chem. Phys.* **2007**, *208*, 1294–1300.
- (46) Ahmed, A. M.; Feast, W. J.; Tsibouklis, J. *Polymer* **1993**, *34*, 1297–1302.
- (47) Shen, P.; Sang, G. Y.; Lu, J. J.; Zhao, B.; Wan, M. X.; Zou, Y. P.; Li, Y. F.; Tan, S. T. *Macromolecules* **2008**, *41*, 5716–5722.
- (48) Shahid, R. A. Ph.D. Thesis. Friedrich-Schiller-University Jena, Jena, Germany, **2005**.
- (49) Shahid, M.; Shahid, R. A.; Klemm, E.; Sensfuss, S. *Macromolecules* **2006**, 7844–7853.
- (50) Wild, A.; Friebe, C.; Winter, A.; Hager, M. D.; Grummt, U. W.; Schubert, U. S. *Eur. J. Org. Chem.* **2010**, DOI: 10.1002/ejoc.200901112.
- (51) In order to obtain an analytical pure sample, a larger number of precipitation steps was required and, thus, a lower isolated yield compared with the other systems was observed.
- (52) Yuan, S. C.; Chen, H. B.; Zhang, Y.; Pei, J. *Org. Lett.* **2006**, *8*, 5700–5704.
- (53) Wild, A.; Schlütter, F.; Pavlov, G. M.; Friebe, C.; Festag, G.; Winter, A.; Hager, M. D.; Schubert, U. S. *Macromol. Rapid Commun.* **2010**, DOI:10.1002/marc.200900889.
- (54) Janitz, S.; Bradley, D. D. C.; Grelly, M.; Giebeler, C.; Inbasekaran, M.; Woo, E. P. *Appl. Phys. Lett.* **1998**, *73*, 2453–2468.
- (55) Chiper, M. Ph.D. Thesis. Eindhoven University of Technology, Eindhoven, The Netherlands, **2008**.
- (56) Ashraf, R. S.; Shahid, M.; Klemm, E.; Al-Ibrahim, M.; Sensfuss, S. *Macromol. Rapid Commun.* **2006**, *27*, 1454–1459.
- (57) Wu, W.-C.; Lee, W.-Y.; Pai, C.-L.; Chen, W.-C.; Tuan, C.-S.; Lin, J.-L. *J. Polym. Sci., Part B: Polym. Phys.* **2006**, *45*, 67–78.
- (58) The synthesis and characterization of the homo polymers **P8** and **P9** based on the donor-bridged bis(terpyridines) **MD1** and **MD2**, respectively, is shown elsewhere.⁵³
- (59) Spehar-Deleze, A. M.; Pellegrin, Y.; Keyes, T. E.; Forster, R. J. *Electrochem. Commun.* **2008**, *10*, 984–986.
- (60) Kelch, S.; Rehahn, M. *Macromolecules* **1999**, *32*, 5818–5828.

Publication A5: “Inkjet printing of zinc(II) *bis*-2,2':6',2''-terpyridine metallopolymers: Printability and film-forming studies by a combinatorial thin-film library approach”

Christian Friebe, Andreas Wild, Jolke Perelaer, Ulrich S. Schubert

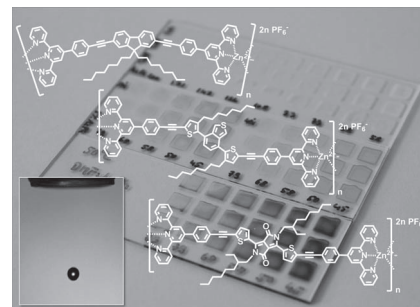
Macromol. Rapid Commun. **2012**, *33*, 503–509.

Reprinted with permission from: WILEY-VCH Weinheim (Copyright 2012)

Inkjet Printing of Zinc(II) Bis-2,2':6',2''-Terpyridine Metallopolymers: Printability and Film-Forming Studies by a Combinatorial Thin-Film Library Approach

Christian Friebe, Andreas Wild, Jolke Perelaer, Ulrich S. Schubert*

For the first time, thin-film libraries of zinc(II) bis-2,2':6',2''-terpyridine metallopolymers are prepared by inkjet printing to study structure–property relationships and their possible usage for organic photovoltaic (OPV) or polymer light-emitting diode (PLED) applications. By using a combinatorial approach, various important parameters, including solvent system, dot spacing, and substrate temperature, as well as UV-vis absorption and emission properties, are screened in a materials efficient and reproducible manner. Homogeneous films with a thickness of 150–200 nm were obtained when printed at 40–50 °C and from a solvent mixture of *N,N*-dimethylformamide and acetophenone in a ratio of 90/10. In applications such as OPV and PLEDs the control over film thickness and homogeneity are central to obtain good device properties.



1. Introduction

On the one hand, 2,2':6',2''-terpyridines show a comprehensive coordination chemistry due to their high binding affinities toward several transition and main group metals. Hence, they are of great interest for functional templates in the fields of supramolecular chemistry.^[1] In particular, the attachment of photo- and electroactive moieties at the easily accessible 4'-position enables the facile tuning

of photophysical and electrochemical properties.^[2] On the other hand, zinc(II) is a suitable and widespread metal to assemble highly ordered metallopolymer structures due to its high coordination flexibility and reversibility.^[3] Consequently, linear, rod-like polymers composed of zinc(II) metal ions and bis-2,2':6',2''-terpyridines, exhibiting π -conjugated spacer units at the 4'-position, are of great interest since they combine optoelectronic properties of the spacer moieties with the favorable processing features of a polymer, in particular, the ability to form smooth thin films.^[2a,4] The fabrication of such coatings is of significant importance for applications in organic photovoltaic (OPV) or polymer light-emitting diodes (PLEDs).

In several studies, the properties of zinc(II)-terpyridine metallopolymers in thin films were investigated,^[4d,5] mainly using spin-coating for film preparation. Beside its advantage of easy preparation of thin films, spin-coating suffers from several drawbacks, for example, high material consumption and the lack of a possible combinatorial workflow.^[6] Alternatively, inkjet printing can be used, showing an efficient material usage, flexible change of processing conditions, and deposition of defined patterns

C. Friebe, A. Wild, Dr. J. Perelaer, Prof. Dr. U. S. Schubert
Laboratory of Organic and Macromolecular Chemistry (IOMC),
Friedrich-Schiller-University Jena,

Humboldtstr. 10, 07743 Jena, Germany
E-mail: ulrich.schubert@uni-jena.de

C. Friebe, A. Wild, Dr. J. Perelaer, Prof. Dr. U. S. Schubert
Jena Center for Soft Matter (JCSM),

Friedrich-Schiller-University Jena,
Humboldtstr. 10, 07743 Jena, Germany

A. Wild, Dr. J. Perelaer, Prof. Dr. U. S. Schubert
Dutch Polymer Institute (DPI), P.O. Box 513, 5600 MB
Eindhoven, The Netherlands

without the necessity of template masks.^[7] Inkjet printing is accepted as a selective and highly efficient material deposition tool for a wide range of applications. It has been used in printed electronics, where conductive features are directly applied onto specific locations for OPV, sensor arrays, thin-film transistors, and radio frequency identification (RFID) tags.^[8] Furthermore, inkjet printing has been used for the screening of numerous compounds and processing parameters, for example, for bulk heterojunction solar cells,^[9] where the critical performance parameters are the donor–acceptor ratio, the film thickness, and the morphology of the resulting films. In particular, the morphology is highly important for the efficiency of an organic solar cell. By using inkjet printing, thin-film libraries can be prepared and film properties can be studied systematically in a fast, reproducible, and simple manner with high material efficiency.^[10]

An often observed phenomenon with inkjet printing is the nonuniform drying, leaving a typical ring structure. The reason of the so-called “coffee-ring” effect was explained by Deegan by a replenishing flow that originates in a drying droplet’s interior and travels toward the substrate–air–liquid interface.^[11]

However, homogeneous films are required for various electronic applications, for instance, for PLEDs, where the device should emit light with an equal intensity at every position of the display. Thus, to achieve a controlled and homogenous film formation, several aspects of the inkjet printing process have to be considered, namely, the used solvent system, drop formation parameters (e.g., nozzle diameter, pulse voltage, and pulse width), printing velocity, dot spacing, and substrate properties (e.g., surface tension and temperature).^[10] Tekin et al.^[12] investigated the influence of various parameters on the reproducibility of inkjet-printed films and presented a detailed study how defined and homogeneous films could be prepared by inkjet printing. Furthermore, the authors showed that the coffee-ring effect in the films could be reduced by using a solvent mixture that consisted of a low- and high-boiling solvent, instead of using a single solvent. Other methods to diminish the coffee-ring effect include increasing the substrate temperature,^[13] making surface energy patterns, which direct the ink to predefined areas on the substrate,^[14] and modifying the shape of the suspended particles.^[15]

In this contribution, we present a combinatorial screening of the preparation of thin films of three zinc(II) bis-2,2′:6′,2″-terpyridine metallopolymers using the inkjet printing technique. The influence of the solvent system, dot spacing, and substrate temperature on the film homogeneity and thickness as well as the UV-vis absorption and emission properties was investigated to identify optimum parameters for the preparation of smooth thin films. To the best of our knowledge, this is

the first time that zinc(II) metallopolymers were deposited via inkjet printing and various film-forming properties were studied in a systematic way.

2. Experimental Section

2.1. Materials

For printing, the zinc(II) bis-2,2′:6′,2″-terpyridine metallopolymers were dissolved in mixtures of *N,N*-dimethylformamide (DMF), acetophenone (AcPh), and *ortho*-dichlorobenzene (*o*-DCB) using concentrations of 5 mg·mL⁻¹ which was the maximum soluble concentration. The solutions were filtered (PTFE filter, pore size 0.45 μm) to prevent nozzle clogging. The solvents were purchased from Sigma–Aldrich (Germany) and used as delivered.

Microscope slides (1″ × 3″) from Marienfeld (Germany) were used as substrates. For cleaning, they were ultrasonicated in demineralized water and iso-propanol, followed by rinsing with iso-propanol and drying with an air flow.

2.2. Instrumentation

The inkjet printing experiments were performed using an Autodrop system from Microdrop Technologies (Germany) equipped with a piezo-based printhead (pipette system) with an inner diameter of 70 μm. The microscope slides were placed onto a heatable table that can be moved in *x*- and *y*-direction. A stable droplet formation could be achieved for both the metallopolymer/DMF/AcPh and the metallopolymer/DMF/*o*-DCB solution applying a voltage of 75 V and a pulse length of 30 μs. The printing velocity was set to 5 mm·s⁻¹ for all experiments. Dot spacing values varied between 50 and 200 μm according to a logarithmic row.

The surface topology was determined using an optical interferometric profiler Wyko NT9100 (Veeco, Germany). The film thicknesses of polymers **2** and **3** were determined measuring the average film height within the central part of the obtained topology cross-sections.

UV-vis absorption and emission spectra of the printed films were measured with a FLASHScan 530 plate reader from Analytik Jena (Germany). The films (5 mm × 5 mm) were printed with a center-to-center distance of 10 mm to fit into a 96-wells microtiter plate pattern that enabled the recording of up to 96 UV-vis spectra within a single measurement. Absorption spectra were referenced to blank microscope slides.

UV-vis absorption measurements of the solutions were carried out with a Specord 250 (Analytik Jena, Germany) and UV-vis emission measurements with an FP 6500 from JASCO Inc. (USA). The measurements were executed using 10⁻⁶ M solutions of the respective solvents (spectroscopy grade) in 1 cm quartz cuvettes at 25 °C with pristine solvent as reference. All emission spectra were obtained by excitation at the wavelength of the maximum absorption.

2.3. Synthesis of Bis-2,2′:6′,2″-Terpyridine Metallopolymers

The synthesis of the printed metallopolymer **1** is part of a former publication,^[4a] the synthesis of metallopolymers **2**, **3**,

and the respective precursors is described in the Supporting Information.

3. Results and Discussion

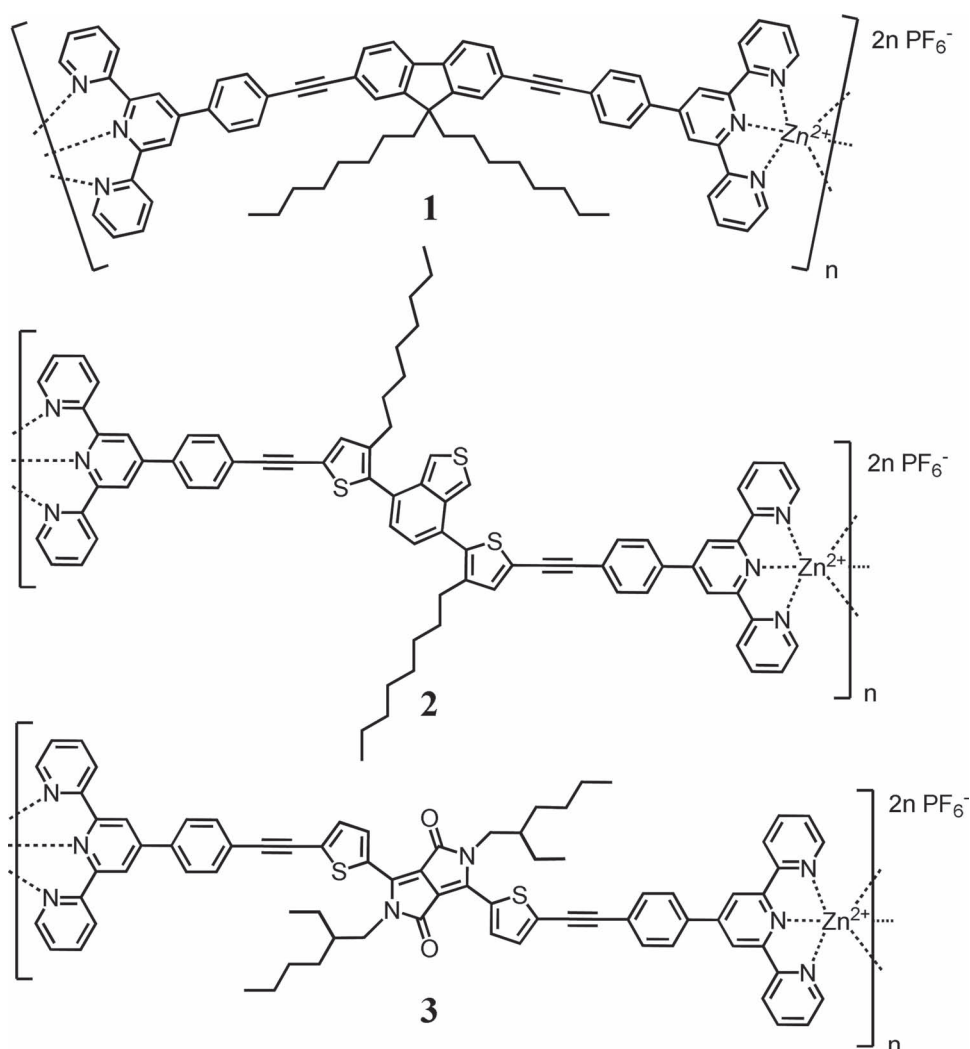
Inkjet-printed films of three zinc(II) terpyridine metallopolymers were prepared, featuring different conjugated spacer units within the bis-2,2':6',2''-terpyridine moiety, namely, 9,9-dioctyl-9H-fluorene (**1**), 4,7-bis(3-octylthiophen-2-yl)benzo[*c*]thiophene (**2**), and 2,5-di(2-ethylhexyl)-3,6-di(thiophen-2-yl)pyrrolo[3,4-*c*]pyrrole-1,4(2*H*,5*H*)-dione (**3**) as depicted in Scheme 1.

Optimization of the printing process was carried out in a combinatorial, two-dimensional way varying multiple parameters at the same time. In contrast to a one-dimensional variation of settings, synergic interactions between different variables could be

recognized.^[10,12] The following sections describe the variation of dot spacing, solvent mixture, and substrate temperature and their influence on film topology and thickness as well as the resulting UV-vis absorption and emission spectra.

3.1. Variation of Solvent Mixture and Dot Spacing

The moderate solubility of the metallopolymers limited the assortment of usable solvents. For successful inkjet printing of solutions, the solvents require a certain boiling temperature, viscosity, and surface tension. *N,N*-Dimethylformamide (bp.: 153 °C) was chosen as it shows a good solubility, printability, and low volatility. With DMF as solvent, a maximum usable concentration of the metallopolymers was 5 mg·mL⁻¹.^[10] Figure S1 (see Supporting Information) presents inkjet-printed films of **1** from pure DMF solutions.



■ Scheme 1. Schematic representation of zinc(II) bis-2,2':6',2''-terpyridine metallopolymers used for film preparation by inkjet printing.

Dot spacing, that is the center-to-center spacing between two adjacent droplets, was varied between 50 and 200 μm according to a logarithmic row. Apparently, film homogeneity is rather poor at all spacings due to a nonuniform drying of the solvent causing a coffee-ring effect which is characterized by the formation of rings and circles.^[11] As mentioned before, a known solution for this problem is the addition of a small amount of a second solvent (usually 5–10 vol%) possessing a higher boiling point that causes a slower and, therefore, more controlled and uniform solvent evaporation.^[14] *Ortho*-dichlorobenzene (bp.: 179 $^{\circ}\text{C}$) was added (5 vol%) and the resulting films are shown in Figure S1b. However, only a small enhancement in film topology can be observed most likely due to a too low boiling point difference. Hence, the minor solvent was changed to acetophenone (bp.: 202 $^{\circ}\text{C}$). Although no homogenous films could be obtained at this point, a considerable improvement is obvious (Figure S1c).

Because of the limited solvent combinations that could be prepared with a sufficient boiling temperature difference with DMF as the major solvent, the DMF/AcPh mixture was chosen as the solvent system to be used for further experiments.

3.2. Variation of Substrate Temperature

The substrate temperature has a significant influence on the drying speed of the as-printed film: at elevated temperatures an accelerated evaporation of the solvents is stimulated, whereas at lower temperature the material has more time to distribute along the film. Polymer **1** was inkjet-printed from DMF/AcPh solution using substrate temperatures ranging from room temperature to 70 $^{\circ}\text{C}$. Figure 1a–c shows that increasing the temperature from room temperature to 40 and 50 $^{\circ}\text{C}$ enhances the uniformity of the film drying, hence resulting in more homogeneous films for a dot spacing in the range from 58 to 108 μm . Noticeable, however, is that at these dot spacings a ring remains around the films, despite the addition of a higher boiling co-solvent.^[12] A complete diminishing of the ring was not possible. When increasing the dot spacing to 200 μm (Figure 1b and c, very right image), lines are visible instead of a continuous film. Because of a faster evaporation of the solvent, the in-flight droplet diameter reduces and leaves a smaller impression at the substrate, which, as a consequence, requires a smaller dot spacing to merge into a continuous feature.^[14] A further increase of the temperature did not result in homogenous films caused by a too quick evaporation of the solvent of the in-flight droplets. The effect of inkjet printing a wet droplet (line) next to a semi-dried droplet (line), that is, an as-printed droplet (line) that is evaporating, may be the cause of the less homogeneous film formation at elevated temperatures.

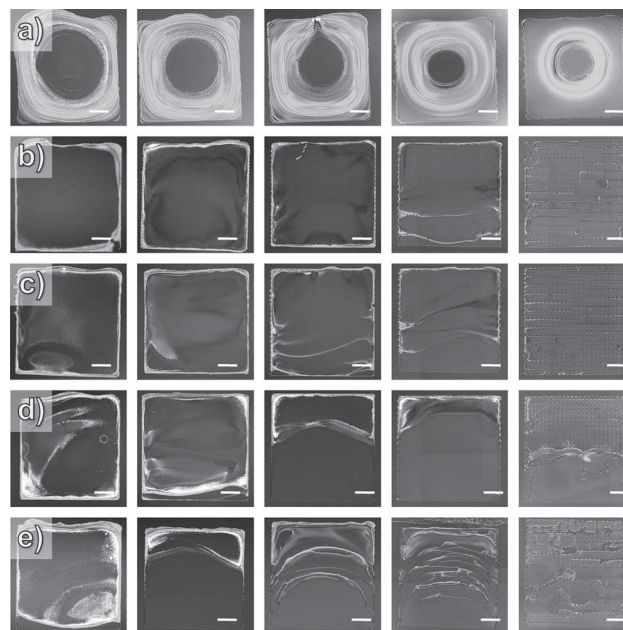


Figure 1. Optical profiler images of films of **1** inkjet-printed with dot spacings of, from left to right, 58, 79, 108, 147, and 200 μm , solvent system DMF/AcPh (95/5). Substrate temperature was room temperature (a), 40 (b), 50 (c), 60 (d), and 70 $^{\circ}\text{C}$ (e). The included scale bars correspond to 1 mm.

3.3. Variation of Solvent Ratio

To further improve the homogeneity of the printed films from DMF/AcPh, the solvent ratio was varied. Films of **1** and **2** were printed from solutions with different DMF/AcPh ratios. Figure 2 shows the optical profiler images of films of **1** printed from the solvent system DMF/AcPh with a volume ratio of 95/5 (Figure 2a and b) and 90/10 (Figure 2c and d). In the case of 10 vol%, the homogeneity of the dried film is significantly improved compared to a lower amount of the higher boiling solvent acetophenone. Furthermore, it is noticeable that the quality of the films is improved over a larger dot spacing range; namely, from 50 to 79 μm , homogeneous films were obtained from a 90/10 solvent mixture, whereas the ratio of 95/5 performs well only with a dot spacing of 50 μm .

In the case of **2**, a similar improvement of the film topology and film boundary was obtained by increasing the higher boiling solvent ratio from 95/5 (Figure 3a and b) to 90/10 (Figure 3c and d), but the appearance of rings in the films remained.

In conclusion, for both polymers an improved performance could be observed using an acetophenone concentration of 10 vol%.

3.4. Optimum Printing Parameters

The obtained data revealed optimum printing conditions for the investigated polymers **1** and **2** to be as follows: first,

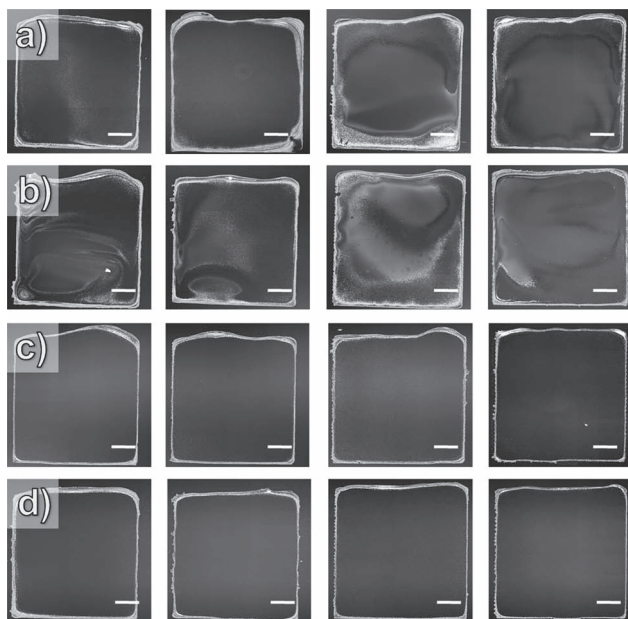


Figure 2. Optical profiler images of films of **1** inkjet-printed with dot spacings of, from left to right, 50, 58, 68, and 79 μm . Solvent system was DMF/AcPh with volume ratios of 95/5 (a, b) and 90/10 (c, d). Substrate temperature was 40 (a, c) and 50 $^{\circ}\text{C}$ (b, d). The included scale bars correspond to 1 mm.

the dot spacing should be chosen within the range from 58 to 79 μm . A mixture of DMF and acetophenone with a volume ratio of 90/10 turned out to be the most convenient solvent system to achieve homogenous films with reduced formation of rings and edging. Furthermore, elevated substrate temperatures of 40–50 $^{\circ}\text{C}$ were necessary for an improved drying behavior of the printed films.

Consequently, the identified printing conditions were applied to a third zinc metallopolymer **3**. The resulting films are shown in Figure 3e and f. The best film performance was achieved using dot spacings of 58 to 79 μm and substrate temperatures of 40–50 $^{\circ}\text{C}$, as concluded for the polymers **1** and **2**.

3.5. Film Thickness

Optical profilometry was used to measure the film thickness of the obtained films, summarized in Table 1. However, we were not able to determine thicknesses of polymer **1**. Although films were clearly visible, profilometer measurements gave thickness values of around 10 nm being highly unrealistic. Also AFM experiments were not successful because of a too sticky surface. Thus, investigations and following discussions about film thicknesses are restricted to systems **2** and **3**.

As expected, for both polymers and substrate temperatures, a decreased film thickness was observed upon increased dot spacing. For organic light-emitting diodes

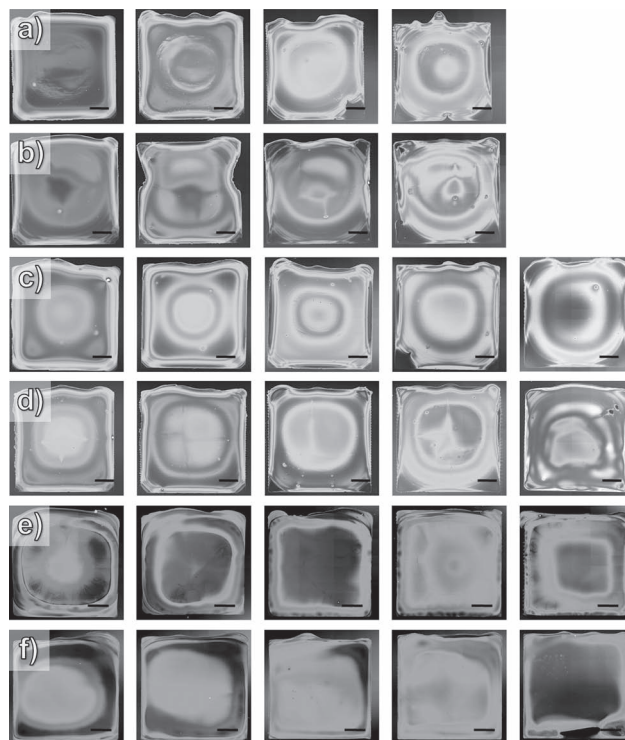


Figure 3. Optical profiler images of films of **2** (a–d) and **3** (e, f) inkjet-printed with dot spacings of, from left to right, 50, 58, 68, 79, and 93 μm (c–f). Solvent system was DMF/AcPh with volume ratios of 95/5 (a, b) and 90/10 (c–f). Substrate temperature was 40 (a, c, e) and 50 $^{\circ}\text{C}$ (b, d, f). The included scale bars correspond to 1 mm.

and photovoltaic devices a film thickness between 100 and 200 nm is required.^[10] These values can be obtained with dot spacings between 79 and 93 μm for both polymers. Notably, the substrate temperature showed a large influence on the standard deviation, that is, the reproducibility of the film thicknesses. While polymer **2** revealed lower deviations for 40 $^{\circ}\text{C}$, polymer **3** performed significantly better using a substrate temperature of 50 $^{\circ}\text{C}$. For the latter, this is even the case throughout the whole series of dot spacing values.

3.6. UV-vis Absorption and Emission Measurements

The UV-vis absorption and emission properties of the studied complexes were investigated in both solution and the inkjet-printed film. On the one hand, spectra of diluted DMF solutions (10^{-6} M) were recorded, on the other hand, measurements on films, which had been printed using optimized conditions, were carried out and are represented in Figure 4. First, all UV-vis features base upon ligand-centered transitions of the conjugated π system of the bis-terpyridine ligands since the zinc(II) does not participate in UV-visible electron transitions. The solution

Table 1. Film thickness and standard deviations at different substrate temperatures and dot spacings. Printed from DMF/AcPh 90/10.

| Polymer | Substrate temperature [°C] | Dot spacing [μm] | Thickness [nm] | Standard deviation [%] |
|---------|----------------------------|------------------|----------------|------------------------|
| 2 | 40 | 50 | 451 | 7.3 |
| | | 58 | 396 | 12.5 |
| | | 68 | 279 | 4.8 |
| | | 79 | 274 | 8.6 |
| | | 93 | 128 | 8.7 |
| | 50 | 50 | 536 | 6.7 |
| | | 58 | 372 | 7.5 |
| | | 68 | 252 | 8.9 |
| | | 79 | 168 | 15.5 |
| | | 93 | 128 | 38.6 |
| 3 | 40 | 50 | 509 | 10.7 |
| | | 58 | 388 | 41.8 |
| | | 68 | 275 | 33.5 |
| | | 79 | 153 | 36.2 |
| | | 93 | 96 | 40.5 |
| | 50 | 50 | 307 | 10.4 |
| | | 58 | 251 | 1.9 |
| | | 68 | 207 | 6.8 |
| | | 79 | 196 | 4.8 |
| | | 93 | 78 | 17.1 |

absorption spectrum of **1** possesses its lowest energy band at around 370 nm while the respective film exhibits a red shift of 2600 cm^{-1} to 410 nm. The observed shift is caused most likely by π - π stacking of the spacer moieties within the solid state leading to a stabilized excited state. Emission measurements revealed a structured peak at 410 nm in solution that is shifted to a broad, structureless emission at 530 nm for the printed film. In comparison to 2600 cm^{-1} in solution, the film features a larger Stokes shift of about 5600 cm^{-1} ; combined with the mentioned change in the band structuring this indicates excimer formation.^[16] In contrast, polymer **2** shows only a small red shift when changing from solution to the printed film indicating a less efficient stacking of the metallopolymer chains. While the absorption shifts from 430 to 445 nm (780 cm^{-1}), the emission exhibits a shift of about 660 cm^{-1} from 605 nm in solution to 630 nm for the printed film. Both solution and film show large Stokes shifts of 6700 and 6600 cm^{-1} , respectively, and broad, unstructured emission bands, caused by the charge-transfer characteristic, namely, intraligand charge transfer (ICT), of the low-energy transitions for this kind of chromophores.^[17] Also metallopolymer **3** possesses only marginal changes between solution and

film absorption. The maximum at around 570 nm remains constant, whereas a low-energy shoulder shifts from 615 to 650 nm. Emission could not be observed for polymer **3** most likely due to a shift to the NIR region, thus not detectable with the available measurement setup.

4. Conclusion

Combinatorial studies have been carried out on zinc(II)-bis-2,2':6',2''-terpyridine metallopolymers with regard to their inkjet printability. The influence of several printing parameters (solvent system, dot spacing, substrate temperature) on film homogeneity and UV-vis properties was investigated. Homogenous films could be obtained when printing from $5\text{ mg}\cdot\text{mL}^{-1}$ solutions using a 90/10 mixture of *N,N*-dimethylformamide and acetophenone as the solvent system. Elevated substrate temperatures of 40 to 50 °C had to be applied to ensure a uniform solvent evaporation. Utilizing dot spacings of 79 to 93 μm allowed achieving film thicknesses below 200 nm, suitable for potential applications in light-emitting or photovoltaic devices. There was, however, a significant influence of the substrate temperature

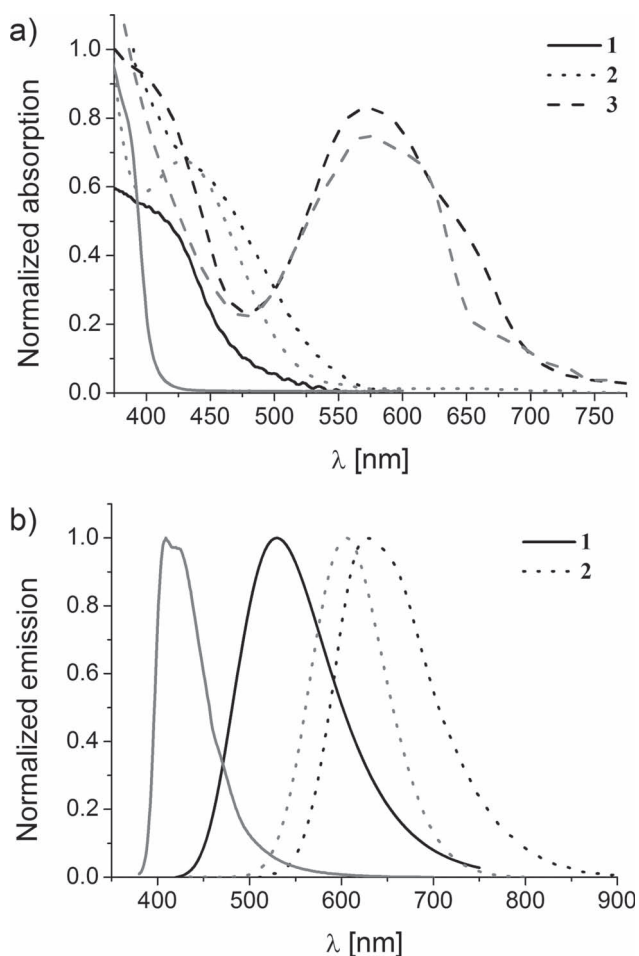


Figure 4. Normalized UV-vis absorption (a) and emission (b) spectra of inkjet-printed zinc(II) metallopolymers **1** (—), **2** (···), and **3** (---) films (black) and the respective solutions (grey; 10^{-6} M in DMF).

on the thickness reproducibility. UV-vis absorption and emission studies reproduced the spectral properties of the respective bis-terpyridine bridging moieties showing excimer emission in case of the fluorene-containing polymer **1** and strong ICT transitions for species **2** and **3** possessing conjugated donor–acceptor systems.

Prospectively, the optimized processing conditions, which were established for the preparation of homogeneous films of zinc(II)-bis-2,2':6',2''-terpyridine metallopolymers by inkjet printing within this contribution, enable the potential usage as photoactive layer within the course of preparation of fully printed optoelectronic devices such as PLEDs or OPVs.

Supporting Information

Supporting Information is available from the Wiley Online Library or from the author.

Acknowledgements: C.F. and A.W. contributed equally to this work. C.F. is grateful to the Fonds der Chemischen Industrie for a PhD scholarship. Furthermore, financial support of this study by the Dutch Polymer Institute (DPI, technology area HTE), the German Federal Ministry of Education and Research (Excellence Research and Innovation in East Germany: PhoNa), and the Thüringer Ministerium für Bildung, Wissenschaft und Kultur (Grant No. B 514-09049: PhotoMic) is kindly acknowledged. We also thank F. Kretschmer for synthetic work.

Received: October 28, 2011; Revised: December 13, 2011; Published online: January 31, 2012; DOI: 10.1002/marc.201100713

Keywords: combinatorial screening; inkjet printing; metal-polymer complexes; terpyridine; thin films

- [1] a) U. S. Schubert, A. Winter, G. R. Newkome, in *Terpyridine-based Materials for Catalytic, Optoelectronic and Life Science Applications*, Wiley-VCH, Weinheim Germany **2011**; b) R. Shunmugam, G. J. Gabriel, K. A. Aamer, G. N. Tew, *Macromol. Rapid Commun.* **2010**, *31*, 784; c) E. C. Constable, *Chem. Soc. Rev.* **2007**, *36*, 246.
- [2] a) A. Wild, A. Winter, F. Schlütter, U. S. Schubert, *Chem. Soc. Rev.* **2011**, *40*, 1459; b) E. A. Medlycott, G. S. Hanan, *Chem. Soc. Rev.* **2005**, *34*, 133.
- [3] a) A. Erxleben, *Coord. Chem. Rev.* **2003**, *246*, 203; b) J. Tao, M.-L. Tong, J.-X. Shi, X.-M. Chen, S. W. Ng, *Chem. Commun.* **2000**, 2043; c) E. B. Fleischer, A. M. Shachter, *Inorg. Chem.* **1991**, *30*, 3763.
- [4] a) A. Wild, F. Schlütter, G. M. Pavlov, C. Friebe, G. Festag, A. Winter, M. D. Hager, V. Cimrová, U. S. Schubert, *Macromol. Rapid Commun.* **2010**, *31*, 868; b) A. R. Rabindranath, A. Maier, M. Schäfer, B. Tieke, *Macromol. Chem. Phys.* **2009**, *210*, 659; c) A. Winter, C. Friebe, M. Chipper, M. D. Hager, U. S. Schubert, *J. Polym. Sci., Part A: Polym. Chem.* **2009**, *47*, 4083; d) S.-C. Yu, C.-C. Kwok, W.-K. Chan, C.-M. Che, *Adv. Mater.* **2003**, *15*, 1643; e) R. Dobrawa, F. Würthner, *Chem. Commun.* **2002**, 1878.
- [5] a) A. Winter, C. Friebe, M. D. Hager, U. S. Schubert, *Macromol. Rapid Commun.* **2008**, *29*, 1679; b) R. Dobrawa, M. Lysetska, P. Ballester, M. Grüne, F. Würthner, *Macromolecules* **2005**, *38*, 1315.
- [6] F. C. Krebs, *Sol. Energy Mater. Sol. Cells* **2009**, *93*, 394.
- [7] M. Singh, H. M. Haverinen, P. Dhagat, G. E. Jabbour, *Adv. Mater.* **2010**, *22*, 673.
- [8] J. Perelaer, P. J. Smith, D. Mager, D. Soltman, S. K. Volkman, V. Subramanian, J. G. Korvink, U. S. Schubert, *J. Mater. Chem.* **2010**, *20*, 8446.
- [9] C. J. Brabec, S. Gowrisanker, J. J. M. Halls, D. Laird, S. Jia, S. P. Williams, *Adv. Mater.* **2010**, *22*, 3839.
- [10] A. Teichler, R. Eckardt, C. Friebe, J. Perelaer, U. S. Schubert, *Thin Solid Films* **2011**, *519*, 3695.
- [11] R. D. Deegan, O. Bakajin, T. F. Dupont, G. Huber, S. R. Nagel, T. A. Witten, *Phys. Rev. E* **2000**, *62*, 756.
- [12] E. Tekin, B. J. de Gans, U. S. Schubert, *J. Mater. Chem.* **2004**, *14*, 2627.
- [13] J. Perelaer, B. J. de Gans, U. S. Schubert, *Adv. Mater.* **2006**, *18*, 2101.
- [14] B.-J. de Gans, U. S. Schubert, *Langmuir* **2004**, *20*, 7789.
- [15] P. J. Yunker, T. Still, M. A. Lohr, A. G. Yodh, *Nature* **2011**, *476*, 308.
- [16] S. A. Jenekhe, J. A. Osaheni, *Science* **1994**, *265*, 765.
- [17] W.-Y. Wong, C.-L. Ho, *Acc. Chem. Res.* **2010**, *43*, 1246.

Publication A6: “Ruthenium(II) photosensitizers of tridentate click-derived cyclometalating ligands: A joint experimental and computational study”

Benjamin Schulze, Daniel Escudero, Christian Friebe, Ronald Siebert, Helmar Görls, Stephan Sinn, Martin Thomas, Sebastian Mai, Jürgen Popp, Benjamin Dietzek, Leticia González, Ulrich S. Schubert

Chem. Eur. J. **2012**, *18*, 4010–4025.

Reprinted with permission from: WILEY-VCH Weinheim (Copyright 2012)



Ruthenium(II) Photosensitizers of Tridentate Click-Derived Cyclometalating Ligands: A Joint Experimental and Computational Study

Benjamin Schulze,^[a, b] Daniel Escudero,^[b, c] Christian Friebe,^[a, b] Ronald Siebert,^[b, d]
Helmar Görls,^[e] Stephan Sinn,^[a, b] Martin Thomas,^[b, c] Sebastian Mai,^[b, c] Jürgen Popp,^[b, d]
Benjamin Dietzek,^{*, [b, d]} Leticia González,^{*, [b, c, f]} and Ulrich S. Schubert^{*, [a, b]}

Abstract: A systematic series of heteroleptic bis(tridentate)ruthenium(II) complexes of click-derived 1,3-bis(1,2,3-triazol-4-yl)benzene N^{^C^N}-coordinating ligands was synthesized, analyzed by single crystal X-ray diffraction, investigated photophysically and electrochemically, and studied by computational methods. The presented comprehensive characterization allows a more detailed understanding of the

radiationless deactivation mechanisms. Furthermore, we provide a fully optimized synthesis and systematic variations towards redox-matched, broadly and intensely absorbing, cyclometalated ruthenium(II) complexes. Most of

them show a weak room-temperature emission and a prolonged excited-state lifetime. They display a broad absorption up to 700 nm and high molar extinction coefficients up to 20000 M⁻¹cm⁻¹ of the metal-to-ligand charge transfer bands, resulting in a black color. Thus, the complexes reveal great potential for dye-sensitized solar-cell applications.

Keywords: click chemistry • computational methods • cyclometalation • photosensitizers • ruthenium

Introduction

Ruthenium(II) polypyridyl complexes are highly prominent in photochemistry, since they allow for a light-driven charge separation in which the ligand becomes photoreduced while the metal is photooxidized and both can undergo subsequent redox reactions in terms of artificial photosynthesis. This metal-to-ligand charge transfer (MLCT) can be fine-tuned by the ligand properties to optimize the photophysical and electrochemical properties. To allow homogeneous, diffusion-controlled photocatalysis, a long excited-state lifetime is most important. A central dilemma is that, in contrast to tris(bidentate) ruthenium(II) complexes, bis(tridentate) ones are more stable and allow an isomer-free functionalization, but typically show only short excited-state lifetimes.^[1] Various optimization strategies to prolong the excited-state lifetime have been developed.^[2] The use of very strong, anionic donors causes slightly prolonged lifetimes, and moreover, interesting properties such as a broadened and red-shifted absorption of visible light and a directed MLCT transition.

An application for which these features become most important and the lifetimes are not that crucial, due to immobilization of the complexes and fast electron injection into the semiconductor, is the dye-sensitized solar cell (DSSC), developed by O'Regan and Grätzel in 1991.^[3] The DSSC applies the principles of natural photosynthesis, namely the spatial separation of the basic functions that are light-driven charge separation and charge transport, and, therefore, allows for modular manipulations of the light-harvesting dyes. Here, the almost pure, and thus predictable and tunable MLCT and reversible redox behavior made Ru^{II} polypyridyl complexes the most attractive candidates. In particu-

[a] B. Schulze, C. Friebe, S. Sinn, Prof. Dr. U. S. Schubert
Laboratory of Organic and Macromolecular Chemistry (IOMC)
Friedrich-Schiller-University Jena
Humboldtstr. 10, 07743 Jena (Germany)
Fax: (+49)3641948202
E-mail: ulrich.schubert@uni-jena.de

[b] B. Schulze, Dr. D. Escudero, C. Friebe, Dr. R. Siebert, S. Sinn,
M. Thomas, S. Mai, Prof. Dr. J. Popp, Prof. Dr. B. Dietzek,
Prof. Dr. L. González, Prof. Dr. U. S. Schubert
Jena Center for Soft Matter (JCSM)
Friedrich-Schiller-University Jena
Humboldtstr. 10, 07743 Jena (Germany)

[c] Dr. D. Escudero, M. Thomas, S. Mai, Prof. Dr. L. González
Laboratory of Theoretical Chemistry
Friedrich-Schiller-University Jena
Helmholtzweg 4, 07743 Jena (Germany)

[d] Dr. R. Siebert, Prof. Dr. J. Popp, Prof. Dr. B. Dietzek
Institute of Physical Chemistry and Abbe Center of Photonics
Friedrich-Schiller-University Jena
Helmholtzweg 4, 07743 Jena (Germany)
and Institute of Photonic Technology Jena
Albert-Einstein-Straße 9, 07745 Jena (Germany)
Fax: (+49)3641206399
E-mail: benjamin.dietzek@uni-jena.de

[e] Dr. H. Görls
Laboratory of Inorganic and Analytic Chemistry
Friedrich-Schiller-University Jena
Lessingstr. 8, 07743 Jena (Germany)

[f] Prof. Dr. L. González
Current address: Prof. Dr. L. González
Institute of Theoretical Chemistry, University of Vienna
Währinger Str. 17, 1090 Vienna (Austria)
Fax: (+43)1427752793
E-mail: leticia.gonzalez@univie.ac.at

Supporting information for this article is available on the WWW
under <http://dx.doi.org/10.1002/chem.201103451>.

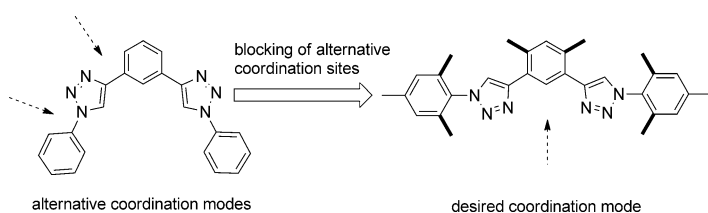
lar, Ru^{II} complexes featuring thiocyanate ligands like the red (N3, N719) and black dyes (N749) still display the benchmark with about 11% solar-cell efficiency.^[4] Their anionic, strong σ - and π -donating thiocyanate ligand enables panchromatic absorption and efficient electron injection into the semiconductor. However, at the same time the main drawback of the classical Ru^{II} dyes is the monodentate thiocyanate ligand limiting their stability and prohibiting further functionalization that could improve the light harvesting. Consequently, Ru^{II} complexes possessing aromatic carbanion donors that essentially adopt the function of the thiocyanate have been employed in DSSCs with great success.^[5] When embedded within a multidentate ligand, this cyclometalation^[6] allows for higher stability and ligand functionalization to optimize the photophysical and electrochemical properties.

Recently, click-derived^[7] ligands have been successfully used as analogues of polypyridyl ligands, in particular of 2,2':6',2''-terpyridine (tpy).^[8] We were interested in extending this analogy to tridentate cyclometalating polypyridyl ligands, namely 1,3-dipyridylbenzene (dpbH).^[9] In this context, we present a new and systematic series of click-derived, tridentate, cyclometalated Ru^{II} complexes^[10] that was studied in detail by experimental and computational methods to elucidate the potential for dye-sensitized solar-cell application.^[11] Thereby, the combination of theoretical investigations and photophysical as well as electrochemical studies enables a consistent and emergent explanatory picture of the new dyes.

Results and Discussion

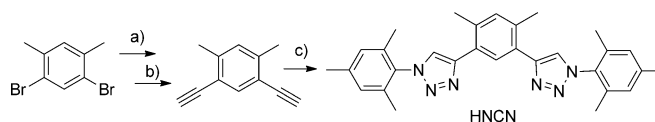
Syntheses: A fully optimized synthetic procedure is presented for the new cyclometalated complexes as well as for a non-cyclometalated model complex.^[8d] The optimization, the design strategy and an exemplary synthetic procedure are explained in the following. For synthetic details, the reader is referred to the Supporting Information.

The ligands were obtained from aryl azides and diethynylbenzene building blocks in good yields using standard click conditions. For the sake of blocking alternative, bidentate coordinations that were observed in initial attempts, methyl groups were placed at strategic positions when possible and reasonable.^[12] Therefore, *o*-xylene was chosen as the central ring as well as mesityl moieties for the clicked-on functionalities (Scheme 1).



Scheme 1. Schematic illustration of the optimization strategy.

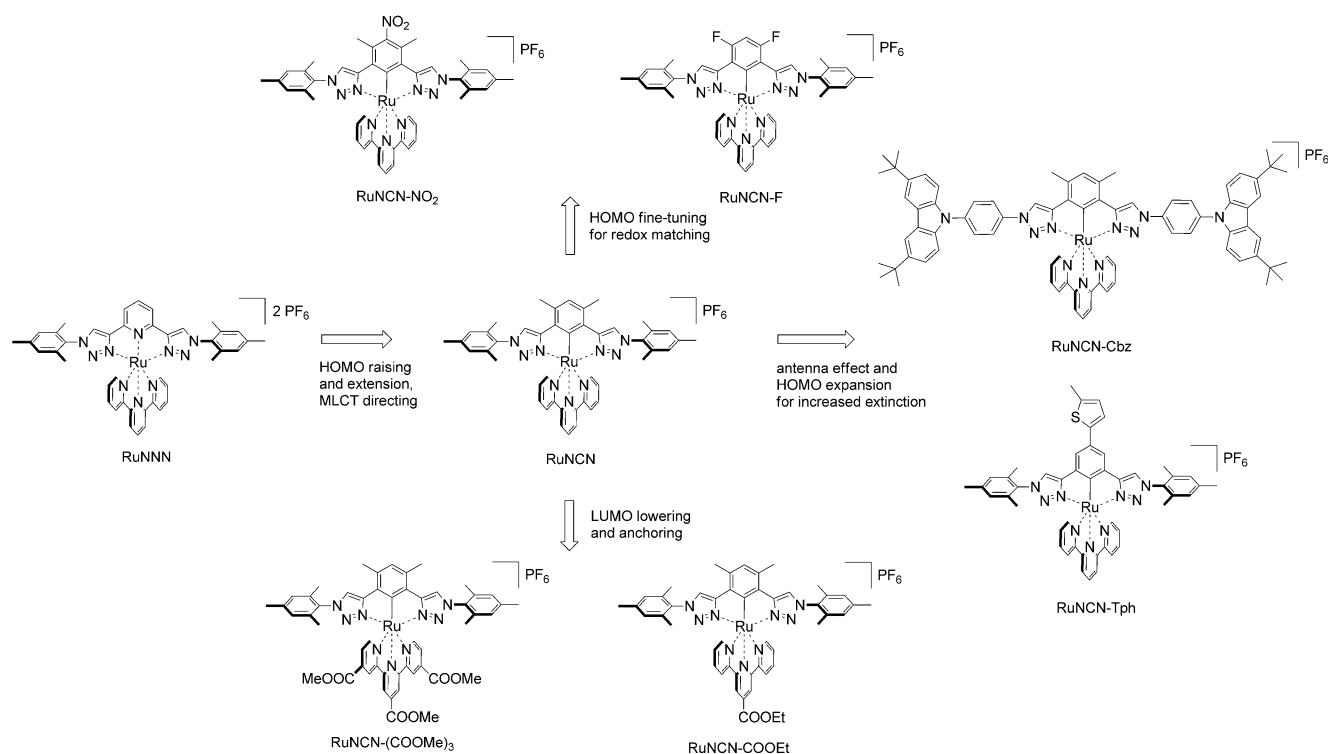
Furthermore, mesityl was chosen as substituent for further reasons: 1) it enables both good solubility and good crystallization behavior, 2) it is electronically decoupled due to its orthogonality and therefore a reasonable electronic reference, 3) it allows for eased NMR interpretations, and 4) it is readily available from mesityl amine through diazotization/azidation and can be considered as a safe azide. The diethynylbenzene building blocks were synthesized under standard Sonogashira conditions with additional LiCl^[13] starting from functionalized dibromobenzenes (Scheme 2).



Scheme 2. Exemplary synthesis of the cyclometalating ligands: a) [Pd(PPh₃)₄], LiCl, CuI, TMS-CCH, NEt₃, PhMe, 50 °C, 72 h; b) KF, THF/MeOH (1:1); 50% over 2 steps; c) CuSO₄·5H₂O, NaAsc., MesN₃, CH₂Cl₂/EtOH/H₂O (1:2:1), 60 °C, 12 h, 90%.

In one case, σ -accepting fluoro substituents replace the methyl groups in the position *meta* to the carbanion to allow blocking as well as electronic fine-tuning.^[5c,e,12] In the case of 1,3,5-tribromobenzene, 2-methylbut-3-yn-2-ol was chosen as protected alkyne to ease the chromatographic separation.^[14] After deprotection and cycloaddition, the according 5-bromo-1,3-bis(triazolyl)benzene allows further ligand-functionalizations by cross-coupling methods in an important position. The subsequent installation of a chromophore at the *para* position of the cyclometalating ring, for example, thiophene, would extend the conjugated system and increase the light absorptivity. Similarly, the mesityl azide reference was changed once to 9-(4-azidophenyl)-3,6-di-*tert*-butyl-9*H*-carbazole to install an organic chromophore at the complex periphery as light-harvesting antenna.^[15] In this case, the conjugation through the triazole ring is not expected^[16] and the increase of light harvesting would be additive only. However, although click chemistry provides facile functionalization within the ligand formation, leading to modular and higher functionalized complexes, we kept the mesityl moiety as reference in all other cases to discuss the more pronounced influences of substituents directly attached to the cyclometalating phenyl ring or the opposed ligand (Scheme 3). In addition, it is questionable if the overall device efficiency profits from the increased absorptivity due to the carbazoles or if it drops due to lowered dye coverage on the semiconductor surface.

To facilitate the coordination and cyclometalation, the common [Ru^{III}(tpy)Cl₃] precursor can be activated in situ by halide abstraction with a silver(I) salt in a weakly coordinating solvent. However, it is known that silver(I) can oxidize the product yielding a homocoupled dimer^[9a] and therefore needs to be filtered off after the activation step. Still, application of a Ru^{III} precursor includes a reduction step towards Ru^{II} after coordination that is normally achieved by alcohols or amines. Since the cyclometalated complexes are oxidized



Scheme 3. Design strategy and overview of the synthesized ruthenium(II) complexes.

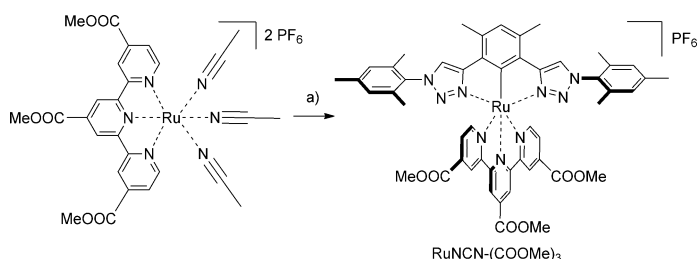
easily, the product is achieved either as Ru^{III} complex or it already underwent side reactions in the position *para* to the cyclometalation that has significant radical character within the Ru^{III} complex. This drawback can be overcome by the use of $[\text{Ru}^{\text{II}}(\text{tpy})(\text{CH}_3\text{CN})_3][\text{PF}_6]_2$ as precursor (see Scheme 4 for a representative example).^[17] In fact, it is

under oxygen-free conditions in a closed vial using an alcohol as solvent and microwave heating to 160°C for 30 min. Isolation of the product by a combination of column chromatography and crystallization afforded the desired complexes, in most cases as X-ray-quality crystals (Figure 1 and the Supporting Information) and in reasonable yields varying from 40 to 70 % (Scheme 4 and the Supporting Information), depending, amongst others, on whether all strategic methyl groups were present.

Since cyclometalated complexes are very electron-rich in the position *para* to the carbanion, they enable targeted homocoupling and post-complexation functionalizations in the presence of oxidants, electrophiles, or both.^[18] This allowed the introduction of a nitro group under Menke conditions and, thereby, the respective manipulation of the carbanion donation by a σ - and π -accepting group in turn.^[5d]

The installation of the anchoring carboxylic acid functions for the DSSC was achieved simply by using ester functionalized ligands and saponification^[5e,f] subsequent to the complexation. Thus, the intermediate, highly soluble, ester-functionalized complexes could be purified and studied, since they are seen as models for the final complexes adsorbed to TiO_2 .^[5k]

Crystal structures: Single crystals of the ligands HNCN and HNCN-F as well as of the three Ru^{II} precursors and of RuNNN, RuNCN, RuNCN- NO_2 , RuNCN-F and RuNCN-Tph could be grown and characterized successfully by X-ray diffraction (Figure 1 and the Supporting Information). The systematic variation allows for comparison although only



Scheme 4. Exemplary synthesis of the cyclometalated ruthenium(II) complexes: a) HNCN, methanol, microwave, 30 min., 160°C , 50%.

easily synthesized from $[\text{Ru}^{\text{III}}(\text{tpy})\text{Cl}_3]$ in acetonitrile/ethanol/water using AgNO_3 and, in contrast to $[\text{Ru}^{\text{III}}(\text{tpy})\text{Cl}_3]$, it can be purified completely, thus simplifying the subsequent complexation. In more detail, after removal of the AgCl by filtration over celite, the product can be isolated either by column chromatography or directly by vapor diffusion of diethyl ether into a concentrated acetonitrile solution yielding large, even X-ray-quality crystals (see the Supporting Information). The subsequent cyclometalation was performed

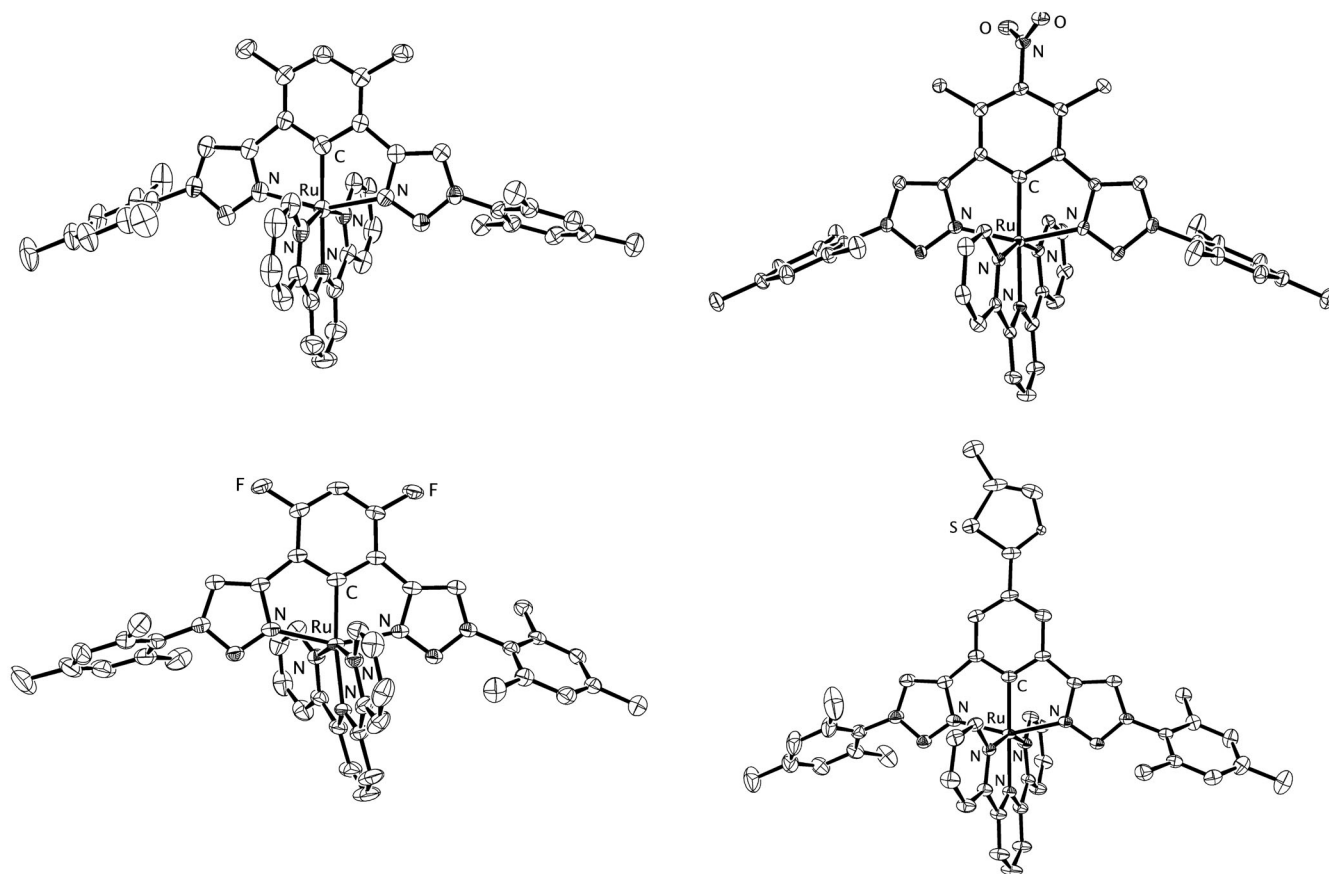


Figure 1. Solid-state structures of RuNCN (top left), RuNCN-NO₂ (top right), RuNCN-F (bottom left) and RuNCN-Tph (bottom right) (50% probability level; counterions, hydrogen atoms and solvent molecules omitted for clarity).

the most pronounced changes are discussed to beware of packing effects (note the strong distortion within RuNCN-F).

The mesityl-triazole torsion angle of the complex series varies between 60° and 90°. The thiophene-phenyl torsion angle in RuNCN-Tph was determined to be 30.7°, thus being in good agreement with the calculated value of 30.2° (see Scheme S9 in the Supporting Information) and allowing for partial extension of the conjugation into the thiophene ring.

The replacement of a dative Ru–N bond of the polypyridyl-type complex RuNNN by a covalent, organometallic Ru–C bond within the cyclometalated RuNCN complex leads to a bond shortening from 2.02 to 1.98 Å, caused by the very good σ donation and additional π donation as well as by electrostatic interactions with the anionic, aromatic carbon donor. Furthermore, the adjacent triazole N–Ru bonds are slightly elongated, most likely due to a declined σ orbital overlap by the smaller bite angle. As a consequence of the good electron donation ability of the carbanion, the opposed Ru–N bond becomes elongated from 1.97 to 2.01 Å which is well-known as *trans* influence. Furthermore, the outer pyridine N–Ru bonds are shortened as result of increased π back donation from the more electron-rich Ru^{II} metal center in the cyclometalated complex (Figure 2 and

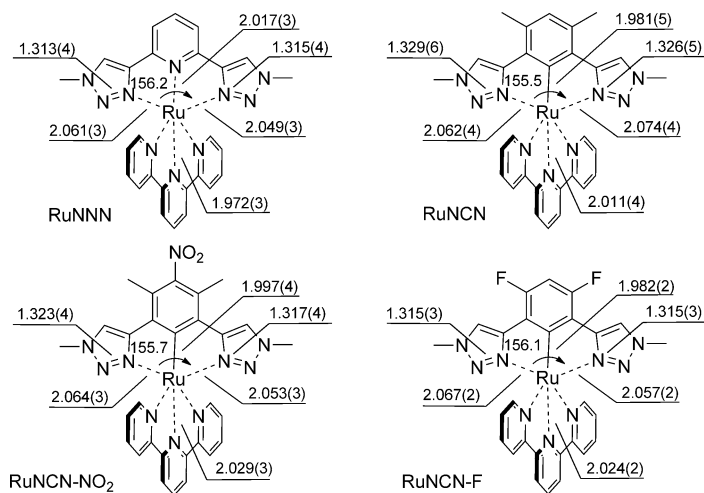
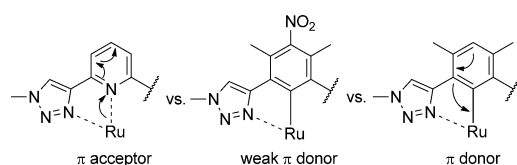


Figure 2. Selected bond lengths (Å) and angles (°) of RuNNN, RuNCN, RuNCN-NO₂ and RuNCN-F.

Scheme 5). Also within the triazole ring, the N²–N³ double bond is elongated as a consequence of the increased π back donation into π^* orbitals.

For RuNCN-NO₂, upon installing an electron-withdrawing group, namely a nitro group that is capable of withdrawal



Scheme 5. Schematic representation of the electronic consequences of the cyclometalation and an electron-withdrawing group.

through the σ and π system, most of the consequences of the cyclometalation are less pronounced than for RuNCN. Even though the π -accepting capability might be reduced due to the dihedral angle of 51.8° (51.6° calculated, see Scheme S9 in the Supporting Information) with the central phenyl ring due to repulsion with the *ortho*-methyl groups, there is a distinct influence on the π system that strongly reduces the π -donation ability of the cyclometalating carbanion in the *para* position. Consequently, the Ru–C bond is elongated to 2.00 \AA (Figure 2 and Scheme 5). In particular in comparison to RuNCN-F, the fluoro substituents that are strongly σ -accepting, but whose moderate π -donation ability does not affect the carbanion because they are in *meta* positions, still allow a very short Ru–C bond of 1.98 \AA . Also the changes in bond lengths within the central phenyl ring are consistent with a participation of a chinoid resonance structure in RuNCN-NO₂. The successive reduction of the electron donation of the carbanion by the fluoro and nitro substituents is demonstrated by the shortening of the triazole N²=N³ double bond due to decreased π back donation. Also the Ru–N bond *trans* to the carbanion is further elongated for the same reason.

Apparently, the fluoro substituent mostly influences the σ donation and might lower the energy of the π system indirectly (inductive effect), while the nitro group causes an additional polarization of the π system that strongly weakens the π donation (mesomeric effect) but to a less extent the σ donation. This is consistent with the electrochemical data: for RuNCN-F only the HOMO is stabilized, located on the Ru^{II} metal center and the fluoro-substituted cyclometalating phenyl ring as well, while RuNCN-NO₂ shows an additional LUMO stabilization that is mediated through the aromatic π system/Ru^{II} d orbitals, since the LUMO is located on the opposed tpy ligand.

Interestingly, within all investigated solid-state structures of triazole-containing ruthenium(II) complexes (see Figure S143 in the Supporting Information), short-contact interactions of the triazole with either the counterions or the solvent are present. Triazoles and triazolium salts are known to allow hydrogen bonding as well as electrostatic interactions.^[19] Similar to triazolium salts, a ruthenium-coordinated triazole is expected to be more polarized than a free triazole. Preliminary results indicate an interaction of the ruthenium(II)-coordinated triazole with iodide (see Figure S144 in the Supporting Information). The question, if hydrogen bonds/electrostatic interactions might allow the preorganization of the redox mediator in a position favorable for ruthenium(III) reduction, will be targeted in the future.

DFT calculations: As a basis for a deeper understanding of the photophysical and electrochemical properties of the presented Ru^{II} complexes, namely to gain insight into detailed structure–property relations, density functional theory (DFT) calculations, and time-dependent (TD) DFT calculations have been performed.

Whilst the description of the UV/Vis characteristics of these complexes is nowadays close to routine, the description of non-adiabatic events occurring after light excitation is more troublesome. Their description would in principle require the use of multiconfigurational methods in combination with a proper description of spin-orbit coupling (SOC) effects. Unfortunately, these methods are practically unaffordable for Ru^{II}–polypyridyl dyes.^[20] Therefore, Δ -SCF-DFT (SCF= self-consistent field) and TDDFT methods remain as valuable alternatives to obtain qualitative and even quantitative information about Ru^{II} complexes and many examples are found in the literature.^[21] DFT calculations provide the geometries and energies of the ground and lowest excited states of each symmetry and spin, whilst information on the higher excited states (i.e., energies, oscillator strengths and associated character of the excitations) can be obtained with the help of TDDFT calculations.

In order to understand the deactivation mechanisms after light excitation for RuNNN and RuNCN, their most relevant structures involved, namely the singlet ground state (S_0) as well as the most stable ³MLCT and triplet metal-centered (³MC) excited state, were optimized. As known for Ru^{II}–polypyridyl complexes, after excitation of the ¹MLCT manifold, ultrafast inter-system crossing (ISC) occurs within less than 100 fs, leading to the formation of the ³MLCT states with near-unity quantum yield. Among the subsequent radiative and non-radiative processes, radiationless deactivation through thermal population of ³MC states is supposed to determine the ³MLCT lifetime.^[1,2] Thus, in addition to the location of the ³MLCT and ³MC states, crossing points between the S_0 and the ³MC potential energy surface determine the non-adiabatic population transfer, as has been recently stated by Boggio-Pasqua et al. for similar Ru^{II}–polypyridyl complexes.^[22]

The electronic nature of the lowest-energy triplet excited states of RuNCN has been confirmed by analysis of the spin density distributions (Figure 3). The most stable ³MLCT state indeed displays unpaired electrons within a Ru $4d_{yz}$ orbital and a π^* orbital of the tpy ligand, while only Ru-based 4d orbitals are involved in the ³MC state. The main geometrical features of both the optimized ³MLCT and ³MC structures for RuNNN and RuNCN are given in Scheme S9 and S10 in the Supporting Information. In comparison to the S_0 geometry, the ³MLCT and also the ³MC geometries of each complex show a weakening of the coordination, attributed to the population of antibonding orbitals, either π^* or “ e_g^* ”, as well as to the weakened π back bonding with the formally oxidized Ru “ t_{2g} ” orbitals. In the ³MC structures the tpy coordination is even distorted (see exemplarily the ³MC structure of RuNCN in Figure 3) due to the weakening, not only of the π back donation but also of the σ donation by the

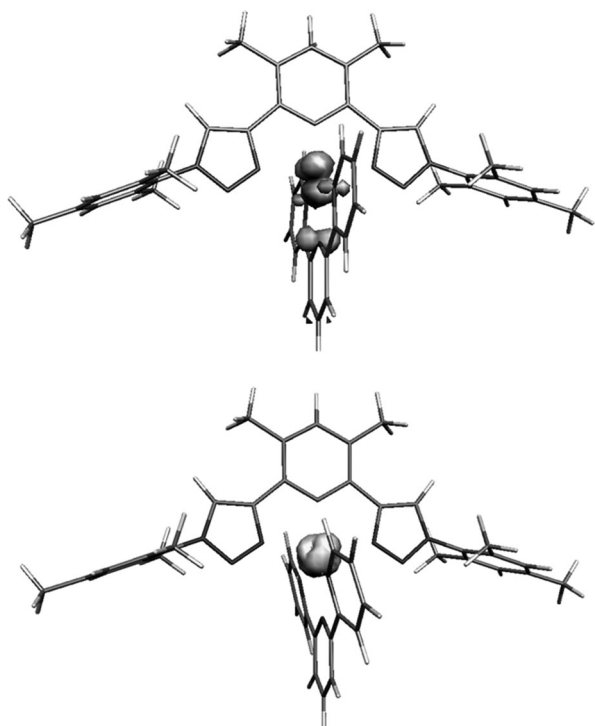


Figure 3. Spin density distribution of the energy optimized $^3\text{MLCT}$ (top) and ^3MC (bottom) geometries of RuNCN.

population of the “ e_g^* ” levels. Thus, repulsive interactions are avoided by ligand distortion, hence lowering the energy of the ^3MC state. This is important, since in the $^3\text{MLCT}$ geometry, due to the strong effective σ donation, the unoccupied, antibonding metal d orbitals are located at high ener-

gies (see below and Figure 4), while in the ^3MC geometry, in which these orbitals are occupied, the destabilizing effects are less pronounced (see the photophysical model section below). Furthermore, while the tridentate ligand is only distorted, a monodentate ligand, such as thiocyanate, can be cleaved off. For all other compounds, only the S_0 and the lowest $^3\text{MLCT}$ states were optimized and the main geometrical features are given in the Supporting Information.

To understand the substituent effects on the photophysical properties, the relevant frontier Kohn–Sham orbitals are plotted in Figure 4. For RuNCN, π donation destabilizes the HOMO that is composed of Ru d_{yz} and NCN π orbitals. In contrast, for RuNNN the HOMO is less destabilized and almost of pure Ru d_{xz} character; only a weak π donation contributes to the HOMO–1, which is therefore lower in energy. In both complexes, the LUMO is formed by the same π^* orbital of the tpy ligand; however, the strongly destabilized HOMO of RuNCN causes an additional indirect LUMO destabilization through the π back donation. Because the LUMO destabilization is less pronounced than for the HOMO, the resulting energy gap is much smaller for RuNCN. A further effect of the strong electron donation within RuNCN is the strongly destabilized “ e_g^* ” orbitals in terms of a strong ligand field. Thus, the d_{z^2} orbital is the LUMO+8 in RuNNN, being 1.9 eV higher in energy than the LUMO, while in RuNCN it is the LUMO+14 with an energy difference of 2.3 eV. This demonstrates that cyclometalation indeed enables destabilization of orbitals that are populated in ^3MC states and that are relevant for the radiationless deactivation. However, the actual electronic situation at the ^3MC geometry might be different as mentioned above. Therefore, although the ^3MC stabilization might be

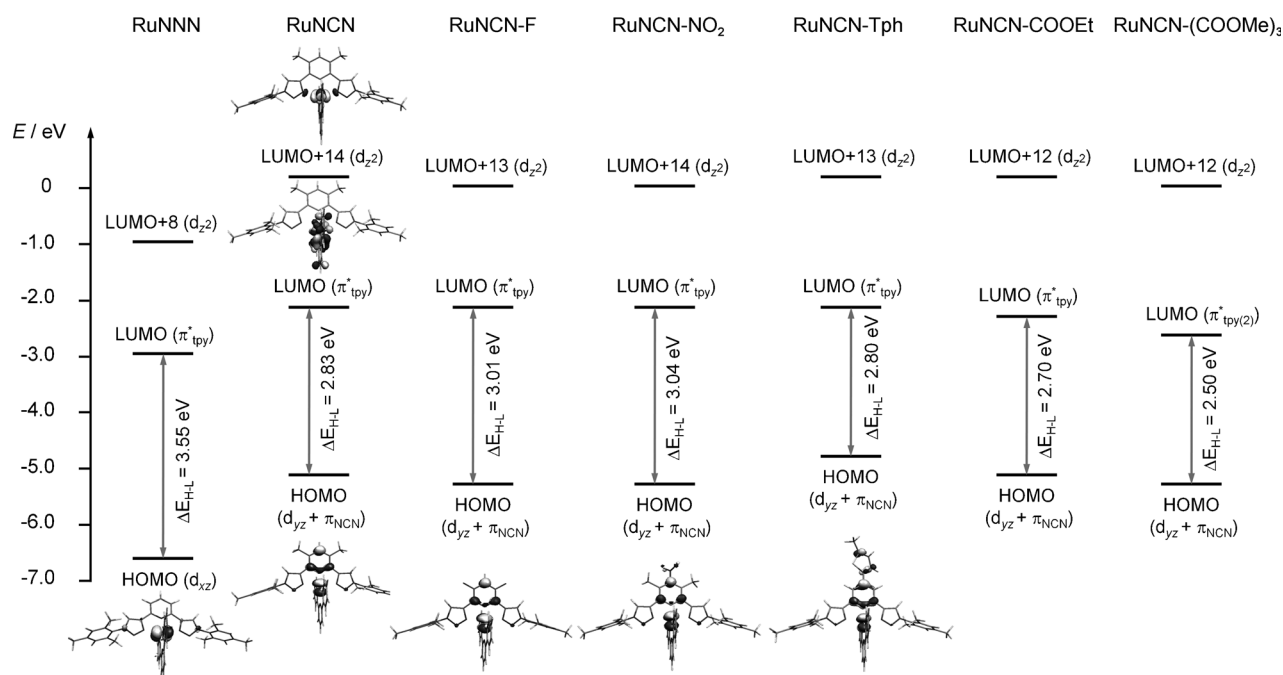


Figure 4. Selected PCM-B3LYP/6-31G* Kohn–Sham orbitals and energy level scheme for the Kohn–Sham orbitals of the Ru^{II} complexes.

helpful, it does not necessarily cause a suppression of the thermal population of the ^3MC from the $^3\text{MLCT}$ states (this issue will be discussed in more detail in the photophysical model section below).

Figure 4 also shows the HOMO orbitals of RuNCN-F, RuNCN-NO₂ and RuNCN-Tph. The introduction of an electron-withdrawing fluoro or nitro group directly attached to the HOMO site leads to HOMO stabilization, since the electronic repulsion and electron donation of the carbanion donor is tempered, but also because the aromatic system, which forms a part of the HOMO itself, is stabilized. In case of RuNCN-Tph, the HOMO and LUMO are slightly destabilized due to electron donation from the thiophene moiety, while the energy gap remains constant. Importantly, the conjugation of the HOMO is extended onto the thiophene ring, which should give rise to an increased light absorptivity (see the photophysical properties). Apparently, stabilization due to extension of the conjugation is overcompensated by electron donation of the thiophene. For complexes of ester-functionalized tpy ligands, the HOMO is slightly stabilized because of the increased π acidity of the ligand. Since they are directly attached to the LUMO site, the LUMO level is strongly stabilized by their electron withdrawal, resulting in smaller energy gaps, in particular for RuNCN-(COOMe)₃. Furthermore, the LUMO, which is not shown for these complexes, is the same orbital throughout the whole series and differs only in energy. As an exception, in RuNCN-(COOMe)₃ the LUMO is a different orbital that is however located on the tpy ligand.

Photophysical properties: A key feature of designated photo-redoxactive Ru^{II} complexes, in particular when aiming at a potential application in dye-sensitized solar cells, is their photophysical behavior. Thus, UV/Vis absorption and emission spectrum measurements as well as photoluminescence quantum yield (Φ_{PL}) and lifetime determinations were executed. Additionally, PCM-TD-B3LYP (PCM = polarizable continuum model) vertical excitations were computed for all the complexes except for RuNCN-Cbz (see the Supporting Information for computational details).

First of all, the free cyclometalating ligands were characterized. Their UV/Vis spectra show a strong absorption peak at around 240 nm with extinction coefficients of 36000–140000 M⁻¹cm⁻¹. Additional bands are located at about 295 nm with weak intensities of 1100 and 4600 M⁻¹cm⁻¹ for HNCN and HNCN-F, respectively. In contrast, HNCN-Cbz and HNCN-Tph, possessing additional chromophores, exhibit strong absorption peaks beyond 290 nm, with ϵ values of 58000 and 46300 M⁻¹cm⁻¹ for HNCN-Cbz and 15400 M⁻¹cm⁻¹ for HNCN-Tph. All ligands are fluorescent, showing emission bands at 325 (HNCN, HNCN-F), 367 (HNCN-Tph), and 404 nm (HNCN-Cbz) (see the Supporting Information).

The absorption and emission features as well as the computed transitions of the studied Ru^{II} complexes are shown in Figure 5 and Table 1. For the assignment of the PCM-TD-B3LYP excitations, see Tables S4–S10 in the Supporting In-

formation. Firstly, the comparison of the parent cyclometalated complex RuNCN with its non-cyclometalated counterpart RuNNN reveals the strong influence of the carbanion donor on the UV/Vis absorption properties. A significant bathochromic shift of the MLCT maxima from 428 to 532 nm, corresponding to 4500 cm⁻¹, is observed upon cyclometalation and well reproduced by the performed calculations. Additionally, an extension of the absorption from 550 to 650 nm is observed that can be explained by destabilization of the Ru-4d orbitals in the RuNCN complex. Indeed, the electronic excitations responsible for these bands involve mainly these orbitals (Table S4 in the Supporting Information). Furthermore, since RuNCN possesses an organometallic, covalent bond, the HOMO is composed of Ru-d orbitals as well as π orbitals of the cyclometalating ligand, while the LUMO (and higher unoccupied molecular orbitals) is π^* -tpy-based. Thus, if the anchoring groups are installed at the tpy acceptor ligand, the transition dipole moment is directed towards the semiconductor surface by the distinct push-pull effect.^[5a] Since these transitions exhibit partial ligand-to-ligand charge-transfer (LLCT) character, they can be described as metal/ligand-to-ligand charge-transfer (MLLCT) excitations. This underlines the feasibility of directly influencing the HOMO by manipulation of the cyclometalating ligand, although usually the MLCT declaration is kept in literature.^[5f,j] Furthermore, the MLCT bands are broadened and even split because of the electronic asymmetry that breaks the orbital degeneracy. Thus, the shorter wavelength transitions around 400 nm exhibit MLCT, MLLCT, and admixed MC character (see S₆, S₁₄ and S₁₇ in Table S4 in the Supporting Information). In the UV region, the high-energy transitions are mainly of π - π^* character (see S₃₄ and S₄₁). However, after thermal relaxation in terms of Kasha's rule, the transferred charge will reside on the acceptor ligand. As a further result of the strong anionic carbon donor, a weak room-temperature emission at 751 nm (Φ_{PL} : 0.006%) was observed for RuNCN (see the photophysical model below).^[6a]

To understand the influence of the triazole moiety, a comparison referring to the corresponding Ru^{II} complexes of pyridine analogues, namely 2,2':6',2''-terpyridine and 1,3-dipyridylbenzene, is helpful. When compared to [Ru(tpy)₂][PF₆]₂, the analogous but heteroleptic RuNNN shows a broadened and blue-shifted absorption. Also the emission at 77 K, which is similar in shape for both, is blue-shifted from 603 to 574 nm. According to the calculations, the emitting state is of $^3\text{MLCT}$ character and tpy-based (see the DFT calculation above). Additionally, the computed emission maxima (adiabatic emission energies obtained with Δ -SCF approach, see the Supporting Information for details), are given in Table 1 and correlate well with the experimental data. The absorption spectra of [Ru(tpy)(dpb)]PF₆ and RuNCN are similar,^[5] except for a slight hypsochromic shift that is observed in the absorption and emission spectra of RuNCN. Interestingly, although still weak, the emission is slightly increased for RuNCN, most likely because of the higher emission energy in accordance with the energy-gap

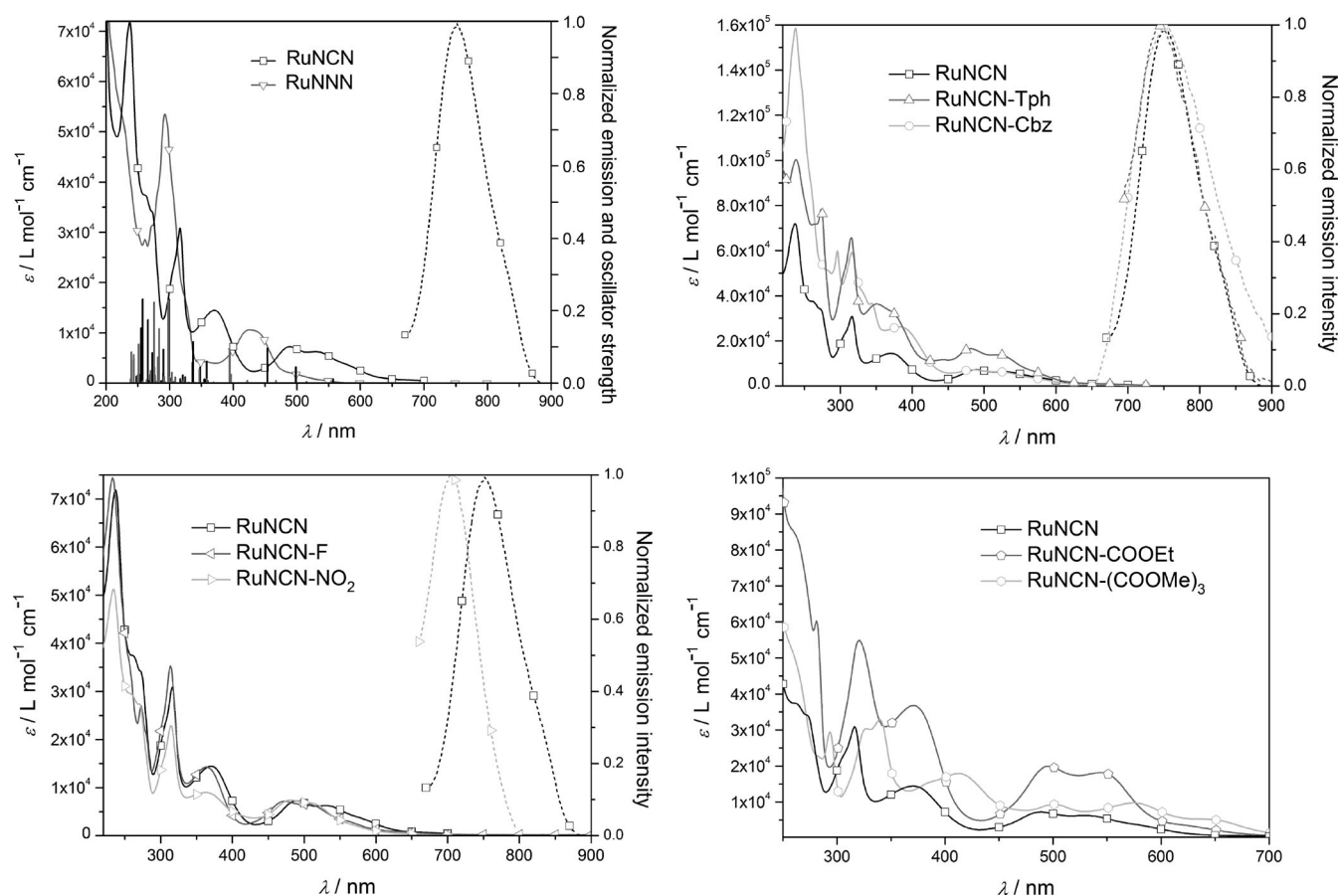


Figure 5. UV/Vis absorption and emission spectra of the investigated ruthenium(II) complexes (10^{-6} M in CH_3CN). For RuNCN and RuNNN, the PCM-TD-DFT/6-31G* computed vertical excitations are superimposed. Solid lines represent the measured curve and symbols are only used for assignment.

law. Furthermore, the extinction coefficients are lowered for RuNCN, attributed to the shorter conjugation that is only partially extended into the triazole.^[8a]

To allow for HOMO fine-tuning (see the electrochemical properties below), electron-withdrawing groups, namely nitro and fluoro substituents, were installed at the central phenyl ring. Consequently, a slight hypsochromic shift (700 cm^{-1}) of the MLCT features in the UV/Vis absorption spectrum was observed due to HOMO stabilization. Accordingly, a room-temperature emission can be observed for RuNCN- NO_2 that is blue-shifted by 870 cm^{-1} (Φ_{PL} : 0.01%). In contrast, RuNCN-F features no measurable photoluminescence (see the temperature-dependent lifetime measurements below). Besides, the π -accepting nitro group, *para* to the Ru-C bond, leads to a decrease of the extinction coefficient by a third compared to the parent RuNCN complex, attributed to interference with the push-pull polarization.

To increase the extinction coefficients, additional chromophores were attached^[5d-g, 15, 23] either directly to the central phenyl ring or as clicked-on antennas. The thiophene moiety that was installed *para* to the Ru-C bond increases the extinction coefficients over the whole UV/Vis absorption spectrum, including the highest wavelength absorption that grows from $7300\text{ M}^{-1}\text{ cm}^{-1}$ for RuNCN to $16500\text{ M}^{-1}\text{ cm}^{-1}$.

Evidently, this is due to extension of the HOMO and, thus, expansion of the optical cross section (see DFT calculations and Figure 4).^[5d] In contrast, the attachment of the carbazole moiety provides an additional but separated chromophore that is not in conjugation with the cyclometalated phenyl ring.^[16] Thereby, the extinction coefficients below 450 nm double with respect to RuNCN, because the carbazole participates in LC transitions, while the absorption bands beyond 450 nm, in analogy to RuNCN assigned mainly to $d_{\text{Ru}}/\pi_{\text{NCN}} \rightarrow \pi_{\text{tpy}}^*$ transitions, remain unchanged in shape and intensity. Furthermore, the room-temperature emission of RuNCN was preserved, thus no additional quenching pathways are introduced; instead, the emission intensity was even slightly increased (Table 1).

For the immobilization on the semiconductor surface in DSSCs, carboxylic groups on the acceptor ligand are necessary. Beside their function as anchoring groups, they also strongly influence the photophysical properties as additional electron-withdrawing groups. Here, the ester-functionalized complexes were seen as models for the TiO_2 -bound dyes.^[5k] The introduction of a single carboxylic ester at the 4'-position of the terpyridine causes a stabilization of the π_{tpy}^* -based LUMO (Figure 4) and an enhanced transition dipole moment, thus leading to a slight bathochromic shift by about 500 cm^{-1} as well as a tripled extinction coefficient in

Table 1. Photophysical data of the complexes.

| Complex | 298 K | | | | 77 K | | $k_r + k_1$ [s ⁻¹] ^[f] | k_2 [s ⁻¹] | k_3 [s ⁻¹] | ΔE_2 [cm ⁻¹] | ΔE_3 [cm ⁻¹] |
|---|--|---|---|--------------------|---|------------------|--|-----------------------------|-----------------------------|-------------------------------------|-------------------------------------|
| | $\lambda_{\text{max}}^{\text{abs}}$ [nm] (ϵ [10 ³ M ⁻¹ ·cm ⁻¹] ^[a,b]) | $\lambda_{\text{max}}^{\text{em}}$ [nm] ^[a,c,d] | Φ_{PL} 10 ⁻⁵ ^[a,e] | τ [ns] | $\lambda_{\text{max}}^{\text{em}}$ [nm] ^[d] | τ [μs] | | | | | |
| RuNNN | 325 (sh), 428 (10.6), 500 (1.8) | – (545) | – | – | 574 | 14 | – | – | – | – | – |
| [Ru(tpy) ₂][PF ₆] ₂ ^[5j,30] | 308 (63.4), 475 (14.7) | – | – | 0.25 | 603 | – | 6.5 × 10 ⁴ | 2.0 × 10 ¹³ | 2.1 × 10 ⁷ | 1700 | 720 |
| RuNCN | 371 (14.5), 488 (7.3), 532 (6.3) | 751 (827) | 6.1 | 4.1 | 719 | 4.1 | 2.44 × 10 ⁵ | 1.1 × 10 ¹² | 3.11 × 10 ⁸ | 1830 | 350 |
| [Ru(tpy)(dpb)]PF ₆ ^[5i] | 424 (9.6), 499 (14.4), ≈ 540 (≈ 10) | 781 | 0.9 | – | – | – | – | – | – | – | – |
| [Ru(tpy)(dpb)]PF ₆ ^[8d] | 504 (10.8), 550 (8.3) | 784 | 4.5 | 4.5 | 752 | 0.48 | – | – | – | – | – |
| RuNCN-F | 363 (14.3), 473 (7.2), 507 (6.5) | – | – | 0.5 ^[h] | 661 | 5.8 | 1.72 × 10 ⁵ | 9.74 × 10 ¹¹ | – | 1290 | – |
| RuNCN-NO ₂ | 365 (9.0), 483 (7.4), 511 (6.8) | 705 (759) | 10.0 | 5.3 | 667 | 5.2 | 1.92 × 10 ⁵ | 6.63 × 10 ¹¹ | – | 1395 | – |
| RuNCN-Cbz | 384 (26.2), 485 (7.3), 523 (6.3) | 750 | 25.0 | 6.7 ^[h] | 712 | 4.5 | 2.22 × 10 ⁵ | 2.04 × 10 ¹¹ | 1.33 × 10 ⁸ | 1570 | 270 |
| RuNCN-Tph | 350 (36.4), 482 (16.5), 518 (13.8) | 745 (802) | 5.3 | 4.1 ^[h] | 722 | 4.3 | 2.33 × 10 ⁵ | 1.89 × 10 ¹¹ | 1.42 × 10 ⁸ | 1452 | 240 |
| RuNCN-COOEt | 372 (36.8), 495 (19.9), 546 (18.2) | – (941) ^[d] | – ^[d] | – ^[d] | – ^[d] | – ^[d] | – | – | – | – | – |
| RuNCN-COOH | 373 (22.0), 491 (10.5), 532 (10.5) | – | – | 12.3 | 745 | 5.7 | 1.75 × 10 ⁵ | 2.02 × 10 ¹⁰ | – | 1135 | – |
| RuNCN-(COOMe) ₃ | 413 (17.9), 500 (9.4), 574 (9.8), 641 (5.3) | – (1032) ^[d] | – ^[d] | – ^[d] | – ^[d] | – ^[d] | – | – | – | – | – |
| RuNCN-(COOH) ₃ | 398 (8.7), 497 (5.0), 572 (5.3), 641 (3.2) | – ^[d] | – ^[d] | – ^[d] | – ^[d] | – ^[d] | – | – | – | – | – |

[a] Measured 10⁻⁶ M in deaerated CH₃CN. [b] sh = shoulder. [c] In brackets: Adiabatic emission energy values ($\Delta\text{SCF-PCM-DFT/6-31G}^*$). [d] The detector limit is at 800 nm. [e] Determined using [Ru(dqp)₂][PF₆]₂ in MeOH/EtOH (1:4; $\Phi_{\text{PL}} = 2.0\%$)^[31] as a reference. [f] The sum of k_r and k_1 is the reciprocal of the 77 K lifetime. [g] tpy = 4'-tolyl-tpy, from reference [32], note that the 4'-tolyl substituent stabilizes the ³MLCT and thereby prolongs the excited state lifetime.^[33] [h] Extrapolated from the temperature-dependent phosphorescence lifetime measurements.

the visible region. When carboxylic ester groups are attached to the *para* positions of all three pyridine moieties of the terpyridine ligand, namely for RuNCN-(COOMe)₃, the absorption is again significantly red-shifted (by 3000 cm⁻¹) and additionally broadened, hence covering almost the whole visible spectrum and causing a black color of the complex. The main visible absorption features are slightly more intense and separated, but they reflect the same transitions as in RuNCN, which becomes evident in comparison to a 77 K excitation spectrum of RuNCN (see Figure S118 in the Supporting Information). A photoluminescence of the complexes bearing carboxylic ester groups was not observed, most likely due to the low energy gap according to the energy-gap law (see below) or the reduced spectrometer sensitivity at low emission energies.^[24] The drop in extinction and the slight blue shift of the saponified complexes, RuNCN-COOH and RuNCN-(COOH)₃, are attributed to the lowered electron acceptance that causes a decreasing polarization and LUMO stabilization.

77 K emission spectroscopy: As all presented coordination compounds show either no or only a weak emission at room temperature, owing to the presence of several non-radiative deactivation pathways that will be discussed in detail later, the exact energy of the lowest-lying excited state is challenging to determine. Emission spectroscopy at low temperatures can enable the determination of these energies if the dominant non-radiative channels are thermally activated.

All the investigated complexes, except RuNCN-COOEt, RuNCN-(COOH)₃ and RuNCN-(COOMe)₃, are emissive at 77 K and show bandshapes typical for ruthenium coordination compounds, namely an intense 0–0 transition that is accompanied by a weaker vibronic satellite (Figure 6, see Fig-

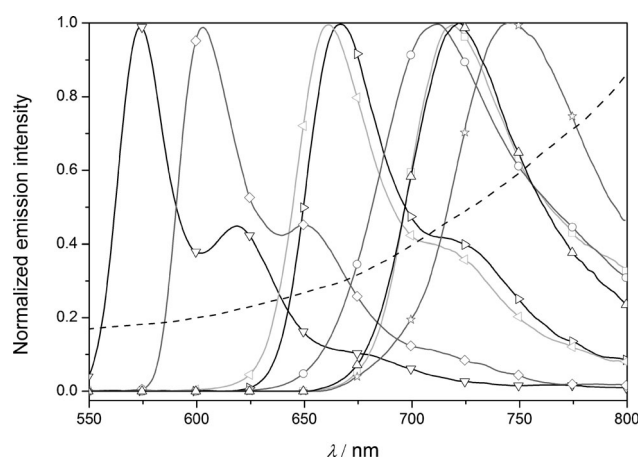


Figure 6. Emission spectra of the complexes: RuNNN (∇), [Ru^{II}(tpy)₂] (\diamond), RuNCN-F (\triangleleft), RuNCN-NO₂ (\triangleright), RuNCN-Cbz (\circ), RuNCN (\square), RuNCN-Tph (\triangle) and RuNCN-COOH (\star) in *n*-butyronitrile glass at 77 K. The spectral resolution decreases at higher wavelengths due to a decreasing spectrometer sensitivity (spectrometer response is given as a dashed line). Solid lines represent the measured curve and symbols are only used for assignment, a color figure is given in the Supporting Information (Figure S119).

ure S118 in the Supporting Information for excitation spectra). The emission maxima are summarized in Table 1. We note that the emission at 77 K is blue-shifted compared to the respective room-temperature emission, because the rigid solvent matrix at low temperatures prevents solvent reorganization and thus avoids the stabilization of the more polar charge-separated excited state (rigidochromic effect).^[25] Still, the comparison of the emission spectra at 77 K reveals a strong bathochromic shift of 3520 cm⁻¹ relative to the non-cyclometalated RuNNN caused by the strong HOMO destabilization in RuNCN. The functionalization of the NCN ligand with the slightly electron-donating thiophene causes no further HOMO destabilization, which might be attributed to the dihedral angle of around 30° which diminishes the conjugation.^[26] In contrast, the functionalization of the NCN ligand with electron-withdrawing groups results in a HOMO stabilization, and thus a blue shift of the emission maximum of about 1130 cm⁻¹ with respect to RuNCN.

Functionalization of the tpy ligand with carboxylic acid esters or free carboxylic acids causes a LUMO stabilization and, as a consequence, a red-shifted absorption and emission. However, it was only possible to measure the emission spectra at 77 K for RuNCN-COOH, which is red-shifted by 490 cm⁻¹ relative to RuNCN. We note that the detector is less sensitive in the near-infrared region as demonstrated by the response function in Figure 6. A theoretically predicted emission of RuNCN-(COOMe)₃ above 1000 nm (Table 1) would thus not be detectable with our measurement setup.

Another important excited-state parameter is its lifetime, which, in contrast to the emission quantum yield, truly reflects the stability of the excited state. Therefore, emission lifetimes were determined at both room temperature and 77 K (Table 1). As a main result, the emission lifetime decreases with decreasing emission energy. Assuming that thermally activated radiationless deactivation pathways are frozen at 77 K, this can be explained by the energy-gap law.^[27] Usually, it can be observed only within a series of very similar complexes or in different solvents,^[28] since other effects, such as delocalization and rigidity, may interfere so that long excited-state lifetimes and small energy gaps do not exclude each other.^[29] Accordingly, RuNCN-COOH has a longer lifetime than RuNCN (Table 1), which is attributed to the modification of the acceptor ligand.

Temperature-dependent lifetime measurements: To gain detailed insight into the deactivation dynamics of the lowest-lying excited state and the stabilizing/destabilizing effects of different substitution patterns, temperature-dependent lifetime measurements were carried out between 300 and 160 K.^[34] The results of these experiments are depicted in Figure 7.

In general, the investigated cyclometalated complexes reveal a steady rise of the emission lifetime with decreasing temperature. However, depending on the specific substitution pattern, the slope of the lifetime increase varies. Similar to the emission spectra at 77 K, the complexes RuNCN-F

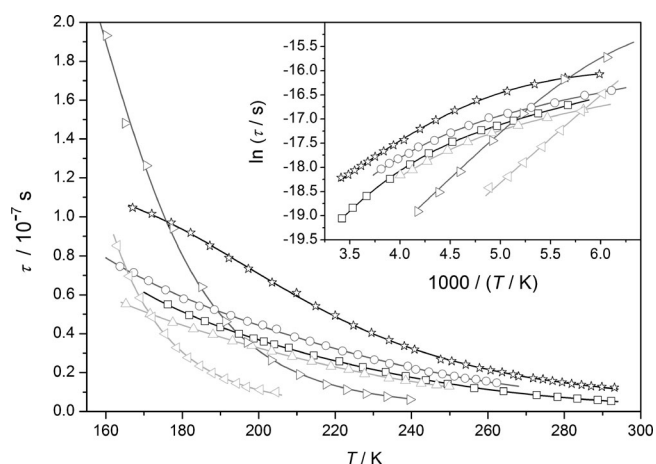


Figure 7. Temperature-dependent emission lifetimes for the complexes: RuNCN-F (∇), RuNCN-NO₂ (\triangleright), RuNCN-Cbz (\circ), RuNCN (\square), RuNCN-Tph (\triangle) and RuNCN-COOH (\star) in *n*-butyronitrile. Symbols correspond to measured lifetimes and solid lines represent a non-linear fit according to equation 1 (RuNCN-COOH, RuNCN-F and RuNCN-NO₂) or equation 2 (RuNCN, RuNCN-Cbz and RuNCN-Tph). A color figure is given in the Supporting Information (Figure S120).

and RuNCN-NO₂ show a different behavior compared to RuNCN, RuNCN-Cbz, and RuNCN-Tph. In detail, for the last three complexes the lifetime starts to increase at higher temperatures and shows a reduced slope than for RuNCN-F and RuNCN-NO₂, thus being shorter-lived at 77 K. In accordance with the literature, the excited-state lifetime at higher temperatures is determined by thermal deactivation via ³MC states.^[1,2] Evidently, the electron-withdrawing groups reduce the donor strength of the carbanion and therefore lower the ³MC states. Consequently, thermal deactivation is facilitated, which can be quantified by fitting an Arrhenius expression to the experimental data [Eqs. (1) or (2)]. Thus, fundamental information about thermally activated, non-radiative deactivation channels can be obtained, for example, their rate constants and activation energies.

$$\tau(T) = \frac{1}{k_r + \sum k_{nr}} = \frac{1}{k_r + k_1 + k_2 \exp(-\Delta E_2/k_B T)} \quad (1)$$

$$\tau(T) = \frac{1}{k_r + \sum k_{nr}} = \frac{1}{k_r + k_1 + k_2 \exp(-\Delta E_2/k_B T) + k_3 \exp(-\Delta E_3/k_B T)} \quad (2)$$

For RuNCN, RuNCN-Cbz, and RuNCN-Tph, two thermally activated (k_2 , ΔE_2 and k_3 , ΔE_3) and one non-activated decay channel (k_1),^[35] in addition to the radiative one (k_r), are necessary to fit the equation to the data [Eq. (2)]. In contrast, for RuNCN-F and RuNCN-NO₂ a model of three channels (a radiative, a non-activated, and a thermally activated non-radiative one) is sufficient to reproduce the data [Eq. (1)]. In principle, there should be a third dark channel for the last two complexes, but due to its low activation energy it is not visible in the experimental temperature

range between 300 and 160 K. The results obtained by analyzing the temperature-dependent lifetime data are summarized in Table 1.

The first activated decay channel (k_2 , ΔE_2) is assigned to the transition from the emitting $^3\text{MLCT}$ to the S_0 via the ^3MC excited state.^[36] Compared to $[\text{Ru}(\text{tpy})_2]^{2+}$ and other complexes of functionalized terpyridines, this activation energy is remarkably low (see the discussion of the ^3MC geometry in the DFT section).^[30,34] We postulate that the room-temperature emission and prolonged excited-state lifetimes, which were observed despite similar or lower activation energies for the $^3\text{MLCT}$ – ^3MC internal conversion than in $[\text{Ru}(\text{tpy})_2]^{2+}$, are caused by a weaker coupling of the ^3MC and the ground state.^[36] This is substantiated by small k_2 rate constants (10^{11} – 10^{12} vs. $1.7 \times 10^{13} \text{ s}^{-1}$ in case of $[\text{Ru}(\text{tpy})_2]^{2+}$). To the best of our knowledge, such a temperature-dependent excited-state lifetime measurement has been performed the first time for cyclometalated ruthenium(II) complexes. In principle, we would expect a similar behavior for $[\text{Ru}(\text{tpy})(\text{dpp})]^+$ or analogous complexes.

Furthermore, for RuNCN-F and RuNCN-NO₂ lower ΔE_2 values were obtained, supporting the assumption of a decreased ^3MC destabilization, but k_2 is again small and even smaller for RuNCN-NO₂. When comparing RuNCN-F and RuNCN-NO₂, the fluoro substituent mainly lowers the ^3MC energy, which is therefore closer to the $^3\text{MLCT}$ state. In contrast, the π -accepting nitro group *para* to the carbanion also affects the $^3\text{MLCT}$ energy (see the LUMO energy in Table 2) resulting in a larger observed $^3\text{MLCT}$ – ^3MC barrier that allows for room-temperature emission. This is also reflected by the displacement of the RuNCN-F curve to lower temperatures (Figure 7).

Despite this good correlation between structure and excited-state dynamics, the temperature-dependent emission properties of RuNCN-COOH need to be discussed separately. Within the whole series, its activation energy for the $^3\text{MLCT}$ – ^3MC internal conversion is the least. Nevertheless, a room-temperature lifetime of 12.3 ns could be measured, which is remarkably high in comparison with the other complexes discussed herein. This can only be explained by the relatively low transition rate for this process, which is one order of magnitude smaller than in the other complexes. Apparently, here the absence of a detectable room-tempera-

ture emission might be due to experimental limitations and does not necessarily mean short excited-state lifetimes.

The second activated decay channel (k_3 , ΔE_3) can be attributed to internal conversion (IC) to an energetically slightly higher-lying MLCT state of increased singlet character (MLCT'), which is also a common feature for ruthenium polypyridyl dyes.^[30,37]

Electrochemistry: Crucial for the potentially photo-redoxactive Ru^{II} complexes, in particular with respect to photovoltaic applications, are their electrochemical properties. Thus, the reversibility of the redox processes and the location of the oxidation and reduction potentials in comparison to the I₃[−]/I[−] couple and the TiO₂ conduction band, respectively, are highly important. Consequently, cyclic voltammetry (CV) measurements were carried out and related results are presented in Figures 8 and 9, Table 2, and the Supporting Information.

Analyzing the influence of cyclometalation by comparing RuNCN to RuNNN shows a strong cathodic shift of the oxidation potential of 900 mV due to the strong σ and π donation as well as electronic repulsion caused by the carbanion.^[6a] Based on the calculations (see above), the first oxidation of RuNCN is not only metal-, but also ligand-based, and corresponds to a transition from $d_{\text{Ru}}/\pi_{\text{NCN}}^+$ to $d_{\text{Ru}}/\pi_{\text{NCN}}^{2+}$ transition. Also the first reduction process, located on the terpyridine ligand, is shifted towards lower potentials by 260 mV, owing to increased π back donation from the more electron-rich Ru^{II} center.^[5j] Both oxidation and reduction process of the RuNCN complex are fully reversible under cyclic voltammetric conditions. Nevertheless, reversibility was investigated in a more detailed fashion by UV/Vis spectroelectrochemical means (see below).

Again, a comparison of the triazole-containing complexes with their pyridine counterparts allows for a relative classification of electronic properties of the ligands. In comparison to the RuNNN-analogous $[\text{Ru}(\text{tpy})_2][\text{PF}_6]_2$, the substitution of a terpyridine ligand by the click-derived 2,6-bis(1,2,3-triazol-4-yl)pyridine leads to a metal-based HOMO of lower energy and tpy-based LUMO of higher energy, indicating a weaker σ -donor and π -acceptor strength of the triazole-containing ligand that would allow the tpy to predominate the π back donation.^[8a–d] In contrast, when comparing

Table 2. Electrochemical data of the complexes.

| Complex | $E_{1/2}^{\text{ox}}$ [V] ($i_{\text{pa}}/i_{\text{pc}}$, ΔE_p [mV]) ^[a] | $E_{1/2}^{\text{red}}$ [V] ($i_{\text{pa}}/i_{\text{pc}}$, ΔE_p [mV]) ^[a] | $E_{\text{S}^{\cdot-}(\text{ox})}$ [V] ^[d] | E_{HOMO} [eV] ^[c] | E_{LUMO} [eV] ^[c] | $E_{\text{gap,el}}$ [eV] | $E_{\text{gap,opt}}$ [eV] |
|--|---|--|---|---------------------------------------|---------------------------------------|--------------------------|---------------------------|
| RuNNN | 0.98 (1.1, 74) | −1.72 (0.9, 80) | −1.22 | −5.78 | −3.22 | 2.56 | 2.20 |
| $[\text{Ru}(\text{tpy})_2][\text{PF}_6]_2$ ^[5j] | 0.89 (64) | −1.66 (63) | – | – | – | – | – |
| RuNCN | 0.08 (1.0, 67) | −1.98 (1.0, 71) | −1.83 | −4.88 | −2.91 | 1.97 | 1.91 |
| $[\text{Ru}(\text{tpy})(\text{dpp})][\text{PF}_6]$ ^[5j] | 0.12 (62) | −1.95 (63) | – | – | – | – | – |
| RuNCN-F | 0.31 (1.0, 74) | −1.95 (1.0, 79) | −1.67 | −5.12 | −2.97 | 2.15 | 1.98 |
| RuNCN-NO ₂ | 0.26 (1.0, 76) | −1.82 (1.0, 88) | −1.77 | −5.07 | −3.11 | 1.96 | 2.03 |
| RuNCN-Cbz | 0.10 (1.0, 83) | −1.97 (irrev.) ^[b] | −1.84 | −4.89 | −3.00 | 1.89 | 1.94 |
| RuNCN-Tph | 0.07 (1.0, 69) | −1.97 (irrev.) ^[b] | −1.93 | −4.87 | −2.93 | 1.94 | 2.00 |
| RuNCN-COOEt | 0.16 (1.0, 70) | −1.79 (1.1, 80) | −1.74 | −4.96 | −3.14 | 1.82 | 1.90 |
| RuNCN-(COOMe) ₃ | 0.26 (1.0, 71) | −1.56 (1.0, 71) | −1.51 | −5.06 | −3.37 | 1.69 | 1.77 |

[a] Measured in CH₃CN with 0.1 M Bu₄NPF₆; with respect to Fc/Fc⁺ as a reference. [b] Irreversible process; $E_{1/2}$ received from DPP. [c] Calculated by using $E_{\text{LUMO/HOMO}} = [-(E_{\text{onset}}^{\text{red/ox}} - E_{\text{onset}}^{\text{Fc/Fc}^+}) - 4.8] \text{ eV}$. [d] Calculated using $E_{\text{S}} = E_{1/2}^{\text{ox}} - E_{\text{gap,opt}}$ ^[3b]

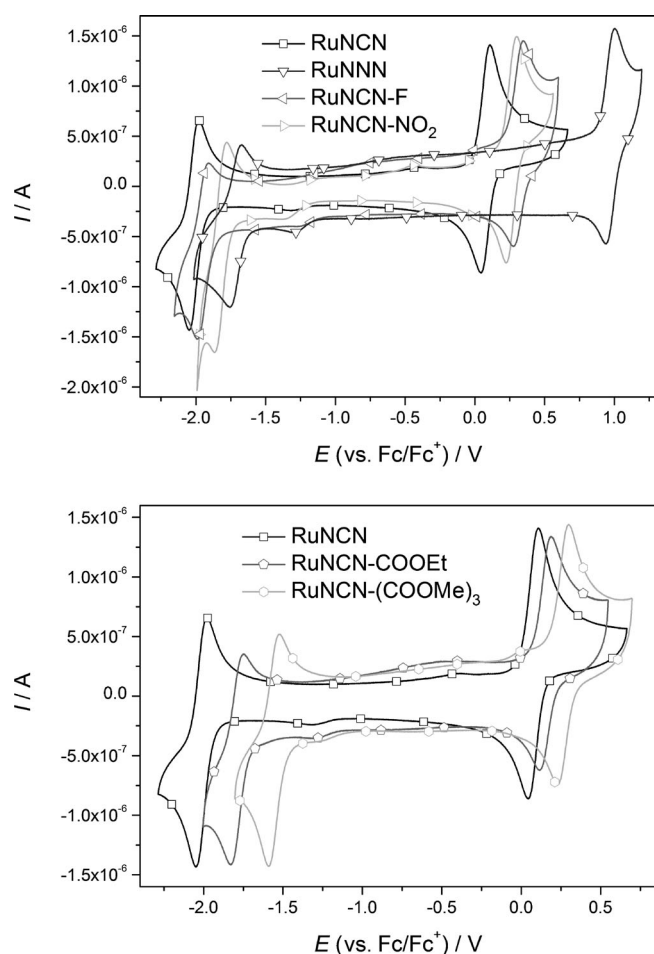


Figure 8. Cyclic voltammograms of the cyclometalated ruthenium(II) complexes and RuNNN as a reference (10^{-5} M in CH_3CN with 0.1 M Bu_4NPF_6). Solid lines represent the measured curve and symbols are only used for assignment.

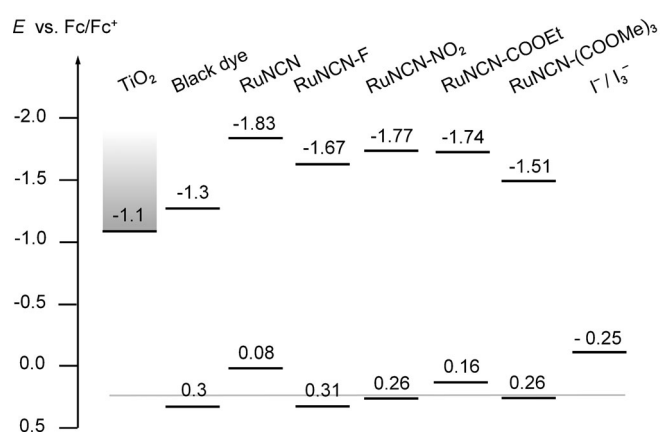


Figure 9. Comparison of the excited-state and ground-state oxidation potentials with the TiO_2 conducting band and the I^-/I_3^- redox couple, respectively. The grey line indicates a potential that ensures enough driving force for the dye regeneration.^[3b,5] The actual TiO_2 conducting band edge depends on the electrolyte composition and is therefore drawn diffusely.^[38]

RuNCN with the analogous $[\text{Ru}(\text{tpy})(\text{dpb})]\text{PF}_6$, for the click-derived complex the oxidation and reduction potentials are cathodically shifted. Evidently, the triazole-containing cyclometalating ligand is a stronger π donor increasing the electron density on the $\text{Ru}^{\text{II}}/\text{NCN}$ -based HOMO and, through increased π back donation from the more electron-rich Ru^{II} to the tpy ligand, the energy of the tpy-based LUMO. This is most likely due to weaker stabilization of the carbanion by the triazole in terms of its electron excess and shorter conjugation length.^[8a] Additionally, for the same reason as for RuNNN, the lower π acceptor strength of the triazole-containing cyclometalating ligand, when compared to its pyridine analogue, might cause the HOMO and tpy-based LUMO of higher energy. Consequently, the more negative excited-state oxidation potential (Figure 9, Table 2) should increase the driving force for the electron injection into the TiO_2 conducting band or would allow for a higher TiO_2 conducting band, which can be achieved by a different electrolyte composition,^[38] and therefore higher cell voltages. At the same time, the lower oxidation potential would lower the driving force for the regeneration of the photooxidized dye (Figure 9). In consistence with the blue shift of absorption and emission, which correspond to the optical gap, the electrochemical HOMO–LUMO gap of RuNCN is increased in comparison with $[\text{Ru}(\text{tpy})(\text{dpb})]\text{PF}_6$.

To still allow efficient dye regeneration, a fine-tuning of the oxidation potential was achieved by installing electron-withdrawing fluoro and nitro groups on the cyclometalated phenyl ring.^[5c–e] Thus, the HOMO is stabilized and the oxidation shows an anodic shift by 230 and 180 mV, respectively, to be about 0.5 V more positive than the I^-/I_3^- redox couple and, thereby, ensure enough driving force for the dye reduction.^[5b,5c,e,i,39] In the case of RuNCN-F, the reduction potential remains nearly unchanged, while for RuNCN-NO₂ a distinct anodic shift from -1.98 to -1.82 V is observed. Most likely, the strong π -accepting nitro group weakens the π donation of the *para*-carbanion and, thereby, the π back donation to the terpyridine. A more detailed discussion of the electronic effects of nitro and fluoro substituents on a cyclometalated phenyl ring depending on their positions can be taken from the literature.^[5d,40]

Introduction of the carbazole and thiophene moieties affects the oxidation and reduction potentials only marginally, but leads to irreversibility of the reduction process under CV conditions in both cases. However, only the dye oxidation and subsequent reduction is the operative process in DSSCs and this process still is reversible. We note that a strategic methyl group was placed in the 5-position of the thiophene to avoid any following reactions, such as radical dimerizations.^[41]

Electrochemical investigations on the ester-substituted complexes RuNCN-COOEt and RuNCN-(COOMe)₃ showed significant anodic shifts of the reduction potentials about 190 and 430 mV, respectively, due to stabilization of the LUMO, which is tpy-based. Still, enough driving force for a fast electron injection would be given. Furthermore, since the π -accepting esters are in *para* position, they in-

crease the overall π -acceptor strength of the polypyridyl ligand, causing a small anodic shift of the oxidation of 80 and 180 mV, respectively. Thus, the oxidation potential of RuNCN-(COOMe)₃ would enable efficient regeneration. However, the strongly electron-withdrawing carboxylic ester can only be seen as approximation of TiO₂-adsorbed carboxylic acids^[5k] and the actual electronic situation depends on the protonation state of the adsorbed complex (see pK_a determinations in the Supporting Information).^[42] Therefore, although electron-withdrawing, the anchoring carboxylic acids most likely will have to be combined with above-mentioned strategies to lower the oxidation potential directly.^[5c,e,i] Consequently, the RuNCN complexes are basically applicable in established DSSCs.

UV/Vis spectroelectrochemical analysis: To obtain a more detailed insight into the electrochemistry of the presented cyclometalated Ru^{II} systems, mainly with regard to reversibility and redox stability, UV/Vis spectroelectrochemical experiments were performed (see Figure 10 for RuNCN and Figures S122–S128 in the Supporting Information for the remaining complexes).

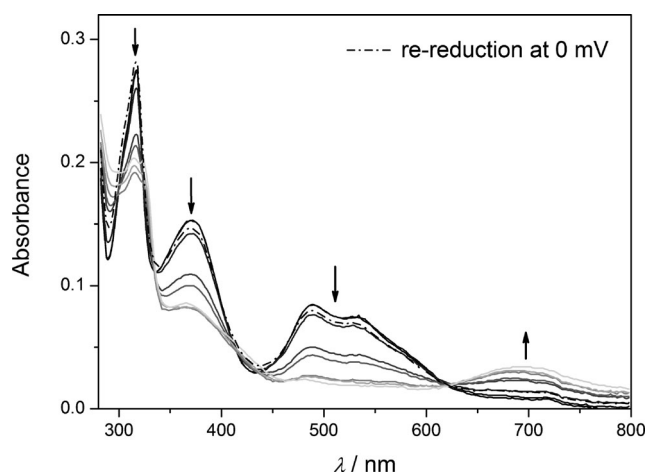


Figure 10. UV/Vis spectroelectrochemical investigation on the oxidation process of RuNCN (voltage varied between 400 and 1000 mV vs. Ag/AgCl; 10⁻⁵ M in CH₃CN with 0.1 M Bu₄NPF₆).

In general, the oxidation processes show several isosbestic points, indicating the temporary presence of only two species to ultimately form the singly oxidized complex in a well-defined reaction. The most evident changes during oxidation are the decrease of MLCT and MLLCT bands between 350 and 600 nm, caused by depopulation of the d_{Ru}/π_{NCN} HOMO, and the appearance of additional, broad peaks between 600 and 850 nm (up to 1000 nm in case of RuNCN-(COOMe)₃), most likely attributed to emerging LMCT ($\pi_{NCN} \rightarrow d_{Ru}$) or LMLCT ($\pi_{NCN} \rightarrow d_{Ru}/\pi_{NCN}$) transitions. Here, the fluoro-substituted RuNCN-F represents an exception that shows no changes beyond 600 nm (Figure S123 in the Supporting Information), probably because of a very low transition dipole moment. Accordingly, for

RuNCN-NO₂ the arising transition is very weak. In contrast, the thiophene-containing complex RuNCN-Tph exhibits the appearance of two intense absorption peaks around 450 and 900 nm (Figure S126 in the Supporting Information), which can be likely assigned to a mixed MC/MLCT (MMLCT, $d_{Ru} \rightarrow d_{Ru}/\pi_{NCN}$), MLCT ($d_{Ru} \rightarrow \pi_{NCN}^*$), or LMLCT transitions that would possess large orbital contributions of the thiophene. Remarkably, the reductions of all oxidized species recreate the original spectra almost completely, thus confirming that the oxidation processes are fully reversible even under these demanding conditions under which the complexes are oxidized for a long time.

The first reductions (studied only for the complexes showing reversible reduction under CV conditions, see the Supporting Information), being located on the terpyridine ligand ($tpy \rightarrow tpy^{\cdot-}$), reveal a less-defined spectral change in spectroelectrochemical measurements. Again, an absorbance decrease in the MLCT/MLLCT region can be observed, caused by the population of a π_{tpy}^* orbital that acts as the acceptor within the longest-wavelength transition processes. Additionally, the absorbance also increases at around 450 nm and several changes occur in the UV region of the spectrum, both originating from appearing, disappearing, or shifted LC and LLCT transitions. In contrast to the oxidation described above, recreation of the initial complex is not successful in most cases, which is likely due to following reactions. As an exception, RuNCN-(COOMe)₃, which possesses three electron-withdrawing ester groups at the terpyridine ligand that enable an enhanced stabilization of the electron-rich $tpy^{\cdot-}$ moiety, allows the nearly full regeneration by re-oxidation.

Photophysical model: Cyclometalated polypyridyl Ru^{II} complexes have been known for some time,^[6,9a] but it was only quite recently that they have been applied to the field of dye-sensitized solar cells.^[5] Although there has been elaborated research on photoactive electron-transfer assemblies, such as homo- and heteronuclear dyads, for the prototypical bis(tridentate), heteroleptic Ru^{II} complex of terpyridine and its cyclometalated analogue 1,3-dipyridylbenzene, a detailed investigation on the excited-state processes is missing up to date.^[32,43] Only a simplified, qualitative explanation of its photophysical properties by relative energies of the S₀, the lowest ³MLCT state and the ³MC state has been reported.^[6a,32] According to that, the lifetime of the charge-separated excited-state is determined by the ³MLCT–³MC energy difference, since the metal-centered excited state shows a strong coupling to the ground state and therefore causes a rapid relaxation once the ³MC state is populated. This is plausible because antibonding orbitals are occupied in the ³MC state, which shows a displacement that typically matches the ground-state geometry at high-energy vibrations; in other words, the transition is highly probable because of a large Franck–Condon factor (strong coupling case of displaced oscillators).^[44] Alternatively, the fast decay to the ground state can be explained in a classical picture assuming the surfaces show a nearly barrierless crossing.^[45]

However, we emphasize that the $^3\text{MC-S}_0$ intersystem crossing not only depends on the ^3MC , but also on the S_0 potential energy surface, which itself is strongly influenced by the electronic nature of the ligand. Thus, several Ru^{II} complexes have been reported, for example, $\text{Ru}(\text{bpy})_2(\text{CN})_2$, that show a weaker $^3\text{MC-S}_0$ coupling.^[36] Despite these studies, the prolonged excited-state lifetime of the cyclometalated $[\text{Ru}(\text{tpy})(\text{dpb})]^+$ in comparison to $[\text{Ru}(\text{tpy})_2]^{2+}$ has only been attributed to the ^3MC destabilization by the carbanion so far.

Nonetheless, temperature-dependent emission lifetime measurements reveal a similar and even lowered activation barrier for the population of the ^3MC state within the RuNCN series compared to $[\text{Ru}(\text{tpy})_2]^{2+}$. At the same time, the non-radiative deactivation rate constant of RuNCN is orders of magnitude smaller than for $[\text{Ru}(\text{tpy})_2]^+$.^[30] We expect a similar behaviour for the analogous $[\text{Ru}(\text{tpy})(\text{dpb})]^+$ complex.

Consequently, Δ -SCF calculations were performed to gain a deeper understanding of the photophysics. In Figure 11 the schematic potential energy surfaces for the complexes RuNCN and RuNNN are depicted. The diabatic energies (DE) are obtained as the energetic differences between the energy minima of the optimized geometries, while the adiabatic energies (AE) are obtained as the actual energy differences at the $^3\text{MLCT}$ and the ^3MC optimized geometries. As shown in Figure 11, the $^3\text{MLCT}$ and ^3MC minima are almost

isoenergetic for RuNCN , while for RuNNN the ^3MC minimum is lower in energy than the $^3\text{MLCT}$ one. This is in agreement with a destabilized ^3MC state for RuNCN as a result of the cyclometalation. As an additional consequence, the S_0 is destabilized as well and both $^3\text{MLCT}$ and ^3MC states appear at lower energies relative to the S_0 . However, for the thermal $^3\text{MLCT-}^3\text{MC}$ internal conversion, the energy barrier and the respective $^3\text{MLCT-}^3\text{MC}$ conversion rate (see ΔE_2 and k_2 in the temperature-dependent lifetime measurements) are determining. Usually, the subsequent $^3\text{MC-S}_0$ intersystem crossing rate is the limiting rate. Thus, referring to the experimental $^3\text{MLCT-}^3\text{MC}$ energy barrier, which is lower for RuNCN than for $[\text{Ru}(\text{tpy})_2]^{2+}$, and the nonetheless prolonged excited-state lifetimes, we postulate a weaker $^3\text{MC-S}_0$ coupling. In agreement with previous reports,^[46] we conclude that the $^3\text{MC-S}_0$ intersystem crossing occurs at high energies on the potential energy surfaces for RuNCN , while for RuNNN and $[\text{Ru}(\text{tpy})_2]^{2+}$ this $^3\text{MC-S}_0$ intersystem crossing point is at low energies and thus readily accessible. This is plausible, since the covalent binding of the cyclometalating ligand has a significant influence on both electronic structure and geometry already of the S_0 affecting also the $^3\text{MC-S}_0$ coupling.

Still, the lifetime of cyclometalated complexes is relatively short and the quantum yield is low in comparison to $[\text{Ru}(\text{bpy})_3]^{2+}$, for example, because of the S_0 destabilization. The resulting small S_0 - $^3\text{MLCT}$ energy gap leads to a more probable thermally non-activated, radiationless deactivation due to an increased Franck-Condon overlap of the S_0 and $^3\text{MLCT}$ vibrational wave functions. The observed decrease of the excited-state lifetime with decreasing emission energy is in accordance with the already mentioned energy-gap law.^[27]

Conclusion

A systematically modified series of new ruthenium(II) complexes of click-derived tridentate cyclometalating ligands aimed towards the application in dye-sensitized solar cells was investigated. An optimized synthetic route was established. The presented cyclometalated ruthenium(II) polypyridyl complexes feature all benefits of established Ru^{II} thiocyanate dyes:

- 1) The HOMO is raised in energy causing a small energy gap and, therefore, a strongly red-shifted absorption.
- 2) The strong electron donation destabilizes ^3MC states and thus offers prolonged excited-state lifetimes.
- 3) The HOMO is extended to the cyclometalating ligand that facilitates the dye regeneration.
- 4) The LUMO is located on the opposite, anchoring ligand. Consequently, the charge transfer is directed towards the semiconductor surface.
- 5) At the same time, the anchoring groups, namely the carboxylic acid functions, strongly lower the LUMO energy, resulting in a panchromatic shift and intense absorption

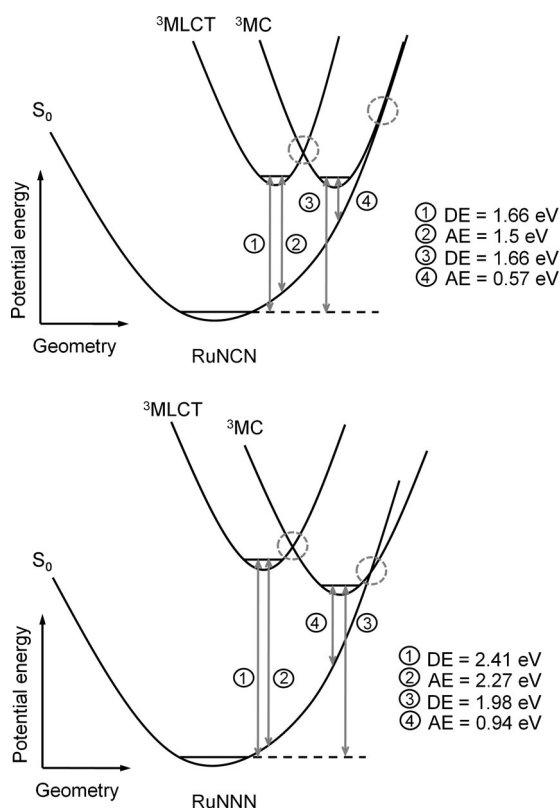


Figure 11. Proposed potential energy surfaces (the MLCT is omitted for clarity) including adiabatic (AE) and diabatic energies (DE) at the Δ SCF-PCM-DFT/6-31G* level of theory for the complexes RuNCN (top) and RuNNN (bottom).

due to the pronounced push–pull effect that heightens the oscillator strengths and the extinction coefficients.

Additionally, the cyclometalated complexes offer further advantages that are essentially absent in thiocyanate complexes:

- 6) The electronic functions of the monodentate thiocyanate ligands are adopted by a multidentate ligand thus preventing photochemical ligand loss and offering higher long-term stability.
- 7) Since the HOMO is extended to the cyclometalating ligand, the optoelectronic properties can be optimized by ligand functionalization. Thus, redox-matching with the electrolyte and improvement of the light harvesting are enabled.

Moreover, the complexes of triazole-containing tridentate cyclometalating ligands offer potential advantages over their pyridyl analogues:

- 8) The stronger effective electron donation allows for longer excited-state lifetimes.
- 9) Their ligands can be readily and modularly functionalized.

A potential drawback might be the lower extinction coefficients, although strategies to increase them have been demonstrated. Still, the determined optoelectronic properties strongly encourage us to test the presented type of complex in a dye-sensitized solar cell. Also, a potential iodide–triazole interaction shall be investigated in the future.

As a result of the combined efforts of experimental and computational methods, a detailed understanding of the photophysical properties is provided, in particular of the crucial radiationless deactivation process of cyclometalated ruthenium(II) complexes.

Experimental Section

Extensive experimental details are given in the Supporting Information. These include synthetic procedures, UV/Vis absorption and emission, CV, NMR and ESI-Tof MS spectra, further solid-state structures and a more detailed discussion thereof, as well as computational details. CCDC-848606 (HNCN), CCDC-848607 (HNCN-F), CCDC-848608 ([Ru(tpy)(CH₃CN)₃][PF₆]₂), CCDC-848609 ([Ru(tpy-COOEt)(CH₃CN)₃][PF₆]₂), CCDC-848610 ([Ru(tpy-(COOMe)₃)(CH₃CN)₃][PF₆]₂), CCDC-848611 (RuNNN), CCDC-848612 (RuNCN), CCDC-848613 (RuNCN-NO₂), CCDC-848614 (RuNCN-F), and CCDC-848615 (RuNCN-Tph) contain the supplementary crystallographic data for this paper. These data can be obtained free of charge from The Cambridge Crystallographic Data Centre via www.ccdc.cam.ac.uk/data_request/cif.

Acknowledgements

Financial support by the Thuringian Ministry for Education, Science and Culture (grant no. B514-09049: Photonische Mizellen, PhotoMIC) is

kindly acknowledged. B.S., C.F., and R.S. are grateful to the Fonds der Chemischen Industrie for Ph.D. scholarships. D.E. is grateful to the DAAD for financial support. B.D. and J.P. thank the Fonds der Chemischen Industrie. We also thank M. Jäger, E. Altuntas, W. Günther and G. Sentis for discussions and performing experiments. Additionally, we thank D. Schrader, S. Ziemann, and J. Türker for experimental assistance.

- [1] a) A. Juris, V. Balzani, F. Barigelletti, S. Campagna, P. Belser, A. von Zelewsky, *Coord. Chem. Rev.* **1988**, *84*, 85–277; b) J. P. Sauvage, J. P. Collin, J. C. Chambron, S. Guillerez, C. Coudret, V. Balzani, F. Barigelletti, L. De Cola, L. Flamigni, *Chem. Rev.* **1994**, *94*, 993–1019.
- [2] a) L. Hammarström, O. Johansson, *Coord. Chem. Rev.* **2010**, *254*, 2546–2559; b) E. A. Medlycott, G. S. Hanan, *Chem. Soc. Rev.* **2005**, *34*, 133–142; c) E. A. Medlycott, G. S. Hanan, *Coord. Chem. Rev.* **2006**, *250*, 1763–1782.
- [3] a) B. O'Regan, M. Grätzel, *Nature* **1991**, *353*, 737–740; b) A. Hagfeldt, G. Boschloo, L. Sun, L. Kloo, H. Pettersson, *Chem. Rev.* **2010**, *110*, 6595–6663.
- [4] a) M. K. Nazeeruddin, A. Kay, I. Rodicio, R. Humphry-Baker, E. Mueller, P. Liska, N. Vlachopoulos, M. Grätzel, *J. Am. Chem. Soc.* **1993**, *115*, 6382–6390; b) M. K. Nazeeruddin, P. Péchy, T. Renouard, S. M. Zakeeruddin, R. Humphry-Baker, P. Comte, P. Liska, L. Cevey, E. Costa, V. Shklover, L. Spiccia, G. B. Deacon, C. A. Bignozzi, M. Grätzel, *J. Am. Chem. Soc.* **2001**, *123*, 1613–1624; c) H. Tributsch, *Coord. Chem. Rev.* **2004**, *248*, 1511–1530.
- [5] a) P. G. Bomben, K. C. D. Robson, P. A. Sedach, C. P. Berlinguette, *Inorg. Chem.* **2009**, *48*, 9631–9643; b) B. D. Koivisto, K. C. D. Robson, C. P. Berlinguette, *Inorg. Chem.* **2009**, *48*, 9644–9652; c) T. Bessho, E. Yoneda, J.-H. Yum, M. Guglielmi, I. Tavernelli, H. Imai, U. Rothlisberger, M. K. Nazeeruddin, M. Grätzel, *J. Am. Chem. Soc.* **2009**, *131*, 5930–5934; d) P. G. Bomben, B. D. Koivisto, C. P. Berlinguette, *Inorg. Chem.* **2010**, *49*, 4960–4971; e) P. G. Bomben, K. D. Thériault, C. P. Berlinguette, *Eur. J. Inorg. Chem.* **2011**, 1806–1814; f) K. C. D. Robson, B. D. Koivisto, A. Yella, B. Spornova, M. K. Nazeeruddin, T. Baumgartner, M. Grätzel, C. P. Berlinguette, *Inorg. Chem.* **2011**, *50*, 5494–5508; g) K. C. D. Robson, B. Spornova, B. D. Koivisto, E. Schott, D. G. Brown, C. P. Berlinguette, *Inorg. Chem.* **2011**, *50*, 6019–6028; h) S. H. Wadman, J. M. Kroon, K. Bakker, M. Lutz, A. L. Spek, G. P. M. van Klink, G. van Koten, *Chem. Commun.* **2007**, 1907–1909; i) P. G. Bomben, T. J. Gordon, E. Schott, C. P. Berlinguette, *Angew. Chem.* **2011**, *123*, 10870–10873; *Angew. Chem. Int. Ed.* **2011**, *50*, 10682–10685; j) S. H. Wadman, M. Lutz, D. M. Tooke, A. L. Spek, F. Hartl, R. W. A. Havenith, G. P. M. van Klink, G. van Koten, *Inorg. Chem.* **2009**, *48*, 1887–1900; k) S. H. Wadman, J. M. Kroon, K. Bakker, R. W. A. Havenith, G. P. M. van Klink, G. van Koten, *Organometallics* **2010**, *29*, 1569–1579.
- [6] a) J.-P. Collin, M. Beley, J.-P. Sauvage, F. Barigelletti, *Inorg. Chim. Acta* **1991**, *186*, 91–93; b) E. C. Constable, J. M. Holmes, *J. Organomet. Chem.* **1986**, *301*, 203–208.
- [7] H. C. Kolb, M. G. Finn, K. B. Sharpless, *Angew. Chem.* **2001**, *113*, 2056–2075; *Angew. Chem. Int. Ed.* **2001**, *40*, 2004–2021.
- [8] a) Y. Li, J. C. Huffman, A. H. Flood, *Chem. Commun.* **2007**, 2692–2694; b) R. M. Meudtner, M. Ostermeier, R. Goddard, C. Limberg, S. Hecht, *Chem. Eur. J.* **2007**, *13*, 9834–9840; c) M. Ostermeier, M.-A. Berlin, R. M. Meudtner, S. Demeshko, F. Meyer, C. Limberg, S. Hecht, *Chem. Eur. J.* **2010**, *16*, 10202–10213; d) B. Schulze, C. Friebe, M. D. Hager, A. Winter, R. Hoogenboom, H. Görls, U. S. Schubert, *Dalton Trans.* **2009**, 787–794; e) B. Happ, C. Friebe, A. Winter, M. D. Hager, R. Hoogenboom, U. S. Schubert, *Chem. Asian J.* **2009**, *4*, 154–163; f) B. Schulze, D. Escudero, C. Friebe, R. Siebert, H. Görls, U. Köhn, E. Altuntas, A. Baumgaertel, M. D. Hager, A. Winter, B. Dietzek, J. Popp, L. González, U. S. Schubert, *Chem. Eur. J.* **2011**, *17*, 5494–5498.
- [9] a) M. Beley, J. P. Collin, R. Louis, B. Metz, J. P. Sauvage, *J. Am. Chem. Soc.* **1991**, *113*, 8521–8522; b) J. A. G. Williams, *Chem. Soc. Rev.* **2009**, *38*, 1783–1801; c) B. Beyer, C. Ulbricht, D. Escudero, C.

- Friebe, A. Winter, L. González, U. S. Schubert, *Organometallics* **2009**, *28*, 5478–5488.
- [10] While this manuscript was in preparation, a communication by Zhong, Yao et al. already introduced this type of click-derived NCN-cyclometalated Ru^{II} complex. However, only a basic characterization was provided and the synthesis was not optimized. W.-W. Yang, L. Wang, Y.-W. Zhong, J. Yao, *Organometallics* **2011**, *30*, 2236–2240.
- [11] Very recently, the use of a 1,2,3-triazolylpyridine within a classical Ru^{II}-thiocyanate complex demonstrated the potential of a click-derived ligand for solar-cell applications. I. Stengel, A. Mishra, N. Poo-trakulchote, S.-J. Moon, S. M. Zakeeruddin, M. Grätzel, P. Bauerle, *J. Mater. Chem.* **2011**, *21*, 3726–3734.
- [12] A. J. Wilkinson, H. Puschmann, J. A. K. Howard, C. E. Foster, J. A. G. Williams, *Inorg. Chem.* **2006**, *45*, 8685–8699.
- [13] C. Amatore, A. Jutand, *Acc. Chem. Res.* **2000**, *33*, 314–321.
- [14] J. G. Rodríguez, T. Laparra, *Tetrahedron* **2009**, *65*, 2551–2555.
- [15] a) C. Y. Chen, H. C. Lu, C. G. Wu, J. G. Chen, K. C. Ho, *Adv. Funct. Mater.* **2007**, *17*, 29–36; b) C. Y. Chen, S. J. Wu, J. Y. Li, C. G. Wu, J. G. Chen, K. C. Ho, *Adv. Mater.* **2007**, *19*, 3888–3891; c) C.-Y. Chen, J.-G. Chen, S.-J. Wu, J.-Y. Li, C.-G. Wu, K.-C. Ho, *Angew. Chem.* **2008**, *120*, 7452–7455; *Angew. Chem. Int. Ed.* **2008**, *47*, 7342–7345; d) C.-Y. Chen, S.-J. Wu, C.-G. Wu, J.-G. Chen, K.-C. Ho, *Angew. Chem.* **2006**, *118*, 5954–5957; *Angew. Chem. Int. Ed.* **2006**, *45*, 5822–5825; e) C.-C. Chou, K.-L. Wu, Y. Chi, W.-P. Hu, S. J. Yu, G.-H. Lee, C.-L. Lin, P.-T. Chou, *Angew. Chem.* **2011**, *123*, 2102–2106; *Angew. Chem. Int. Ed.* **2011**, *50*, 2054–2058; f) F. Gao, Y. Wang, D. Shi, J. Zhang, M. Wang, X. Jing, R. Humphry-Baker, P. Wang, S. M. Zakeeruddin, M. Grätzel, *J. Am. Chem. Soc.* **2008**, *130*, 10720–10728; g) F. Gao, Y. Wang, J. Zhang, D. Shi, M. Wang, R. Humphry-Baker, P. Wang, S. M. Zakeeruddin, M. Grätzel, *Chem. Commun.* **2008**, 2635–2637; h) N. Hirata, J.-J. Lagref, E. J. Palomares, J. R. Durrant, M. K. Nazeeruddin, M. Grätzel, D. Di Censo, *Chem. Eur. J.* **2004**, *10*, 595–602.
- [16] R. Westlund, E. Glimsdal, M. Lindgren, R. Vestberg, C. Hawker, C. Lopes, E. Malmström, *J. Mater. Chem.* **2008**, *18*, 166–175.
- [17] a) M. Jäger, R. J. Kumar, H. Görls, J. Bergquist, O. Johansson, *Inorg. Chem.* **2009**, *48*, 3228–3238; b) H. F. Suen, S. W. Wilson, M. Pomerantz, J. L. Walsh, *Inorg. Chem.* **1989**, *28*, 786–791.
- [18] M. Gagliardo, D. J. M. Snelders, P. A. Chase, R. J. M. Klein Gebbink, G. P. M. van Klink, G. van Koten, *Angew. Chem.* **2007**, *119*, 8710–8726; *Angew. Chem. Int. Ed.* **2007**, *46*, 8558–8573.
- [19] a) Y. Li, A. H. Flood, *Angew. Chem.* **2008**, *120*, 2689–2692; *Angew. Chem. Int. Ed.* **2008**, *47*, 2649–2652; b) Y. Li, A. H. Flood, *J. Am. Chem. Soc.* **2008**, *130*, 12111–12122; c) S. Liu, P. Müller, M. K. Takase, T. M. Swager, *Inorg. Chem.* **2011**, *50*, 7598–7609; d) B. Schulze, C. Friebe, M. D. Hager, W. Günther, U. Köhn, B. O. Jahn, H. Görls, U. S. Schubert, *Org. Lett.* **2010**, *12*, 2710–2713.
- [20] L. González, D. Escudero, L. Serrano-Andrés, *ChemPhysChem* **2012**, *13*, 28–51.
- [21] a) B. Happ, D. Escudero, M. D. Hager, C. Friebe, A. Winter, H. Görls, E. Altuntaş, L. González, U. S. Schubert, *J. Org. Chem.* **2010**, *75*, 4025–4038; b) A. Vlček Jr., S. Zálšíš, *Coord. Chem. Rev.* **2007**, *251*, 258–287; c) M.-F. Charlot, A. Aukauloo, *J. Phys. Chem. A* **2007**, *111*, 11661–11672.
- [22] J. Heully, F. Alary, M. Boggio-Pasqua, *J. Chem. Phys.* **2009**, *131*, 184308.
- [23] a) K. C. D. Robson, B. D. Koivisto, T. J. Gordon, T. Baumgartner, C. P. Berlinguette, *Inorg. Chem.* **2010**, *49*, 5335–5337; b) R. Siebert, A. Winter, B. Dietzek, U. S. Schubert, J. Popp, *Macromol. Rapid Commun.* **2010**, *31*, 883–888.
- [24] R. Englman, J. Jortner, *Mol. Phys.* **1970**, *18*, 145–164.
- [25] a) F. Barigelletti, P. Belser, A. Von Zelewsky, A. Juris, V. Balzani, *J. Phys. Chem.* **1985**, *89*, 3680–3684; b) M. Wrighton, D. L. Morse, *J. Am. Chem. Soc.* **1974**, *96*, 998–1003.
- [26] a) M. Presselt, B. Dietzek, M. Schmitt, J. Popp, A. Winter, M. Chiper, C. Friebe, U. S. Schubert, *J. Phys. Chem. C* **2008**, *112*, 18651–18660; b) M. Presselt, B. Dietzek, M. Schmitt, S. Rau, A. Winter, M. Jäger, U. S. Schubert, J. Popp, *J. Phys. Chem. A* **2010**, *114*, 13163–13174.
- [27] a) J. V. Caspar, T. J. Meyer, *J. Phys. Chem.* **1983**, *87*, 952–957; b) K. R. Barqawi, Z. Murtaza, T. J. Meyer, *J. Phys. Chem.* **1991**, *95*, 47–50; c) J. V. Caspar, E. M. Kober, B. P. Sullivan, T. J. Meyer, *J. Am. Chem. Soc.* **1982**, *104*, 630–632.
- [28] J. V. Caspar, B. P. Sullivan, E. M. Kober, T. J. Meyer, *Chem. Phys. Lett.* **1982**, *91*, 91–95.
- [29] J. A. Treadway, B. Loeb, R. Lopez, P. A. Anderson, F. R. Keene, T. J. Meyer, *Inorg. Chem.* **1996**, *35*, 2242–2246.
- [30] A. C. Benniston, G. Chapman, A. Harriman, M. Mehrabi, C. A. Sams, *Inorg. Chem.* **2004**, *43*, 4227–4233.
- [31] M. Abrahamsson, M. Jäger, R. J. Kumar, T. Österman, P. Persson, H.-C. Becker, O. Johansson, L. Hammarström, *J. Am. Chem. Soc.* **2008**, *130*, 15533–15542.
- [32] M. Beley, S. Chodorowski, J.-P. Collin, J.-P. Sauvage, L. Flamigni, F. Barigelletti, *Inorg. Chem.* **1994**, *33*, 2543–2547.
- [33] C. R. Hecker, A. K. I. Gushurst, D. R. McMillin, *Inorg. Chem.* **1991**, *30*, 538–541.
- [34] a) R. Siebert, C. Hunger, J. Guthmüller, F. Schlütter, A. Winter, U. S. Schubert, L. González, B. Dietzek, J. Popp, *J. Phys. Chem. C* **2011**, *115*, 12677–12688; b) R. Siebert, A. Winter, U. S. Schubert, B. Dietzek, J. Popp, *Phys. Chem. Chem. Phys.* **2011**, *13*, 1606–1617.
- [35] As a non-radiative temperature-independent channel is assumed to contribute to the excited-state dynamics the experimental phosphorescence rate at 77 K can be expressed as $1/\tau_{77K} = k_r + k_1$.
- [36] a) G. H. Allen, R. P. White, D. P. Rillema, T. J. Meyer, *J. Am. Chem. Soc.* **1984**, *106*, 2613–2620; b) W. F. Wacholtz, R. A. Auerbach, R. H. Schmehl, *Inorg. Chem.* **1986**, *25*, 227–234; c) F. Barigelletti, A. Juris, V. Balzani, P. Belser, A. Von Zelewsky, *J. Phys. Chem.* **1987**, *91*, 1095–1098; d) A. Islam, N. Ikeda, A. Yoshimura, T. Ohno, *Inorg. Chem.* **1998**, *37*, 3093–3098.
- [37] a) B. J. Coe, D. W. Thompson, C. T. Culbertson, J. R. Schoonover, T. J. Meyer, *Inorg. Chem.* **1995**, *34*, 3385–3395; b) R. S. Lumpkin, E. M. Kober, L. A. Worl, Z. Murtaza, T. J. Meyer, *J. Phys. Chem.* **1990**, *94*, 239–243; c) M. Sykora, J. R. Kincaid, *Inorg. Chem.* **1995**, *34*, 5852–5856; d) H. Yersin, E. Gallhuber, A. Vogler, H. Kunkely, *J. Am. Chem. Soc.* **1983**, *105*, 4155–4156.
- [38] B. Enright, G. Redmond, D. Fitzmaurice, *J. Phys. Chem.* **1994**, *98*, 6195–6200.
- [39] G. Boschloo, A. Hagfeldt, *Acc. Chem. Res.* **2009**, *42*, 1819–1826.
- [40] Z. Wang, E. Turner, V. Mahoney, S. Madakuni, T. Groy, J. Li, *Inorg. Chem.* **2010**, *49*, 11276–11286.
- [41] J. Heinze, B. A. Frontana-Urbe, S. Ludwigs, *Chem. Rev.* **2010**, *110*, 4724–4771.
- [42] Y. Tachibana, M. K. Nazeeruddin, M. Grätzel, D. R. Klug, J. R. Durrant, *Chem. Phys.* **2002**, *285*, 127–132.
- [43] M. Beley, J. P. Collin, J. P. Sauvage, *Inorg. Chem.* **1993**, *32*, 4539–4543.
- [44] K. Freed, J. Jortner, *J. Chem. Phys.* **1970**, *52*, 6272–6291.
- [45] J. H. Alstrum-Acevedo, M. K. Brennaman, T. J. Meyer, *Inorg. Chem.* **2005**, *44*, 6802–6827.
- [46] I. M. Dixon, F. Alary, J.-L. Heully, *Dalton Trans.* **2010**, *39*, 10959–10966.

Received: November 3, 2011

Published online: February 29, 2012

Publication A7: “A heteroleptic *bis*(tridentate) ruthenium(II) complex of a click-derived abnormal carbene pincer ligand with potential for photosensitizer application”

Benjamin Schulze, Daniel Escudero, Christian Friebe, Ronald Siebert, Helmar Görls, Uwe Köhn, Esra Altuntas, Anja Baumgaertel, Martin D. Hager, Andreas Winter, Benjamin Dietzek, Jürgen Popp, Leticia González, Ulrich S. Schubert

Chem. Eur. J. **2011**, *17*, 5494–5498.

Reprinted with permission from: WILEY-VCH Weinheim (Copyright 2011)

A Heteroleptic Bis(tridentate) Ruthenium(II) Complex of a Click-Derived Abnormal Carbene Pincer Ligand with Potential for Photosensitizer Application

Benjamin Schulze,^[a] Daniel Escudero,^[b] Christian Friebe,^[a] Ronald Siebert,^[c] Helmar Görls,^[d] Uwe Köhn,^[a] Esra Altuntas,^[a] Anja Baumgaertel,^[a] Martin D. Hager,^[a] Andreas Winter,^[a] Benjamin Dietzek,^[c] Jürgen Popp,^[c] Leticia González,^{*[b]} and Ulrich S. Schubert^{*[a]}

Ruthenium(II) polypyridyl complexes have received particular interest with respect to photosensitizer applications, because they are stable and inert complexes that show a defined metal-to-ligand charge transfer (MLCT).^[1] A central dilemma is that trisbidentate complexes (e.g., of 2,2'-bipyridine, bpy) show long excited-state lifetimes, whereas bis(tridentate) complexes (e.g., of 2,2':6',2''-terpyridine, tpy) allow the isomer-free construction of linear assemblies for vectorial electron-transfer processes.^[2] The quest of diminishing the fast radiationless deactivation of the ³MLCT state through the triplet metal-centered state (³MC) of bis(tridentate) ruthenium(II) polypyridyl complexes^[3] has motivated numerous approaches^[4-6] that aim at ³MLCT lowering or ³MC raising or both. Ideally, electronic manipulations are realized

by direct incorporation of stronger donors, that is, by cyclometalation^[7] or coordination through anionic N-heterocycles^[8] and N-heterocyclic carbenes (NHCs).^[9] Thereby, strong σ and π donation by coordination through anionic carbon or nitrogen donors lead to a destabilized ground state and, thus, a lowered ³MLCT, resulting in a radiationless deactivation governed by the energy-gap law^[10] and a low driving force for the potential electron-transfer processes. In contrast, classical NHC ligands are strong, charge-neutral σ donors and π acceptors, thus causing a favorable ³MC destabilization, but also undesirably blue-shifted MLCT transitions. Alternatively, the expansion to six-membered ring chelators^[6] leads to excellent excited-state lifetimes by a more favorable bite angle, but can also cause the formation of isomers (*fac*, *mer*) that show very different properties and that are hard to separate.

In this regard, abnormal or mesoionic carbene ligands^[11] provide superior σ -donating and only moderate π -accepting properties that ideally would lead to strongly destabilized ³MC states and a maintained ³MLCT energy. 1,2,3-Triazolylidenes match these demands and are readily accessible by modular click chemistry. Herein we present a heteroleptic bis(tridentate) ruthenium(II) complex (RuCNC) of the new 2',6'-bis(1-mesityl-3-methyl-1,2,3-triazol-4-yl-5-idene)pyridine (CNC) ligand and the parent tpy. A heteroleptic complex with tpy is particularly interesting, because it preserves the elaborated terpyridine chemistry, including a variety of ruthenium precursors, allows for asymmetric functionalization, and includes a reference ligand. The electronic and optical properties of RuCNC were investigated by experimental and theoretical studies.

The synthesis of RuCNC was achieved under mild reaction conditions with a high selectivity and reasonable yield (Scheme 1). For the preparation of 2',6'-bis(1-mesityl-3-methyl-1,2,3-triazolium-4-yl)pyridine tetrafluoroborate (H₂CNC), the parent click-derived 2',6'-bis(1-mesityl-1,2,3-triazol-4-yl)pyridine (tripy)^[12] could be methylated selectively with Meerwein's salt^[13] as evidenced by single-crystal X-ray diffraction (Figure 1), spectroscopic, and spectrometric methods. Because free 1,2,3-triazolylidenes undergo a 5–3-methyl shift,^[11] a stable silver(I)-precursor (AgCNC) was

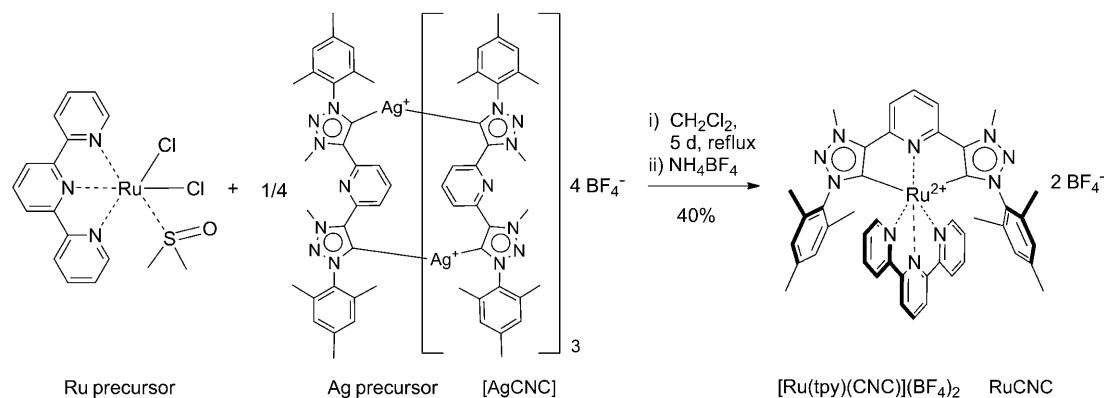
[a] Dipl.-Chem. B. Schulze, Dipl.-Chem. C. Friebe, Dr. U. Köhn, E. Altuntas, Dipl.-Chem. A. Baumgaertel, Dr. M. D. Hager, Dr. A. Winter, Prof. Dr. U. S. Schubert
Laboratory of Organic and Macromolecular Chemistry (IOMC)
Jena Center for Soft Matter (JCSM)
Friedrich-Schiller-University Jena
Humboldtstr. 10, 07743 Jena (Germany)
Fax: (+49) 3641948202
E-mail: ulrich.schubert@uni-jena.de

[b] D. Escudero, Prof. Dr. L. González
Laboratory of Theoretical Chemistry
Jena Center for Soft Matter (JCSM)
Friedrich-Schiller-University Jena
Helmholtzweg 4, 07743 Jena (Germany)
Fax: (+49) 3641948302
E-mail: leticia.gonzalez@uni-jena.de

[c] Dipl.-Chem. R. Siebert, Dr. B. Dietzek, Prof. Dr. J. Popp
Institute of Physical Chemistry and Abbe Center of Photonics
Jena Center for Soft Matter (JCSM)
Friedrich-Schiller-University Jena
Helmholtzweg 4, 07743 Jena (Germany)
and
Institute of Photonic Technology Jena
Albert-Einstein-Straße 9, 07745 Jena (Germany)

[d] Dr. H. Görls
Laboratory of Inorganic and Analytic Chemistry
Friedrich-Schiller-University Jena
Lessingstr. 8, 07743 Jena (Germany)

Supporting information for this article is available on the WWW under <http://dx.doi.org/10.1002/chem.201100045>.



Scheme 1. Schematic representation of the synthesis RuCNC.

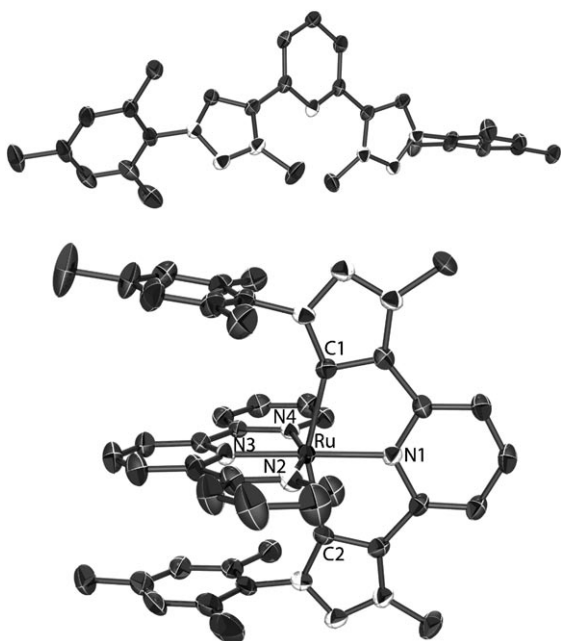


Figure 1. Solid-state structures of H₂CNC (top) and RuCNC (bottom, ellipsoids at 50% probability level; hydrogen atoms, solvents molecules, and tetrafluoroborate anions are omitted for clarity). Selected bond lengths (Å) and angles (°) of RuCNC: Ru–C1, 2.058(4); Ru–C2, 2.051(4); Ru–N1, 2.083(4); Ru–N2, 2.068(4); Ru–N3, 1.962(4); Ru–N4, 2.052(4); C1–Ru–C2, 154.34(17); N2–Ru–N4, 158.25(15); N1–Ru–N3, 178.48(15).

prepared by utilizing silver(I) oxide. ESI-ToF MS, MALDI-ToF MS, and MS/MS measurements revealed isotopically resolved peaks of up to tetrameric cycles (see Figure S36 in the Supporting Information for an optimized structure of the tetrameric complex).^[14] In the milder ESI MS, mainly the 4:4 complex, beside 3:3 and 1:1 fragments, were observed. Diffusion-ordered NMR-spectroscopy (DOSY) measurements proved the uniformity of the proton signals and the formation of a higher aggregate. In the ¹³C NMR spectra, the abnormal carbene signals appeared with a typical ^{107/109}Ag coupling at around 170 ppm that was shifted to higher field by 10 ppm compared with a silver complex of a normal imidazolylidene carbene with a carbon sextet.^[14] For

the subsequent transmetalation, common ruthenium(II) and ruthenium(III) monocomplexes of tpy were tested, but only *cis*-[Ru(tpy)(DMSO)Cl₂]^[15] proved to be a sufficiently selective and reactive precursor. Single crystals of RuCNC suitable for X-ray diffraction were grown by vapor diffusion of diethyl ether into a methanolic solution (Figure 1). The C,N,C-pincer coordination as well as an intramolecular tweezer-like π stacking was clearly confirmed. The ruthenium–carbon bond lengths are identical to those reported for a related heteroleptic ruthenium(II) complex of the classical 2',6'-bis(3-methylimidazol-1-yl-2-ylidene)pyridine and terpyridine, other bond lengths are comparable and the bite angles are slightly larger.^[9] The identity and purity of the complex were proven by MS and various NMR techniques. The triazolium protons vanished and characteristic high-field shifts due to the π stacking were visible in the ¹H NMR spectrum. Furthermore, a strong low-field shift to around 185 ppm can be observed for the coordinating carbons in the ¹³C NMR spectrum, but again less pronounced than for classical NHC ligands.^[9]

The UV/Vis absorption spectrum of RuCNC shows a typical MLCT transition, but, due to the reduced symmetry of the heteroleptic complex, it exhibits a comparatively low extinction coefficient and a band splitting. The absorption profile is similar to the related heteroleptic complex with *N,N,N*-bound tripy.^[12] Noteworthy, the MLCT absorption is only marginally blue-shifted in comparison to the parent [Ru(tpy)₂](PF₆)₂ (see above and Table 1). The room-temperature emission measurement revealed an intense red and unstructured emission with quantum yields close to the [Ru(bpy)₃](PF₆)₂ reference value (Table 1). Furthermore, the emission showed a slow and monoexponential decay, thus arising from a single phosphorescent triplet state (Figure 2). The excited-state lifetime of 633 ns can almost compete with [Ru(bpy)₃](PF₆)₂ and is 2500 times longer than for [Ru(tpy)₂](PF₆)₂.

In comparison to ruthenium(II) complexes of charge-neutral polypyridyl ligands, the redox potentials show a cathodic shift, most likely due to the anionic carbon of the mesoionic carbene, but a similar energy gap. The HOMO and LUMO energies calculated from the cyclovoltammetry results

Table 1. Selected photophysical and electrochemical data.

| | [Ru(tpy) ₂](PF ₆) ₂ | [Ru(bpy) ₃](PF ₆) ₂ | RuCNC |
|---|--|--|--|
| $\lambda_{\text{max}}^{\text{Abs}}$ [nm] ^[a] | 474 | 450 | 463 |
| ϵ [10 ⁴ M ⁻¹ cm ⁻¹] ^[a] | 1.8 | 1.4 | 1.0 |
| $\lambda_{\text{ma}}^{\text{Em}}$ [nm] | – | 597 | 643 (634) ^[b] |
| τ [ns] | 0.21 ^[c] | 860; ^[d] 680 ^[d,e] | 633; 615 ^[e] |
| Φ_{PL} [%] | – | 6.2 ^[f] | 4.4; ^[g] 5.5 ^[e,g] |
| $E_{1/2}^{\text{Ox}}$ [V] ^[h] | 0.90 | 0.90 | 0.60 |
| $E_{1/2}^{\text{Red}}$ [V] ^[h] | –1.64 | –1.71 | –1.95 |
| E_{LUMO} [eV] ^[i] | –3.20 | –3.28 | –2.70 |
| E_{HOMO} [eV] ^[i] | –5.71 | –5.70 | –5.38 |

Measured in deaerated acetonitrile at 298 K, unless stated otherwise. [a] Maximum of the MLCT band. [b] Theoretical predicted AEE value (PCM-B3LYP/6-31G*). [c] Measured in butyronitrile at 290 K; from ref. [3a]. [d] From ref. [16]. [e] Measured in deaerated CH₂Cl₂. [f] From ref. [17a]. [g] Against [Ru(bpy)₃](PF₆)₂ as standard. [h] Measured in CH₃CN containing 0.1 M NBu₄PF₆ and with Fc/Fc⁺ as a reference. [i] Calculated by using $E_{\text{LUMO/HOMO}} = [- (E_{\text{onset}}^{\text{Red/Ox}} - E_{\text{onset}}^{\text{Fc/Fc}^+}) - 4.8]$ eV.

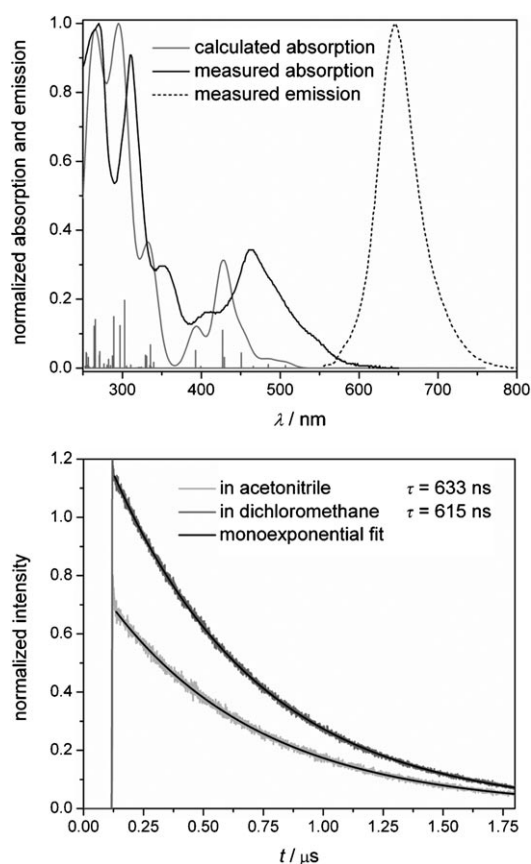


Figure 2. Calculated and measured UV/Vis absorption and measured emission spectra (top). Emission decay (bottom).

(Table 1) are raised in energy and, additionally, the oxidation appears to be reversible. To obtain a more detailed insight into the oxidation process, UV/Vis spectroelectrochemical experiments were executed (see Figure S31 in the Supporting Information). Several isosbestic points suggest the presence of only two species and, thus, a well-defined oxidation process. The most obvious spectral change is the strong decrease of the MLCT bands at 463, 410, and 352 nm, con-

sistent with the assignment of the oxidation process as a ruthenium(II)/ruthenium(III) transition. Additionally, a weak and broad band at around 600 to 800 nm appears, most likely due to ligand-to-metal charge transfer (LMCT, $\pi \rightarrow d$) transitions, whereas the bands below 330 nm, in the region dominated by ligand-centered (LC) transitions, appear essentially unchanged. Remarkably, the reduction of the oxidized species regenerates the parent complex quantitatively. This highlights the potential of RuCNC to act as an electron donor.

To understand the electronic properties and the bonding of the abnormal carbene ligand to the ruthenium center, energy-decomposition analysis (EDA)^[18] was performed (see computational details in the Supporting Information). The EDA (BP86-ZORA/TZP) calculation revealed that the interaction energy between the carbene and the ruthenium(II)-tpy fragment is -256 kcal mol⁻¹. Former EDA calculations on ruthenium complexes of normal (C2-bound) and abnormal (C4-bound) imidazolylidenes revealed interaction energies of -60 to -70 kcal mol⁻¹ for a single ruthenium-carbene bond.^[19] Assuming these values for a tridentate system still leaves a significant energy difference, this means that CNC enables very strong ruthenium-abnormal carbene bonds. The global interaction energy stems roughly 1:1 from covalent and ionic interactions due to the mesoionic character of the carbene donor ligand. Concerning the covalency of the bond, strong σ -donating as well as π -accepting interactions contribute to the global energy (see Figure S37 and Table S3 in the Supporting Information). Furthermore, time-dependent DFT (TD-DFT) calculations in the presence of acetonitrile (PCM-TD-B3LYP/6-31G*) were performed to rationalize the absorption and emission spectra. The geometry-optimization calculations show that the HOMOs are centered on the ruthenium, whereas the LUMOs are localized on both ligands (Figure 3b). Thus, several transitions, mainly of MLCT character and directed towards both ligands, are observable in the visible region of the absorption spectrum (see Figure 3a and Table S4 in the Supporting In-

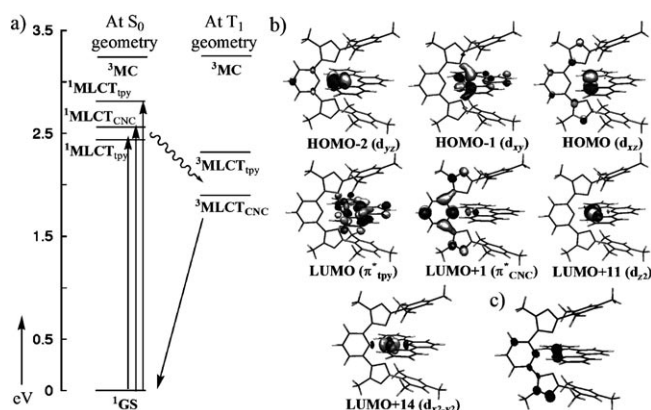


Figure 3. a) Energy-level scheme of the lowest excited states of RuCNC at both the S₀- and T₁-optimized geometries (GS = ground state). b) Most relevant Kohn-Sham orbitals computed at the PCM-B3LYP/6-31G* level of theory. c) Spin-density plot of the T₁ state.

formation). The calculated UV/Vis spectrum is slightly blue-shifted in comparison with the measured spectrum, but both are consistent in shape (see Figure 2). Also, the computed emission maximum is in good agreement with the experiment (see the value of the theoretical predicted adiabatic electronic emission, AEE, in Table 1). Thereby, the longest-wavelength ¹MLCT absorption involves the tpy ligand, whereas, the ³MLCT emission originates from the carbene ligand after redistribution of electron density in the course of vibrational relaxation and intersystem crossing. The MLCT nature of the T₁ state was confirmed by spin-density analysis (see Figure 3c). Remarkably, due to the strong σ donation, the ³MC states are of very high energies, 32 kcal mol⁻¹ above the ³MLCT, thus hardly populated thermally and therefore, the radiationless deactivation is suppressed efficiently (see Figure 3a and Table S5). Oppositely, for the parent compound [Ru(tpy)₂]²⁺, it was found, with the help of ΔDFT calculations, that the ³MC state is even 4 kcal mol⁻¹ lower in energy than the ³MLCT.^[6f]

In conclusion, click chemistry and subsequent methylation was employed to introduce tridentate 2',6'-bis(1,2,3-triazolylidene)pyridine ligands with mesoionic carbene donors. Ruthenium(II) complexation was achieved by transmetalation from a tetrameric silver(I) cycle. Due to the superior σ donation of the mesoionic carbene, the heteroleptic ruthenium(II) complex of the new ligand and the parent terpyridine possesses promising photophysical and electrochemical properties with respect to photosensitizer applications. As a bis(tridentate), heteroleptic system, the complex allows for the construction of isomer-free, linear, and asymmetric substituted assemblies.

Experimental Section

Experimental and computational details are provided in the Supporting Information. CCDC-787332 (H₂CNC) and -787333 (RuCNC) contain the supplementary crystallographic data for this paper. These data can be obtained free of charge from The Cambridge Crystallographic Data Centre via www.ccdc.cam.ac.uk/data_request/cif.

Acknowledgements

B.S., C.F., and R.S. are grateful to the Fonds der Chemischen Industrie for PhD scholarships. D.E. is grateful to the Carl-Zeiss-Stiftung for a PhD scholarship. B.D. thanks the Fonds der Chemischen Industrie. We also thank M. Jäger, W. Günther, and G. Sentis for discussions and performing experiments.

Keywords: carbenes • click chemistry • computational chemistry • photosensitizer • ruthenium

- [1] a) A. Juris, V. Balzani, F. Barigelletti, S. Campagna, P. Belser, A. von Zelewsky, *Coord. Chem. Rev.* **1988**, *84*, 85–277; b) J.-P. Sauvage, J.-P. Collin, J.-C. Chambron, S. Guillerez, C. Coudret, V. Balzani, F. Barigelletti, L. De Cola, L. Flamigni, *Chem. Rev.* **1994**, *94*, 993–1019.

- [2] a) E. A. Medlycott, G. S. Hanan, *Chem. Soc. Rev.* **2005**, *34*, 133–142; b) E. A. Medlycott, G. S. Hanan, *Coord. Chem. Rev.* **2006**, *250*, 1763–1782.
- [3] a) D. W. Fink, W. E. Ohnesorge, *J. Am. Chem. Soc.* **1969**, *91*, 4995–4998; b) A. Amini, A. Harriman, A. Mayeux, *Phys. Chem. Chem. Phys.* **2004**, *6*, 1157–1164.
- [4] For the multichromophore approach, see: a) J. Wang, G. S. Hanan, F. Loiseau, S. Campagna, *Chem. Commun.* **2004**, 2068–2069; b) J. H. Wang, Y. Q. Fang, L. Bourget-Merie, M. I. J. Poisson, G. S. Hanan, A. Juris, F. Loiseau, S. Campagna, *Chem. Eur. J.* **2006**, *12*, 8539–8548.
- [5] For electronic manipulations, see: a) M. Maestri, N. Armaroli, V. Balzani, E. C. Constable, A. M. W. Cargill Thompson, *Inorg. Chem.* **1995**, *34*, 2759–2767; b) Y.-Q. Fang, N. J. Taylor, G. S. Hanan, F. Loiseau, R. Passalacqua, S. Campagna, H. Nierengarten, A. V. Dorsse-laer, *J. Am. Chem. Soc.* **2002**, *124*, 7912–7913; c) R. Siebert, A. Winter, B. Dietzek, U. S. Schubert, J. Popp, *Macromol. Rapid Commun.* **2010**, *31*, 883–888.
- [6] For structural manipulations, see: a) L. Hammarström, O. Johansson, *Coord. Chem. Rev.* **2010**, *254*, 2546–2559; b) M. Abrahamsson, M. Jäger, T. Österman, L. Eriksson, P. Persson, H.-C. Becker, O. Johansson, L. Hammarström, *J. Am. Chem. Soc.* **2006**, *128*, 12616–12617; c) M. Abrahamsson, M. Jäger, R. J. Kumar, T. Österman, P. Persson, H.-C. Becker, O. Johansson, L. Hammarström, *J. Am. Chem. Soc.* **2008**, *130*, 15533–15542; d) F. Schramm, V. Meded, H. Fliegl, K. Fink, O. Fuhr, Z. Qu, W. Klopfer, S. Finn, T. E. Keyes, M. Ruben, *Inorg. Chem.* **2009**, *48*, 5677–5684; e) A. Breivogel, C. Förster, K. Heinze, *Inorg. Chem.* **2010**, *49*, 7052–7056; f) O. Anders Borg, S. S. M. C. Godinho, M. J. Lundqvist, S. Lunell, P. Persson, *J. Phys. Chem. A* **2008**, *112*, 4470–4476; as apparent from the last reference, an ideal octahedral symmetry avoids admixing of ruthenium(II) d orbitals to the LUMO; this lowers the probability of the ³MLCT-to-³MC transition and, consequently, the energy of the MC state becomes less crucial.
- [7] a) J.-P. Collin, M. Beley, J.-P. Sauvage, F. Barigelletti, *Inorg. Chim. Acta* **1991**, *186*, 91–93; b) S. H. Wadman, M. Lutz, D. M. Tooke, A. L. Spek, F. Hartl, R. W. A. Havenith, G. P. M. van Klink, G. van Koten, *Inorg. Chem.* **2009**, *48*, 1887–1900; c) M. Jäger, A. Smeigh, F. Lombeck, H. Görls, J.-P. Collin, J.-P. Sauvage, L. Hammarström, O. Johansson, *Inorg. Chem.* **2010**, *49*, 374–376; d) P. G. Bomben, K. C. D. Robson, P. A. Sedach, C. P. Berlinguette, *Inorg. Chem.* **2009**, *48*, 9631–9643.
- [8] a) M. Duati, S. Fanni, J. G. Vos, *Inorg. Chem. Commun.* **2000**, *3*, 68–70; b) M. Duati, S. Tasca, F. C. Lynch, H. Bohlen, J. G. Vos, *Inorg. Chem.* **2003**, *42*, 8377–8384.
- [9] a) S. U. Son, K. H. Park, Y.-S. Lee, B. Y. Kim, C. H. Choi, M. S. Lah, Y. H. Jang, D.-J. Jang, Y. K. Chung, *Inorg. Chem.* **2004**, *43*, 6896–6898; b) H.-J. Park, K. H. Kim, S. Y. Choi, H.-M. Kim, W. I. Lee, Y. K. Kang, Y. K. Chung, *Inorg. Chem.* **2010**, *49*, 7340–7352.
- [10] a) R. Englman, J. Jortner, *Mol. Phys.* **1970**, *18*, 145–164; b) J. V. Caspar, B. P. Sullivan, E. M. Kober, T. J. Meyer, *Chem. Phys. Lett.* **1982**, *91*, 91–95.
- [11] a) P. Mathew, A. Neels, M. Albrecht, *J. Am. Chem. Soc.* **2008**, *130*, 13534–13535; b) G. Guisado-Barrios, J. Bouffard, B. Donnadieu, G. Bertrand, *Angew. Chem.* **2010**, *122*, 4869–4872; *Angew. Chem. Int. Ed.* **2010**, *49*, 4759–4762; c) O. Schuster, L. Yang, H. G. Raubenheimer, M. Albrecht, *Chem. Rev.* **2009**, *109*, 3445–3478; d) R. Lalrempuia, N. D. McDaniel, H. Müller-Bunz, S. Bernhard, M. Albrecht, *Angew. Chem.* **2010**, *122*, 9959–9962; *Angew. Chem. Int. Ed.* **2010**, *49*, 9765–9768.
- [12] a) Y. Li, J. C. Huffman, A. H. Flood, *Chem. Commun.* **2007**, 2692–2694; b) R. M. Meudtner, M. Ostermeier, R. Goddard, C. Limberg, S. Hecht, *Chem. Eur. J.* **2007**, *13*, 9834–9840; c) B. Schulze, C. Friebe, M. D. Hager, A. Winter, R. Hoogenboom, H. Görls, U. S. Schubert, *Dalton Trans.* **2009**, 787–794; d) M. Ostermeier, M.-A. Berlin, R. M. Meudtner, S. Demeshko, F. Meyer, C. Limberg, S. Hecht, *Chem. Eur. J.* **2010**, *16*, 10202–10213.
- [13] a) B. Schulze, C. Friebe, M. D. Hager, W. Günther, U. Köhn, B. O. Jahn, H. Görls, U. S. Schubert, *Org. Lett.* **2010**, *12*, 2710–2713;

- b) K. J. Kilpin, U. S. D. Paul, A.-L. Lee, J. D. Crowley, *Chem. Commun.* **2011**, 47, 328–330; c) K. M. Mullen, J. Mercurio, C. J. Serpell, P. D. Beer, *Angew. Chem.* **2009**, *121*, 4875–4878; *Angew. Chem. Int. Ed.* **2009**, *48*, 4781–4784; d) T. Karthikeyan, S. Sankararaman, *Tetrahedron Lett.* **2009**, *50*, 5834–5837.
- [14] a) M. L. Gower, J. D. Crowley, *Dalton Trans.* **2010**, 39, 2371–2378; b) C. Radloff, H.-Y. Gong, C. Schulte to Brinke, T. Pape, V. M. Lynch, J. L. Sessler, F. E. Hahn, *Chem. Eur. J.* **2010**, *16*, 13077–13081.
- [15] R. Ziessel, V. Grossshenny, M. Hissler, C. Stroh, *Inorg. Chem.* **2004**, *43*, 4262–4271.
- [16] B. Durham, J. V. Caspar, J. K. Nagle, T. J. Meyer, *J. Am. Chem. Soc.* **1982**, *104*, 4803–4810.
- [17] a) J. M. Calvert, J. V. Caspar, R. A. Binstead, T. D. Westmoreland, T. J. Meyer, *J. Am. Chem. Soc.* **1982**, *104*, 6620–6627; b) K. Suzuki, A. Kobayashi, S. Kaneko, K. Takehira, T. Yoshihara, H. Ishida, Y. Shiina, S. Oishic, S. Tobita, *Phys. Chem. Chem. Phys.* **2009**, *11*, 9850–9860. The second reference reported the photoluminescence quantum yield of [Ru(bpy)₃](PF₆)₂ to be 9.2%. According to that, the quantum yields of RuCNC would be 6.5 and 8.2%, respectively.
- [18] a) F. M. Bickelhaupt, E. J. Baerends, *Kohn–Sham Density Functional Theory: Predicting and Understanding Chemistry in Reviews in Computational Chemistry, Vol. 15* (Eds.: K. B. Lipkowitz, D. B. Boyd), Wiley-VCH, Weinheim, **2000**, pp. 1–86; b) M. Lein, G. Frenking in *Theory and Applications of Computational Chemistry: The First 40 Years* (Eds.: C. E. Dykstra, G. Frenking, K. S. Kim, G. E. Scuseria), Elsevier, Amsterdam, **2005**, pp. 291–367.
- [19] a) R. Tonner, G. Heydenrych, G. Frenking, *Chem. Asian J.* **2007**, *2*, 1555–1567; b) N. S. Antonova, J. J. Carbó, J. M. Poblet, *Organometallics* **2009**, *28*, 4283–4287.

Received: January 5, 2011
Published online: April 12, 2011

Publication A8: “Ruthenium(II) metallo-supramolecular
polymers of click-derived tridentate ditopic ligands”

Benjamin Schulze, Christian Friebe, Stephanie Hoepfener,
Georges M. Pavlov, Andreas Winter, Martin D. Hager,
Ulrich S. Schubert

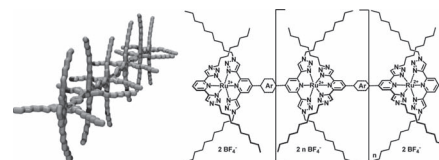
Macromol. Rapid Commun. **2012**, *33*, 597–602.

Reprinted with permission from: WILEY-VCH Weinheim (Copyright 2012)

Ruthenium(II) Metallo-Supramolecular Polymers of Click-Derived Tridentate Ditopic Ligands

Benjamin Schulze, Christian Friebe, Stephanie Hoepfener, Georges M. Pavlov, Andreas Winter, Martin D. Hager, Ulrich S. Schubert*

New ditopic 2,6-*bis*(1,2,3-triazol-4-yl)pyridine ligands featuring a π -conjugated spacer and clicked-on solubilizing groups were employed in the synthesis of Ru^{II} metallo-supramolecular polymers that exhibit an intense metal-to-ligand charge transfer absorption in the visible light region. The coordination polymers obtained were studied in solution by means of size exclusion chromatography and analytical ultracentrifugation, revealing a comparably high molar mass and moderate rigidity. Investigations in the solid state by atomic force and transmission electron microscopy confirmed the formation of rod-like polymers. Furthermore, film preparation by drop-casting showed good film-forming properties. Thus, the solution-processable, photoredoxactive polymers might be applicable in solar cells.



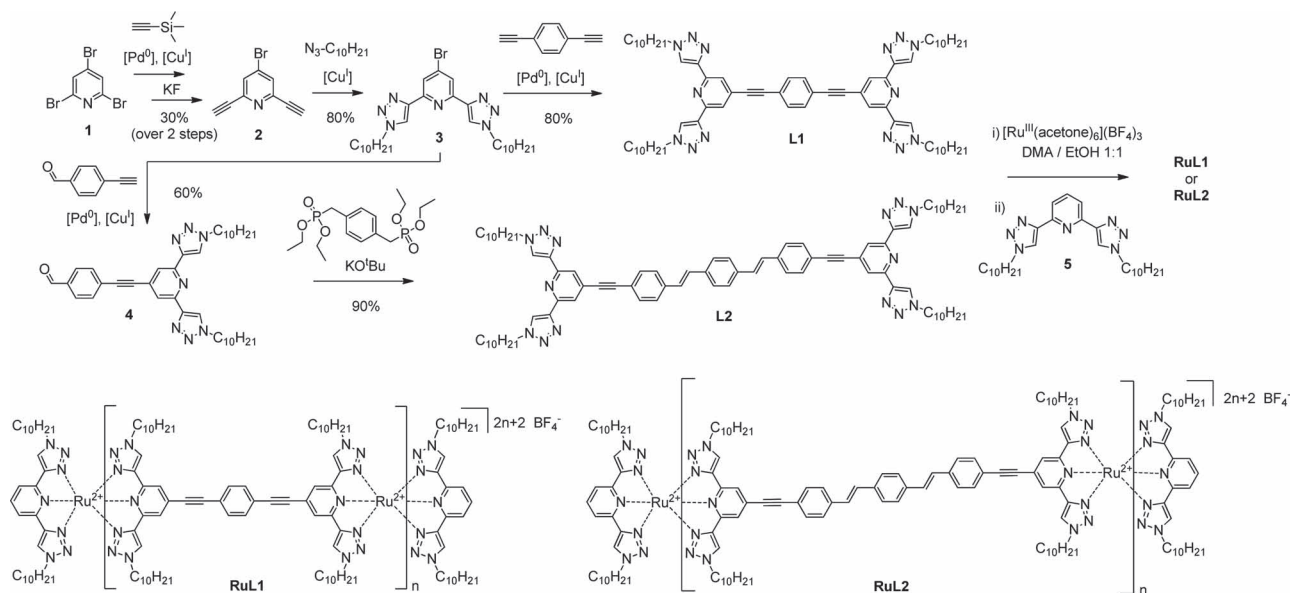
1. Introduction

The assembly of molecular building blocks to supramolecular architectures via non-covalent interactions represents an emerging field of research in modern macromolecular chemistry and materials science.^[1] Thereby, the defined properties of small molecules and the processing advantages of polymers (i.e. good film formation) can be merged. Besides hydrogen bonding and ionic/electrostatic interactions, metal-to-ligand coordination is most

commonly applied in this respect.^[2] In particular, tridentate ligands, for example the 2,2':6',2''-terpyridine moiety,^[3] when employed as a linear, ditopic ligand, enable the construction of high-molar-mass coordination polymers.^[4] Depending on the metal ions (in particular Ru^{II}, Fe^{II}, and Zn^{II}), one can achieve a broad range of properties suitable for different optoelectronic applications, e.g., in photovoltaics, electrochromic displays and light-emitting diodes. Most of these applications make use of a π -conjugated backbone that enables (Zn^{II}) or modulates (Ru^{II}) photoredox activity. In general, these linear rod-like metallopolymers suffer from their poor solubility in common solvents. In order to offer solution processability, e.g., printability and film-forming ability, solubilizing groups that prevent π interactions are required.^[5] Commonly, alkoxy or even polymer side chains are thus introduced to the building blocks of the π -conjugated backbone.^[4b] By application of the Cu^I-catalyzed azide-alkyne 1,3-dipolar cycloaddition (CuAAC),^[6] tridentate terpyridine-analog ligands, namely 2,6-*bis*(1*H*-1,2,3-triazol-4-yl)pyridines (tripy),^[7] are accessible that are modularly and readily terminal functionalized. Thus, solubilizing groups can be installed most easily on the ligand, which, moreover, enables a free design of the π -conjugated spacer. Furthermore, the use of Ru^{II} ions allows the synthesis of stable and inert coordination

B. Schulze, C. Friebe, Dr. S. Hoepfener, Dr. G. M. Pavlov, Dr. A. Winter, Dr. M. D. Hager, Prof. U. S. Schubert
Laboratory of Organic and Macromolecular Chemistry (IOMC),
Friedrich-Schiller-University Jena,
Humboldtstr. 10, 07743 Jena, Germany
E-mail: ulrich.schubert@uni-jena.de

B. Schulze, C. Friebe, Dr. S. Hoepfener, Dr. G. M. Pavlov, Dr. A. Winter, Dr. M. D. Hager, Prof. U. S. Schubert
Jena Center for Soft Matter (JCSM), Friedrich-Schiller-
University Jena, Humboldtstr. 10, 07743 Jena, Germany
Dr. G. M. Pavlov, Dr. A. Winter, Dr. M. D. Hager,
Prof. U. S. Schubert
Dutch Polymer Institute (DPI), P.O. Box 902, 5600 AX
Eindhoven, The Netherlands



■ Scheme 1. Schematic representation of the synthesis of Ru^{II} metallopolymers **RuL1** and **RuL2**.

polymers that enable a detailed characterization. As Ru^{II} polypyridyl-analog polymeric complexes,^[8] they typically exhibit photogenerated charge separation that makes them potentially suitable for applications in solution-processable photovoltaic devices.^[9]

In this communication we describe the synthesis and characterization of two linear π -conjugated ditopic bis-tripty ligands (**L1** and **L2**). The self-assembly with Ru^{II} ions yields the metallopolymers **RuL1** and **RuL2** that have extensively been studied in solution (i.e. size exclusion chromatography, analytical ultracentrifugation, optoelectronic properties) as well as in the solid state (i.e. atomic force and transmission electron microscopy).

2. Experimental Section

All experimental details are provided in the Supporting Information.

3. Results and Discussion

3.1. Synthesis

Ditopic bis-tripty ligands were recently introduced by Chandrasekar et al.,^[7a] however, the syntheses of these back-to-back ligands involved a long eight-reaction-step sequence and only Eu^{III} complexes thereof have been prepared that are insoluble due to crosslinking (formation of 3:1 complexes). In an optimized protocol that allows for late-stage clicking – thereby preserving a modular character – 2,4,6-tribromopyridine (**1**) was reacted via a regioselective

Sonogashira reaction^[10] to yield 2,6-diethynyl-4-bromopyridine (**2**) as a versatile building block. Subsequently, decyl azide was used to build up the 4-halide-functionalized precursor ligand **3**, bearing already solubilizing groups and allowing for the introduction of a π -conjugated spacer by metal-catalyzed cross-coupling reactions (Scheme 1). The ditopic ligands were obtained either directly by Sonogashira cross-coupling with 1,4-diethynylbenzene or by Sonogashira reaction with 4-ethynylbenzaldehyde (to yield **4**) followed by a Horner-Wadsworth-Emmons reaction with an appropriate diphosphonate to give bis-tripty ligands with π -conjugated spacers of phenylene-ethynylene (**L1**) and phenylene-ethynylene/phenylene-vinylene (**L2**) connectivity, respectively, in high yields (Scheme 1). For the preparation of the Ru^{II} metallopolymers, a coordination polymerization as described by Rehahn et al. was used.^[4c,11] For this purpose, the highly active [Ru(acetone)₆](BF₄)₃ precursor complex was reacted with 1 eq. of either **L1** or **L2** in a mixture of *N,N*-dimethylacetamide (DMA) and ethanol, i.e. under reducing conditions.^[4c,11] According to the theory of step-growth polymerization,^[12] high-molar-mass polymers can only be achieved at very high degrees of conversion that require, in turn, a 1:1 stoichiometry of both functional groups. For two complementary bifunctional monomers (A-A and B-B), this requirement is hard to achieve. However, the point of equivalence can be approached by very slow “titration” with the metal precursor ion since the once formed complexes are inert and stable and, thus, the polymer will not disassemble (depolymerize) when the metal precursor is added in excess. The progress of the polymerization was monitored by size exclusion chromatography (SEC). To ensure defined Ru^{II} end groups and to

remove excessive Ru^{III}, a monotopic tripy ligand (**5**) was added at the end of the reaction. The crude product was purified simply by evaporation of all volatile compounds in vacuo and repeated swelling of the polymeric material with dichloromethane and acetonitrile.

3.2. Hydrodynamic Investigations

The molar masses (\bar{M}_n) of the resulting Ru^{II} polymers were estimated relatively by SEC (in DMA containing 0.08 wt.% NH₄PF₆) against a linear polystyrene standard using a photodiode array detector (PDA, Figure 1). **RuL1** and **RuL2** had average \bar{M}_n values of 85,000 and 59,000 g·mol⁻¹, and polydispersity indices (PDIs) of 3.3 and 2.4, respectively. For **RuL2** this is close to the theoretical value of 2 for a step-growth polymerization, while for **RuL1** the broader size distribution still is within an acceptable range for this polymerization method. Furthermore, both \bar{M}_n values are apparently overestimated due to the anticipated chain stiffness of the metallopolymer that leads to a larger hydrodynamic volume than for the coiled polystyrene of the same molar mass. Indeed, absolute molar mass determination by NMR integration (see Figure S 17) revealed \bar{M}_n values of 41,000 and 39,000 g·mol⁻¹, corresponding to a degree of polymerization of 30 and 25 for **RuL1** and **RuL2**, respectively. However, these values are based on the assumption that the end-capping was complete and that no cyclic structures were formed. Consequently, absolute molar mass determination by analytical ultracentrifugation (AUC) was performed, which, moreover, provides hydrodynamic, thus structural information. The differential distribution of the sedimentation coefficient of **RuL1** and **RuL2** is shown in Figure 1, S 25 and S 26. The molar masses of the polymer samples were calculated by the modified Svedberg equation^[13] (Equation 1) as well as by the concept of the hydrodynamic invariant^[14] (Equation 2); these estimations are presented in Table 1. Thereby, a combination of the velocity sedimentation coefficient (s_0) and the value of the frictional ratio

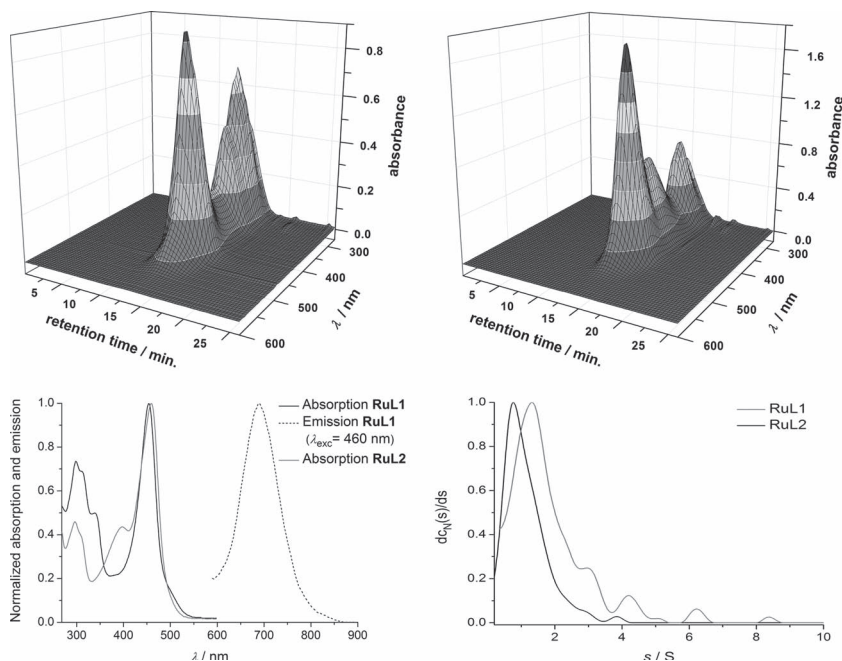


Figure 1. SEC traces (PDA detector, in DMA cont. 0.08% NH₄PF₆) of **RuL1** (top, left) and **RuL2** (top, right). Normalized differential distributions $dc_N(s)/ds$ of the sedimentation coefficient (bottom, right) of **RuL1** (black, $c = 1.85 \cdot 10^{-3}$ g·cm⁻³) and **RuL2** (grey, $c = 5.5 \cdot 10^{-4}$ g·cm⁻³ in DMF cont. 1 wt.% of NH₄BF₄). UV-vis absorption and emission of **RuL1** (black) and **RuL2** (grey) in DMF solution (bottom, left).

(f/f_{sph}) led to the modified Svedberg equation used for M_{sf} determination from the hydrodynamic data,^[13]

$$M_{\text{sf}} = 9\pi \times 2^{1/2} N_A ([s](f/f_{\text{sph}}))^{3/2} v^{1/2} \quad (1)$$

where v is the partial specific volume, $[s] = s_0 \eta_0 / (1 - v\rho_0)$ is the intrinsic sedimentation coefficient and N_A is the Avogadro constant. The frictional ratio (f/f_{sph}) is the weight-average frictional ratio of all species in the sample with f being the frictional coefficient of the dissolved macromolecule and f_{sph} being the frictional coefficient of a rigid sphere with the same “anhydrous” volume (free of solvent) as the macromolecule. The values of the partial specific volume were evaluated from the velocity sedimentation experiment performed in DMF and in deuterated DMF. Alternatively, molar masses were estimated also from the velocity sedimentation coefficient and intrinsic viscosity values using the hydrodynamic invariant A_0 ,^[14]

Table 1. Results of the hydrodynamic studies.

| Polymer | s_0 | f/f_{sph} | $[\eta]$ | M_{sf} | $M_{s\eta}$ | $\bar{M}_n(\text{NMR})$ | $\bar{M}_n(\text{SEC})$ | PDI _{SEC} |
|-------------|-------|--------------------|-------------------------------------|------------------------|------------------------|-------------------------|-------------------------|--------------------|
| | [S] | | [cm ³ ·g ⁻¹] | [g·mol ⁻¹] | [g·mol ⁻¹] | [g·mol ⁻¹] | [g·mol ⁻¹] | |
| RuL1 | 1.7 | 3.2 | 90 | 36,000 | 34,000 | 41,000 | 85,000 | 3.3 |
| RuL2 | 1.1 | 3.8 | 80 | 29,000 | 17,000 | 39,000 | 59,000 | 2.4 |

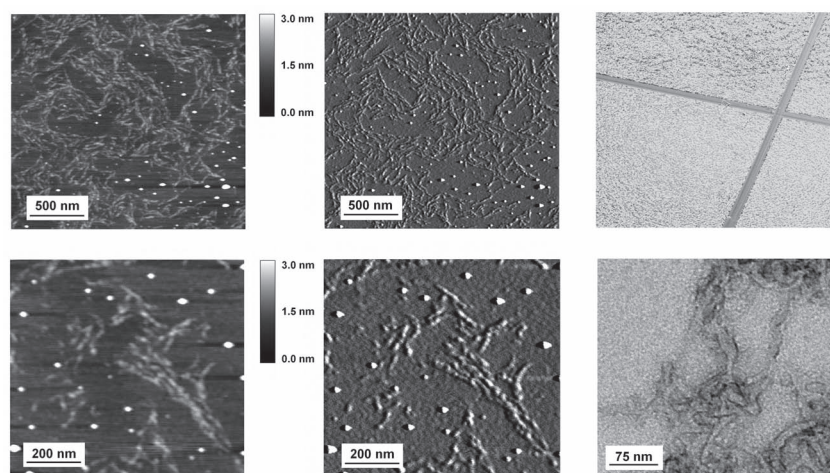


Figure 2. Representative microscopy images of **RuL1**: AFM height (left) and amplitude images (middle) on a mica slide. Optical profilometer image (top, right) of a drop-casted and scratched film on a quartz slide. TEM image (bottom, right, negatively stained with uranyl acetate) on a carbon-coated grid.

$$M_{s\eta} = (R/A_0)^{3/2} [s]^{3/2} [\eta]^{1/2} \quad (2)$$

where $[\eta]$ is the intrinsic viscosity value, A_0 is the hydrodynamic invariant value, and R is the gas constant. The values of M_{sf} and $M_{s\eta}$ are in satisfactory agreement and show that synthesized species belong to the macromolecular compounds. The determined M_{sf} values of 36,000 and 29,000 $\text{g}\cdot\text{mol}^{-1}$ correspond to 25 and 18 repeating units for **RuL1** and **RuL2**, respectively. Furthermore, viscosity measurements in DMA (containing 1 wt.% NH_4PF_6 to exclude a polyelectrolyte effect) allowed to estimate the intrinsic viscosity $[\eta]$ to be 90 and 80 $\text{cm}^3\cdot\text{g}^{-1}$ for **RuL1** and **RuL2**, respectively, which reflects a moderate rigidity of the polymer chains. When compared to Ru^{II} coordination polymers of linear and rigid ditopic terpyridines, these M and $[\eta]$ values are lower than reported by Rehahn et al. and comparable to the values reported by our group.^[4c,9c] The lower intrinsic viscosity can be attributed to a lower molar mass and/or a more flexible connectivity within this new π -conjugated backbone. Furthermore, it has been shown by Flood et al. that *bistridentate* complexes of tripy ligands offer more steric freedom with respect to interligand interactions and, therefore, might allow a stronger bending.^[7b]

In addition, for both polymers the persistence length (a) could be estimated using the classical relationships which connect the mean-square end-to-end distance ($\langle h^2 \rangle$) and the molar mass.^[14a] Accordingly, the persistence length of the polymer chains is $a > 6$ nm meaning that these structures may be considered as stiff polymer chains. Taking the obtained degrees of polymerization into account, the polymers have ca. 9 times of their persistence lengths. Given that 20 to 30 times of the persistence length is

needed to allow intramolecular ring closure,^[15] the metallopolymers thus are relatively rigid and should not have formed circular structures during synthesis.

3.3. Morphological Characterization

To gain insights into the nature of the metallo-supramolecular polymers in the solid state, several microscopic techniques were applied to investigate thin films (Figure 2). Large rod-like polymer structures were observed, which exhibit a length of 120 to 200 nm for **RuL1** and 100 to 150 nm for **RuL2**. The typical thickness measured by AFM is about 18 nm. These lateral dimensions are in the range of the tip size and, as a result of the convolution of the molecular structure with the AFM tip, the exact width of the rods cannot be determined. Nonetheless, inspection of the rod-like structures, in particular by amplitude imaging, revealed that the rods exhibit a substructure, which however cannot be clearly resolved due to the limited AFM resolution. Still, the height of the polymer strands could be estimated to be around 0.5 nm which correlates roughly with the Ru^{II} complex fragment laying on the surface, i.e. the flexible alkyl chains are not visible by the AFM tip. Furthermore, TEM images were acquired. Uranyl-acetate staining was performed to increase the contrast of the polymer structures. Here, the rod thickness could be determined to be around 12 nm. Unfortunately, also these measurements do not provide evidence if the rod-like structures are helically twisted. Still, the higher resolution revealed partial coiling and entangling of the polymeric structures. Taking the hydrodynamic results into account, it can be concluded that aggregates have formed since thickness and length are approximately three and five times, respectively, larger than the dimensions of an individual polymer chain. Furthermore, the results of the AFM and TEM imaging, namely the formation of rods as well as partial coiling and entangling, are consistent with the AUC results that gave the picture of a relatively rigid but still flexible polymer.

Although aggregation was observed in AFM and TEM images, the solubilizing alkyl chains still allowed solution processability and good film-forming properties. This was demonstrated by preparation of a smooth film by drop-casting of a concentrated DMA solution (ca. 5 $\text{mg}\cdot\text{mL}^{-1}$) on a quartz slide and subsequent evaporation. The thickness of the film was determined by scratching and revealed a thickness of 300 nm (**RuL1**) and 600 nm (**RuL2**) depending on the concentration of the solution (see Figure 2, S 27 and S 28).

3.4. Photophysical and Electrochemical Properties

The *bistripy* ligands featured large extinction coefficients and medium to high photoluminescence quantum yields (**L1**: $\Phi_{\text{PL}} = 0.53$, **L2**: $\Phi_{\text{PL}} = 0.97$, see Figure S 18). In comparison to **L1**, the absorption of **L2** is more intense and red-shifted due to the extension of the conjugated system; similarly the emission maximum is red-shifted for **L2**. The emission of both ligands features a vibronic structure. In contrast to **L2**, the emission of **L1** is weakened and red-shifted at higher concentrations (see Figure S 18) which is attributed to the presence of aggregates. Due to its low solubility, **L2** is expected to form aggregates as well, which apparently do not influence the emission since the fluorescence quantum yield is close to unity.

The electrooptical properties of the metallopolymers were investigated by UV-vis absorption and emission spectroscopy as well as by cyclic voltammetry and spectroelectrochemistry. For comparison, mononuclear Ru^{II} *bis*-complexes of unsubstituted tripy ligands (**5**) showed a reversible metal-based oxidation at 0.95 V and a quasi-reversible ligand-based reduction at -2.20 V against Fc/Fc⁺ in acetonitrile.^[7b,7d] Furthermore, a metal-to-ligand charge-transfer (MLCT) absorption is located at around 400 nm and no room-temperature emission is observable due to rapid radiationless deactivation via energetically low lying thermally accessible metal-centered triplet (³MC) states. In contrast, both polymers **RuL1** and **RuL2** showed a broad and intense MLCT transition at around 450 nm thus featuring a red shift of about 50 nm. Obviously, the conjugated spacer expands and stabilizes the tripy-centered lowest unoccupied molecular orbital (LUMO). Moreover, a weak emission at 700 nm ($\Phi_{\text{PL}} = 2 \cdot 10^{-5}$) was observed for metallopolymer **RuL1** at room temperature in solution that can be explained by a stabilization of the ³MLCT state by the π -conjugated spacer^[8,16] and/or an excited-state equilibrium with ³ $\pi\pi^*$ states.^[17] The electrochemical investigations (see Figure S 21 and S 22) revealed an irreversible oxidation process at 0.40 V that is located on the π -conjugated spacer since it only affects ligand-centered (LC) transitions in spectroelectrochemical measurements (see Figure S 23 and S 24). Unfortunately, a metal-based oxidation process could not be studied as it was not observed up to the DMA solvent cut-off at 1 V. On the other hand, four reduction waves could be observed for **RuL1** (-1.60 V, -1.85 V, -2.20 V, -2.45 V) while for **RuL2** two reductions were present (-1.78 V, -2.50 V). Compared with the model complex, the MLCT band of the metallopolymers was shifted from 400 nm to 450 nm which corresponds to 0.35 eV. Regarding the reduction potential of the model complex at -2.20 V, that was assigned to the population of tripy-centered π^* orbitals, the reduction around -1.80 V that is present for both metallopolymers is likewise assigned to be tripy-based. Further reduction

processes are located on the π -conjugated spacer as they are absent in the model complex.

4. Conclusions

Two new Ru^{II}-based metallopolymers of click-derived ditopic tridentate ligands possessing rigid, linear and π -conjugated spacers have been prepared and their properties have been investigated in solution as well as in the solid state, i.e. in thin films. The metallo-supramolecular materials exhibited relatively high molar masses and their moderate rigidity was concluded from hydrodynamic experiments. They allow for solution processability as well as film formation which – together with their optoelectronic properties, namely photogenerated charge-separated excited states – suggest their potential utilization in printable photovoltaic devices.

Supporting Information

Supporting Information is available from the Wiley Online Library or from the author.

Acknowledgements: Financial support by the *Fonds der Chemischen Industrie* (PhD scholarships for B.S. and C.F.), the *Dutch Polymer Institute* (technology area HTE), the *German Federal Ministry of Education and Research* (Excellence Research and Innovation in East Germany: PhoNa) and the *Thüringer Ministerium für Bildung, Wissenschaft und Forschung* (Grant No. B 514-09049: PhotoMic) is kindly acknowledged. The authors thank Dr. G. Festag for the size exclusion chromatography measurements.

Received: November 15, 2011; Revised: January 30, 2012; Published online: March 19, 2012; DOI: 10.1002/marc.201100782

Keywords: analytical ultracentrifugation; click chemistry; metallopolymers; ruthenium; supramolecular structures

- [1] J.-M. Lehn, *Angew. Chem. Int. Ed.* **1988**, *27*, 89.
- [2] a) P. R. Andres, U. S. Schubert, *Adv. Mat.* **2004**, *16*, 1043; b) R. Dobrawa, F. Würthner, *J. Polym. Sci., Part A: Polym. Chem.* **2005**, *43*, 4981; c) V. A. Friese, D. G. Kurth, *Coord. Chem. Rev.* **2008**, *252*, 199; d) V. A. Friese, D. G. Kurth, *Curr. Opin. Colloid Interface Sci.* **2009**, *14*, 81; e) C.-L. Ho, W.-Y. Wong, *Coord. Chem. Rev.* **2011**, *255*, 2469; f) M. Rehahn, *Acta Polym.* **1998**, *49*, 201; g) G. R. Whittell, M. D. Hager, U. S. Schubert, I. Manners, *Nat. Mater.* **2011**, *10*, 176; h) G. R. Whittell, I. Manners, *Adv. Mater.* **2007**, *19*, 3439; i) K. A. Williams, A. J. Boydston, C. W. Bielawski, *Chem. Soc. Rev.* **2007**, *36*, 729; j) C.-A. Fustin, P. Guillet, U. S. Schubert, J.-F. Gohy, *Adv. Mater.* **2007**, *19*, 1665.
- [3] U. S. Schubert, A. Winter, G. R. Newkome, in *Terpyridine-Based Materials*, Wiley-VCH Verlag GmbH & Co. KGaA, **2011**, pp. 65.

- [4] a) M. Chiper, R. Hoogenboom, U. S. Schubert, *Macromol. Rapid Commun.* **2009**, *30*, 565; b) A. Wild, A. Winter, F. Schlütter, U. S. Schubert, *Chem. Soc. Rev.* **2011**, *40*, 1459; c) S. Kelch, M. Rehahn, *Macromolecules* **1999**, *32*, 5818; d) D. G. Kurth, M. Higuchi, *Soft Matter* **2006**, *2*, 915; e) A. Winter, C. Friebe, M. Chiper, M. D. Hager, U. S. Schubert, *J. Polym. Sci., Part A: Polym. Chem.* **2009**, *47*, 4083; f) S. Schmatloch, A. M. J. van den Berg, A. S. Alexeev, H. Hofmeier, U. S. Schubert, *Macromolecules* **2003**, *36*, 9943.
- [5] a) S. R. Amrutha, M. Jayakannan, *J. Phys. Chem. B* **2008**, *112*, 1119; b) E. Tekin, E. Holder, V. Marin, B.-J. de Gans, U. S. Schubert, *Macromol. Rapid Commun.* **2005**, *26*, 293.
- [6] H. C. Kolb, M. G. Finn, K. B. Sharpless, *Angew. Chem. Int. Ed.* **2001**, *40*, 2004.
- [7] a) N. Chandrasekhar, R. Chandrasekar, *J. Org. Chem.* **2010**, *75*, 4852; b) Y. Li, J. C. Huffman, A. H. Flood, *Chem. Commun.* **2007**, 692; c) R. M. Meudtner, M. Ostermeier, R. Goddard, C. Limberg, S. Hecht, *Chem. Eur. J* **2007**, *13*, 9834; d) B. Schulze, C. Friebe, M. D. Hager, A. Winter, R. Hoogenboom, H. Görls, U. S. Schubert, *Dalton Trans.* **2009**, 87.
- [8] a) E. A. Medlycott, G. S. Hanan, *Chem. Soc. Rev.* **2005**, *34*, 133; b) J. P. Sauvage, J. P. Collin, J. C. Chambron, S. Guillerez, C. Coudret, V. Balzani, F. Barigelletti, L. De Cola, L. Flamigni, *Chem. Rev.* **1994**, *94*, 993.
- [9] a) H. Padhy, D. Sahu, I. H. Chiang, D. Patra, D. Kekuda, C.-W. Chu, H.-C. Lin, *J. Mater. Chem.* **2011**, *21*, 1196; b) P. D. Vellis, J. A. Mikroyannidis, C.-N. Lo, C.-S. Hsu, *J. Polym. Sci., Part A: Polym. Chem.* **2008**, *46*, 7702; c) A. Wild, F. Schlütter, G. M. Pavlov, C. Friebe, G. Festag, A. Winter, M. D. Hager, V. Cimrová, U. S. Schubert, *Macromol. Rapid Commun.* **2010**, *31*, 868.
- [10] H. Benmansour, R. D. Chambers, G. Sandford, D. S. Yufit, J. A. K. Howard, *ARKIVOC* **2007**, *XI*, 46.
- [11] S. Kelch, M. Rehahn, *Chem. Commun.* **1999**, 123.
- [12] A. Cifferi, in *Supramolecular Polymers*, Marcel Dekker, New York **2000**.
- [13] G. M. Pavlov, D. Amorós, C. Ott, I. I. Zaitseva, J. Garcia de la Torre, U. S. Schubert, *Macromolecules* **2009**, *42*, 7447.
- [14] a) V. N. Tsvetkov, P. N. Lavrenko, S. V. Bushin, *J. Polym. Sci. Polym. Chem.* **1984**, *22*, 3447; b) V. N. Tsvetkov, *Rigid-chain Polymers. Hydrodynamic and Optical Properties in Solution.*, Consultants Bureau, New York **1989**.
- [15] T. Odijk, *Macromolecules* **1983**, *16*, 1340.
- [16] a) A. Juris, V. Balzani, F. Barigelletti, S. Campagna, P. Belser, A. von Zelewsky, *Coord. Chem. Rev.* **1988**, *84*, 85; b) E. A. Medlycott, G. S. Hanan, *Coord. Chem. Rev.* **2006**, *250*, 1763.
- [17] R. Siebert, C. Hunger, J. Guthmüller, F. Schlütter, A. Winter, U. S. Schubert, L. González, B. Dietzek, J. Popp, *J. Phys. Chem. C* **2011**, *115*, 12677.

Publication A9: “Linear metallopolymers from ruthenium(II)-
2,6-di(quinolin-8-yl)pyridine complexes by
electropolymerization – Formation of redox-stable and
emissive films”

Christian Friebe, Helmar Görls, Michael Jäger, Ulrich S. Schubert

Eur. J. Inorg. Chem. **2013**, 4191–4202.

Reprinted with permission from: WILEY-VCH Weinheim (Copyright 2013)

DOI:10.1002/ejic.201300359

Linear Metallopolymers from Ruthenium(II)-2,6-di(quinolin-8-yl)pyridine Complexes by Electropolymerization – Formation of Redox-Stable and Emissive Films

Christian Friebe,^[a,b] Helmar Görls,^[c] Michael Jäger,^{*[a,b]} and Ulrich S. Schubert^{*[a,b]}

Keywords: Electropolymerization / Ruthenium / N ligands / Thin films / Density functional calculations

Two rodlike ruthenium(II) complexes of 2,6-di(quinolin-8-yl)pyridines (dqp) were synthesized and possess a pair of 2-thienyl moieties attached to the 4-positions of the quinoline units of one ligand or at the 4-positions of the pyridine rings of both ligands. The heteroleptic and homoleptic complexes were characterized by UV/Vis absorption and emission spectroscopy as well as electrochemical and X-ray crystallographic means. The subsequent electropolymerization of the thiophene units led to the controlled formation of thin solid

films onto electrode surfaces as proven by X-ray photoelectron spectroscopy (XPS). The electrochemical analysis of the films was complemented by UV/Vis spectroscopy and UV/Vis/NIR spectroelectrochemistry, which revealed their stability towards oxidation, red emission, and reversible redox switching of their optical properties. Density functional theory (DFT) calculations were executed on the monomer complexes and respective dimeric systems to gain insight into their spectroscopic and electrochemical properties.

Introduction

Ruthenium(II) polypyridyl complexes are favorable building units for photophysical applications, in particular as sensitizers within light-harvesting devices, because of their ability to undergo efficient and long-lived light-induced charge separation.^[1] The prototypical Ru(bpy)₃²⁺ (bpy = 2,2'-bipyridine) shows a long excited-state lifetime of 860 ns, which allows subsequent redox reactions to occur.^[2] However, the tris(bidentate) ligand assembly can lead to the formation of enantiomeric and diastereomeric mixtures and impedes the ideal *trans* arrangement of donor and acceptor moieties with maximal separation to prevent back-reactions.^[3] On the other hand, the bis(tridentate) congener Ru(tpy)₂²⁺ (tpy = 2,2':6',2''-terpyridine) allows for the stringent *trans* alignment of the substituents,^[4] but possesses a very short excited-state lifetime of 0.25 ns, which

precludes efficient utilization of the excited states.^[5] The observed short lifetimes are caused by the efficient interaction of the triplet metal-to-ligand charge-transfer (³MLCT) excited state with the triplet metal-centered (³MC) states and their fast and radiationless deactivation towards the singlet ground state within Ru(tpy)₂²⁺ and analogous systems.^[6]

The different strategies to overcome this limitation mainly focus on the enlargement of the ³MLCT–³MC energy gap by stabilization of the ³MLCT state, destabilization of the ³MC state, or both. The most promising approaches are based on the incorporation of strong electron donors by cyclometalation^[6a,7] or N-heterocyclic carbenes^[8] and structural modifications,^[9] whereas the attachment of additional energy-storing chromophores only enhances the apparent lifetime.^[10] Hammerström et al. demonstrated that the utilization of tridentate ligands with a bite angle of 180° leads to a less distorted octahedral complex geometry, which causes a decreased admixing of metal d orbitals into the lowest unoccupied molecular orbital (LUMO). Thus, the orbital overlap between the ligand-centered LUMOs and the e_g orbitals is diminished and a deactivation via the ³MC state becomes less probable.^[6b] Applying this concept, the family of substituted Ru(dqp)₂²⁺-based complexes [dqp = 2,6-di(quinolin-8-yl)pyridine] combines excellent properties for light-harvesting applications with an excited-state lifetime in the μs time scale.^[11]

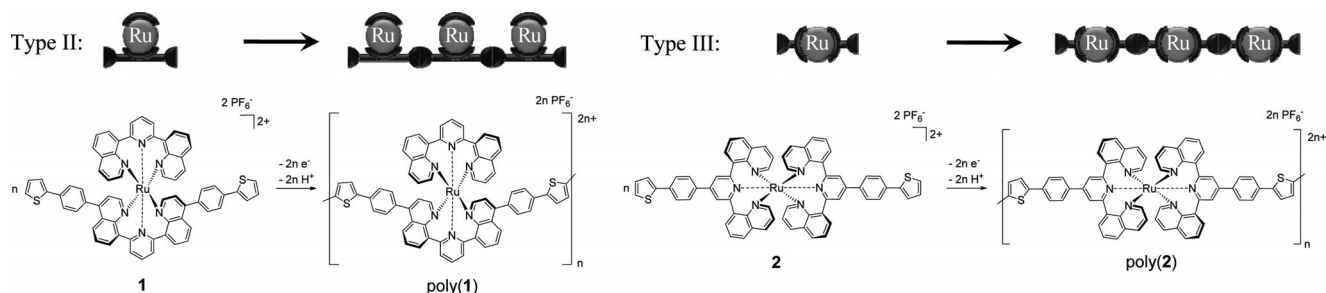
The subsequent incorporation into photovoltaic devices requires thin-film processing of the respective sensitizers, that is, the deposition of a layer that is thin and homogen-

[a] Laboratory of Organic and Macromolecular Chemistry (IOMC), Friedrich Schiller University Jena, Humboldtstr. 10, 07743 Jena, Germany
E-mail: michael.jaeger.iomc@uni-jena.de
ulrich.schubert@uni-jena.de
Homepage: <http://www.schubert-group.com/>

[b] Jena Center for Soft Matter (JCSM), Friedrich Schiller University Jena, Philosophenweg 7, 07743 Jena, Germany

[c] Laboratory of Inorganic and Analytic Chemistry (IAAC), Friedrich Schiller University Jena, Lessingstr. 8, 07743 Jena, Germany

Supporting information for this article is available on the WWW under <http://dx.doi.org/10.1002/ejic.201300359>.



Scheme 1. Type II and type III arrangement of metal-containing polymers as applied for $\text{Ru}(\text{dqp})_2^{2+}$ complexes in this contribution.

ous enough to allow efficient charge transport onto an electrode surface. For this purpose, a convenient and widespread technique is the electrochemical polymerization of a metal-containing monomer solution to enable the direct preparation of an insoluble polymeric coating on the surface^[12] and, thus, numerous ruthenium(II) polypyridyl-type complexes have been processed by electropolymerization.^[13] In this contribution, we present two $\text{Ru}(\text{dqp})_2^{2+}$ complexes featuring 2-thienyl units linked either to the quinoline (**1**) or the pyridine moieties (**2**) and their subsequent incorporation into a photoactive film by electropolymerization (Scheme 1). The two investigated substitution patterns enable a lateral attachment to the polymer main chain or a direct incorporation into the backbone (metal-containing polymers of type II and III, respectively, Scheme 1)^[14] with equal spatial separation of the ruthenium(II) centers. First density functional theory (DFT) and time-dependent DFT (TD-DFT) calculations were performed to explore the structural, spectroscopic, and electrochemical properties of the designed systems. The second part describes the synthesis and characterization of the monomer complexes as well as the resulting polymer films by UV/Vis spectroscopy and cyclic voltammetry. Additionally, X-ray crystallographic analysis for the monomers and UV/Vis/NIR spectroelectrochemical experiments and X-ray photoelectron spectroscopy (XPS) studies of the obtained polymer films were executed.

Results and Discussion

DFT Calculations

DFT and TD-DFT calculations were performed to investigate the electronic structures and transitions of the two different conjugation paths. Firstly, the geometries of the complexes were optimized with the given charge and multiplicity and subsequently confirmed by vibrational analysis. The optical properties were further investigated by TD-DFT to obtain absorption spectra. In addition to the monomers, the respective dimetallic complexes were investigated to explore the effect of dimerization on the electronic structure (for optimized geometries, see Supporting Information).

The structural features of the complexes closely resemble those previously obtained for the parent $\text{Ru}(\text{dqp})_2^{2+}$ with a different basis set (see Supporting Information).^[11b] Notably, both substitution patterns differ in the degree of coplanarity (dihedral angle) between the dqp and the outer phenyl ring, which suggests an increased interaction with the dqp-based molecular orbitals (MOs) from **1** (49°) to **2** (30°). However, no significant differences between the phenyl and thiophene twists were observed (a comparison to the experimental data is provided below). The related dimeric complexes display very similar structural parameters and have identical Ru–N bond lengths and torsional angles. The twist between the phenyl and thiophene unit is slightly smaller, whereas the torsion angle between the bridging thiophene units is 10° . On the basis of the dihedral angles, phenyl–bithiophene–phenyl conjugation within the bridge is reasonable ($<22^\circ$) and also allows coupling to the $\text{Ru}(\text{dqp})_2^{2+}$ fragments ($<49^\circ$).

The frontier MO energies and respective contributions of the involved fragments of the complexes in the ground state are depicted in the Supporting Information. Importantly, the highest occupied molecular orbitals (HOMO and HOMO–1) are mainly metal-based, whereas the nearby orbitals (HOMO–2 and HOMO–3) show significant admixing of the thiophene units. The lowest unoccupied molecular orbitals (LUMO to LUMO+5) are primarily localized on the dqp ligands. For the asymmetric complex **1**, the contribution of the thiophene-substituted dqp fragment to the LUMO and LUMO+1 is larger than that of nonfunctionalized dqp, whereas the opposite holds for the LUMO+2 and LUMO+3. For the symmetric complex **2**, the contribution of each dqp ligand to the LUMOs is equal because of the symmetry of the molecule. Upon dimerization, the orbital energy of the bithiophene fragments is significantly lowered and constitutes the new HOMO with only minor admixing of d orbitals from both ruthenium centers. However, the lower occupied orbitals remain metal-based. The LUMOs of the dimers are ligand-based and display a higher contribution of the dqp fragment connected to the bridge. The electronic structure of the complexes can be qualitatively summarized as follows: (1) The HOMO manifold is essentially ruthenium-based, (2) the dimers show a delocalized HOMO on the bridge with minor contributions of both metal centers, (3) the LUMO manifold is ligand-

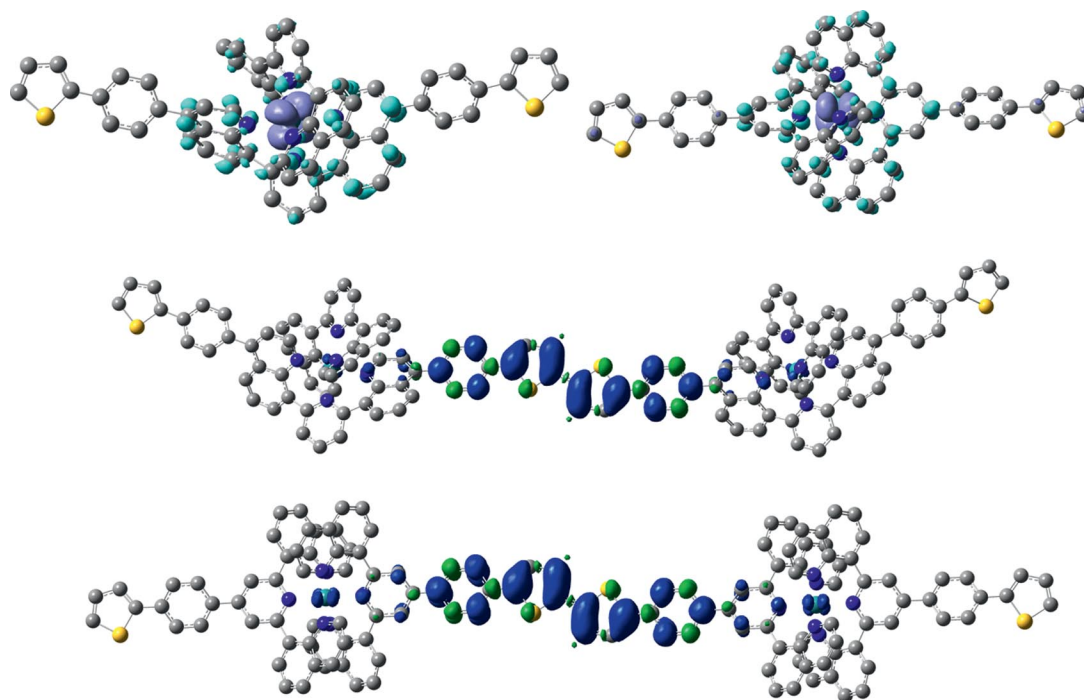


Figure 1. EDDM plots of the lowest-energy ground state absorptions (isovalue = 0.0016, decrease in blue, increase in cyan) of **1** (top left) and **2** (top right). Electron density from spin-density difference calculations of dimer(**1**) (middle) and dimer(**2**) (bottom, isovalue = 0.001) in the singly oxidized state.

based throughout the series and shows a larger contribution from the substituted dqp ligand. However, the computational results of the HOMOs of the dimers should be interpreted with care owing to the well-known artificial stabilization of delocalized states.^[15]

The vertical excitations were investigated by TD-DFT calculations (see Supporting Information). Electron-density difference maps (EDDM) are often used to visualize electronic redistribution,^[16] in particular if the discussion is complicated by many contributing MOs. The monomers **1** and **2** display low-energy transitions with MLCT character (Figure 1), whereas the higher-energy transitions revealed an extended delocalization across the aromatic units and an increased admixing of thiophene-based orbitals. Furthermore, the EDDM analysis shows the principle effect of the substitution pattern. The alignment of the thiophene- and metal-based d orbitals leads to higher oscillator strengths of the respective transitions. For complex **1**, this combination is less favorable and the strong MLCT transition is found at 505 nm, whereas this transition in complex **2** shows a pronounced redshift to 536 nm, in line with the lower dihedral angle between the dqp fragment and the phenyl ring (see above).

The dimers display a similar behavior, except for an additional very intense intraligand charge-transfer (ILCT) transition of the bis(thiophene). For dimer(**1**), the asymmetric substitution pattern induces a localization on the quinoline unit connected to the bridge, whereas the accepting LUMO of dimer(**2**) is almost evenly distributed over both dqp ligands. This behavior is consistent with the more ef-

ficient conjugation through the metal-based d orbitals in dimer(**2**), as described above.

The changes in the electronic structures of the complexes upon oxidation were examined by spin-density difference plots (see Supporting Information). Upon oxidation of the monomeric complexes, the first electron is removed from a metal-centered orbital, whereas the second one originates from one 4-(2-thienyl)phenyl unit. Hence, the intended redox-mediated coupling becomes reasonable upon a second oxidation, according to the accepted mechanism involving an oxidized thiophene radical.^[17] In contrast, both dimers show first oxidations that reside primarily on the bridge with minor contributions from both ruthenium centers. The second and third oxidation processes are localized on the individual ruthenium centers (see Supporting Information).

Notably, the order of the successive oxidation steps may be reversed, owing to the discussed artificial stabilization of delocalized states.^[15] However, the observed low energetic differences between the metal- and bridge-based orbitals as well as their spatial overlap suggest significant interactions between them.

The combined computational results of the monomeric and dimeric structures show their promising potential in electropolymerized films. As the polymerization process is expected to start upon the oxidation of the thiophene unit, the (easier) ruthenium-centered oxidation may serve as a valuable tool to monitor the course of the electropolymerization. The MO analysis of the dimeric structures reveals an extended delocalization across the bridge, that is, a weak communication between the two metal centers in the oxid-

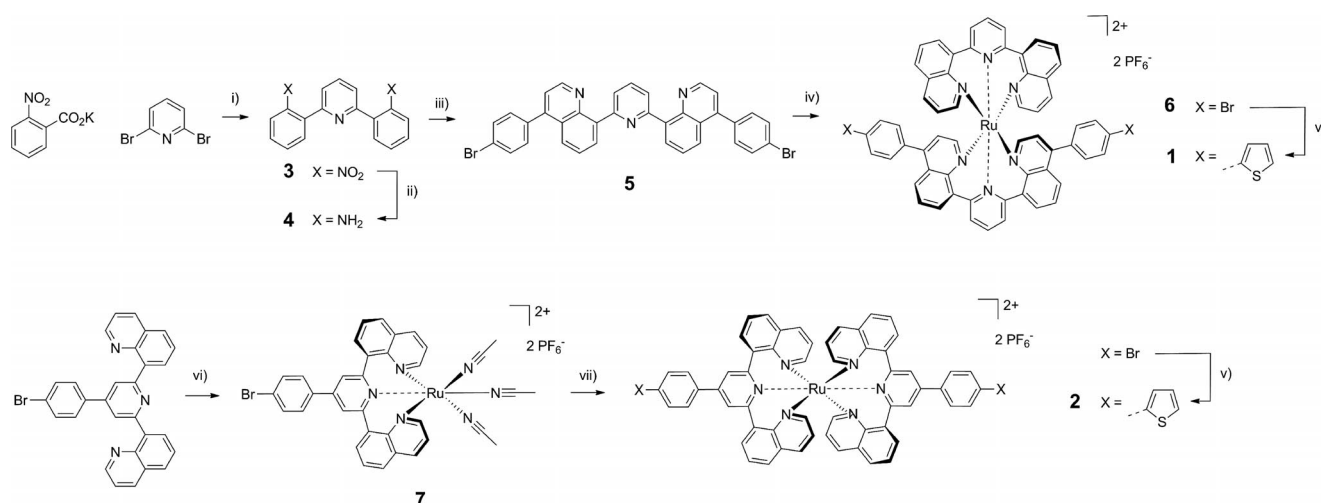
ized state, which is beneficial for efficient charge migration within the films. However, a more detailed analysis, for example, modeling of polymeric structures, is beyond the scope of this study.

Syntheses of Monomers

The synthetic strategy towards the electropolymerizable thiophene-equipped complexes is shown in Scheme 2 and is based on the synthesis of the bromo-functionalized ligands, followed by the stepwise coordination to ruthenium, and the introduction of the thiophene moieties in the final step. This sequence was chosen to prevent any side reactions of the thiophene units owing to the harsh conditions during the coordination steps and to enable easy removal of the small amounts of the inevitably formed facial isomers by crystallization. In addition, this route also explores the versatility of the intermediate bromo complex, for example, for subsequent cross-coupling reactions. To construct the framework of the quinoline-functionalized ligand, the original route by C–C coupling was adjusted to tolerate the reactive peripheral bromo substituents. In this regard, 2-nitrobenzoic acid represents a valuable quinoline precursor, as shown by the efficient decarboxylative cross coupling with a variety of aryl halides.^[18] To suppress the protonation of the formal C nucleophile after decarboxylation, the potassium salt was used instead.^[19] The twofold coupling with 2,6-dibromopyridine gave **3** (48% yield), which was subsequently reduced to the corresponding bis(aniline) **4** by using hydrazine hydrate and palladium on charcoal. Finally, the quinoline ring formation was achieved by a twofold Skraup reaction with a commercial bromophenyl-substituted C₃ synthon.^[20] Although this route gave only a low yield (15%) of bis(bromophenyl)-substituted dqp (**5**), it is comparable with related single Skraup reactions and bene-

fits from the direct access to the bis-functionalized ligand. The related pyridine-substituted ligand 8,8'-[4-(4-bromophenyl)pyridine-2,6-diyl]diquinoline was synthesized by a Kröhnke reaction of acetylquinoline and *p*-bromobenzaldehyde as described in the literature.^[21] The next step involved the coordination to a suitable ruthenium precursor and separation from facial isomers^[11a] by fractionalized crystallization. Heating ligand **5** with [Ru(dqp)(CH₃CN)₃](PF₆)₂ afforded complex **6** in excellent yield (95%). The subsequent conversion to the thiophene-functionalized complex (**1**) was quantitative without any detectable debromination according to the ¹H NMR signal intensity ratios of the thiophene- and the quinoline-related protons. The related homoleptic complex **2** was synthesized in a similar stepwise fashion; the initial reaction of RuCl₃ with 8,8'-[4-(4-bromophenyl)pyridine-2,6-diyl]diquinoline was followed by a reduction and halide abstraction with Ag^I to yield the intermediate complex **7**. The next step is the coordination of a second equivalent of 8,8'-[4-(4-bromophenyl)pyridine-2,6-diyl]diquinoline; however, some debromination occurred and isolation of the bis(bromo) complex by chromatography and crystallization failed. We tentatively assign this failure to the small structural difference between the H and Br substituents among the complexes. Hence, the crude material was converted into the thiophene-equipped complexes, which were successfully separated by crystallization. The origin of the unexpected debromination is unknown and the isolated yields of **2** are lower (38% over both steps).

The ¹H NMR spectra of **1** and **2** show the characteristic pattern of the coordinated ligands in the aromatic region (Figure 2) and are supported by 2D NMR spectroscopic data (see Supporting Information). The spectrum of the asymmetric complex **1** has two overlapping sets of signals for each ligand. However, the subunits can be identified according to their characteristic chemical shifts and coupling



Scheme 2. Schematic representation of the synthetic route towards the heteroleptic complex **1** (top) and the homoleptic complex **2** (bottom): (i) CuI, Pd/C, 1,10-phenanthroline, *N*-methyl-2-pyrrolidinone (NMP), 180 °C, 15 h, 48%; (ii) Pd/C, hydrazine hydrate, EtOH, 80 °C, 1 h, 86%; (iii) 1-(4-bromophenyl)-3-chloropropan-1-one, arsenic pentoxide, phosphoric acid, 140 °C, 2 h, 15%; (iv) [Ru(dqp)(CH₃CN)₃](PF₆)₂, ethylene glycol, 140 °C, 14 h, 95%; (v) thiophen-2-ylboronic acid, Pd(dba)₂, S-PHOS, CH₃CN/H₂O, potassium carbonate, 100 °C, 16 h, 92 (**1**) and 55% (**2**); (vi) 1. RuCl₃·3H₂O, EtOH, 115 °C, 13 h; 2. AgNO₃, CH₃CN/EtOH/H₂O, 90 °C, 17 h, then NH₄PF₆, 60%; (vii) 8,8'-[4-(4-bromophenyl)pyridine-2,6-diyl]diquinoline, ethylene glycol, 140 °C, 14 h, 68%.

patterns, in agreement with the literature.^[11a,21] The proton in the 3-position of the quinoline unit is noticeable as a doublet in ligand **5** or as a double doublet in unsubstituted dqp. The protons in the 4-position of the pyridine rings appear as overlapping triplets owing to a small chemical shift difference. Two of the thiophene protons are well resolved and can be used to validate the thiophene content. A direct comparison by means of the adjacent phenyl ring is complicated owing to superposition with the remaining signals. Complex **2** shows a less complicated spectrum owing to the axial symmetry of the molecule. Similar features of the quinoline and thiophene units are present, whereas the 3- and 5-protons of the pyridine rings appear as singlets in the spectrum.

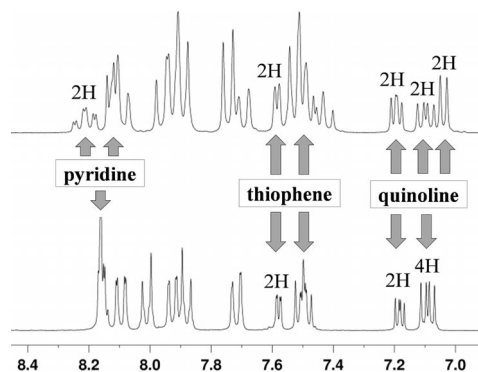


Figure 2. ¹H NMR spectra (CD₃CN, 300 MHz, expanded region) of **1** (top) and **2** (bottom) with assignment of the characteristic protons.

X-ray Crystallography

The structures of the complexes with both substitution patterns were also investigated by X-ray crystal analysis (Figure 3 and Table 1). All attempts to crystallize complex **1** gave only plates, and the quality of the collected X-ray data was not sufficient to allow discussion of the structure beyond the configuration and conformation (see Supporting Information). Hence, the related bromo precursor **6** was also investigated to supplement the structural discussion with respect to **2**. The geometrical features of the coordination site, that is, the mutual arrangement of the N and Ru atoms, are preserved in comparison to the parent Ru-(dqp)₂²⁺. Reinvestigation of the available X-ray data of Ru(dqp)₂²⁺ showed a large deviation between the two com-

plexes within the unit cell,^[11b] which is seen in the large absolute difference of the respective bond lengths. However, the average value agrees well with the numbers derived from complexes **6** and **2**. In general, the Ru–N bond length of the central pyridine ring is shortened by 0.026 Å compared with that of the outer quinoline unit. A similar behavior was found for the calculated structures, despite the known typical overestimation of the calculated bond lengths (+0.04 Å). The internal N–Ru–N angles are all close to the ideal octahedral coordination, as are the dihedral angles between the quinoline and pyridine unit as calculated from their respective mean planes.

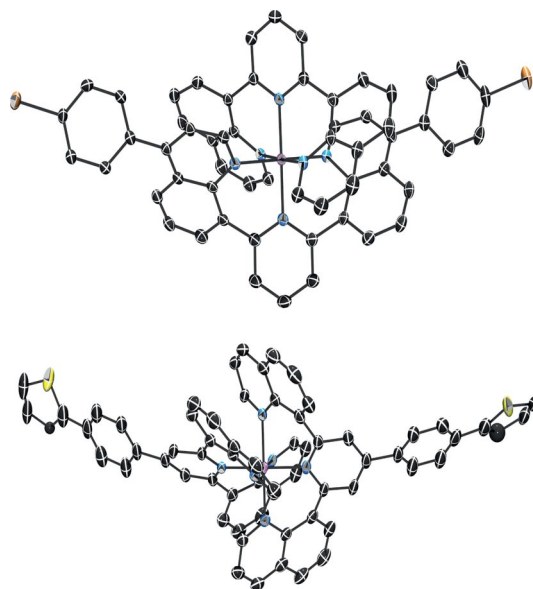


Figure 3. Top: Solid-state structure of **6** (ellipsoids drawn at 50% probability, hydrogen atoms are omitted for clarity). Bottom: Solid-state structure of **2** (ellipsoids drawn at 50% probability, hydrogen atoms are omitted and only one conformation of the thiophene units is displayed for clarity, spherical carbon atoms are isotropic).

The numbers agree well with those of the computed structures (37°); somewhat larger variations were found for **2**. This observation is tentatively attributed to crystal packing effects and indicates a certain flexibility of the coordinated ligand. This distortion is also visible from the “bending” away from the C₂ axis of the molecule in **2** (Figure 3). In addition, two conformations of the thiophene unit with respect to the neighboring phenyl group were found in the solid state and arise from the very similar steric demand

Table 1. Solid-state structural data for Ru(dqp)₂²⁺, **6**, and **2**.

| Compound | Ru–N ^[a] [Å] | | dqp | | N–Ru–N [°] | | Torsion angle ^[c] [°] | | |
|---|---|-------------------|-----------------|-------------------|------------|---------|----------------------------------|-------|---------------------|
| | dqp–thiophene ^[b] N ^{py} | N ^{quin} | N ^{py} | N ^{quin} | Adjacent | Axial | py–quin | py–ph | ph–tph |
| Ru(dqp) ₂ ²⁺ ^[d] | – | – | 2.034 (0.030) | 2.063 (0.050) | 88–92 | 176–180 | 35–40 | – | – |
| 6 | 2.036 (–) | 2.073 (0.002) | 2.039 (–) | 2.070 (0.005) | 89–90 | 179–180 | 37–41 | 46–47 | 4–33 ^[e] |
| 2 | 2.028 (–) | 2.064 (0.007) | – | – | 89–91 | 179–180 | 29–44 | 26 | 13 |

[a] Numbers in parentheses are the absolute differences between the experimental minimum and maximum values. [b] Thiophene-containing ligand {i.e., **3** or 8,8′-[4-(4-bromophenyl)pyridine-2,6-diyl]diquinoline}. [c] Calculated angles spanned by the mean planes defined by all heteroatoms of the aromatic unit (py = pyridine, quin = quinoline, ph = phenyl, tph = thiophene). [d] Calculated from the crystallographic data (average of both complexes of the unit cell) from ref.^[11b] [e] Data taken from the structural motif of **1**.

after a 180° rotation along the connecting C–C bond. The structural motif of **1** displays a similar torsion angle between the pyridine and phenyl rings (45°) as that in **6**, but a large variation for the phenyl and thiophene unit (4 and 33°). The average experimental values agree very well with the DFT calculations; however, the larger numerical variations, for example, between the pyridine and quinoline units and the peripheral aromatic units, may be induced by the crystal packing (see Supporting Information).

Photophysical and Electrochemical Characterization of Monomers

The monomeric complexes were further characterized by UV/Vis spectroscopy (Figure 4 and Table 2). The absorption spectrum of the heteroleptic complex **1** shows characteristic bands between 400 and 600 nm, which are assigned to MLCT transitions. Complex **2** exhibits similar absorption bands, but displays a pronounced shoulder at longer wavelength and an additional peak at 425 nm. The experimental absorption data are in very good agreement with the DFT results (see also the electronic transitions in the DFT Calculations section). The UV/Vis emission measurements revealed structureless room-temperature emission bands at 698 (**1**) and 678 nm (**2**) with Stokes shifts of 4900 and 3300 cm⁻¹, respectively, which indicate significant differences between the two conjugation pathways in the emissive excited states. Furthermore, photoluminescence quantum yields (Φ_{PL}) of 0.8 and 3.1% for **1** and **2**, respectively, could be determined in deaerated solutions at room temperature. The excitation spectra support the assignments

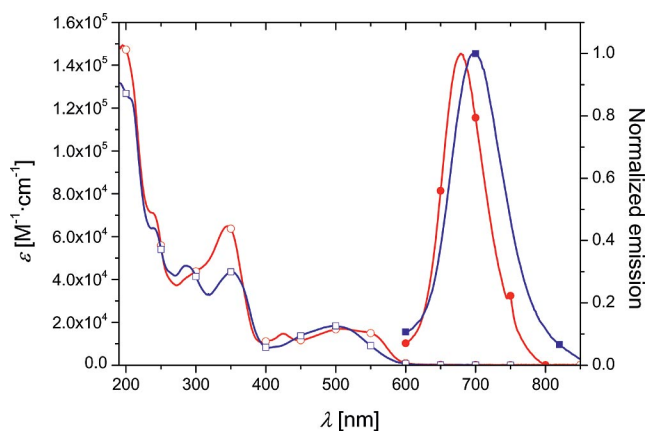


Figure 4. UV/Vis absorption (hollow symbols) and emission (filled symbols) spectra of the monomeric complexes **1** (blue) and **2** (red) (10⁻⁶ M in CH₃CN).

Table 2. UV/Vis spectroscopic properties and electrochemical data of the monomer complexes (in CH₃CN, 10⁻⁶ M for UV/Vis spectroscopy, 10⁻⁴ M with 0.1 M Bu₄NPF₆ for electrochemistry).

| | λ_{Abs} [nm] (ϵ [10 ³ M ⁻¹ cm ⁻¹])[^a] | λ_{Em} [nm] | Φ_{PL} [^b] [%] | $E_{1/2}^{[c]}$ [V] ($i_{\text{pa}}/i_{\text{pc}}$, ΔE_{p} [mV]) |
|----------|---|----------------------------|---|---|
| | | | | $2^+ \rightarrow 3^+$ / $2^+ \rightarrow 1^+$ |
| 1 | 521s (16.6), 500 (18.5), 350 (43.9), 285 (46.4) | 698 | 0.8 | 0.70 (1.05, 70) / -1.68 (0.94, 79) |
| 2 | 553s (15.0), 507 (17.1), 425 (14.7), 345 (64.7), 290 (41.7) | 678 | 3.1 | 0.67 (1.06, 68) / -1.70 (0.90, 73) |

[a] s = shoulder. [b] Measured by using [Ru(dqp)₂](PF₆)₂ (Φ_{PL} = 2% in MeOH/EtOH, 1:4) as reference.^[11b] [c] Measured vs. Fc⁺/Fc.

and agree with the reported data of the parent Ru(dqp)₂²⁺ complex.^[11b]

Cyclic voltammetric (CV) measurements (Table 2 and Supporting Information) showed reversible first oxidations at 0.70 V vs. Fc⁺/Fc for **1** and 0.67 V for **2**, which are attributed to single-electron Ru^{III}/Ru^{II} redox processes. A second, irreversible oxidation wave was observed at ca. 1.3 V for both complexes and is assigned to the formation of thiophene radical moieties. Furthermore, the first reduction signals at ca. -1.70 V featured reversible behavior for both complexes.

The optical changes of **1** and **2** upon oxidation were investigated by UV/Vis/NIR spectroelectrochemistry. Firstly, a decrease of the MLCT absorption band at 500 nm was observed as well as the formation of a broad absorption band between 600 and 1100 nm featuring several unassigned low-energy transitions from lower-lying occupied orbitals to the metal-based singly occupied molecular orbital (SOMO, see the Supporting Information). These results are in line with those for the parent Ru(dqp)₂²⁺ and are further discussed with regard to the electropolymerized films (see below).

Electropolymerization

Complex **1** was electropolymerized in acetonitrile containing 5 vol.-% BF₃·OEt₂ and 0.1 M Bu₄NPF₆ as conductive electrolyte, according to the proposed reaction in Scheme 1. The electropolymerization was not possible in pure acetonitrile/Bu₄NPF₆. Hence, the Lewis acid boron trifluoride diethyl etherate was used as it interacts with the aromatic system of the thiophene and reduces its aromaticity and, thus, leads to a lowered oxidation potential for the thiophene moieties and enables electropolymerization.^[22] The polymerization was conducted potentiodynamically by cycling between -0.5 and 1.7 V vs. Fc⁺/Fc; the thiophene moieties are oxidized at ca. 1.2 V to form reactive thienyl cation radicals.^[17] Figure 5 shows the development of the cyclic voltammogram over the first 50 cycles: It exhibits a well-defined growth of the characteristic electrochemical response at 0.7 V, and the signal corresponding to oxidation of the mono-thiophene decreases over the first cycles owing to the consumption of monomeric complexes near the electrode surface. Notably, a small cathodic peak at ca. 0.9 V occurs after two cycles and is tentatively assigned to the reduction of oxidized thiophene moieties, which may originate from trapped units within the (formed) film or from

unreacted units owing to a decrease in the rate of oxidative dimerization as the monomer is depleted. The increase of the peak current corresponding to the ruthenium(II)- and/or bis(thiophene) oxidation shows a slope change around the fifteenth cycle, most likely because of the complete coverage of the electrode surface with polymer, and, thus, a decreased charge transport, which causes a diminished polymerization rate.^[23]

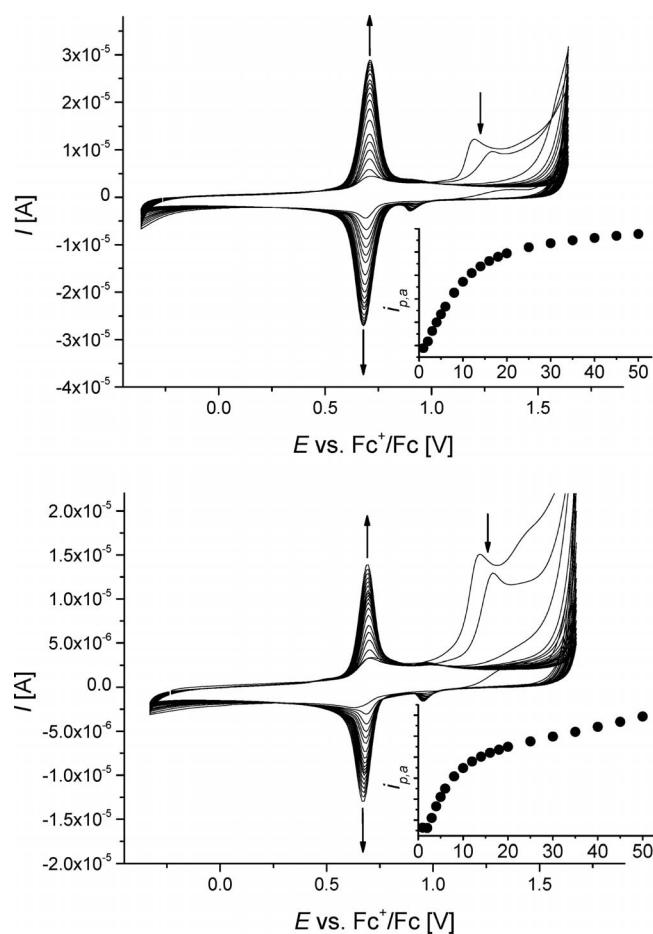


Figure 5. First 50 CV cycles of the electropolymerization of **1** (top) and **2** (bottom) on a glassy carbon disk electrode. Insets: Peak current increase at 0.70 V with cycle number (10^{-4} M in CH_3CN with 5 vol.-% $\text{BF}_3\cdot\text{OEt}_2$ and 0.1 M Bu_4NPF_6).

Likewise, electropolymerization of homoleptic **2** was performed and monitored by recording the respective cyclic voltammograms (Figure 5). As for the heteroleptic counterpart, a decrease of the current slope is observable at around the fifteenth cycle, but is less pronounced than for **1**. However, further studies are required to reveal the effect of other factors, such as counterion diffusion and charge mobility, on the film growth.

The elemental composition of the deposited films on indium tin oxide (ITO) coated glass substrates was investigated by X-ray photoelectron spectroscopy (XPS, see Supporting Information). Analysis of the spectra revealed the signals for the expected characteristic elements (namely, ru-

thenium, carbon, nitrogen, and sulfur) as well as Ru/S ratios of 1:2.1 and 1:1.9 for poly(**1**) and poly(**2**), respectively, consistent with the theoretical value.

The obtained CV data prove a successful electrochemical polymerization process and show a continuous growth of the peak current of the redox wave of the ruthenium(II) complex. This is attributed to deposition of the complex moieties and is accompanied by the disappearance of the thienyl-related signal, which is assigned to irreversible consecutive reactions of the formed thienyl radical cations, namely coupling reactions to generate oligomeric and polymeric chains. The utilization of boron trifluoride diethyl etherate, which is known to enhance the oxidative electropolymerization ability of aromatics by lowering of the redox potential, was necessary to enable the polymerization process.

Electrochemical and Photophysical Characterization of the Polymers

The films were rinsed with pure solvent to remove soluble monomer species after electropolymerization, and the coated working electrodes were immersed in fresh solvent with 0.1 M Bu_4NPF_6 and showed no dissolution at all. The electrochemical and photophysical data are summarized in Table 3. Figure 6 shows cyclic voltammograms of the oxidation of the polymers at different scan rates. The half-wave potential of poly(**1**) is only marginally shifted (towards 0.76 V vs. Fc^+/Fc) compared to that of the dissolved monomer complex. However, the involvement of the bis(thiophene) unit in the oxidation process cannot be excluded as the respective potential of the bis(phenylthienyl) (1.14 V vs. SCE, ca. 0.73 V vs. Fc^+/Fc)^[24] is close to the observed redox potential. Furthermore, the redox process is reversible: The charge density is the same for oxidation and reduction (ca. 5×10^{-4} C cm^{-2}). The linear relationship between peak current and applied scan rate up to 500 mVs^{-1} indicates the formation of a conductive film with redox processes that are only weakly limited by charge diffusion.^[17,25] For poly(**2**), the oxidation signal appears well-defined and reversible (charge transfer of around 3×10^{-4} C cm^{-2} for both oxidation and subsequent reduction) at a potential of 0.72 V vs. Fc^+/Fc . In contrast to poly(**1**), the linearity of the peak-current-scan-rate function is retained up to the maximum applied scan rate of 2000 mVs^{-1} (Figure 6). This behavior can be explained by a higher charge mobility than in poly(**1**), which is further supported by the smaller $E_{\text{pa}} - E_{\text{pc}}$ separation as well as the already mentioned smaller de-

Table 3. UV/Vis spectroscopic and electrochemical data of electropolymerized films.

| | $\lambda_{\text{Abs, poly}}$ [nm] | $\lambda_{\text{Abs, mono}}^{\text{[a]}}$ [nm] | $\lambda_{\text{Em, poly}}$ [nm] | $\lambda_{\text{Em, mono}}^{\text{[a]}}$ [nm] | $E_{1/2, \text{ox}}^{\text{[b]}}$ [V] |
|------------------|--------------------------------------|---|-------------------------------------|--|--|
| Poly(1) | 537 | 527 | 767 | 746 | 0.76 |
| Poly(2) | 567 | 551 | 745 | 717 | 0.72 |

[a] UV/Vis properties of spin-coated films of the monomer complexes. [b] Measured vs. Fc^+/Fc .

crease of the current slope during electropolymerization for poly(2).

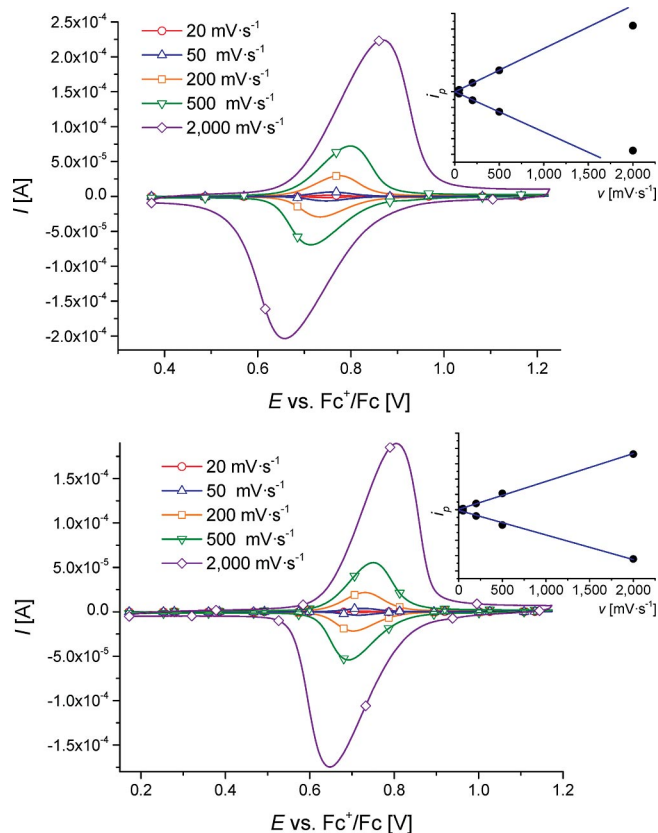


Figure 6. Cyclic voltammograms of the electropolymerized film of poly(1) (top) and poly(2) (bottom) at different scan rates. Insets: Peak-current dependence on scan rate [coated glassy carbon electrode in CH_3CN with $0.1 \text{ M Bu}_4\text{NPF}_6$; linear fit for poly(1) is valid up to 500 mV s^{-1}].

The UV/Vis absorption and emission characteristics of films of poly(1) and poly(2) on ITO-coated glass substrates were determined. The films of poly(1) and its respective monomer **1** (Figure 7) show a significant redshift of absorption of about 1400 and 1000 cm^{-1} , respectively, in comparison to that of the monomer dissolved in acetonitrile, but there are only marginal differences between the monomer and the polymer in the solid state. Similarly, the thin-film absorption of poly(2) exhibits a large redshift between the dissolved monomer complex **2** and the spin-coated film thereof, and only a small shift of 500 cm^{-1} occurs for the polymer relative to the monomer film (Figure 7). Furthermore, the additional peak at 425 nm , which was observed for **2** in solution, is also present for the films as an absorption shoulder at ca. 430 nm . Notably, the absorbance of the formed bis(phenylthienyl) moieties is expected at ca. 374 nm ^[24] and is, thus, overlaid with features of the ruthenium(II) complexes. Both polymeric films showed weak photoluminescence. In comparison to the emission of the complexes in solution, the solid-state emission of the spin-coated monomers is bathochromically shifted by approximately 800 to 900 cm^{-1} , and the emission of the electropolymerized films is shifted by ca. 1300 cm^{-1} (see Figure 7). The

spectral shifts towards higher wavelengths were observed likewise for ruthenium(II) polypyridyl systems in previous studies and are assigned to the presence of low-energy trap sites, which are available through electronic interaction between the ligand π systems of the closely packed complexes in the solid state.^[26] For the polymerized systems, an even more efficient interaction is plausible and leads to the more pronounced redshift. However, no significant effect of the conjugation path on the excited-state properties was found.

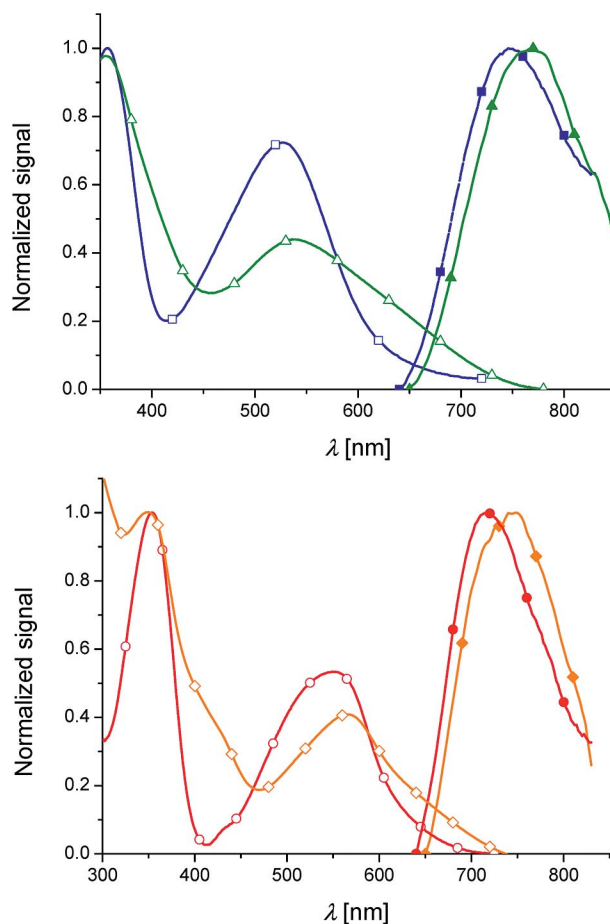


Figure 7. UV/Vis absorption (hollow symbols) and emission (filled symbols) spectra of films of poly(1) (green), **1** (blue) (top), poly(2) (orange), and **2** (red) (bottom) on ITO-coated glass substrates.

The electrosynthesized polymer films were studied by UV/Vis/NIR spectroelectrochemistry [Figure 8 shows an exemplary spectra for poly(1), and those of the other compounds are in the Supporting Information]. Poly(1) showed a bleaching of the low-energy MLCT absorption band, caused by the depletion of the respective metal-located orbitals, as well as the appearance of a broad band at 600 – 1100 nm , similar to that of the related monomer species. This leads to a color change of the polymer film from deep red to light yellow. However, no clear evidence of the oxidized bis(thiophene) moieties can be deduced from the data owing to the spectral overlap [the bis(phenylthienyl) radical cation absorbs at ca. 932 nm],^[24] despite the occurrence of some distinct bands in comparison to $\text{Ru}(\text{dqp})_2^{2+}$ and the respective monomers. Subsequent application of a potential

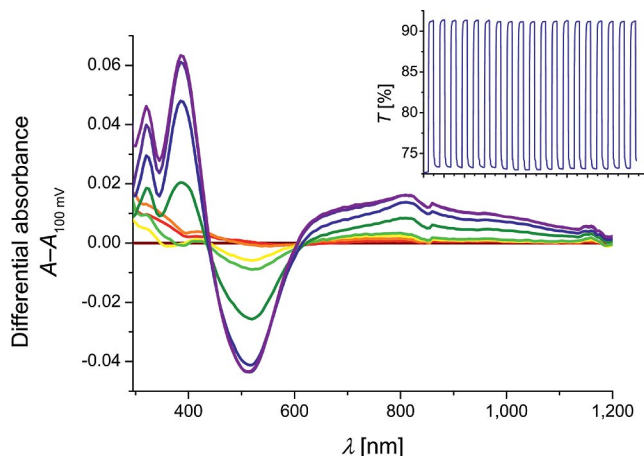


Figure 8. Exemplary change of the UV/Vis absorption spectrum of a film of poly(1) during the oxidation process. Inset: Change of transmission at 515 nm over 20 cycles of switching between initial and oxidized state.

able to reduce the oxidized species recovered fully the starting spectrum; the repeatable change of film transmission at 515 and 810 nm with switching potential over 20 cycles indicates a reversible and stable redox process with switching times (defined by achieving 95% of the full transmission change^[27]) of approximately 2 s.

Likewise, the application of an oxidative potential to poly(2) films caused the disappearance of the bands between 400 and 600 nm and the increase of absorption intensity in the NIR region with a peak at 800 nm. The re-reduction of poly(2) produced the initial spectrum nearly completely and, at least over 20 cycles, a reversible and stable redox switching with response times of ca. 2.5 s could be observed.

Conclusions

Two new ruthenium(II) complexes based on 2,6-di(quinolin-8-yl)pyridines were synthesized by a straightforward and efficient modular route to introduce electropolymerizable 2-thienyl units. The linear arrangement within the heteroleptic and homoleptic complexes assures identical spatial separation of the metal centers within the rodlike type II (lateral incorporation) and type III (incorporation into the backbone) metallopolymers.

The monomer complexes were structurally investigated by X-ray crystallography and show a sizeable deviation from the ideal linear arrangement. The principle physicochemical characteristics of the incorporated Ru(dqp)₂²⁺ moiety were preserved, that is, broad and strong long-wavelength UV/Vis absorption features, photoluminescence quantum yields up to 3% as well as reversible redox processes. Both monomers allowed well-defined potentiodynamic electropolymerization in the presence of a Lewis acid to directly yield insoluble polymer films on the electrode surfaces. The (spectro)electrochemical measurements confirmed the stability of the films towards oxidation and revealed reversible redox-triggered switching of their optical

properties. A small difference between both conjugation paths was observed, namely a faster electrochemical response, which is attributed to a higher charge-carrier mobility for the type III polymer (obtained from the homoleptic monomer complex); this finding is in accordance with the higher film growth rate and DFT calculations, which revealed a more efficient π conjugation within the type III system.

However, additional parameters (e.g., counterion mobility, film morphology, and thickness) may also contribute and are under investigation. The presented approach to photoredox-active films benefits from facile instrumentation, the modular design of the monomers, and the preservation of photophysical and electrochemical properties.

Experimental Section

General Methods: All starting materials were purchased from commercial sources [dba is dibenzylideneacetone, S-PHOS is dicyclohexyl(2',6'-dimethoxybiphenyl-2-yl)phosphane, Pd/C is activated palladium on charcoal (10 wt.-% from Aldrich)] and were used as obtained unless otherwise noted; potassium 2-nitrobenzoate,^[19] 8,8'-[4-(4-bromophenyl)pyridine-2,6-diyl]diquinoline,^[21] and [Ru(dqp)(MeCN)₃](PF₆)₂^[11a,21] were prepared according to literature procedures. Flash column chromatography was conducted with a Biotage Isolera One System with Biotage SNAP Cartridges KP-Sil and a UV/Vis detector. Microwave reactions were performed with a Biotage Initiator Sixty Microwave synthesizer.

UV/Vis absorption spectra of solutions and films were recorded with a Perkin-Elmer Lambda 750 UV/Vis spectrophotometer, emission spectra of solutions were recorded with a Jasco FP6500, and emission spectra of films were recorded with a Tecan infinite M200 Pro microplate reader. Solution measurements were performed by using concentrations of 10⁻⁶ M in respective solvents (spectroscopy grade; deaerated for emission measurements) in 1 cm quartz cuvettes at 25 °C; emission spectra were taken by excitation at the longest-wavelength absorption maximum.

Electrochemical measurements were performed with a Metrohm Autolab PGSTAT30 potentiostat with a standard three-electrode configuration (a glassy carbon disk working electrode, a platinum-rod auxiliary electrode, and a Ag/AgCl reference electrode); scan rates from 20 to 2000 mV s⁻¹ were applied. The experiments were performed at concentrations of 10⁻⁴ M in degassed solvents (spectroscopy grade) containing 0.1 M Bu₄NPF₆ (dried previously by heating at 110 °C and stored under vacuum). At the end of each measurement, ferrocene was added as an internal standard.

Electropolymerization experiments were executed with the same set-up by using either a glassy carbon disk electrode or an ITO-coated glass slide (Sigma Aldrich, 0.5 × 1") as working electrode. The polymerization was performed potentiodynamically by applying velocities of 200 mV s⁻¹.

Spectroelectrochemical experiments were performed in a thin-layer quartz cuvette containing a 0.1 M Bu₄NPF₆ dichloromethane solution with an ITO-coated glass slide with the deposited polymer as the working electrode, a platinum wire auxiliary electrode, and a Ag/AgCl reference electrode. The potential was controlled by using a Metrohm Autolab PGSTAT30 potentiostat. The oxidation process was monitored by UV/Vis spectroscopy by using a Perkin-Elmer Lambda 750 UV/Vis spectrophotometer and was considered complete when there were no further spectral changes.

For comparison, films of the monomer complexes were prepared by spin-coating solutions of the monomers (5 mg mL⁻¹ in acetonitrile) with a spin coater from Laurell Technologies Corporation (30 s at 1500 rpm) onto ITO-coated glass substrates (Sigma Aldrich, 1 × 1").

NMR spectra were recorded with a 250 or 300 MHz NMR spectrometer (Bruker AVANCE) with samples in deuterated solvents at 25 °C, if not noted otherwise. Chemical shifts are reported in parts per million (ppm, δ scale) relative to the residual solvent signal.^[28]

ESI HRMS spectrometry was performed with an ESI-(Q)-TOFMS MICROTOF II (Bruker Daltonics GmbH) mass spectrometer.

X-ray photoelectron spectra were recorded with an EA200-ESCA system (SPECS) by using a non-monochromatic Al-K α radiation source ($h\nu = 1486.6$ eV).

2,6-Bis(2-nitrophenyl)pyridine (3): A flask was charged with potassium 2-nitrobenzoate (13.171 g, 64.2 mmol), 2,6-dibromopyridine (6.901 g, 29.1 mmol), Pd/C (0.340 g, 0.287 mmol), copper(I) iodide (0.380 g, 1.995 mmol), 1,10-phenanthroline (0.367 g, 2.037 mmol), and *N*-methyl-2-pyrrolidinone (20 mL). The reaction mixture was heated to 180 °C for 15 h and allowed to cool to room temperature. The reaction mixture was quenched by addition of water and extracted three times with dichloromethane. The combined organic layers were dried with sodium sulfate, filtered, and the excess solvent was removed under reduced pressure (20 mbar) at 70 °C. The crude product was adsorbed on silica and purified by flash chromatography (silica gel, SNAP 50 g, eluted with hexane/CH₂Cl₂, 30:70 to 0:100, followed by evaporation of solvent under reduced pressure) to yield **3** (4.501 g, 14.01 mmol, 48%). ¹H NMR (CD₂Cl₂, 300 MHz): $\delta = 7.89$ (t, $J = 7.8$ Hz, 1 H), 7.86 (d, $J = 7.8$ Hz, 2 H), 7.71–7.61 (m, 4 H), 7.55 (td, $J = 7.5, 2.0$ Hz, 2 H), 7.49 (d, $J = 7.9$ Hz, 2 H) ppm. ¹³C NMR (CD₂Cl₂, 75 MHz): $\delta = 155.3, 149.3, 137.8, 134.7, 132.7, 131.5, 129.5, 124.4, 122.0$ ppm. HRMS (ESI): calcd. for C₁₇H₁₁N₃O₄Na [M + Na]⁺ 344.0642; found 344.0658. C₁₇H₁₁N₃O₄ (321.29): calcd. C 63.55, H 3.45, N 13.08; found C 63.31, H 3.39, N 12.91.

2,2'-(Pyridine-2,6-diyl)dianiline (4): A flask was charged with **3** (4.501 g, 14.01 mmol), Pd/C (0.100 g, 0.084 mmol), ethanol (60 mL), and hydrazine hydrate (3 mL, 61.5 mmol) in portions. The reaction mixture was heated to 80 °C for 1 h. The reaction mixture was allowed to cool to room temperature, filtered, and the remaining solid was washed with dichloromethane. The filtrates were combined, and the excess solvent was removed under reduced pressure to yield **4** (3.150 g, 12.05 mmol, 86%). ¹H NMR (CD₂Cl₂, 300 MHz): $\delta = 7.87$ (t, $J = 8.0$ Hz, 1 H), 7.53 (d, $J = 8.0$ Hz, 2 H), 7.52 (dd, $J = 7.8, 1.3$ Hz, 2 H), 7.17 (td, $J = 7.7, 1.4$ Hz, 2 H), 6.80–6.72 (m, 4 H), 5.32 (br. s, 4 H) ppm. ¹³C NMR (CD₂Cl₂, 75 MHz): $\delta = 157.8, 146.3, 138.2, 130.0, 129.8, 122.8, 120.1, 117.6, 116.9$ ppm. HRMS (ESI): calcd. for C₁₇H₁₆N₃ [M + H]⁺ 284.1158; found 284.1092. C₁₇H₁₆N₃ (261.33): calcd. C 78.13, H 5.59, N 16.08; found C 77.77, H 5.68, N 16.07.

2,6-Bis[4-(4-bromophenyl)quinolin-8-yl]pyridine (5): A flask was charged with **4** (0.400 g, 1.531 mmol), arsenic pentoxide (1.055 g, 4.59 mmol), and phosphoric acid (85%, 15 mL). The reaction mixture was heated to 100 °C to form a yellow solution, and 1-(4-bromophenyl)-3-chloropropan-1-one (0.871 g, 3.52 mmol) was added in portions. After 30 min, the reaction mixture was heated to 140 °C for 2 h. The mixture was cooled to room temperature, neutralized by dropwise addition of aqueous sodium hydroxide (to pH 8), and extracted three times with dichloromethane. The combined organic layers were washed with water and brine, dried with sodium sulfate, filtered, and adsorbed on silica. The excess solvent

was removed under reduced pressure. The crude product was purified by flash chromatography (silica gel, SNAP 50 g, adsorbed on silica, eluted with a gradient of hexane/EtOAc, 10:90 to 0:100, followed by evaporation of solvent under reduced pressure). The solid was triturated and heated to reflux in ethanol; the solids were collected from the hot solution by filtration. The obtained solids were dried under reduced pressure to yield **5** (0.150 g, 0.233 mmol, 15%).^[29] ¹H NMR (CD₂Cl₂, 300 MHz): $\delta = 8.97$ (d, $J = 4.3$ Hz, 2 H), 8.19 (dd, $J = 7.1, 1.3$ Hz, 2 H), 8.06 (d, $J = 7.8$ Hz, 2 H), 7.92 (dd, $J = 8.5, 1.5$ Hz, 2 H), 7.92 (dd, $J = 8.3, 7.3$ Hz, 2 H), 7.44 (dm, $J = 8.4$ Hz, 4 H), 7.62 (dd, $J = 8.3, 7.3$ Hz, 2 H), 7.44 (dm, $J = 8.4$ Hz, 4 H), 7.36 (d, $J = 4.3$ Hz, 2 H) ppm. ¹³C NMR (CD₂Cl₂, 75 MHz): $\delta = 157.1, 149.8, 147.5, 146.6, 140.0, 137.5, 134.5, 131.9, 131.5, 131.3, 127.0, 126.7, 126.4, 125.7, 122.8, 121.4$ ppm. HRMS (ESI): [M + H]⁺ calcd. for C₃₅H₂₂⁷⁹Br⁸¹BrN₃ 644.0158; found 644.0080.

[Ru(5)(dqp)](PF₆)₂ (6): A flask was charged with [Ru(dqp)-(CH₃CN)₃](PF₆)₂ (0.165 g, 0.156 mmol), **5** (0.100 g, 0.155 mmol), and ethylene glycol (4 mL), purged with N₂ for 30 min, and heated to 140 °C for 14 h under a N₂ atmosphere. The crude reaction mixture was allowed to cool to room temperature and added dropwise into aqueous NH₄PF₆. The red solid was filtered, washed with water, and purified by column chromatography (silica, SNAP, CH₃CN/H₂O/neat KNO₃, 40:4), the red band was collected and the counterion exchanged with NH₄PF₆. Recrystallization by vapor diffusion of diethyl ether into an acetonitrile solution yielded **6** (0.202 g, 0.148 mmol, 95%). ¹H NMR (CD₃CN, 300 MHz): $\delta = 8.20$ (apparent td, $J = 8.1, 1.2$ Hz, 2 H), 8.14 (d, $J = 5.5$ Hz, 2 H), 8.11–8.07 (m, 4 H), 7.94 (d, $J = 8.1$ Hz, 2 H), 7.91 (d, $J = 8.0$ Hz, 4 H), 7.80 (d, $J = 8.3$ Hz, 4 H), 7.73 (d, $J = 7.2$ Hz, 2 H), 7.69–7.63 (m, 4 H), 7.50–7.39 (m, 8 H), 7.09 (dd, $J = 8.2, 5.5$ Hz, 2 H), 7.01 (d, $J = 5.3$ Hz, 2 H) ppm. ¹³C NMR (CD₃CN, 75 MHz): $\delta = 159.6, 158.8, 157.9, 157.7, 149.4, 148.0, 147.8, 139.4, 139.2, 138.8, 136.2, 134.2, 133.9, 133.2, 133.1, 133.1, 132.6, 131.9, 129.3, 129.2, 129.2, 128.1, 127.8, 127.8, 125.8, 124.4, 123.3, 123.2$ ppm. HRMS (ESI): calcd. for C₅₈H₃₆⁷⁹Br⁸¹BrN₆Ru [M – 2PF₆]²⁺ 539.0200; found 539.0232.

[Ru{2,6-bis[4-(4-(thiophen-2-yl)phenyl)quinolin-8-yl]pyridine}(dqp)](PF₆)₂ (1): A microwave vial was charged with **6** (0.117 g, 0.086 mmol), thiophen-2-ylboronic acid (0.043 g, 0.336 mmol), Pd(dba)₂ (0.0025 mg, 4.35 μ mol), dicyclohexyl(2',6'-dimethoxybiphenyl-2-yl)phosphane (0.0035 g, 8.53 μ mol), and potassium carbonate (0.076 g, 0.550 mmol). After the addition of acetonitrile (3 mL) and water (1.5 mL), the vial was sealed, purged for 10 min with N₂, and conventionally heated to 100 °C for 16 h. The crude reaction mixture was allowed to cool to room temperature and was purified as described for **6** to yield **1** (0.108 g, 0.079 mmol, 92%). ¹H NMR (CD₃CN, 250 MHz): $\delta = 8.22$ (t, $J = 8.1$ Hz, 1 H), 8.21 (t, $J = 8.1$ Hz, 1 H), 8.14–8.05 (m, 6 H), 7.99–7.85 (m, 10 H), 7.74 (d, $J = 8.1$ Hz, 4 H), 7.69 (d, $J = 8.2$ Hz, 2 H), 7.58 (d, $J = 3.6$ Hz, 2 H), 7.56–7.39 (m, 10 H), 7.19 (dd, $J = 4.9, 3.6$ Hz, 2 H), 7.10 (dd, $J = 8.1, 5.1$ Hz, 2 H), 7.04 (d, $J = 5.5$ Hz, 2 H) ppm. ¹³C NMR (CD₃CN, 62 MHz): $\delta = 159.5, 158.8, 157.9, 157.8, 150.0, 148.0, 147.8, 143.8, 139.4, 139.2, 138.8, 136.3, 136.1, 134.2, 133.9, 133.3, 133.2, 131.9, 131.6, 129.8, 129.4, 129.3, 129.2, 127.9, 127.8, 127.8, 127.4, 127.0, 125.9, 125.5, 123.2, 123.2$ ppm. HRMS (ESI): calcd. for C₆₆H₄₂N₆RuS [M – 2PF₆]²⁺ 542.0981; found 542.1057.

[Ru(8,8'-(4-(4-bromophenyl)pyridine-2,6-diyl)diquinoline)-2-(CH₃CN)₃](PF₆)₂ (7): A microwave vial was charged with 8,8'-(4-(4-bromophenyl)pyridine-2,6-diyl)diquinoline^[21] (0.300 g, 0.614 mmol), ruthenium trichloride hydrate (0.164 g, 0.585 mmol), and ethanol (10 mL). The vial was sealed and conventionally

heated to 115 °C for 13 h. The reaction mixture was allowed to cool to room temperature, filtered, and washed thoroughly with ethanol and dichloromethane. The dark brown solid was dried under reduced pressure to yield crude Ru{8,8'-[4-(4-bromophenyl)pyridine-2,6-diyl]diquinoline}Cl₃ (0.352 g, 0.506 mmol, 86%).

A flask was charged with crude Ru{8,8'-[4-(4-bromophenyl)pyridine-2,6-diyl]diquinoline}Cl₃ (0.352 g, 0.506 mmol), silver nitrate (0.301 g, 1.771 mmol), acetonitrile (7 mL), ethanol (1.5 mL), and water (1.5 mL). The suspension was heated to 90 °C for 17 h. The white solids were removed by filtration, and the orange-brown solution was reduced in volume under reduced pressure and purified as described for **6** to yield **7** (0.305 g, 0.304 mmol, 60%). ¹H NMR (CD₃CN, 300 MHz): δ = 9.08 (dd, *J* = 5.2, 1.2 Hz, 2 H), 8.67 (br. d, *J* = 7.5 Hz, 2 H), 8.62 (dd, *J* = 8.4, 1.2 Hz, 2 H), 8.28 (d, *J* = 8.2 Hz, 2 H), 8.18 (s, 2 H), 7.93 (t, *J* = 7.8 Hz, 2 H), 7.87 (dm, *J* = 8.5 Hz, 2 H), 7.77 (dm, *J* = 8.5 Hz, 2 H), 7.67 (dd, *J* = 8.2, 5.2 Hz, 2 H), 2.45 (s, 3 H), 1.96 (s, 6 H) ppm. ¹³C NMR (CD₃CN, 63 MHz): δ = 159.8, 158.6, 150.0, 147.3, 139.7, 136.2, 135.3, 135.2, 133.5, 133.0, 130.4, 129.7, 129.2, 127.8, 127.3, 126.3, 125.5, 123.2, 4.5, 3.8 ppm. HRMS (ESI): calcd. for C₃₅H₂₇⁷⁹BrN₆Ru [M - 2PF₆]²⁺ 356.0259; found 355.8804.

[Ru{8,8'-[4-(4-(thiophen-2-yl)phenyl)pyridine-2,6-diyl]diquinoline}]₂(PF₆)₂ (2**):** A flask was charged with **7** (0.195 g, 0.195 mmol), 8,8'-[4-(4-bromophenyl)pyridine-2,6-diyl]diquinoline (0.095 g, 0.195 mmol), and ethylene glycol (10 mL) and heated to 140 °C under N₂ for 14 h. The crude reaction mixture was allowed to cool to room temperature and was worked up as described for **6** to yield crude [Ru(8,8'-[4-(4-bromophenyl)pyridine-2,6-diyl]diquinoline)₂](PF₆)₂ containing some monodebrominated product (0.180 g, 0.132 mmol, 68%).

A microwave vial was charged with crude [Ru(8,8'-[4-(4-bromophenyl)pyridine-2,6-diyl]diquinoline)₂](PF₆)₂ (0.180 g, 0.132 mmol), thiophen-2-ylboronic acid (0.067 g, 0.526 mmol), Pd(dba)₂ (0.0038 g, 6.58 μmol), dicyclohexyl(2',6'-dimethoxybiphenyl-2-yl)phosphane (0.0054 g, 0.013 mmol), and potassium carbonate (0.111 g, 0.790 mmol). After the addition of acetonitrile (3 mL) and water (1.5 mL), the vial was sealed, purged for 10 min with N₂, and conventionally heated to 100 °C for 16 h. The reaction mixture was worked up as described for **6** to yield the title compound **2** (0.100 g, 0.073 mmol, 55%). ¹H NMR (CD₃CN, 300 MHz): δ = 8.18–8.13 (m, 8 H), 8.09 (dd, *J* = 8.1, 1.2 Hz, 4 H), 8.01 (d, *J* = 8.5 Hz, 4 H), 7.93 (dd, *J* = 7.4, 1.2 Hz, 4 H), 7.88 (d, *J* = 8.5 Hz), 7.72 (dd, *J* = 8.2, 1.2 Hz, 4 H), 7.58 (dd, *J* = 3.6, 1.0 Hz, 2 H), 7.50 (t, *J* = 7.5 Hz, 4 H), 7.50 (dd, *J* = 5.1, 1.0 Hz, 2 H), 7.18 (dd, *J* = 5.1, 3.7 Hz, 2 H), 7.09 (dd, *J* = 8.2, 5.2 Hz, 4H) ppm. ¹³C NMR (CD₃CN, 75 MHz): δ = 159.6, 158.1, 149.8, 147.7, 143.7, 138.6, 137.2, 135.8, 134.5, 133.0, 131.6, 129.7, 129.2, 127.9, 127.6, 127.5, 127.4, 126.1, 125.7, 123.1 ppm. HRMS (ESI): calcd. for C₆₆H₄₂N₆RuS₂ [M - 2PF₆]²⁺ 542.0981; found 542.0990.

X-ray Crystallography: The intensity data for the compounds were collected with a Nonius KappaCCD diffractometer with graphite-monochromated Mo-*K*_α radiation. The data were corrected for Lorentz and polarization effects but not for absorption effects.^[30]

The structures were solved by direct methods (SHELXS^[31]) and refined by full-matrix least-squares techniques against *F*_o² (SHELXL-97^[31]). All hydrogen atoms were included at calculated positions with fixed thermal parameters. All non-hydrogen, non-disordered atoms were refined anisotropically.^[31] The crystals of **1** were extremely thin and of low quality and resulted in a standard data set; however, the structure is sufficient to show the connectivity and geometry despite the high final *R* value. We will only publish the conformation of the molecule and the crystallographic

data. We will not deposit the data in the Cambridge Crystallographic Data Centre. Crystallographic data as well as structure solution and refinement details are summarized in the Supporting Information. XP (Siemens Analytical X-ray Instruments, Inc.) was used for structure representations.

CCDC-888462 (for **6**) and -888463 (for **2**) contain the supplementary crystallographic data for this paper. These data can be obtained free of charge from The Cambridge Crystallographic Data Centre via www.ccdc.cam.ac.uk/data_request/cif.

Computational Methods: All calculations were performed with the Gaussian 09 (G09) program package^[32] by employing the DFT method and using Becke's three-parameter hybrid functional^[33] and the Lee–Yang–Parr gradient-corrected correlation functional^[34] (B3LYP). The ruthenium atoms were treated by the 28-electron relativistic effective core potential MWB^[35] for the inner shells, whereas the outer shells (4s, 4p, 4d, and 5s electrons) were treated separately. The remaining atoms (C, H, N, and S) were treated with the 6-31G(d) double- ζ basis set.^[36] Bulk solvent effects (acetonitrile) were included by using the integral equation formalism of the polarizable continuum model of Tomasi and co-workers.^[37] The geometry optimizations of the singlet and triplet states were performed without any constraints and the true nature was confirmed by normal-mode analysis. The molecular orbitals and electron/spin densities were visualized by using the GaussView 5.0 package.^[38] The vertical excitations were computed by TD-DFT at the same level of theory. The electronic transitions were determined from the changes in electronic distribution by using electron-density difference maps (EDDMs),^[39] which were computed with the GaussSum 2.2 package.^[40] The triplet excited states were visualized by spin-density plots, expressed as a difference between α and β spin densities, by using the GaussView 5.0 package.^[38] The density of states (DOS) and crystal orbital overlap population (COOP) analysis was performed by using the GaussSum 2.2 package.^[40]

Supporting Information (see footnote on the first page of this article): Spectral data (UV/Vis, UV/Vis/NIR spectroelectrochemistry, XPS), DFT calculation results, and X-ray crystallographic data.

Acknowledgments

The authors acknowledge the Bundesministerium für Bildung und Forschung, the European Social Fund (ESF), the Thüringer Aufbaubank (TAB), and the Thuringian Ministry of Economy, Employment and Technology (TMWAT) for financial support. M. J. is grateful for financial support from the Carl-Zeiss-Stiftung. The authors also thank Esra Altuntas for ESI measurements and Dr. Bernd Schröter for XPS measurements.

- 1) a) A. Juris, V. Balzani, F. Barigelletti, S. Campagna, P. Belser, A. von Zelewsky, *Coord. Chem. Rev.* **1988**, *84*, 85–277; b) T. J. Meyer, *Pure Appl. Chem.* **1986**, *58*, 1193–1206.
- 2) B. Durham, J. V. Caspar, J. K. Nagle, T. J. Meyer, *J. Am. Chem. Soc.* **1982**, *104*, 4803–4810.
- 3) J.-P. Sauvage, J.-P. Collin, J.-C. Chambron, S. Guillerez, C. Coudret, V. Balzani, F. Barigelletti, L. De Cola, L. Flamigni, *Chem. Rev.* **1994**, *94*, 993–1019.
- 4) a) E. C. Constable, *Chem. Soc. Rev.* **2007**, *36*, 246–253; b) H. Hofmeier, U. S. Schubert, *Chem. Soc. Rev.* **2004**, *33*, 373–399.
- 5) J. R. Winkler, T. L. Netzel, C. Creutz, N. Sutin, *J. Am. Chem. Soc.* **1987**, *109*, 2381–2392.
- 6) a) B. Schulze, D. Escudero, C. Friebe, R. Siebert, H. Görls, S. Sinn, M. Thomas, S. Mai, J. Popp, B. Dietzek, L. González, U. S. Schubert, *Chem. Eur. J.* **2012**, *18*, 4010–4025; b) O. A.

- Borg, S. S. M. C. Godinho, M. J. Lundqvist, S. Lunell, P. Persson, *J. Phys. Chem. A* **2008**, *112*, 4470–4476; c) A. Amini, A. Harriman, A. Mayeux, *Phys. Chem. Chem. Phys.* **2004**, *6*, 1157–1164; d) D. W. Fink, W. E. Ohnesorge, *J. Am. Chem. Soc.* **1969**, *91*, 4995–4998.
- [7] a) M. Jäger, A. Smeigh, F. Lombeck, H. Görls, J.-P. Collin, J.-P. Sauvage, L. Hammarström, O. Johansson, *Inorg. Chem.* **2010**, *49*, 374–376; b) S. H. Wadman, M. Lutz, D. M. Tooke, A. L. Spek, F. Hartl, R. W. A. Havenith, G. P. M. van Klink, G. van Koten, *Inorg. Chem.* **2009**, *48*, 1887–1900; c) P. G. Bomben, K. C. D. Robson, P. A. Sedach, C. P. Berlinguette, *Inorg. Chem.* **2009**, *48*, 9631–9643; d) J.-P. Collin, M. Beley, J.-P. Sauvage, F. Barigelletti, *Inorg. Chim. Acta* **1991**, *186*, 91–93.
- [8] a) H.-J. Park, K. H. Kim, S. Y. Choi, H.-M. Kim, W. I. Lee, Y. K. Kang, Y. K. Chung, *Inorg. Chem.* **2010**, *49*, 7340–7352; b) B. Schulze, D. Escudero, C. Friebe, R. Siebert, H. Görls, U. Köhn, E. Altuntas, A. Baumgaertel, M. D. Hager, A. Winter, B. Dietzek, J. Popp, L. González, U. S. Schubert, *Chem. Eur. J.* **2011**, *17*, 5494–5498.
- [9] a) L. Hammarström, O. Johansson, *Coord. Chem. Rev.* **2010**, *254*, 2546–2559; b) A. Breivogel, C. Förster, K. Heinze, *Inorg. Chem.* **2010**, *49*, 7052–7056; c) F. Schramm, V. Meded, H. Fliegl, K. Fink, O. Fuhr, Z. Qu, W. Klopfer, S. Finn, T. E. Keyes, M. Ruben, *Inorg. Chem.* **2009**, *48*, 5677–5684.
- [10] a) J. Wang, Y.-Q. Fang, L. Bourget-Merle, M. I. J. Polson, G. S. Hanan, A. Juris, F. Loiseau, S. Campagna, *Chem. Eur. J.* **2006**, *12*, 8539–8548; b) J. Wang, G. S. Hanan, F. Loiseau, S. Campagna, *Chem. Commun.* **2004**, 2068–2069.
- [11] a) M. Jäger, R. J. Kumar, H. Görls, J. Bergquist, O. Johansson, *Inorg. Chem.* **2009**, *48*, 3228–3238; b) M. Abrahamsson, M. Jäger, T. Österman, L. Eriksson, P. Persson, H.-C. Becker, O. Johansson, L. Hammarström, *J. Am. Chem. Soc.* **2006**, *128*, 12616–12617.
- [12] a) C. Friebe, M. D. Hager, A. Winter, U. S. Schubert, *Adv. Mater.* **2012**, *24*, 332–345; b) M. O. Wolf, *J. Inorg. Organomet. Polym. Mater.* **2006**, *16*, 189–199.
- [13] a) Y.-W. Zhong, C.-J. Yao, H.-J. Nie, *Coord. Chem. Rev.* **2013**, *257*, 1357–1372; b) C.-J. Yao, Y.-W. Zhong, H.-J. Nie, H. D. Abruña, J. Yao, *J. Am. Chem. Soc.* **2011**, *133*, 20720–20723; c) X. J. Zhu, B. J. Holliday, *Macromol. Rapid Commun.* **2010**, *31*, 904–909; d) J. Hjelm, R. W. Handel, A. Hagfeldt, E. C. Constable, C. E. Housecroft, R. J. Forster, *Inorg. Chem.* **2005**, *44*, 1073–1081; e) R. M. Leasure, T. Kajita, T. J. Meyer, *Inorg. Chem.* **1996**, *35*, 5962–5963; f) C. P. Horwitz, Q. Zuo, *Inorg. Chem.* **1992**, *31*, 1607–1613; g) T. F. Guarr, F. C. Anson, *J. Phys. Chem.* **1987**, *91*, 4037–4043; h) C. D. Ellis, L. D. Margerum, R. W. Murray, T. J. Meyer, *Inorg. Chem.* **1983**, *22*, 1283–1291; i) P. Denisevich, H. D. Abruña, C. R. Leidner, T. J. Meyer, R. W. Murray, *Inorg. Chem.* **1982**, *21*, 2153–2161.
- [14] M. O. Wolf, *Adv. Mater.* **2001**, *13*, 545–553.
- [15] a) M. L. Naklicki, S. I. Gorelsky, W. Kaim, B. Sarkar, R. J. Crutchley, *Inorg. Chem.* **2012**, *51*, 1400–1407; b) M. Lundberg, P. E. M. Siegbahn, *J. Chem. Phys.* **2005**, *122*, 224103.
- [16] Y. Sun, M. El Ojaimi, R. Hammitt, R. P. Thummel, C. Turro, *J. Phys. Chem. B* **2010**, *114*, 14664–14670.
- [17] J. Heinze, B. A. Frontana-Uribe, S. Ludwigs, *Chem. Rev.* **2010**, *110*, 4724–4771.
- [18] L. J. Goossen, N. Rodríguez, B. Melzer, C. Linder, G. Deng, L. M. Levy, *J. Am. Chem. Soc.* **2007**, *129*, 4824–4833.
- [19] L. J. Goßen, B. Zimmermann, C. Linder, N. Rodríguez, P. P. Lange, J. Hartung, *Adv. Synth. Catal.* **2009**, *351*, 2667–2674.
- [20] D. Pomeranc, V. Heitz, J.-C. Chambron, J.-P. Sauvage, *J. Am. Chem. Soc.* **2001**, *123*, 12215–12221.
- [21] M. Jäger, L. Eriksson, J. Bergquist, O. Johansson, *J. Org. Chem.* **2007**, *72*, 10227–10230.
- [22] S. Jin, G. Xue, *Macromolecules* **1997**, *30*, 5753–5757.
- [23] P. J. Hochgesang, R. D. Bereman, *Inorg. Chim. Acta* **1988**, *149*, 69–76.
- [24] J. J. Apperloo, L. B. Groenendaal, H. Verheyen, M. Jayakanan, R. A. J. Janssen, A. Dkhissi, D. Beljonne, R. Lazzaroni, J.-L. Brédas, *Chem. Eur. J.* **2002**, *8*, 2384–2396.
- [25] a) A. J. Bard, L. R. Faulkner, *Electrochemical Methods*, 2nd ed., John Wiley & Sons, New York, **2001**; b) the relationship between the peak current and scan rate may also be strongly influenced by film thickness.
- [26] a) M. Devenney, L. A. Worl, S. Gould, A. Guadalupe, B. P. Sullivan, J. V. Caspar, R. L. Leasure, J. R. Gardner, T. J. Meyer, *J. Phys. Chem. A* **1997**, *101*, 4535–4540; b) J. L. Colón, C. Y. Yang, A. Clearfield, C. R. Martin, *J. Phys. Chem.* **1988**, *92*, 5777–5781.
- [27] C. L. Gaupp, D. M. Welsh, R. D. Rauh, J. R. Reynolds, *Chem. Mater.* **2002**, *14*, 3964–3970.
- [28] H. E. Gottlieb, V. Kotlyar, A. Nudelman, *J. Org. Chem.* **1997**, *62*, 7512–7515.
- [29] A small amount of inseparable impurities remained and were readily removed after the coordination step.
- [30] a) COLLECT, *Data Collection Software*, Nonius B. V., The Netherlands, **1998**; b) Z. Otwinowski, W. Minor, in: *Processing of X-ray diffraction data collected in oscillation mode*, in: *Methods in Enzymology*, vol. 276: *Macromolecular Crystallography*, Part A (Eds.: C. W. Carter, R. M. Sweet), Academic Press, New York, **1997**, p. 307–326.
- [31] G. M. Sheldrick, *Acta Crystallogr., Sect. A* **2008**, *64*, 112–122.
- [32] M. J. Frisch, G. W. Trucks, H. B. Schlegel, G. E. Scuseria, M. A. Robb, J. R. Cheeseman, G. Scalmani, V. Barone, B. Mennucci, G. A. Petersson, H. Nakatsuji, M. Caricato, X. Li, H. P. Hratchian, A. F. Izmaylov, J. Bloino, G. Zheng, J. L. Sonnenberg, M. Hada, M. Ehara, K. Toyota, R. Fukuda, J. Hasegawa, M. Ishida, T. Nakajima, Y. Honda, O. Kitao, H. Nakai, T. Vreven, J. A. Montgomery Jr., J. E. Peralta, F. Ogliaro, M. Bearpark, J. J. Heyd, E. Brothers, K. N. Kudin, V. N. Staroverov, R. Kobayashi, J. Normand, K. Raghavachari, A. Rendell, J. C. Burant, S. S. Iyengar, J. Tomasi, M. Cossi, N. Rega, J. M. Millam, M. Klene, J. E. Knox, J. B. Cross, V. Bakken, C. Adamo, J. Jaramillo, R. Gomperts, R. E. Stratmann, O. Yazyev, A. J. Austin, R. Cammi, C. Pomelli, J. W. Ochterski, R. L. Martin, K. Morokuma, V. G. Zakrzewski, G. A. Voth, P. Salvador, J. J. Dannenberg, S. Dapprich, A. D. Daniels, Ö. Farkas, J. B. Foresman, J. V. Ortiz, J. Cioslowski, D. J. Fox, *Gaussian 09*, revision A.1, Gaussian, Inc., Wallingford, **2009**.
- [33] A. D. Becke, *J. Chem. Phys.* **1993**, *98*, 5648–5652.
- [34] C. T. Lee, W. T. Yang, R. G. Parr, *Phys. Rev. B* **1988**, *37*, 785–789.
- [35] D. Andrae, U. Häußermann, M. Dolg, H. Stoll, H. Preuß, *Theor. Chim. Acta* **1990**, *77*, 123–141.
- [36] P. C. Hariharan, J. A. Pople, *Theor. Chim. Acta* **1973**, *28*, 213–222.
- [37] J. Tomasi, B. Mennucci, R. Cammi, *Chem. Rev.* **2005**, *105*, 2999–3094.
- [38] *GaussView*, v. 5.0.8, R. D. Dennington, T. A. Keith, J. M. Millan, Semicchem, Inc., Shawnee KS, **2008**.
- [39] W. R. Browne, N. M. O’Boyle, J. J. McGarvey, J. G. Vos, *Chem. Soc. Rev.* **2005**, *34*, 641–663.
- [40] a) *GaussSum*, v. 2.2.5, N. M. O’Boyle, J. G. Vos, Dublin City University, Dublin, Ireland, **2009**; available at <http://gausssum.sourceforge.net>; b) N. M. O’Boyle, A. L. Tenderholt, K. M. Langner, *J. Comput. Chem.* **2008**, *29*, 839–845.

Received: March 15, 2013
Published Online: June 26, 2013

Publication A10: “Emitting electrode coatings with redox-switchable conductivity: Incorporation of ruthenium(II)-2,6-di(quinolin-8-yl)pyridine complexes into polythiophene by electropolymerization”

Christian Friebe, Michael Jäger, Ulrich S. Schubert

RSC Adv. **2013**, 3, 11686–11690.

Reprinted with permission from: The Royal Society of Chemistry (Copyright 2013)

Emitting electrode coatings with redox-switchable conductivity: incorporation of ruthenium(II)-2,6-di(quinolin-8-yl)pyridine complexes into polythiophene by electropolymerization†

Cite this: *RSC Advances*, 2013, 3, 11686

Christian Friebe,^{ab} Michael Jäger^{*ab} and Ulrich S. Schubert^{*ab}

Received 14th January 2013,
Accepted 28th March 2013

DOI: 10.1039/c3ra41356j

www.rsc.org/advances

Polythiophenes doped with ruthenium(II)-2,6-di(quinolin-8-yl)pyridine complexes are prepared *via* an electrochemical polymerization approach. The influence of the ruthenium(II)-thiophene ratios and different complex assemblies on the electrochemical, conductivity, and optical properties of the polymer are studied. The polymers feature an enhanced redox stability with increasing ruthenium(II) content and reversibly switchable conductivities (up to 10^{-5} S cm⁻¹), combined with the characteristic emission of the complexes at around 750 nm under ambient conditions.

The last decade has shown great advancement in the preparation of tailored photo- and electro-active materials, *e.g.*, to generate light in electroluminescent devices,^{1–3} in sensing applications,^{4–6} or to harvest solar energy.^{7–9} In view of photovoltaic devices, the following functions of the material are crucial: the efficient absorption of visible light, charge separation, and the transport of the mobile charge carriers, *i.e.*, through the active layer towards the adjacent electrodes.^{10,11} Different materials have been developed for this purpose, including inorganic nanoparticles,^{12,13} small-molecule and metal-complex systems,^{14–17} and (semi-)conducting organic polymers.^{18–20} The latter, polymer-based systems offer various advantages in comparison to conventional inorganic semiconductor-based systems, *e.g.*, the applicability of a variety of modern polymerization techniques, established assembling and processing techniques for device integration, but also the possibility to tailor the optical and electrochemical properties on the molecular scale. In particular, π -conjugated polymers, *e.g.*, polythiophenes and poly(phenylene-vinylene)s, are attractive solar-cell dyes due to their visible-light absorbance combined with a high intrinsic charge-carrier mobility as well as excellent thin-film processability.¹⁸ However, these purely organic polymers suffer from both electrochemical instability and charge trapping due to irreversible redox processes.^{21–23} Alternatively, the incorporation of metal complexes into semi-

conducting polymers gives access to reversible redox properties combined with enhanced optical characteristics of the metallo-polymer,^{24–26} *e.g.*, stability towards molecular oxygen. A facile yet efficient approach to assemble metallopolymers is provided by the electrochemical polymerization process; the respective metal complex is equipped with a pair of electro-connectable functionalities that allow the formation of a linear polymeric system upon electrochemical treatment.^{27,28} If the solvent system is chosen carefully with regard to solubility, the resulting polymer can be deposited directly onto the working-electrode surface without an additional processing step. Like this, in particular ruthenium(II) and osmium(II) complexes of polypyridyl-type ligands were used for the preparation of photoactive, conductive thin films by electropolymerization.^{29–35} There, polymer coatings containing ruthenium(II)-*bis*(2,2':6',2''-terpyridine) and ruthenium(II)-*tris*(2,2'-bipyridine) complexes showed electrical conductivities up to 10^{-3} S cm⁻¹.^{32,33}

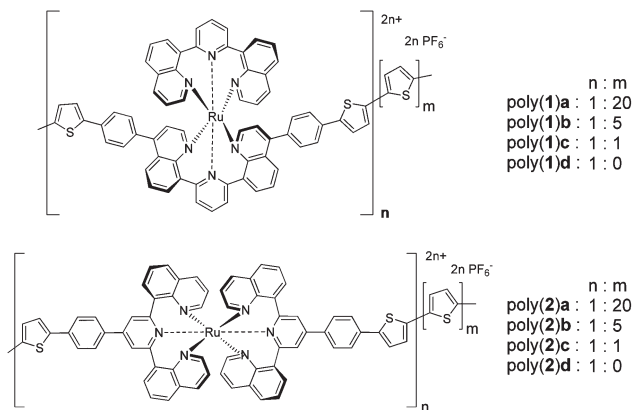
We have recently demonstrated the thin-film preparation by electrochemical polymerization of two photo-redox-active ruthenium(II) complexes with 2,6-di(quinolin-8-yl)pyridine (dqp) ligands possessing 2-thienyl groups.³⁶ The films exhibited the typical [Ru(dqp)₂]²⁺-based absorption and emission profiles^{37,38} combined with the reversible redox properties.³⁶ In this contribution, we describe the subsequent incorporation of the complexes into polythiophene to form conjugated metallo-*co*-polymers (Scheme 1). In addition to the characterization of the films by UV-vis absorption and emission spectroscopy as well as cyclic voltammetry, a detailed analysis of the conductivity behaviour depending on the oxidation state is provided by *in situ* electrochemical impedance spectroscopy (EIS).

^aLaboratory of Organic and Macromolecular Chemistry (IOMC), Friedrich Schiller University Jena, Humboldtstr. 10, 07743 Jena, Germany.

E-mail: ulrich.schubert@uni-jena.de; michael.jaeger.iomc@uni-jena.de

^bJena Center for Soft Matter (JCSM), Friedrich Schiller University, Philosophenweg 7, 07743 Jena, Germany

† Electronic supplementary information (ESI) available: Experimental details, detailed electrochemical and photophysical characterization. See DOI: 10.1039/c3ra41356j



Scheme 1 Schematic representation of the polymers obtained *via* electro-*co*-polymerization of ruthenium(II) complexes and thiophene. The *co*-monomer ratios refer to the content in the applied electrolyte solution.

The electro-*co*-polymerization of the ruthenium(II) complexes with varying amounts of thiophene was performed in acetonitrile with 0.1 M Bu_4NPF_6 as the conductive electrolyte and 5 vol% $\text{BF}_3 \cdot \text{OEt}_2$, which facilitates the polymerization process by lowering the thiophene-related oxidation potentials.^{39,40} The polymerization was conducted potentiodynamically by cycling between -0.1 and 1.5 V vs. Fc^+/Fc , thus oxidizing the thiophene moieties at around 1.2 V to form reactive thienyl cation radicals, which lead to polymerization.²⁸ The cyclic voltammetric changes during the *co*-polymerization of **1** and **2** with increasing thiophene content are depicted exemplarily for poly(**1**)**a** and poly(**1**)**d** in Fig. 1a and

Fig. 1b, respectively, and for all polymers in the ESI† In general, a steady increase of the respective current with the cycle number occurs. In all cases, the slope decreases after about 10 to 20 cycles, indicating a reduced polymerization rate. The absolute peak current is twice to four times as high for the *co*-polymers as for the $\text{Ru}(\text{dqp})_2$ *homo*-polymers, attributed to the additional high thiophene content. Furthermore, the changes in the cyclic voltammograms (CVs) during electropolymerization differ significantly among the films. The final CV cycles of the 1 : 20 polymerizations are mostly determined by polythiophene characteristics, *i.e.*, broad oxidation waves due to various overlapping, chain-length-dependent redox states.^{28,41} In contrast, the *homo*-polymers and the 1 : 1 mixtures feature the sharp signal of the complex's $\text{Ru}^{\text{III}}/\text{Ru}^{\text{II}}$ redox process. In addition, the characteristic peaks of unreacted thiophene upon re-reduction can be observed.³⁶ In the case of the 1 : 5 ratios, a broader electrochemical response caused by the incorporation of polythiophene moieties in the polymer system is present.

By this procedure, metallic-red (*homo*-polymers) to deep-black (1 : 20 *co*-polymers) films were prepared on a platinum electrode for cyclovoltammetric analysis in a fresh electrolyte solution (Fig. 1c and Fig. 1d for poly(**1**)**a** and poly(**1**)**d**, respectively; see ESI† for all polymers). As already observed during the polymerization, the CV of a complex–thiophene ratio of 1 : 20 resembles primarily polythiophene. Notably, a reduced electrochemical stability was noticed as indicated by the decreasing peak currents from cycle to cycle during the CV experiments. For a lower thiophene content (1 : 5), the films show improved electrochemical characteristics, *i.e.*, reversible signals at scan rates below 50 mV s^{-1} , resembling the

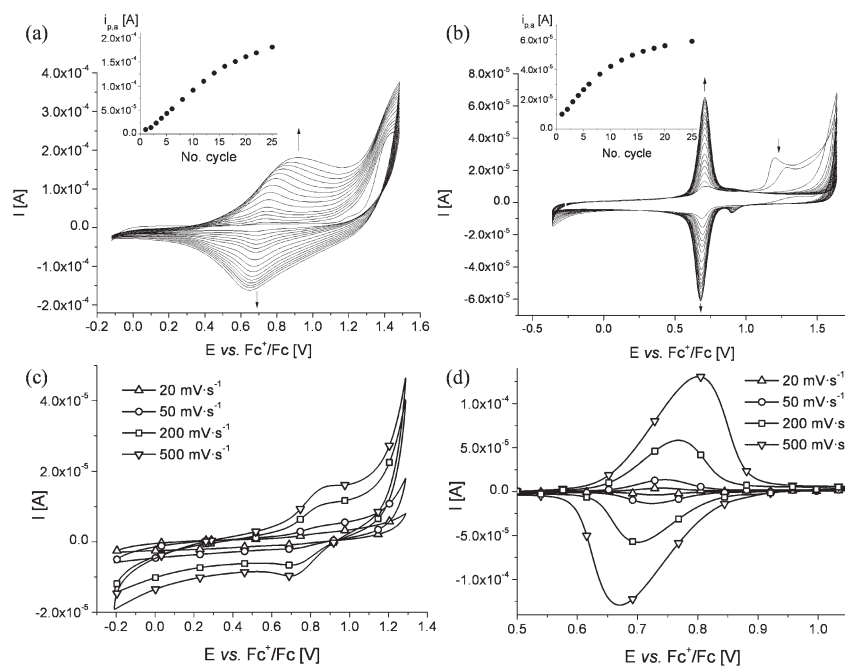


Fig. 1 Exemplary presentation of CV development during electro-*co*-polymerization of complex **1** with thiophene (1 : 20) (a) and pure **1** (b). Exemplary cyclic voltammograms of films of poly(**1**)**a** (c) and poly(**1**)**d** (d) on a platinum disk electrode at different scan rates.

complex's Ru^{III}/Ru^{II} redox process with half-wave potentials of 0.77 and 0.74 V vs. Fc⁺/Fc for poly(**1b**) and poly(**2b**), respectively. At higher scan rates the waves are broader and display a larger peak split indicating electron transfer processes on the timescale of the experiment. In contrast, a *co*-monomer ratio of 1 : 1 leads to CVs that are dominated by the complexes' characteristics and closely resemble the case of the *homo*-polymers. The respective peak-current dependence on the scan rate exhibits a linear behaviour up to 500 mV s⁻¹ as well as small peak splits (10 to 15 mV at 20 mV s⁻¹), both indicating the formation of a conductive film where redox processes are only weakly limited by charge diffusion (see ESI†).^{28,42}

Electrochemical impedance spectroscopy represents a versatile tool to elucidate the charge-transfer characteristics of conducting polymer films.^{43–45} In particular, the changes in conductivity of different ruthenium(II)-thiophene ratios can be deduced for varying degrees of film oxidation. The Nyquist plots generally display two semi-circles and a straight line at lower frequencies (see the example in Fig. 2 for poly(**1d**) and the ESI†). The first semi-circle remains almost unaffected by varying the dc potential for all polymers. It spans from around 60 to 500 Ω on the Re(Z)-axis and represents the charge transfer from the electrolyte to the polymer film, which is similar in all measurements and is adequately described by an equivalent-circuit element consisting of a resistor (R), corresponding to the interfacial charge-transport resistance, and a parallel constant phase element (CPE), representing the interface charging and accounting also for film inhomogeneities.⁴³ The second semi-circle structure varies vastly with changing dc potential and reflects the charge-transport phenomena within the polymer film. Likewise, it can be fitted best by an R-CPE equivalent-circuit element where the resistor is equivalent to the film's bulk resistance, while the CPE correlates to its charge-separation capacitance. The affiliated straight line represents the Warburg impedance reflecting ion diffusion that is necessary to sustain electroneutrality within the film (Fig. 2).

The analysis of the second semi-circles yields the electron-transfer resistance and the conductivity of the polymer film in

the different oxidation levels. Fig. 3 illustrates the conductivity–potential behaviour for the first polymer series, while the related cyclic voltammograms are provided to assist the comparison. In case of the polythiophene-dominated poly(**1a**), the conductivity increases with the onset of oxidation over a wide range and reaches a peak value at 1.5×10^{-5} S cm⁻¹ at +800 mV. The magnitude of conductance is determined by the product of charge mobility and charge-carrier concentration.^{43,46} Hence, the oxidation of the film introduces charge carriers at the polythiophene moieties, leading to an increased hole conductance. Once too many units are oxidized, the conductivity drops again (2×10^{-6} S cm⁻¹) since less accepting sites are available for a hole-hopping mechanism. The reverse scan reveals the effect of overoxidation and the associated degradation of the conjugated π systems,^{28,47–49} which leads to an unspecific decrease of conductivity. In line with this explanation, poly(**1b**) shows a later onset of oxidation and conductivity increase with a maximum value of 5×10^{-6} S cm⁻¹, ascribed to the lower polythiophene content. In contrast, the reverse scan showed a distinct but small peak (10^{-6} S cm⁻¹), which is attributed to less pronounced anodic degradation of the polythiophene's conjugated π system. The highest conductivities are observed around the half-wave potential of the Ru^{III}/Ru^{II} couple, which suggests a significant contribution of the ruthenium centres to the conductance. In agreement with the CV data, the redox processes of the complexes are fully reversible, although the influence of oligo- and polythiophene moieties is clearly apparent by the broadened CV. The 1 : 1 polymer poly(**1c**) exhibits a similar behaviour, but the higher ruthenium content leads to an almost reversible redox chemistry with a comparable maximum conductivity of 5×10^{-6} S cm⁻¹. In case of the *homo*-polymer poly(**1d**), the conductivity reaches a maximum of about 1.5×10^{-5} S cm⁻¹ for a dc potential of 700 mV, which corresponds to the half-wave potential of the Ru^{III}/Ru^{II} redox process. At this potential, the maximum conductance is expected due to the optimal 1 : 1 ratio of charge-carrying and charge-accepting units, *i.e.*, Ru^{III} : Ru^{II} centres.⁴⁶ The polymers derived from complex **2** show, in principal, a similar behaviour as their already discussed counterparts (see ESI†).

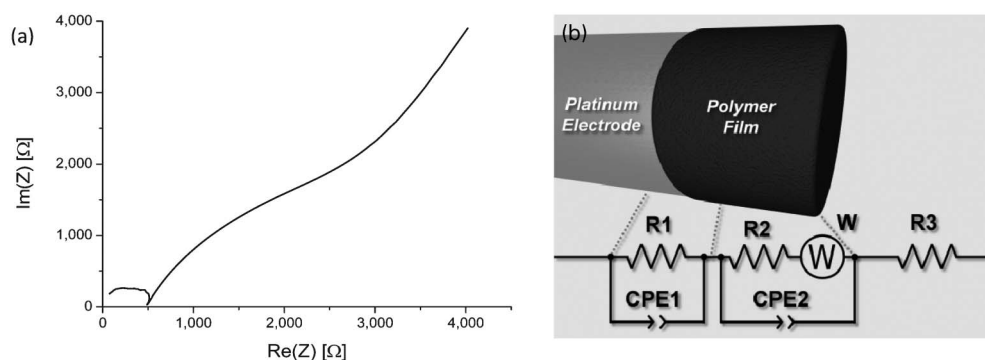


Fig. 2 (a) Exemplary Nyquist plot for poly(**1d**) at 950 mV. (b) Equivalent circuit used for the fit of the EIS data (R1: electrolyte–polymer charge-transfer resistance; CPE1: electrolyte–polymer interface charging; R2: polymer-film charge-transport resistance; CPE2: polymer-film charge-separation capacitance; W: Warburg impedance due to ionic diffusion; R3: electrolyte resistance).

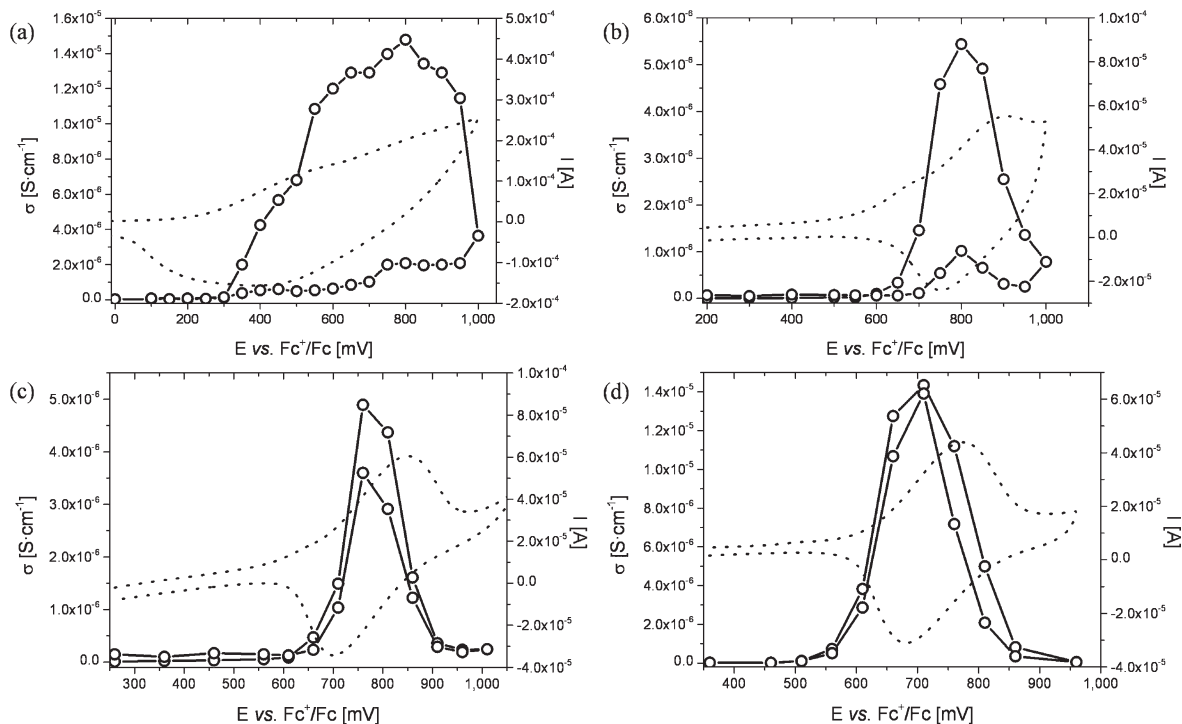


Fig. 3 Conductivities of a) poly(1)a, b) poly(1)b, c) poly(1)c, and d) poly(1)d films on a platinum electrode depending on the applied dc potential (solid line; dotted line: respective CV).

Co-polymers poly(2)a and poly(2)b exhibit a vast conductivity drop during the backward scan decreasing from 10^{-5} S cm^{-1} and 3×10^{-6} S cm^{-1} , respectively, to 10^{-6} S cm^{-1} in both cases. Again, this behaviour is most likely attributed to the diminished π conjugation within the polythiophene chains caused by anodic degradation. For poly(2)c and poly(2)d, the ruthenium(II) unit is determinant, leading to a sharp increase of conductivity when oxidizing the metal complex with peak values of 8×10^{-6} S cm^{-1} and 1.3×10^{-5} S cm^{-1} , respectively. The backwards scans reveal reversible behaviour without any significant loss in conductivity. At this point, it is important to realize that the absolute conductivity values are also a property of the (inhomogeneous) material. Hence, a more detailed analysis and discussion of the charge transport would involve the separate measurement of the charge mobility and charge concentration, which is beyond the scope of this study.

The optical properties of the films were investigated by UV-vis absorption and steady-state emission spectroscopy (see ESI†). In the case of the *homo*-polymers, absorption bands are centred around 530 and 565 nm for poly(1)d and poly(2)d, respectively, assigned to the metal-to-ligand charge-transfer (MLCT) absorptions of the ruthenium(II) complex units. Admixing thiophene with a 1 : 5 ratio leads to a blue shift of the peak maxima towards 520 and 510 nm for poly(1)b and poly(2)b, respectively. The absorption spectra of the 1 : 20-ratio *co*-polymers exhibit the typical broad band of polythiophene,⁵⁰ *i.e.*, a maximum around 450 nm, and a long-wavelength shoulder at around 600 nm, arising from the additional MLCT contributions of the complexes.

The UV-vis emission measurements display peaks at 760 and 735 nm for the polymers obtained from 1 and 2, respectively, even under ambient conditions, *i.e.*, at room temperature in the presence of oxygen, which is unique for a film of a tridentate ruthenium(II) system. The signals do not shift with changing thiophene content indicating that the emission is purely based on the metal complex, even for the polythiophene-dominated 1 : 20 *co*-polymers.

Conclusions

In summary, we presented the defined electrochemical preparation of a series of *co*-polymers consisting of ruthenium(II)-2,6-di(quinolin-8-yl)pyridine complexes with varying contents of thiophene. The electro-*co*-polymerization was monitored by cyclic voltammetry, which showed the facile deposition of the polymers onto the electrode. The electrochemical properties of the thin films were studied by cyclic voltammetry and electrochemical impedance spectroscopy, which revealed conductivities up to 10^{-5} S cm^{-1} . An increased ruthenium(II)-complex content leads to well-behaved, reversible switching of conductivity combined with a remarkably enhanced electrochemical stability upon oxidation. Notably, all films show luminescence around 750 nm originating from the ruthenium(II) units under ambient conditions in the presence of oxygen – a common challenge for conventional organic chromophores in functional devices. Hence, the presented approach benefits from a facile and well-defined

preparation *via* electro-*co*-polymerization, enhanced electrochemical stability, redox-chemical switching of the conductivities, and the typical favourable excited-state properties of the metal complex. Future work will be directed to utilize this unique combination of optical and electrochemical properties in photovoltaic devices, light-emitting materials, or light- and redox-driven sensors.

Acknowledgements

The authors acknowledge the “Bundesministerium für Bildung und Forschung”, the European Social Fund (ESF), the “Thüringer Aufbaubank” (TAB), and the Thuringian Ministry of Economy, Employment and Technology (TMWAT) for financial support. M. J. is grateful for financial support of the Carl-Zeiss-Stiftung. We also thank Prof. Dr Anna Ignaszak for instrumental support and discussions.

References

- 1 A. P. Kulkarni, C. J. Tonzola, A. Babel and S. A. Jenekhe, *Chem. Mater.*, 2004, **16**, 4556–4573.
- 2 L. Akcelrud, *Prog. Polym. Sci.*, 2003, **28**, 875–962.
- 3 L. S. Hung and C. H. Chen, *Mater. Sci. Eng., R*, 2002, **39**, 143–222.
- 4 U. Lange, N. V. Roznyatovskaya and V. M. Mirsky, *Anal. Chim. Acta*, 2008, **614**, 1–26.
- 5 X. Luo, A. Morrin, A. J. Killard and M. R. Smyth, *Electroanalysis*, 2006, **18**, 319–326.
- 6 P. D. Beer and E. J. Hayes, *Coord. Chem. Rev.*, 2003, **240**, 167–189.
- 7 G. Dennler, M. C. Scharber and C. J. Brabec, *Adv. Mater.*, 2009, **21**, 1323–1338.
- 8 H. Hoppe and N. S. Sariciftci, *J. Mater. Res.*, 2004, **19**, 1924–1945.
- 9 M. Grätzel, *J. Photochem. Photobiol., C*, 2003, **4**, 145–153.
- 10 A. Facchetti, *Chem. Mater.*, 2011, **23**, 733–758.
- 11 A. Pivrikas, N. S. Sariciftci, G. Juška and R. Österbacka, *Progr. Photovolt.: Res. Appl.*, 2007, **15**, 677–696.
- 12 I. Robel, V. Subramanian, M. Kuno and P. V. Kamat, *J. Am. Chem. Soc.*, 2006, **128**, 2385–2393.
- 13 J. B. Baxter and E. S. Aydil, *Appl. Phys. Lett.*, 2005, **86**, 053114.
- 14 M. Riede, T. Mueller, W. Tress, R. Schueppel and K. Leo, *Nanotechnology*, 2008, **19**, 424001.
- 15 M. K. Nazeeruddin and M. Grätzel, in *Photofunctional Transition Metal Complexes*, ed. V. W. W. Yam, Springer, Berlin, 2007, vol. 123, pp. 113–175.
- 16 P. Peumans, A. Yakimov and S. R. Forrest, *J. Appl. Phys.*, 2003, **93**, 3693–3723.
- 17 A. Hagfeldt and M. Grätzel, *Acc. Chem. Res.*, 2000, **33**, 269–277.
- 18 S. Günes, H. Neugebauer and N. S. Sariciftci, *Chem. Rev.*, 2007, **107**, 1324–1338.
- 19 K. M. Coakley and M. D. McGehee, *Chem. Mater.*, 2004, **16**, 4533–4542.
- 20 C. J. Brabec, N. S. Sariciftci and J. C. Hummelen, *Adv. Funct. Mater.*, 2001, **11**, 15–26.
- 21 Z. Li and C. R. McNeill, *J. Appl. Phys.*, 2011, **109**, 074513.
- 22 C. Groves, J. C. Blakesley and N. C. Greenham, *Nano Lett.*, 2010, **10**, 1063–1069.
- 23 I. Hwang, C. R. McNeill and N. C. Greenham, *J. Appl. Phys.*, 2009, **106**, 094506.
- 24 G. R. Whittell, M. D. Hager, U. S. Schubert and I. Manners, *Nat. Mater.*, 2011, **10**, 176–188.
- 25 C.-L. Ho and W.-Y. Wong, *Coord. Chem. Rev.*, 2011, **255**, 2469–2502.
- 26 G. R. Whittell and I. Manners, *Adv. Mater.*, 2007, **19**, 3439–3468.
- 27 C. Friebe, M. D. Hager, A. Winter and U. S. Schubert, *Adv. Mater.*, 2012, **24**, 332–345.
- 28 J. Heinze, B. A. Frontana-Urbe and S. Ludwigs, *Chem. Rev.*, 2010, **110**, 4724–4771.
- 29 C.-J. Yao, J. Yao and Y.-W. Zhong, *Inorg. Chem.*, 2012, **51**, 6259–6263.
- 30 C.-J. Yao, Y.-W. Zhong, H.-J. Nie, H. D. Abruña and J. Yao, *J. Am. Chem. Soc.*, 2011, **133**, 20720–20723.
- 31 X. J. Zhu and B. J. Holliday, *Macromol. Rapid Commun.*, 2010, **31**, 904–909.
- 32 J. Hjelm, R. W. Handel, A. Hagfeldt, E. C. Constable, C. E. Housecroft and R. J. Forster, *Inorg. Chem.*, 2005, **44**, 1073–1081.
- 33 S. S. Zhu, R. P. Kingsborough and T. M. Swager, *J. Mater. Chem.*, 1999, **9**, 2123–2131.
- 34 R. M. Leasure, T. Kajita and T. J. Meyer, *Inorg. Chem.*, 1996, **35**, 5962–5963.
- 35 P. Denisevich, H. D. Abruña, C. R. Leidner, T. J. Meyer and R. W. Murray, *Inorg. Chem.*, 1982, **21**, 2153–2161.
- 36 C. Friebe, H. Görls, M. Jäger and U. S. Schubert, *Eur. J. Inorg. Chem.*, DOI: 10.1002/ejic.201300359.
- 37 M. Abrahamsson, M. Jäger, R. J. Kumar, T. Österman, P. Persson, H.-C. Becker, O. Johansson and L. Hammarström, *J. Am. Chem. Soc.*, 2008, **130**, 15533–15542.
- 38 M. Abrahamsson, M. Jäger, T. Österman, L. Eriksson, P. Persson, H.-C. Becker, O. Johansson and L. Hammarström, *J. Am. Chem. Soc.*, 2006, **128**, 12616–12617.
- 39 W. Chen and G. Xue, *Prog. Polym. Sci.*, 2005, **30**, 783–811.
- 40 S. Alkan, C. A. Cutler and J. R. Reynolds, *Adv. Funct. Mater.*, 2003, **13**, 331–336.
- 41 K. Meerholz, H. Gregorius, K. Müllen and J. Heinze, *Adv. Mater.*, 1994, **6**, 671–674.
- 42 A. J. Bard and L. R. Faulkner, *Electrochemical Methods*, John Wiley & Sons, Inc., New York, 2nd ed., 2001.
- 43 J. F. Rubinson and Y. P. Kayinamura, *Chem. Soc. Rev.*, 2009, **38**, 3339–3347.
- 44 C. H. Hamann, A. Hamnett and W. Vielstich, *Electrochemistry*, Wiley-VCH, Weinheim, 2nd ed., 2007.
- 45 B. W. Johnson, D. C. Read, P. Christensen, A. Hamnett and R. D. Armstrong, *J. Electroanal. Chem.*, 1994, **364**, 103–109.
- 46 C. E. D. Chidsey and R. W. Murray, *J. Phys. Chem.*, 1986, **90**, 1479–1484.
- 47 A. Zykwincka, W. Domagala, B. Pilawa and M. Lapkowski, *Electrochim. Acta*, 2005, **50**, 1625–1633.
- 48 U. Barsch and F. Beck, *Electrochim. Acta*, 1996, **41**, 1761–1771.
- 49 Z. Qi and P. G. Pickup, *Anal. Chem.*, 1993, **65**, 696–703.
- 50 K. Kaneto, K. Yoshino and Y. Inuishi, *Solid State Commun.*, 1983, **46**, 389–391.

Publication A11: “Designing cyclometalated ruthenium(II)
complexes for anodic electropolymerization”

Christian Friebe, Benjamin Schulze, Helmar Görls, Michael Jäger,
Ulrich S. Schubert

Chem. Eur. J., DOI: 10.1002/chem.201301439.

Reprinted with permission from: WILEY-VCH Weinheim (Copyright 2013)

Designing Cyclometalated Ruthenium(II) Complexes for Anodic Electropolymerization

Christian Friebe,^{[a, b]‡} Benjamin Schulze,^{[a, b]‡} Helmar Görls,^[c] Michael Jäger,^[a, b] and Ulrich S. Schubert*^[a, b]

[a] C. Friebe, B. Schulze, Dr. M. Jäger, Prof. Dr. U. S. Schubert
Laboratory of Organic and Macromolecular Chemistry (IOMC)
Friedrich Schiller University Jena
Humboldtstr. 10, 07743 Jena, Germany
E-mail: ulrich.schubert@uni-jena.de

[b] C. Friebe, B. Schulze, Dr. M. Jäger, Prof. Dr. U. S. Schubert
Jena Center for Soft Matter (JCSM)
Friedrich Schiller University Jena
Philosophenweg 7, 07743 Jena, Germany

[c] Dr. H. Görls
Laboratory of Inorganic and Analytic Chemistry
Friedrich Schiller University Jena
Humboldtstr. 8, 07743 Jena, Germany

‡ C. Friebe and B. Schulze contributed equally to this work.

Supporting information for this article is available on the WWW under <http://www.chemeurj.org/> or from the author.

Abstract: For the first time, anodic electropolymerization of cyclometalated ruthenium(II) complexes is shown. Competing oxidative decomposition reactions can be overcome through modification of the involved redox

potentials by introduction of electron-withdrawing substituents, namely nitro groups, at the cyclometalating phenyl ring. The generated functionalized ruthenium(II) complexes allow the electrochemical preparation of thin

polymer films, which show a broad UV-vis absorption as well as stable and reversible redox switchability. The presented complexes, thus, reveal potential for photovoltaic applications based on photoredox-active films.

Introduction

The ruthenium(II)-polypyridyl motif represents a highly favorable building block, with regard to applications as photosensitizer units (*e. g.* in solar cells, light-driven catalysis, water splitting).^[1] In particular the incorporation of strong electron-donating ligands enables the formation of ruthenium(II) complexes providing long excited-state lifetimes and broad absorption features, both being crucial for an efficient photosensitizer dye.^[2] Thereby, ruthenium(II) complexes that contain thiocyanate ligands have been applied very successfully.^[3] However, the monodentate thiocyanates cause a lowered complex stability and impede further functionalization with regard to dye optimization. Hence, alternative, polydentate ligands that feature strong electron donors, namely anionic carbon^[4] and nitrogen^[5] atoms as well as classical^[6] and mesoionic^[7] *N*-heterocyclic carbenes, were designed for sensitizer application. In this regard, we recently presented a series of complexes based on a cyclometalating, tridentate ligand that possesses 1,2,3-triazole moieties, which were introduced by copper(I)-catalyzed azide-

alkyne 1,3-dipolar cycloaddition (CuAAC) allowing the facile assembly of functionalized ligands. The complexes showed prolonged excited-state lifetimes, redox stability, and the suitability for application in dye-sensitized solar cells.^[4a, 8]

Most of the photosensitizer applications require the processing of the dye in thin films to allow light absorption as well as efficient charge transfer to the affiliated reaction site. Thereby, an instrumentally simple technique for the formation of defined layers is the electropolymerization, *i. e.* the formation of insoluble polymers by coupling of electrochemically generated monomer radicals on an electrode surface.^[9] Like that, different ruthenium(II) complexes of polypyridyl-type ligands were already successfully used to form polymeric coatings.^[10] Lately, also cyclometalated systems were polymerized *via* electrochemical reduction^[11] and, very recently, also by an anodic approach.^[12] However, up to now, successful oxidative electropolymerization of cyclometalated ruthenium(II) complexes was reported only rarely in literature, although the anodic polymerization allows the usage of aromatic electropolymerizable units like thiophene, 3,4-ethylenedioxythiophene (EDOT), pyrrole, etc. These enable the assembly of

metallopolymers^[13] that feature π -conjugated spacer units providing additional chromophores and potentially enabling an intramolecular electron transfer after photooxidation of the complex.^[14] This, in turn, leads to a more efficient UV-vis absorption and an extended charge separation, respectively. A potential challenge is the high reactivity of the electron-rich central phenyl ring of the cyclometalating ligand, which possesses high spin density and forms radicals when the required potentials are applied and lead possibly to electrochemical coupling.^[15] Nevertheless, redox stability could be shown in UV-vis-NIR spectroelectrochemical experiments, at least for the first oxidation state.^[4a] Still, the electron-rich aromatic moiety may give rise to side reactions or decomposition under the highly positive potentials required for the electropolymerization.

In this work, we present the preparation and electrochemical polymerization of ruthenium(II) complexes based on 1,2,3-triazole-containing, cyclometalating ligands. Two structural motifs are introduced, varying in the presence and absence of methyl groups at the linking phenyl rings, which prevent and allow, respectively, a *co*-planarization of the phenyl-thiophene and the central metal-coordinating triazole moieties and may, thus, affect the extent of π conjugation between thiophene and triazole. However, electronic coupling through the triazole is not expected.^[16] The synthesized monomer complexes were fully characterized; the prepared polymer films were studied by cyclic voltammetry, UV-vis absorption spectroscopy, and UV-vis-NIR spectroelectrochemistry. Furthermore supporting computational calculations based on density functional theory (DFT) were carried out to gain further insight into the electrochemical behavior.

Results and Discussion

Synthesis and electrochemical behavior of thiophene-equipped complexes: To gain a first survey of the ability of the cyclometalated ruthenium(II) complexes to undergo anodic electropolymerization, two complexes possessing 4-(2-thienyl)-phenyl moieties at the triazole rings were synthesized (Scheme 1) and studied by electrochemical means.

In order to allow a rapid and modular access to the thiophene-functionalized cyclometalating ligands, we rely on a click-derived triazole-based framework. It has been demonstrated that the involved triazole units can be used as analogues for pyridine donors.^[17] Initial attempts to directly couple 2-thienylboronic acid to the corresponding bromo-functionalized HNCN ligand framework *via* Suzuki cross-coupling were not successful (sluggish reaction, intractable reaction mixtures). Likewise, an attempted cyclometalation using a bromo-functionalized HNCN ligand in order to install the thiophene after the complexation was precluded by a partial debromination resulting in an inseparable mixture of complexes.^[18] The alternative approach to first install the thiophene on the azide-functionalized bromobenzene afforded the desired 2-(4-azidophenyl)thiophene building blocks in reasonable yields. Interestingly, the Suzuki cross-coupling tolerated the presence of aryl azides despite their known tendency to form phosphazides and phosphimines with free or coordinated phosphines of the palladium catalyst.^[19] The subsequent copper(I)-catalyzed azide-alkyne 1,3-dipolar cycloaddition (CuAAC) afforded the thiophene-containing 1,3-bis(1,2,3-triazolyl)benzene ligands in good yields. In contrast to the initially attempted cross-coupling method, the CuAAC greatly simplifies the purification as the educt and byproducts are readily removed, which is particularly important in the case of low product solubility, *e. g.* for **HTph**. For **HTphMe**, the solubility is much higher due to the steric interactions between the triazoles and the

ortho methyl groups of the outer phenyl rings, which enforce a twisting out of plane and thereby preclude π stacking. As a result, X-ray-quality single crystals could be grown by vapor diffusion of diethyl ether into a concentrated dichloromethane solution (see Figure S42). The cyclometalation was achieved in fair yields using $[\text{Ru}^{\text{II}}(\text{tpy})(\text{CH}_3\text{CN})_3][\text{PF}_6]_2$ (tpy = 2,2':6',2''-terpyridine) as precursor.^[4a]

Subsequently, the monomer complexes were electrochemically characterized; the obtained cyclic voltammograms (CVs) and differential pulse voltammograms (DPPs) are depicted in the Supporting Information (Figure S45 and S46), the first redox potential values are given in Table 1. The CV of **RuTph** and **RuTphMe** reveal a reversible redox process with a half-wave potential of 0.10 V, which is, based on preceding computational investigations on related systems,^[4a] assigned to the depopulation of a mixed ruthenium- and cyclometalating ligand-based orbital. In the region around 1.1 V to 1.4 V, further oxidation processes appear, including the thienyl radical cation formation being crucial for the electropolymerization. Thereby, the thienyl-based signals possess a significantly larger peak current than the first redox processes. This is attributed to a lack of electronic coupling since the 1,2,3-triazole is known to interrupt π conjugation,^[16] which leads to simultaneous oxidation of both thiophene moieties at the same redox potential. The first, ligand-based reduction appears at -2.04 V for **RuTph** and at -2.06 V for **RuTphMe** and is irreversible in both cases.

The electropolymerization experiments were carried out potentiodynamically in different solvents using 0.1 M Bu_4NPF_6 as electrolyte. The first studies were executed in acetonitrile. Including the higher oxidations at 1.2 to 1.4 V into the potential cycling, both **RuTph** and **RuTphMe** show a rapid decrease of all redox signals indicating decomposition of the complexes (see Figure S47). Since changing the potential range or scan rate did not lead to a successful polymerization, the solvent was changed to dichloromethane, which has a lower nucleophilicity than acetonitrile possibly leading to a diminished rate of side reactions^[9] (see Figure S48 and Figure 1 exemplarily for **RuTphMe**). For **RuTph**, the cyclic voltammetric development is divided in two phases: During the first eleven cycles, an increase of the original ruthenium-based redox signal occurs, indicating the formation of the desired polymer, which is, however, accompanied by the arising of additional signals at around -0.1 and 0.9 V, suggesting the formation of byproducts. After the eleventh cycle, the redox signals in the region between -0.4 and 0.4 V start to decrease, which is most likely due to the electrochemical decomposition of the formed compounds. For **RuTphMe**, likewise, additional redox processes appear at around -0.2 V, but already during the third cycle a signal decrease, *i. e.* decomposition, starts. Also further studies involving the use of Lewis acids (*e. g.* $\text{BF}_3\cdot\text{OEt}_2$, borate esters)^[20] or weak bases (*e. g.* water, 2,6-di-*tert*-butylpyridine),^[9] did not result in a successful electropolymerization. $\text{BF}_3\cdot\text{OEt}_2$ in acetonitrile even caused the displacement of the cyclometalating ligand leading to the undesired recovery of the $[\text{Ru}^{\text{II}}(\text{tpy})(\text{CH}_3\text{CN})_3]^{2+}$ precursor species (see Figure S43 and S49).

We assumed that the decomposition is caused by an inherent electrochemical process of the complexes. This assumption was supported by comparison of the cyclic voltammograms of the thiophene-equipped system with its parent complex devoid of thiophene units (**Ru**, Figure 2), revealing an additional, irreversible redox process at around 1.2 V, which would be overlaid by the thienyl-based signals. Thus, oxidation of the thienyl units would not be possible without inducing an irreversible oxidation reaction of the complex core moiety.

Synthesis and electrochemical behavior of redox-modified NO₂ complexes: To overcome the problem of electrochemical decomposition, we attempted to shift the respective irreversible oxidation potential beyond the thiophene-based one. Therefore, a nitro group was introduced at the 4-position of the central phenyl ring of the cyclometalating ligand to increase the redox potentials as observable for the respective thiophene-free parent complex (**RuNO₂**, Figure 2).

The nitro groups were directly attached on the cyclometalated phenyl ring using Cu(NO₃)₂ (Scheme 2). Here, the common Menke conditions^[4a, 21] had to be attenuated to prevent the nitration of the thiophene moiety.^[22] In fact, even if a high excess of Cu(NO₃)₂ is used in dichloromethane / methanol as a solvent mixture, solely the nitration on the cyclometalated phenyl ring is observed, which underlines the high reactivity in the position *para* to the carbanion and, conversely, the ease of manipulating the carbanion donation in cyclometalated complexes. The pure complexes were obtained after counterion exchange to hexafluorophosphate and crystallization by vapor diffusion of diethyl ether into a concentrated DMF solution. The desired nitro-functionalization was proven unambiguously by single crystal X-ray diffraction (Figure 3).^[23] Bond lengths and bite angles as well as the dihedral angles of the nitro group relative to the central phenyl ring (52°) and of the mesityl ring relative to the triazole (62–72°) are comparable to the previously reported crystallographic data.^[4a] Accordingly, the electron-withdrawing character of the nitro group is attenuated and the π conjugation between the complex and the *N*-substituents of the triazole is broken. Note that also only a weak π conjugation into the triazoles for **RuTph** is indicated by DFT (*vide infra*), in line with literature.^[16] On the other hand, small torsion between thiophene and mesityl allows for extended conjugation, which may give rise to an additional chromophore after the electropolymerization (*vide infra*). In addition, a bromo function was introduced exemplarily to the central phenyl ring of **RuTph** using CuBr₂ in dichloromethane / methanol^[24] aiming on blocking the reactive *para* position of the central phenyl ring, while maintaining the oxidation potential reasonably constant. However, for the latter, the electropolymerization control experiments resulted, as for the non-brominated species, in non-defined electrochemical processes (see Figure S50), thus ruling out potential side reactions in the position *para* to the carbanion.

Electrochemical characterization of **RuTphMeNO₂** and **RuTphNO₂** showed that both the first oxidation and the first reduction potentials are anodically shifted by about 200 mV (see Table 1) due to the electron-withdrawing influence of the nitro group. As for the nitro-free counterparts, the first, reversible anodic signal is assigned to an oxidation of the mixed ruthenium(II) / cyclometalating-ligand moiety.^[4a] Importantly, as intended, the second oxidation is easier to achieve than the irreversible oxidation of the parent **RuNO₂** complex (see Figure 2). Hence, this redox process is assigned to the thienyl-based oxidation, which should, in turn, enable electrochemical polymerization without decomposition. In contrast to the preceding complexes, the first reduction is reversible and a further process occurs at -2.10 V.

Additionally, DFT calculations were executed to examine the energies and spin-density distributions of the singly and doubly oxidized states of the four complexes (see Figure 4 and Figure S68 to S77): Firstly, for all complexes, the assignment of the first oxidation to a metal- and cyclometalating ligand-based process is confirmed. The second oxidation process may formally lead to a singlet or a triplet state, depending whether the removed electron has alpha or beta spin, respectively. Applying a closed-shell

configuration upon the second oxidation formally enforces a metal-ligand-based oxidation, which requires a potential that is anodically shifted by 1.33 to 1.55 V in comparison to the first oxidation process. While the triplet configuration of the parent complexes **Ru** and **RuNO₂** displays a small stabilization, the thiophene-containing complexes reveal the localization of the second spin on one phenyl-thiophene unit causing a potential difference of only 0.80 to 1.15 V compared to the first oxidation. Notably, the computed second oxidation should be regarded as an upper limit, considering the artificial stabilization of extended π -systems,^[25] the effect of the surrounding charges,^[26] and the challenges to accurately treat spin-spin interactions,^[27] which becomes particularly important in strongly-coupled open-shell systems.^[28] The introduction of the nitro substituent leads to an anodic shift of the metal-ligand-based oxidations by approximately 0.25 V, whereas the thiophene-phenyl-based oxidation remains almost unchanged. Hence, the calculations support the observed behavior of the systems upon nitration, but could not definitely support the considerations concerning the electrochemical decomposition *via* a second irreversible oxidation process. However, the observed deviations between experiment and calculations for the model complex **Ru**, namely the difference for the second oxidation, have to be taken into account also for the thiophene-functionalized complexes.

The electropolymerization of **RuTphMeNO₂** in dichloromethane was studied and the respective cyclic voltammograms are shown in Figure 5. The peak current of the first oxidation of the complex rises during the first five to ten cycles, as expected for a successful electropolymerization. However, the slope is comparatively low, indicating a low polymerization rate, and decreases afterwards, reaching a plateau at the twentieth cycle.^[29] Hence, the obtained films are very thin (the apparent surface coverage was determined to be only $\Gamma = 1 \cdot 10^{-9}$ mol·cm⁻²). Nevertheless, their characterization by cyclic voltammetry, depicted in Figure 6, and UV-vis spectroscopy (*vide infra*) was possible. The CV shows a reversible first oxidation with a half-wave potential of 0.28 V, slightly cathodically shifted compared to the dissolved monomer complex. Furthermore, the peak current grows linearly with increasing scan rate up to 500 mV·s⁻¹, indicating the formation of conductive films with only weakly diffusion-controlled charge migration.^[9, 30]

In a similar manner, anodic polymerization attempts were also carried out for the non-methylated congener **RuTphNO₂**. Notably, only relatively low concentrations (around 50 μ g·mL⁻¹ or 5·10⁻⁵ M) could be applied due to the poor solubility of the complex. However, in contrast to its methylated counterpart, a linear increase with a steady slope of the monitored peak current occurred within the 30 cycles that were conducted (Figure 7)^[31] and a surface coverage of $\Gamma = 2 \cdot 10^{-9}$ mol·cm⁻² was obtained. Additional signals appeared at 0.45 and -0.05 V, which are tentatively assigned to non-reacted radicals that were not incorporated into the polymer. Comparable features had already been observed in former electropolymerization studies.^[18] The characterization of the obtained thin polymer films by CV displayed a reversible oxidation signal at 0.25 V, thus slightly cathodically shifted with respect to both its respective monomer and the **RuTphMeNO₂** polymer film. As for the latter, the peak-current scan-rate relationship shows a linear behavior up to 500 mV·s⁻¹ (Figure 8). Notably, the accompanying signals at 0.45 and -0.05 V are not present in the film CVs, supporting the assignment to non-reacted species.

Additionally, electropolymerization studies on the nitro-functionalized complexes using higher vertex potentials were carried out, which resulted in a non-defined reaction process, like

already observed for the non-nitro species (Figure S52 and S53). Thus, the enhanced electropolymerization ability upon nitro-functionalization can be indeed attributed to shifted redox potentials, but not to blocked reaction sites.

Co-polymerization experiments: To further enhance the electropolymerization performance of the **RuTphMeNO₂** complex, *co*-polymerization attempts with 3,4-ethylenedioxythiophene (EDOT) as the second *co*-monomer were carried out. Since the ruthenium(II) complexes are diluted within the resulting polymers, diminishing of undesirable side reactions between the metal complexes is expected. Thus, different molar ratios were used to identify the EDOT content that leads to an improved electropolymerization. The resulting CVs during the potentiodynamic anodic polymerization experiments are shown exemplarily for a ratio of 1:1 in Figure 9 (see Figure S54 for complex-EDOT ratios of 5:1, 2:1, and 1:5). Using a 5:1 ratio, no improvement of the polymerization process is noticeable at all. Like for the pure complex, the peak-current development indicates an interruption around the fifteenth cycle. However, an additional plateau arises between -0.2 and 0.6 V, which is assigned to the formation of PEDOT chains (see Figure S58 for comparison). For a molar ratio of 2:1, an enhanced PEDOT generation is observable, but, still, the slope of the ruthenium(II)-based peak-current increase is reduced after 15 cycles and the further current development parallels the pure PEDOT-based one. This indicates that only PEDOT is formed from that cycle on and no more ruthenium(II) complex is included. Eventually, increasing the EDOT molar ratio to 50% leads to a significantly improved polymerization: The ruthenium(II)-related current increases linearly at least up to the fortieth cycle with a larger slope than the EDOT-related current, indicating that the ruthenium(II) moiety is still incorporated into the generated *co*-polymer. A similar behavior was observed for an excess of EDOT, namely for a ruthenium(II)-complex-EDOT ratio of 1:5, with an expectedly higher current for the PEDOT-related background. This way, *co*-polymer films containing the cyclometalated ruthenium(II) complex were prepared and characterized. Cyclic voltammetry revealed a reversible oxidation process for both the 1:1 and the 1:5 *co*-polymers at around 0.27 V accompanied by a broad, undefined redox current assigned to the electrochemical doping of PEDOT chains. In both cases, the peak-current-scan-rate relationship is linear up to 500 mV·s⁻¹ (Figure 10 and S56) and an apparent surface coverage of 5·10⁻⁹ mol·cm⁻² and 8·10⁻⁹ mol·cm⁻² (with respect to the complex moieties) for the 1:1 and the 1:5 ratio, respectively, was determined.

Like for its methylated analogue, *co*-polymers of **RuTphNO₂** and EDOT were electrochemically prepared using molar ratios of 1:1 and 1:5 (see Figure S55). For an equimolar ratio, only marginal differences, namely a small current plateau between -0.2 and 0.5 V, occur, compared to the *homo*-polymerization. This behavior is most likely attributed to the very low concentration (below 10⁻⁴ M) of the EDOT, which is required because of the low complex solubility. In contrast, the fivefold EDOT excess led to the distinct formation of PEDOT moieties, indicated by the development of a broad current plateau. As for **RuTphMeNO₂**, the peak current that corresponds to the Ru^{III}/Ru^{II} redox couple increases faster than the subjacent PEDOT-related current, showing that both the ruthenium(II) complex and EDOT are polymerized. Subsequent electrochemical characterization confirmed the achieved findings: The cyclic voltammogram of the 1:1 polymer (Figure S57) resembles in principle the *homo*-polymer with only small deviations, while the films from the higher EDOT ratio revealed significant PEDOT influence, namely a broad, underlying current plateau. Analysis of

the Ru^{III}/Ru^{II}-related current revealed an apparent surface coverage of ca. 2·10⁻⁹ mol·cm⁻² in both cases.

UV-vis spectroscopy and UV-vis-NIR spectroelectrochemistry:

The UV-vis absorption and emission features of the monomer complexes are depicted in Table 2 and the Supporting Information (Figure S59). The absorption spectra exhibit a set of bands between 450 and 700 nm that are assigned to metal-to-ligand and metal/ligand-to-ligand charge-transfer (MLCT and MLLCT, respectively) transitions.^[4a] In case of **RuTphMeNO₂** and **RuTphNO₂**, these bands are blue-shifted due to the electron-withdrawing nature of the nitro group, causing a stabilization of the highest occupied molecular orbitals, which are located on the cyclometalating ligand and the metal.^[4a] An additional band can be found at around 400 nm. Here, the introduction of methyl groups at the phenyl spacer moieties causes a hypsochromic shift as well as a decreasing extinction coefficient. This is most likely because of a diminished π conjugation within the triazole-phenyl-thienyl fragment due to sterical hindrance by the methyl groups precluding a complete *co*-planarization. Emission measurements revealed photoluminescence at around 740 nm for the nitro-free **RuTph** and **RuTphMe**, while the emission maxima for the nitro-substituted species are, as expected, blue-shifted by about 900 to 1,000 cm⁻¹.

Comparison of the UV-vis absorption spectrum of the **RuTphMeNO₂** polymer film with the monomer complex showed an only negligible red shift of the MLCT maximum of 110 cm⁻¹ from 520 nm for the drop-casted monomer film to 523 nm for the polymer, accompanied by a broadening and a loss of structural features for the MLCT band (Figure 11, top). Additionally, an intense peak arises at 341 nm, which is assigned to LC transitions that are located on the *bis*-phenylthienyl moiety,^[32] being only present in the polymer, but not in the monomer, and thus confirming the coupling of the monomer complexes. Unfortunately, spectroelectrochemical investigations could not be executed since the obtained films were too thin to give an observable absorption signal within the used setup.

For the polymer film from **RuTphNO₂**, UV-vis absorption measurements exhibited a prominent, MLCT-based band at 531 nm, slightly red-shifted by 220 cm⁻¹ with respect to the monomer film (525 nm) (Figure 11, bottom) and by 290 cm⁻¹ compared with the methylated analog, suggesting a higher degree of conjugation in the non-methylated polymer. Likewise, the additional band that is present in the UV region, assigned to *bis*-phenylthienyl units^[32] formed through the polymerization, is red-shifted by 590 cm⁻¹ to 348 nm. Additionally, UV-vis-NIR spectroelectrochemical studies on the polymer film were carried out and are exemplarily shown in Figure 12. The spectral changes during the oxidation process with a half-wave potential of 0.25 V resemble in principle the characteristic features observed for the present cyclometalated ruthenium(II) complex moiety, namely a bleaching of the MLCT absorption, on the one hand, and the rise of a broad and weak band between 700 and 900 nm, which is assigned to ligand-to-metal charge-transfer transitions.^[4a] Repeated switching between the initial and the oxidized state turned out to be reversible for at least the 30 cycles that were run, proving the redox stability of the prepared polymer film, and revealed switching times (defined by the time that is necessary to undergo 95% of the full transmission change^[33]) of 1.8 s.

The UV-vis absorption spectra of the 1:1 and 1:5 *co*-polymer films of **RuTphMeNO₂** show absorption maxima at 523 nm and 341 nm, accompanied by a broad band in the NIR region (see Figure S60). With increasing EDOT ratio, the relative intensity of

the latter rises; this is assigned to a growing content of PEDOT moieties, which exhibit a strong NIR absorption (see Figure S62 for comparison). Simultaneously, the band at 341 nm, related to *bis*-phenylthienyl moieties, decreases with respect to the MLCT absorption since the *bis*-thienyl bridges are replaced by *oligo*-EDOT blocks for the *co*-polymers. UV-vis-NIR spectroelectrochemical studies of the *co*-polymer films showed a combination of **Ru** and PEDOT characteristics, namely the vanishing of the MLCT band between 400 and 600 nm and the rise of a broad, intense band in the NIR region, respectively. In the long-wavelength visible region, also the behavior of the metal complex, *i. e.* the formation of a new absorption band, is dominant, but, in particular for the 1:5 *co*-polymer, superimposed by a PEDOT-related absorption decrease. Notably, for the 1:1 *co*-polymer, the PEDOT-based NIR absorption is blue-shifted with respect to the 1:5 polymer, indicating the presence of shorter *oligo*-EDOT chains, which possess a smaller conjugated π system, while the 1:5 system exhibits an NIR absorption maximum similar to the pure-PEDOT reference study, indicating that the maximum conjugation length is already achieved. Applying a re-reducing potential recovered the initial spectrum in both cases and, similarly, monitoring the UV-vis transmission while repeatedly changing between oxidizing and re-reducing potential showed reversible and stable redox switchability for at least 30 cycles.

The UV-vis absorption spectrum of the **RuTphNO₂** 1:1 *co*-polymer (see Figure S61) equals basically the *homo*-polymer. In contrast, the 1:5 film shows an enhanced absorption in the NIR region, characteristic of PEDOT. Remarkably, in contrast to its methylated counterpart, a notable red shift of 1,300 cm⁻¹ between the *homo*-polymer and the 1:5 *co*-polymer appears for the absorption band that occurs around 520 nm, indicating interactions between the metal complex centers and the *poly*- and *oligo*-EDOT moieties. UV-vis-NIR spectroelectrochemical studies on the *co*-polymer films revealed the typical spectral changes during oxidation: For the ruthenium(II)-complex-dominated 1:1 polymer, as soon as the oxidation of the metal center begins, the MLCT absorption band at around 500 nm vanishes, while, beyond 600 nm, a very broad, weak absorption arises, which spans, in contrast to the *homo*-polymer (*vide supra*), the region up to 1,600 nm, attributed to the *oligo*-EDOT chains that were incorporated. However, their influence is significantly smaller than for the 1:1 *co*-polymer of the **RuTphMeNO₂** complex. An isosbestic point at 590 nm, which was not present for the other *co*-polymer studies, supports the presence of only one electrooptically determinant species, namely the ruthenium(II) complex, while the behavior of the other *co*-polymers is composed of metal-complex and PEDOT features. In case of the 1:5 *co*-polymer, both the metal complex moiety and PEDOT chains determine the spectra; a decrease of the complex' MLCT absorption between 400 and 600 nm is accompanied by the emerging of a strong NIR absorption peaking at 1,350 nm. Re-reduction of the polymer films recovered the initial UV-vis-NIR absorption spectra, demonstrating redox stability of the systems. However, for the 1:5 *co*-polymer, repetitive switching of the redox state over 30 cycles showed a diminishing of the maximum absorption change to 95% of the initial value, which could not be observed for the other systems.

Conclusion

Oxidative electrochemical polymerization could successfully be applied to incorporate electron-rich ruthenium(II) complexes of cyclometalating, 1,2,3-triazole-based polypyridyl-type ligands readily equipped with electropolymerizable thiophene moieties into

polymeric thin-film coatings. The use of non-functionalized thiophene-containing complexes led to decomposition reactions during the electropolymerization process, which are attributed to an irreversible, accessible second oxidation of the electron-rich cyclometalating phenyl ring. The subsequent selective introduction of a nitro group at the phenyl ring caused an anodic shift of the decomposition-related electrochemical potentials, but not of the thiophene-assigned ones. Hence, the maximum potential during the potentiodynamic polymerization could be chosen at such a value that the generation of thienyl radicals, which are crucial for the formation of the polymer chains, is possible without competing degradation. Since the problem of undesired side reactions is expected to be a general issue for the oxidative electropolymerization of cyclometalated complexes, this approach is believed to be a generally applicable strategy for the processing of cyclometalated ruthenium(II)-polypyridyl systems. Alternatively, the incorporation of 3,4-ethylenedioxythiophene (EDOT) moieties instead of the thiophene groups into the ruthenium(II) complex represents a possible future approach for an improved electropolymerization as the oxidation potential that is required for radical formation would be lowered. Besides modifications of the metal complexes themselves, an additional *co*-monomer can be used to further enhance the polymerization performance. Consequently, EDOT was utilized to form *co*-polymers with different monomer ratios.

The obtained *homo*-polymer films showed UV-vis absorption up to 700 nm as well as stable redox switchability associated with electrochromicity. The *co*-polymers exhibited UV-vis absorption that is expanded to the NIR region, which is attributed to incorporated *oligo*-/*poly*-EDOT chains, as well as a reversible electrochemical and spectroelectrochemical behavior, reflecting the mixed characteristics of the ruthenium(II) and the EDOT moieties.

In the end, a method is presented to generate conductive photo-redox-active and -stable films featuring a low energy gap, which are believed to show a great potential for application in photovoltaic and electrochromic devices.

Experimental Section

General methods and detailed synthetic procedures can be found in the Supporting Information (further electrochemical and photophysical data?). Crystallographic data (excluding structure factors) has been deposited in the Cambridge Crystallographic Data Centre as supplementary publication CCDC-929252 for **HTphMe**, CCDC-929253 for [Ru^{II}(tpy)(CH₃CN)₂][BF₄]₂, and CCDC-929254 for **RuTphMeNO₂**. Copies of the data can be obtained free of charge on application to CCDC, 12 Union Road, Cambridge CB2 1EZ, UK [E- mail: deposit@ccdc.cam.ac.uk].

Acknowledgements

The authors acknowledge the "Bundesministerium für Bildung und Forschung", the European Social Fund (ESF), the "Thüringer Aufbaubank" (TAB), and the Thuringian Ministry of Economy, Employment and Technology (TMWAT) for financial support. C. F. and B. S. thank the Fonds der Chemischen Industrie for Ph. D. scholarships. M. J. is grateful for financial support of the Carl-Zeiss-Stiftung. We also thank Prof. Dr. Anna Ignaszak for discussions and Peter Schulze for synthetic support.

- [1] a) J.-P. Sauvage, J.-P. Collin, J.-C. Chambron, S. Guillerez, C. Coudret, V. Balzani, F. Barigelletti, L. De Cola, L. Flamigni, *Chem. Rev.* **1994**, *94*, 993-1019; b) A. Juris, V. Balzani, F. Barigelletti, S. Campagna, P. Belser, A. von Zelewsky, *Coord. Chem. Rev.* **1988**, *84*, 85-277; c) T. J. Meyer, *Pure Appl. Chem.* **1986**, *58*, 1193-1206.
- [2] K. Kalyanasundaram, M. Grätzel, *Coord. Chem. Rev.* **1998**, *177*, 347-414.
- [3] a) A. Hagfeldt, G. Boschloo, L. Sun, L. Kloo, H. Pettersson, *Chem. Rev.* **2010**, *110*, 6595-6663; b) H. Tributsch, *Coord. Chem. Rev.* **2004**, *248*, 1511-1530; c)

- M. K. Nazeeruddin, P. Péchy, T. Renouard, S. M. Zakeeruddin, R. Humphry-Baker, P. Comte, P. Liska, L. Cevey, E. Costa, V. Shklover, L. Spiccia, G. B. Deacon, C. A. Bignozzi, M. Grätzel, *J. Am. Chem. Soc.* **2001**, *123*, 1613-1624; d) M. K. Nazeeruddin, A. Kay, I. Rodicio, R. Humphry-Baker, E. Müller, P. Liska, N. Vlachopoulos, M. Grätzel, *J. Am. Chem. Soc.* **1993**, *115*, 6382-6390; e) B. O'Regan, M. Grätzel, *Nature* **1991**, *353*, 737-740.
- [4] a) B. Schulze, D. Escudero, C. Friebe, R. Siebert, H. Görls, S. Sinn, M. Thomas, S. Mai, J. Popp, B. Dietzek, L. González, U. S. Schubert, *Chem. Eur. J.* **2012**, *18*, 4010-4025; b) K. C. D. Robson, B. D. Koivisto, A. Yella, B. Spornova, M. K. Nazeeruddin, T. Baumgartner, M. Grätzel, C. P. Berlinguette, *Inorg. Chem.* **2011**, *50*, 5494-5508; c) P. G. Bomben, T. J. Gordon, E. Schott, C. P. Berlinguette, *Angew. Chem. Int. Ed.* **2011**, *50*, 10682-10685; d) T. Bessho, E. Yoneda, J.-H. Yum, M. Guglielmi, I. Tavernelli, H. Imai, U. Rothlisberger, M. K. Nazeeruddin, M. Grätzel, *J. Am. Chem. Soc.* **2009**, *131*, 5930-5934; e) Y. Eiji, M. Grätzel, M. K. Nazeeruddin, Eur. Pat. Appl. (2009), EP 2036955; f) S. H. Wadman, J. M. Kroon, K. Bakker, M. Lutz, A. L. Spek, G. P. M. van Klink, G. van Koten, *Chem. Commun.* **2007**, 1907-1909.
- [5] a) C.-C. Chou, K.-L. Wu, Y. Chi, W.-P. Hu, S. J. Yu, G.-H. Lee, C.-L. Lin, P.-T. Chou, *Angew. Chem. Int. Ed.* **2011**, *50*, 2054-2058; b) K.-L. Wu, H.-C. Hsu, K. Chen, Y. Chi, M.-W. Chung, W.-H. Liu, P.-T. Chou, *Chem. Commun.* **2010**, *46*, 5124-5126.
- [6] a) H.-J. Park, K. H. Kim, S. Y. Choi, H.-M. Kim, W. I. Lee, Y. K. Kang, Y. K. Chung, *Inorg. Chem.* **2010**, *49*, 7340-7352; b) S. U. Son, K. H. Park, Y.-S. Lee, B. Y. Kim, C. H. Choi, M. S. Lah, Y. H. Jang, D.-J. Jang, Y. K. Chung, *Inorg. Chem.* **2004**, *43*, 6896-6898.
- [7] a) D. G. Brown, P. A. Schauer, J. Borau-Garcia, B. R. Fancy, C. P. Berlinguette, *J. Am. Chem. Soc.* **2013**; b) B. Schulze, D. Escudero, C. Friebe, R. Siebert, H. Görls, U. Köhn, E. Altuntas, A. Baumgaertel, M. D. Hager, A. Winter, B. Dietzek, J. Popp, L. González, U. S. Schubert, *Chem. Eur. J.* **2011**, *17*, 5494-5498; c) O. Schuster, L. Yang, H. G. Raubenheimer, M. Albrecht, *Chem. Rev.* **2009**, *109*, 3445-3478.
- [8] a) B. Schulze, D. G. Brown, K. C. D. Robson, C. Friebe, M. Jäger, E. Birkner, C. P. Berlinguette, U. S. Schubert, *Chem. Eur. J.*, DOI: 10.1002/chem.201301440; b) W. Yang, Y. Zhong, *Chin. J. Chem.* **2013**, *31*, 329-338; c) W.-W. Yang, L. Wang, Y.-W. Zhong, J. Yao, *Organometallics* **2011**, *30*, 2236-2240.
- [9] J. Heinze, B. A. Frontana-Urbe, S. Ludwigs, *Chem. Rev.* **2010**, *110*, 4724-4771.
- [10] a) X. J. Zhu, B. J. Holliday, *Macromol. Rapid Commun.* **2010**, *31*, 904-909; b) J. Hjeltn, R. W. Handel, A. Hagfeldt, E. C. Constable, C. E. Housecroft, R. J. Forster, *Inorg. Chem.* **2005**, *44*, 1073-1081; c) J. A. Moss, J. C. Yang, J. M. Stipkala, X. Wen, C. A. Bignozzi, G. J. Meyer, T. J. Meyer, *Inorg. Chem.* **2004**, *43*, 1784-1792; d) R. M. Leasure, T. Kajita, T. J. Meyer, *Inorg. Chem.* **1996**, *35*, 5962-5963; e) C. P. Horwitz, Q. Zuo, *Inorg. Chem.* **1992**, *31*, 1607-1613; f) T. F. Guarr, F. C. Anson, *J. Phys. Chem.* **1987**, *91*, 4037-4043; g) C. D. Ellis, L. D. Margerum, R. W. Murray, T. J. Meyer, *Inorg. Chem.* **1983**, *22*, 1283-1291; h) P. Denisevich, H. D. Abruña, C. R. Leidner, T. J. Meyer, R. W. Murray, *Inorg. Chem.* **1982**, *21*, 2153-2161.
- [11] a) C.-J. Yao, J. Yao, Y.-W. Zhong, *Inorg. Chem.* **2012**, *51*, 6259-6263; b) C.-J. Yao, Y.-W. Zhong, H.-J. Nie, H. D. Abruña, J. Yao, *J. Am. Chem. Soc.* **2011**, *133*, 20720-20723.
- [12] C.-J. Yao, Y.-W. Zhong, J. Yao, *Inorg. Chem.*, DOI: 10.1021/ic401288g.
- [13] a) C. Friebe, M. D. Hager, A. Winter, U. S. Schubert, *Adv. Mater.* **2012**, *24*, 332-345; b) W. K. Chan, *Coord. Chem. Rev.* **2007**, *251*, 2104-2118; c) M. O. Wolf, *J. Inorg. Organomet. Polym. Mater.* **2006**, *16*, 189-199; d) Y. Liu, Y. Li, K. S. Schanze, *J. Photoch. Photobio. C* **2002**, *3*, 1-23; e) T. Hirao, *Coord. Chem. Rev.* **2002**, *226*, 81-91; f) P. G. Pickup, *J. Mater. Chem.* **1999**, *9*, 1641-1653.
- [14] K. Hu, K. C. D. Robson, P. G. Johansson, C. P. Berlinguette, G. J. Meyer, *J. Am. Chem. Soc.* **2012**, *134*, 8352-8355.
- [15] a) W.-W. Yang, J. Yao, Y.-W. Zhong, *Organometallics* **2012**, *31*, 1035-1041; b) M. Beley, S. Chodorowski, J.-P. Collin, J.-P. Sauvage, L. Flamigni, F. Barigelletti, *Inorg. Chem.* **1994**, *33*, 2543-2547; c) M. Beley, J. P. Collin, R. Louis, B. Metz, J. P. Sauvage, *J. Am. Chem. Soc.* **1991**, *113*, 8521-8522.
- [16] a) S. Potratz, A. Mishra, P. Bäuerle, *Beilstein J. Org. Chem.* **2012**, *8*, 683-692; b) I. Stengel, C. A. Strassert, E. A. Plummer, C.-H. Chien, L. De Cola, P. Bäuerle, *Eur. J. Inorg. Chem.* **2012**, *2012*, 1795-1809; c) A. Wild, C. Friebe, A. Winter, M. D. Hager, U.-W. Grummt, U. S. Schubert, *Eur. J. Org. Chem.* **2010**, *2010*, 1859-1868.
- [17] J. D. Crowley, D. A. McMorran, in *Click Triazoles*, Vol. 28 (Ed.: J. Košmrlj), Springer Berlin Heidelberg, **2012**, p. 31-83.
- [18] C. Friebe, H. Görls, M. Jäger, U. S. Schubert, *Eur. J. Inorg. Chem.* **2013**, 4191-4202.
- [19] M. Lamberti, G. C. Fortman, A. Poater, J. Broggi, A. M. Z. Slawin, L. Cavallo, S. P. Nolan, *Organometallics* **2012**, *31*, 756-767.
- [20] a) W. Chen, G. Xue, *Prog. Polym. Sci.* **2005**, *30*, 783-811; b) S. Jin, G. Xue, *Macromolecules* **1997**, *30*, 5753-5757.
- [21] M. Gagliardo, D. J. M. Snelders, P. A. Chase, R. J. M. Klein Gebbink, G. P. M. van Klink, G. van Koten, *Angew. Chem. Int. Ed.* **2007**, *46*, 8558-8573.
- [22] A. R. Katritzky, E. F. V. Scriven, S. Majumder, R. G. Akhmedova, N. G. Akhmedov, A. V. Vakulenko, *ARKIVOC* **2005**, *iii*, 179-191.
- [23] L. Farrugia, *J. Appl. Crystallogr.* **1997**, *30*, 565.
- [24] S. H. Wadman, R. W. A. Havenith, M. Lutz, A. L. Spek, G. P. M. van Klink, G. van Koten, *J. Am. Chem. Soc.* **2010**, *132*, 1914-1924.
- [25] M. Lundberg, P. E. M. Siegbahn, *J. Chem. Phys.* **2005**, *122*, 224103.
- [26] M. L. Naklicki, S. I. Gorelsky, W. Kaim, B. Sarkar, R. J. Crutchley, *Inorg. Chem.* **2012**, *51*, 1400-1407.
- [27] A. J. Cohen, P. Mori-Sánchez, W. Yang, *Science* **2008**, *321*, 792-794.
- [28] D. H. Ess, T. C. Cook, *J. Phys. Chem. A* **2012**, *116*, 4922-4929.

Received: ((will be filled in by the editorial staff))

Revised: ((will be filled in by the editorial staff))

Published online: ((will be filled in by the editorial staff))

Scheme 1. Synthesis of the thiophene-containing cyclometalated ruthenium(II) complexes: a) Pd(PPh₃)₄, K₂CO₃, DMF, 50 °C, 12 h, 40%; b) CuSO₄·5H₂O, NaAsc., CH₂Cl₂/EtOH/H₂O (1:2:1), 50 °C, 12 h, 70%; c) EtOH/toluene (1:1) or DMF, 140 to 160 °C, 30 to 120 min., 50%. **Ru** was prepared previously in an analogous synthesis.^[4a]

Scheme 2. Synthesis of the nitro-functionalized thiophene-containing cyclometalated ruthenium(II) complexes: a) Cu(NO₃)₂, CH₂Cl₂/MeOH (2:1 to 3:1), rt, 96 h, 67 to 85%. **RuNO₂** was prepared previously in an analogous synthesis.^[4a]

Figure 1. CV development during electropolymerization attempts for **RuTphMe** in CH₂Cl₂ (10⁻⁴ M with 0.1 M Bu₄NPF₆).

Figure 2. Cyclic voltammograms depicting the oxidation processes of **RuTphMe** and **RuTphMeNO₂** in comparison to the parent **RuNCN** and **RuNCN-NO₂** (10⁻⁴ M in CH₃CN with 0.1 M

Figure 3. ORTEP plot^[23] of **RuTphMeNO₂**, thermal ellipsoids drawn at 50% probability level, solvent molecules, counterion, and hydrogen atoms omitted for clarity. Disorder of a thiophene omitted for clarity. Selected bond lengths (Å) and angles (°): Ru–C1, 1.981(4); Ru–N1, 2.085(4); Ru–N2, 2.032(3); Ru–N3, 2.075(4); Ru–N4, 2.082(3); Ru–N5, 2.052(3); N4–Ru–N5, 155.56(13); N1–Ru–N3, 155.89(14).

Figure 4. Spin density of singly oxidized (top) and doubly oxidized triplet (bottom) state of **RuTphNO₂** (dark and light regions indicate excess of alpha and beta-spin, respectively; iso value 0.002).

Figure 5. CV and peak-current development during the electropolymerization of **RuTphMeNO₂** in CH₂Cl₂ (10⁻⁴ M with 0.1 M Bu₄NPF₆).

Figure 6. CVs of **RuTphMeNO₂** showing the first oxidation process at different scan rates. Inset: Relationship between peak currents and applied scan rate. (Film on glassy-carbon disk electrode in CH₂Cl₂ with 0.1 M Bu₄NPF₆.)

Figure 7. CV and peak-current development during the electropolymerization of **RuTphNO₂** in CH₂Cl₂ (10⁻⁵ M with 0.1 M Bu₄NPF₆).

Figure 8. CVs of **RuTphNO₂** showing the first oxidation process at different scan rates. Inset: Relationship between peak currents and applied scan rate. (Film on glassy-carbon disk electrode in CH₂Cl₂ with 0.1 M Bu₄NPF₆.)

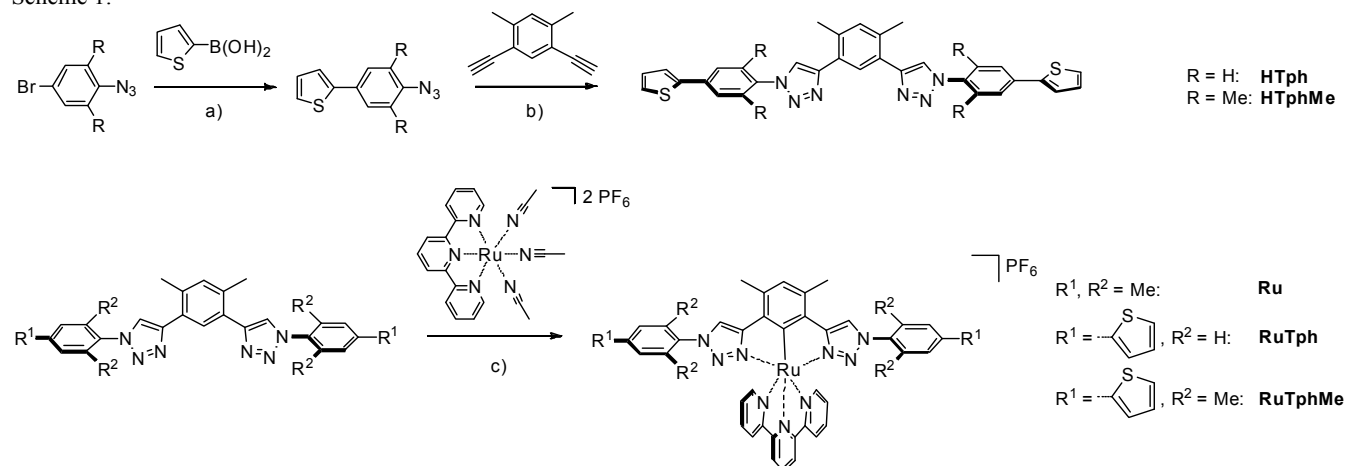
Figure 9. CV and peak-current development during the *co*-electropolymerization of **RuTphMeNO₂** with EDOT in CH₂Cl₂ (10⁻⁴ M with 0.1 M Bu₄NPF₆) using a molar ratio of 1:1.

Figure 10. CVs of electropolymerized *co*-polymer films from **RuTphMeNO₂** and EDOT showing the first oxidation process at different scan rates and relationship between peak currents and applied scan rate (films on glassy-carbon disk electrode in CH₂Cl₂ with 0.1 M Bu₄NPF₆) for a molar ratio of 1:1.

Figure 11. UV-vis absorption spectrum of electropolymerized films (□) from **RuTphMeNO₂** (top) and **RuTphNO₂** (bottom) in comparison to the drop-casted monomer (Δ) (films on ITO-coated glass) and the dissolved monomer (○) (10⁻⁶ M in CH₂Cl₂).

Figure 12. Change of the UV-vis absorption spectrum of an electropolymerized film of **RuTphNO₂** during the oxidation and re-reduction (●) process. (Note that the underlying absorbance between 800 and 1,100 nm (*) is attributed to the ITO substrate.) Inset: Change of transmission at 510 nm over 30 cycles of switching between initial and oxidized state. (Film on ITO-coated glass in CH₂Cl₂ with 0.1 M Bu₄NPF₆.)

Scheme 1:



Scheme 2:

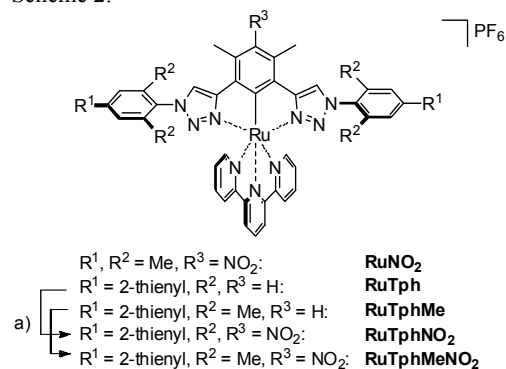


Figure 1:

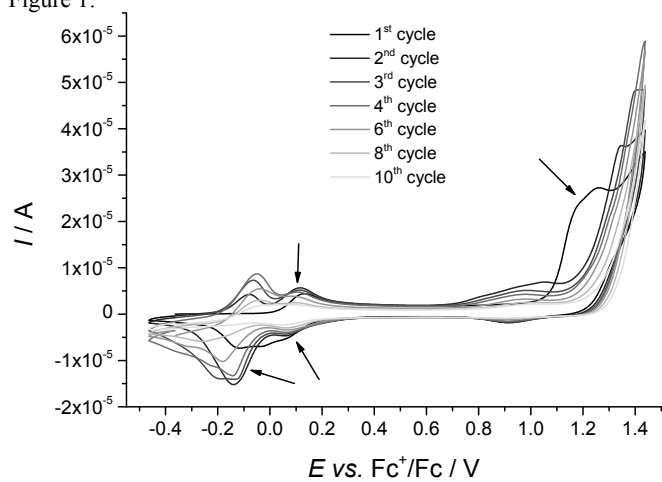


Figure 2:

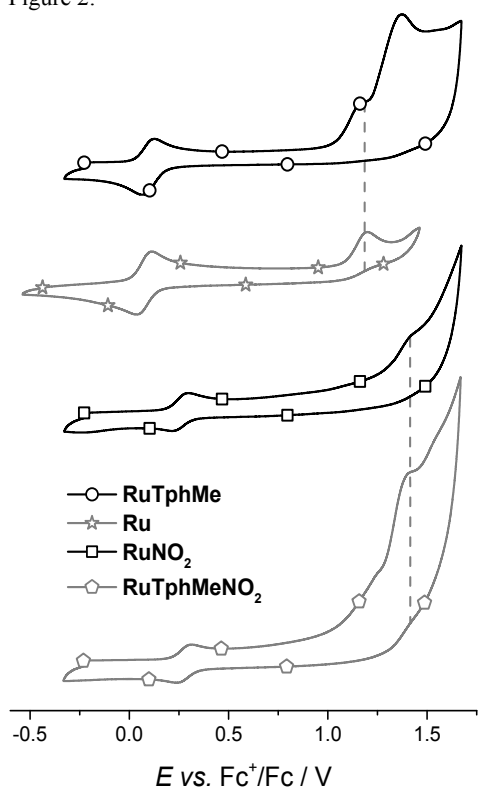


Figure 3:

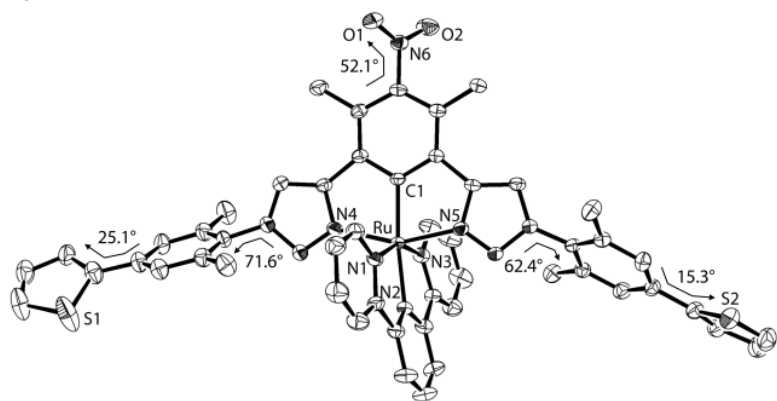


Figure 4:

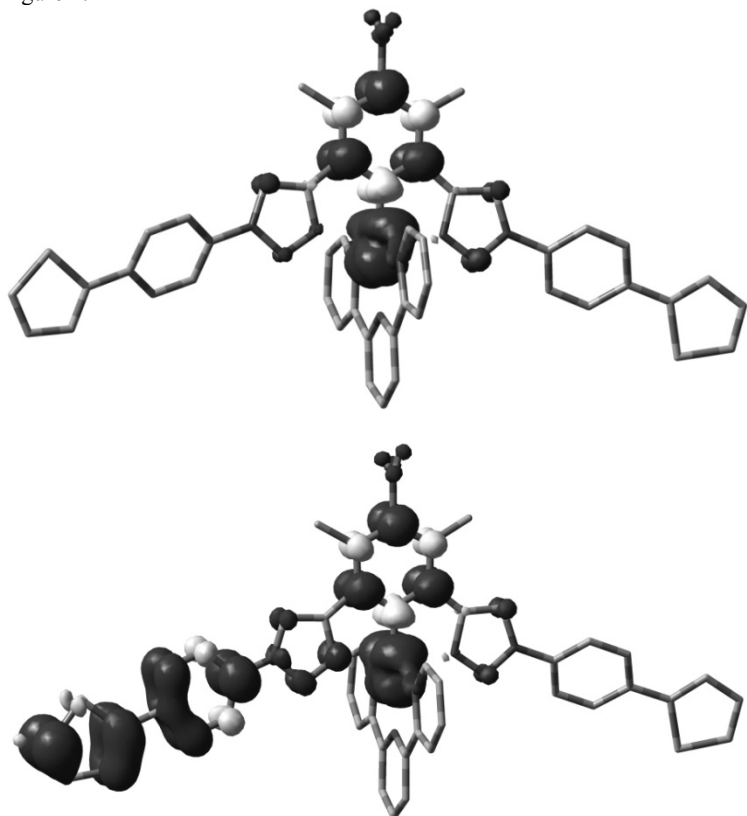


Figure 5:

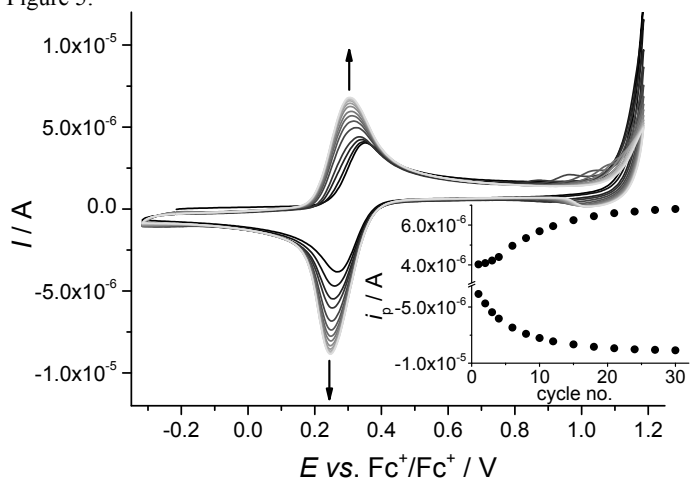


Figure 6:

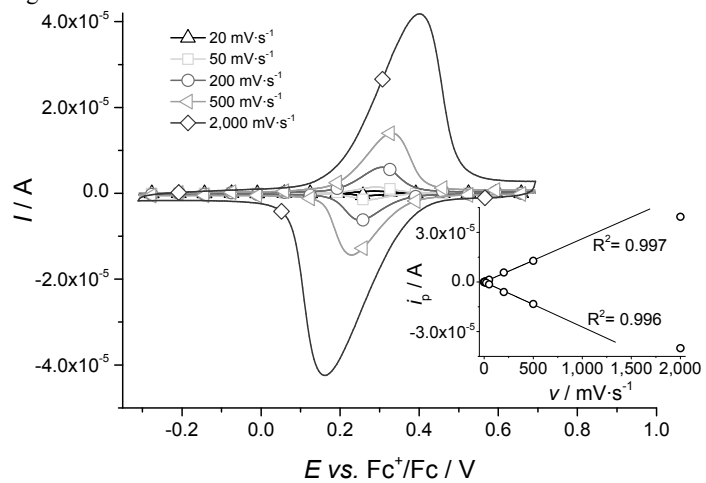


Figure 7:

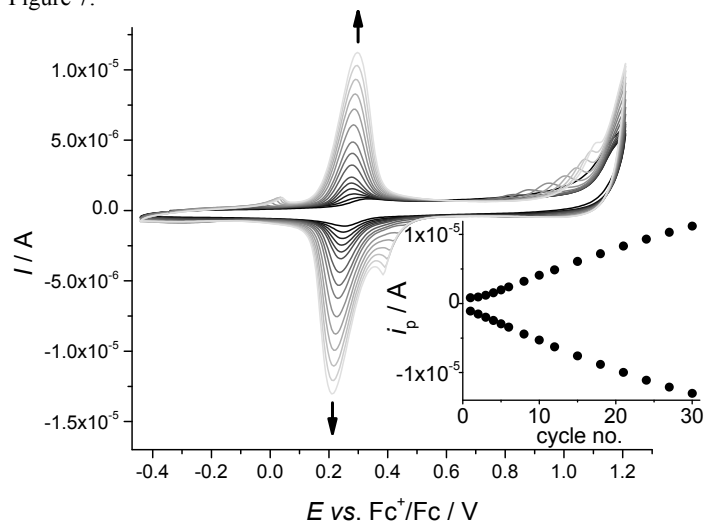


Figure 8:

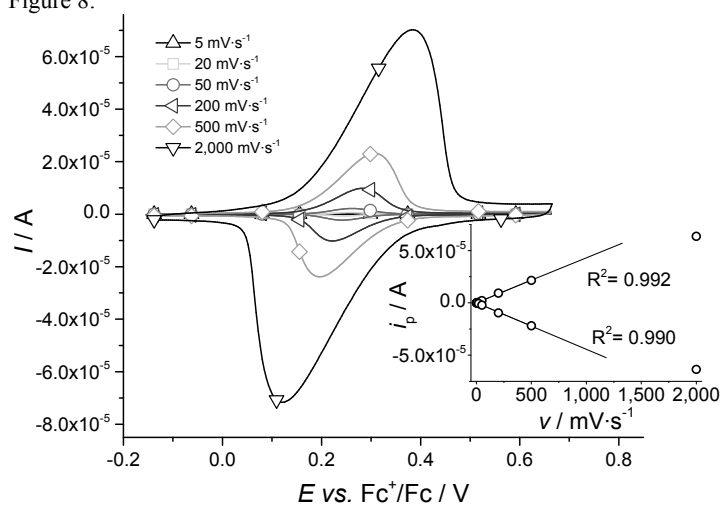


Figure 9:

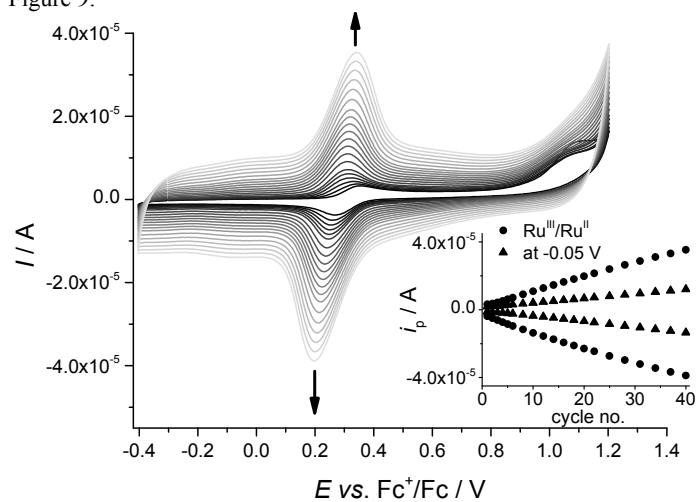


Figure 10:

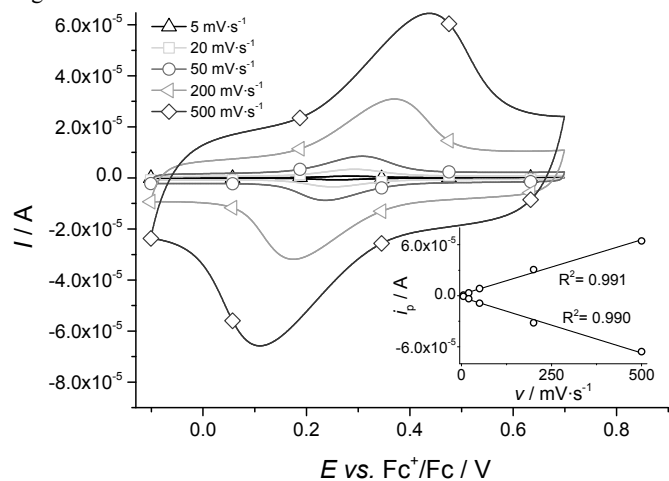


Figure 11:

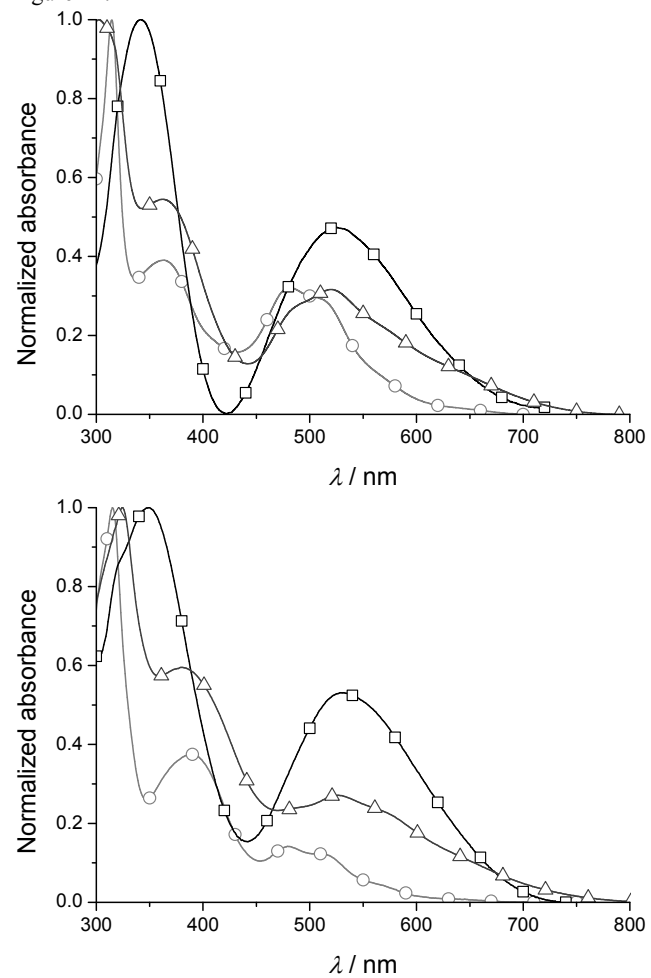
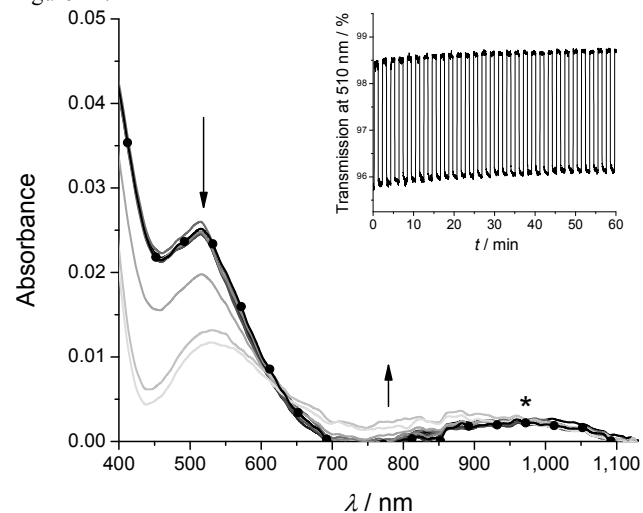


Figure 12:

Table 1. Electrochemical characteristics of the monomer complexes (10^{-4} M in CH_2Cl_2 with 0.1 M Bu_4NPF_6).

| Complex | $E_{1/2} / \text{V}$ (i_{pa}/i_{pc} , $\Delta E_p / \text{mV}$) ^[a] | |
|------------------------------|--|-------------------------------|
| | +1 → +2 | +1 → 0 |
| RuTph | 0.10 (1.05, 65) | -2.12 (irrev.) ^[b] |
| RuTphMe | 0.10 (1.0, 74) | -2.17 (irrev.) ^[b] |
| RuTphNO₂ | 0.29 (1.0, 67) | -1.87 (1.0, 75) |
| RuTphMeNO₂ | 0.31 (1.0, 72) | -1.88 (1.05, 78) |

[a] Potentials vs. Fc^+/Fc . [b] Peak potential of the cathodic wave.Table 2. UV-vis spectroscopical characteristics of the monomer complexes (10^{-6} M in CH_2Cl_2).

| Complex | $\lambda_{\text{Abs}} / \text{nm}$ ($\epsilon / 10^3 \text{ M}^{-1} \cdot \text{cm}^{-1}$) ^[a] | $\lambda_{\text{Em}} / \text{nm}$ |
|------------------------------|---|-----------------------------------|
| RuTph | 685s (0.7), 586s (5.0), 533 (9.5), 491 (11.0), 388 (43.8) | 733 |
| RuTphMe | 689s (0.8), 590s (5.5), 536 (10.5), 491 (12.8), 372 (32.1) | 743 |
| RuTphNO₂ | 645s (0.7), 570s (4.0), 507 (11.8), 479 (13.7), 389 (36.3) | 689 |
| RuTphMeNO₂ | 642s (0.7), 560s (5.6), 515 (14.3), 482 (16.5), 361 (26.1) | 690 |

[a] s...shoulder.